AD NUMBER: AD0511990
CLASSIFICATION CHANGES
TO: Unclassified
FROM: Confidential
LIMITATION CHANGES
TO: Approved for public release; distribution is unlimited.
FROM: Distribution authorized to U.S. Gov't. agencies and their contractors; Export Control; 31 Oct 1970. Other requests shall be referred to Air Force System Command, Air Force Rocket Propulsion Laboratory, Edwards AFB, CA
AUTHORITY
31 Oct 1982 C TO U GROUP 4. ST-A AFRPL LTR 5 FEB 1986

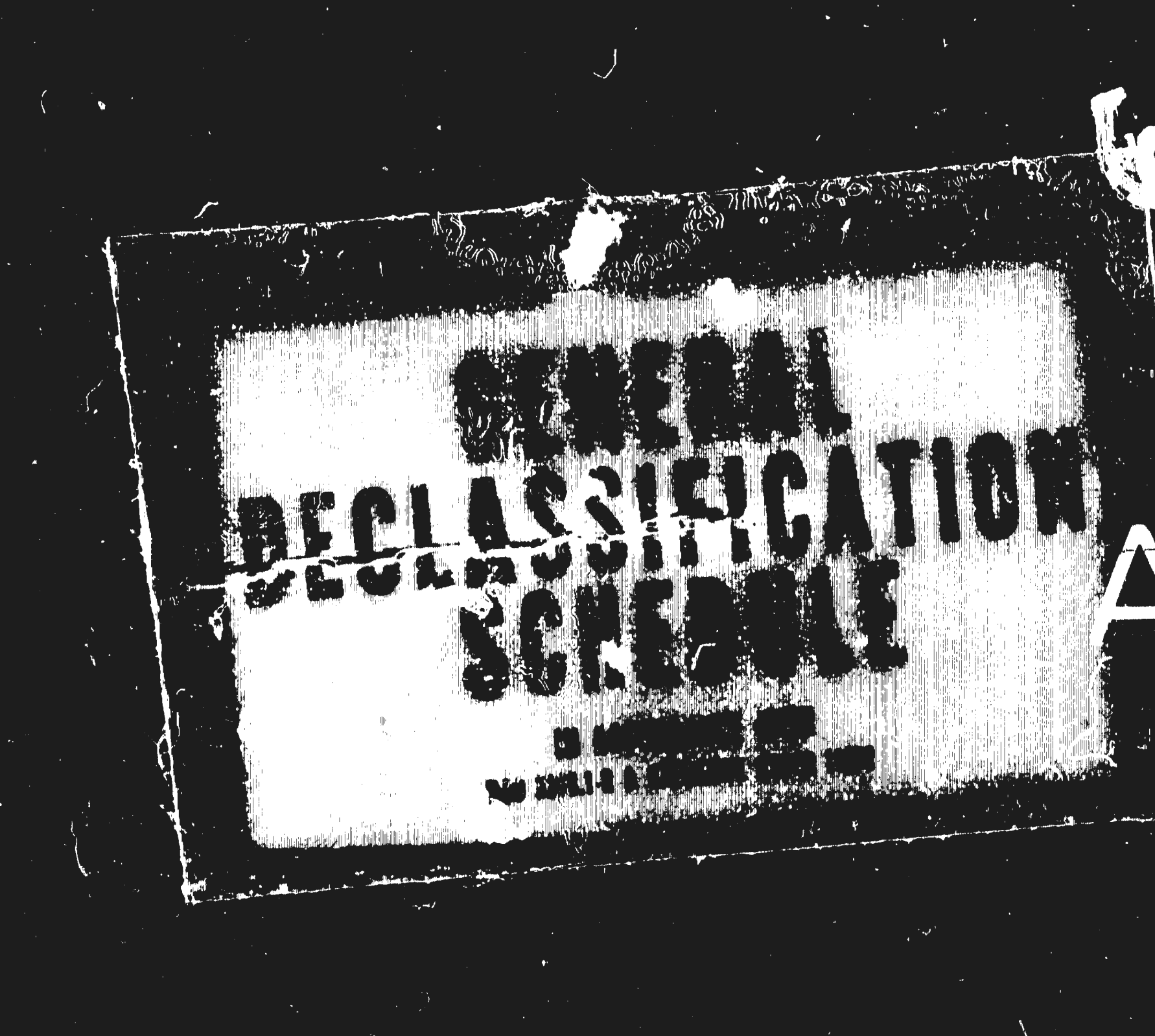
GENERAL
DECLASSIFICATION
SCHEDULE

SECURITY MARKING

The classified or limited status of this report applies to each page, unless otherwise marked.

Separate page printouts MUST be marked accordingly.

THIS DOCUMENT CONTAINS INFORMATION AFFECTING THE NATIONAL DEFENSE OF THE UNITED STATES WITHIN THE MEANING OF THE ESPIONAGE LAWS, TITLE 18, U.S.C., SECTIONS 793 AND 794. THE TRANSMISSION OR THE REVELATION OF ITS CONTENTS IN ANY MANNER TO AN UNAUTHORIZED PERSON IS PROHIBITED BY LAW.

NOTICE: When government or other drawings, specifications or other data are used for any purpose other than in connection with a definitely related government procurement operation, the U. S. Government thereby incurs no responsibility, nor any obligation whatsoever; and the fact that the Government may have formulated, furnished, or in any way supplied the said drawings, specifications, or other data is not to be regarded by implication or otherwise as in any manner licensing the holder or any other person or corporation, or conveying any rights or permission to manufacture, use or sell any patented invention that may in any way be related thereto.

CONFIDENTIAL

AFRPL-TR-70-127

(UNCLASSIFIED TITLE)

ADVANCED MANEUVERING PROPULSION TECHNOLOGY PROGRAM - INTERIM FINAL REPORT

(VOLUME II: FLUORINE/HYDROGEN ENGINE CRITICAL COMPONENT DEMONSTRATION TESTING)

Rocketdyne
A Division of North American Rockwell Corporation
6633 Canoga Avenue
Canoga Park, California

Technical Report AFRPL-TR-70-127

October 1970

Group 4
Downgraded at 3-Year Intervals
Declassified After 12 Years

In addition to security requirements which must be met, this document is subject to special export controls and each transmittal to foreign governments or foreign nationals may be made only with prior approval of AFRPL(RPPR/STINFO), Edwards, California, 93523.

Air Force Rocket Propulsion Laboratory
Air Force Systems Command
United States Air Force
Edwards Air Force Base, California

CONFIDENTIAL

CONFIDENTIAL

(18) (19) AFRPL-TR-70-127-Vol-2

(6) (UNCLASSIFIED TITLE)

ADVANCED MANEUVERING PROPULSION TECHNOLOGY PROGRAM - [redacted]

VOLUME II. [FLUORINE/HYDROGEN] ENGINE CRITICAL COMPONENT DEMONSTRATION TESTING (U). (8)

(9) Interim final rept. Nov 67 - Jun 70.

ROCKETDYNE
A Division of North American Rockwell Corporation
6633 Canoga Avenue
Canoga Park, California

Technical Report AFRPL-TR-70-127

(11) Oct[redacted]70

(12) 441 p.

(17) R-8280-Vol-2

Group 4
Downgraded at 3-Year Intervals
Declassified After 12 Years

(15) F04611-67-C-0116

Air Force Rocket Propulsion Laboratory
Air Force Systems Command
United States Air Force
Edwards Air Force Base, California

308 000

1473

mk

CONFIDENTIAL

(U) FOREWORD

(U) This technical report presents the results of Task I, Engine System Analysis and Design, and Task II, Engine Critical Component Demonstration Testing, conducted as part of the Advanced Maneuvering Propulsion Technology (AMPT) Program. The program conducted by Rocketdyne, a Division of North American Rockwell, during the period of November 1967 to June 1970, was authorized by the USAF Rocket Propulsion Laboratory under contract F04611-67-C-0116.

(U) The Air Force program manager was Mr. R. L. Wiswell and the Air Force project engineer was Mr. W. W. Wells. Mr. R. R. Morin was the Rocketdyne program manager, Mr. H. G. Diem the Rocketdyne assistant program manager, and Mr. D. H. Huang the Rocketdyne project engineer.

(U) This report was submitted on 31 July 1970 as Rocketdyne report number R-8280, Volumes I and II. These volumes are:

I. Engine System Analysis and Design
II. Engine Critical Component Demonstration Testing

(U) Task III of the program, Propellant Feed System Analysis and Design, was conducted by two vehicle company subcontractors (General Dynamics/Convair and Lockheed Missiles and Space Company), and the results are published separately as reports AFRPL-TR-70-103 and AFRPL-TR-70-104, respectively.

(U) A separate Materials and Processes report was published as AFRPL-TR-70-126.

(U) This technical report has been reviewed and is approved.

R. L. Wiswell,
AFRPL AMPT Program Manger,
RPRES

(This page is Unclassified)

(U) ABSTRACT

(U) The results of the Advanced Maneuvering Propulsion System (AMPS) engine critical component evaluations are presented. The components included segments of the main aerospike thrust chamber, complete main aerospike thrust chamber assembly, and main and secondary engine LF_2 pump bearings and seals.

(U) Performance, regenerative cooling, and combustion stability were demonstrated on aerospike thrust chamber segment firing tests. Fabrication of a complete 12-segment thrust chamber assembly was completed.

(U) Dyanmic testing of the pump bearings and seals was accomplished; however, sufficient durations were not accumulated at design conditions to demonstrate feasibility and durability of the bearings and seals.

CONTENTS

ILLUSTRATIONS

TABLES

ABBREVIATIONS AND SYMBOLS

A	area
ADP	advanced development program
B-4A	test stand designation
c*	characteristic velocity
C_F	thrust coefficient
c_p	specific heat
CR	Chicago Rawhide
CRES	corrosion-resistant steel
D/N	diameter-to-speed ratio
EB	electron beam
EDM	electrical-discharge machining
G_c	chamber contour designation
h_c	coolant side heat transfer coefficient
h_g	gas-side heat transfer coefficient
ID	inside diameter
K	chamber contour designation
k	thermal conductivity
LF_2	liquid fluorine
LH_2	liquid hydrogen
LN_2	liquid nitrogen
MOV	main oxidizer valve
MR	mixture ratio
NFL	Nevada Field Laboratory
P_r	Prandtl number = $\frac{\mu c_p}{k}$

OD	outside diameter
p	pressure
P_c	chamber pressure
P/N	part number
$\dot{Q}$	heat transfer per second
scim	standard cubic inch per minute
S/N	serial number
St	Stanton number = $\frac{h_g}{V \rho c_p}$
T	temperature
T_{AB}	temperature, adiabatic wall
T_b	temperature, bulk
T_{wg}	temperature, gas wall
U/N	unit number
V	velocity
$\dot{w}$	weight flowrate
1-D	one dimensional
2-D	two dimensional
ΔH	enthalpy change
ΔP	pressure change
ΔT	temperature change
ϵ	expansion area ratio
μ	viscosity
ρ	density

SECTION I

(U) INTRODUCTION

(U) The Advanced Maneuvering Propulsion Technology (AMPT) Program is being conducted to provide technology advancements applicable to future high-energy advanced maneuvering propulsion systems. The first portion of the program, reported in this volume, was conducted during the period of November 1967 to June 1970, and was devoted to a fluorine/hydrogen (F_2/H_2) propulsion system. A typical system is illustrated in Fig. 1 with some of the basic design parameters for the Advanced Development Program (ADP), together with some of the design variations that were also considered.

(C) The fluorine/hydrogen engine configuration (Fig. 2) utilizes concentric thrust chambers. The outer main thrust chamber (30,000 pounds thrust) incorporates the toroidal-aerodynamic spike design concept. The inner secondary thrust chamber (3300 pounds thrust) is a bell-type design. The thrust chambers are fed from independent turbopumps that are driven by hot gases from each thrust chamber. Each thrust chamber can be throttled over a 9:1 thrust range, which gives the engine system an overall throttle ratio of 81:1. The normal mode of operation is for the thrust chambers to fire one at a time.

(C) The fluorine/hydrogen propellant feed system consists of the main propellant tankage; thermal conditioning and support structure; zero-gravity expulsion system; fill, vent, feed, and drain lines; propellant management system; and a pressurization system. The 18,000-pound weight for the complete propulsion system, together with a 2000-pound payload (20,000 pounds total), is compatible with the present Titan III-D launch vehicle for polar orbit launches from the Air Force Western Test Range. A gimbal angle of ±10 degrees was selected to provide the capability for rapid turning maneuvers. System thermal design provides the capability of at least 14 days in orbit with no fluorine loss and with very little hydrogen loss, depending on the mission duty cycle.

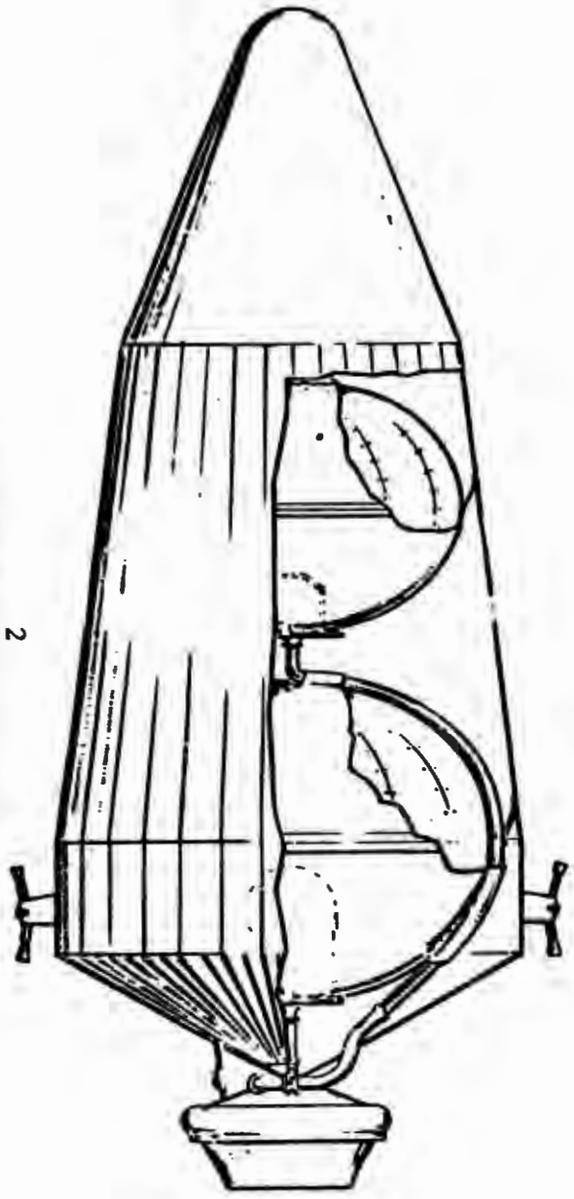

	DESIGN POINT FOR ADP	DESIGN VARIATIONS BEING CONSIDERED
PROPULSION SYSTEM WEIGHT, LB	18,000	10,000 TO 75,000
PAYLOAD WEIGHT, LB	2,000	1,000 TO 25,000
THRUST (MAXIMUM), LB	30,000	VARIATIONS WITH STAGE SIZE & APPLICATION
LAUNCH VEHICLE	TITAN III D	FAMILY OF LAUNCH VEHICLES
SPACE RESIDENCE TIME	14 DAYS (NO F_2 VENTING)	UP TO 180 DAYS
RESTARTS	30 MINIMUM	VARIATIONS WITH MISSION REQUIREMENTS
PAD HOLD CAPABILITY	• NO F_2 VENTING • H_2 VENTING & TOPPING	NEAR INSTANT LAUNCH READINESS
FLIGHT PLAN	• NO SUBORBITAL BURN • 100 NM, CIRCULAR POLAR ORBIT	DEPENDENT ON APPLICATION

CONFIDENTIAL

Figure 1. System Characteristics (U)

CONFIDENTIAL

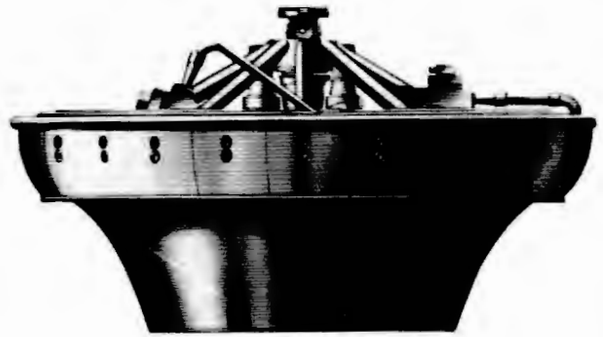

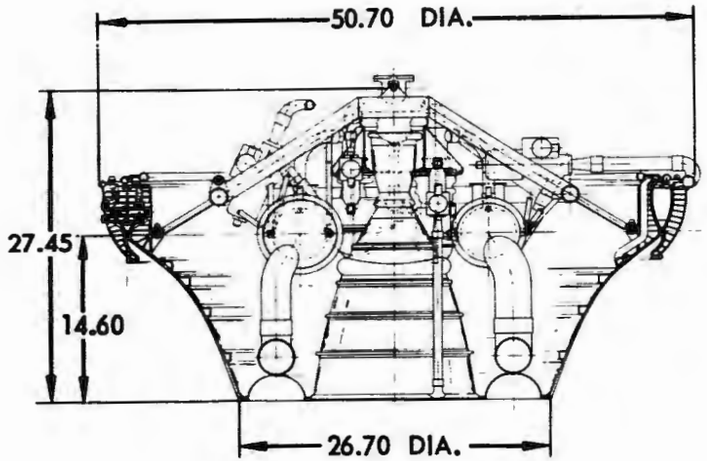

PARAMETER	MAIN ENGINE	SECONDARY ENGINE
THRUST, POUNDS	30,000	3,300
CHAMBER PRESSURE, PSIA	650	750
VACUUM SPECIFIC IMPULSE, SECONDS	460	457.5
MIXTURE RATIO, O/F	12:1	12:1
THROTTLE RATIO	9:1	9:1
AREA RATIO	60:1	60:1

CONFIDENTIAL

Figure 2. Engine System for Advanced Maneuvering Propulsion System (U)

(C) The AMPT Program for the fluorine/hydrogen propulsion system originally consisted of two phases, Phase I of the program, which was for a 32-month period, included the following three tasks:

Task I: Engine Analysis and Design

Task II: Engine Critical Component Demonstration Testing

Task III: Propellant Feed System Analysis and Design

(U) Tasks I and II were accomplished by Rocketdyne, and Task III was performed by two vehicle company subcontractors--General Dynamics/Convair and Lockheed Missiles and Space Company.

(U) Phase II of the program was to provide for detail design, fabrication, and demonstration test of the complete propulsion system. The system, of flight-type design, was to be based on engine and propellant feed system design analyses and layout drawings generated in Phase I. Phase II of the program was not accomplished, however, because of redirection of the program by the Air Force. This volume of the report covers the work performed on the engine critical component demonstration testing (Task II) for the fluorine/hydrogen propulsion system.

SECTION II

(U) ## SUMMARY

(U) This report presents the results of the work accomplished on Task II, Fluorine/Hydrogen Engine Critical Component Demonstration Testing, which was conducted as part of the Advanced Maneuvering Propulsion Technology Program. The critical engine components included segments of the main aerospike thrust chamber, complete main aerospike thrust chamber assembly, and main and secondary engine LF_2 pump bearings and seals. A schedule of the Task II effort, together with Tasks I and III, is shown in Fig. 3 .

(U) ## 1. AEROSPIKE THRUST CHAMBER DESIGN APPROACH

(U) The AMPS aerospike thrust chamber utilizes the segmentation design approach. The chamber is made up of 12 segments, each of which is a 30-degree sector of the complete chamber. Each segment is a regeneratively cooled individual combustion chamber compartment consisting of an outer body wall, an inner body wall, two end plates, and an injector. The end plates extend from the injector end of the chamber, through the throat section to the end of the outer body expansion shroud. This provides for full combustion chamber compartmentation; a feature desirable for stable combustion.

(U) The aerospike thrust chamber is assembled using 12 segments that are bolted together at their end plates. A one-piece nozzle skirt--which attaches to the assembled segment ring, a base closure, a thrust mount, and propellant manifolding--completes the main thrust chamber assembly.

(U) The segmentation design approach permits significant development advantages. Testing of individual segments provides an economical and rapid means for evaluating basic combustion performance, heat transfer, and structural characteristics of the design. After basic development problems are solved with segment testing, the full thrust chamber is fabricated, assembled, and tested for verification of overall performance and operating characteristics.

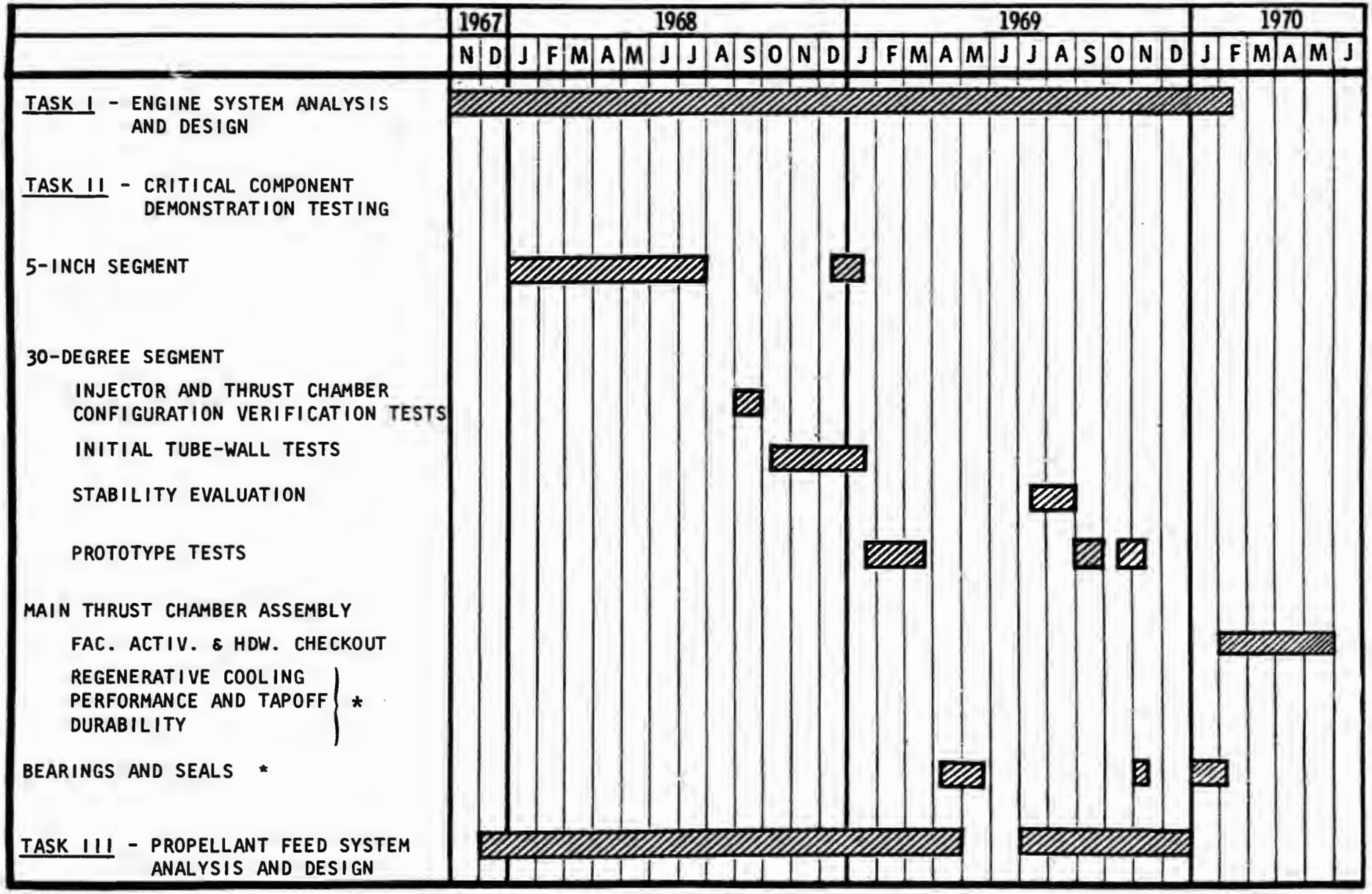

*NOT COMPLETED

Figure 3. AMPT Phase I Program (U)

(U) Another advantage of the segmentation design approach is that it lends itself readily to production fabrication methods because a significant number of parts of identical design (segments) are manufactured. This inherently results in reduced fabrication costs.

(U) The segmentation design approach also provides the capability for individual segment removal, replacement, and refurbishment. This should greatly enhance the reusability and operational life of the engine. A significant cost factor is that complete chamber scrappage may be avoided in the event the combustion chamber is damaged locally during fabrication or testing.

(U) The aerospike thrust chamber design for Phase I utilizes a heavyweight support structure because it was not an early program objective to demonstrate flightweight components. However, the geometrical and functional related aspects of the chamber (e.g., cooling, performance, etc.) were of flight prototype design. Subsequent program phases would incorporate lightweight support structure.

(U) 2. AEROSPIKE THRUST CHAMBER DEVELOPMENT

(C) The aerospike thrust chamber development included testing of both water-cooled and regeneratively cooled segments with the objectives of demonstrating performance, combustion stability, and regenerative cooling over the complete throttle range of 9:1. The performance goal was to demonstrate 97 percent of theoretical c* efficiency (shifting composition) over the complete throttle range; this goal was achieved. Regenerative cooling was demonstrated at design flowrates with the flight prototype cooling circuit design.

(U) The sequence of segment testing, illustrated in Fig. 4, included a total of 255 firings. Initial segment firings were conducted with segments of 5-inch equivalent circumferential length and provided performance and heat transfer characterization of candidate injectors and combustion chamber geometries.

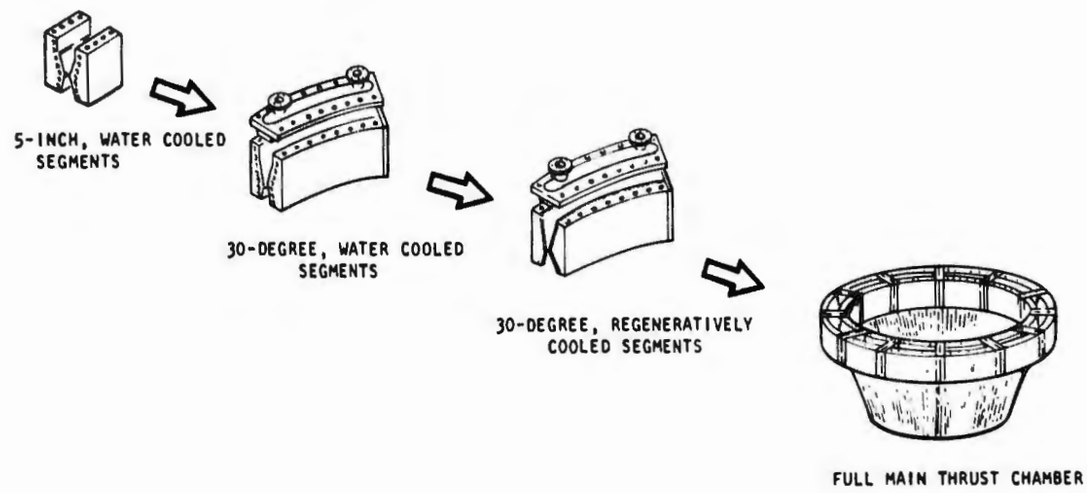

Figure 4. Main Thrust Chamber Hardware Development Sequence (U)

(U) The selected chamber geometry and injector design were then verified in the full-size, 30-degree, water-cooled segment hardware. Following these tests, two candidate regenerative coolant circuit designs (tubular and channel wall) were evaluated in full-size, 30-degree segment hardware. From the results of this testing, the prototype 30-degree segment channel-wall design was finalized for the aerospike thrust chamber.

(U) The complete aerospike thrust chamber was assembled using 12 segment units, a nozzle extension, base closure, propellant distribution manifolds, thrust mount, and miscellaneous plumbing for purges, instrumentation, etc. The assembly is shown in Fig. 5 and was to undergo hot-firing tests at Rocketdyne's Nevada Field Laboratory. The testing, however, was not accomplished because of a facility incident which occurred during facility activation checkouts. Serious facility damage resulted, and the testing was not accomplished.

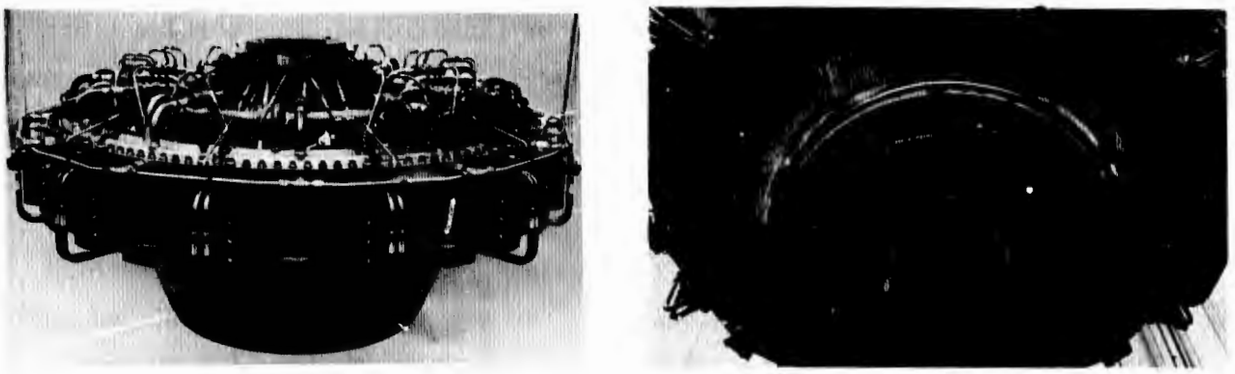

SIDE VIEW AFT VIEW

Figure 5 . Main Thrust Chamber Assembly (U)

(U) 3. FLUORINE TURBOPUMP BEARINGS AND SEALS

(U) Dynamic testing of the main and secondary fluorine turbopump bearings and seals was accomplished using testers which simulated the operating conditions and environments of the actual turbopump. Sufficient durations, however, were not accumulated at maximum design conditions to fully demonstrate feasibility and durability of the designs.

(U) Tester operational difficulties were encountered during the program. The bearings, however, were in satisfactory condition after each test (except where damage attributed to other causes occurred) in spite of overspeed, lack of coolant flow, and abnormal loading conditions. Insufficient testing was accomplished to demonstrate durability; however, the bearings were run for short periods at full load and speed without failure.

(C) The bellows-type primary fluorine seal with the plasma-sprayed Al_2O_3 nose performed satisfactorily during the limited testing at normal operating conditions. Insufficient testing was accomplished to establish wear rates and demonstrate durability; however, the sealing efficiency was satisfactory during the limited testing that was performed. Kentanium K162B and solid Al_2O_3 insert configurations leaked excessively at high pressure due to thermal distortion of the seal face.

(C) The Am-Cer-Met 701-65, floating ring purged intermediate seal proved to be very effective for the separation of the oxidizer and turbine drain cavities. The seal survived extremes of operation with very little damage and performed very satisfactorily. The rubbing characteristics of the material against the BaF_2-CaF_2 coated mating surface were satisfactory.

(U) The main turbine bellows face-type carbon seal performed satisfactorily during the limited testing; however, the secondary turbine seal bellows failed after short periods on all the seals tested. The failure mode appeared to be fatigue of the bellows plate adjacent to the weld due to resonant vibration excited by running in a dry atmosphere of nitrogen gas. Nonlubricated seal faces will initiate a resonance frequency vibration due to a stick-slip condition (difference between static and dynamic coefficients of friction) at the rubbing face. The secondary seal does not have vibration dampers due to the small size and limited space available. Redesign of the seal to add a damper similar to the one used on the main seal would be possible. In the actual turbine, however, sufficient lubrication would probably be present from the hot gas products.

SECTION III

MAIN THRUST CHAMBER

1. THRUST CHAMBER ASSEMBLY DESCRIPTION

(U) The Phase I main engine thrust chamber (Fig. 6) consists of an annular combustion chamber with regeneratively cooled inner and outer bodies and a regeneratively cooled nozzle extension which is attached to the inner body. The annular combustion chamber is divided into 12 equal segments by structural end plates (baffles) that extend from the injector face to the end of the expansion shroud on the outer body. The complete thrust chamber is assembled by joining 12 of these segments together at the inner end plates. The segmentation design approach is illustrated in Fig. 7 .

(C) A single-pass, channel-wall, regenerative cooling system is used in the combustion chamber, and a two-pass, tubular wall, regenerative system is used in the nozzle. The combined cooling circuit is illustrated in Fig. 8 with the full-thrust pressure and temperature conditions shown. The minimum thrust conditions are shown in Fig. 9 . Hydrogen from the pump discharge is ducted to the inboard side of the segment end plate. The end plate is cooled in a single downpass. The coolant is then transferred (through an external duct) to the outboard, upper end of the segment end plate. The hydrogen is then distributed along the segment outer body and cools the outer body in a single downpass. The coolant is then collected and transferred, through the lower portion of the segment end plate, to a distribution manifold at the lower end of the chamber segment inner body. The inner body is then cooled in a single up-pass. The coolant is collected and transferred through external tubes to the nozzle manifold. The coolant flows through a two-pass cooling circuit in the nozzle and is routed through transfer tubes back to the segment injectors.

(U) The 12 main thrust chamber injectors are provided with independent manifolding. Propellant inlets are located in the center of each segment.

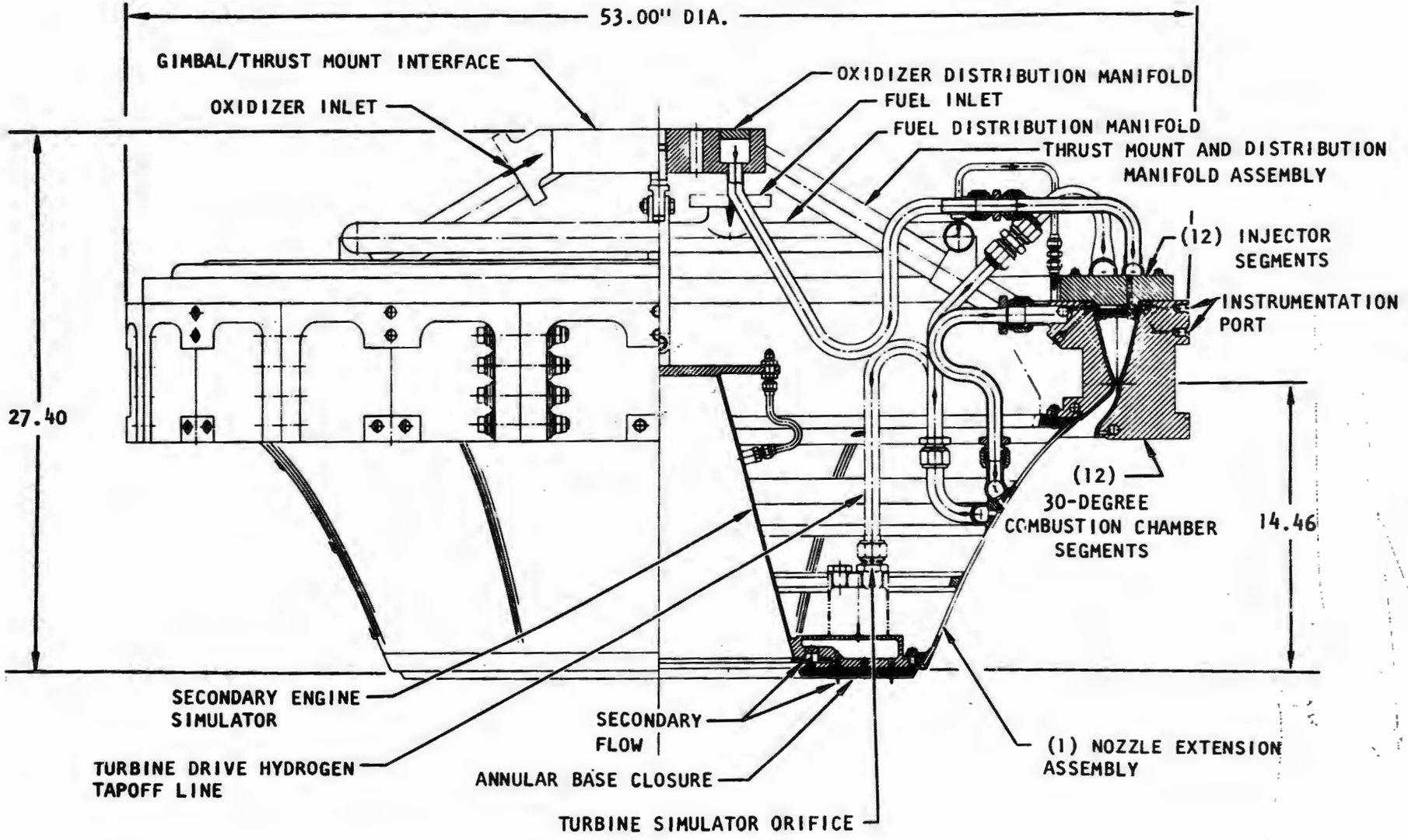

Figure 6. Phase I Main Engine Thrust Chamber Assembly (U)

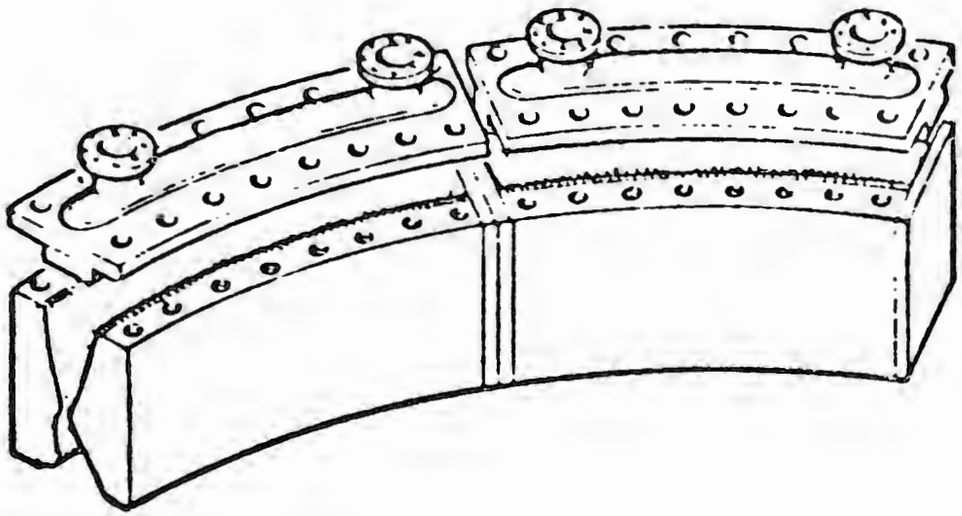

TWO 30-DEGREE THRUST CHAMBER SEGMENTS

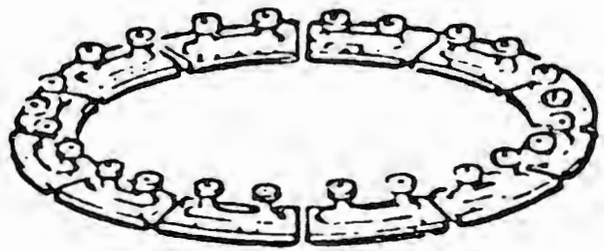

FULL SEGMENTED
INJECTOR AND MANIFOLD

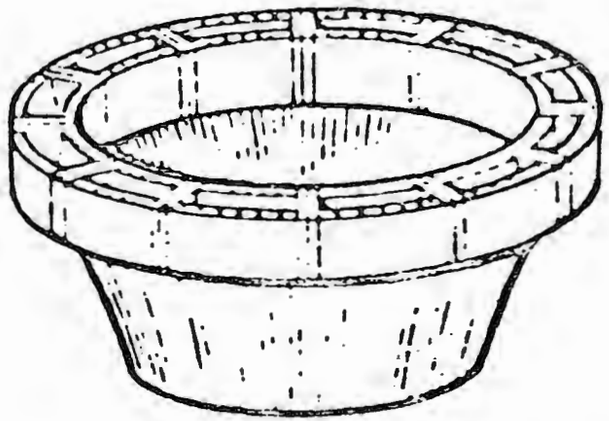

FULL SEGMENTED THRUST CHAMBER

Figure 7. AMPT Program Thrust Chamber and Injector Segments (U)

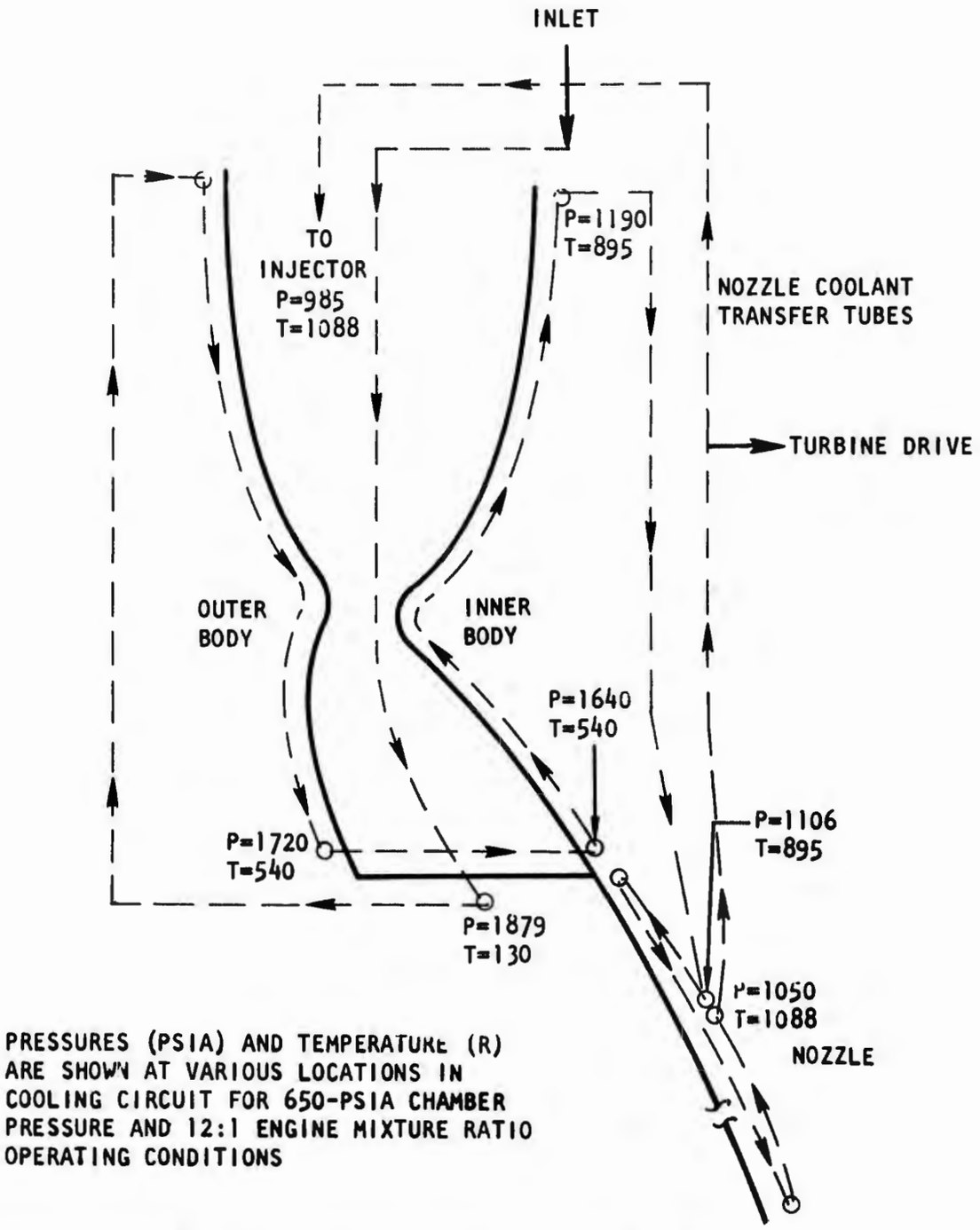

Figure 8. Main Engine Thrust Chamber Cooling Circuit (full-thrust operation) (U)

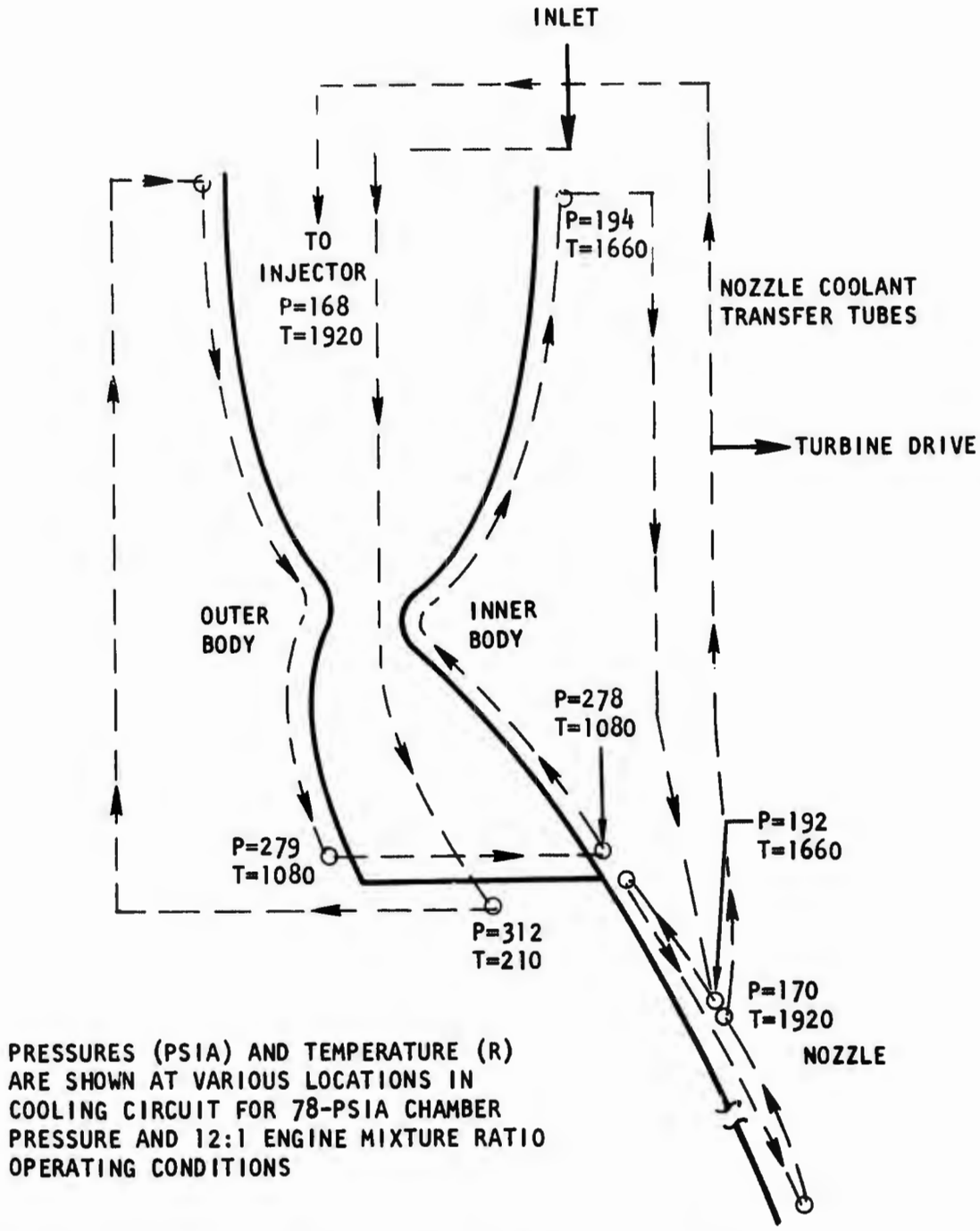

Figure 9 Main Engine Thrust Chamber Cooling Circuit (minimum-thrust operation) (U)

(U) The thrust chamber basic design parameters are shown in Table 1.

TABLE 1

(C) MAIN THRUST CHAMBER DESIGN CONDITIONS

Thrust (maximum), pounds	30,000
Chamber Pressure (maximum), psia	650
Engine Mixture Ratio	12:1
Chamber Diameter (at throat centerline), inches	45.83
Geometric Throat Area, sq in.	25.163
Aerodynamic Throat Area, sq in.	25.050
Throat Gap*, inch	0.187
Expansion Area Ratio	
Geometric	59.30
Aerodynamic	59.57
Hot Hydrogen Tapoff Turbine Drive	

*Chamber at ambient temperature

(U) Design and fabrication of the main thrust chamber was completed after the segment testing had demonstrated satisfactory operation of the injector/combustion chamber configuration.

(U) The main thrust chamber assembly included the following components:

1. 30-degree channel-wall thrust chamber assembly segments
2. Thrust mount and propellant inlet manifold assembly
3. Nozzle extension and base closure assembly
4. Associated propellant feed tubes, seals, and connecting hardware

(U) The completed, main, 360-degree thrust chamber assembly is shown in Fig. 10 through 13, and an assembly drawing is shown in Fig. 6 .

(U) Twelve, 30-degree channel-wall thrust chamber segment assemblies were used to assemble the full thrust chamber. Baffles, which form end plates for each segment, extend from the sealed injector end through the throat to the end of the outer body shroud. The segments were bolted together with eight bolts (four inner and four outer) at each interface (end plate) to form the 360-degree combustion chamber.

(U) After assembly of the combustion chamber, the nozzle mating surfaces were machined, and the one-piece nozzle extension with the base closure assembly was bolted to the combustion chamber. Assembly was completed by installation of the thrust mount assembly and propellant feed tubing.

(U) Development of the 30-degree segments used in the main thrust chamber assembly was accomplished by the following sequential hardware evaluations:

1. 5-inch segments
2. 30-degree water-cooled segment
3. 30-degree tube-wall regeneratively cooled segments
4. Initial 30-degree channel-wall regeneratively cooled segment
5. Prototype 30-degree channel-wall regeneratively cooled segment

(U) Injector development was conducted in conjunction with the chamber segment development. The design, fabrication, and test results for each of the above steps is presented in the sections that follow. The types of segment hardware are illustrated in Fig. 14.

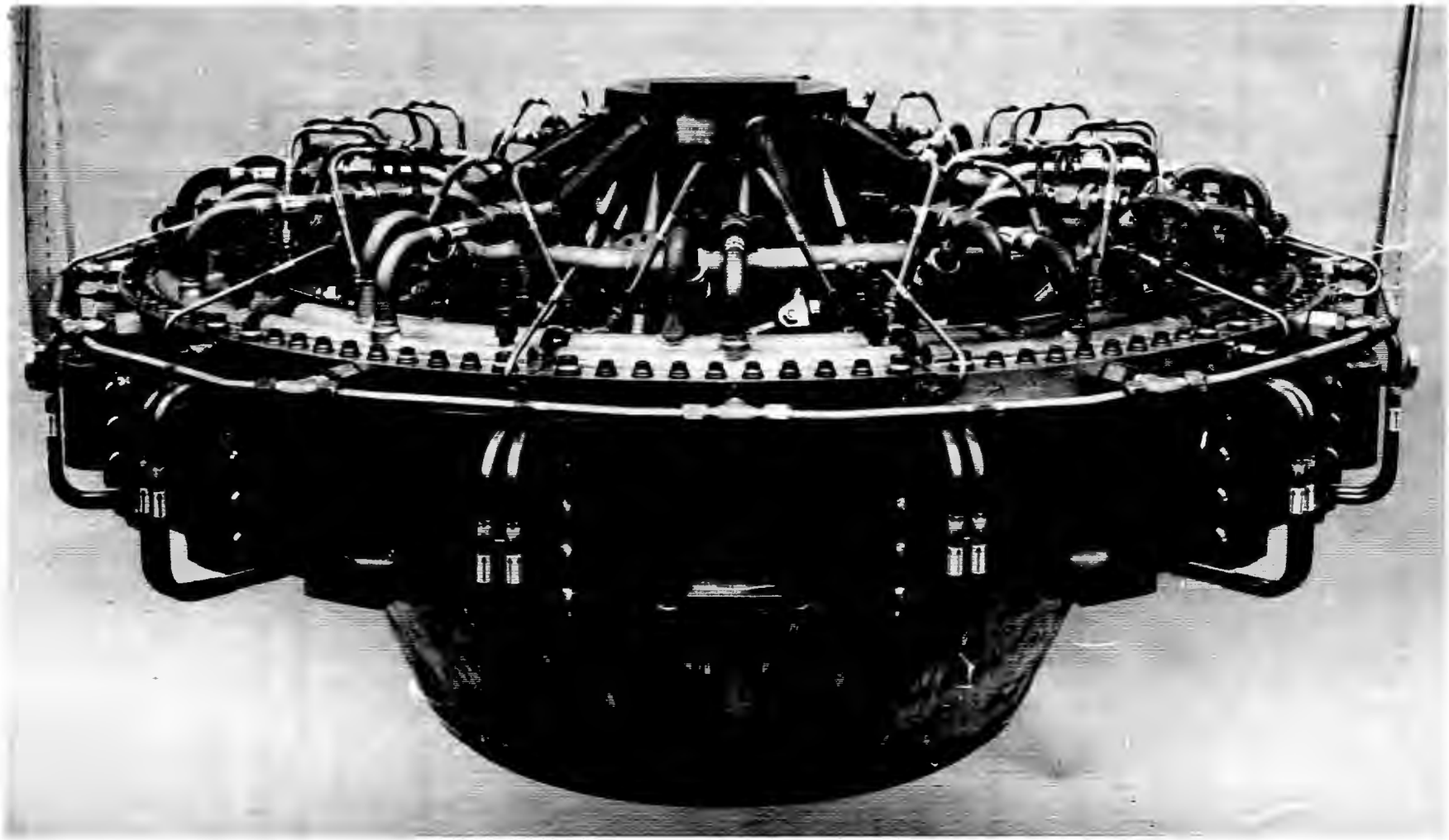

1EH32-2/18/70-C1G

Figure 10. Thrust Chamber Assembly (U)

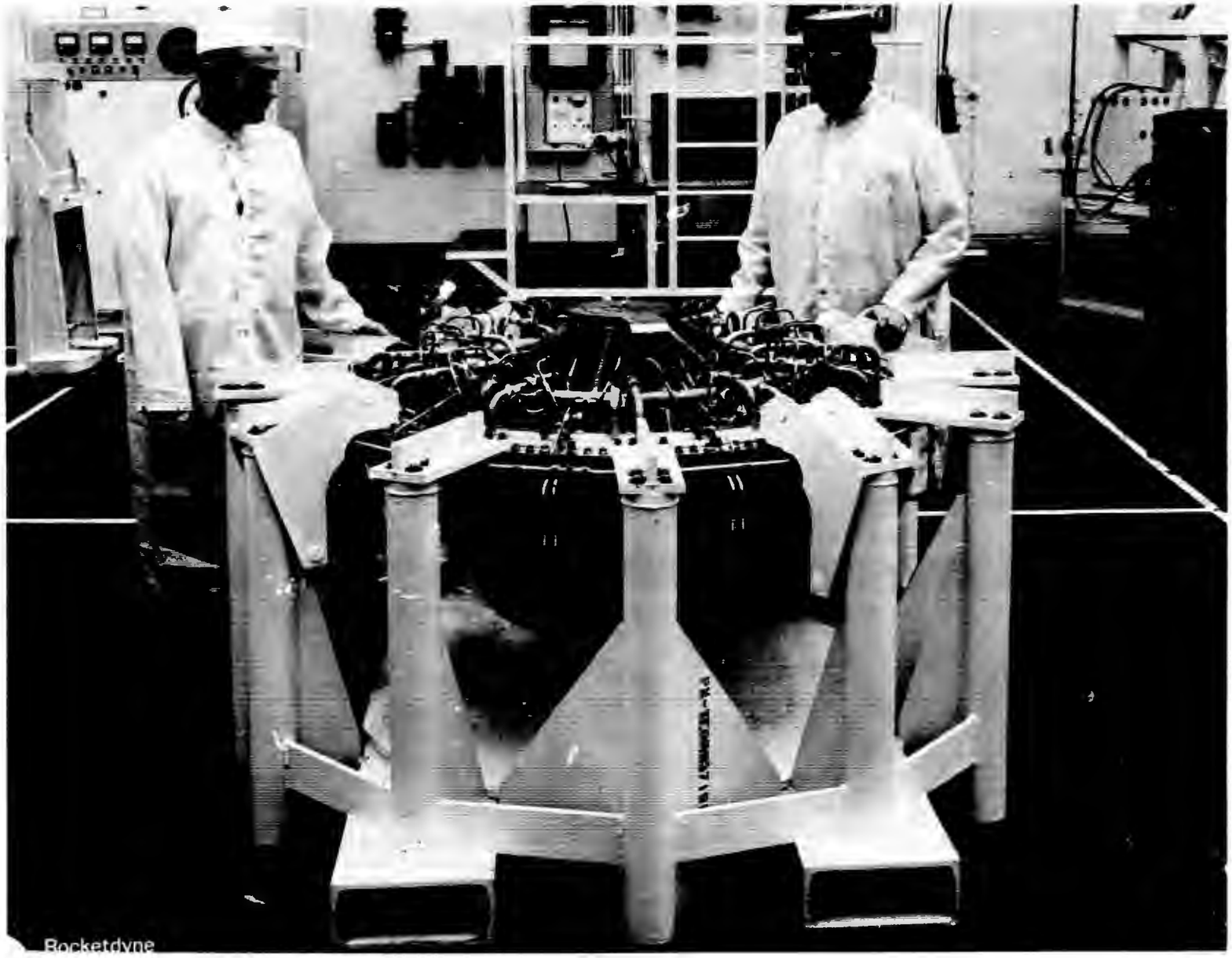

1EH32-2/20/70-C1A

Figure 11. Main Thrust Chamber Assembly in Handling Dolly (U)

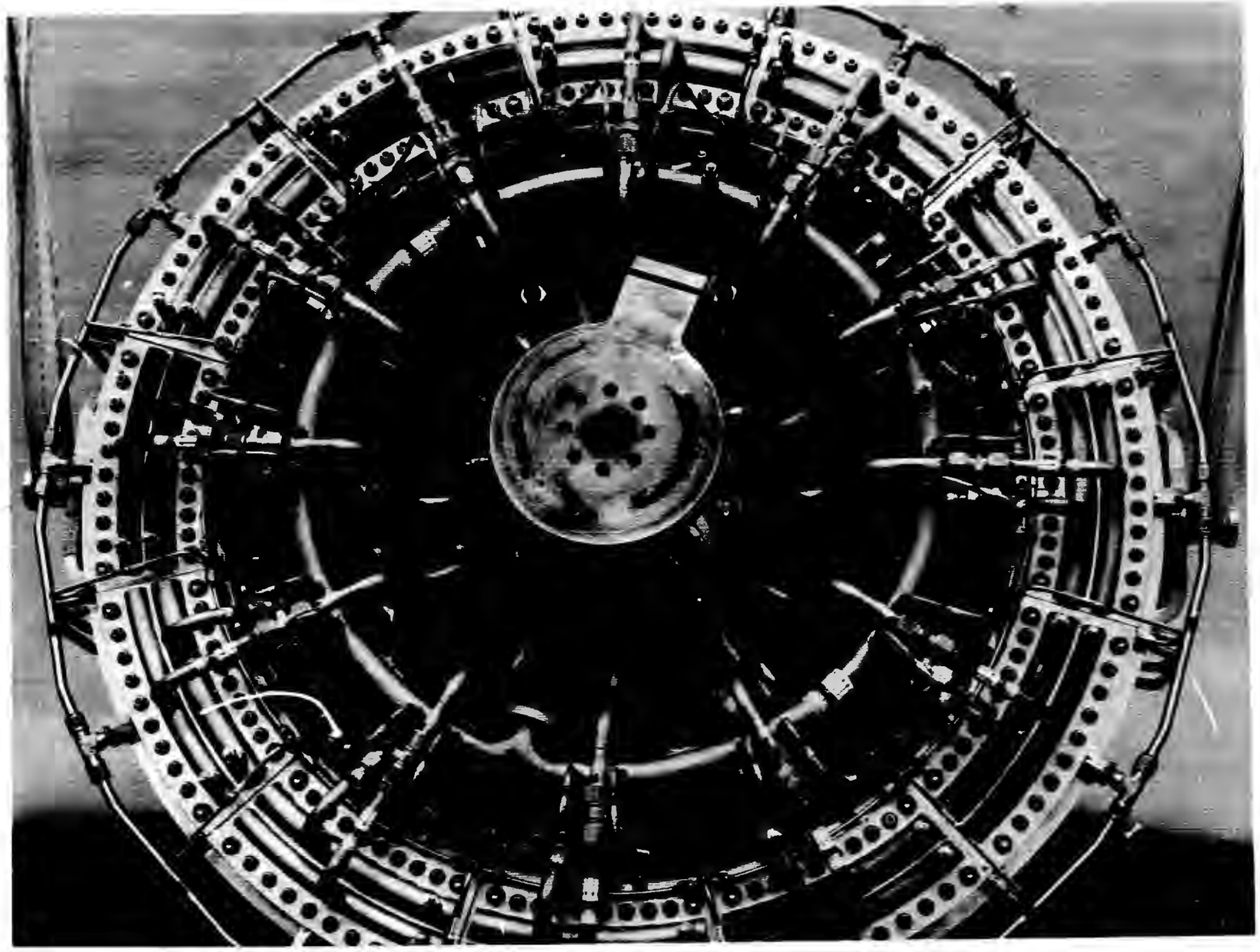

1EH32-2/18/70-C1A

Figure 12. Thrust Chamber Assembly (Forward View) (U)

1EH32-2/18/70-C1H

Figure 13. Thrust Chamber Assembly (Aft View) (U)

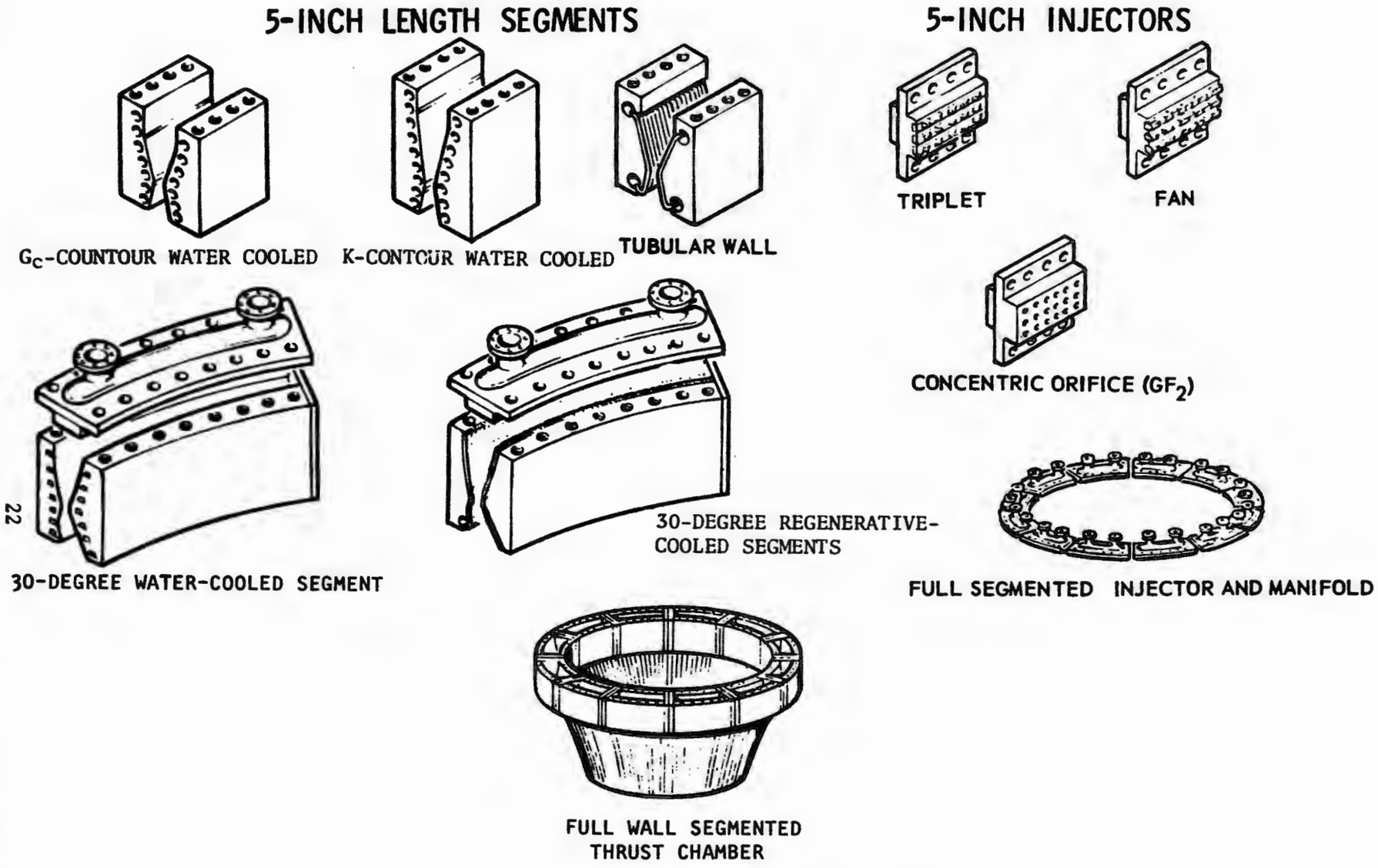

Figure 14. Building-Block Development Approach for the Main Engine Aerospike Thrust Chamber (U)

2. 5-INCH SEGMENT EVALUATION

(U) Several injector patterns and combustion chamber geometry variations were evaluated with 5-inch size segments. The test evaluation provided the performance and heat transfer characterization data necessary to define the combustion chamber contour and injector configuration for the subsequent 30-degree segments and full main thrust chamber segments.

(U) In the sections that follow, the 5-inch segment hardware is first described, followed by a discussion of the testing, analysis, and results obtained.

a. Hardware Design and Fabrication

(1) 5-Inch Segment Thrust Chambers

(U) The 5-inch segment thrust chambers evaluated on this program included three water-cooled, copper, calorimetry assemblies and one tube-wall assembly. The water cooled assemblies were designated according to their combustion chamber wall contours. The configurations evaluated included the G_c, K, and shortened G_c contours.

(a) G_c Contour

(U) Two G_c contour chambers were fabricated. The G_c contour (Fig. 15) was a refinement of the most successful configuration developed during the previous experimental program (Ref. 1). The refinement was mainly in the throat area to obtain a contour that would provide maximum regenerative coolant curvature enhancement for the subsequent tubular-wall thrust chamber segments.

(C) The chambers were fabricated from copper for good heat transfer and were designed to overcome some of the detrimental factors determined during the previous program (Ref. 1). This consisted of fabricating the chamber

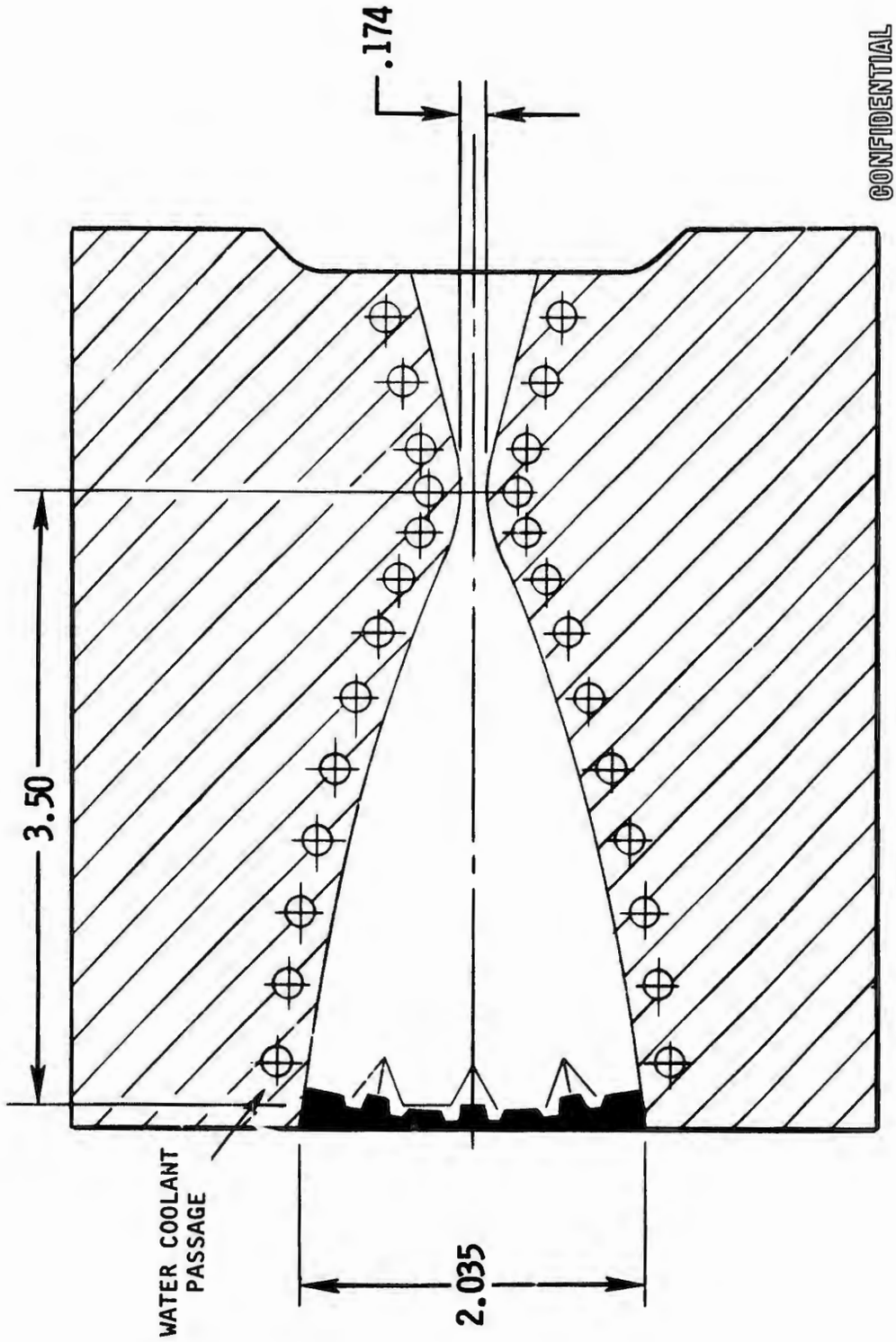

Figure 15. 5-Inch, Solid-Wall Segment, G_c Combustion Chamber Contour, Symmetrical Nozzle (U)

(C) of two halves that were brazed together (Fig. 16 and 17) to provide a continuous hot-gas surface with no transverse (to hot-gas flow direction) interruptions. The chambers were then drilled (0.174-inch diameter) to provide the water-cooling passages.

(C) The coolant passages in the combustion zone and nozzle (Fig. 15) were individually fed and instrumented. Each circuit cooled both contour walls and side plates and was designed for the coolant water to be in the nucleate boiling regime, with coolant passage pressures maintained above 1000 psig and coolant velocity maintained above 125 ft/sec. With these coolant conditions, the analysis predicted adequate chamber wall cooling, with local heat fluxes up to 40 $Btu/in.^2$-sec.

(U) Previous experience at Rocketdyne had indicated that progressive deterioration (roughening) of the copper walls, particularly in the throat region, would occur. This detrimental effect was noted during testing, and the throat regions were hand polished prior to the start of a day's test series. The chamber hot-gas surfaces were not plated or otherwise treated to prevent this deterioration.

(C) All chambers had a symmetrical 15-degree half-angle divergent nozzle with a 4.5 expansion ratio. The combustion chamber at the injector mounting flange was 5 inches long by approximately 2 inches wide, and the distance from injector face-to-throat was 3.5 inches.

(b) K Contour

(C) One K contour chamber segment was fabricated to specifically evaluate the effect of increased combustion zone length on local heat transfer rates at the throat and the total integrated heat rejection rate. The contour is shown in Fig. 18 and was similar to the G_c contour chamber, except the distance from injector face-to-throat was 5.0 inches. The same fabrication technique was used for the K contour chamber as was used for the G_c contour chambers.

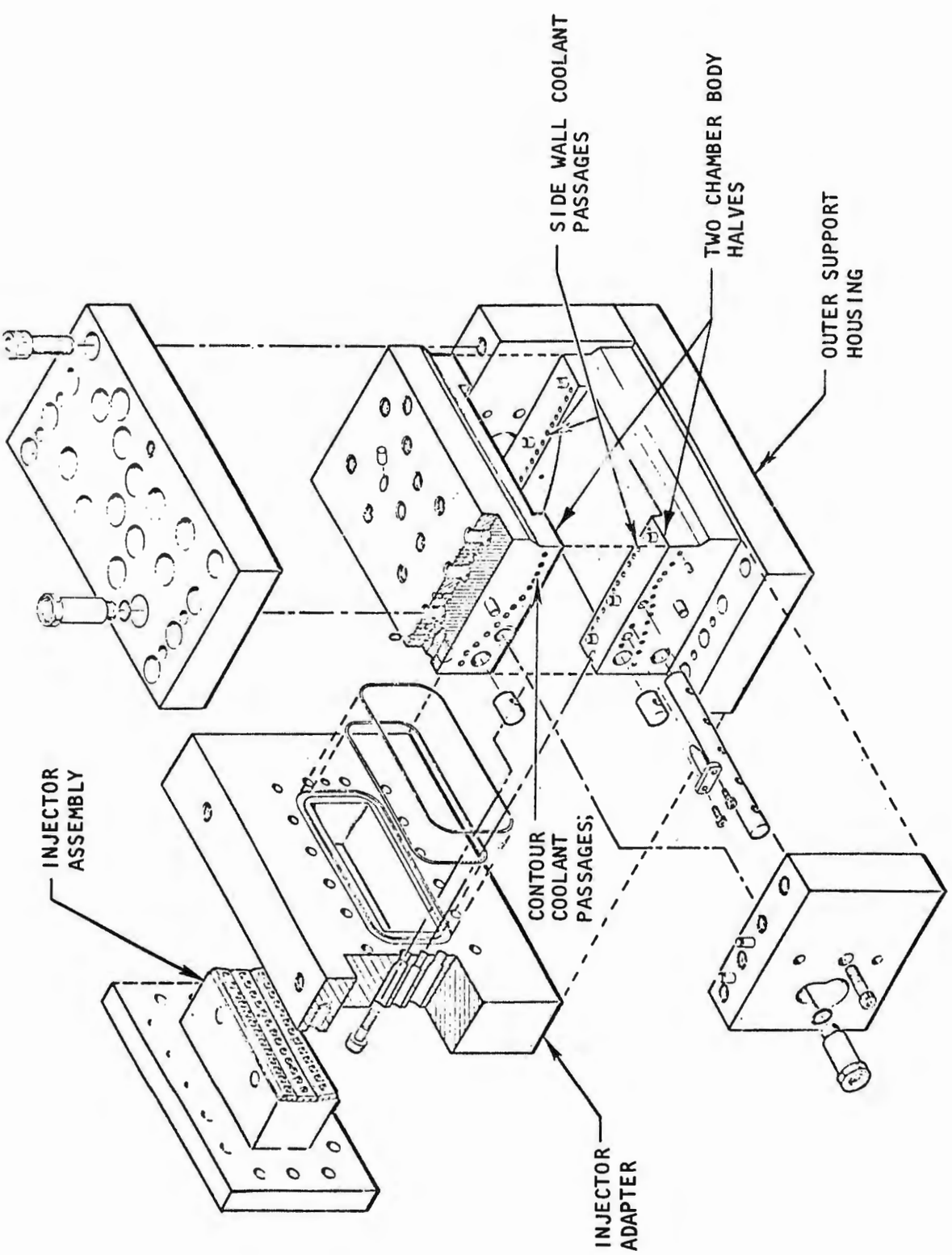

Figure 16. Exploded View of 5-Inch Solid Wall Segment With Chamber Support Housing (U)

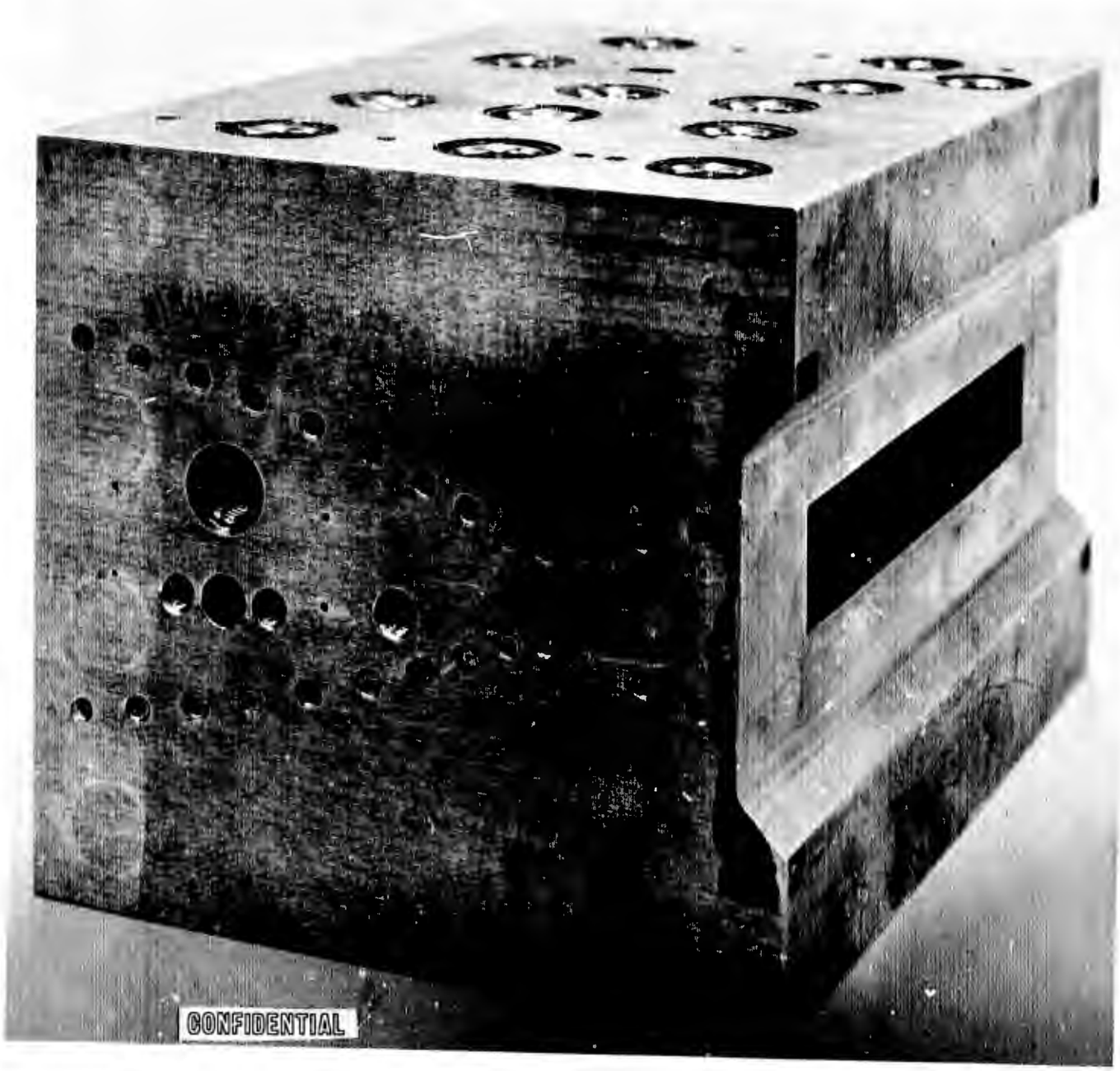

LXE32-12/12/67-C1C

Figure 17. External View of Assembled 5-Inch Solid Wall Thrust Chamber Segment Halves (G_c Contour) (U)

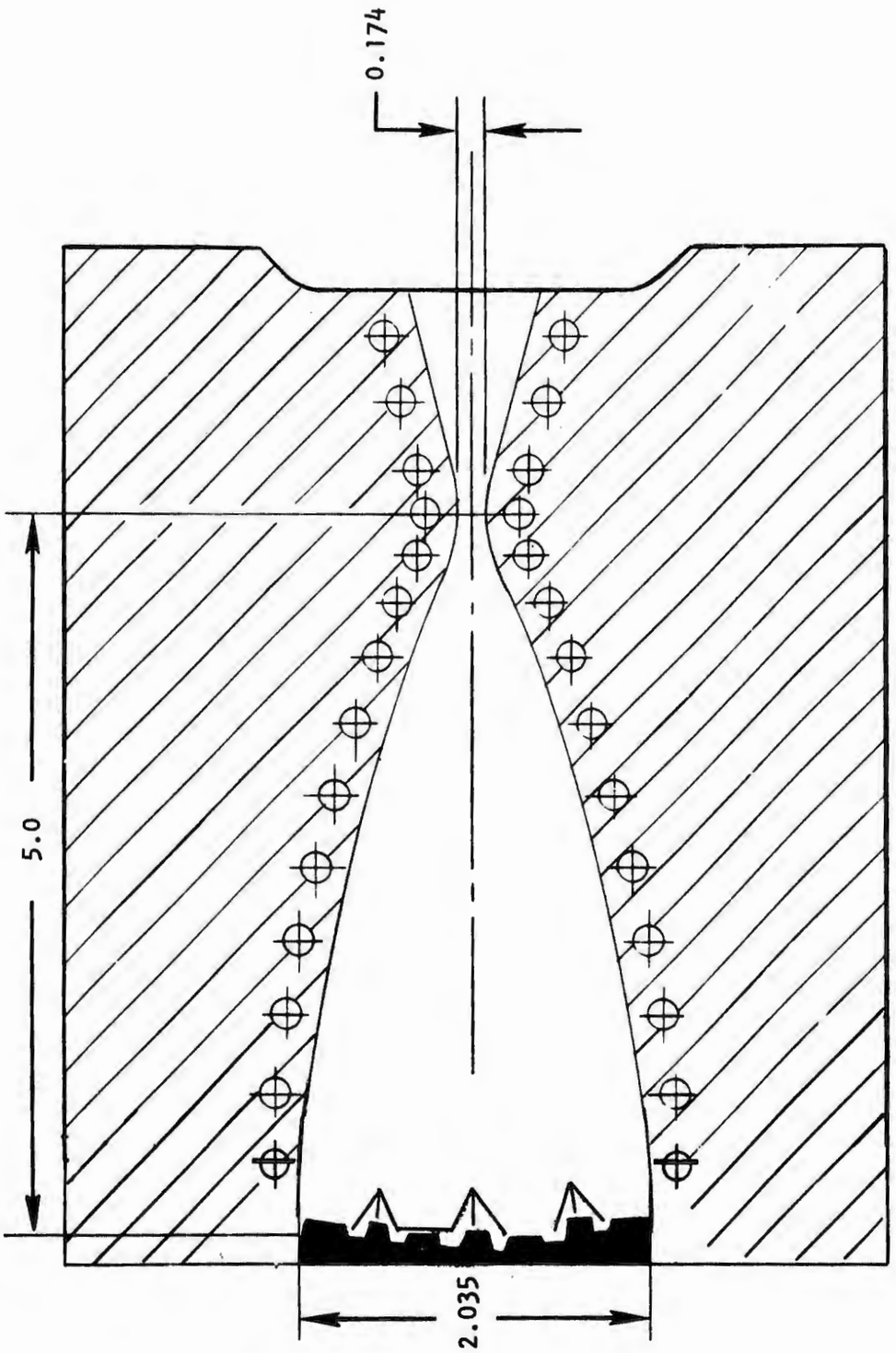

Figure 18. 5-Inch Solid-Wall Segment With K Combustion Chamber Contour (U)

(c) Shortened G_c Contour

(C) As an approach for reducing the overall chamber heat load by reducing the chamber wall surface area, a shortened combustion chamber was evaluated. A basic 5-inch, water-cooled, G_c contour segment thrust chamber was reworked by machining the injector mounting block to permit the injector to extend 0.82 inch closer to the throat. The chamber walls in the upper combustion zone also were machined to permit the deepter penetration of the injector. The effective combustion zone length was reduced from 3.5 to 2.68 inches, and the combustion zone wall surface area was reduced by 22.8 percent. The segment configuration is illustrated in Fig. 19.

(U) The modification for the shortened chamber was devised to be accomplished easily and quickly, and the test results proved the contour to be somewhat non-ideal from the standpoint of heat transfer. The results led to the design of a second reduced size configuration called the short contour segment.

(d) Short Contour

(U) This chamber segment was designed as a further evaluation of the approach for reducing the overall heat load by reducing the chamber wall surface area. A second benefit of the design would be reduced thrust chamber and engine weight.

(C) The chamber contour, shown in Fig. 20, incorporated a straight, constant-convergence combustion zone contour (12-degree half-angle) with an injector face-to-throat distance of 2.7 inches. The throat radius of curvature was maintained at 0.875 and the throat gap was 0.187 inch. The throat gap change from the 0.174 inch value, used on previous chamber contours, was a result of a refined engine performance balance conducted in the Task I studies (Vol. I, Section III).

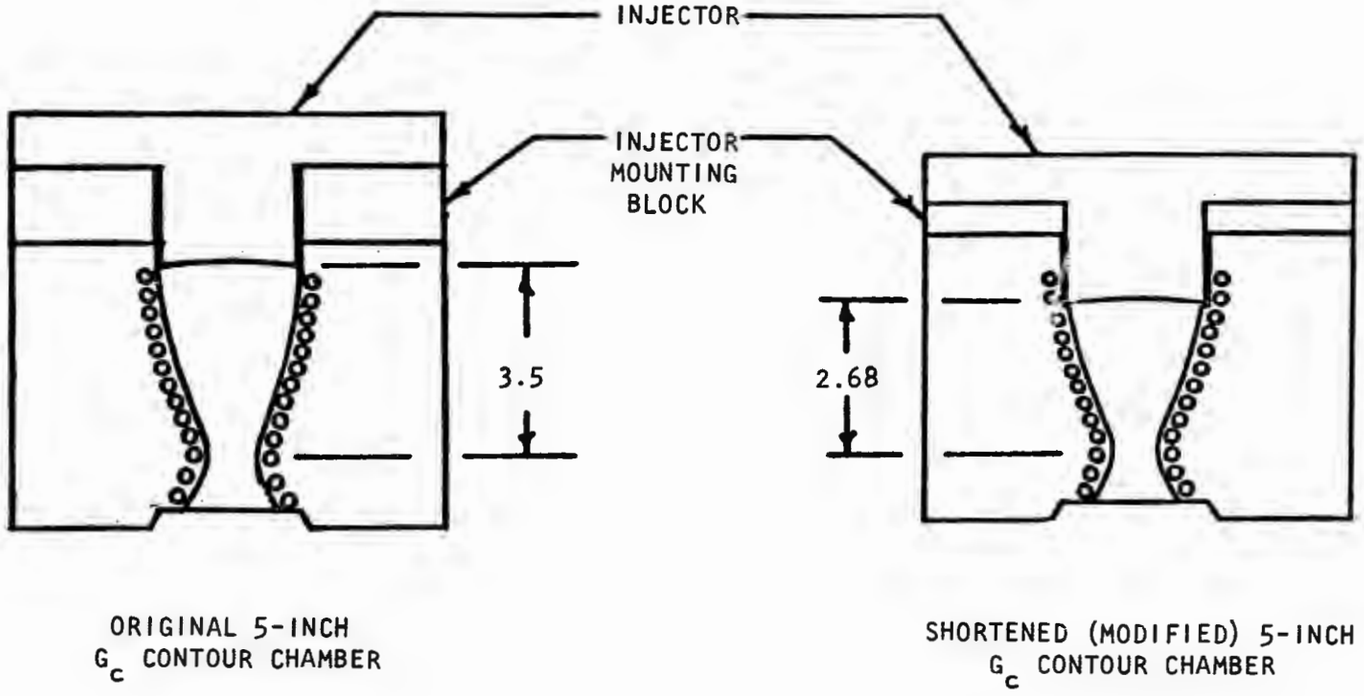

Figure 19. 5-Inch Water Cooled Chamber Segment; Original and Shortened Combustion Zone Configurations (U)

CONFIDENTIAL

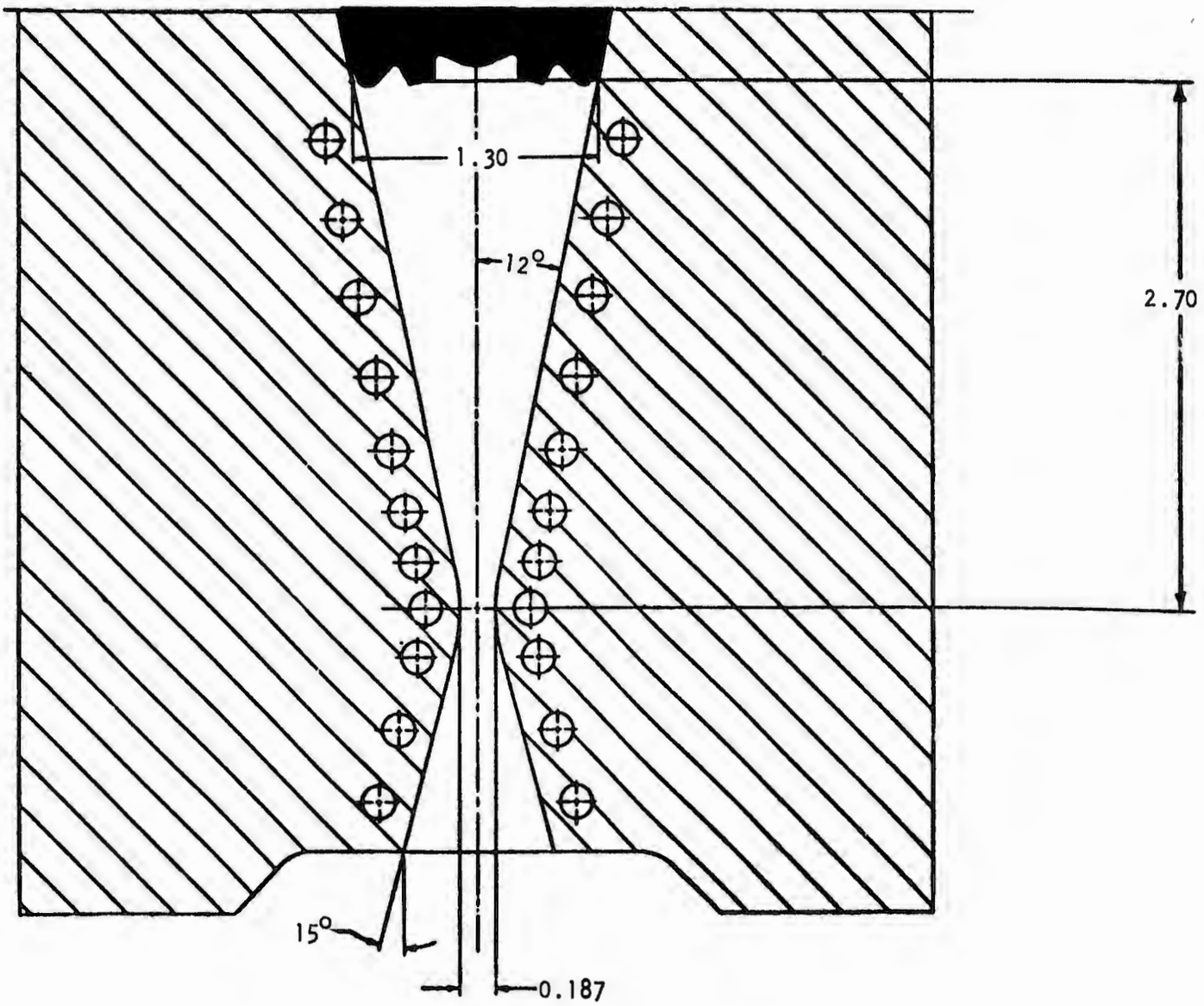

Figure 20. Short Contour 5-Inch Water Cooled Segment Design (U)

(C) Straight combustion zone walls, as compared to contoured walls (Fig. 20 versus Fig. 15), were selected for design simplicity and because the straight wall was not expected to be detrimental to the boundary layer buildup and associated heat transfer characteristics based on previous work accomplished (Ref. 1). The wall curvature upstream of the throat in the G_c design was originally thought to be necessary to provide curvature enhancement for the regeneratively cooled design.

(U) Fabrication of the short contour segment was only partially completed in this program because other approaches to the reduction in heat load proved successful (refer to Section III, subsections 3 and 5).

(e) 5-Inch Tubular Wall Segment Thrust Chamber

(U) The design and fabrication of a 5-inch tubular-wall segment was accomplished coincident with the design, fabrication, and test evaluation of the 5-inch, water-cooled chambers and injectors. The primary purpose of the thrust chamber was to provide total integrated heat rejection rate data for a regeneratively cooled assembly and also provide coolant pressure drop information. The chamber design utilized the G_c contour.

(C) An exploded view of the tube-wall segment assembly is shown in Fig. 21. The basic subassembly consisted of Nickel 200 tubes of 0.017-inch wall thickness, with each tube electron-beam-welded to an adjacent tube to form a panel. The electron beam welding technique did not produce an entirely flat panel. The tube-to-tube height varied in a transverse direction across the panel. This variation could produce lack of braze attachment to the backup structure and possible failure. Because of this possibility, the electron beam welded panel approach was not used for the subsequent 30-degree tubular-wall segment thrust chambers. The flat panels had electroformed nickel applied at the ends for manifolding and were subsequently formed to the required combustion zone and nozzle contour. The panels were then furnace brazed to the chamber back-up

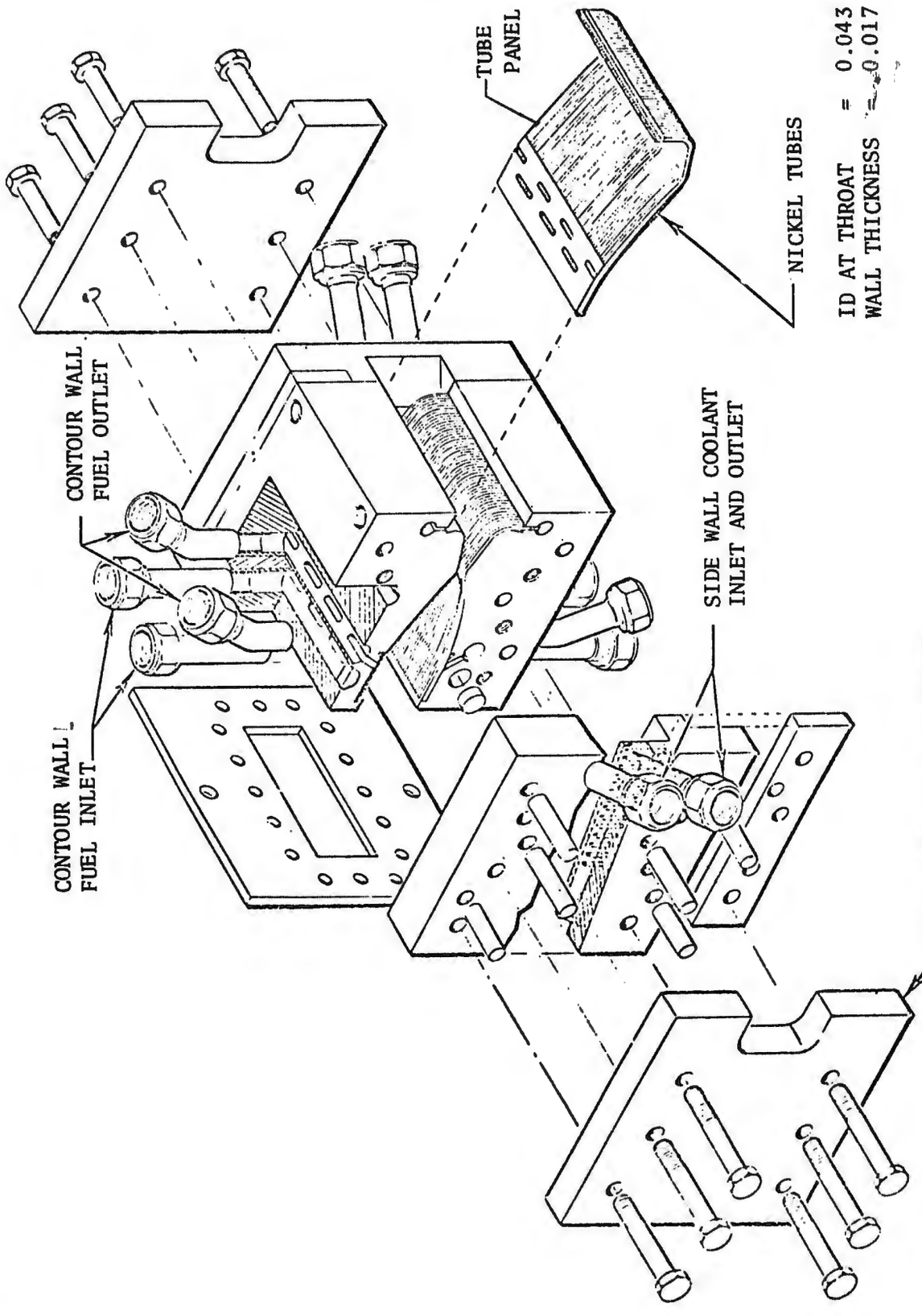

Figure 21. Five-Inch Tube Wall Segment Assembly (U)

(C) structure. Coolant manifolding was provided so that up- and down-pass cooling would be used on each individual contour wall. The side plates were fabricated of copper with drilled coolant passages and were individually water cooled. The complete assembly (Fig. 22) was furnace braze assembled to minimize the number of seals exposed to hot combustion gas.

(2) 5-Inch Injector Assemblies

(U) Based on results of the previous experimental program (Ref. 1), two basic injector patterns were selected for potential favorable performance and chamber wall heat transfer characteristics. The injectors incorporated triplet and impinging fan orifice patterns. An additional injector configuration, which was a concentric orifice type, was also included in the evaluation because of the potential for more complete oxidizer vaporization within the injector orifices and resulting improved operating characteristics.

(U) The mechanical design parameters for all the 5-inch injectors are presented in Table 2 .

(a) Triplet Injector

(U) The triplet injector assembly consisted of a body and three face strips (Fig. 23). The injector body performed the following functions: (1) provided containment and primary distribution of both injected propellants; (2) provided a base for attachment of the injector face strips; (3) provided a flange for attachment of the injector to the thrust chamber. Three triplet injector assemblies were fabricated.

(U) The injector body was machined by conventional techniques to provide internal propellant feed passages and lands at the injector face strip-to-body joint. The purpose of the lands (Fig. 23) was to provide a combination

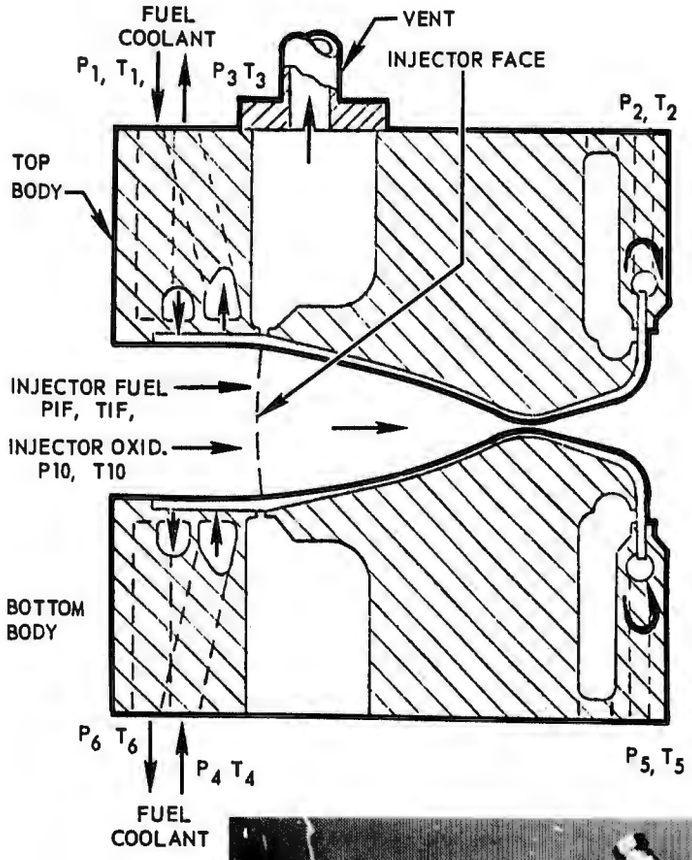

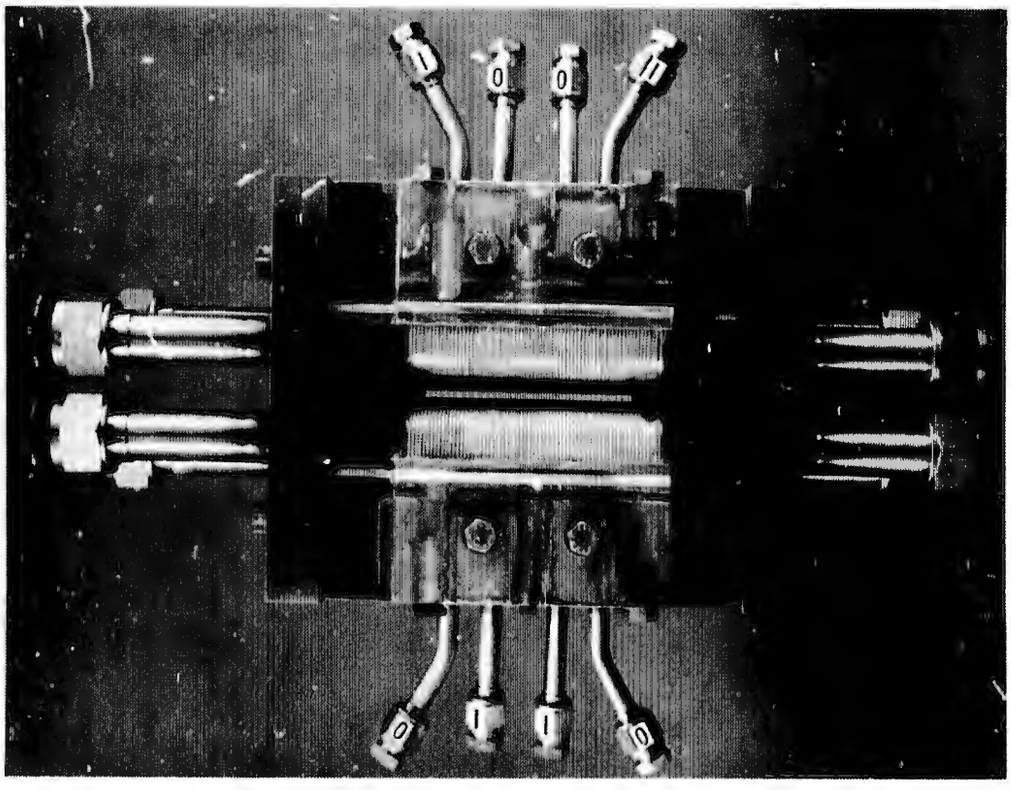

Figure 22. 5-Inch Tubular-Wall Thrust Chamber Segment (U)

TABLE 2

5-INCH SEGMENT INJECTOR DESIGN CHARACTERISTICS

Item	Triplet U/N 1	Triplet U/N 2	Triplet U/N 3	Fan U/N 1	Fan U/N 2	Fan U/N 3	Fan U/N 4	Concentric Orifice
Orifice Diameter, inches								
Fuel	0.0483	0.0483	0.035	0.026 and 0.037	0.018 and 0.028	0.018 and 0.028	0.020 and 0.028	0.008
Oxidizer	0.020	0.020	0.018	0.016	0.016	0.016	0.015	0.033
Number of Orifices								
Fuel	39	39	48	117	117	117	108	33
Oxidizer	78	82	96	156	156	156	144	33
Total Orifice Area, sq in.								
Fuel	0.07146	0.07146	0.04618	0.0833	0.04386	0.04386	0.04690	0.09265
Oxidizer	0.0245	0.02576	0.02443	0.0314	0.0314	0.0314	0.02710	0.02822
Impingement Length-to-Diameter Ratio								
Fuel	2.98	2.98	5.20	5.9 and 8.4	7.8 and 12.2	7.8 and 12.2	5.86 and 8.2	- -
Oxidizer	13.5	13.5	16.81	3.9 and 19.6	3.9 and 19.6	4.0 and 19.5	3.5 and 15.8	- -
Included Oxidizer Impingement Angle, degrees								
Oxidizer Preimpingement	- -	- -	- -	55	55	55	35	- -
Final Impingement With Fuel Showerhead	68	68	60	65	65	65	71	- -
Impingement Distance (Fuel Orifice Face to Impingement Point), inches	0.144	0.144	0.182	0.219	0.219	0.219	0.164	- -
Number of Strips	3	3	3	3	3	3	0(Integral)	- -
Number of Elements	39	39	48	39	39	39	36	33
Injector Face Size, inches	2 x 5	2 x 5	2 x 5	2 x 5	2 x 5	2 x 5	2 x 5	2 x 5
Calculated Pressure Drop at 650-psia Chamber Pressure, psid								
Fuel	216	216	350	202	350	350	306	100
Oxidizer	316	286	316	272	272	272	360	306
Injection Density, elements/sq in.	3.9	3.9	4.8	3.9	3.9	3.9	3.6	3.3
Element-to-Wall Cant Angle, degrees	30	30	30	30	30	30	50	- -

CONFIDENTIAL

AD 511990

AUTHORITY: AFRPL.
ltr 5 Feb 86

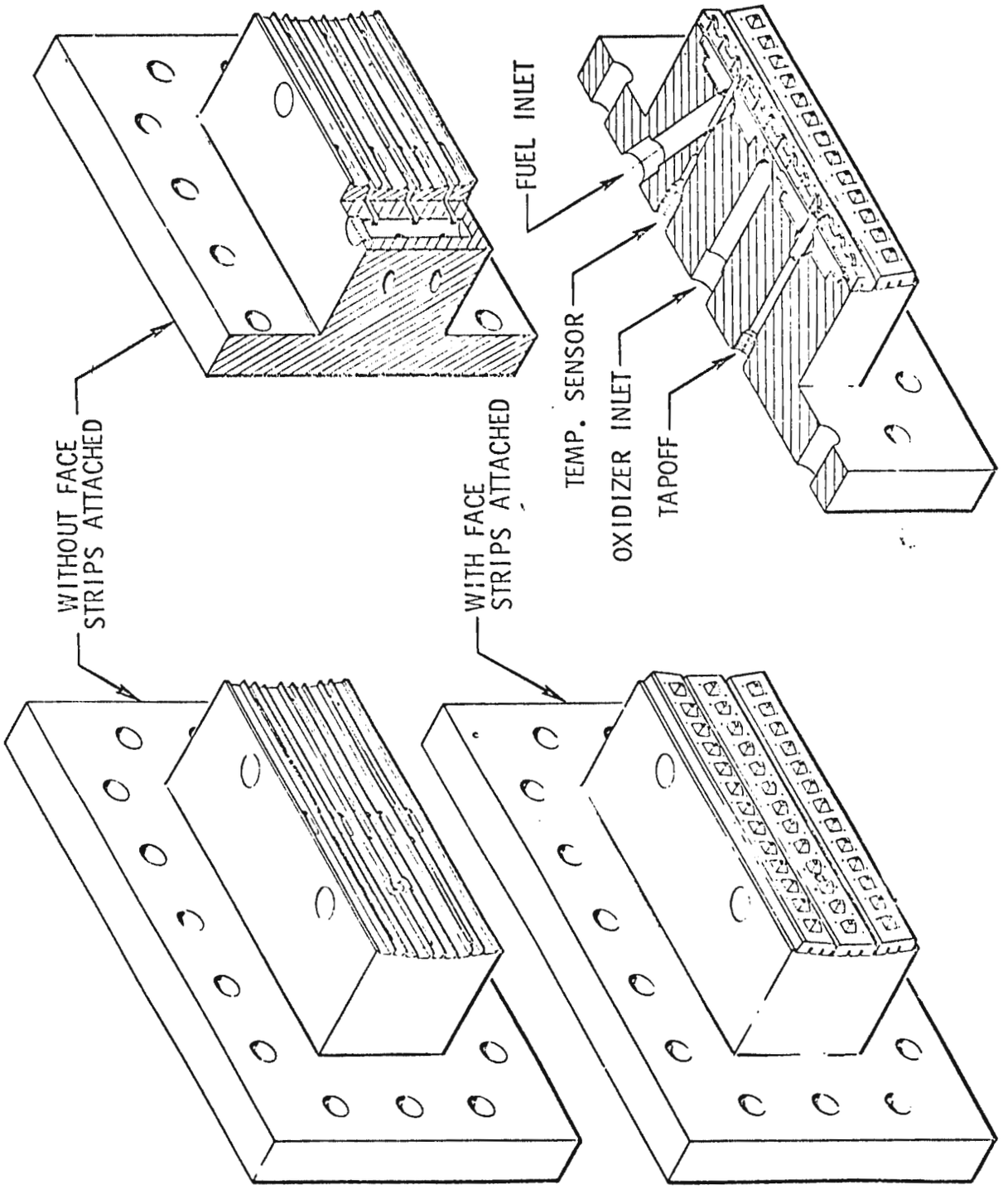

Figure 23. Five-Inch Triplet Injector Assembly (U)

(U) shear and tension-type braze joint for injector face strip attachment. The injector body material was 347 CRES. The injector face strips provided final distribution of the propellant to the injector orifices for injection into the combustion chamber.

(U) The injector strips contained the triplet elements. Each element consisted of two oxidizer streams impinging on a showerhead fuel stream (Fig. 24). The basic element configuration, orifice spacing, orientation, orifice diameter, etc., was established from results obtained during the previous program (Ref. 1) and is presented in Table 2 .

(C) The injector strips were fabricated from Nickel 200 to provide a material which : (1) had a very high auto-ignition temperature with fluorine (1253 to 1266 C); (2) had a high melting point since fuel injection temperatures of 1000 to 1100 F were predicted; and (3) had good thermal conductivity for face cooling to prevent melting and erosion. The initial injector strips were fabricated by conventional machining. Later strips were machined by use of EDM. All orifices were drilled.

(U) The first and second triplet injectors (U/N 1 and 2) were essentially identical in design and fabrication technique, except for minor modification of U/N 2 as a result of the testing. Injector U/N 3 incorporated a number of design changes for improved injector face cooling. Among the changes was the addition of oxidizer feed control webs (Fig. 25) for the purpose of increasing the oxidizer flow velocity parallel to the face (refer to Section III, 2, b, (1)).

(U) Following completion of fabrication, all the injectors were flow tested with filtered (40-micron) water to ensure that no orifice blockage or misimpingement existed and to provide pressure drop calibration data. Typical calibration data are shown in Fig. 26 , and a typical flow test shown in Fig. 27 .

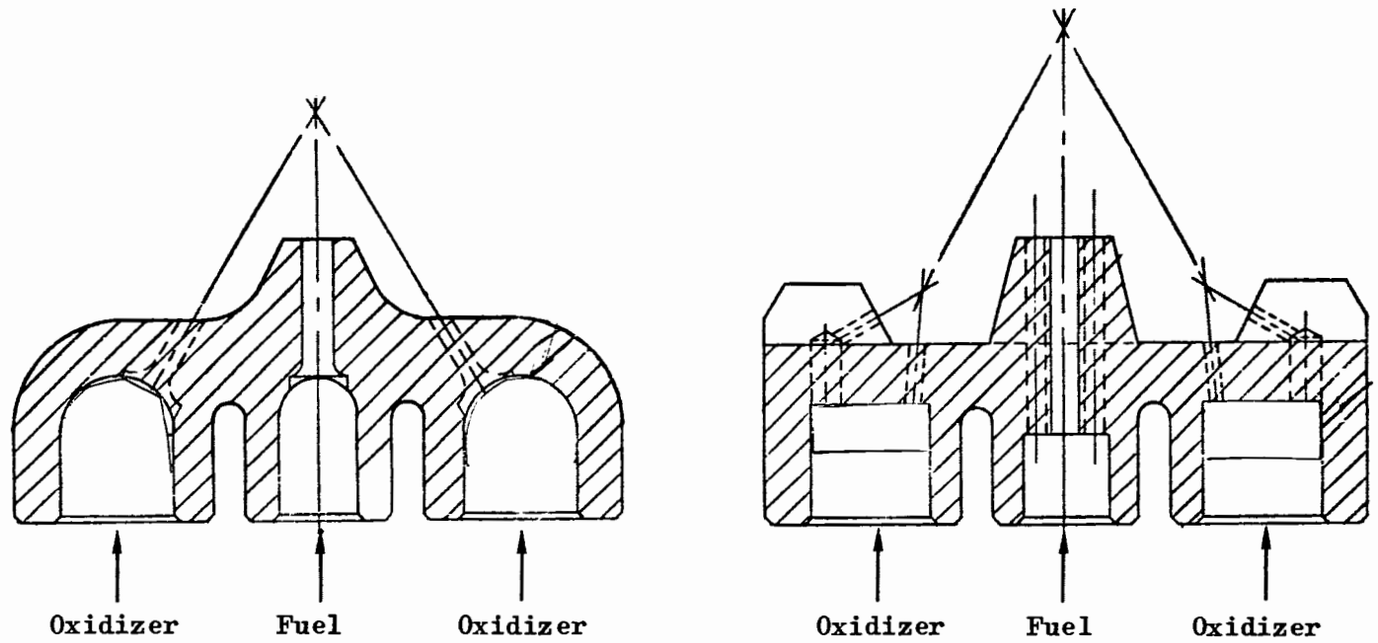

CONFIDENTIAL

Figure 24. Original Triplet and Fan Injector Strip Configurations (U)

CONFIDENTIAL

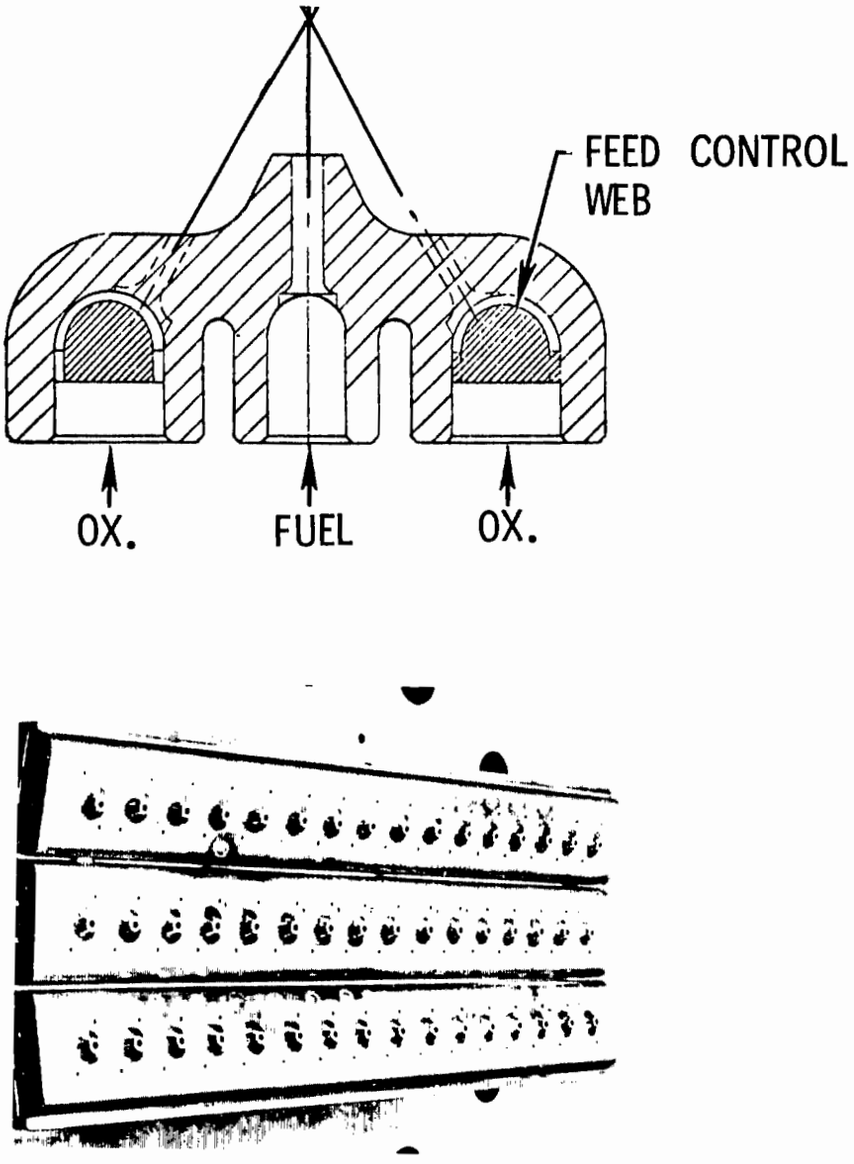

Figure 25. Modified 5-Inch Triplet Injector Segment (U/N 3) (U)

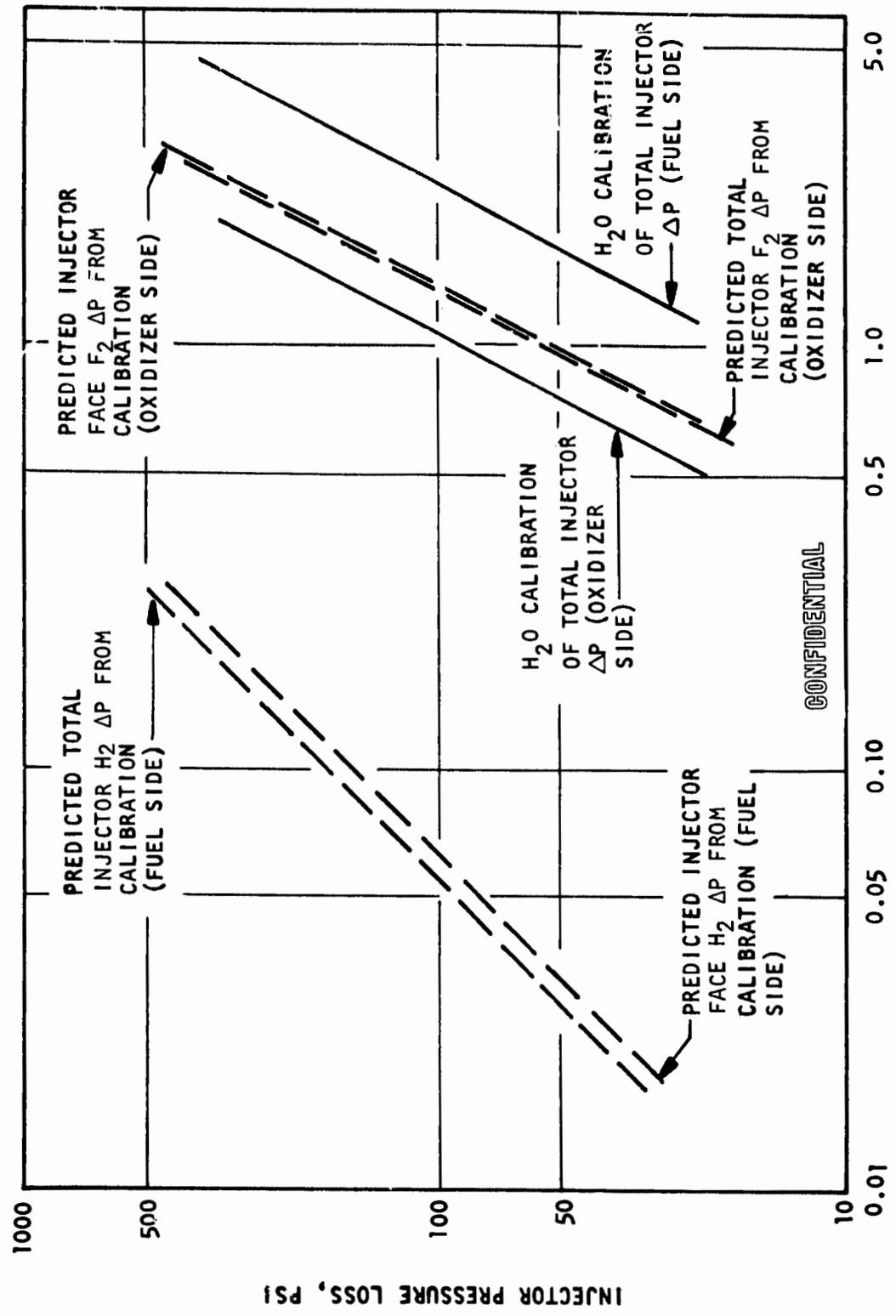

Figure 26. Flow Calibration of 5-Inch U/N 1 Triplet Injector (U)

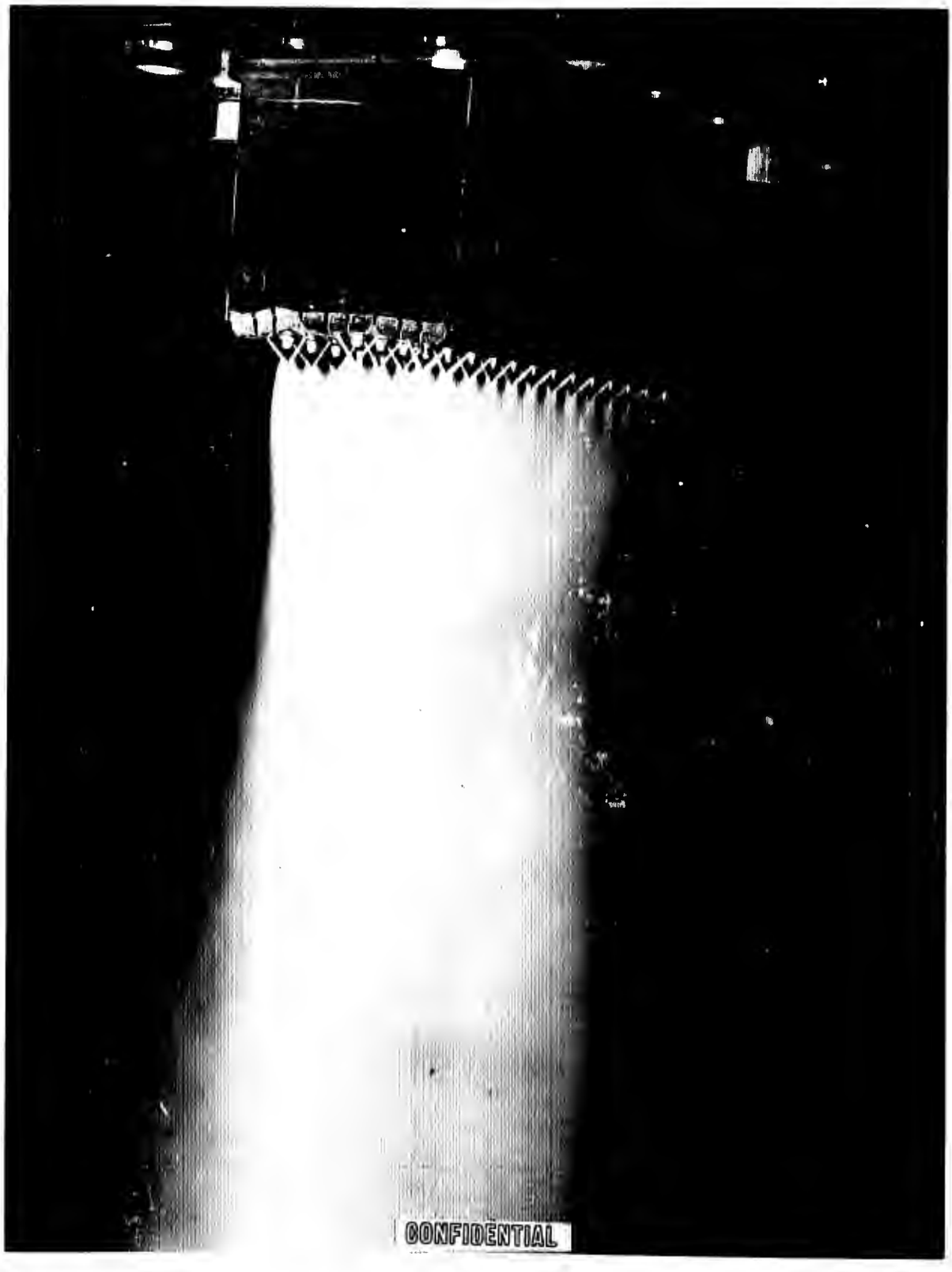

1EH44-12/28/67-C1G

Figure 27. 5-Inch Triplet Injector Water Flow Test (Oxidizer Side)(U)

(U) The injectors were flushed with deionized water following flow test and then thoroughly cleaned by:

1. Vacuum dry at 212 ±10 F for 2 hours
2. Vapor degrease with trichlorethane
3. Ultrasonic clean with total immersion in Freon for three, 3-minute cycles
4. Vacuum dry at 212 ±10 F for 2 hours after part has been heated to 212 ±10 F
5. Double package

(U) The injectors were then sent to the test area for fluorine passivation prior to installation in the segment test assembly.

(b) Fan Injector

(C) The impinging fan injector design was based on the work accomplished in the previous program (Ref. 1). The injector elements each have three fuel orifices and two pairs of oxidizer orifices. A single element and the complete face of the U/N 1 injector are shown in Fig. 24 and 28, respectively. Gaseous hydrogen was injected from the three central shower head orifices. The fluorine was injected from the two pairs of doublet orifices, forming fans whose flat side face the central gaseous hydrogen streams. The fluorine fans and hydrogen streams, in turn, impinged at a central common point.

(U) Four fan injectors were fabricated, and significant design details of each is shown in Table 2. Impinging fan injectors (U/N 1, 2, and 3) were similar to the triplet injector design and consisted of a body and three face strips. The face strips were furnace-braze attached to the body. Both body and face strips performed the same functions on the fan injector as for the triplet injector. The face strip material was Nickel 200,

1EH44-2/1/68-C1B

Figure 28. 5-Inch Fan Injector Assembly U/N 1 (U)

CONFIDENTIAL

(U) but the injector body material was changed from CRES 347, used on the triplet injectors, to 304L stainless steel for the fan injectors to provide a low carbon content material with better weld characteristics. The initial impinging fan injector, U/N 1 (Fig. 28), face strips and body were machined by conventional methods, and a combination tension-shear furnace braze joint was used for face attachment. The injector did not incorporate feed control webs in the oxidizer feed passages. Drilled vent holes were utilized for disposal of possible propellant leakage past the face strip-to-body braze joint, similar to the U/N 2 and U/N 3 triplet injectors.

(C) The fan injector design parameters (Table 2) and fabrication techniques were similar for the U/N 1 and U/N 2 injectors, with two important changes:

1. The fuel orifice area for U/N 2 injector (Table 2) was significantly decreased compared to U/N 1. This decrease was made after examination of the U/N 1 injector test data, and data from other programs at Rocketdyne, which indicated that increased fuel velocity would increase η_{c*} due to more vigorous secondary atomization of the oxidizer droplets and, also, decrease upper combustion zone local heat flux.
2. Feed control webs were incorporated into the oxidizer passages to increase the flow velocity behind the injector face to approximately 40 ft/sec for improved face cooling. The feed control webs are shown in Fig. 29.

(C) The U/N 3 injector (Fig. 30) was modified to improve the face-cooling capability. The feed control webs were designed to increase the oxidizer velocity between the strip backside and feed control to 60 ft/sec. Turbulence inducers (swirlers), formed from wire, were attached to the feed control webs for improved heat transfer. The feed control web installation is shown in Fig. 30, and the detail webs with turbulence inducers are shown in Fig. 31.

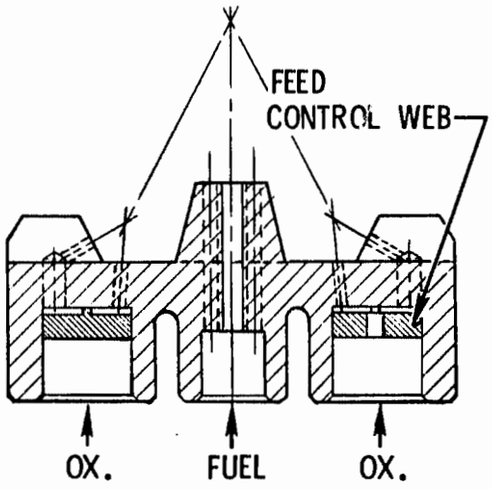

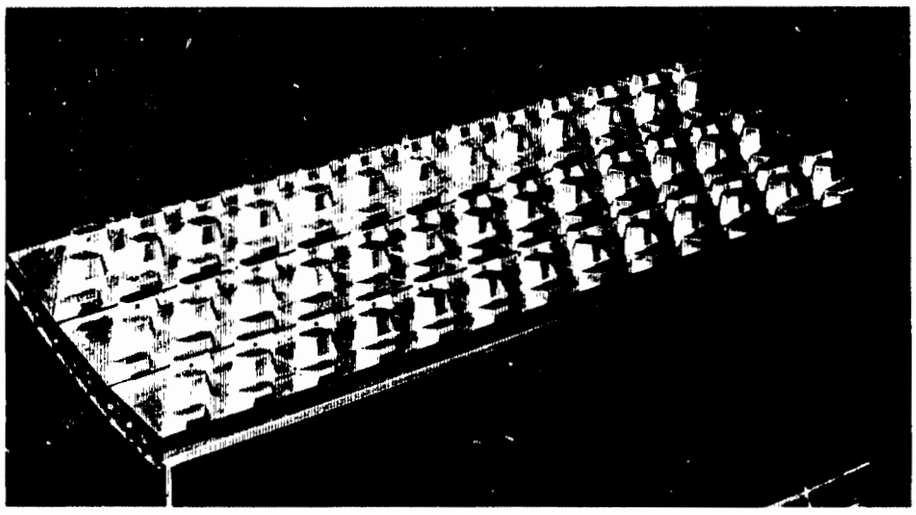

Figure 29. 5-Inch Fan Injector Segment (U/N 2) (U)

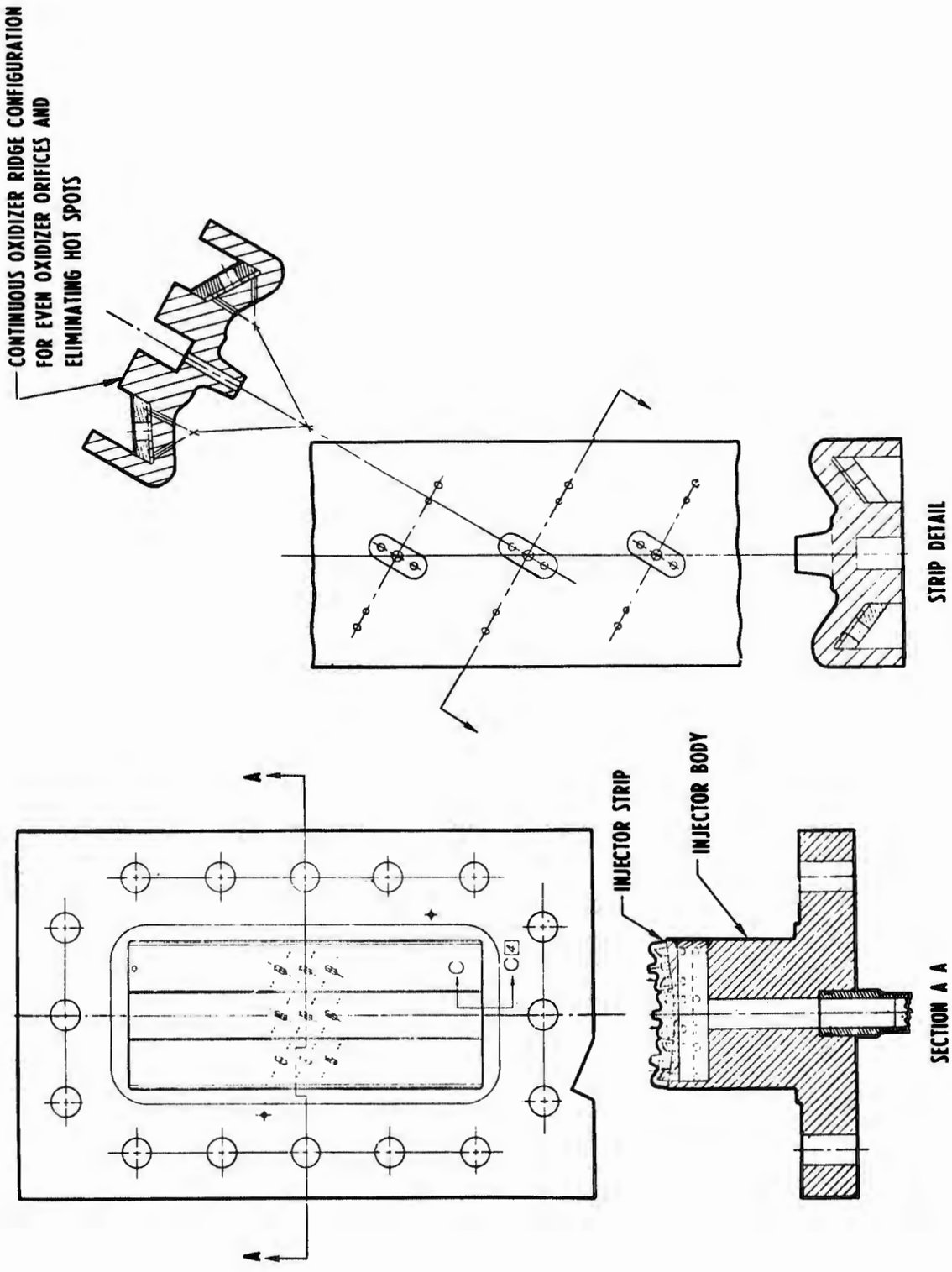

Figure 30. Modified 5-Inch Fan Injector (U/N 3) (U)

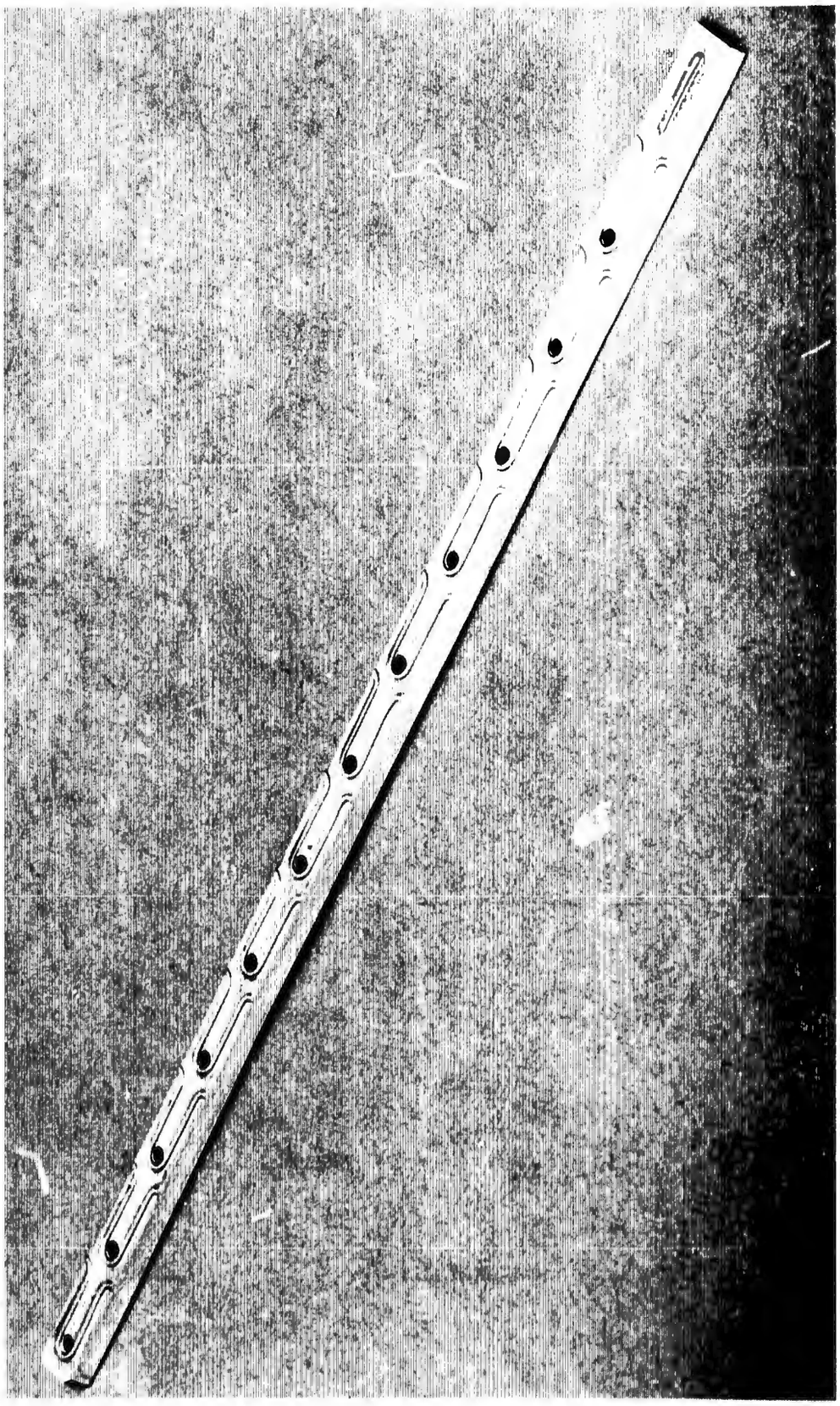

1EH42-5/8/68-C1B

Figure 31. Oxidizer Feed Web (Face Side) for 5-Inch U/N 3 Injector (U)

(U) The oxidizer element protrusions on the injector face, typical of U/N 1 and U/N 2 fan injectors, were replaced on injector U/N 3 with continuous contoured strips to increase the durability and improve performance. U/N No. 1 and 2 injectors had experienced minor melting of the oxidizer protrusions during testing. Also, a possible hydraulic imbalance at the low chamber pressures was believed to contribute to a loss in characteristic velocity efficiency of the U/N 2 fan injector. The imbalance consisted of a geometrical difference in oxidizer orifice length. The continuous contoured oxidizer strip provided orifices of equal length (see Fig. 29 and 30).

(U) Internally pressurized static purge passages were incorporated into the U/N 3 injector at the bipropellant braze joints to ensure positive separation of propellants. The static purge pressure in the purge passages was always maintained at value higher than the injection pressure of either propellant. The purge passage design can be seen in Fig. 32.

(U) Some fabrication problems were encountered with the U/N 3 fan injector. The injector was flow tested following initial furnace braze attachment of the face strips, and many orifices in the center strip were found plugged with braze alloy. Machine removal of the center strip, fabrication of a replacement strip and a second furnace-braze cycle for strip attachment was required. The injector was subsequently flow tested satisfactorily and structurally tested to verify braze joint integrity.

(U) Design and fabrication techniques used for the U/N 4 injector were changed, compared to U/N 1, 2, and 3, in an effort to simplify manufacture. The injector is shown in Fig. 33 and consists of an integral face and body with no braze joints. The injector was completely fabricated from nickel 200 material. The injector face was electrical-discharge machined in one operation. Oxidizer feed control webs were incorporated similar to the U/N 3 injector (Fig. 34).

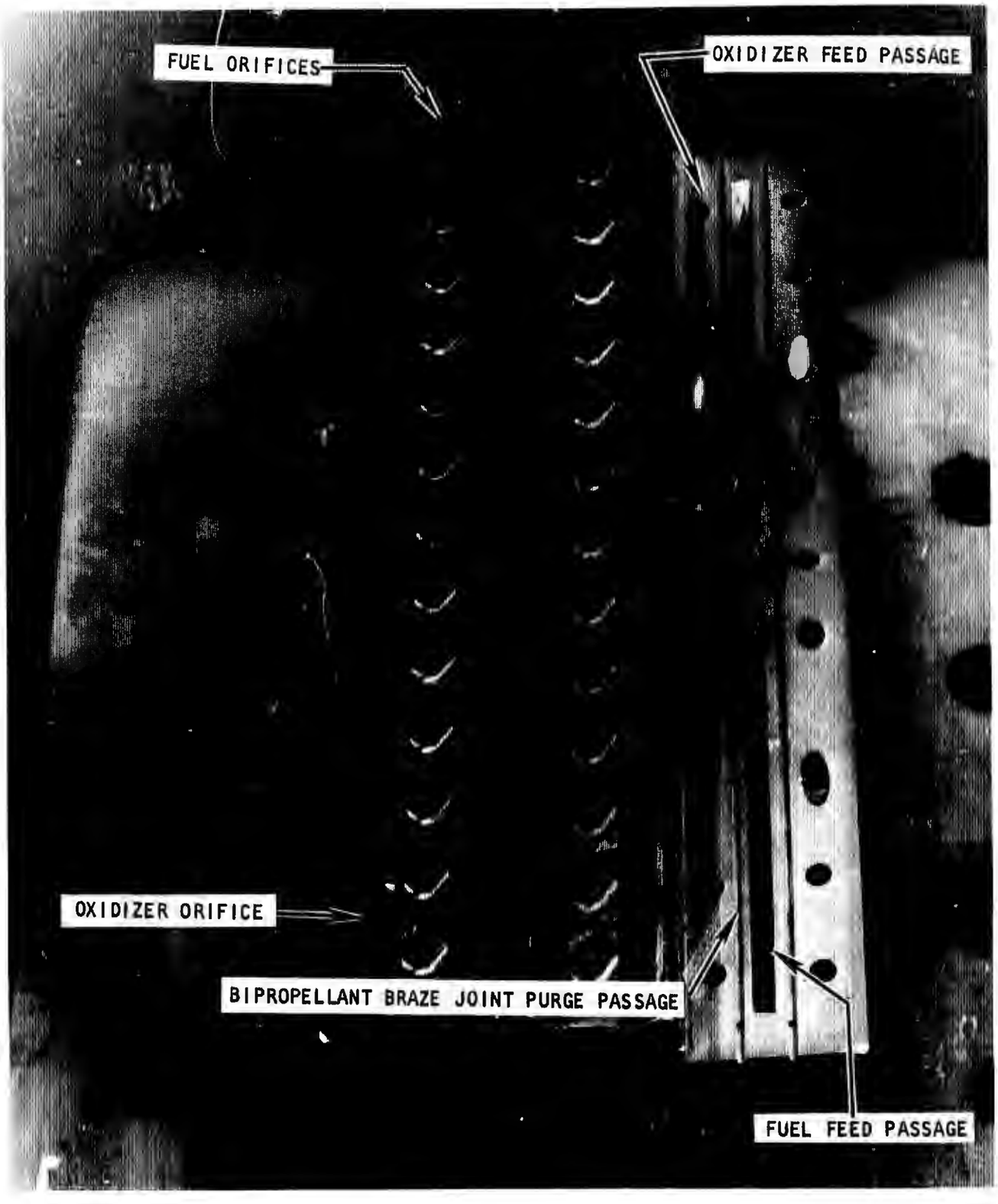

1EH42-5/9/68-C1E

Figure 32. Five-Inch Fan Injector (U/N 3) (U)

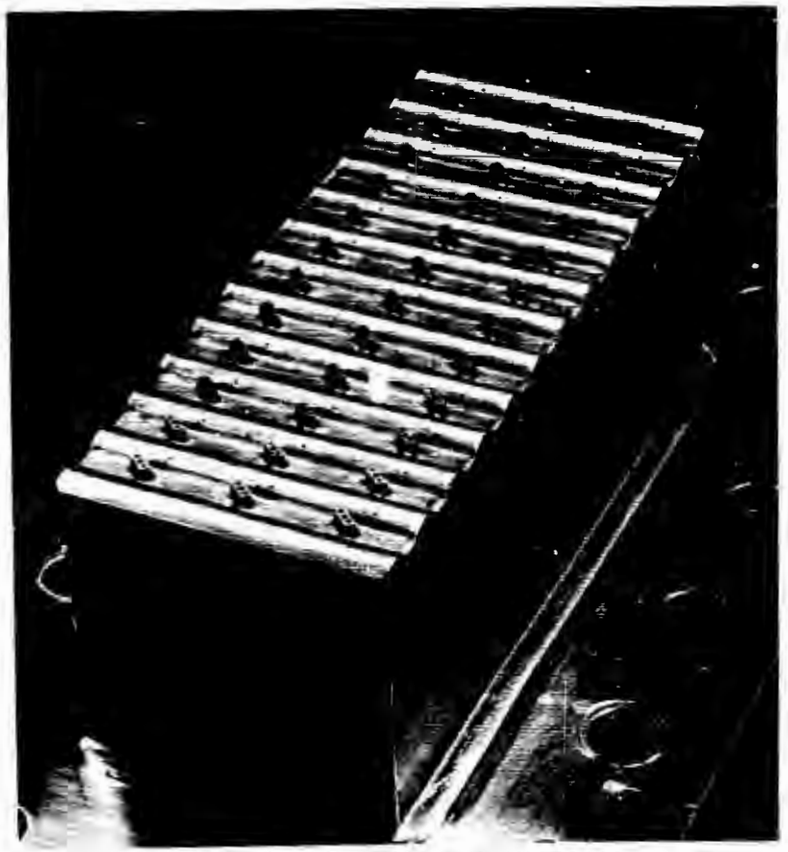

A. 5-INCH FAN INJECTOR

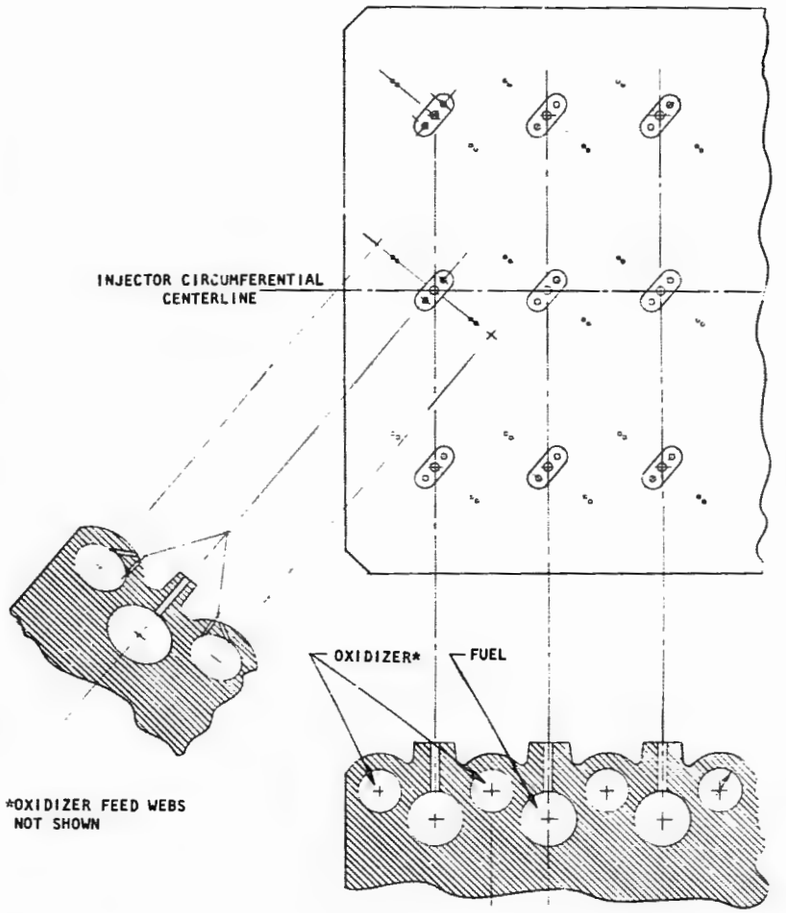

B. INJECTOR WITH RADIAL DRILLED PROPELLANT FEED PASSAGES

Figure 33. Integral Face Injector (U/N 4) (U)

1EH42-7/5/68-C1C

Figure 34. Oxidizer Feed Web (Back Side) for 5-Inch U/N 4 Injector (U)

(U) Following completion of manufacturing, the injectors were flow tested and cleaned, as described earlier for the triplet injectors. Typical flow calibration data is shown in Fig. 35.

(c) Concentric Orifice Injector

(U) The concentric orifice injector was designed and fabricated as a backup approach to the impinging stream-type injectors (triplet and fan). The injector concept was considered to offer a potential for achieving high performance over the throttle range be virtue of oxidizer vaporization within the injector. The injector element posts were designed to achieve heat exchange between the relatively warm hydrogen and the colder fluorine.

(U) The injector design is shown in Fig. 36, and design details are given in Table 2. Nickel 200 material was used in fabrication of all major details. The injector had 33 elements arranged in three rows and the face area between elements utilized Rigimesh for face cooling with hydrogen.

(d) Short Contour Segment Injector

(C) As discussed earlier in Section III, 2, a, (1), (d), a short contour segment was designed for evaluation of an approach for reducing overall heat load. The injector for this segment, shown in Fig. 37, had a reduced face width of 1.3 inches. Decreasing the face area simplified the face cooling requirements and also permitted a more compact and lighter weight design. The element spacing of the injector face remained the same as the fan U/N 3 injector, with the exception of the outermost, diagonally opposed fuel elements. These elements were more closely spaced to the adjacent element and canted inward to prevent baffle impingement. The number of elements per segment was decreased, with a resultant increase in thrust per element and injection density. A comparison of the injection density for the 2-inch width fan and reduced face area injectors is shown in Table 3. The injector construction technique was identical to the 2-inch fan injector (U/N 3).

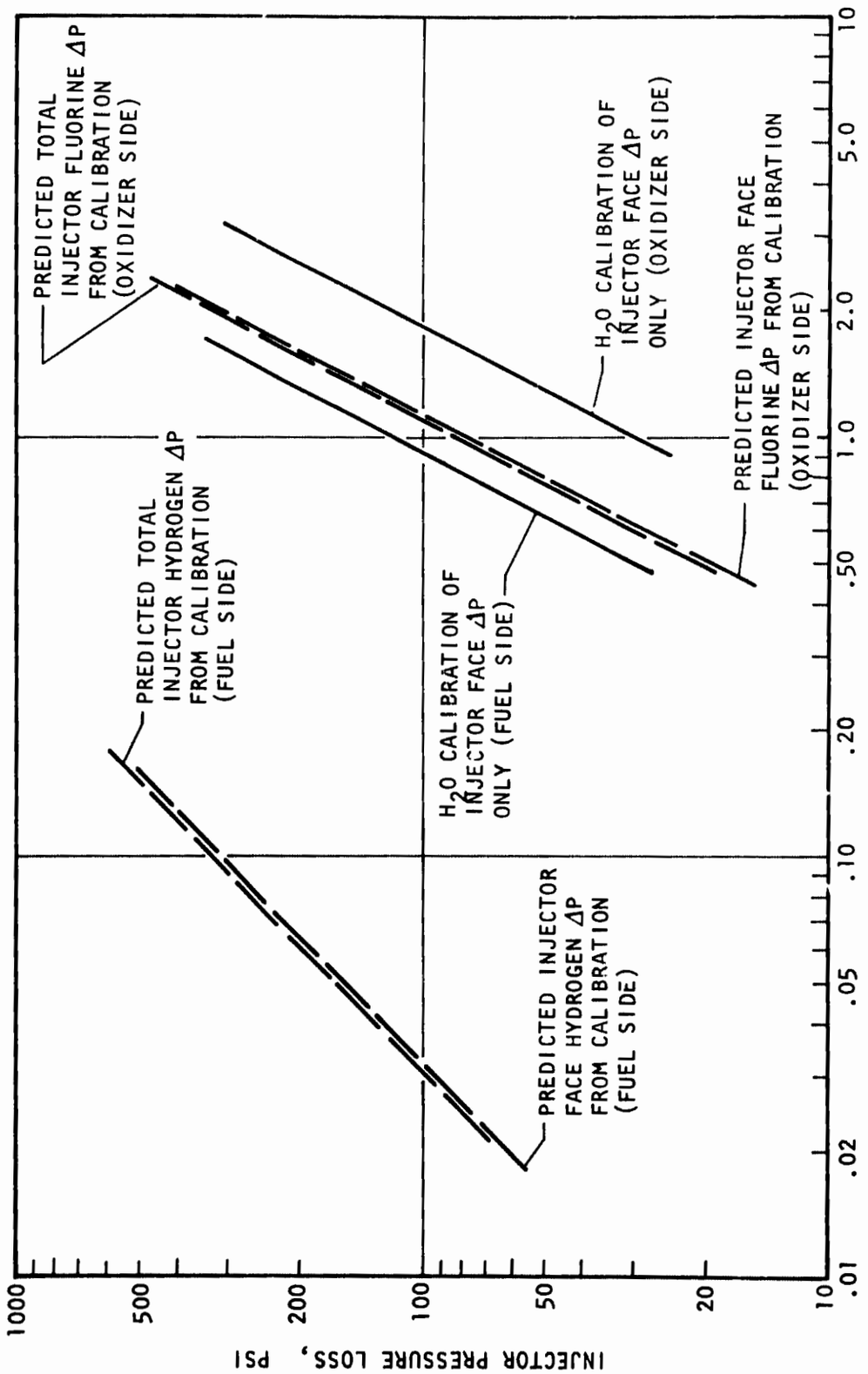

Figure 35. Flow Calibration of 5-Inch U/N 3 Fan Injector (U)

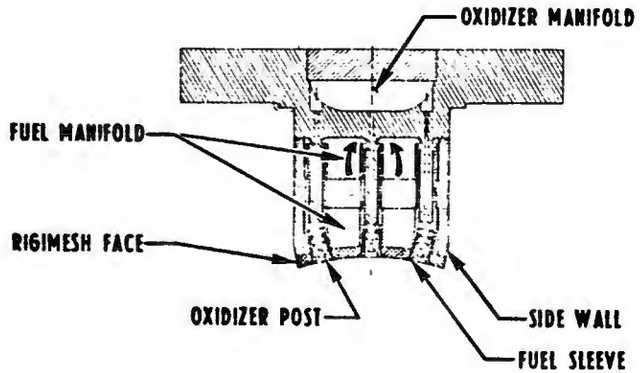

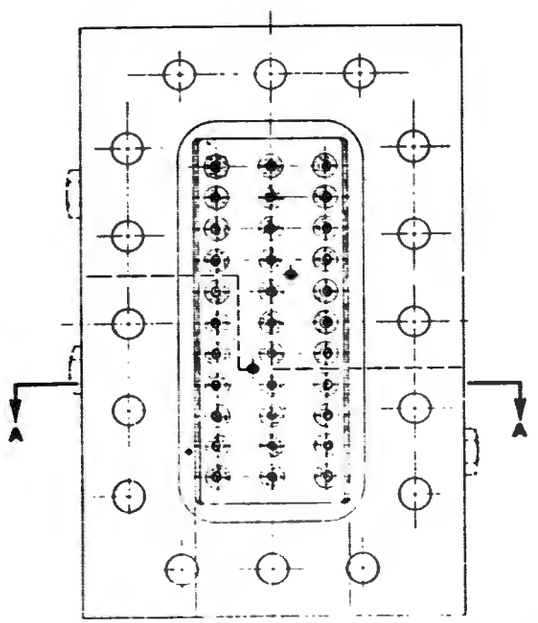

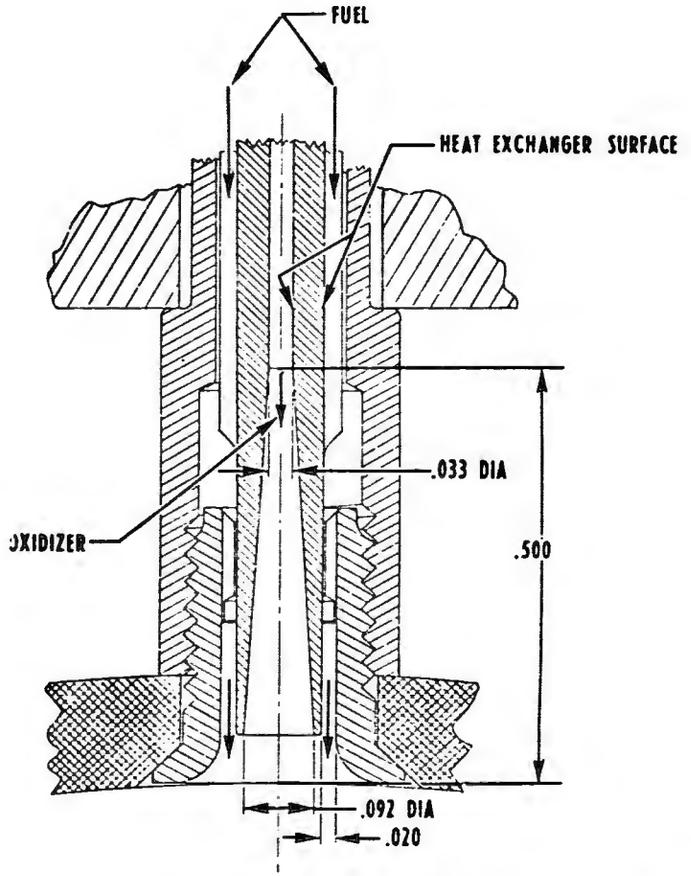

INJECTOR POST DETAIL CONFIDENTIAL

Figure 36. 5-Inch Concentric Orifice GF_2 Injector (U)

CONFIDENTIAL

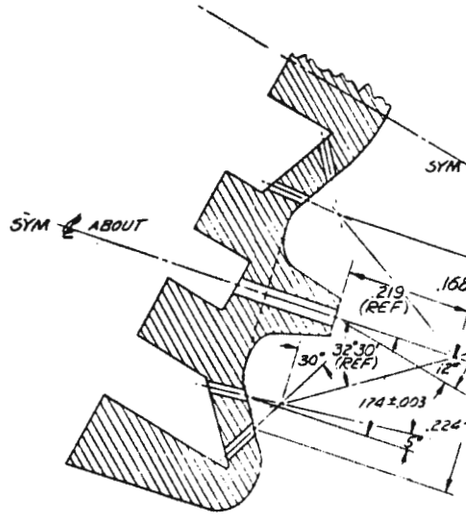

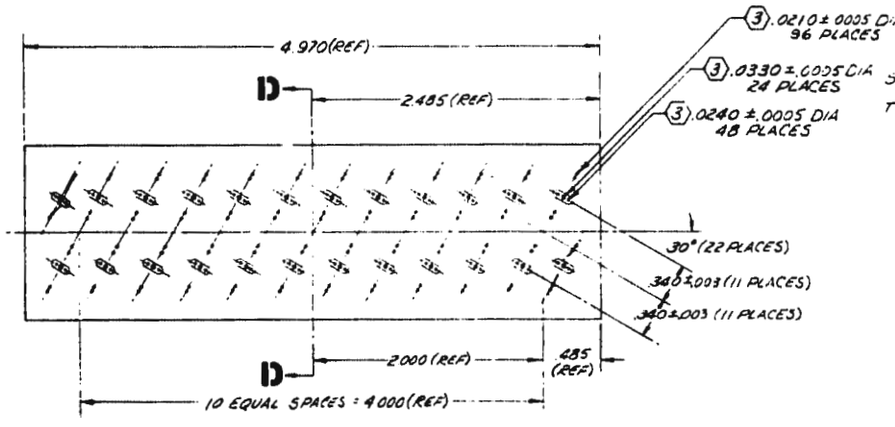

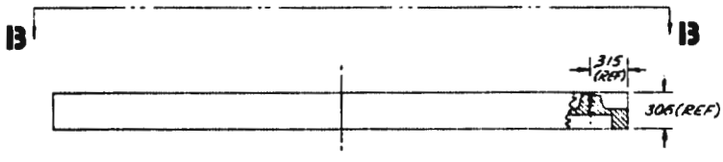

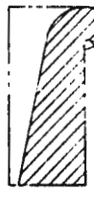

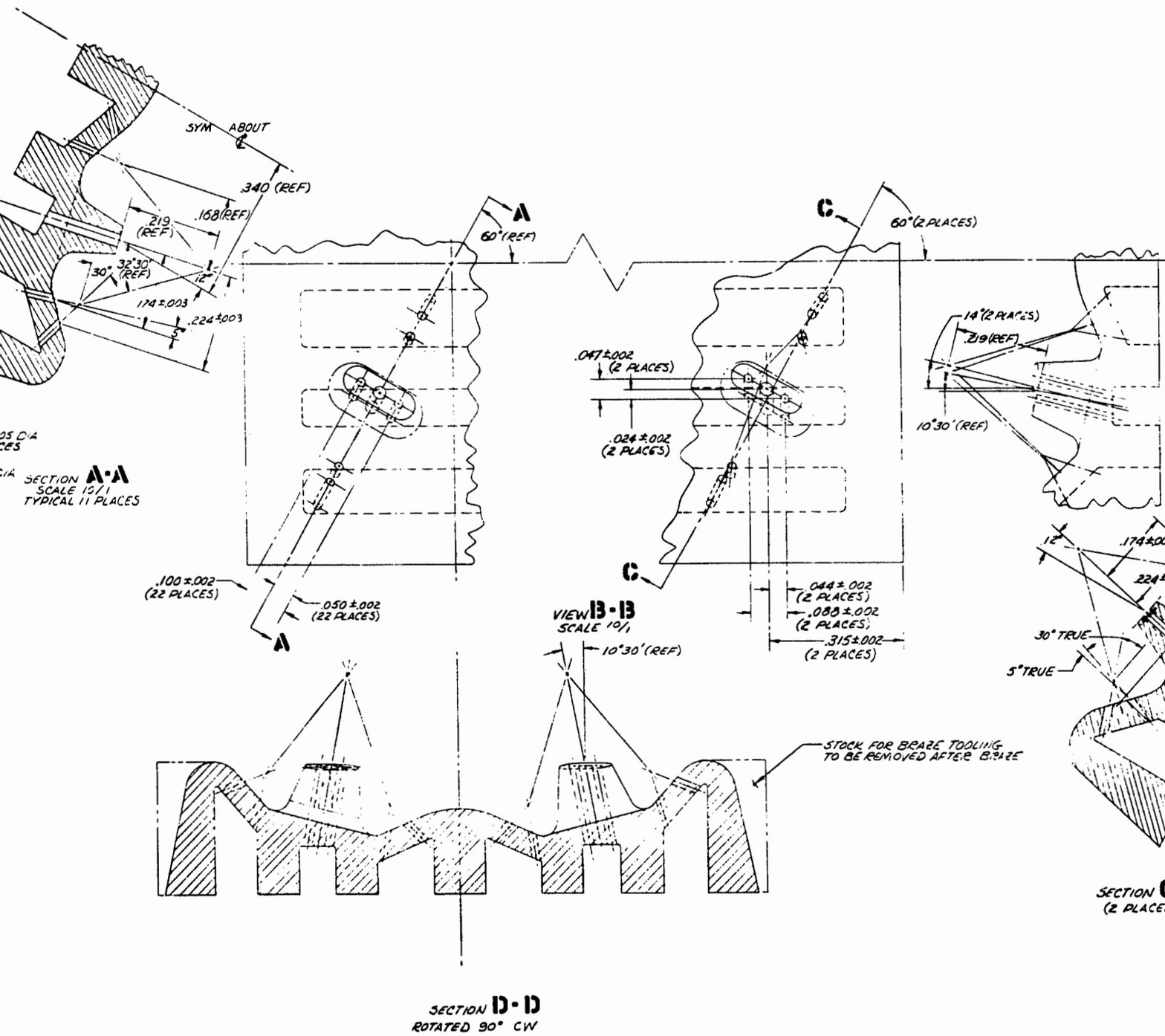

SECTION A-A
SCALE 10/1
TYPICAL 11 PLACES

VIEW B-B
SCALE 10/1

SECTION D-D
ROTATED 90° CW

4. USE SULPHUR FRE
PROCESSING TO P
NICKEL AS DESCR
(3) EDGE OF ORIFICE
AT INJECTOR FA
2. IDENTIFY PER R
1. MACHINE PER RA

2

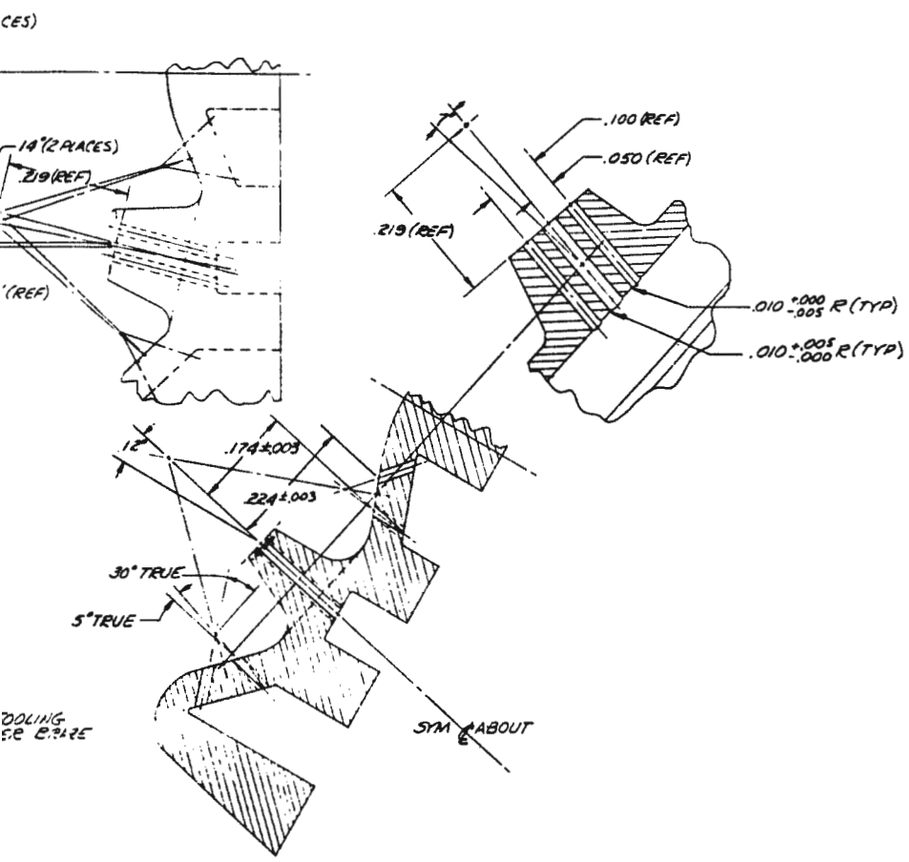

SECTION C-C
(2 PLACES OPPOSITE CORNERS)

4. USE SULPHUR FREE MATERIALS WHEN PROCESSING TO PREVENT EMBRITTLEMENT OF NICKEL AS DESCRIBED IN RA0102-014
3. EDGE OF ORIFICE TO BE SHARP AT INJECTOR FACE
2. IDENTIFY PER RA0104-008 (TAG ONLY)
1. MACHINE PER RA0103-002

Figure 37. Reduced Size Injector Face Strip (U)

TABLE 3

COMPARISON OF INJECTION PARAMETERS FOR 2-INCH WIDE* AND 1.3-INCH WIDE FAN INJECTORS (C)

Configuration	Number of Rows	Number of Elements	Injection Density, LB_m/sec per in^2 of Face Area
2-Inch Wide	3	39	0.2186 at Maximum Thrust 0.0263 at Minimum Thrust
1.3-Inch Wide	2	24	0.337 at Maximum Thrust 0.0405 at Minimum Thrust

*U/N 1, 2, and 3

(U) As mentioned earlier, for the short contour segment chamber, fabrication of the injector was only partially completed in this program because other approaches to the reduction in heat load proved successful (refer to Section III, 5.0, d).

b. 5-Inch Thrust Chamber Segment Testing and Analysis

(U) The segment firing tests were conducted at Victor test stand, at the Propulsion Research Area, Santa Susana Field Laboratory. A description of the facility and operation is presented in Appendix I.

(C) The primary test objectives of the 5-inch segment test program were to provide data that would:

1. Establish the performance (c*) capabilities of the candidate triplet- and fan-type injectors
2. Establish the heat transfer characteristics of the G_c contour (3.5-inch length, injector face-to-throat) thrust chambers

(U) These data would then establish design criteria for the injector and thrust chamber configuration to be selected for the 30-degree thrust chamber assembly.

(U) Additional test objectives were to:

1. Evaluate injector face heat transfer characteristics and durability
2. Determine injector-thrust chamber compatibility
3. Evaluate the cooling capability of the 5-inch regeneratively cooled tubular-wall segment
4. Determine compatibility of the injector design and fabrication techniques with fluorine

(C) Seventy-nine, 5-inch-segment, thrust chamber assembly tests were conducted at site altitude conditions for a total duration of 451.6 seconds. Summaries of the tests are shown in Tables 4 and 5 . A typical test facility installation is shown in Fig. 38.

(1) Triplet Injector-G_c Contour Chamber Test Evaluation

(C) Three triplet injectors (U/N 1, 2, and 3) were tested. The first test hardware assembly consisted of the triplet injector U/N 1 and the G_c water-cooled thrust chamber segment. The initial two firing tests were conducted at chamber pressures of 350 and 355 psia. Upon removal of the segment from the facility for detail hardware inspection following test 2, the injector O-ring seal (dual-pressurized O-ring seals) was found not to have been installed and film coolant (ambient temperature, seal pressurant GN_2) had been introduced in the upper combustion zone. A low (3 Btu/in.^{2}-sec) upper combustion zone heat transfer rate resulted.

(U) Test No. 3, at a chamber pressure of 345 psia, was terminated prematurely because of exhaust flame pattern changes. Posttest inspection revealed overheating and

TABLE 4

5-INCH INJECTOR WATER-COOLED SEGMENT THRUST CHAMBER TEST SUMMARY (U)

(by test numbers)

Test No.	Date, 1968	Chamber Segment	Injector	Test Duration, seconds	Chamber Pressure, psia	Injector Flow, lb/sec	Mixture Ratio, o/f	Fuel Injection Temperature, R	Throat Heat Flux Btu/sq in.-sec	Injector-End Heat Flux Btu/sq in.-sec	Characteristic Velocity (From Chamber Pressure), ft/sec	Corrected Characteristic Velocity Efficiency, percent		Momentum Ratio $\frac{\dot{w}_f v_f}{\dot{w}_o v_o}$	$\frac{\dot{w}_o}{\dot{w}_f v_f} \times 10^3$	Remarks
												From Chamber Pressure	From Thrust			
1	1-5	G_c #1	Triplet U/N 1	0.6	350	0.91	8.1	Instrument Malfunction	11.7	2.97	—	—	—	—	—	No Hardware Damage
2	1-5	G_c #1	Triplet U/N 1	1.6	355	0.94	8.4	Instrument Malfunction	13.4	3.63	*	*	*	*	*	Slight Injector Face Overheating
3	1-9	G_c #1	Triplet U/N 1	2.2	345	0.91	9.1	1083	14.05	10.1	*	*	*	*	*	Injector Irreparably Damaged
4																
5								Facility Checkout Tests With Stand Activation Hardware								
6																
7	1-19	G_c #1	Triplet U/N 2	1.0	337	1.14	12.7	798	12.1	3.9	*	*	*	*	*	Slight Injector Face Overheating
8	1-23	G_c #1	Triplet U/N 2	1.15	322	1.270	14.35	1018	12.5	7.81	*	*	*	*	*	Slight Injector Face Overheating
9	1-23	G_c #1	Triplet U/N 2	1.15	197	7.878	14.5	980	8.5	5.99	*	*	*	*	*	Slight Injector Face Overheating
10	1-26	G_c #1	Triplet U/N 2	1.0	559	1.954	13.58	1222	21.3	13.1	*	*	*	*	*	Injector Irreparably Damaged
11	2-2	G_c #1	Fan U/N 1	0.6	352	1.270	14.76	1144	14.2	2.0	*	*	*	*	*	No Hardware Damage
12	2-2	G_c #1	Fan U/N 1	1.0	353	1.239	14.16	954	14.75	2.12	*	*	*	*	*	No Hardware Damage
13	2-5	G_c #1	Fan U/N 1	0.7	484	1.769	14.49	1266	17.4	3.44	*	*	*	*	*	No Hardware Damage
14	2-5	G_c #1	Fan U/N 1	1.25	509	1.799	14.61	1162	18.4	3.21	*	*	*	*	*	No Hardware Damage
15	2-5	G_c #1	Fan U/N 1	0.75	643	2.233	13.88	1344	19.55	3.34	*	*	*	*	*	No Hardware Damage
16	2-7	G_c #1	Fan U/N 1	3.0	627	2.216	14.15	1127	21.97	4.46	*	*	*	*	*	No Hardware Damage
17	2-7	G_c #1	Fan U/N 1	1.4	655	2.250	13.5	1433	22.9	3.73	*	*	*	*	*	No Hardware Damage; Instrumentation Difficulty
18	2-10	K	Fan U/N 1	2.0	260	0.760	7.9	1285		3.20	*	*	*	*	*	No Hardware Damage; Low Mixture Ratio
19	2-10	K	Fan U/N 1	2.0	256	0.760	9.5	1310	11.5	1.52	*	*	*	*	*	No Hardware Damage; Low Mixture Ratio

*Instrumentation difficulty

CONFIDENTIAL

TABLE 4

(Continued)

Test No.	Date, 1968	Chamber Segment	Injector	Test Duration, seconds	Chamber Pressure, psia	Injector Flow, lb/sec	Mixture Ratio, o/f	Fuel Injection Temperature, R	Throat Heat Flux Btu/sq in.-sec	Injector-End Heat Flux Btu/sq in.-sec	Characteristic Velocity (From Chamber Pressure), ft/sec	Corrected Characteristic Velocity Efficiency, percent		Momentum Ratio $\frac{\dot{w}_f v_f}{\dot{w}_o v_o}$	$\frac{\dot{w}_o}{\dot{w}_f v_f} \times 10^3$	Remarks
												From Chamber Pressure	From Thrust			
20	2-10	K	Fan U/N 1	2.0	355	1.2143	13.80	1319	14.2	2.97	8000	95.7	95.6	4.08	4.268	No Hardware Damage
21	2-10	K	Fan U/N 1	2.0	506	1.727	13.6	1356	17.6	2.64	8050	96.6	97.6	2.80	4.385	No Hardware Damage
22	2-10	K	Fan U/N 1	1.8	645	2.086	12.9	1446	20.33	3.4	8460	97.3	97.7	2.62	3.88	Slight Fuel Trapezoid Melting
23	2-13	K	Fan U/N 1	1.0	638	2.165	13.6	524	17.1	9.45	8075	97.2	100.6	0.855	11.438	Injector Face Overheating
24	2-16	K	Fan U/N 1	19.0	355	1.1492	13.16	1432	11.07	3.22	8467	95.2	95.9	4.45	4.125	No Additional Hardware Damage
25	2-16	K	Fan U/N 1	9.0	236	0.7670	14.60	1371	10.9	1.91	8415	100.4	100.3	5.65	4.807	No Additional Hardware Damage
26	2-23	G_c #2	Fan U/N 1	3.5	65	0.248*	14.7	1128	5.64	3.75	**	**	**	**	**	No Additional Hardware Damage; Instrumentation Difficulty**
27	2-23	G_c #2	Fan U/N 1	9.0	65	0.248*	14.7	1243	6.1	4.14	**	**	**	**	**	Injector Irreparably Damaged; Instrumentation Difficulty**
28	3-1	G_c #2	Triplet U/N 3	0.7	368	1.280	14.40	1240	15.4	1.67	8005	96.7	99.0	4.27	3.001	No Hardware Damage
29	3-1	G_c #2	Triplet U/N 3	2.3	371	1.296	14.60	1380	16.3	2.21	7961	96.0	98.3	4.4	2.877	No Hardware Damage
30	3-1	G_c #2	Triplet U/N 3	7.0	374	1.304	14.90	1407	16.71	3.47	7970	96.2	99.4	4.56	2.738	No Hardware Damage
31	3-5	G_c #2	Triplet U/N 3	0.7	611	2.170	13.91	1360	22.5	5.5	7823	95.78	96.0	2.90	2.50	No Hardware Damage; Slight Oxidizer Strip Overheating
32	3-5	G_c #2	Triplet U/N 3	0.1	—	—	—	1330	—	—	—	—	—	—	—	Chamber Burnout Due to Lack of Water Coolant, No Injector Damage
33	3-8	G_c #1	Triplet U/N 3	1.2	361	1.278	14.28	1160	15.2	2.3	7852	96.8	97.4	3.88	3.28	No Hardware Damage
34	3-8	G_c #1	Triplet U/N 3	15.0	375.6	1.264	14.15	1452	16.92	2.41	8257	96.2	97.4	5.38	2.65	No Additional Hardware Damage
35	3-8	G_c #1	Triplet U/N 3	2.6	515.9	1.772	13.84	1310	20.4	3.65	8090	98.6	96.3	3.45	2.67	Slight Additional Oxidizer Strip Overheating
36	3-12	G_c #1	Triplet U/N 3	0.7	513.2	1.765	14.11	1285	19.9	4.27	8075	100.1	100.6	3.16	2.85	No Additional Hardware Damage

*Estimated

**Instrumentation difficulty

CONFIDENTIAL

TABLE 4

(Continued)

Test No.	Date, 1968	Chamber Segment	Injector	Test Duration, seconds	Chamber Pressure, psia	Injector Flow, lb/sec	Mixture Ratio, o/f	Fuel Injection Temperature, R	Throat Heat Flux Btu/sq in.-sec	Injector-End Heat Flux Btu/sq in.-sec	Characteristic Velocity (From Chamber Pressure), ft/sec	Corrected Characteristic Velocity Efficiency, percent		Momentum Ratio $\frac{\dot{w}_f V_f}{\dot{w}_o V_o}$	$\frac{\dot{w}_o}{\dot{w}_f V_f} = 10^3$	Remarks
												From Chamber Pressure	From Thrust			
37	3-12	G_c #1	Triplet U/N 3	0.3	—	—	—	1175	—	—	—	—	—	—	—	Injector Overheating and Strip Fatigue Failure; Instrumentation Difficulty
38	3-25	G_c #1	Fan U/N 2	0.7	382.5	1.402	16.02	1445	17	1.4	8260	99.4	99.2	5.4	3.12	No Hardware Damage
39	3-27	G_c #1	Fan U/N 2	2.6	377.6	1.292	14.69	1324	18.3	1.01	8018	98.3	98.9	6.4	2.66	No Hardware Damage
40	3-27	G_c #1	Fan U/N 2	10.0	385.6	1.449	16.67	1460	18.2	1.48	8163	98.5	99.3	6.2	2.62	No Hardware Damage
41	3-29	G_c #1	Fan U/N 2	1.5	520.4	1.757	14.39	1340	21.35	2.14	8218	98.6	98.5	4.17	2.80	No Hardware Damage
42	3-29	G_c #1	Fan U/N 2	10.0	525.8	1.752	14.33	1423	21.4	2.49	8268	98.5	99.4	2.07	2.66	No Hardware Damage
43	3-29	G_c #1	Fan U/N 2	1.5	654.8	2.2042	14.39	1342	24.8	2.92	8243	97.3	98.7	3.38	2.76	No Hardware Damage
44	4-3	G_c #1	Fan U/N 2	9.2	661	2.1996	13.70	1493	25.1	3.53	8329	97.5	100.0	4.10	2.25	Slight Fuel and Oxidizer Trapezoid Melting
45	4-3	G_c #1	Fan U/N 2	3.0	220.8	0.7874	14.94	1269	12.6	0.81	*	*	*	*	*	No Additional Hardware Damage; Oxidizer Contamination
46	4-3	G_c #1	Fan U/N 2	8.0	222.2	0.792	15.16	1362	13.3	0.93	*	*	*	*	*	No Additional Hardware Damage; Oxidizer Contamination
47	4-5	G_c #1	Fan U/N 2	18.5	207.9	0.7642	13.92	1449	13.2	0.93	*	*	*	*	*	No Additional Hardware Damage; Oxidizer Contamination
48	4-5	G_c #1	Fan U/N 2	19.0	130.9	0.4783	12.94	1405	8.5	1.9	*	*	*	*	*	No Additional Hardware Damage; Oxidizer Contamination
49	4-5	G_c #1	Fan U/N 2	8.3	94.6	0.3611	14.63	1269	7.2	1.63	*	*	*	*	*	No Additional Hardware Damage; Oxidizer Contamination
50	4-5	G_c #1	Fan U/N 2	4.0	72.3	0.3041	14.1	1027	6.0	1.63	*	*	*	*	*	No Additional Hardware Damage; Oxidizer Contamination
51	4-30	5" TWTC	Fan U/N 2	0.300	439	1.295	8.6	1482	—	—	—	—	—	—	—	Thrust Chamber and Injector Irreparably Damaged

*Oxidizer contamination

CONFIDENTIAL

TABLE 4
(Continued)

Test No.	Date, 1968	Chamber Segment	Injector	Test Duration, seconds	Chamber Pressure, psia	Injector Flow, lb/sec	Mixture Ratio, o/f	Fuel Injection Temperature, R	Throat Heat Flux Btu/sq in.-sec	Injector-End Heat Flux Btu/sq in.-sec	Characteristic Velocity (From Chamber Pressure), ft/sec	Corrected Characteristic Velocity Efficiency, percent		Momentum Ratio $\frac{\dot{w}_f v_f}{\dot{w}_o v_o}$	$\frac{\dot{w}_o}{\dot{w}_f v_f} \times 10^3$	Remarks
												From Chamber Pressure	From Thrust			
52	6-5	G_c #1	Fan U/N 3	0.5	365.0	1.266	14.5	1502	17.3	1.1	8042	97.2	97.7	4.53	2.92	No Hardware Damage
53	6-5	G_c #1	Fan U/N 3	2.6	368.0	1.266	14.9	1296	17.3	1.1	8114	97.9	96.7	4.66	2.84	No Hardware Damage
54	6-5	G_c #1	Fan U/N 3	9.0	370.5	1.270	14.6	1302	17.3	1.1	8118	97.8	98.4	4.76	2.77	No Hardware Damage
55	6-5	G_c #1	Fan U/N 3	2.8	660.4	2.196	14.2	1317	25.4	2.33	8392	100.0	100.0	8.75	2.76	Slight Fuel Post Melting
56	6-7	G_c #1	Fan U/N 3	8.5	218.6	0.758	14.0	1231	12.8	0.94	8042	98.4	100.3	0.48	2.81	Additional Fuel Post Melting
57	6-7	G_c #1	Fan U/N 3	8.3	145.8	0.512	13.84	1126	10.9	1.4	7948	97.93	—	0.42	2.74	Additional Fuel Post Melting
58	6-7	G_c #1	Fan U/N 3	7.6	106.5	0.3892	13.69	1047	9.1	1.63	7739	96.07	—	0.32	2.91	No Further Hardware Damage
59	6-7	G_c #1	Fan U/N 3	7.2	77.7	0.2865	14.63	902	7.25	1.8	7572	95.69	—	0.34	3.70	No Further Hardware Damage
60	6-7	G_c #1	Fan U/N 3	35.5	77.1	0.2870	14.54	952	7.17	2.5	7493	94.80	—	0.34	3.45	Additional Fuel Post Melting
61	6-10	G_c #1	Fan U/N 3	9.5	655.8	2.189	14.1	1544	25	2.9	8360	98.5	99.6	3.05	2.30	Additional Fuel Post Melting Plus Erosion Spot in Throat
62	6-18	G_c #1	Fan U/N 3	9.5	295.4	1.022	14.9	1394	16.0	1.05	8031	97.3	98.5	5.87	2.94	Erosion of Spot Repair
63	6-18	G_c #1	Fan U/N 3	9.5	215.6	0.756	14.4	1310	13.7	0.76	7933	96.5	—	9.15	2.66	Additional Erosion of Spot Repair
64	6-18	G_c #1	Fan U/N 3	9.5	145.6	0.5095	14.19	1378	10.5	1.39	8054	99.07	—	0.49	2.70	Additional Erosion of Spot Repair
65	6-18	G_c #1	Fan U/N 3	9.5	71.2	0.2716	13.44	1216	6.8	1.94	7385	92.36	—	0.48	2.44	No Additional Damage
66	7-10	K	Fan U/N 4	1.5	Varied During Test	—	—	1170	9.6	6.46	—	—	—	--	--	Melting of Injector Face and Fuel Posts
67	7-17	K	Fan U/N 4	1.1	367.8	1.259	14.76	1237	14.05	3.16	8044	97.15	96.85	5.52	3.31	No Damage
68	7-17	K	Fan U/N 4	4.5	348.7	1.17	13.7	1326	13.9	4.79	8210	98.49	98.74	7.17	2.72	Slight Fuel Post Melting

CONFIDENTIAL

TABLE 4

(Concluded)

Test No.	Date, 1968	Chamber Segment	Injector	Test Duration, seconds	Chamber Pressure, psia	Fuel Injector Flow, lb/sec	Mixture Ratio, o/f	Injection Temperature, R	Throat Heat Flux Btu/sq in.-sec	Injector-End Heat Flux Btu/sq in.-sec	Characteristic Velocity (From Chamber Pressure), ft/sec	Corrected Characteristic Velocity Efficiency, percent		Momentum Ratio $\frac{\dot{w}_f V_f}{\dot{w}_o V_o}$	$\frac{\dot{w}_o}{\dot{w}_f V_f} \times 10^3$	Remarks
												From Chamber Pressure	From Thrust			
69	7-17	K	Fan U/N 4	1.3	671.3	2.191	14.38	1306	25.5	5.0	8436	99.04	99.1	3.57	3.12	No additional damage
70	7-17	K	Fan U/N 4	3.8	675.5	1.193	14.38	1401	26.39	5.33	8482	99.4	99.4	3.76	2.92	No additional damage
71	7-18	K	Fan U/N 4	2.4	75.5	0.2811	14.23	1037	5.59	3.28	7396	92.25	--	0.43	3.48	No additional damage; observer cutoff
72	7-18	K	Fan U/N 4	2.0	Varied During Test	--	--	1175	9.6	4.2	--	--	--	--	--	No additional damage; observer cutoff
73	7-29	K	Fan U/N 4	5.0	368.9	1.251	14.45	1320	14.0	1.46	8123	98.36	97.87	6.35	2.94	No additional damage
74	7-29	K	Fan U/N 4	1.5	Varied During Test	--	--	1272	18.3	10.0	--	--	--	--	--	Facility malfunction; injector irreparably damaged
103	12/22	G_c No.1*	Fan U/N 3	0.5	65	--	--	--	--	--	--	--	--	--	--	No additional damage
104	12/22	G_c No.1*	Fan U/N 3	33.5	75.3	0.278	14.09	1402	7.79	2.02	7521	93.7	--	0.231	2.35	
105	12/22	G_c No.1*	Fan U/N 3	24.0	149.6	0.532	14.76	1394	11.37	1.59	7797	96.0	--	0.565	2.67	No additional damage
106	12/22	G_c No.1*	Fan U/N 3	19.6	217.4	0.765	14.49	1416	14.09	1.56	8003	97.3	--	0.651	2.57	No additional damage
107	12/22	G_c No.1*	Fan U/N 3	14.5	367.4	1.246	13.62	1434	19.39	1.26	8302	98.76	--	0.957	2.33	No additional damage
009-69	1969 1/16	G_c No.1*	Fan U/N 3	3.0	664.3	2.284	14.14	1383	30.03	2.22	8822	102	--	0.629	2.35	Throat erosion
010-69	2/7	G_c No.1*	Fan U/N 3	3.6	632.7	2.12	12.4	1379	30.7	2.00	8399	101	--	0.716	2.04	Throat erosion
011-69	2/7	G_c No.1*	Fan U/N 3	4.5	623.1	2.09	12.7	1445	32.07	1.97	8368	101	--	0.717	2.02	Throat erosion

*Shortened combustion chamber to 2.68 inches

CONFIDENTIAL

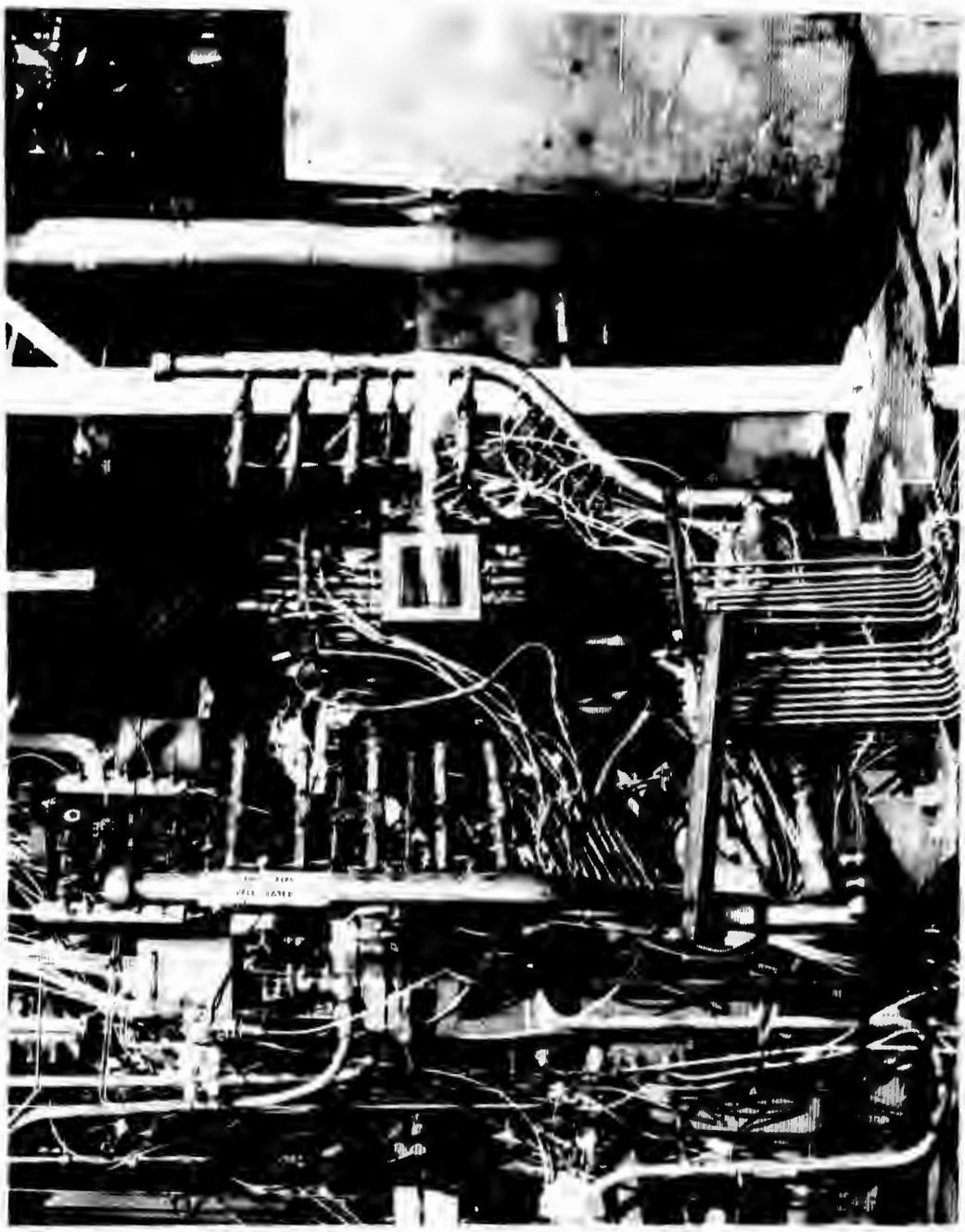

Figure 38. 5-Inch Solid-Wall Thrust Chamber Segment at Victor Test Stand (U)

(U) melting of the oxidizer strips and overheating of the fuel strips. In addition, low-cycle thermal fatigue of all strips had occurred, as evidenced by the transverse cracks that were visible. The upper combustion zone local heat transfer rates, when all required seals were installed and GN_2 was not introduced into the upper combustion zone, were approximately three times as great as they had been during tests 1 and 2.

(U) The second triplet injector (U/N 2) was modified slightly, by incorporating vent holes into the bipropellant vent areas instead of machining continuous slots, as in the U/N 1 injector configuration. The slots and vent holes were to permit escape of possible propellant leakage past the braze joint. Vent holes instead of slots provided additional heat conduction paths between the fuel and oxidizer sections of the strips for improved face cooling.

TABLE 5

5-INCH SEGMENT THRUST CHAMBER TEST SUMMARY (U)

(By Hardware Type)

Hardware Configuration		Testing*	
Thrust Chamber	Injector	No. of Tests	Duration, seconds
5-Inch Segment**			
G_c Contour, Water-Cooled, U/N 1 (3.5-inch combustion zone, 46 tests, 263 seconds)	Triplet, U/N 1	3	4.4
	Triplet, U/N 2	4	4.3
	Fan, U/N 1	7	8.7
	Triplet, U/N 3	5	19.8
	Fan, U/N 2	13	96.3
CONFIDENTIAL	Fan, U/N 3	14	129.5
K Contour, Water-Cooled	Fan, U/N 1	8	38.8
	Fan, U/N 4	9	23.1
G_c Contour, Water-Cooled, U/N 2	Fan, U/N 1	2	12.5
	Triplet, U/N 3	5	10.8
G_c Shortened Contour, Water-Cooled, U/N 1 Mod (2.68-inch combustion zone)	Fan, U/N 3	8	103.1
Tube Wall, U/N 1	Fan, U/N 2	1	0.3

*Test Series: 001-68 through 074-68, 103-68 through 107-68 (107-68 final test in 1968), 009-69 through 011-69

(U) Four test firings were conducted with the U/N 2 triplet injector over a range of chamber pressure of 559 to 197 psia. Overheating of the injector face was again encountered and caused irrepairable damage to the injector.

(U) Overheating of the face on triplet injectors U/N 1 and 2 presented a critical problem that resulted in a complete reappraisal of the original design criteria. In addition to the examination of design criteria and comparison to that developed during the previous program (Ref. 1), the following analyses were performed. A complete metallurgical analysis of the overheated U/N 1 injector was made to determine mode of failure, verify strip material, type, determine if contamination was present, and to examine for nickel embrittlement.

(U) The analysis indicated that:

1. The strip material was Nickel 200 with no significant embrittlement.
2. Transverse cracks in the strips were a result of thermal fatigue failure by overheating.
3. Residue found on the back side of the strips resulted from the reaction of fluorine and overheated nickel. No other contaminants were found.

(C) An extension of the three-dimensional conduction heat transfer analysis performed during initial design was made to cover heat flux ranges of 9 to 10 Btu/in.^{2}-sec. The initial analysis had been performed for heat fluxes of 2 to 4 Btu/in.^{2}-sec. The higher range was found to be necessary to define the injector temperature profile when the injector-end heat flux was determined to be 10.1 Btu/in.^{2}-sec on test 003. The conclusion from the analysis was that there was inefficient use of the propellants for face strip cooling and that fluorine was vaporizing in the strip. The analysis also showed that the injector strips should be modified to increase the velocity of the propellant on the back side of the strips, and improve the distribution into the strips.

(C) The following modifications were made to accomplish these objectives for the triplet injector U/N 3:

1. Incorporated oxidizer feed control webs to increase the oxidizer flow velocity parallel to the face to a design value of 40 ft/sec (Fig. 25)
2. Oxidizer orifice impingement angle changed from 68 to 60 degrees (included angle) to move the flame front farther from the injector face
3. Number of elements per strip increased from 13 to 16 with oxidizer orifices diameter (0.018 ±0.0005) fuel orifices (0.035 ±0.0005)
4. Oxidizer strip thickness decreased from 0.062 to 0.045 $^{+0.000}_{-0.005}$ inch
5. Modified the oxidizer strips to control flow distribution and strip cross celocity
6. Incorporated spacers in the fuel strips to increase flow velocity
7. Modified the oxidizer strip end element pattern in two places to re-orient the oxidizer fan and eliminate strip end burning
8. Replaced interstrip relief grooves with vent holes to improve strength and conduction paths (modification previously made on triplet U/N 2 injector)
9. Modified the body to provide additional oxidizer manifold volume for better distribution

(C) A three-dimensional heat transfer analysis of the modified triplet pattern (described above) was conducted for face materials of copper and nickel, using a face heat flux of 9 Btu/in.^{2}-sec. The results are presented in Fig. 39 and 40. As observed in Fig. 39, the maximum predicted face temperature with the copper strip was 1700 F. This temperature is relatively close to the melting temperature (1900 F) of copper. By comparison, the maximum temperature predicted for the nickel strip was 2200 F. The melting temperature of nickel is 2650 F and, therefore, would provide a safer operating margin. Based on this analysis, the conclusion was that nickel material should be retained for the injector face strips.

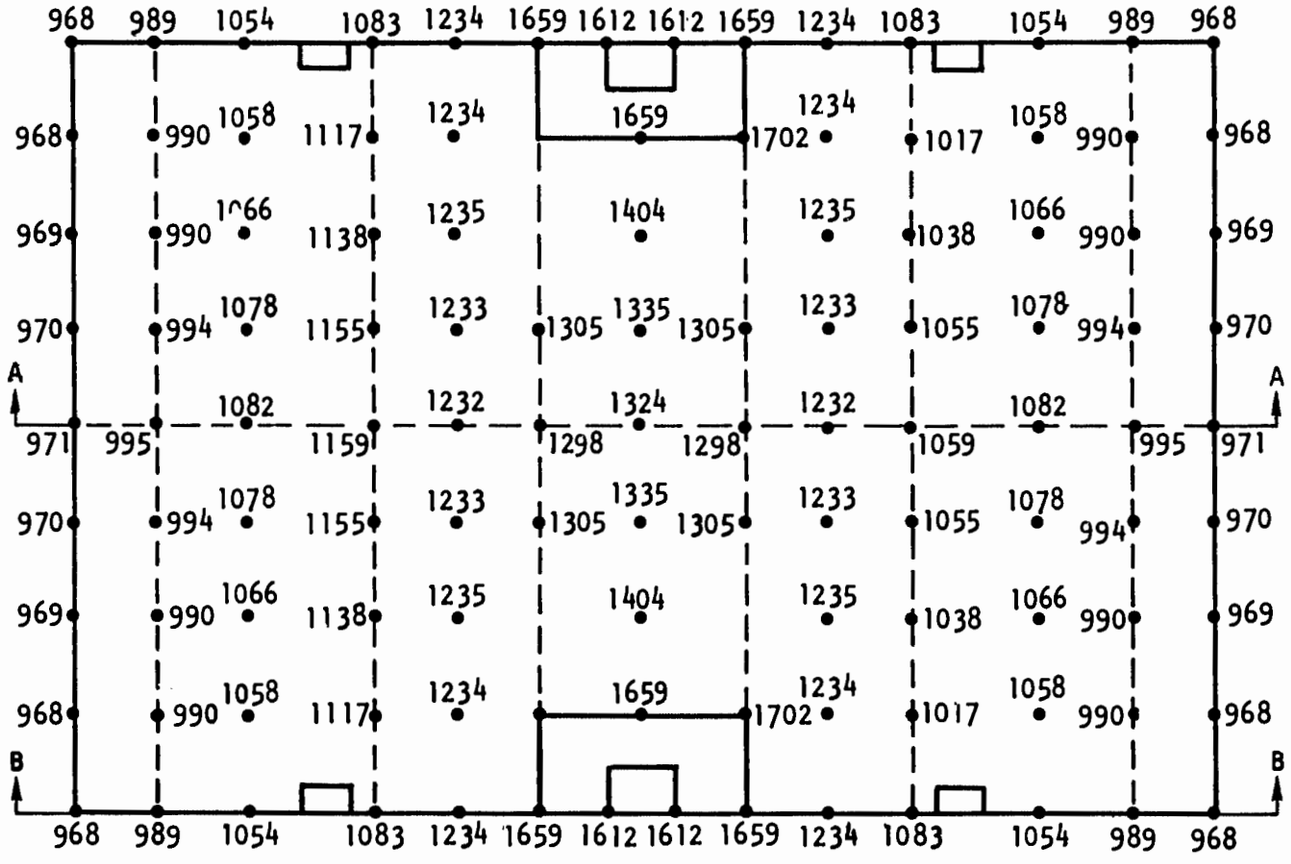

INJECTOR FACE INDICATING GAS-SIDE
WALL TEMPERATURE DISTRIBUTION

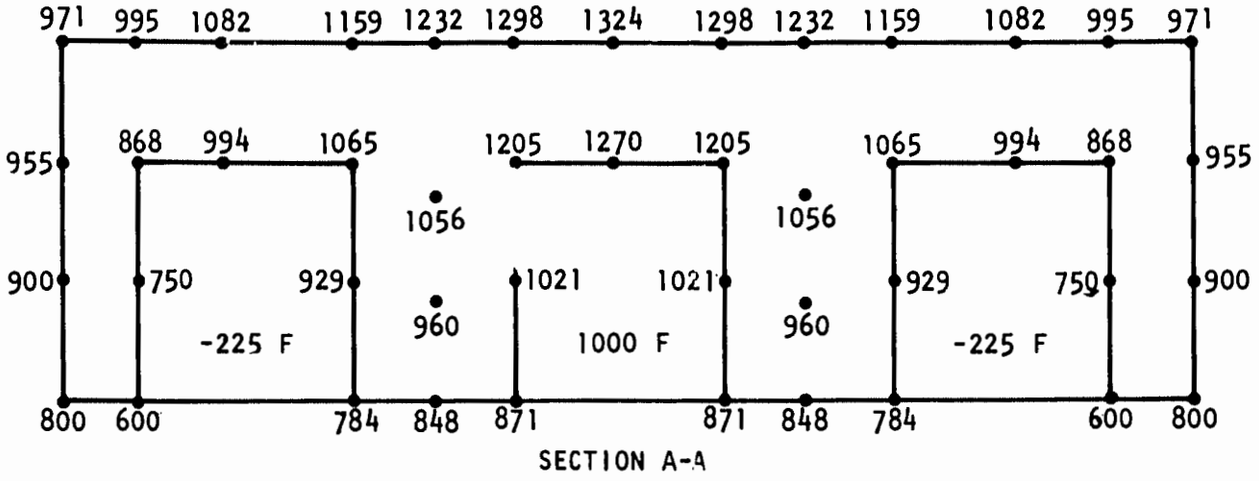

Figure 39. 5-Inch Triplet Copper Strip, 3-D Conduction Model Temperature Distribution (Face Q/A = 9 Btu/in.^{2}-sec) (U)

2

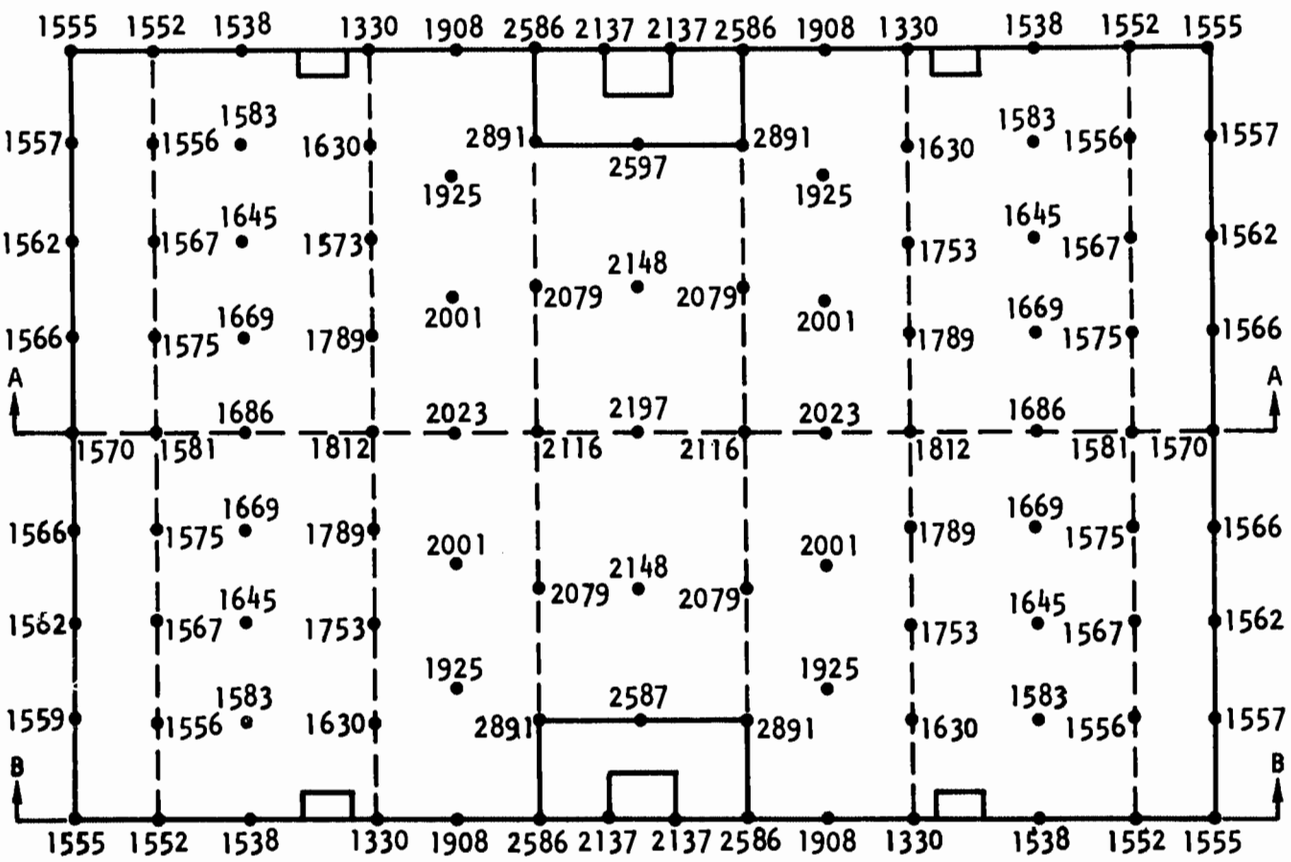

INJECTOR FACE INDICATING GAS-SIDE
WALL TEMPERATURE DISTRIBUTION

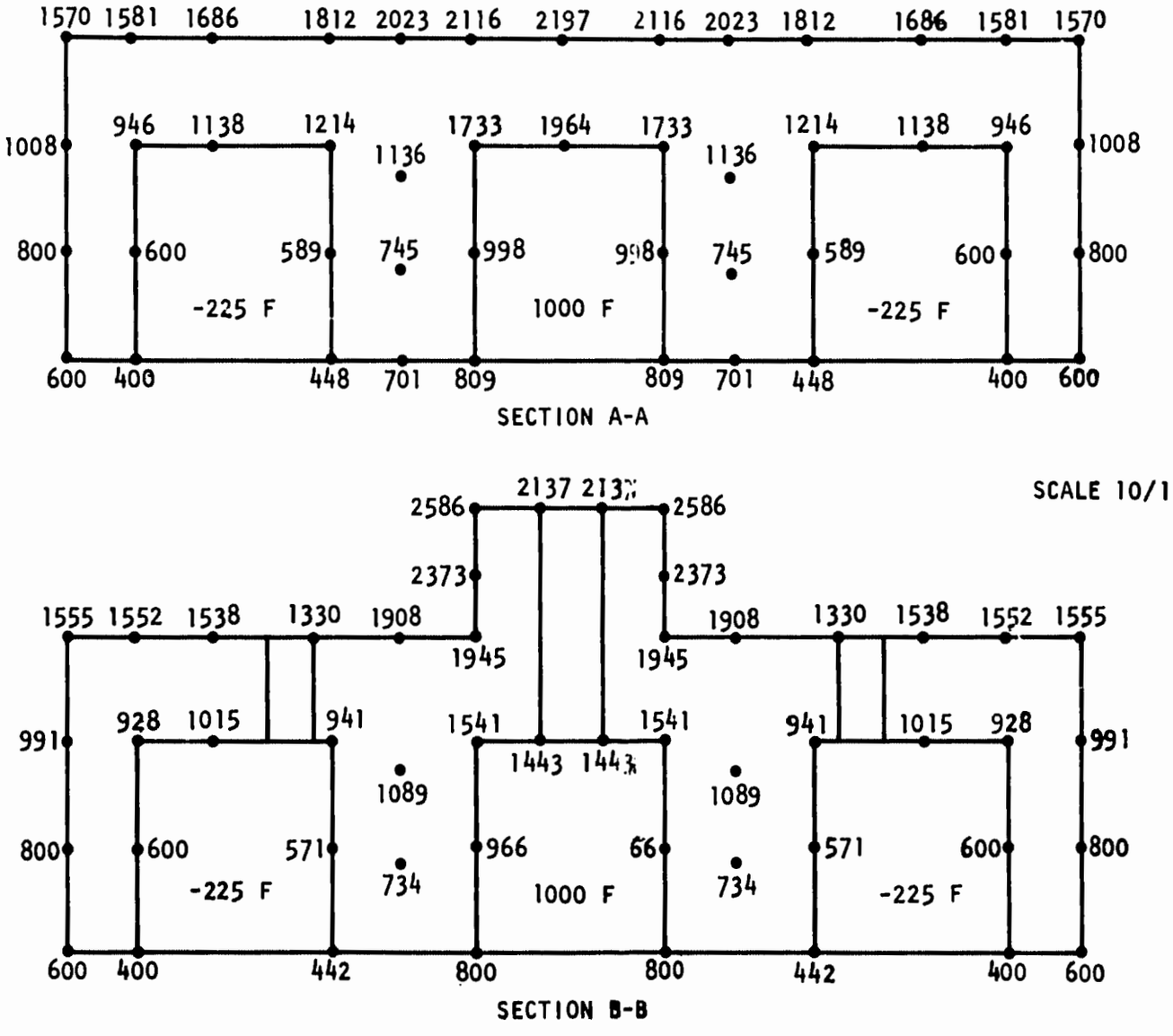

Figure 40. 5-Inch Triplet Nickel Strip, 3-D Conduction Model Temperature Distribution (Face Q/A = 9 Btu/in.^{2}-sec) (U)

(C) After incorporating the above-described modifications into triplet injector U/N 3, 10 firing tests were conducted at chamber pressures ranging from 611 to 361 psia. The injector face cooling was much improved compared to the results obtained previously with triplet injectors U/N 1 and U/N 2. Slight face overheating did occur during the testing, however, and on the last test the injector failed from apparent thermal fatigue of the injector oxidizer strips.

(U) No further development effort was expended on the triplet injector, because results from tests with the fan injector showed greater promise of satisfactory operation for the fan injector type.

(2) Fan Injector U/N 1-G_c Contour Chamber Test Evaluation

(C) Four fan injectors (U/N 1, 2, 3, and 4) were fabricated and tested. The initial series of seven tests on U/N 1 fan injector covered a range of chamber pressures of 655 to 352 psia and indicated acceptable injector-chamber compatibility, local heat flux in the combustion zone and throat, and injector face durability. Slight erosion of several fuel trapezoids (face extensions required to maintain proper orifice L/D, however, occurred. The overall injector physical condition was good, and there was no evidence of face overheating or thermal fatigue failure of the injector face strips.

(C) Low-frequency chamber pressure oscillations, at approximately 3 Hz, were noted on the longer duration tests. The oscillations were apparent in the chamber pressure, fuel injection pressure, and oxidizer injection pressure measurements. The oxidizer injection pressure oscillations had the greatest magnitude and apparently caused the oscillations in chamber pressure and fuel injection pressure.

(C) A combined heat transfer and hydrodynamic analysis was conducted to determine the cause of the oscillations and provide corrective design criteria. A total

(C) quantitative solution could not be obtained, although the following qualitative conclusions were drawn:

1. The oxidizer in the injector feed passages was undergoing a phase change, liquid to two-phase, in the subcritical and supercritical pressure regimes.
2. Unstable film boiling and temperature stratification of the oxidizer were occurring in the feed passages behind the injector face.

These results were subsequently used in making design modifications for the U/N 2 injector. The design change was the incorporation of oxidizer feed webs as described in Section III, 2, a, (2), (b).

(3) Fan Injector U/N 1-K Contour Chamber Test Evaluation

(C) Eight satisfactory tests were conducted with the U/N 1 fan injector and the K contour chamber over a range of chamber pressures of 645 to 236 psia. The tests were conducted to obtain performance and heat transfer data for comparison with the G_c contour.

(C) The results are shown in Fig. 41 and summarized in the following:

1. The total integrated heat rejection rate, Btu/sec, of the K contour was 25-percent greater than that of the G_c contour. This increase was a result of the much larger chamber wall surface area for the K contour, and would result in a 25-percent increase in coolant bulk temperature and increased chamber wall hot-gas-side wall temperature, T_{wg}.
2. The local heat transfer rate, heat flux expressed as Btu/in.^{2}-sec, at the throat of the K contour chamber was 20.35 Btu/in.^{2}-sec at 638-psia chamber pressure, as compared to the G_c contour chamber of 21.97 Btu/in.^{2}-sec at 627 psia. This slight decrease for the K chamber was believed to be a result of the more favorable boundary layer buildup for the greater length K contour wall.

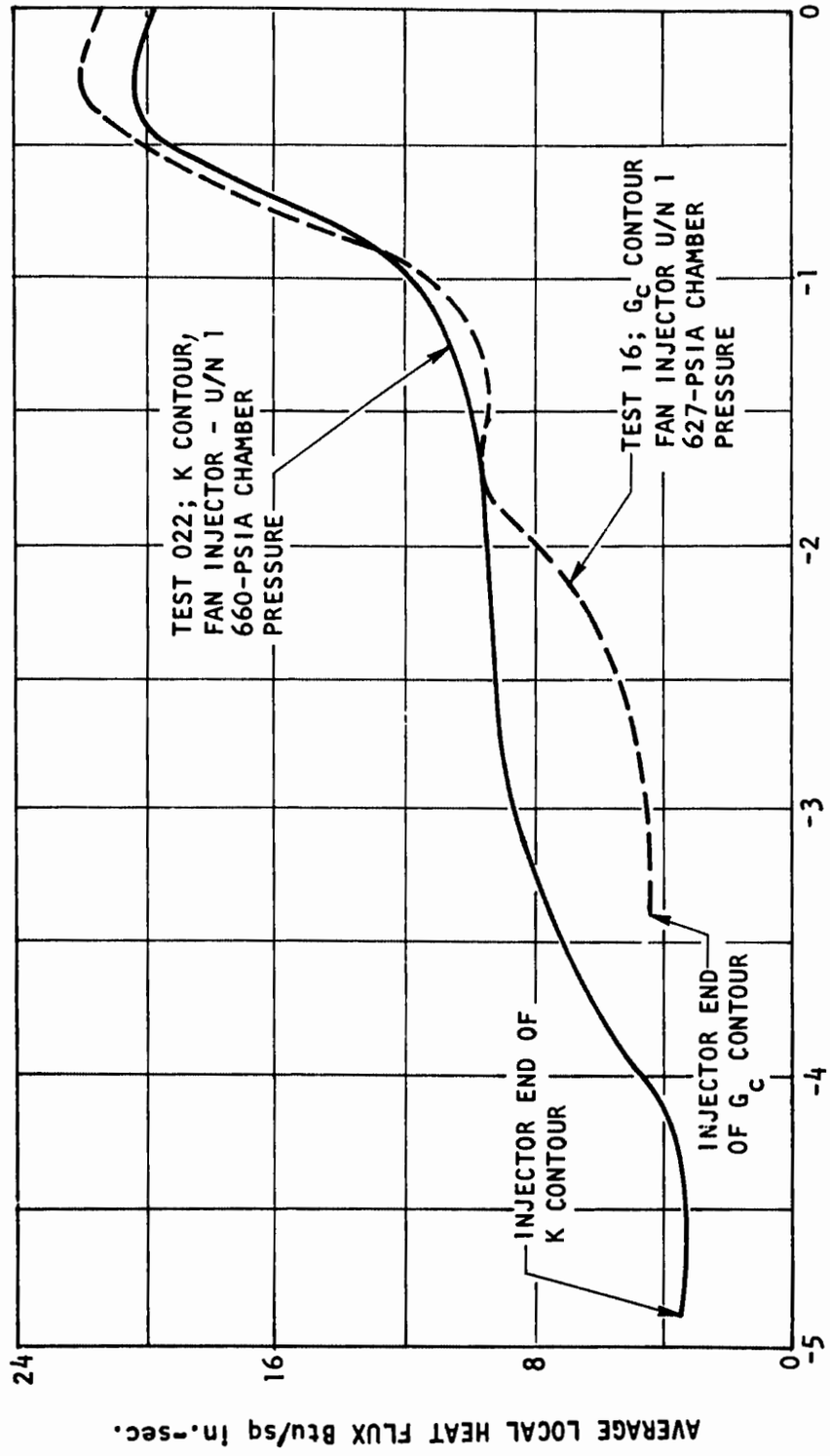

Figure 41. Heat Flux Distribution Measured in Contour K and G_c Contour Solid-Wall Thrust Chambers (U)

(U) Based upon item 1 above, and the recognizable weight advantage afforded by the shorter length chamber, the G_c contour was selected for the 30-degree segment thrust chamber combustion zone configuration.

(C) Because of the low-frequency chamber pressure oscillations which occurred previously, with the U/N 1 fan injector and G contour chamber, a test (23) was conducted to evaluate the effect of hydrogen injection temperature on the oxidizer injector flow instability. The hypothesis was that the oscillations were caused by unstable heat transfer conditions in the oxidizer feed passages of the injector, which was enhanced by the elevated-temperature hydrogen (900 F) in the injector. The hypothesis was investigated on the firing test by the use of ambient (70 F) temperature hydrogen which had a resultant decreased heat transfer potential relative to the colder fluorine. The use of ambient hydrogen rather than heated hydrogen did result in the cessation of chamber pressure oscillations, but an increased injector face heat flux also resulted, due to a lower hydrogen injection velocity. Overheating of the injector face occurred; however, continued testing was possible with this injector.

(4) Fan Injector, U/N 2--G_c Contour Chamber Test Evaluation

(C) The U/N 2 fan injector was tested 13 times in the G_c water-cooled chamber over a chamber pressure range of 661 to 72.3 psia. The test objectives were:

1. Determine injector face heat transfer and cooling capability
2. Determine injector-chamber contour c* performance capability
3. Evaluation of the injector-chamber contour heat transfer characteristics

(U) Test objectives were met; however, the G_c chamber throat heat transfer rates with the U/N 2 fan injector were slightly higher than on previous tests. The numerous thermal cycles experienced by the G_c, U/N 1, thrust chamber led to a

(U) degeneration of the chamber wall in the throat region. This degeneration consisted of slight waviness of the wall, and surface roughness, which was believed to have caused the increased heat transfer. The throat region was repeatedly polished between tests for removal of the roughness.

(C) During the test series excessively high injector face heat flux was encountered at low chamber pressures. A detail analysis of the problem was conducted. The investigation revealed that the injector mechanics (relationship of propellant phase, mixing length, injection angle, etc.) and resultant face heat flux were primarily a function of the fluorine condition, e.g., liquid, two-phase, saturated vapor, etc. Injector operation in the low chamber pressure region resulted in higher than predicted face heat flux because of a change in basic injector mechanics that was self-sustaining and progressive. The increased face heat flux resulted in less dense fluorine injection, which in turn resulted in an increased face heat flux, and the cycle continued until a true gas-gas injection mechanism existed.

(C) To evaluate the condition of the fluorine injected into the chamber, a thermodynamic analysis was performed using the face heat flux as the source of an enthalpy change. As the pressure drop in the injector is primarily through the orifices, the properties of the fluorine as it reaches the orifices can be found assuming a constant pressure process. This condition is only an approximation, because the face heat flux is measured at the wall and the actual face area cooled by the fluorine is not exactly known. If this area is assumed to be 2/3 of the face (hydrogen cools 1/3), the change in enthalpy can be calculated, and the fluorine quality entering the orifice can be determined. Figure 42 shows the face heat flux necessary to effect the vaporization process as a function of chamber pressure (oxidizer flow). Also plotted is the heat flux measured for the fan injector U/N 2 during testing. As shown, the test data curve is discontinuous near the point of saturated liquid fluorine injection (tests 46 and 47). This condition indicates higher face heat flux with two-phase fluorine than with liquid. The discontinuity is attributed to a basic change in injector mechanics.

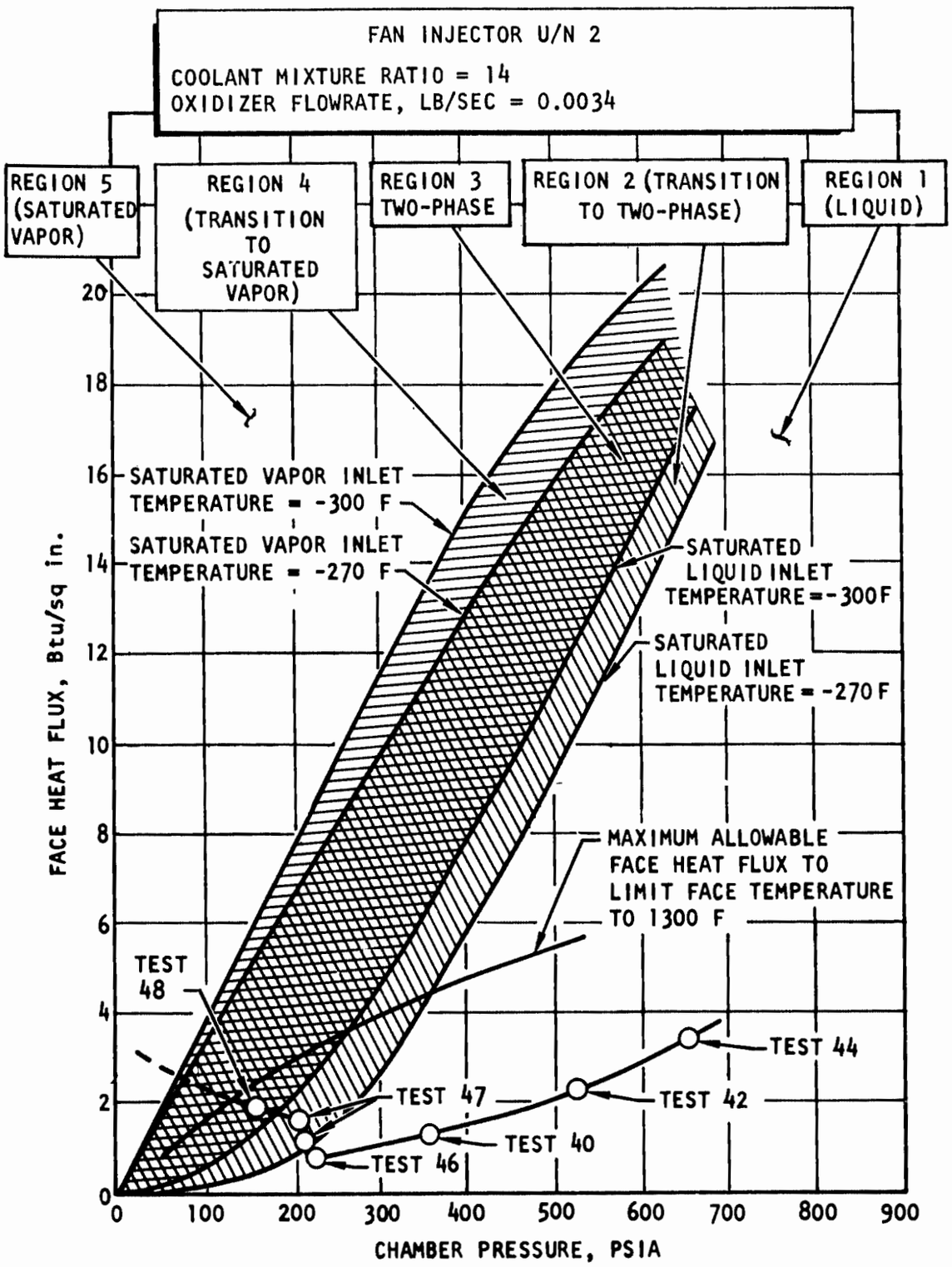

Figure 42. Heat Flux vs Chamber Pressure Showing Quality of Fluorine Injected on a Bulk Basis (U)

(U) A curve that designates the maximum allowable heat flux as a function of chamber pressure is also shown in Fig. 42. The values derived from this curve were used for test redline values and also as design criteria.

(U) The fan injector fluorine orifice pressure drop (U/N 2) as a function of flowrate is shown in Fig. 43. The change in slope as a result of operation in the two-phase flow region can be seen.

(U) Based on the above results, additonal design modifications were incorporated into the U/N 3 injector. These modifications were principally to increase the oxidizer flow velocity between the feed web and injector face for improved heat transfer (refer to Section III, 2, a, (2) (b)).

(5) Fan Injector U/N 3--G_c Contour Chamber Test Evaluation

(C) The U/N 3 fan injector and G_c water-cooled chamber assembly was tested 14 times, over a chamber pressure range of 71.2 to 660.4 psia. All tests were satisfactory. Slight erosion of the segment chamber throat, however, was experienced during the test series. The erosion was attributed to a reduction in the liquid side heat transfer coefficient due to scale formation in the coolant passage. An attempt was made to repair the erosion with dalic-plating, but it was not completely satisfactory. The chamber coolant passages were acid-flushed to remove the scale.

(C) Four tests were conducted to specifically investigate the low chamber pressure retion with respect to c* performance. Previous experience indicated that an increase in fuel injection velocity could be beneficial for c* performance. The increase in fuel injection velocity from a normal 5000 to 6000 ft/sec was obtained by increasing the fuel injection temperature while maintaining the proper mixture ratio, 14.1 (o/f). There was no apparent increase in performance indicating that c* efficiency was insensitive to fuel injection velocity increases above a minimum value of approximately 4500 ft/sec.

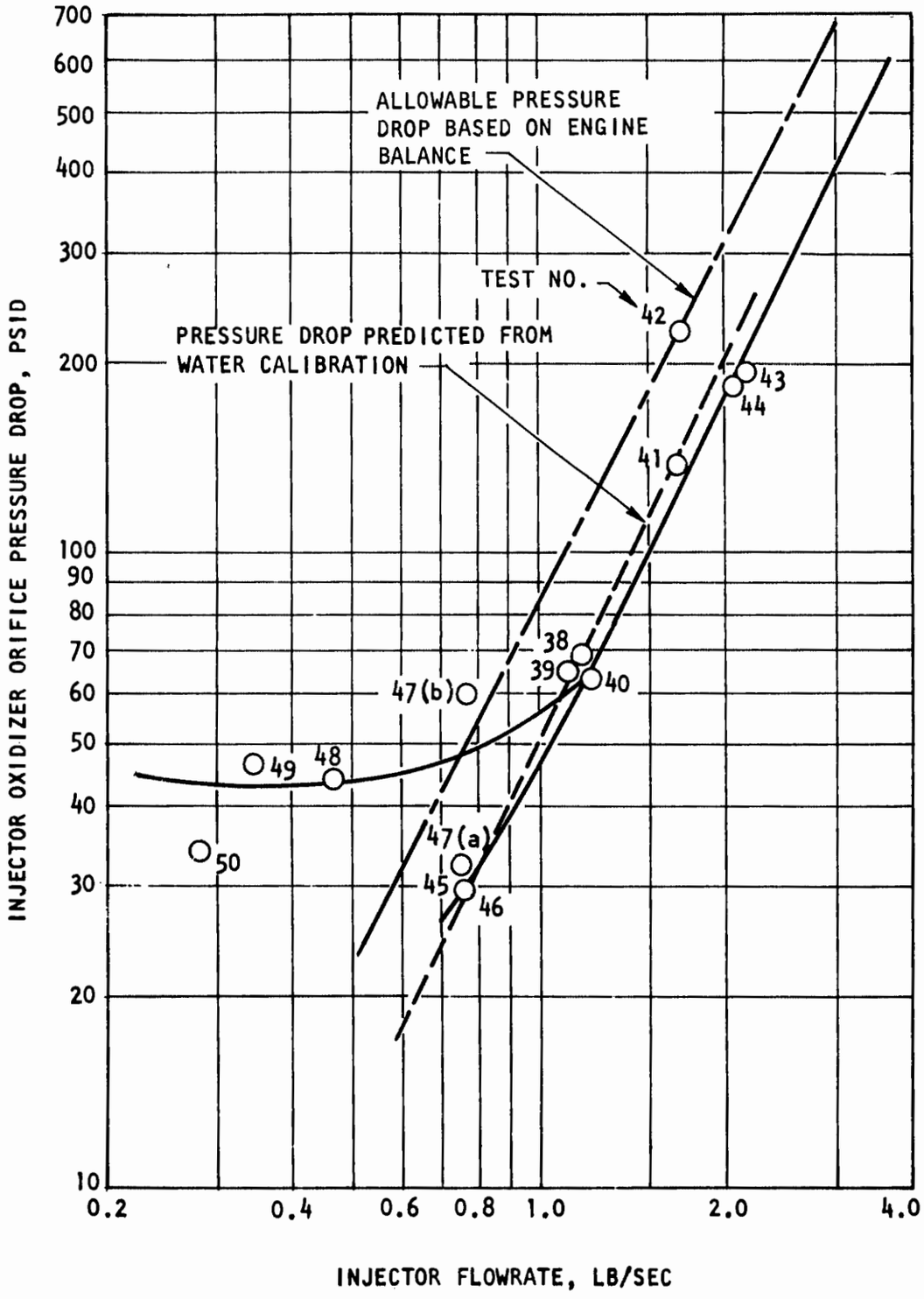

Figure 43. 5-Inch Fan Injector Orifice Pressure Drop vs Flowrate (U/N 2) (U)

(U) The c* performance for the U/N 2 and U/N 3 fan injectors is presented in Fig. 44 for tests of 5 seconds or greater duration. The performance was determined according to the methods outlined in Appendix II. The methods included determination of c* efficiency from both thrust and chamber pressure measurements.

(6) Fan Injector U/N 4--K Contour Chamber Test Evaluation

(C) Nine tests were conducted with the U/N 4 fan injector and the K contour chamber over a chamber pressure range of 675.5 to 75.5 psia. The U/N 4 fan injector was fabricated by a different technique (integral face) as described earlier in Section III, 2, a, (2),(b)). The K contour chamber was used because of the poor throat condition of the G_c chamber as a result of repeated use.

(C) The initial test was programmed for 1.5 seconds duration at 370-psia chamber pressure. Injector operation was unsatisfactory, and some hardware damage was apparent due to excessive injector face and upper combustion zone heat flux. The fuel protrusions were melted on the tips, and six melted areas were noted on the oxidizer strips. The injector was reworked by increasing the oxidizer orifice diameter (thereby decreasing the oxidizer injection velocity) and cutting back the fuel protrusions approximately 0.035 inch so that they were equal in height to the oxidizer strip. Previous tests of the fan injectors had indicated that the upper combustion zone heat flux was directly influenced by oxidizer injection velocity. That is, as oxidizer velocity increases, so did upper combustion zone heat flux. This effect is shown in Fig. 45, which is a plot of upper combustion zone heat flux (Measured immediately below the injector face) as a function of oxidizer injection velocity. Fuel injection velocity was reasonably constant over the throttle range.

(C) The next four tests with the modified injector were conducted at chamber pressures of approximately 370 and 650 psia, and the test data verified the effectiveness of the injector modification. The injector and combustion chamber wall heat flux were significantly reduced by the decrease in the oxidizer injection

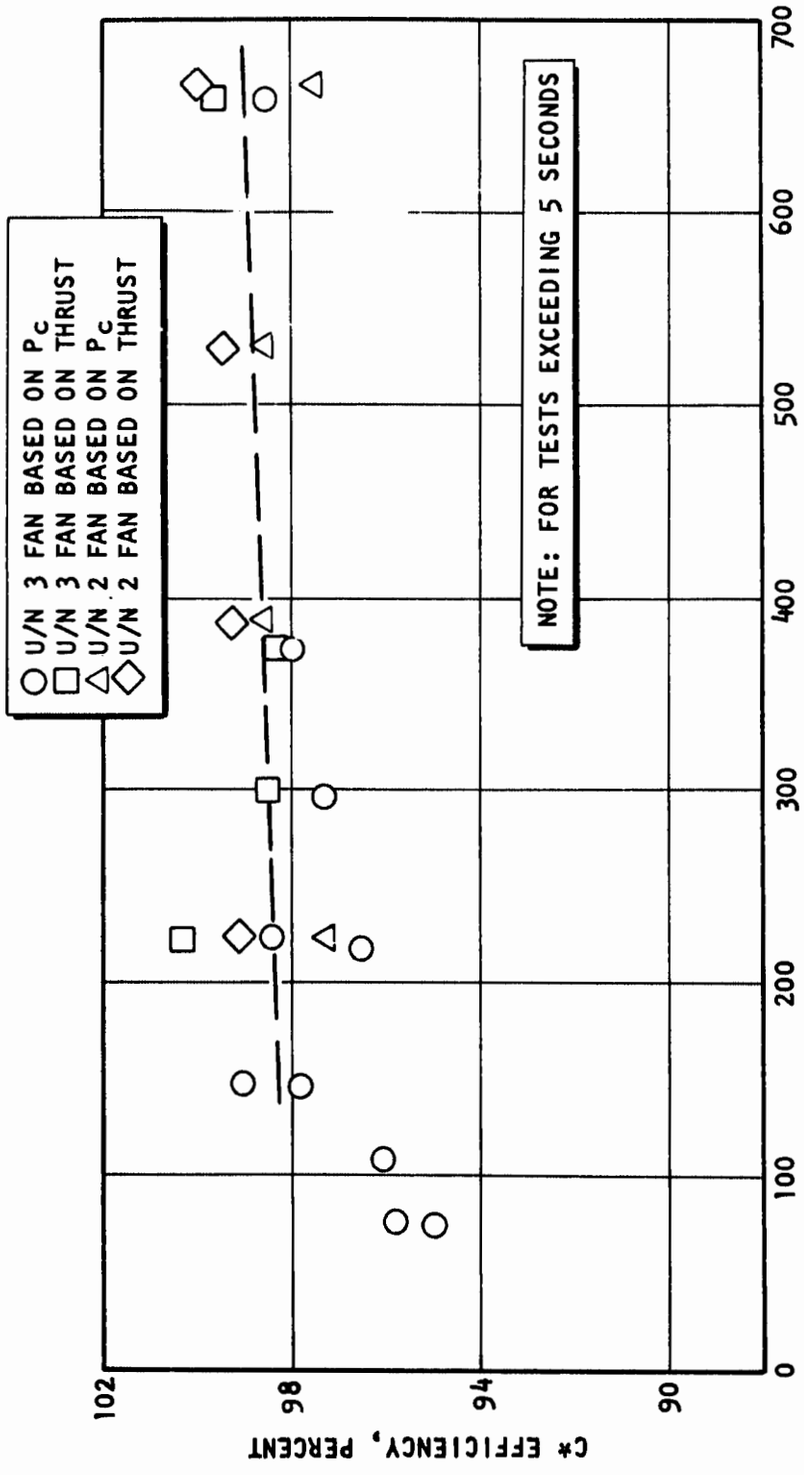

Figure 44. c* Efficiency for 5-Inch Fan Injector and G_c Contour Chamber (U)

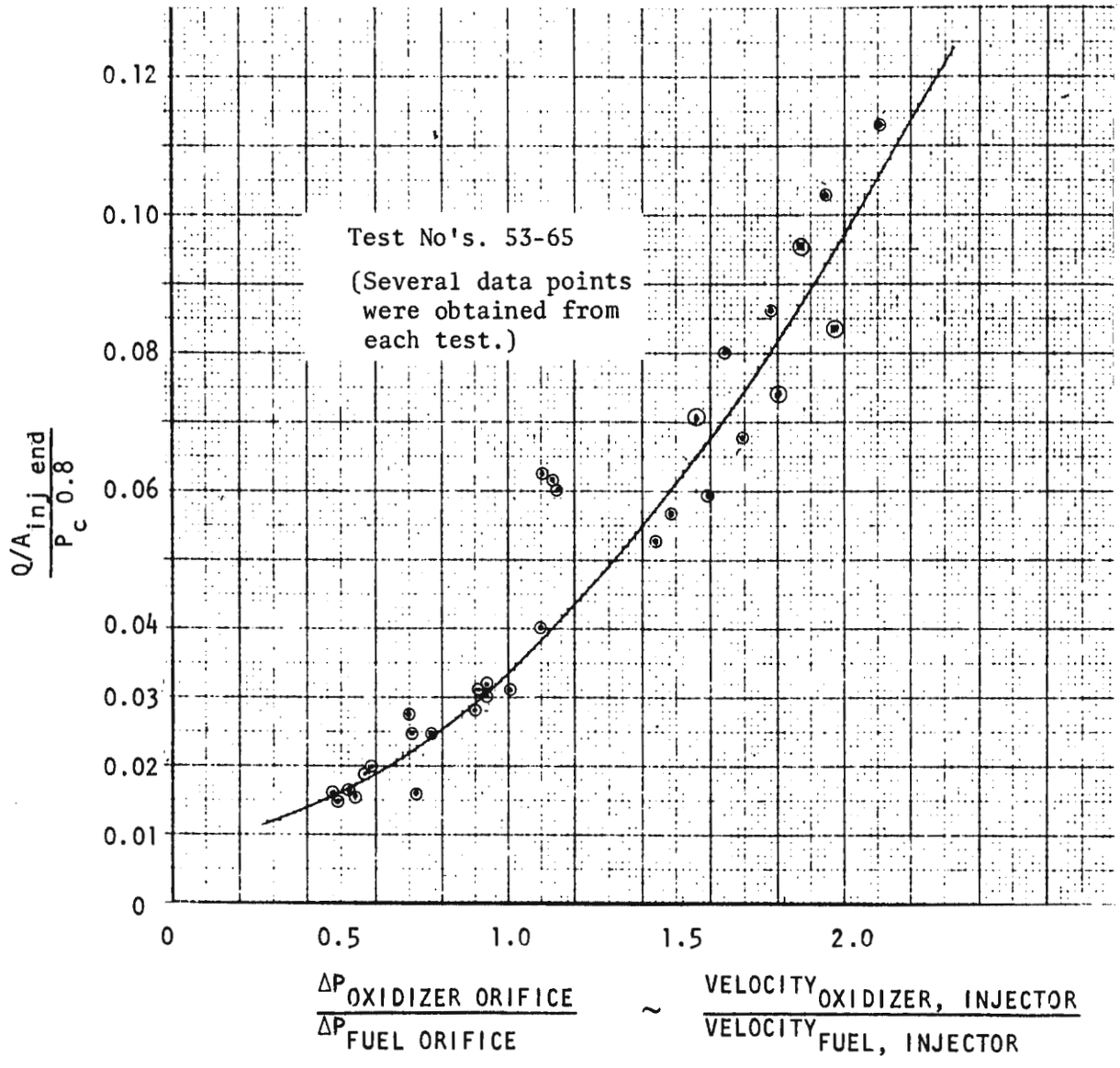

Figure 45. Test Results With 5-Inch Segment Fan Injector (U/N 3) and 5-Inch G_c Solid-Wall Thrust Chamber (U)

(C) velocity. However, the local heat transfer rates were still higher than had been previously experienced with the fan injector U/N 3. The performance and heat transfer characteristics of this injector at lower operating chamber pressures were then investigated for complete evaluation.

(C) Test number 71 was targeted for 75-psia chamber pressure but, during the test, the injector-end heat flux was noted to continually increase, and the test was terminated to avoid possible overheating of the injector face. The next test, number 72, was then conducted with a targeted chamber pressure of 220 psia. The resulting high injector-end heat flux caused an increase in the oxidizer injector pressure drop, and the facility oxidizer cavitating venturi came out of cavitation. Chamber pressure began to decrease, and the test was terminated.

(C) A hypothesis was that an injection parameter change, (oxidizer impingement angle, Table 2) was instrumental in the decreased injector capability, as compared to fan injector U/N 3. A review of the design revealed that the fuel streams diverging from the showerhead orifices were not completely enveloped by the oxidizer fans. This condition permitted fuel to circulate to the walls of the chamber, where chemical reaction-induced turbulence could greatly enhance the local gas-side film coefficient. The injector was overheated during test 074, because of a facility malfunction involving high oxidizer feed temperature. The injector was irreparably damaged and, therefore, no further testing was conducted on this unit.

(7) Fan Injector U/N 3--Shortened G_c Chamber Test Evaluation

(C) As an approach to reducing the overall chamber heat load, the G_c contour chamber was modified to provide a shorter length combustion zone; 2.68 inches from injector face to throat rather than the 3.5 inches. (Refer to Section III, 2, a, (1), (c).) The primary test objectives were to evaluate the effect of the shortened combustion zone on the total heat rejection rate, local heat transfer rate, and η_{c^*} over the throttle range. Eight tests were conducted over a chamber pressure range of 664.3 to 65 psia.

(C) Inspection of the injector after the fifth test revealed that a leakage path existed between an oxidizer braze joint and the inert purge/bipropellant separation groove. The leak was detected when pressure applied to the groove produced an audible flow of gas. The injector was removed from the test assembly, and inspection revealed that the leakage path was restricted to an oxidizer braze joint only and bipropellant leakage did not exist. The injector was subsequently tested at the 650-psia chamber pressure level during test 009-69 with no problems. Inspection subsequent to test 009-69 revealed no increase in purge leakage or bipropellant leakage in the injector.

(C) Slight erosion of the thrust chamber throat was again noted after test 009-69. This is the same region where erosion had occurred on previous 650-psia chamber pressure tests. Previously, the eroded zone had been dalic-plated with copper to its original configuration. The same repair technique was used again after test 009-69.

(U) Two additional tests (010-69 and 011-69) were conducted to evaluate modifications to the U/N 3, 5-inch fan injector in the shortened water-cooled thrust chamber segment. The injector modification consisted of a realignment of the fuel elements on the injector face to diminsh the fuel jet and chamber wall interaction. The elements in the outer row were mechanically canted inward, toward the throat, so that the centerline of the showerhead fuel jets would converge and impinge at the geometrical throat plane and not on the walls. A hypothesis was that the increased throat heat transfer rate that had been experienced during the previous tests with this chamber segment was attributable to (1) an increase in boundary layer turbulence from the fuel jet impingement on the combustion chamber wall upstream of the throat, and (2) the higher resultant jet velocity at the wall from the shortened combustion zone. The plan was that the wall impingement aspect would be evaluated by the change in alignment described above.

(U) The two tests were satisfactory programmed duration tests. No injector damage resulted. The previous erosion of the throat was enlarged and finally opened up into the throat water passage on test 011-69.

(U) The throat heat flux rates were essentially the same as on the previous test, 009-69, indicating that the injector modification was ineffective in reducing the local throat heat transfer rate to the value of the nominal length chamber. A definite decrease in upper combustion zone local heat flux, however, was obtained. This effect is significant and would be useful for any future design refinement of the injector.

(U) A major variable, existent between the short and the nominal length chamber, was the fuel element-to-wall spacing. By virtue of the injector geometry and modification of the thrust chamber to the short configuration, the fuel elements were moved closer to the wall (see Fig. 19). There was not a practical test scheme that could readily provide an effective evaluation of this effect, although the increased momentum of the fuel jets, closer to the wall, would have a tendency to increase the convective film coefficient.

(C) The analytical prediction was that shortening the 5-inch-diameter combustion zone (injector face to throat) from 3.5 to 2.68 inches would result in a decrease in total integrated heat load (heat rejection rate to the walls) of 13 percent at 78-psia chamber pressure. The effects on the local heat transfer rates, particularly at the throat, and the characteristic velocity performance could not be determined analytically, although they were not expected to be significant.

(C) The analytical prediction was, also, that the same change to the 30-degree chamber segment would result in a 7-percent decrease in heat rejection rate. The reduced effect (compared to the 5-inch segment) was caused by a decreased contribution of the combustion zone to the total heat rejection rate in the full 30-degree segment.

Data from previous tests on the unmodified 5-inch thrust chamber segment are compared with the shortened thrust chamber segment data in Fig. 46 and 47 for the total heat load and the injector-end heat flux, respectively. A significant

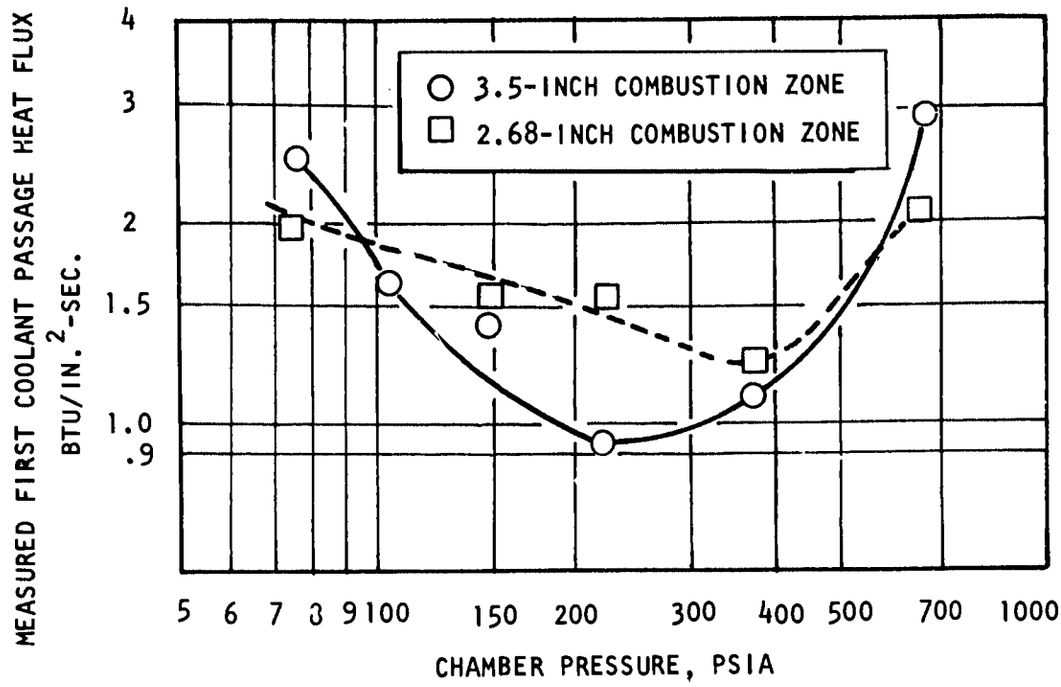

Figure 46. Measured Injector-End Heat Flux for Shortened and Original G_c Contour Chambers With U/N 3 Fan Injector (U)

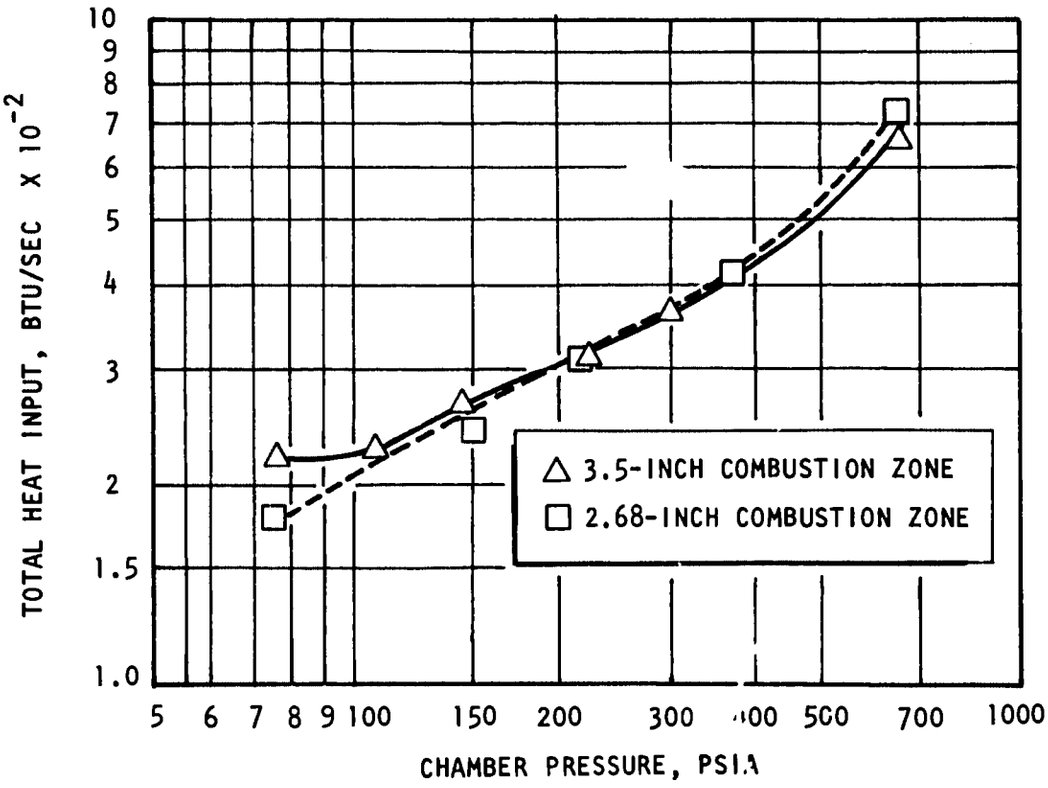

Figure 47. Total Heat Input to Coolant for Shortened and Original G_c Contour Chambers With U/N 3 Fan Injector (U)

(C) improvement (approximately 20-percent reduction) in the heat load was realized at the 78-psia chamber pressure level with the shortened segment. As chamber pressure increased, the heat load difference between the two chambers decreased, and, at 250 and 350 psia, there appeared to be no significant difference. At 650 psia, the heat rejection rate for the modified chamber segment was approximately 6 percent higher than the original 3.5-inch combustion zone segment. In relation to the 30-degree segment with a short combustion zone, the heat rejection rate increase would be expected to be approximately 2 percent.

(C) Relating these data to the 30-degree segment indicated that a 10-percent reduction in total heat load at 78 psia could be expected with the shorter combustion zone with no appreciable difference in local throat heat transfer rates. A comparison of the measured local heat flux values for the modified and nonmodified 5-inch chambers is presented in Fig. 48 through 52.

(C) The results from the 650-psia test on the shortened chamber indicated an excessively high local throat heat flux (30 Btu/in.^{2}-sec, compared to 25 Btu/in.^{2}-sec for the unmodified chamber) for this particular injector chamber combination. In addition, the results of the modified injector tests (010-69 and 011-69) did not indicate a reduction in local throat heat flux.

(C) One concern in shortening the combustion zone of the thrust chamber was that some compromise may result in the performance. To evaluate this possibility, a comparison was made between the characteristic velocity efficiency data from the shortened chamber and the original chamber. The comparison shown in Fig. 53 was made for the tests in which the unmodified U/N 3 injector was tested, thereby reducing the differences in the hardware to only the differences in the combustion chamber. Figure 53 shows that the data from the shortened chamber appear to be of the same population as the previous data.

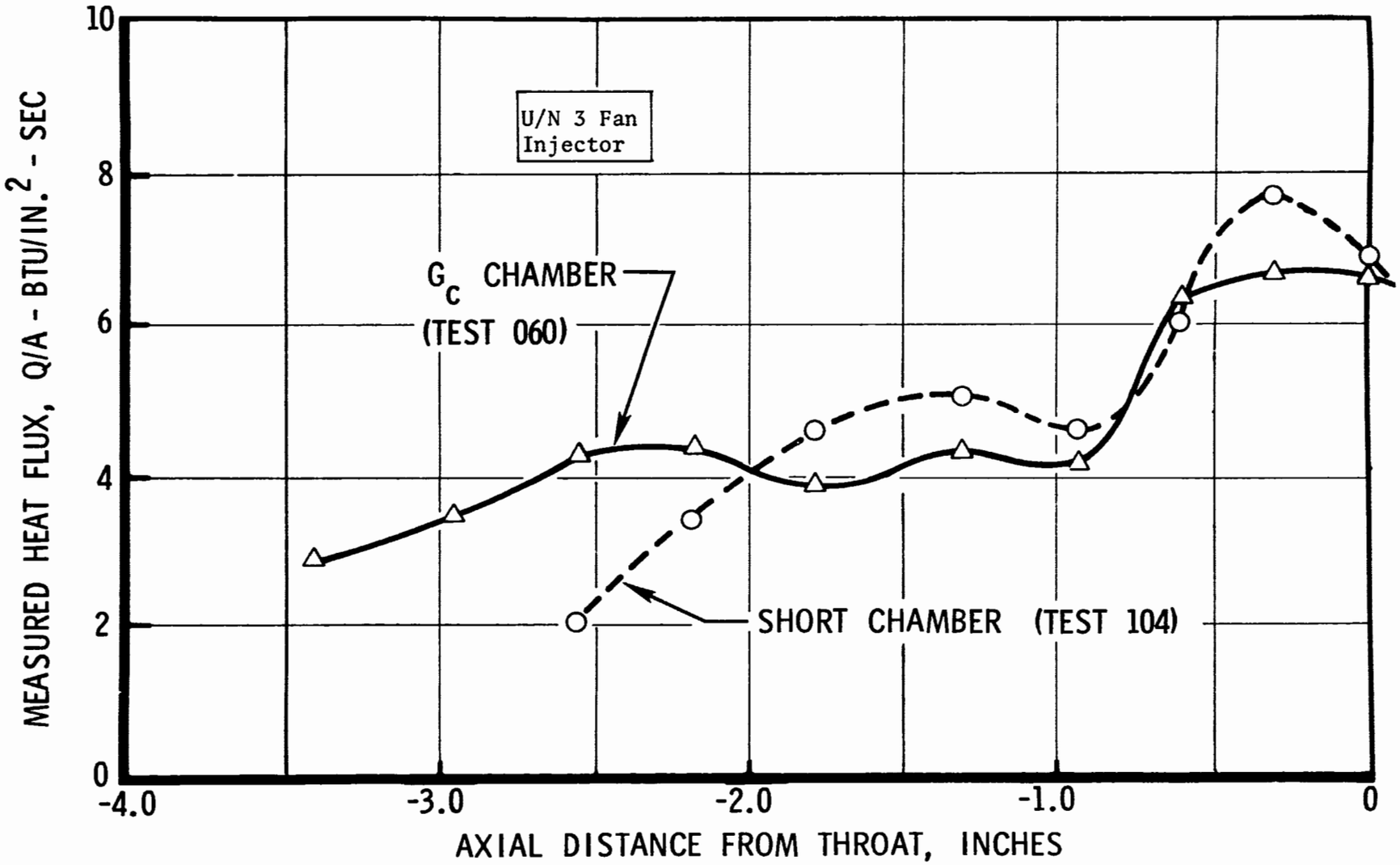

Figure 48. 5-Inch Chamber Segment Heat Flux Profile Comparison, 78-Psia Chamber Pressure (C)

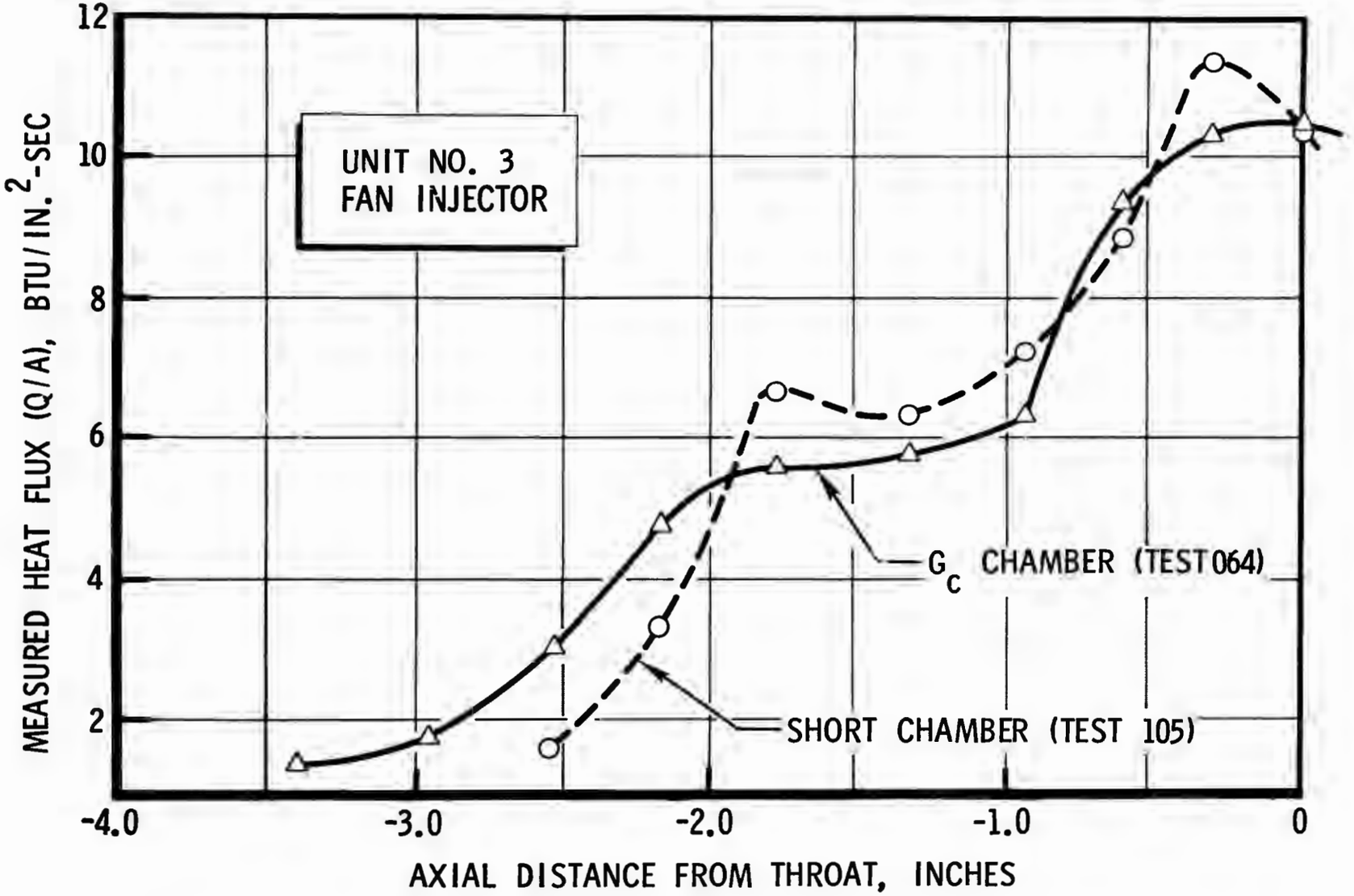

Figure 49. 5-Inch Chamber Segment Heat Flux Profile Comparison, 150-Psia Chamber Pressure (C)

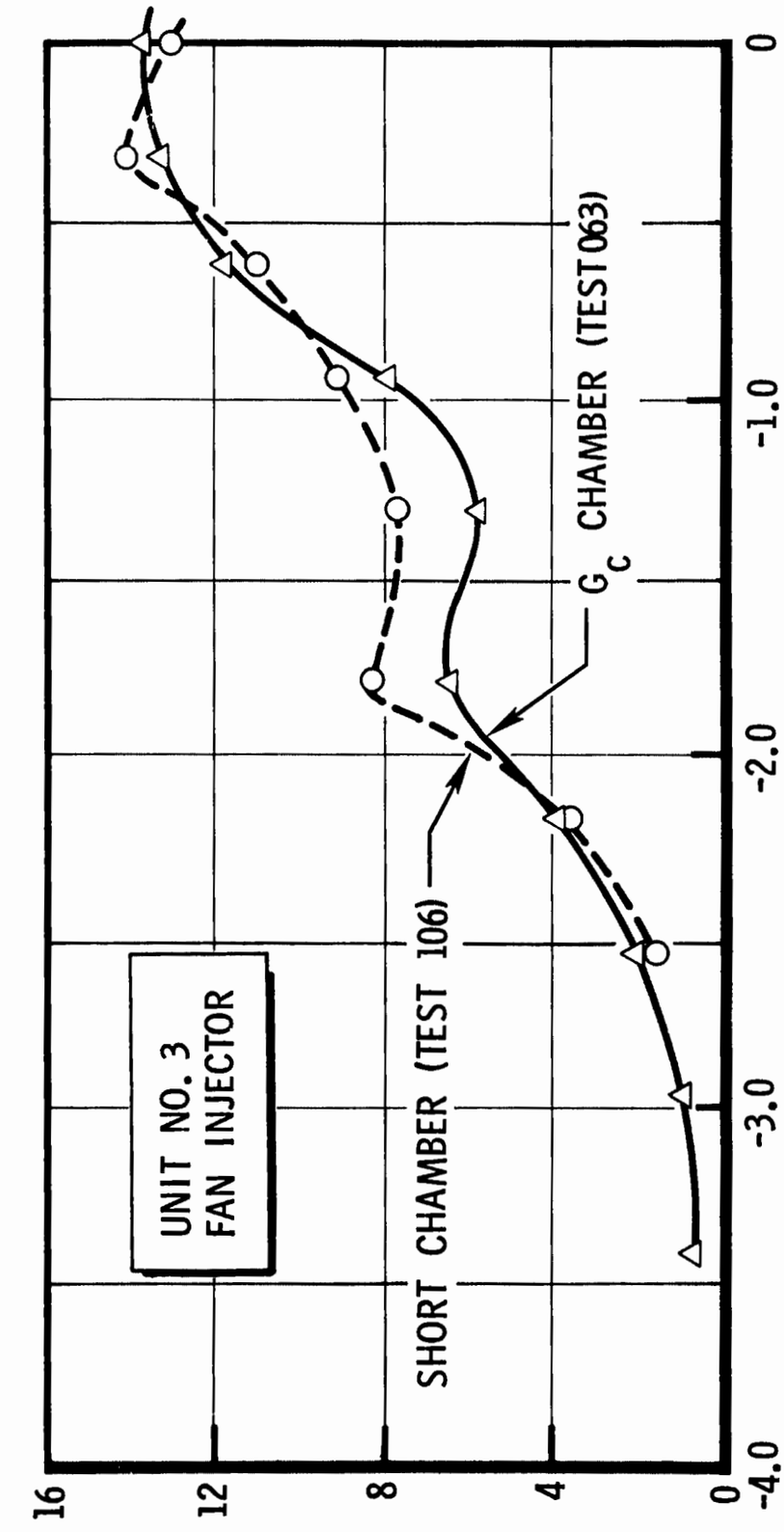

Figure 50. 5-Inch Chamber Segment Heat Flux Profile Comparison, 220-Psia Chamber Pressure (C)

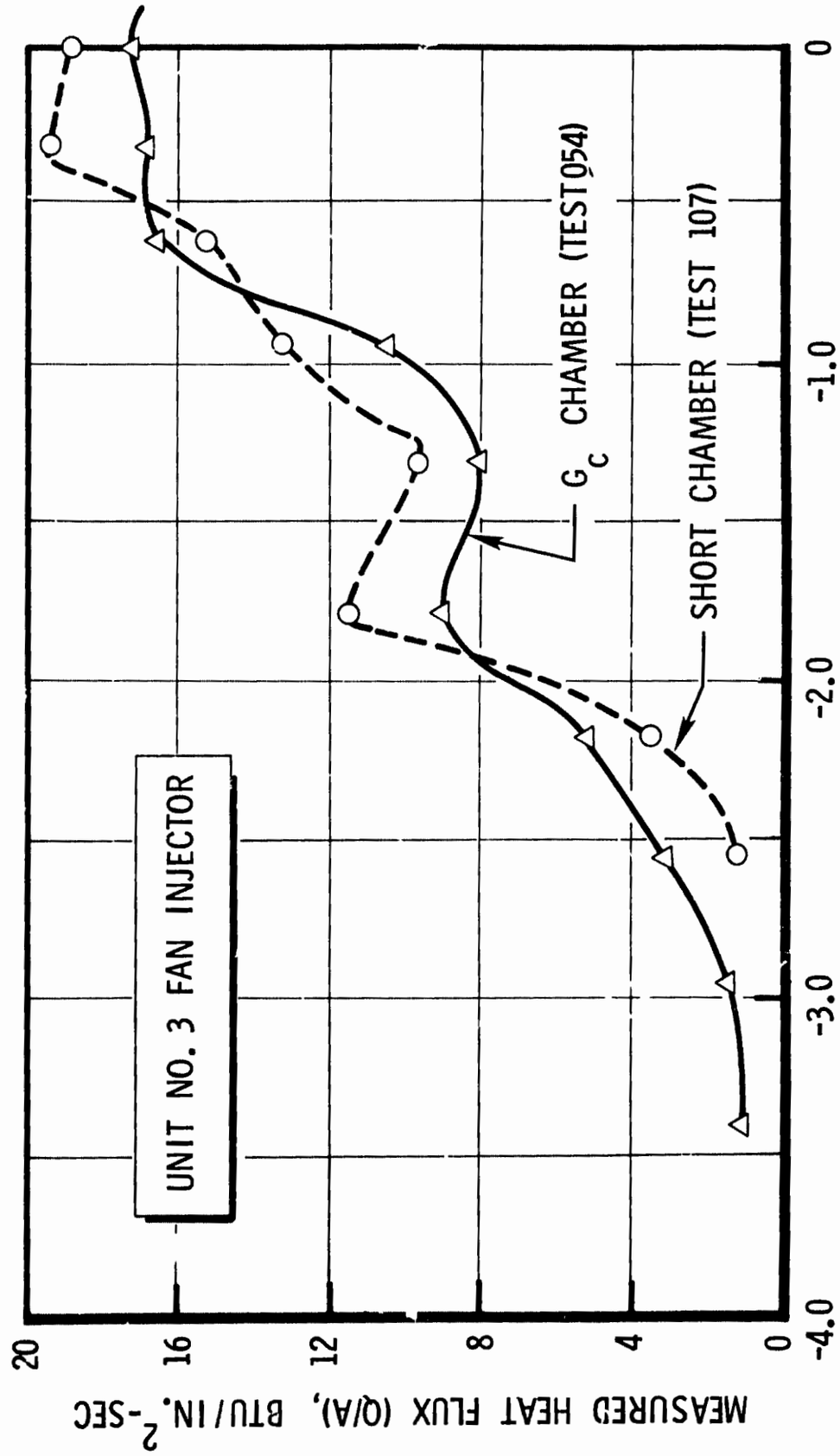

Figure 51. 5-Inch Chamber Segment Heat Flux Profile Comparison, 370-Psia Chamber Pressure (C)

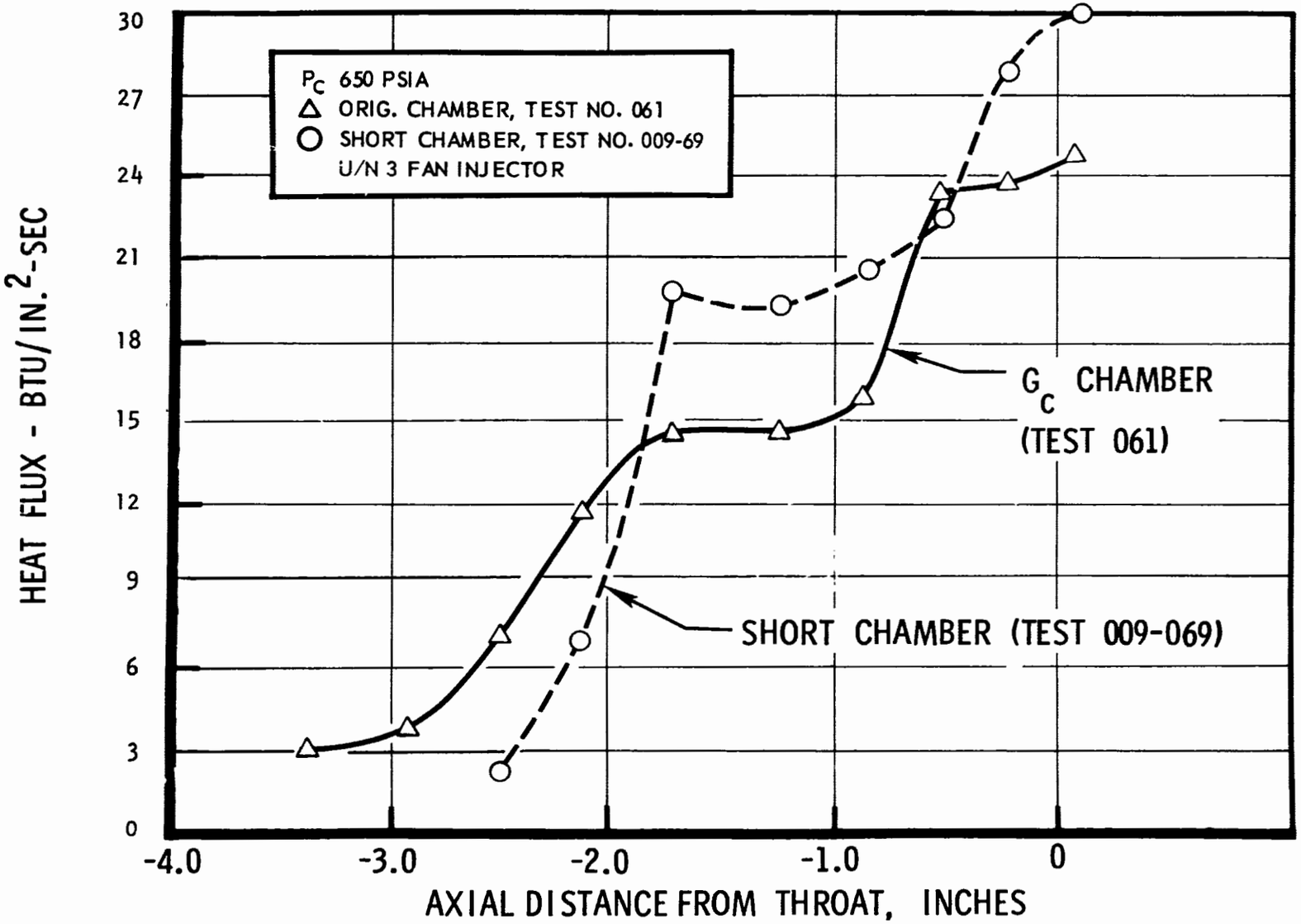

Figure 52. 5-Inch Chamber Segment Heat Flux Profile Comparison, 650-Psia Chamber Pressure (C)

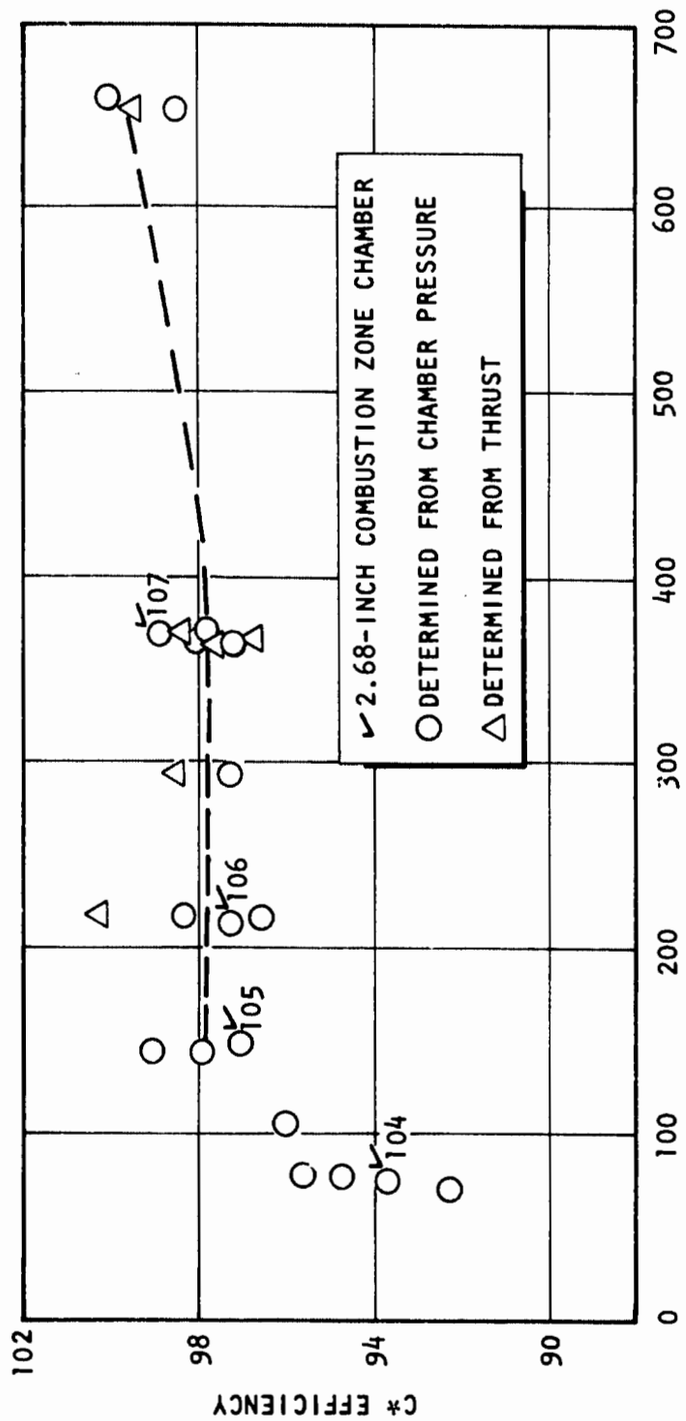

Figure 53. 5-Inch Fan Injector c* Efficiency (U)

(8) Concentric Orifice Injector-K Contour Chamber Test Evaluation

(U) The concentric orifice injector was hot-fire tested four times in the K contour chamber.* The K contour chamber, which had an injector face-to-throat length of 5 inches was used to provide maximum propellant residence time in the combustion zone and, thus, provide the injector the best opportunity to obtain maximum performance. The data from the tests are summarized in Table 6.

(C) The initial two tests indicated extremely poor η_{c*} performance (76 and 79 percent), and corresponding low local throat heat transfer rates. The test data, together with data on similar types of injectors being developed on other programs, indicated that additional propellant mixing was required to increase η_{c*} performance. A 0.100-inch recess of the oxidizer post was made in an attempt to promote better mixing.

(C) Two additional tests were accomplished with a resulting increase in η_{c*} to 97 percent; however, face overheating and erosion occurred. No additional modification or testing was accomplished on this injector because the fan injector design appeared more promising.

(9) 5-Inch Tubular-Wall Thrust Chamber Test Evaluation

(C) The test hardware assembly consisted of the modified fan injector (U/N 2) and the 5-inch tubular-wall thrust chamber. The basic test objectives were:

1. Determine heat rejection rate to the contoured walls with liquid hydrogen as coolant.
2. Determine cooling capability of the Nickel 200, 0.017-inch wall thickness tubes.
3. Determine the total heat rejection rate to the water-cooled copper side walls.

*Tests conducted under company sponsorship.

TABLE 6

5-INCH CONCENTRIC INJECTOR TEST SUMMARY (U)

(K Contour Chamber)

Test No.	Duration, seconds	Chamber Pressure, psia	Injector Flow, lb/sec	Mixture Ratio	Fuel Injection Temperature, F	Cutoff	Throat Heat Flux, Btu/in.^{2}-sec	Injector End Heat Flux, Btu/in.^{2}-sec	η_{c^*}
552	0.75	468	2.161	14.55	Ambient	Programmed	16.75	2.74	76
553	1.55	508	2.173	14.7	1310	Programmed	16.65	2.23	79
554	0.6	574	Not Stabilized	--	1361	Programmed	--	--	--
555	2.9	607	2.079	14.4	1378	Observer	18.95	6.19	97

CONFIDENTIAL

(C) 4. Determine pressure drop characteristics of the contour tube walls with hydrogen as the coolant flow.

(U) The segment chamber assembly with the coolant circuit illustrated is shown in Fig. 22. The initial test (51), following coolant system blowdown, was scheduled for 1-second duration as a checkout test. The test was terminated prematurely because of irreparable damage to the thrust chamber and injector. A detailed investigation of the failure incident was conducted and the failure was attributed to a defective facility check valve installed in a line which was common to the fuel propellant and coolant systems and the fuel coolant purge system. Reverse flow through the check valve resulted in the diversion of fuel coolant flow into the fuel propellant system. The system flow schematic is shown in Fig. 54.

(10) 5-Inch Thrust Chamber Segment Test Evaluation Summary

(U) Three copper, water-cooled, calorimetry 5-inch chamber segments were fabricated and tested. Eight 5-inch injectors were fabricated. The results are summarized as follows.

(C) The G_c contour segments (No. 1 and 2), 3.5 inches from injector face to throat, were fired successfully on 53 tests for 287 seconds duration. Degeneration and erosion of the copper hot-gas wall at the throat occurred.

(C) The shortened G_c contour segment (2.68 inches from injector face-to-throat) was fired successfully on eight tests for 103.1 seconds duration. A reduction in total heat rejection rate was obtained at low chamber pressures; however, the local throat heat flux at 650-psia chamber pressure was excessive.

(C) The K-contour, solid-wall thrust chamber, 5 inches from injector face-to-throat, was used successfully on 17 test firings for 61.9 seconds duration without sustaining any damage. The heat transfer results were used as a basis for a

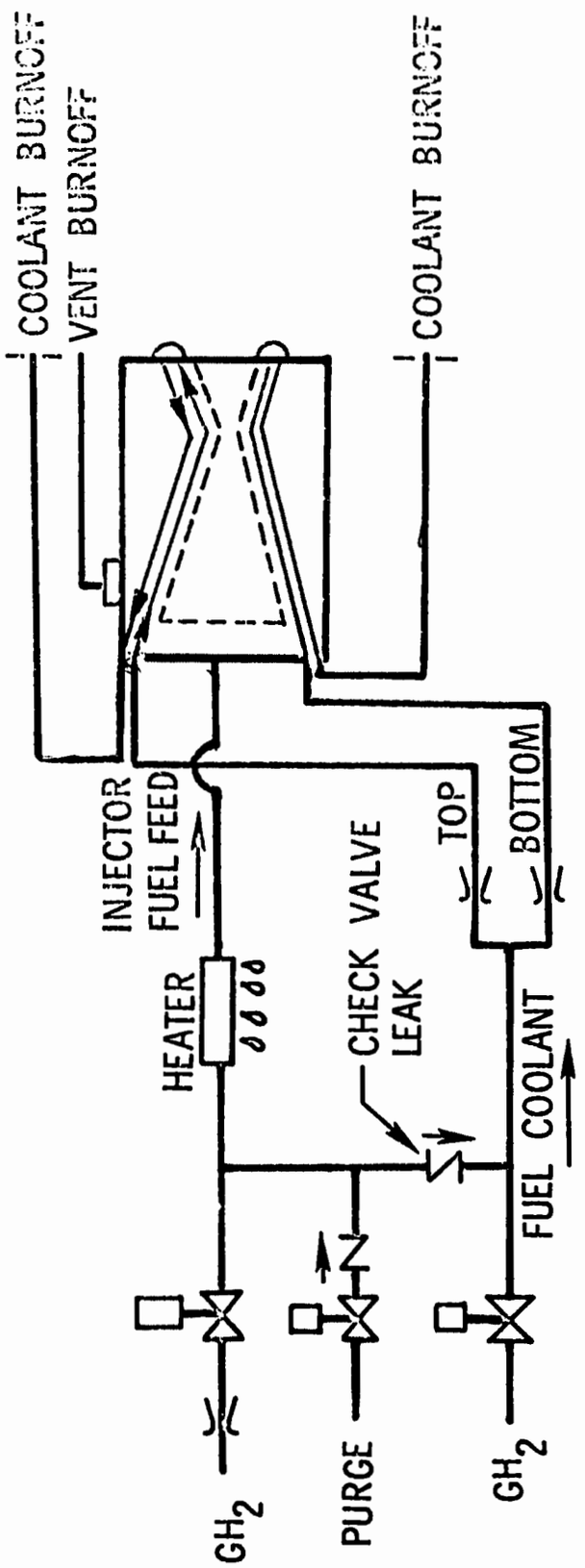

Figure 54. Fuel Flow System for 5-Inch Tube-Wall Segment (U)

(C) comparison of tubular-wall thrust chamber designs having either a 3.5- or 5.0-inch injector face-to-throat length. The results of the analysis indicated that the use of the K contour would be less desirable with respect to cooling inlet pressure requirements, tube gas-side wall temperatures at the inner body up-pass due to the increased enthalpy in the coolant, and weight due to increased length. The heat flux distribution in the two types of chambers was very similar in the throat region, but the K contour had more surface area in the combustion zone and provided more coolant temperature rise.

(U) High-frequency chamber pressure transducers, Kistler Type 614A4, were used on tests 10 through 50 to aid in the identification of any high-frequency acoustic oscillations that might be occurring in the combustion chamber. An examination of these data showed that no significant oscillations of this type were encountered.

(C) The following specific results were obtained:

1. The G_c combustion zone contour, and the impinging fan type-injector provided the most satisfactory results and were chosen for final evaluation with the subsequent 30-degree segment thrust chamber hardware.
2. Satisfactory characteristic velocity efficiency was demonstrated for the chosen injector and chamber configuration.
3. Total integrated heat rejection rates and local heat fluxes for the thrust chamber segment were obtained and used for the 30-degree segment combustion chamber design.
4. Satisfactory injector durability and face cooling were demonstrated after injector modifications were made.
5. The ability to decrease the total integrated heat rejection rate, by decreased combustion zone length, was demonstrated.

3. 30-DEGREE WATER-COOLED SEGMENT EVALUATION

(U) Based on the results of the 5-inch segment tests, two variations of the fan injector were evaluated with full size, 30-degree segment hardware. The segment chamber, with a G_c contour, was water cooled, curved, and included a skewed nozzle expansion section. Test evaluations with this hardware were conducted to make the final 30-degree injector design selection, investigate methods for reducing chamber heat load (film cooling), and investigate acoustic modes of combustion instability (pulsing tests).

(U) In the sections that follow, the hardware is first described, followed by a discussion of the testing, analysis, and results obtained.

a. Hardware Design and Fabrication

(1) 30-degree Water-Cooled Segment Thrust Chamber

(U) The purpose of the 30-degree water-cooled thrust chamber segment was to:

1. Provide overall and local heat transfer data, particularly in the skewed nozzle aft of the throat, which was not obtained during 5-inch segment testing.
2. Provide combustion stability information.
3. Provide an evaluation of the two variations of the fan injector (brazed-face versus the integral-face).
4. Provide an evaluation of oxidizer and fuel boundary layer coolant.
5. Provide characteristic velocity efficiency (c*) data.

(U) The design of the segment chamber is shown in Fig. 55, with significant details noted. The fabrication technique was similar to that used for the 5-inch copper segment thrust chambers. The completed chamber is shown in Fig. 56.

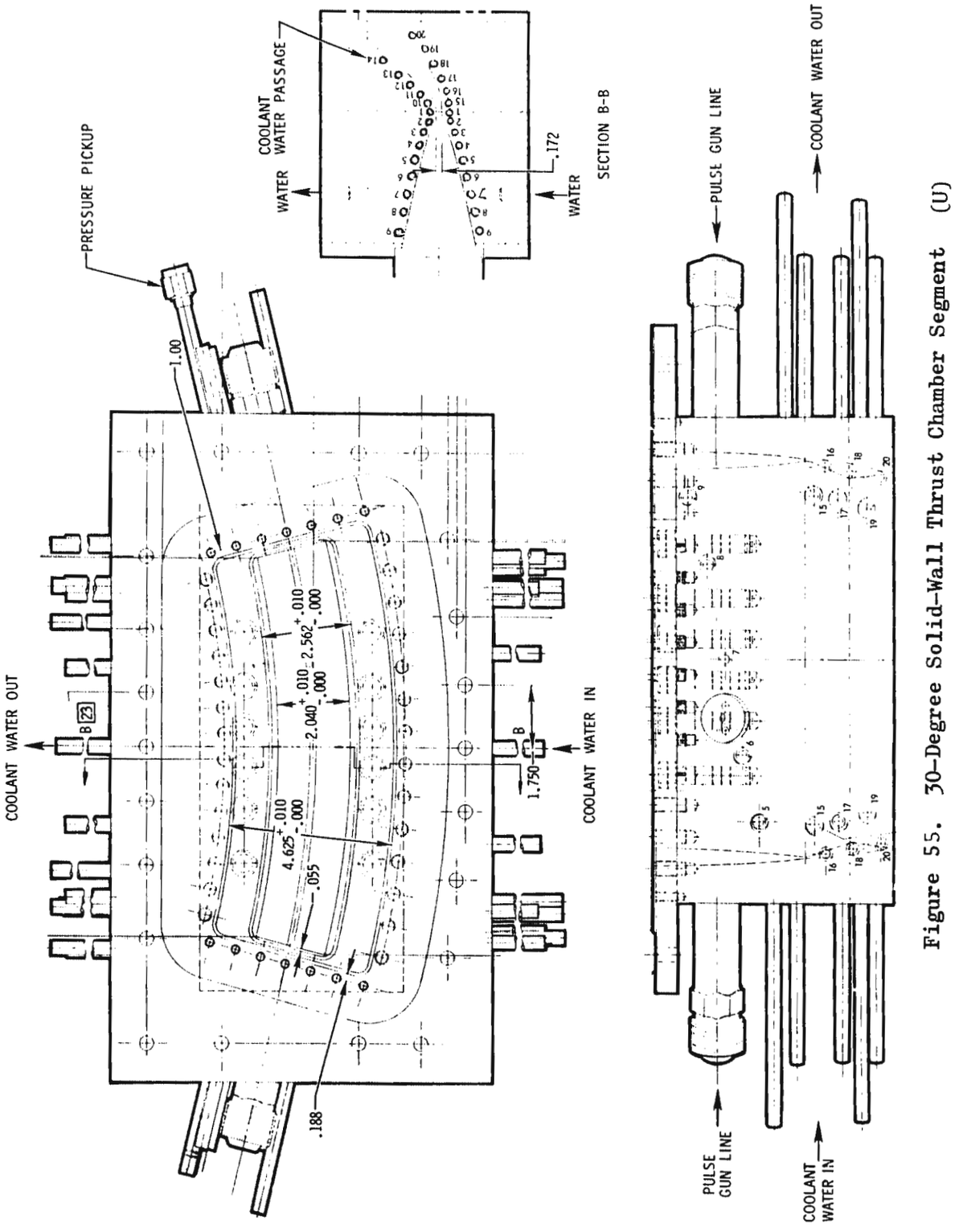

Figure 55. 30-Degree Solid-Wall Thrust Chamber Segment (U)

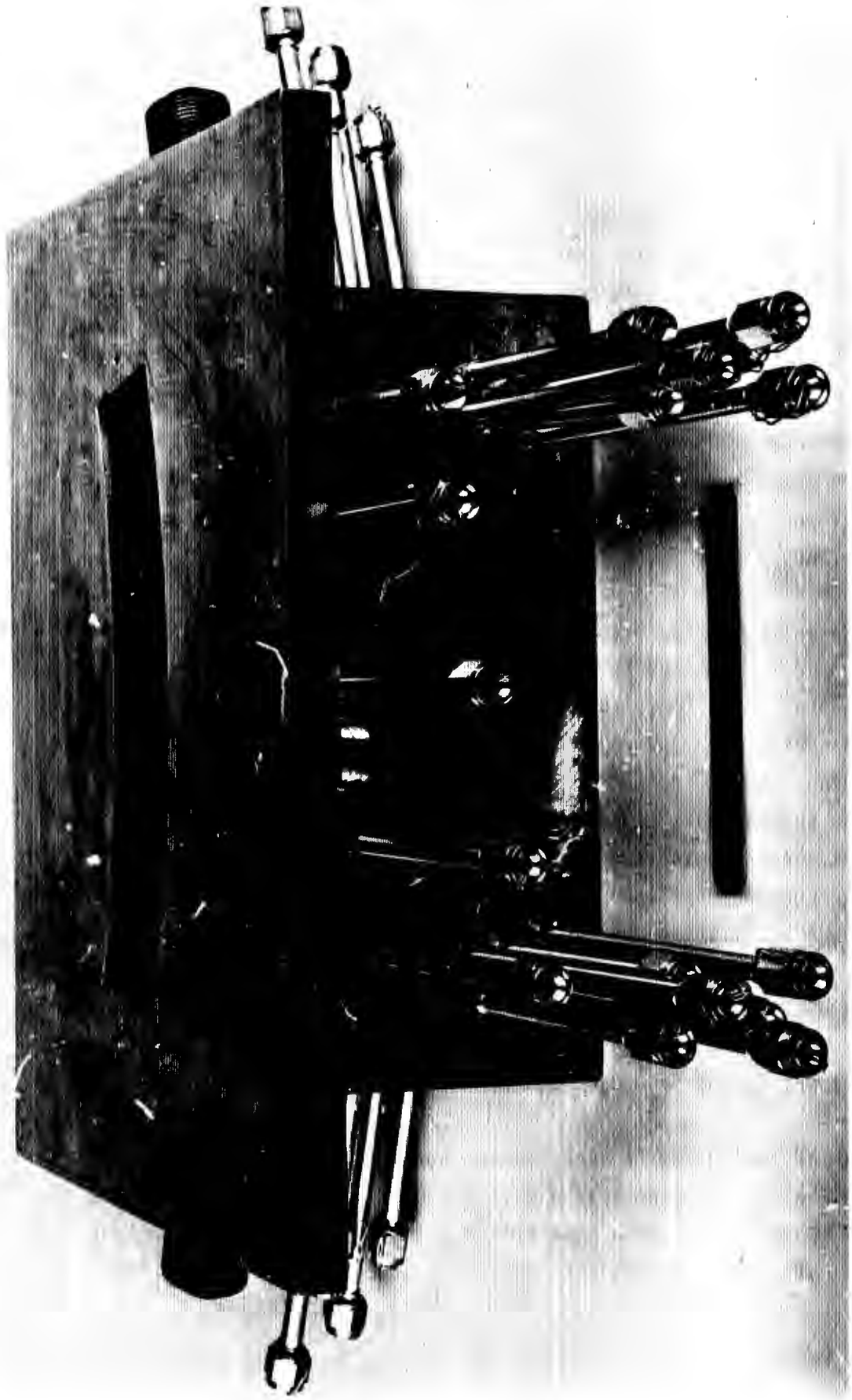

1EH32-7/19/68-C1B*

Figure 50. 30-Degree Solid-Wall Thrust Chamber (Complete Assembly) (U)

(U) The segment experienced coolant water leakage during the test program. The leakage occurred in the pulse gun-to-chamber braze joint (Fig.), and also at the throat plane in the axial braze joint of the outer body. The axial braze joints were made during assembly brazing of three detail parts that form the complete outer body. This assembly technique was used to simplify coolant passage drilling. Temporary repairs were made to the chamber to enable completion of injector selection testing. The leakage was temporarily stopped with the use of a particle suspension liquid sealant (DuPont heavy duty stop-leak) and verified by high pressure, 1350-psig inlet pressure, water blowdowns.

(U) The thermal cycling of the chamber was believed to have caused the leaks, but that the thermal expansion of the copper wall during the test firing prevented leakage during the test, and most of the leakage occurred during the shutdown (cooling) cycle.

(U) Water blowdowns at operating pressure after each test revealed that most of the water leakage occurred at the throat. The combustion zone leakage did not exceed 1 drop per second. Therefore, the assumption was made that the effect of the leakage on c* performance and combustion zone heat transfer was negligible. A later attempt was made to permanently repair the chamber by machining out the area where the throat leakage had occurred and furnace brazing a special plug into the voids. A new pulse gun assembly was also furnace braze installed. The plug and pulse gun assembly incorporated the required coolant passages that were removed during the machining process.

(U) The deficient braze joint region at the throat was removed in one piece with the use of a hollow mill and was subjected to metallurgical analysis. Gross voids in the braze joint caused by oxygen contamination were found.

(U) A modification of the 30-degree water-cooled segment chamber was made to provide a means of evaluating the effect of a fuel-rich region along the combustion chamber walls (fuel bias) on the heat transfer and performance. The modification consisted of adding fuel manifolds to the inner and outer bodies into which 108

(U) passages were drilled. Spray tubes were then brazed into the passages (Fig. 57) to provide fuel injection to the chamber between the walls and the outer row of injector oxidizer holes.

(U) The throat region of the 30-degree water-cooled segment chamber continued to deteriorate during the testing so that minor repair was not possible. A major repair technique was devised that consisted of removal of the damaged section from immediately upstream of the throat to the nozzle exit, and replacement with a new nozzle section. The replacement section was brazed to the original section (Fig. 58).

(2) 30-Degree Segment Injectors

(U) Two variations of the fan injector were designed and fabricated for 30-degree segment testing. The injector designs resulted from the previous 5-inch water-cooled segment tests and differed primarily in the type of injector face plate (integral versus non-integral).

(U) The first design was a two-piece configuration with a nickel face brazed to a corrosion-resistant steel body similar to the 5-inch U/N 3 design (Fig. 59). The second was an all-nickel integral face and body design, as shown in Fig. 60 and was similar to the 5-inch U/N 4 design. The propellant feed passages of the integral injector ran radially, which was 90 degrees from those in the two-piece brazed injector. In addition, the face of the integral injector was flat (Fig. 61), whereas the two-piece brazed injector had a curved face with an angle of 12 degrees (Fig. 62). Table 7 presents the design characteristics of the two injectors.

(U) Both injectors incorporated flow devices (inserts) that increased the oxidizer velocity at the back side of the injector face and improved cooling of the injector face. The insert designs were similar to those used for the 5-inch integral and brazed face injectors described earlier in Section III, 2, a(2)(b).

Figure 57. 30-Degree Water-Cooled Segment Modified for Fuel Bias (U)

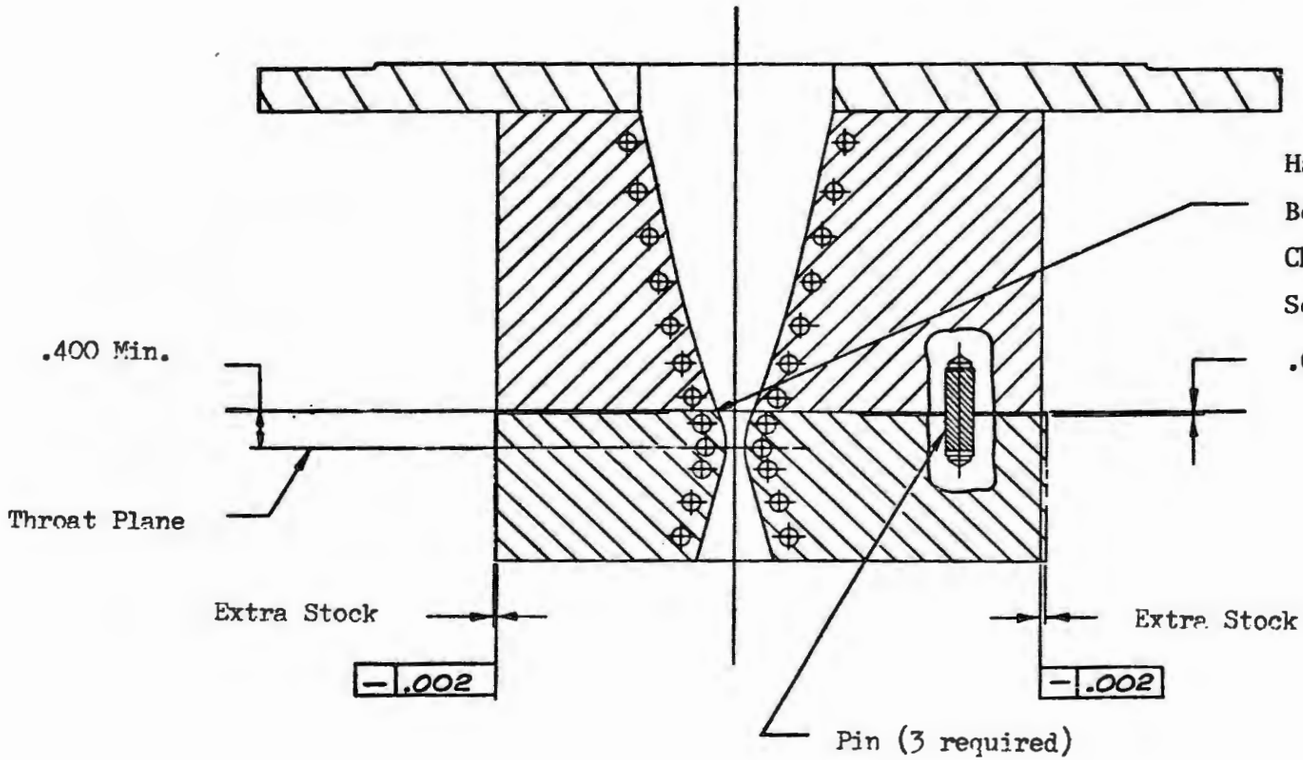

Figure 58. 30-Degree Water-Cooled Thrust Chamber Segment Repair (U)

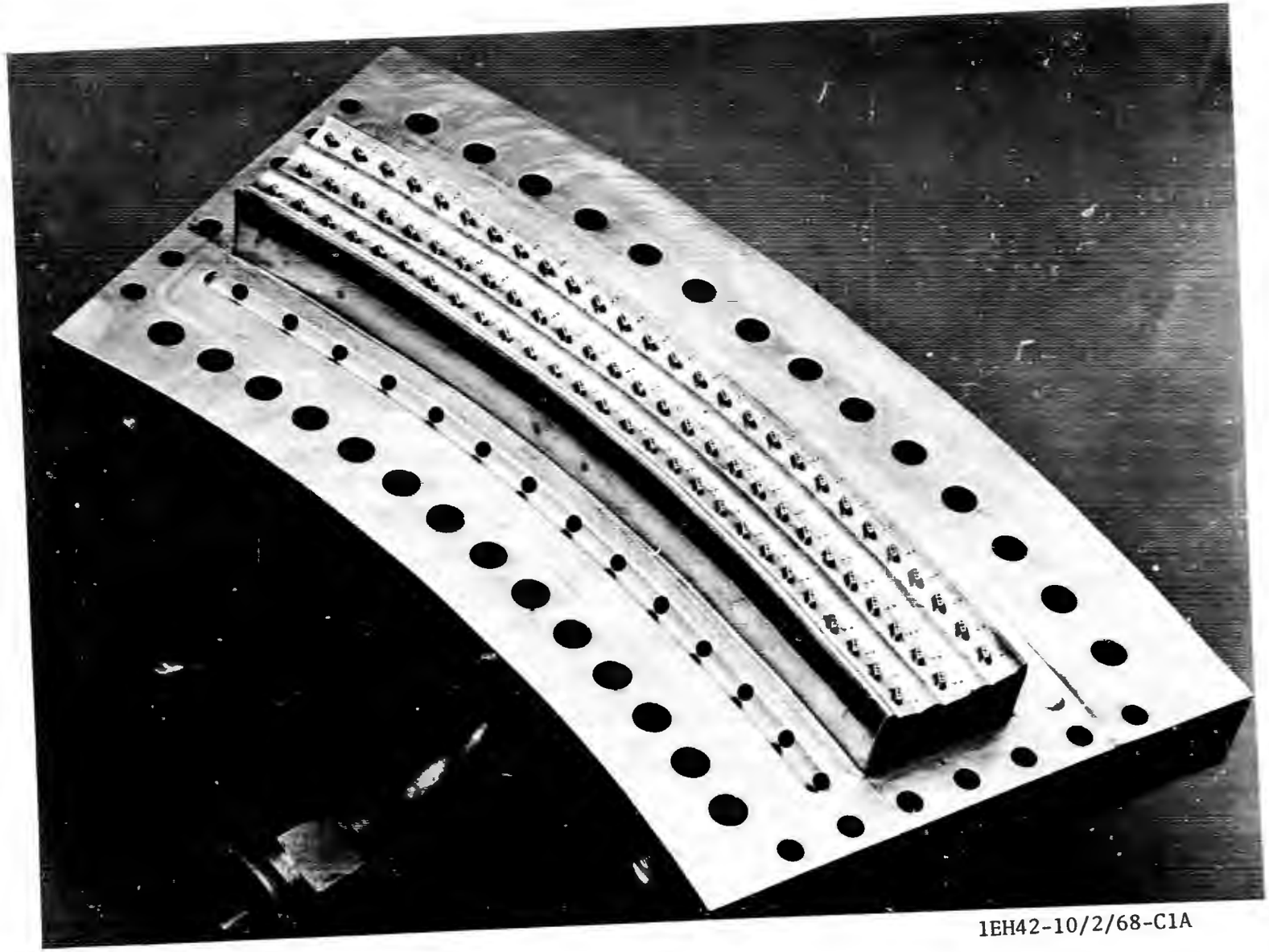

1EH42-10/2/68-C1A

Figure 59. 30-Degree Injector With Brazed Face (U/N 1 Posttest 081)(U)

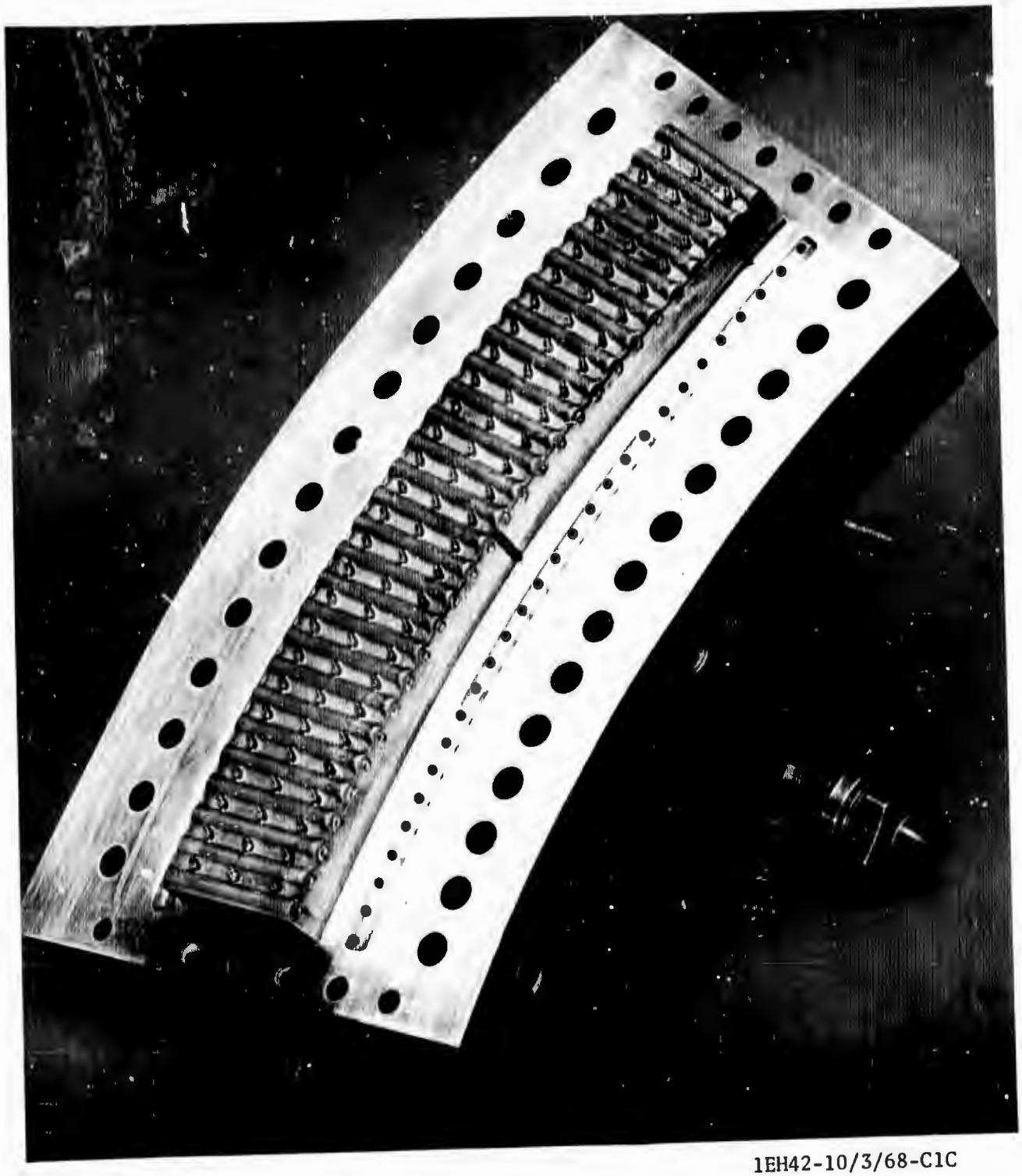

1EH42-10/3/68-C1C

Figure 60. 30-Degree Injector With Integral Face (Posttest 076) (U)

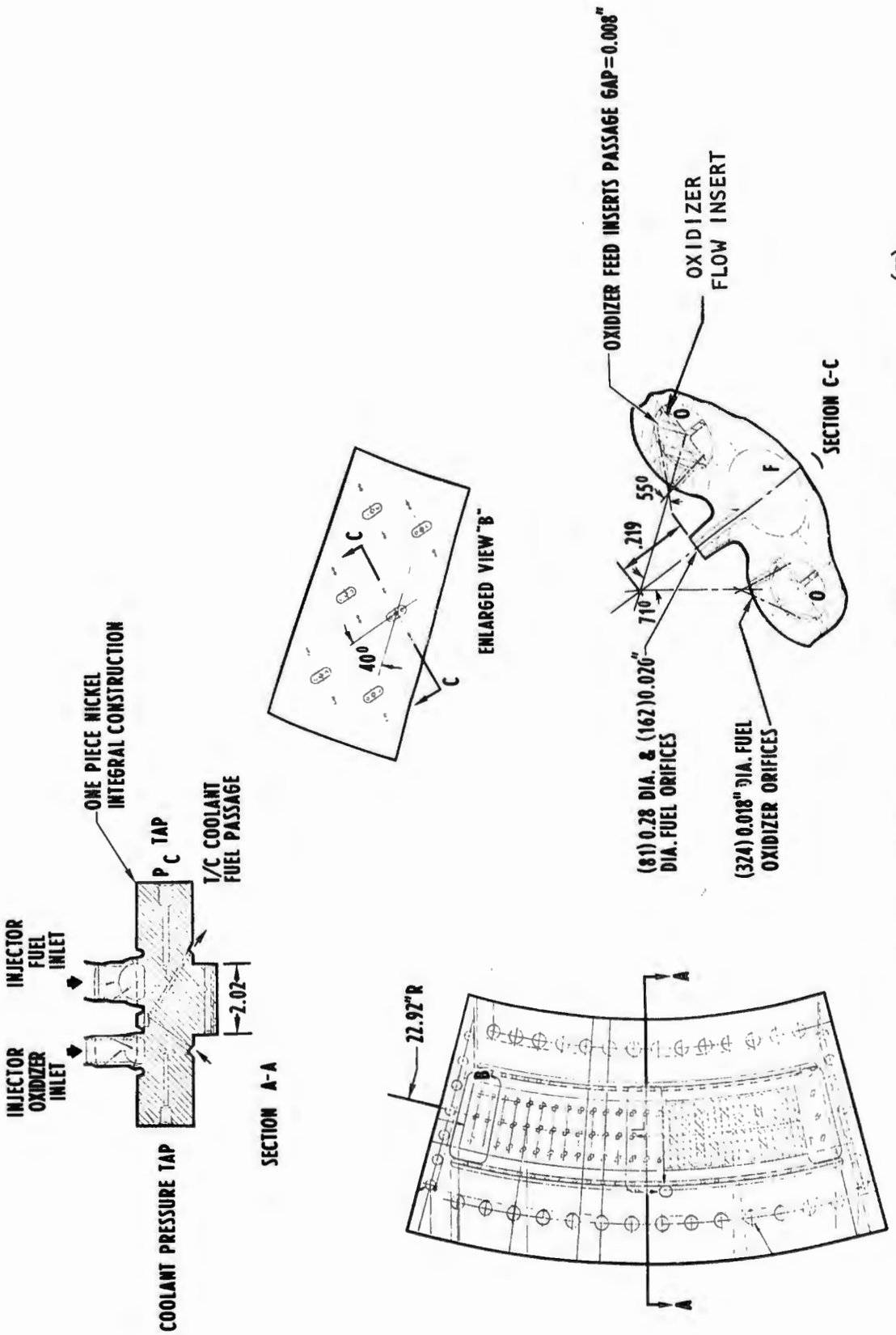

Figure 61. 30-Degree Integral Face Fan Injector Segment (U)

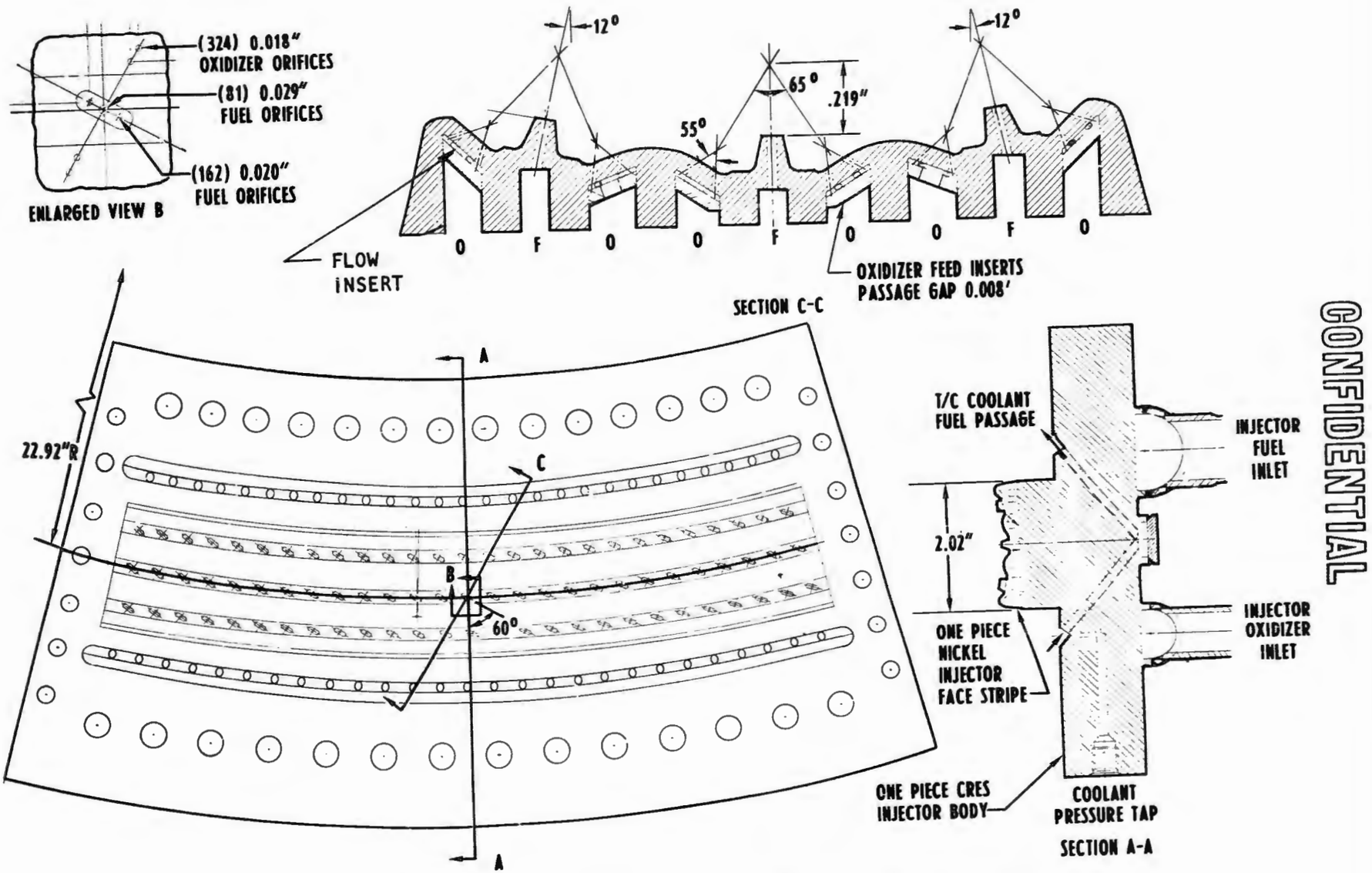

Figure 62. 30-Degree Brazed Face Fan Injector Segment (U)

CONFIDENTIAL

TABLE 7. 30-DEGREE SEGMENT INJECTOR DESIGN CHARACTERISTICS (U)

Item	Brazed Face Fan Injector	Integral Face Fan Injector
Orifice Diameter, inches		
Fuel	0.020 (162 ea) and 0.029 (81 ea)	0.020 (150 ea), & 0.028 (81 ea), & 0.025 (12 ea, 6 end elements)
Oxidizer	0.018 (324 ea)	0.018 (324 ea)
Number of Orifices		
Fuel	243	243
Oxidizer	324	324
Total Orifice Area, sq in.		
Fuel	0.105	0.103
Oxidizer	0.082	0.082
Impingement Length-to-Diameter Ratio		
Fuel	7.5 and 11.0	7.8 and 11.0
Oxidizer	3.6 and 17.4	1.9 and 17.0
Included Oxidizer Impingement Angle, degrees		
Oxidizer Preimpingement	55	55
Final Impingement With Fuel Showerhead	65	71
Impingement Distance (Fuel Orifice to Impingement Point), inches	0.219	0.219
Number of Strips	1	0 (Integral)
Number of Elements	81	81
Injector Face Size, inches	2 x 11	2 x 11
Calculated Pressure Drop at 650-psia Chamber Pressure, psid		
Fuel	350	370
Oxidizer	236	236
Injection Density, elements/in.^{2}	3.7	3.7
Element-to-Wall Cant Angle, degrees	30	45
Incline Angle, degrees	12	0

CONFIDENTIAL

CONFIDENTIAL

(C) The brazed face injector body was made of stainless steel, which was drilled and machined to feed both propellants to the injection face. The back (inlet) side contains the two propellant manifolds, which are butt welded to weld ribs that a are turned and milled into the body. Each manifold (Fig. 63) has one propellant inlet and several bosses for pressure taps and thermocouples (future injectors would have manifolds with inlets, shells, and bosses cast in one piece). A series of holes is drilled into the body block to feed the propellants to cross ports just behind the injector face. These cross ports are drilled and plugged from alternate sides of the body island. Small holes are then drilled into these cross ports to distribute propellants to the face grooves. Details of this porting are shown in Fig. 64.

(C) The Nickel 200 face for the brazed face injector was electrically discharge machined (EDM) on both sides. The hot-gas side was cut with curved oxidizer humps and fuel pyramids, as shown in Fig. 65. The feed side is cut with deep propellant grooves (six for oxidizer and three for fuel), as shown in Fig. 66 . Each oxidizer groove is fitted with a feed insert that is electron-beam welded in place. These inserts are nickel strips with wire spacers shaped to give the 60 ft/sec oxidizer groove velocity that is needed to cool the face. Proper fit of the feed strips is checked by radiograph inspection. The face is drilled with conventional twist drills to provide fan injection pattern elements consisting of three fuel and four oxidizer holes.

(C) The face and insert assembly is brazed to the body in a hydrogen atmosphere furnace. The braze alloy that is used consists of gold-palladium nickel (Palniro 7) foil 0.001-inch thick. Prior to brazing, the body interface is electrolytically plated with nickel to a thickness of 0.0002 to 0.0004 inch. The braze bond between the face and body occurs at 10 interfaces that are all in a common plane to ensure good fitup and lack of thermal stresses from differential contractions. Three of the interfaces are between dissimilar propellant manifolds and are, therefore, separated by isolation passages that are interconnected to a proof-pressure and purge system (see Fig. 64). Chamber pressure taps are routed down the sides of the injector center body block so as not to interfere with the braze interface.

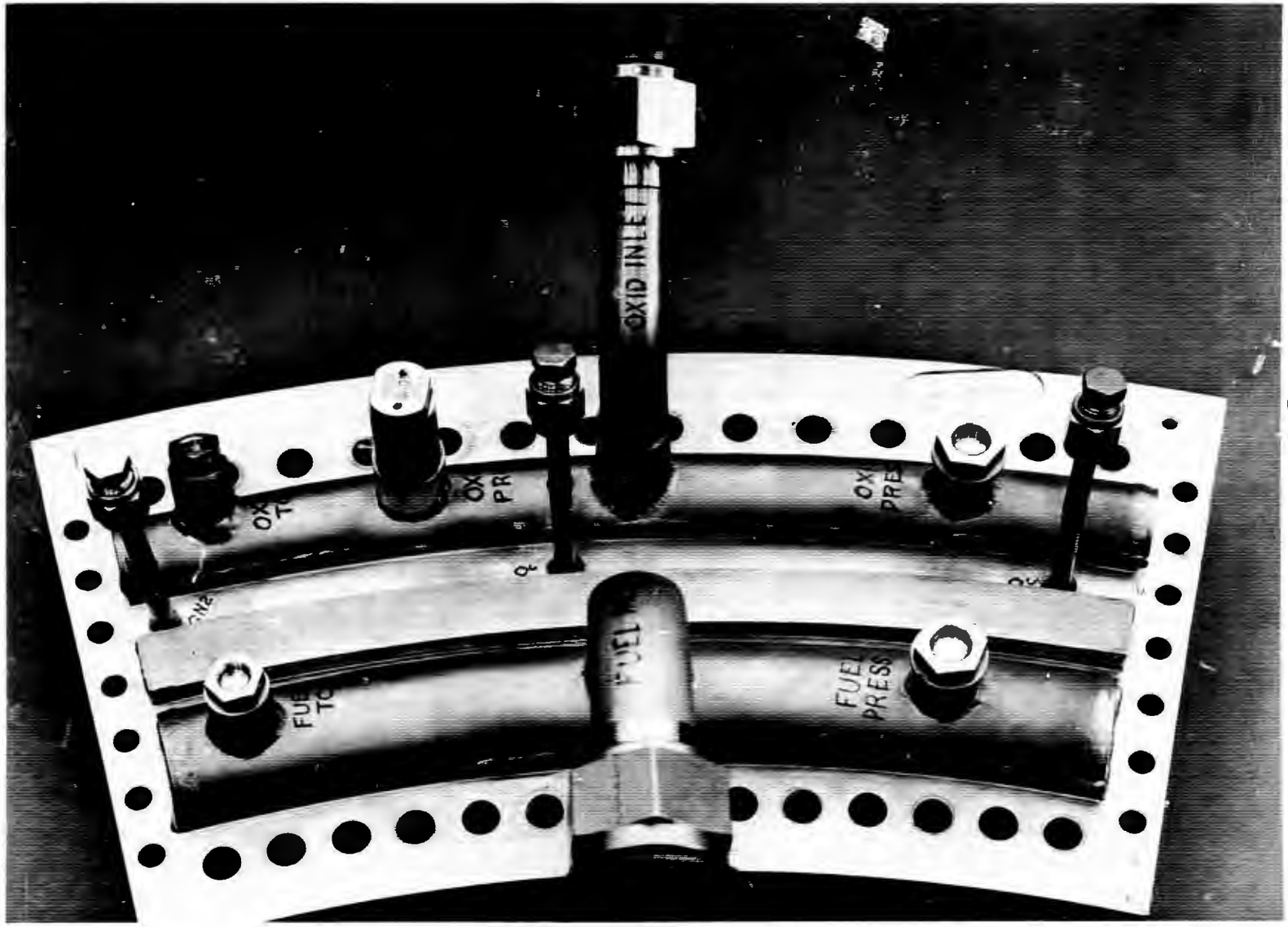

1EH44-9/17/68-C1H

Figure 63. 30-Degree Injector Segment Manifolds and Ports (Brazed Injector)(U)

CONFIDENTIAL

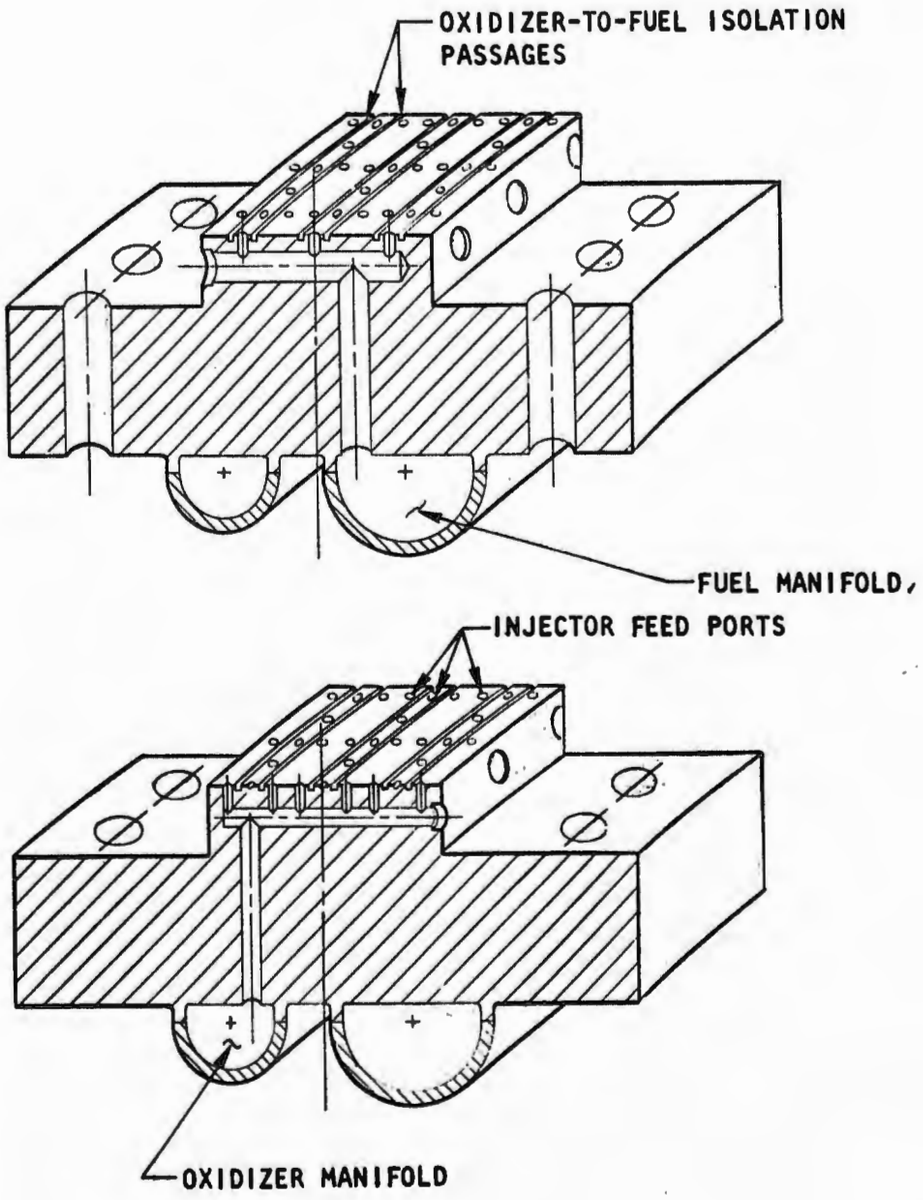

Figure 64. 30-Degree Injector, U/N 1 (Brazed Injector) (U)

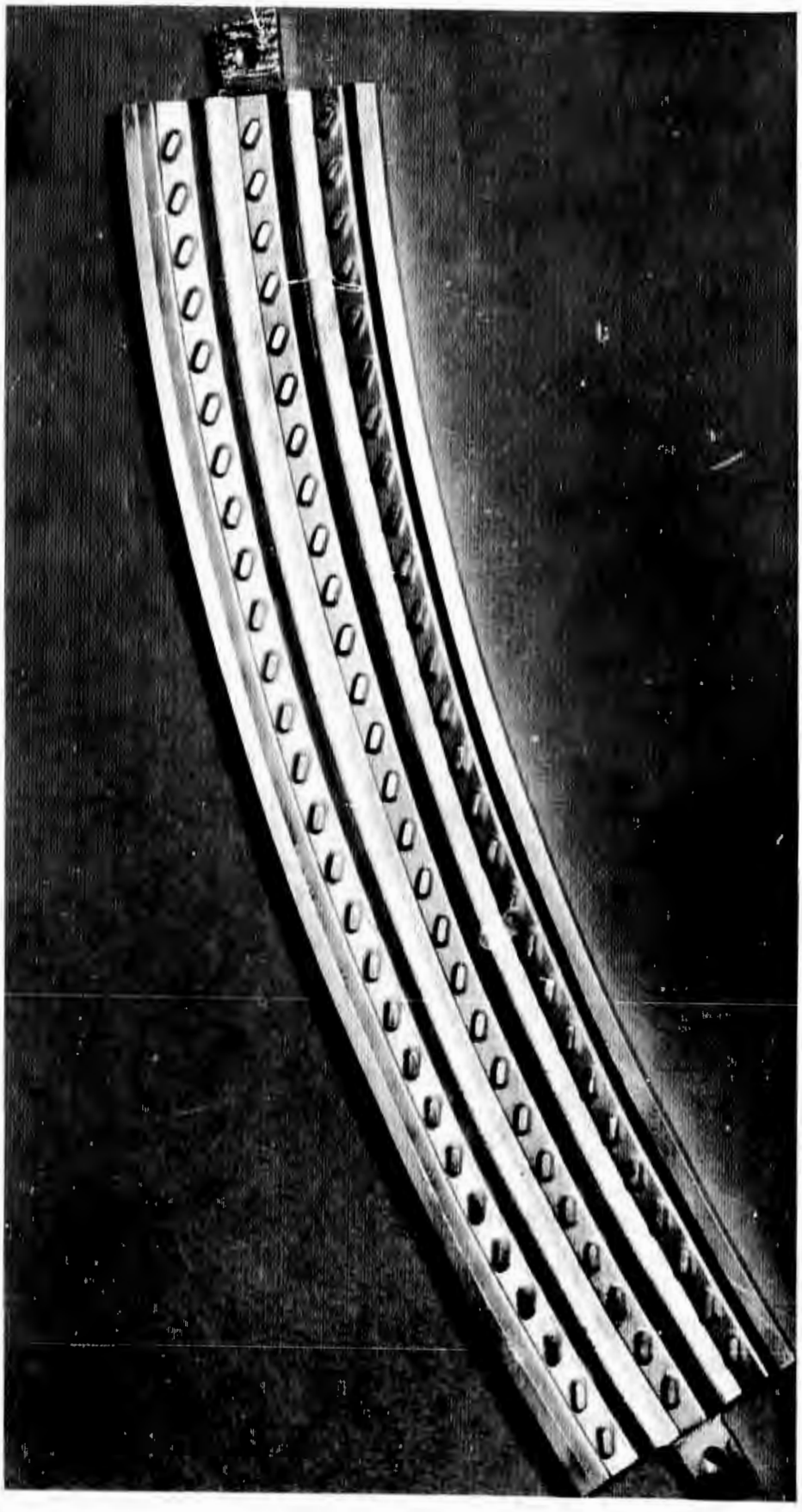

1EH42-7/31/68-C1A

Figure 65. 30-Degree Brazed Injector Face Plate (U/N 1) (U)

Figure 66. 30-Degree Injector Face Plate Back Side (Brazed Injector) (U)

(C) The completed injectors were vacuum leak checked, proof pressure checked to 11,000 psi (purge slots), flow calibrated, and cleaned according to applicable procedures.

(C) During the test program the 30-degree brazed face injector (U/N 1) was modified to provide oxidizer film coolant orifices adjacent ot the original outer row oxidizer doublets, as shown in Fig. 67. The modification was made for the test evaluation of reducing the overall chamber wall heat load by use of oxidizer film coolant. The film coolant orifice sizes were initially 0.018-inch diameter and were later enlarged to 0.021-inch diameter.

(U) The prototype brazed-face injector design with the 0.018-inch oxidizer bias holes is shown in Fig. 68 through 70.

b. Thirty-Degree Water-Cooled Thrust Chamber Segment Testing and Analysis

(C) The hot-fire testing of the 30-degree thrust chamber segment assemblies was also conducted at the Victor Test Stand, Propulsion Research Area, Santa Susana Field Laboratory. The primary test objectives were:

1. Evaluate the performance, compatability, and durability of the two versions of the fan injector.
2. Determine the heat transfer characteristics of the 30-degree segment configuration, which include the skewed nozzle and circumferential curvature
3. Evaluate the combustion stability characteristics of the final injector segment/chamber configuration with pulse gun-induced combustion chamber oscillations
4. Evaluate the use of oxidizer and fuel film cooling for reduction of upper combustion zone heat rejection rate
5. Verify characteristic velocity (c*) performance of the final 30-degree injector design over the design throttle range
6. Evaluate durability of the final 30-degree injector design.

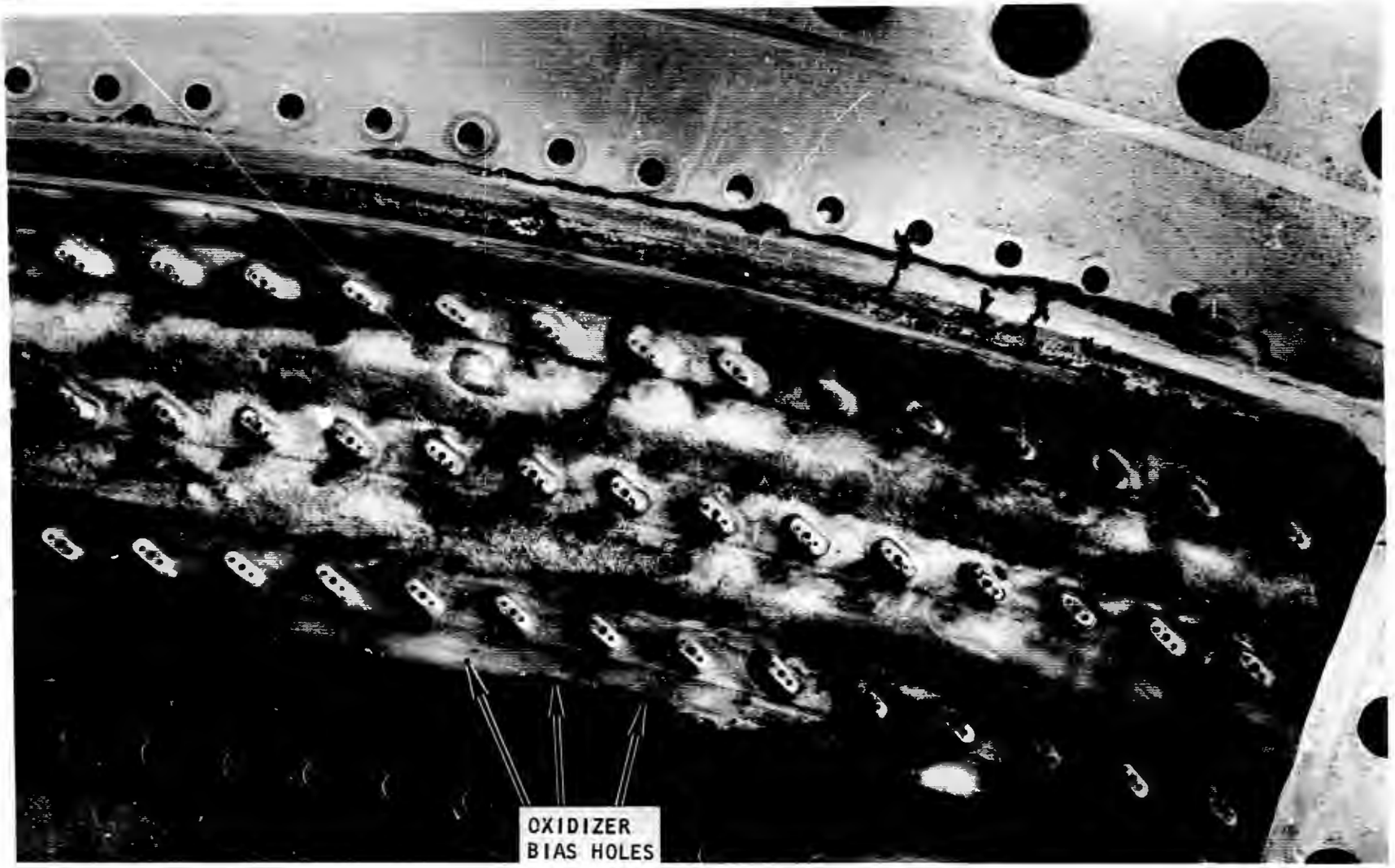

1EH45-3/24/69-C1A

Figure 67. 30-Degree Injector (U/N 1) Modified for Oxidizer Bias (Posttest 020) (U)

CONFIDENTIAL

CONFIDENTIAL

DASH NO.	M DIA
-5	.296±.005
-7	.202±.005
-9	.140±.005
-13	.187±.005

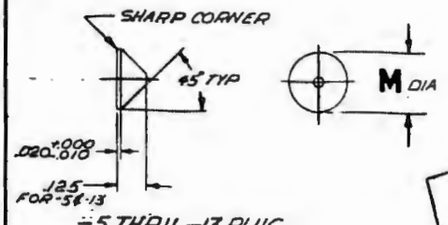

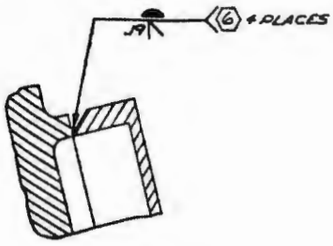

SECTION **J-J**

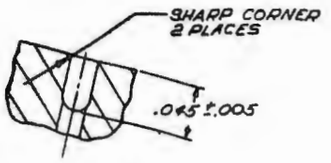

DETAIL **H**
6 PLACES
SCALE 20/1

SECTION **E-E**

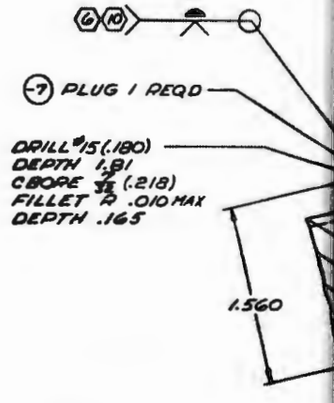

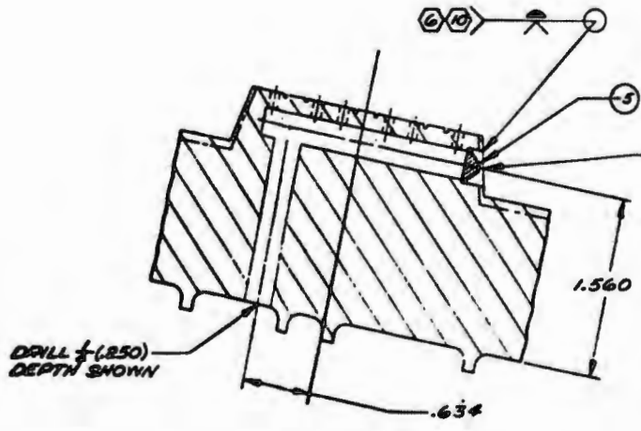

SECTION **D-D**

2.

.739 +.003 -.000 2 PLACES
.727±.002 2 PLACES
.715 +.003 -.000 2 PLACES
.554 +.003 -.000 2 PLACES
.542±.002 2 PLACES
.530 +.003 -.000 2 PLACES
.103 +.003 -.000 2 PLACES
.091±.002 2 PLACES
.079 +.003 -.000 2 PLACES
DRILL #76 (.020) DEPTH .28
6 HOLES LOCATED AS SHOWN

(9) PLUG 1 REQD
DRILL 1/4 (.125)
DEPTH 1.90
C'BORE 5/16 (.156)
DEPTH .165
FILLET R .010 MAX

.838±.005 28 PLACES
.429±.005 28 PLACES
.203±.005 28 PLACES
DRILL #47 (.078)
DEPTH .308
84 PLACES
SHARP CORNER TYP
DRILL 5/32 (.156)
DEPTH 2.000
C'BORE 17/64 (.203)
FILLET R .010 MAX
DEPTH .130
12 PLACES
(13) PLUG 12 REQD
DRILL 3/16 (.187)
DEPTH SHOWN
12 PLACES
1.560
12 PLACES
.634 12 PLACES

SECTION A-A

.250 DIA REF
SHARP CORNER
DRILL #47 (.078) TO FULL INTERSECTION OF CROSS PASSAGE
29°

SECTION C-C
3 PLACES
SCALE 4/1

22.918 R REF
90°±2° 39 PLCS
.635±.002 26 PLACES

SHARP CORNER 36 PLACES
35° 36 PLCS
DRILL #47 (.078) DEPTH TO FULL INTERSECTION OF CROSS PASSAGE 36 PLACES

DETAIL F
SCALE 4/1

(4)
1.560
DRILL #15 (.180)
DEPTH SHOWN
.318

SECTION C-C

(5) PLUG 1 REQD
FLAT BOTTOM DRILL 1/4 (.250)
DEPTH 2.000
C'BORE 5/16 (.312)
FILLET R .010 MAX
DEPTH .165
1.560

DRILL 1/4 (.250)
DEPTH 1.81
C'BORE 5/16 (.312)
FILLET R .010 MAX
DEPTH .165
13 PLACES
SHARP CORNER TYP
.635±.002 54 PLACES
(5) PLUG 13 REQD
DRILL #47 (.078)
THRU ONE WALL
42 PLACES
EXTRA S
1.560 13 PLACES
4 PLACES (6) .09
.318 13 PLACES
DRILL 1/4 (.250)
DEPTH SHOWN
13 PLACES

SECTION B-B

3

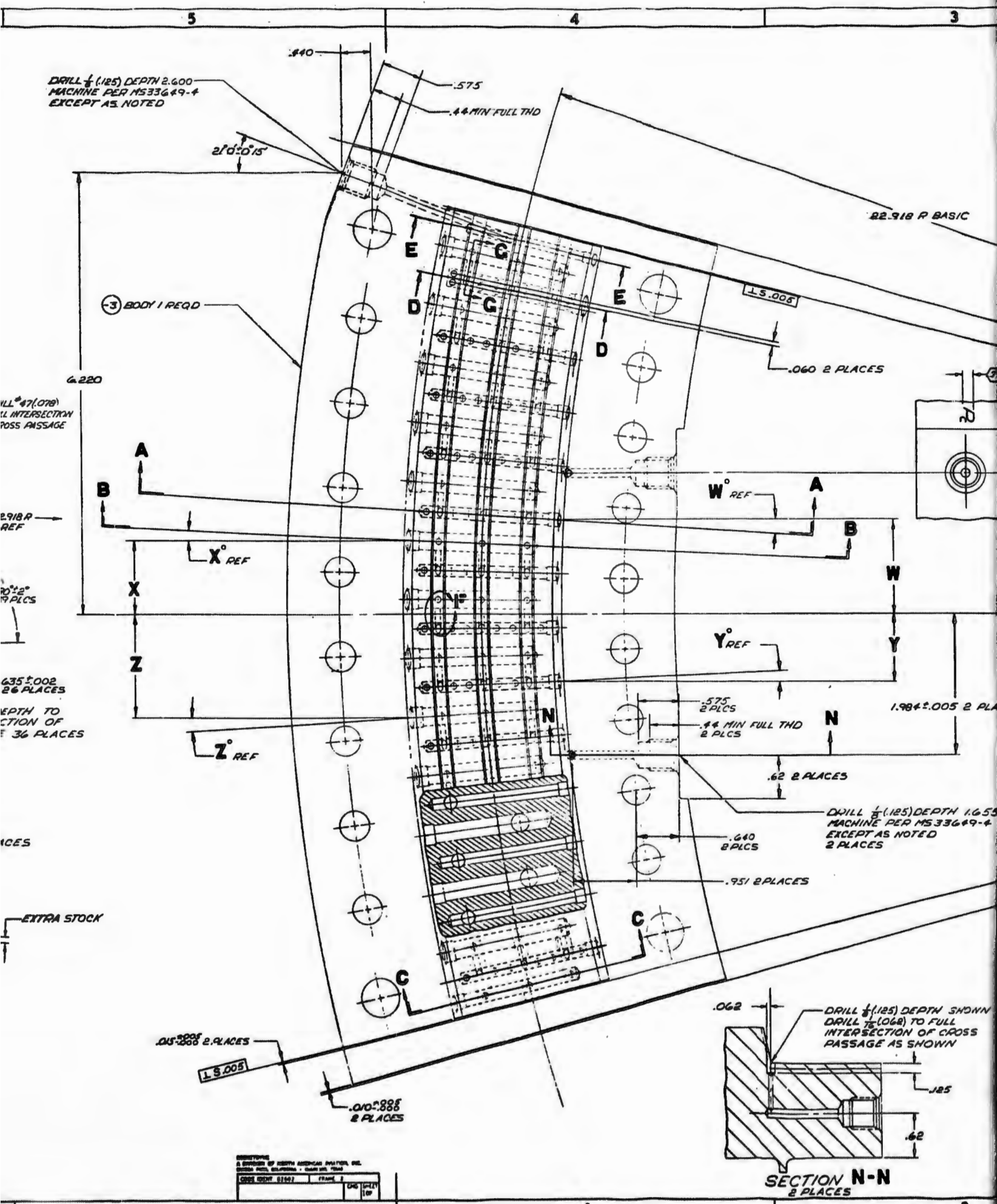

X ±.005	X° REF
.210	0° 30'
1.048	2° 30'
1.884	4° 30'
2.719	6° 30'
3.550	8° 30'
4.376	10° 30'
5.198	12° 30'

Z ±.005	Z° REF
.629	1° 30'
1.466	3° 30'
2.302	5° 30'
3.135	7° 30'
3.964	9° 30'
4.788	11° 30'
5.504	13° 15'

W ±.005	W° REF
.571	1° 30'
1.332	3° 30'
2.092	5° 30'
2.848	7° 30'
3.602	9° 30'
4.351	11° 30'
5.002	13° 15'

Y ±.005	Y° REF
.190	0° 30'
.952	2° 30'
1.712	4° 30'
2.470	6° 30'
3.225	8° 30'
3.977	10° 30'
4.723	12° 30'

REVISIONS

ZONE	DESCRIPTION	DATE	APPROVED
	1. NEW SIZ REWORKED 3. RECORD CHANGE 2. CURRENT SIP REWORKED 4. NOW SHOP PRACTICE 5. PARTS MADE OS		

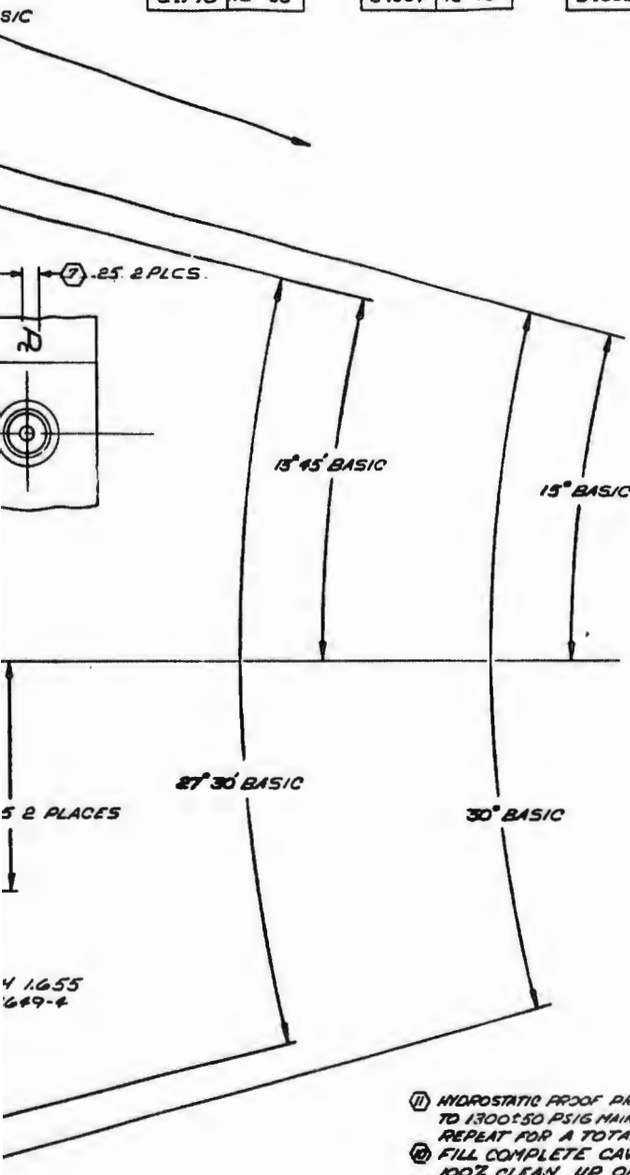

⑪ HYDROSTATIC PROOF PRESS TEST WITH DEIONIZED WATER TO 1300±50 PSIG MAINTAIN PRESS FOR 2 MIN REPEAT FOR A TOTAL OF 5CYCLES NO LEAKAGE ALLOWED
⑩ FILL COMPLETE CAVITY TO ASSURE 100% CLEAN UP ON NEXT ASSY
⑨ HYDROSTATIC PROOF PRESS TEST WITH DEIONIZED WATER TO 2750±50 PSIG MAINTAIN PRESSURE FOR 2 MINUTES REPEAT FOR A TOTAL OF 5 CYCLES NO LEAKAGE ALLOWED
8. CAP AND PLUG PORTS PER RA0116-054
⑦ IMPRESSION STAMP LETTERING AS SHOWN, LETTERING TO BE LEGIBLE AND NOT RESULT IN CRACKS OR DISTORTION
⑥ WELD PER RA0107-087 CLASS II
⑤ STRESS RELIEVE AFTER WELDING PER RA0111-018 EXCEPT COOLING RATE NOT TO EXCEED 650°F PER HOUR
④ ELECTROLYTIC NICKEL PLATE INJECTOR BODY FACE .0002-.0004 THICK PER RA0109-005 PLATING ON REMAINING SURFACES OPTIONAL WELD PRIOR TO PLATING
3. CLEAN PER STO1106A0002
2. MACHINE PER RA0103-002
① IDENTIFY PER RA0104-008

Figure 68. 30-Degree Prototype Injector Body (U)

NO	MATERIAL	SIZE	SPECIFICATION
-13	304L CRES BAR	½ DIA x .18	005763 CONDA CL 304L
-9	304L CRES BAR	½ DIA x .18	005763 CONDA CL 304L
-7	304L CRES BAR	½ DIA x .18	005763 CONDA CL 304L
-5	304L CRES BAR	½ DIA x .18	005763 CONDA CL 304L
-3	MAKE FROM EWR 116151		

117/118

DES BY E.SYP 4-25-67	ROCKETDYNE A DIVISION OF NORTH AMERICAN AVIATION, INC. CANOGA PARK, CALIFORNIA · NEOSHO, TEXAS		
CHK BY	BODY-30° INJECTOR ASSY OF		
DES			
ENGR			
CODE IDENT NO 02602	SIZE J	EWR 116336	
SCALE 2/1	SHEET 1 OF		

CONFIDENTIAL

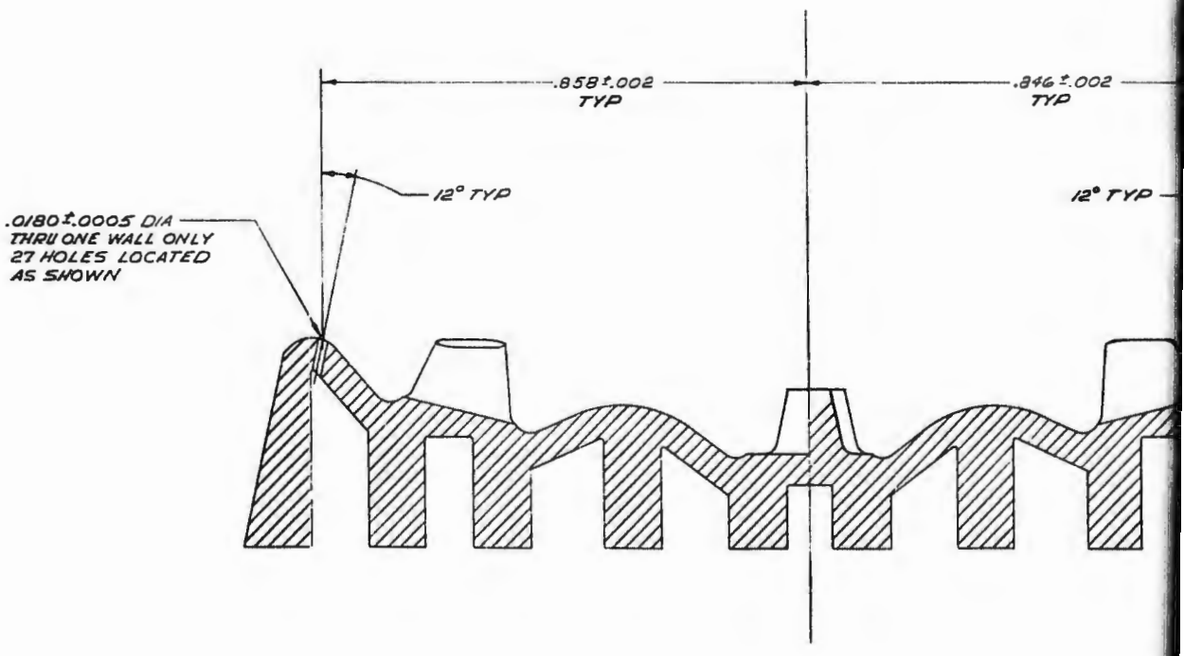

SECTION D-D
SCALE 10/1

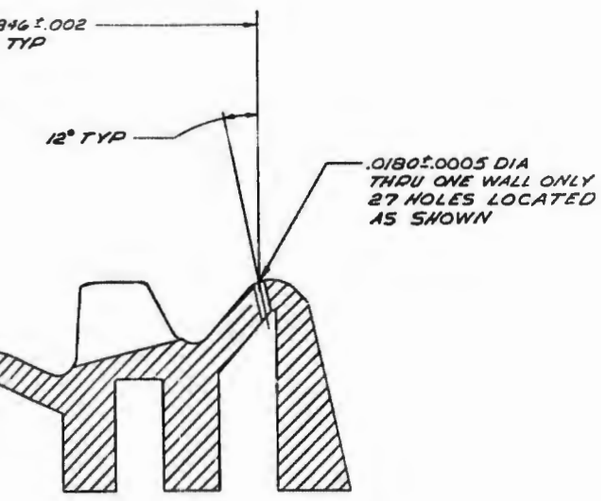

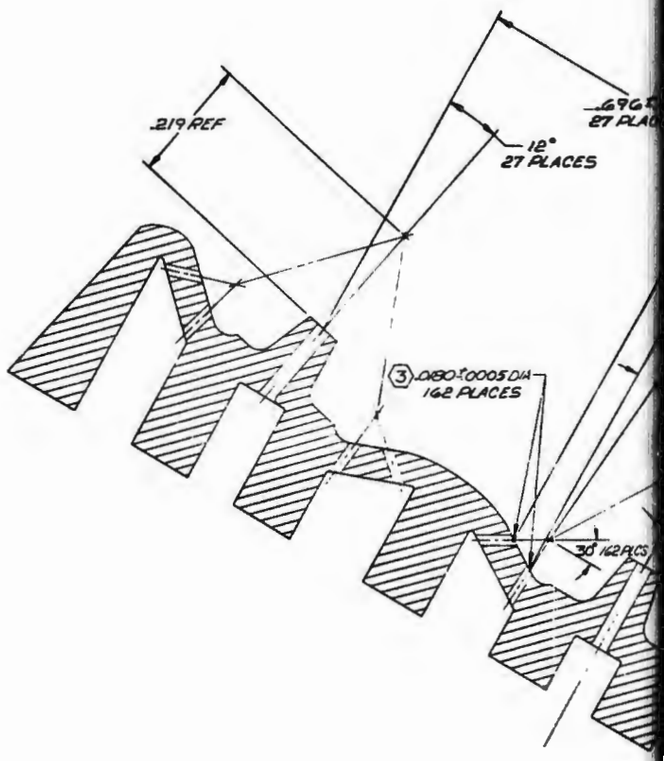

SECTION A-A
SCALE 10/1

2

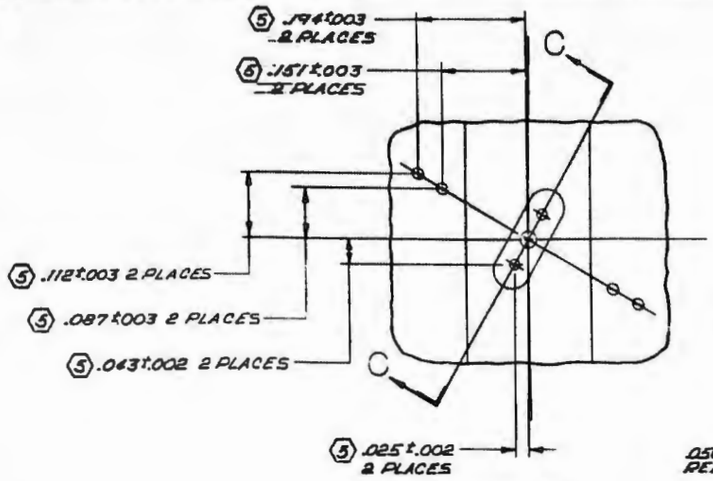

DETAIL B
81 PLACES
SCALE 10/1

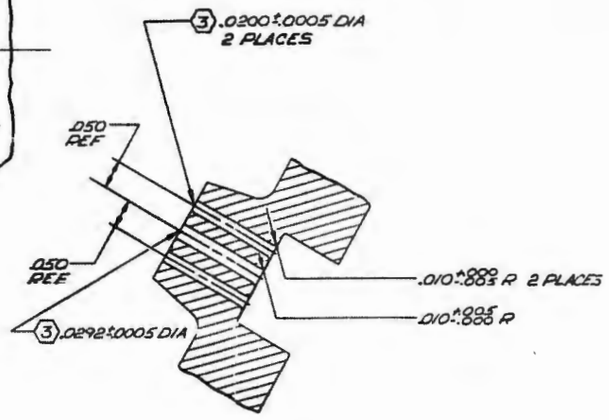

SECTION C-C
A4 79 PLACES
SCALE 10/1

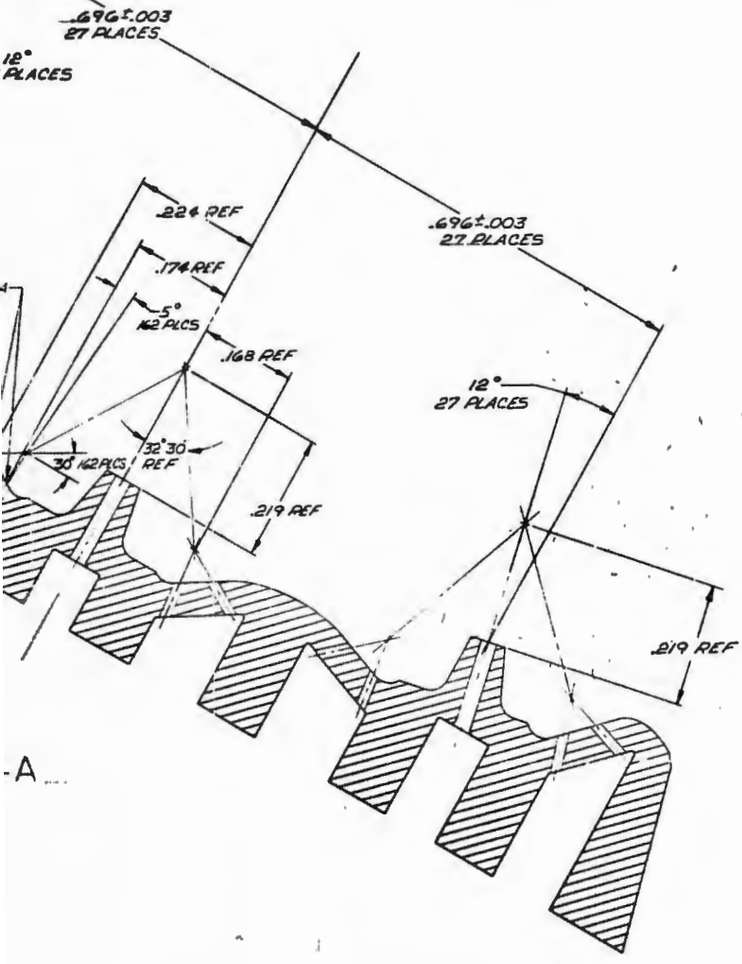

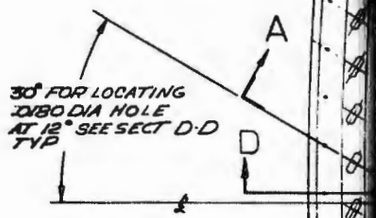

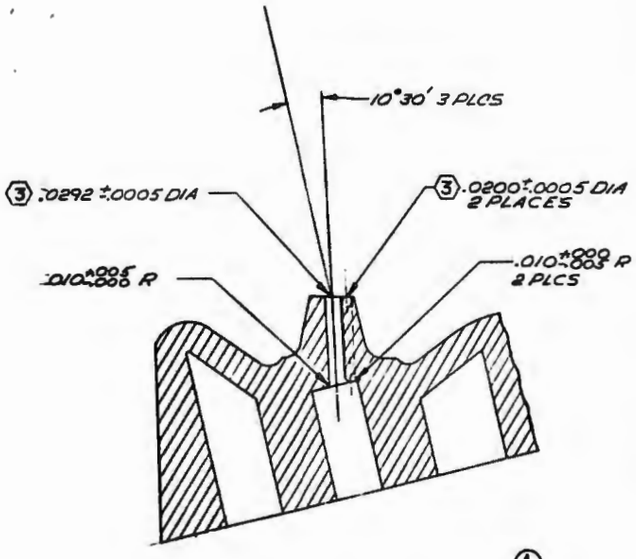

SECTION G-G
A4
SCALE 10/1

G

3

CONFIDENTIAL

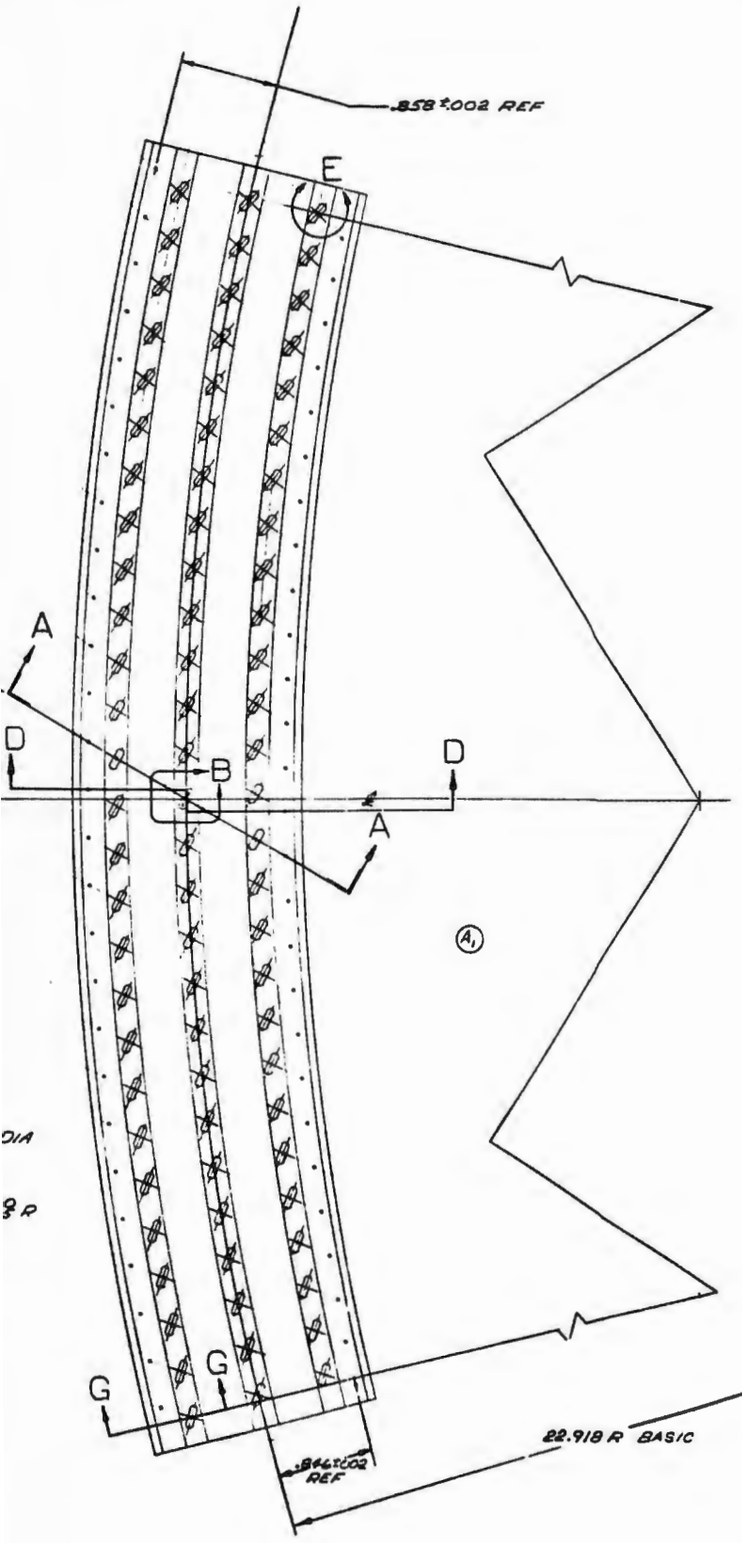

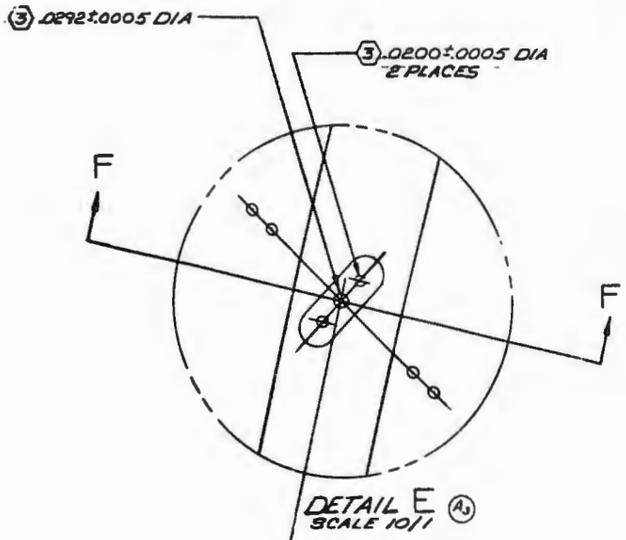

DETAIL E (A3)
SCALE 10/1

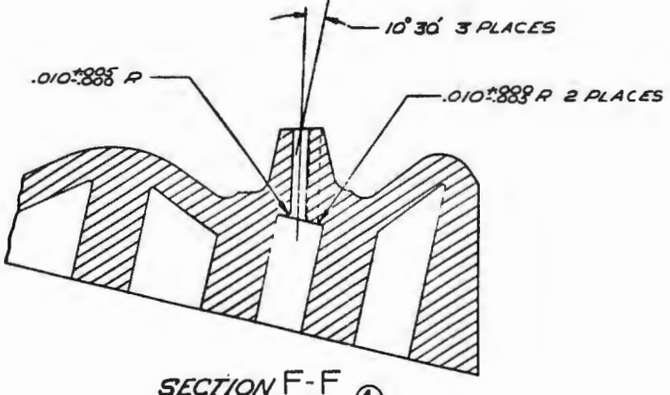

SECTION F-F (A3)
SCALE 10/1

5 LOCATE FROM CENTER ORIFICE AS SHOWN
4 USE SULPHUR FREE MATERIALS WHEN PROCESSING TO PREVENT EMBRITTLEMENT OF NICKEL AS DESCRIBED IN RA0102-014
3 EDGE OF ORIFICE TO BE SHARP AT INJECTOR FACE
2 IDENTIFY PER RA0104 0.8 (EXCEPT TAG ONLY)
1 MACHINE PER RA0103-008

UNLESS OTHERWISE SPECIFIED

MAKE FR
EWR100

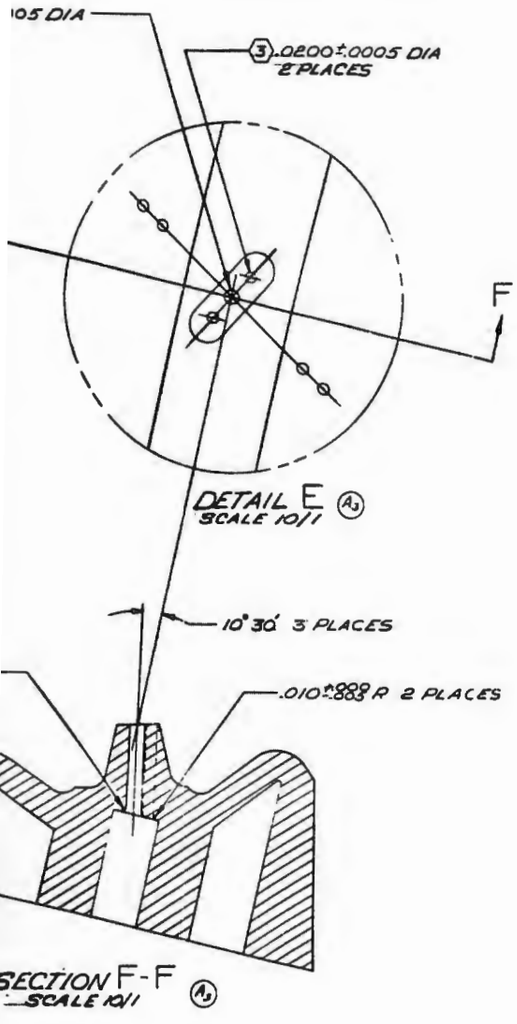

REVISIONS				
SYM	ZONE	DESCRIPTION	DATE	APPROVED
		1. MAY BE REWORKED 3. RECORD CHANGE 2. CANNOT BE REWORKED 4. NOW SHOP PRACTICE 5. PARTS MADE OR		
		A		
#		1) REMOVED: DRILL #(.031) THRU 2 PLCS, .316±.002 2 PLCS, .478B±.002, 12°3'32" REF .776±.002 @ 1°56'28" REF	5	
7/66		2) ADDED SECT D-D	5	
8		3) ADDED DETAIL E & SECT F-F	5	
5		4) ADDED SECT G-G	5	
6		71 PLACES WAS 91 PLACES	5	6 JAN 67

EWR 100750 A1

CONFIDENTIAL
(LEGEND UNCLASSIFIED)

GROUP 4
DOWNGRADED AT 3 YEAR INTERVALS
DECLASSIFIED AFTER 12 YEARS

6633 CANOGA AVE., CANOGA PARK 91304

(3) LOCATE FROM CENTER ORIFICE AS SHOWN
4. USE SULPHUR FREE MATERIALS WHEN PROCESSING TO PREVENT EMBRITTLEMENT OF NICKEL AS DESCRIBED IN RADIO2-014
(3) EDGE OF ORIFICE TO BE SHARP AT INJECTOR FACE
2. IDENTIFY PER RADIO4 01.8 (EXCEPT TAG ONLY)
1. MACHINE PER RADIO3-008

REF. UNLESS OTHERWISE SPECIFIED

HEAT TREAT

FINISH

MATL MAKE FROM EWR100705

UNLESS OTHERWISE SPECIFIED DIMENSIONS ARE IN INCHES AND APPLY PRIOR TO FINISH
125 MAX ELIM ROUGHNESS
TOLERANCES ON
DECIMALS ANGLES
.XX ± .010 ANGLES ± 30'
.XXX ± .010
HOLES NOTED "DP (4)"
.000 THRU .060 ± .015 — .001
.061 THRU .120 ± .020 — .001
.121 THRU .180 ± .025 — .001
.181 THRU .240 ± .030 — .001
.241 THRU .300 ± .035 — .001
.301 THRU .360 ± .040 — .001
.361 THRU .420 ± .045 — .001
.421 THRU 1.000 ± .050 — .001
1.001 THRU 2.000 ± .060 — .001

DO NOT SCALE PRINT

DR BY	E. SIP	7/6/67
CHK BY		
DES		
ENG		
DEV		
FRAME	3	

ROCKETDYNE
A DIVISION OF NORTH AMERICAN AVIATION, INC
CANOGA PARK, CALIFORNIA • MCGREGOR, TEXAS

PLATE-DRILLED, 30° INJECTOR FACE

CODE IDENT NO	SIZE	
02602	J	EWR 100750

SCALE 2/1 SHEET 1 OF

CONFIDENTIAL

Figure 69. 30-Degree Prototype Injector Face (U)

CONFIDENTIAL

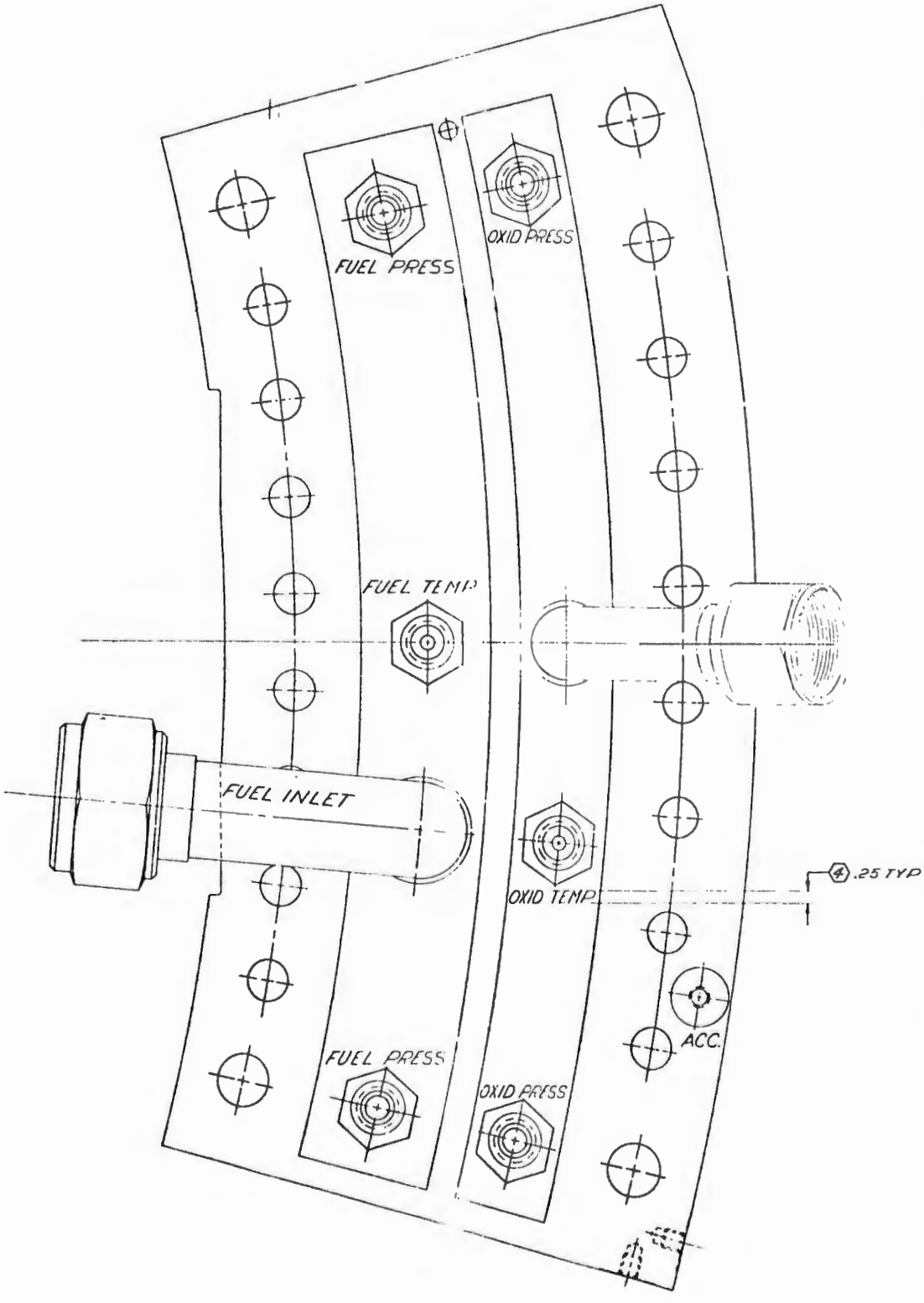

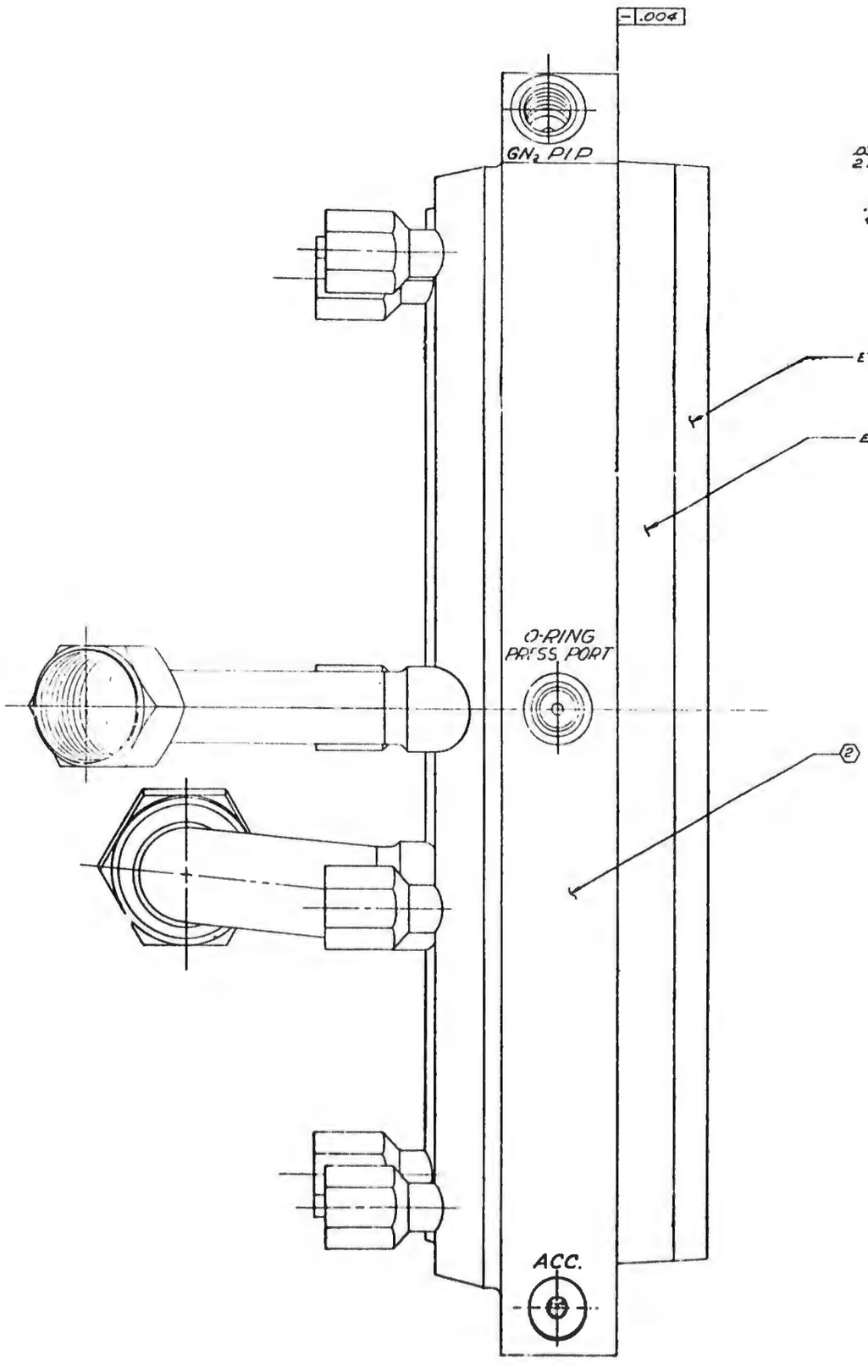

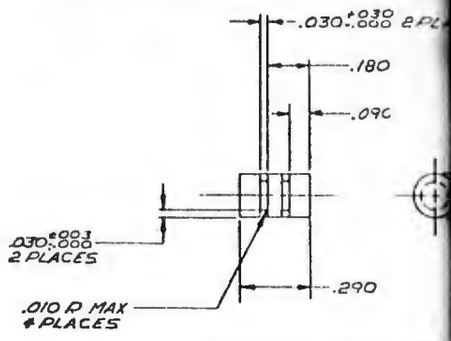

⑨ – 3 PLUG DETA
SCALE 4/1

EWR 100740 INJECTOR FACEPLATE 1
EWR 116336 INJECTOR BODY 1 REQ

CENTERLINE
CENTERLINE
TO BE IN LI

2

MICROFILM OVERLAP AREA

D.$^{.838}_{.838}$ 2 PLACES

—.180

—.090

.1850 $^{+.0008}_{-.0018}$ DIA

.290

UG DETAIL
ALE 4/1

EPLATE 1 REQD

DY 1 REQD

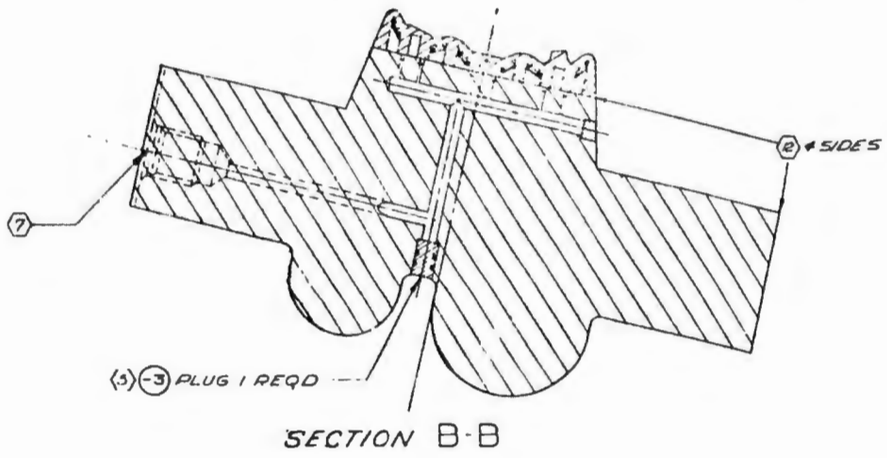

SECTION B-B

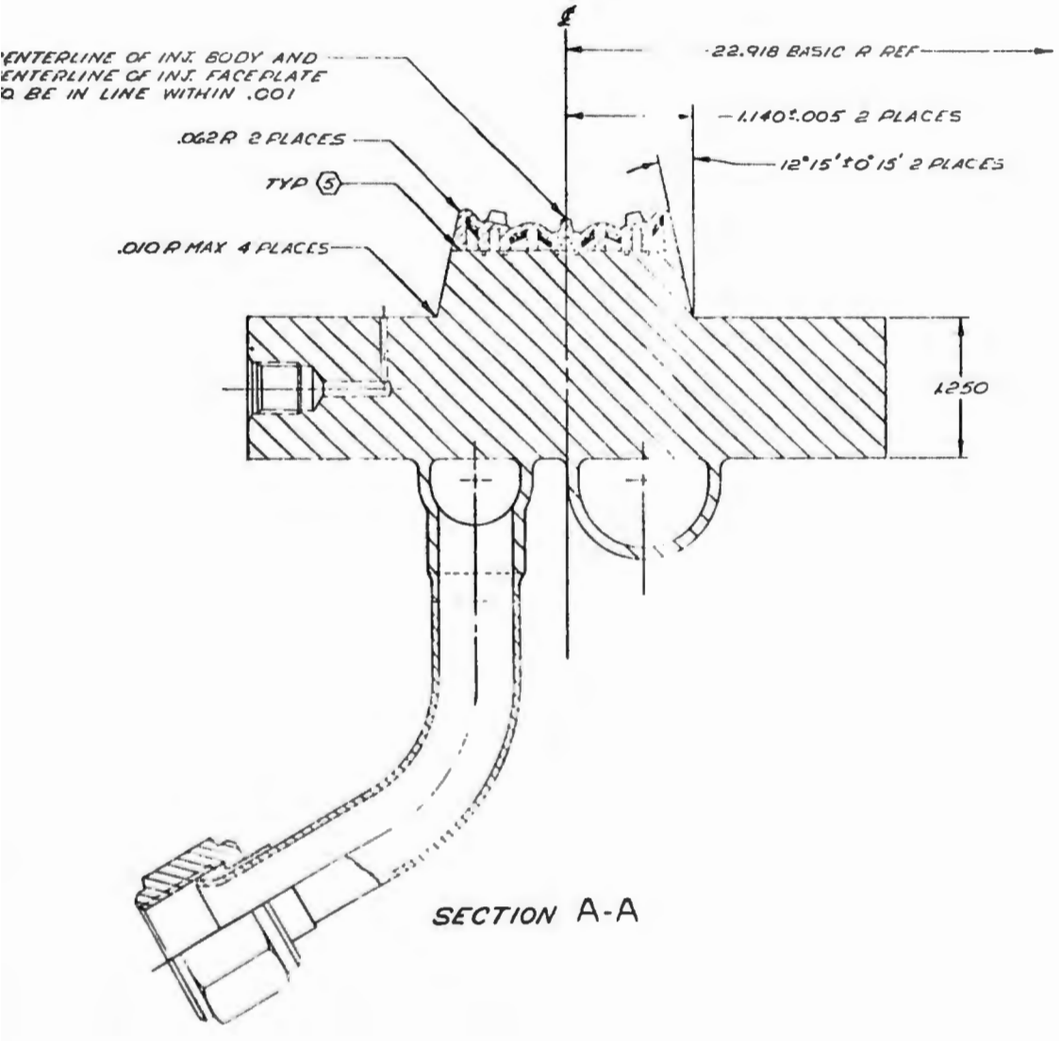

SECTION A-A

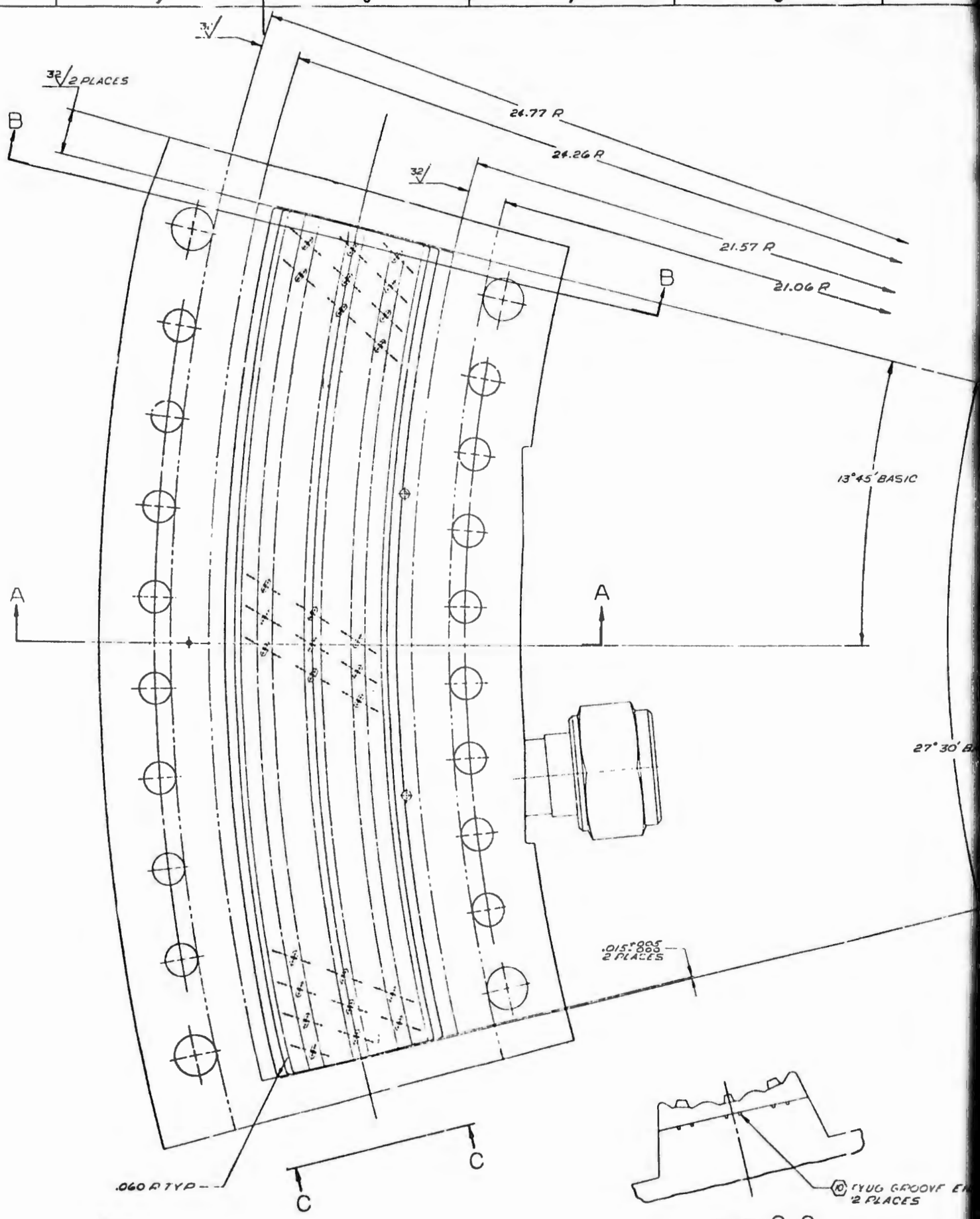

10 9 8 7 6

• MICROFILM OVERLAP AREA •

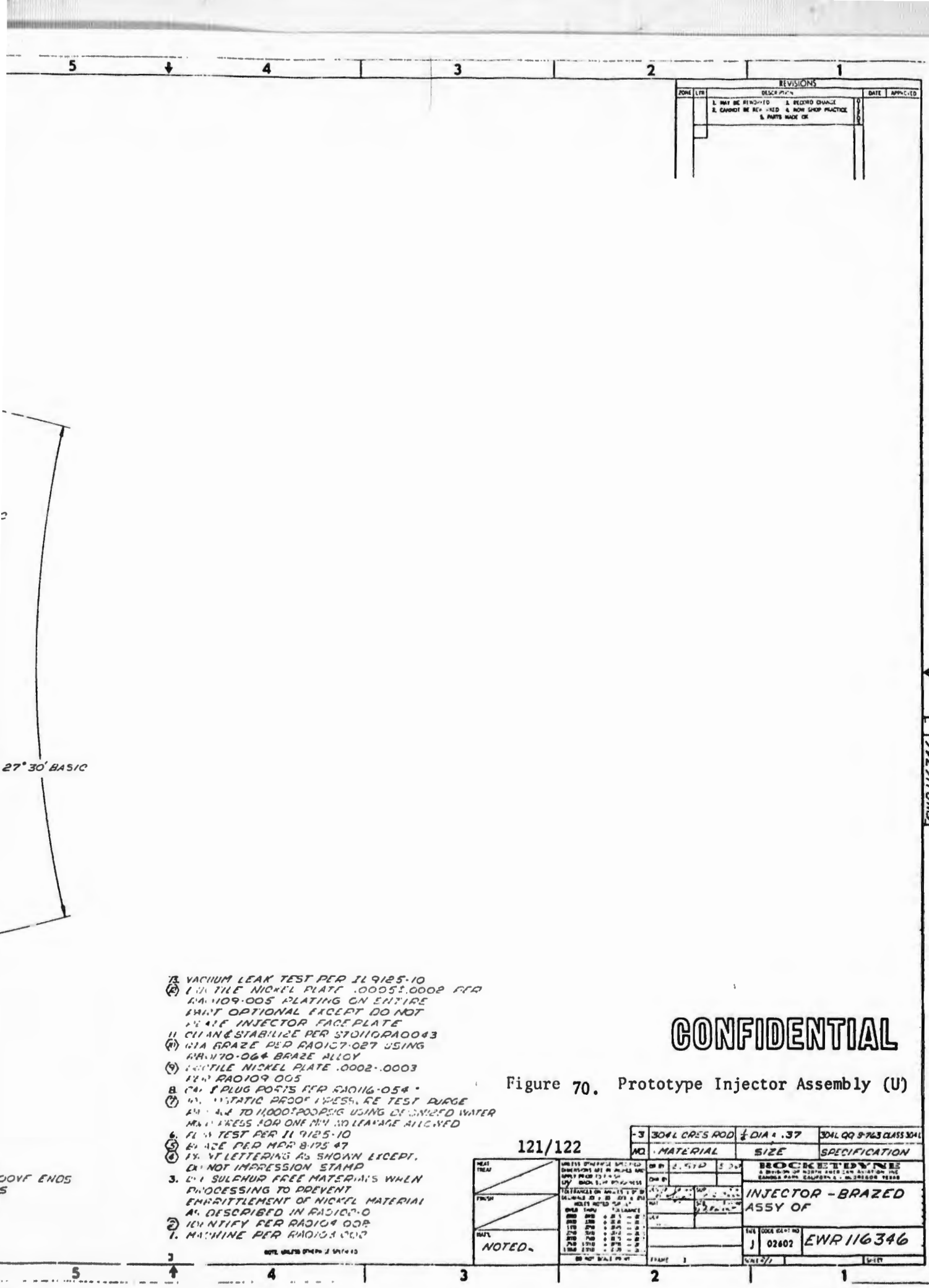

CONFIDENTIAL

Figure 70. Prototype Injector Assembly (U)

(1) Injector Test Evaluation

(U) The initial tests were specifically intended for evaluation of two candidate 30-degree injector types to ascertain which was most suitable for regenerative thrust chamber segment assembly testing. The injectors consisted of the curved, brazed-face, impinging fan type (Fig. 59), and the integral flat-face impinging fan injector (Fig. 60). A summary of this test series is provided in Table 8.

(U) Another test objective of these initial tests was to obtain heat transfer data, local heat flux and total integrated heat rejection rate to the coolant, for the 30-degree segment thrust chamber configuration, which had the typical aerospike skewed divergent nozzle. These data were required so that the cooling characteristics of the 30-degree regenerative-cooled segment could be accurately predicted. Additional test objectives included:

1. Demonstration of injector face-cooling capability and structural integrity
2. Evaluation of characteristic velocity (c*) efficiency of the injector
3. Determination of operational characteristics of the injector, i.e., propellant pressure loss

(C) Evaluation of the integral injector was completed in two tests when the test data indicated that the total integrated heat rejection rate to the solid-wall thrust chamber was considerably higher than predicted from the 5-inch, water-cooled calorimetry chamber results.

(C) Evaluation of the curved, brazed-face injector was satisfactorily completed in five tests. All test objectives were met, and the injector demonstrated suitability for use with the regenerative-cooled thrust chamber segments, although the final determination of injector-chamber compatibility remained to be accomplished in the regeneratively cooled hardware.

TABLE 8

30-DEGREE WATER-COOLED THRUST CHAMBER SEGMENT AND INJECTOR EVALUATION TEST SUMMARY (U)

TEST NO.	CHAMBER SEGMENT	INJECTOR	DURATION, SECONDS	CHAMBER, PRESSURE, PSIA	INJECTOR FLOW, LB/SEC.	MIXTURE RATIO	FUEL INJECTOR TEMPERATURE, R	THROAT HEAT FLUX, BTU/IN.^{2} SEC	INJECTOR END HEAT FLUX, BTU/IN.^{2} SEC	η_{c^*}
075	30-DEGREE SOLID WALL	INTEGRAL	1.0	327	2.32	14.37	1398	15.2	2.88	98.1
076		INTEGRAL	4.0	332	2.51	14.15	1391	16.4	1.90	96.9
077		BRAZED (UNIT NO. 1)	1.0	330	2.60	14.46	1258	11.3	0.43	---
078		BRAZED (UNIT NO. 1)	3.75	343	2.51	14.06	1423	17.5	0.32	98.7
079		BRAZED (UNIT NO. 1)	1.0	647	4.71	13.87	1359	25.4	1.07	97.1
080		BRAZED (UNIT NO. 1)	5.0	152	1.16	13.20	1311	11.5	0.67	96.2
081		BRAZED (UNIT NO. 1)	15.0	89	0.68	13.54	1280	8.0	0.82	96.6

CONFIDENTIAL

(U) The water-cooled calorimetry chamber segment was instrumented to obtain coolant flowrate and temperature rise in each coolant passage. The combustion zone region was cooled with a parallel coolant circuit wherein the inlet flow was split to cool a one-half baffle, the inner, or outer body, and then a one-half baffle, as shown in Fig. 71. Because of the circuit configuration, it was not possible to determine the separate inner- and outer-body heat inputs in the combustion zone. Aft of the throat, the inner body, outer body, and baffles were cooled separately, as shown in Fig. 72. This arrangement permitted separate computation of the inner body heat inputs aft of the throat and enabled determination of the combustion and nozzle total integrated heat inputs directly.

(U) The injector end heat flux, as determined from measurements taken at the first water coolant passage, is shown in Fig. 73 for both injectors over the range of chamber pressure tested. Also shown are the analytically determined maximum allowable values. As indicated in Fig. 73, the brazed-face injector exhibited much lower values of injector end heat flux than did the integral injector, and were well below the maximum allowable curve.

(C) The measured chamber heat flux profiles for both type injectors are shown in Fig. 74 for a chamber pressure of approximately 340 psia and a nominal mixture ratio of 14.0. The computed Stanton-Prandtl No. ($N_{St} \times (N_{Pr})^{2/3}$) profiles (determined by using the techniques presented in (Ref. 1) for both configurations are compared in Fig. 75 . As observed in the figures, use of the integral flat-face injector resulted in higher local heat fluxes in the combustion chamber region, and was believed to be due to more direct impingement of the injector fans on the chamber wall. Any boundary condition established on the chamber wall upstream of the impingement point is disturbed at that point. The brazed curved-face injector was indicated to have a more gradual and continuous boundary layer attachment mechanism.

(C) The total integrated heat input of the integral flat face injector was also considerably greater (29 percent) than with the curved-face injector. The heat transfer results of the tests (075 through 081) are tabulated in Table 9.

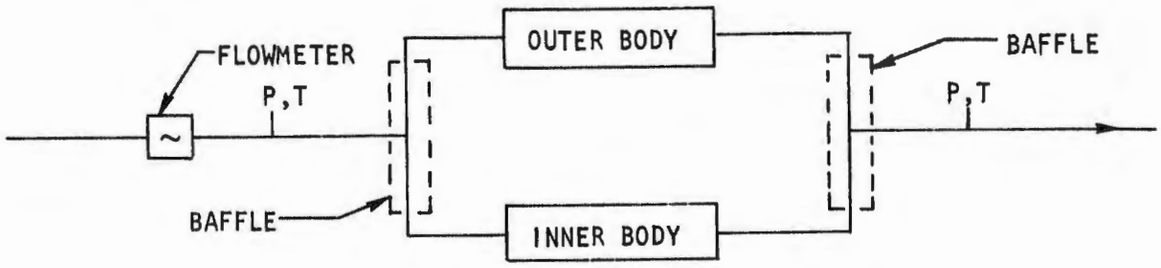

Figure 71. Combustion Zone Coolant Circuit for the 30-Degree Water Cooled Segment (U)

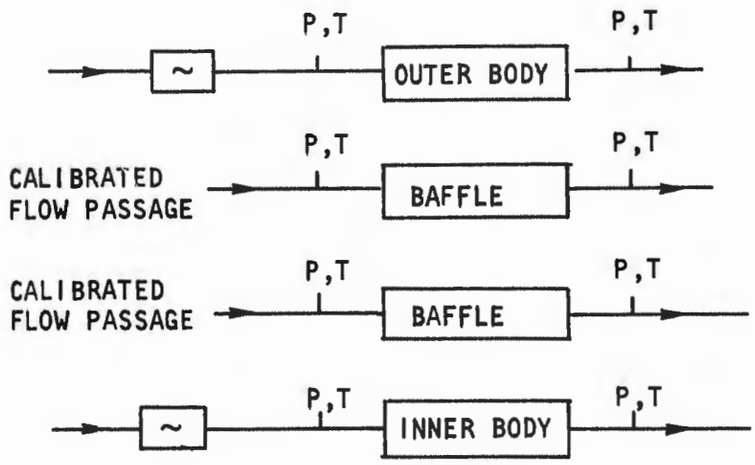

Figure 72. Nozzle Section Coolant Circuit for the 30-Degree Water Cooled Segment (U)

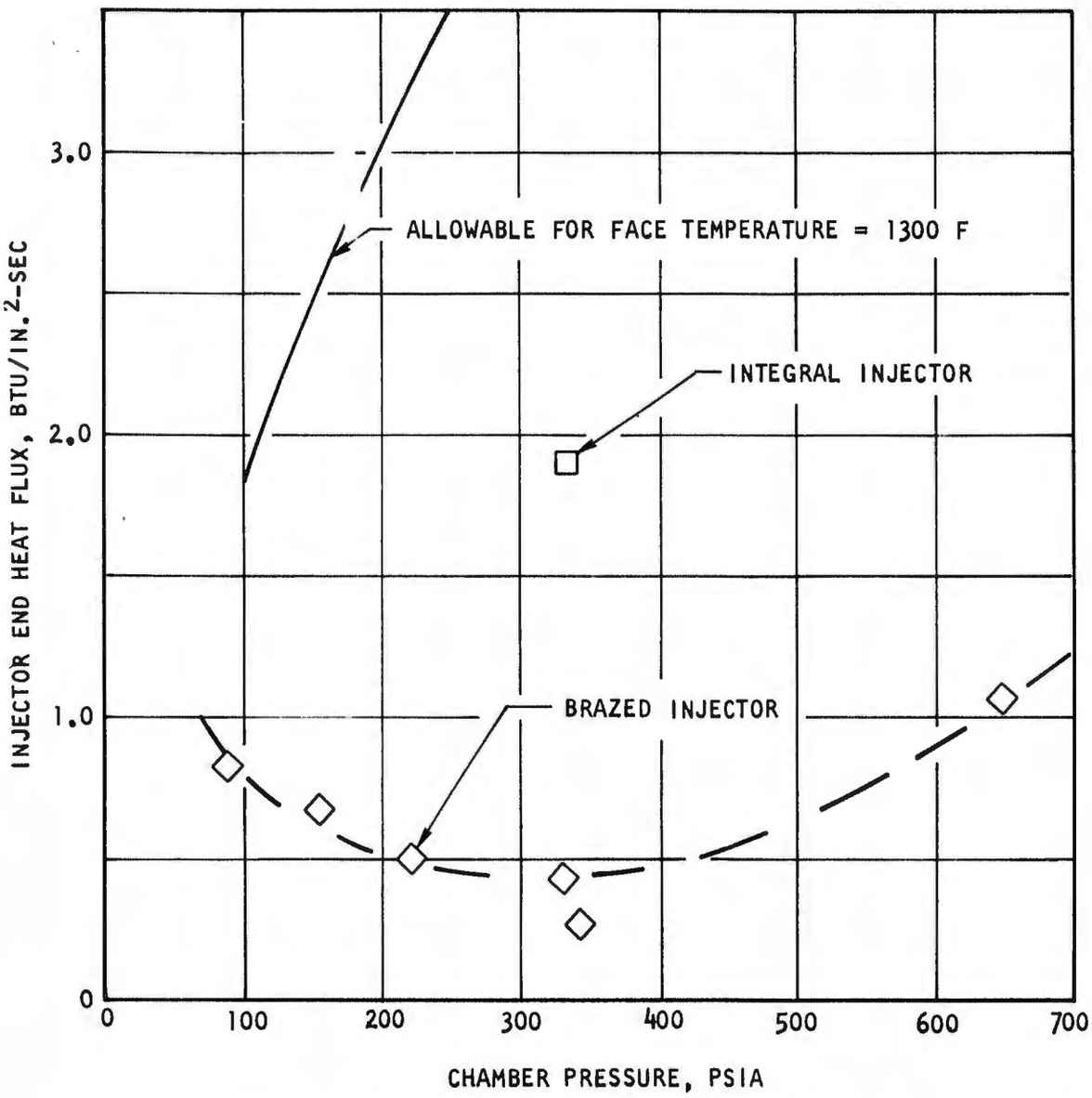

Figure 73. Injector End (Face) Heat Flux for 30-Degree Injectors (U)

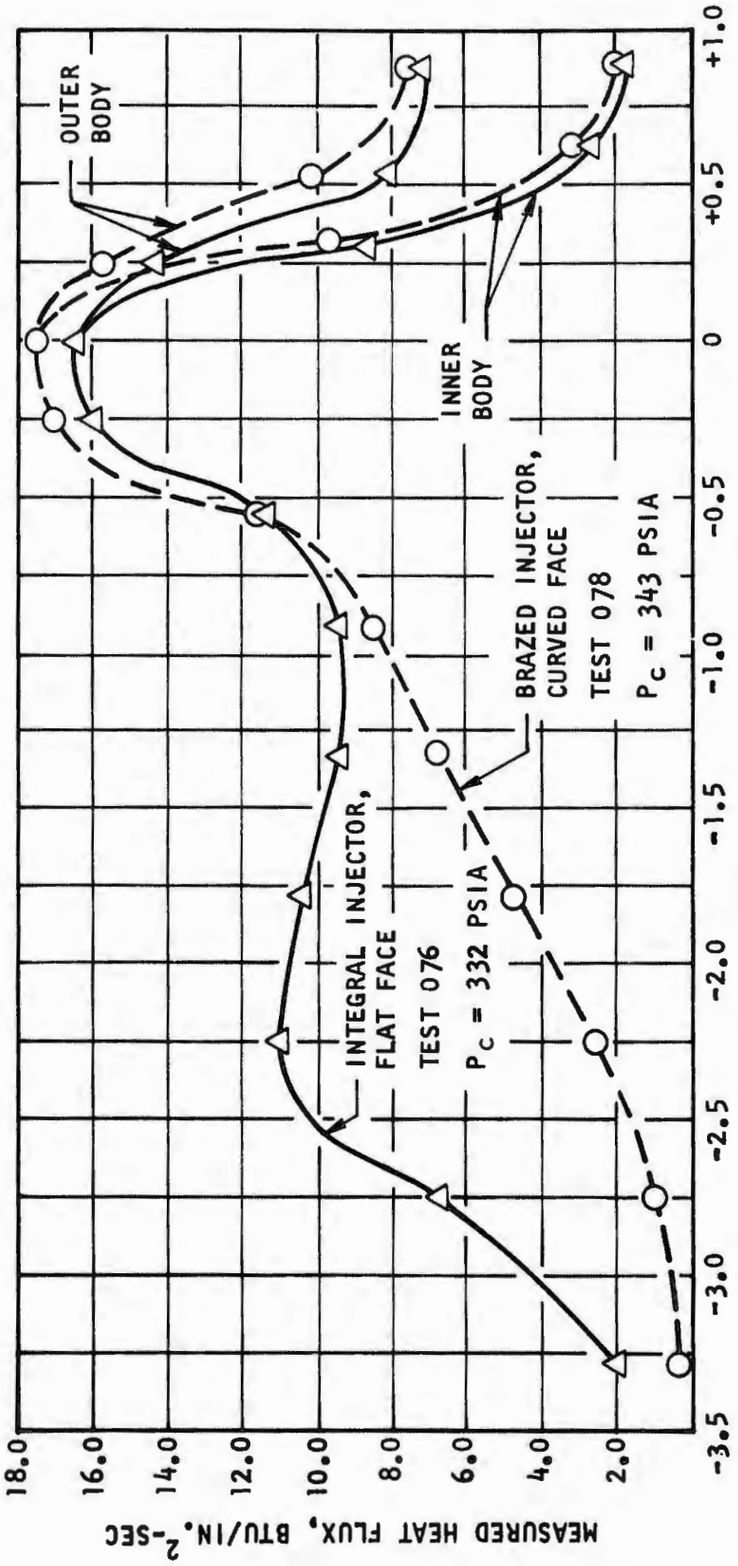

Figure 74. Measured Heat Flux Versus Chamber Length Comparison of 30-Degree Injectors (U)

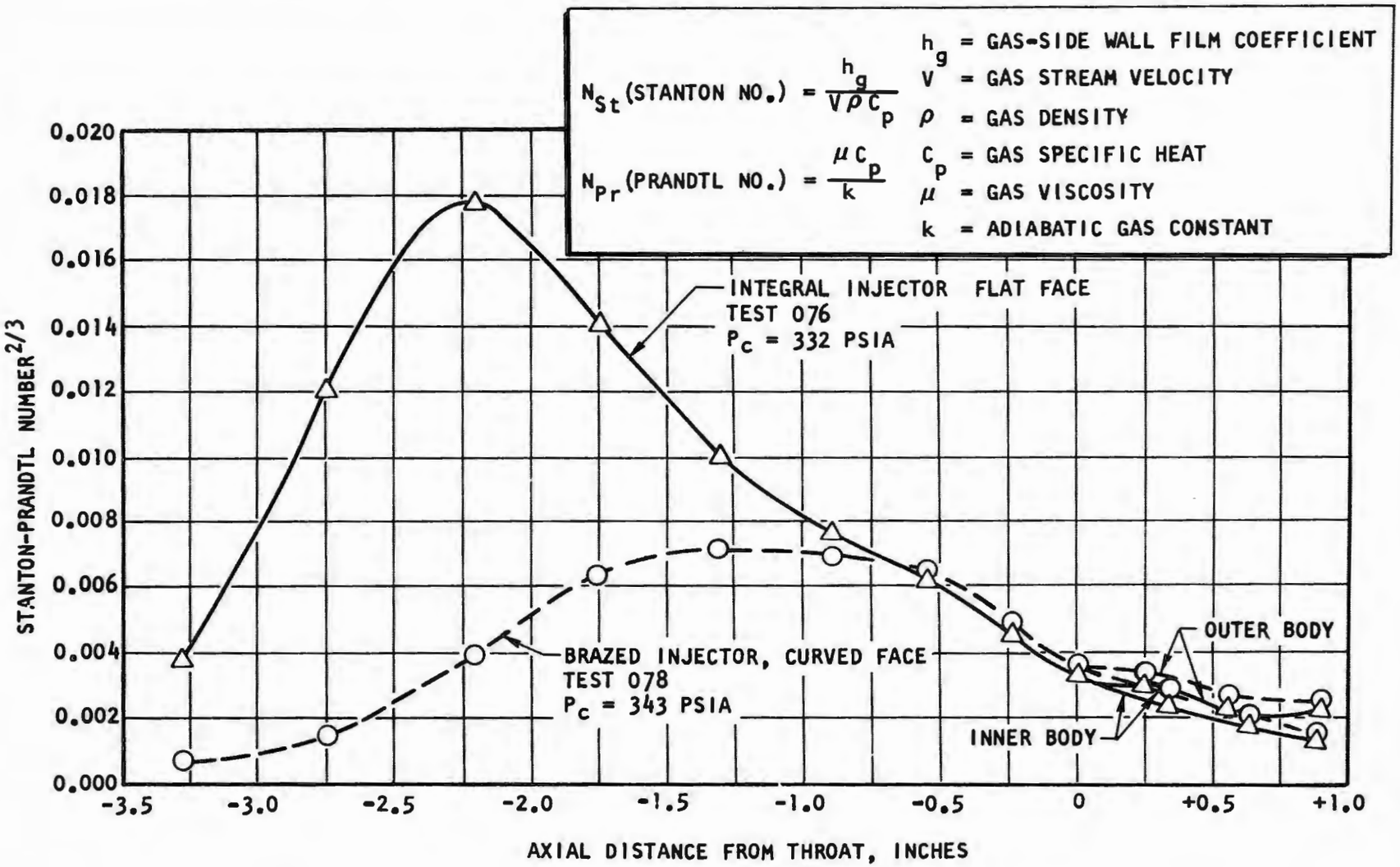

Figure 75. Stanton-Prandtl No. Versus Chamber Length Comparison of 30-Degree Injectors (U)

TABLE 9

30-DEGREE WATER-COOLED SEGMENT CHAMBER HEAT TRANSFER DATA FOR INJECTOR EVALUATION (U)

Test No.	Injector Configuration	Chamber Pressure, psia	Injector Flow, lb/sec	Throat Heat Flux, $Btu/in.^2$-sec	Injector End Heat Flux[2], $Btu/in.^2$-sec	Total Heat[4] Load, Btu/lbm	Combustor[4] Heat Load, Btu/lbm	Nozzle[4] Heat Load, Btu/lbm	Total[4] Heat Load, Btu/sec	Inner Body Nozzle Heat Load, Btu/sec	Outer Body[3] Nozzle Heat Load, Btu/sec
075[1]	Integral Face (Unit No. 1)	327	2.32	15.2	2.88	449	324	125	1041.5	89	201
076	Integral Face (Unit No. 1)	332	2.51	16.4	1.90	451	321	130	1129.8	95	230
077[1]	Brazed Face (Unit No. 1)	330	2.60	11.3	0.43	237	140	96	614.5	--	--
078	Brazed Face (Unit No. 1)	343	2.51	17.6	0.32	347	206	141	870.8	106	228
079	Brazed Face (Unit No. 1)	647	4.71	25.4	1.07	302	171	131	1422	172	411
080	Brazed Face (Unit No. 1)	152	1.16	11.5	0.67	541	363	178	627	54	152
081	Brazed Face (Unit No. 1)	89	0.68	8.1	0.828	717	472	245	478	34	126

(1) Short duration: 1 second

(2) Determined from coolant passage closest to injector face

(3) Includes baffle heat input from throat to exit

(4) Includes baffle heat inputs

NOTE: Heat load, Btu/lb = $\frac{\text{Total Head Load, Btu/sec}}{\text{Injector Flowrate, lbm/sec}}$

CONFIDENTIAL

(C) The higher (N_{St} x $(N_{Pr})^{2/3}$) (i.e., gas-side film coefficient, hg) values obtained with the integral injector would result in gas-wall temperatures that would be higher than those produced by the brazed-face injector.

(C) Comparisons of the total integrated heat load per pound of injected reactants obtained during the previous program (Ref. 1) for contour G chamber with an impinging fan injector and the 30-degree, water-cooled, contour G_c chamber data with the two impinging fan injectors (integral and brazed face) are presented in Fig. 76 . The curve drawn for the brazed-face injector with contour G_c has the same shape as that shown for the G contour, indicating the same nonlinear relationship between P_c and heat load. Two data points are shown for the integral injector, and the curve shape was drawn to reflect the shape established by the other injectors. The lower integrated heat input obtained with the brazed-face injector would result in lower gas-side wall temperature and lower coolant bulk temperature. Based on these results, the brazed-face injector was selected for use in further 30-degree, water-cooled segment testing and regenerative cooled segment testing.

(C) Another objective of the above series of tests (075 to 081) was to evaluate the heat transfer in the skewed nozzle section and the influence of separation from the inner body and recompression on the outer body during sea level operation. Separation and recompression occured at all chamber pressures below approximately 180 psia.

(C) Without the separation/recompression effects, the heat load versus chamber pressure would have a straight line relationship when plotted on log-log paper ($\Delta H \sim P^n$). The test data showing the effect of these phenomena for the water cooled segment are shown in the curves of Fig. 77 and 78. The coolant passages are identified in Fig. 55. The separation of the gas from the inner body results in a decrease in coolant enthalpy change in that body, while the recompression on the outer body results in an increase in coolant enthalpy change in that body. The net result is an increase in total coolant enthalpy change and associated coolant bulk temperature when the chamber pressure is below 180 psia and the test is at sea-level conditions. The effect is nonexistent at altitude but applies to the

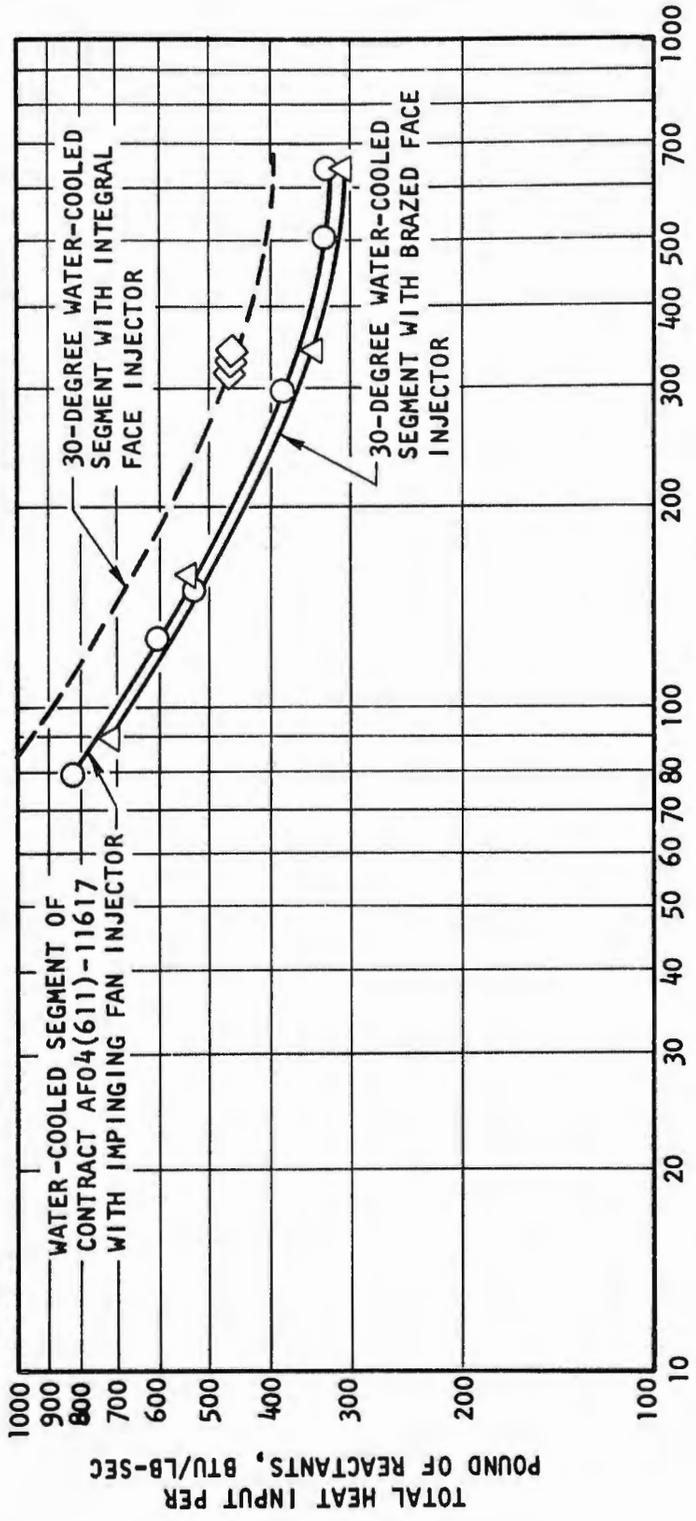

Figure 76. Comparison of Total Integrated Heat Input (Includes End Plates) (U)

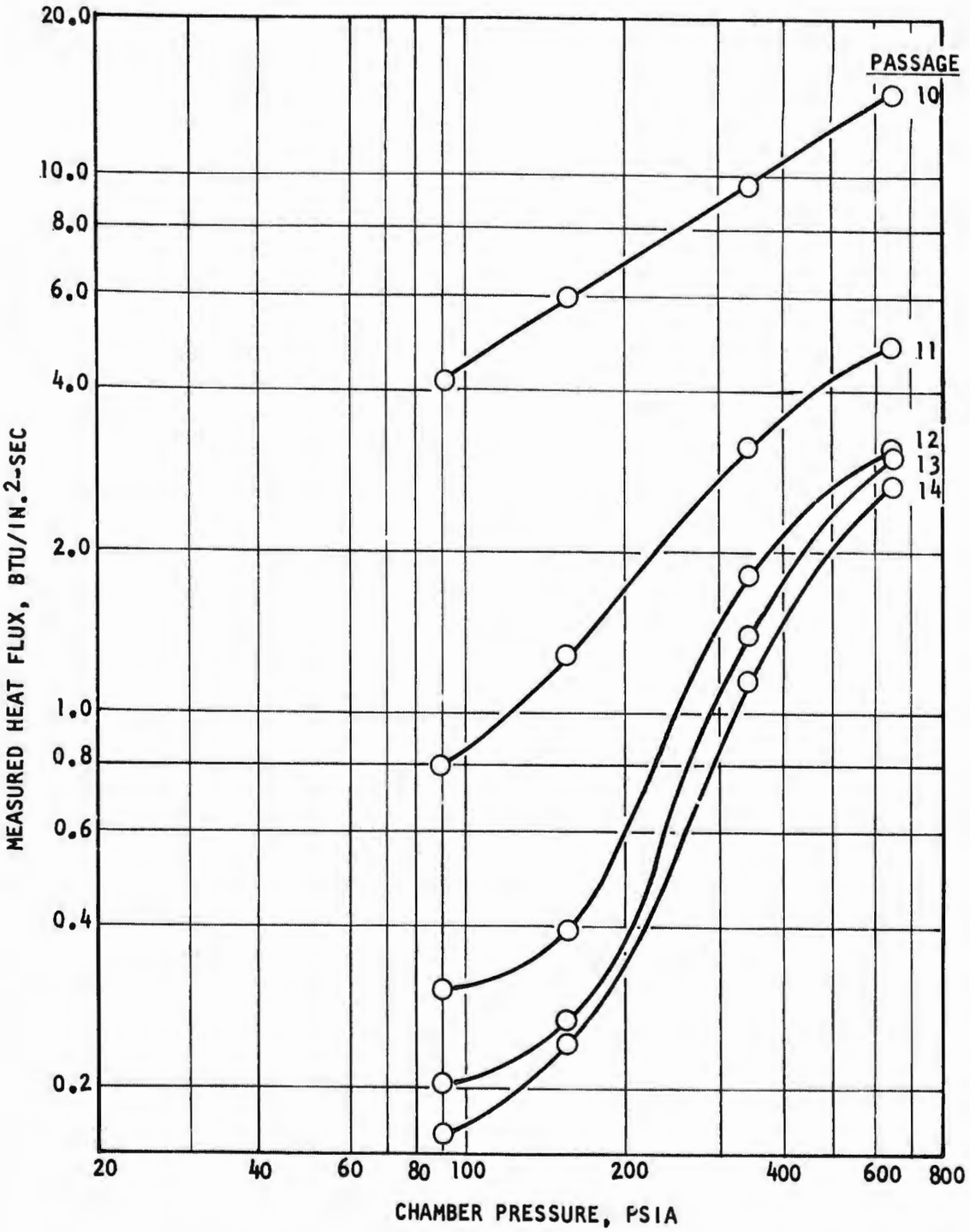

Figure 77. Nozzle Inner Body Measured Heat Flux Versus Chamber Pressure, 30-Degree Solid-Wall Segment (Tests 078-081) (U)

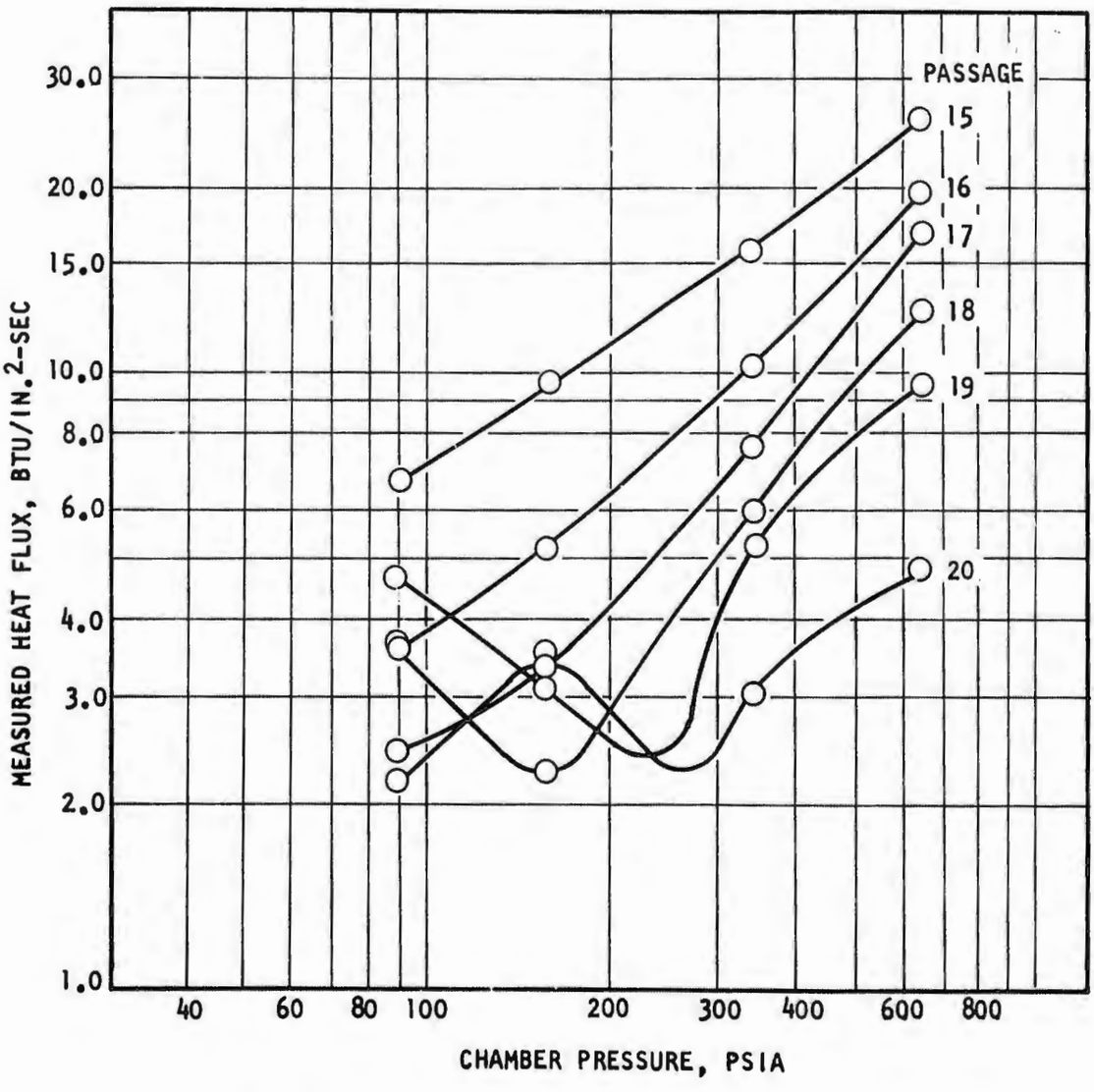

Figure 78. Nozzle Outer Body Measured Heat Flux Versus Chamber Pressure, 30-Degree Solid-Wall Segment (Tests 078-081) (U)

(C) analysis of 30-degree segment thrust chamber data. The empirical percentage magnitude of the effect can be determined from Fig. 79. The values used in Fig. 79 were obtained by linear interpolation of Fig. 77 and 78.

(U) The characteristic velocity efficiency (ηc^*) data derived from the 30-degree solid-wall test data in tabulated in Table 8.

(2) Mixture Ratio Bias Evaluation

(U) As an approach for reduction of overall chamber segment heat load, a series of tests was conducted with the 30-degree water-cooled segment for evaluation of mixture ratio bias. A summary of the test series is shown in Table 10 . Five tests were conducted with the 30-degree water-cooled thrust chamber segment that incorporated the previously described fuel and oxidizer bias modifications (see Section III, 3, a, (2)) to evaluate these effects on the total heat rejection rate and local heat flux.

(C) The first test (013-69), was conducted at 226-psia chamber pressure and used the fuel bias test configuration. The degree of fuel bias was varied during the test by control of facility fuel supply pressure. The test results, shown in Fig. 80 , indicated a definite increase in the upper combustion zone local heat flux and total heat rejection rate. However, the local heat flux in the throat decreased slightly. The results of an oxidizer bias test and a nonbiased test are shown in Fig. 80 form comparison. Based on the results obtained, no further fuel bias testing was conducted.

(C) Four tests (014-69 through 017-69) were conducted with the injector oxidizer bias modification. The first two tests were made with a bias hole size of 0.018-inch diameter. This hole size was selected to provide an oxidizer bias flow of approximately 15 percent of the total oxidizer flow. The intent was to obtain a chamber wall heat transfer reduction without significant loss in combustion efficiency.

(C) The last two oxidizer bias tests were conducted with a bias hole size of 0.021-inch diameter, which gave an oxidizer bias flow of approximately 20 percent of the total oxidizer flow.

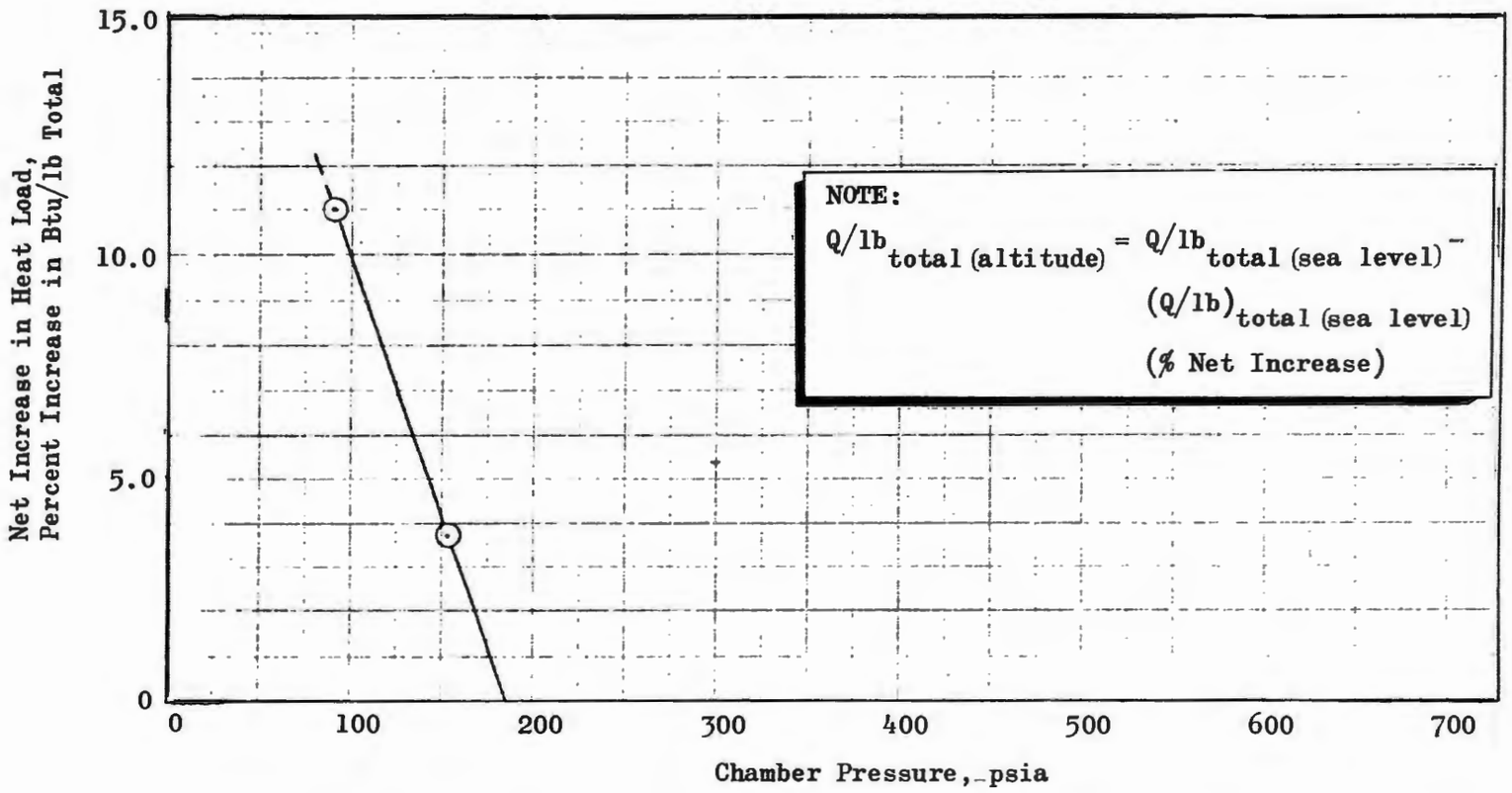

Figure 79. Net Increase in Total Heat Load From Separation and Recompression Based on Solid-Wall Segment Tests (U)

TABLE 10

30-DEGREE WATER-COOLED THRUST CHAMBER SEGMENT WITH MIXTURE RATIO BIAS TEST SUMMARY (U)

Test No.	Injector U/N	Duration, seconds	Chamber Pressure, psia	Injector Flow, lb/sec	Mixture Ratio	Fuel Injection Temperature, R	Fuel Injection Temperature, η_{c^*}	Cutoff	Throat Heat Flux Btu/in^2-sec	Injector End Heat Flux Btu/in^2-sec	Remarks
013-69	3	54.4	226	1.558	12.92	1552	99.6	Programmed	13.2	2.52	Fuel bias by chamber modification
014-69	1	20.7	222	1.519	14.57	1600	100	Programmed	15.4	0.49	Oxidizer bias by injector modification (0.018 inch diameter) holes added) ↓
015-69	1	37.4	80.4	0.555	15.18	1382	103	Programmed	6.08	0.67	
016-69	1	13.8	74.1	0.566	14.74	1382	93	Programmed	6.08	0.53	Oxidizer bias by injector modification (0.021 inch diameter holes added)
017-69	1	3.2	613	4.458	14.41	1492	93	Programmed	25.05	0.81	↓

CONFIDENTIAL

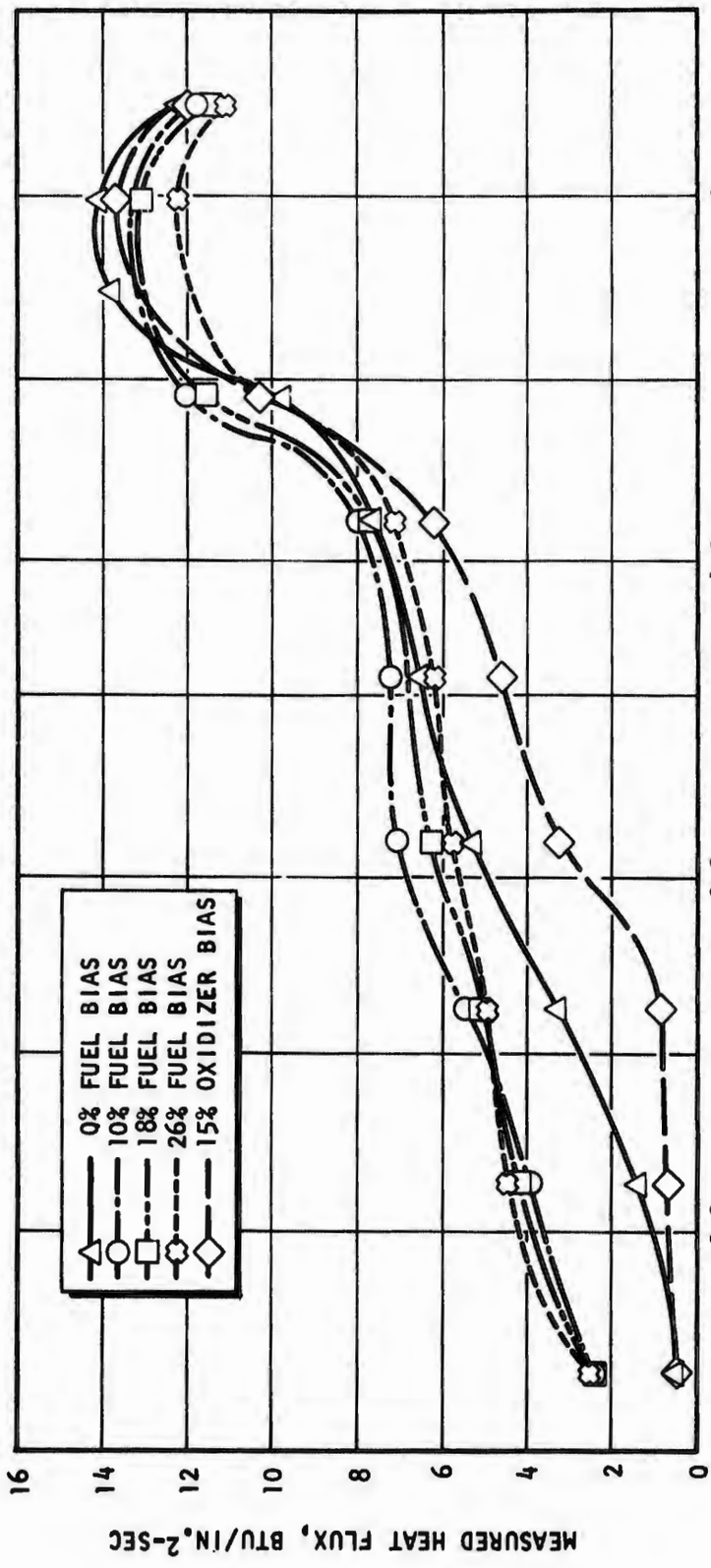

Figure 80. 30-Degree Water-Cooled Segment Heat Flux Profile With Injector Outer Zone Fuel Bias (Chamber Pressure = 226 psia) (C)

(U) A comparison of the heat flux profiles obtained at various chamber pressures is shown in Fig. 81 through 83. Previous tests at similar operating conditions, but without oxidizer bias, also are shown for comparison purposes. The 0.018-inch diameter hole oxidizer bias resulted in substantially (15 percent) decreased total heat rejection rates without any loss in the characteristic velocity efficiency. The 0.021-inch diameter hole oxidizer bias orifice size resulted in some additional reduction ($\approx$4 percent) in the total heat rejection rate relative to the results obtained with the 0.018-inch oxidizer bias orifice. However, there was an apparent significant loss in c* efficiency based on the results of these tests.

(C) The overall effect of the oxidizer bias (both bias hole sizes) on the total heat input is shown in Fig. 84 over the full range of operating chamber pressures. This figure compares the total heat input to the coolant per pound of injected propellants for a series of tests conducted with and without oxidizer bias. The total heat loads are indicated for each test point and the injected propellant flowrates were determined from the operating conditions at each chamber pressure. The figure shows that the greatest difference in the two curves occurs at the critical low chamber pressure level. Here, the heat load per pound of injected propellant is approximately 15 percent lower with the oxidizer bias based on an average of the values obtained with the two bias percent flows at the low chamber pressure level.

(C) Based on the favorable results obtained from the above testing, the oxidizer bias modification was incorporated into the 30-degree brazed-face injector design. The 0.018-inch-diameter oxidizer bias hole size was selected because nearly the same heat load reduction was obtained with this hole size, compared to the 0.021-inch-diameter hole size, while not resulting in any apparent combustion efficiency loss.

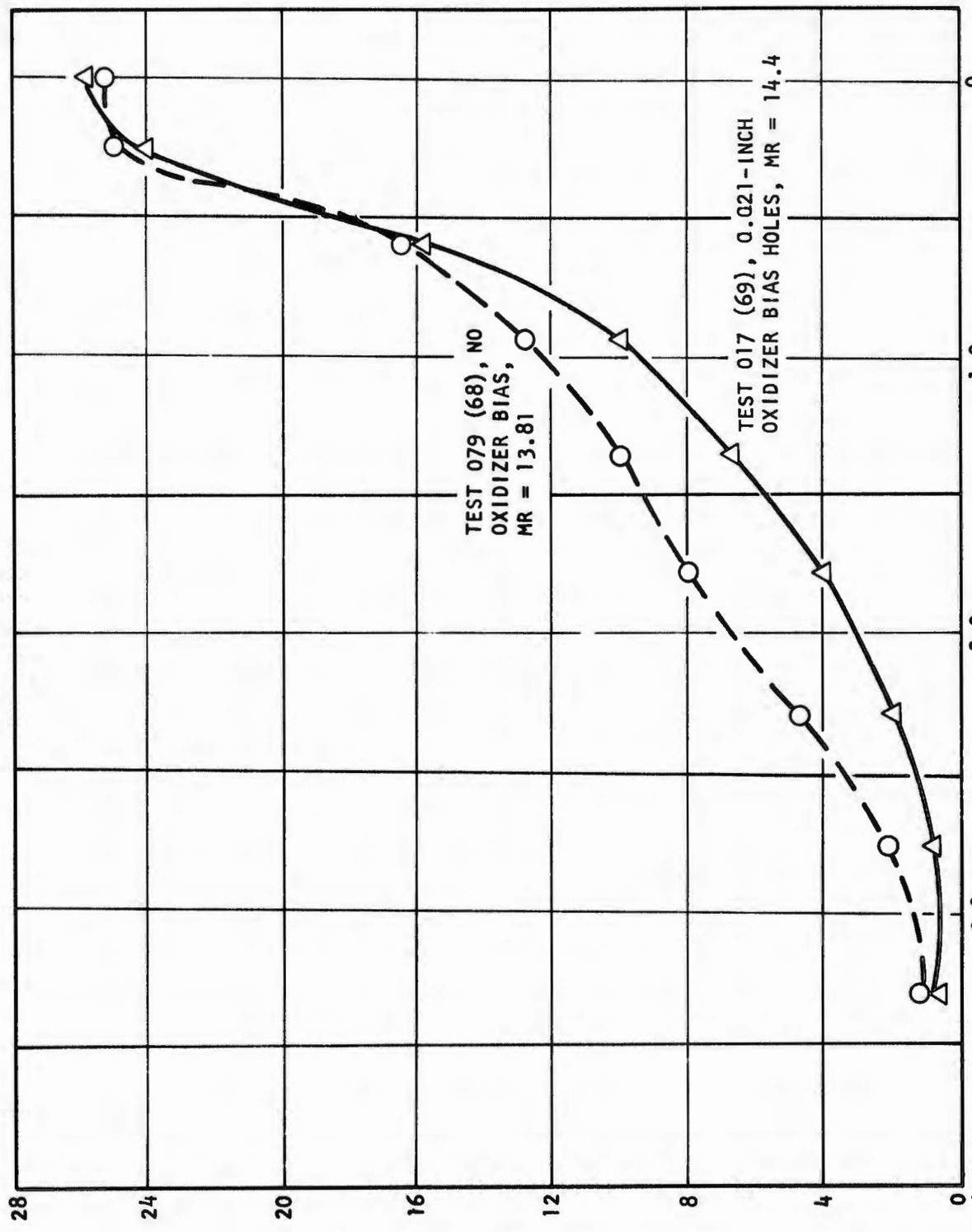

Figure 81. 30-Degree Solid-Wall Segment Heat Flux Profile With and Without Oxidizer Bias (Chamber Pressure = 647 psia) (C)

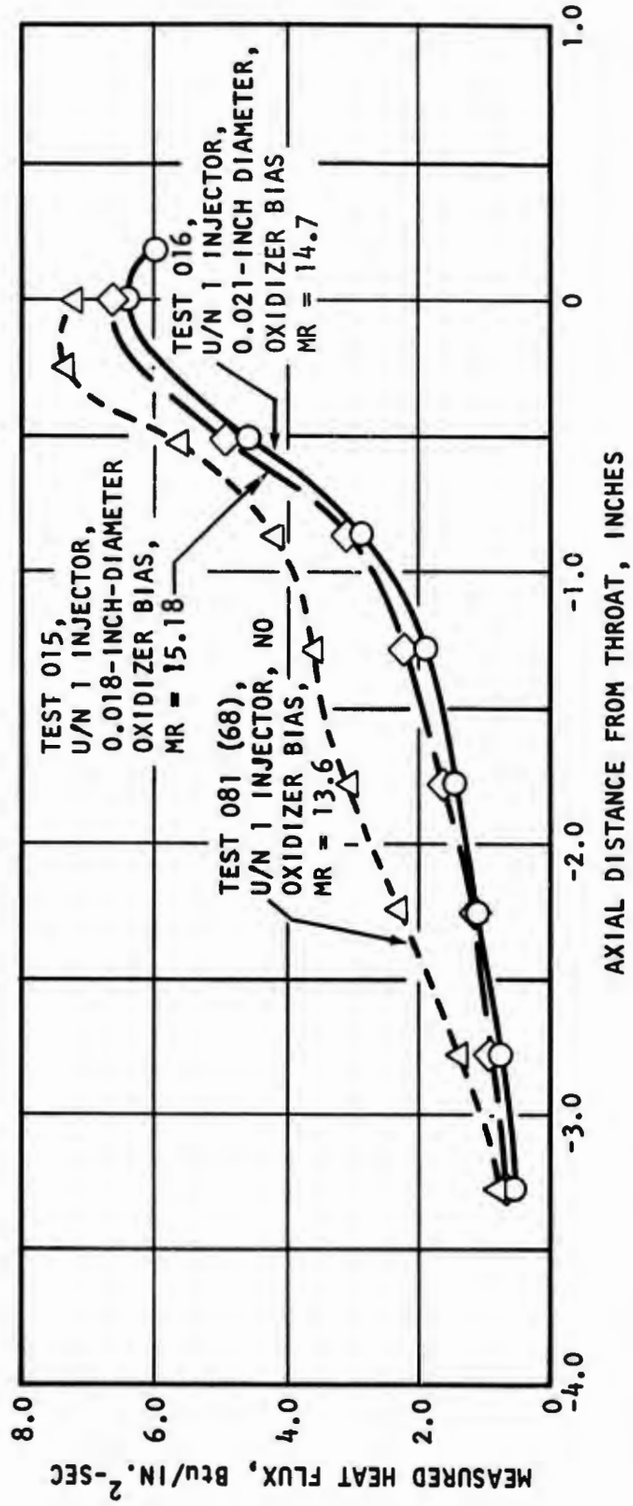

Figure 82. 30-Degree Water-Cooled Segment Heat Flux Profile With and Without Oxidizer Bias (Chamber Pressure = 78 psia) (C)

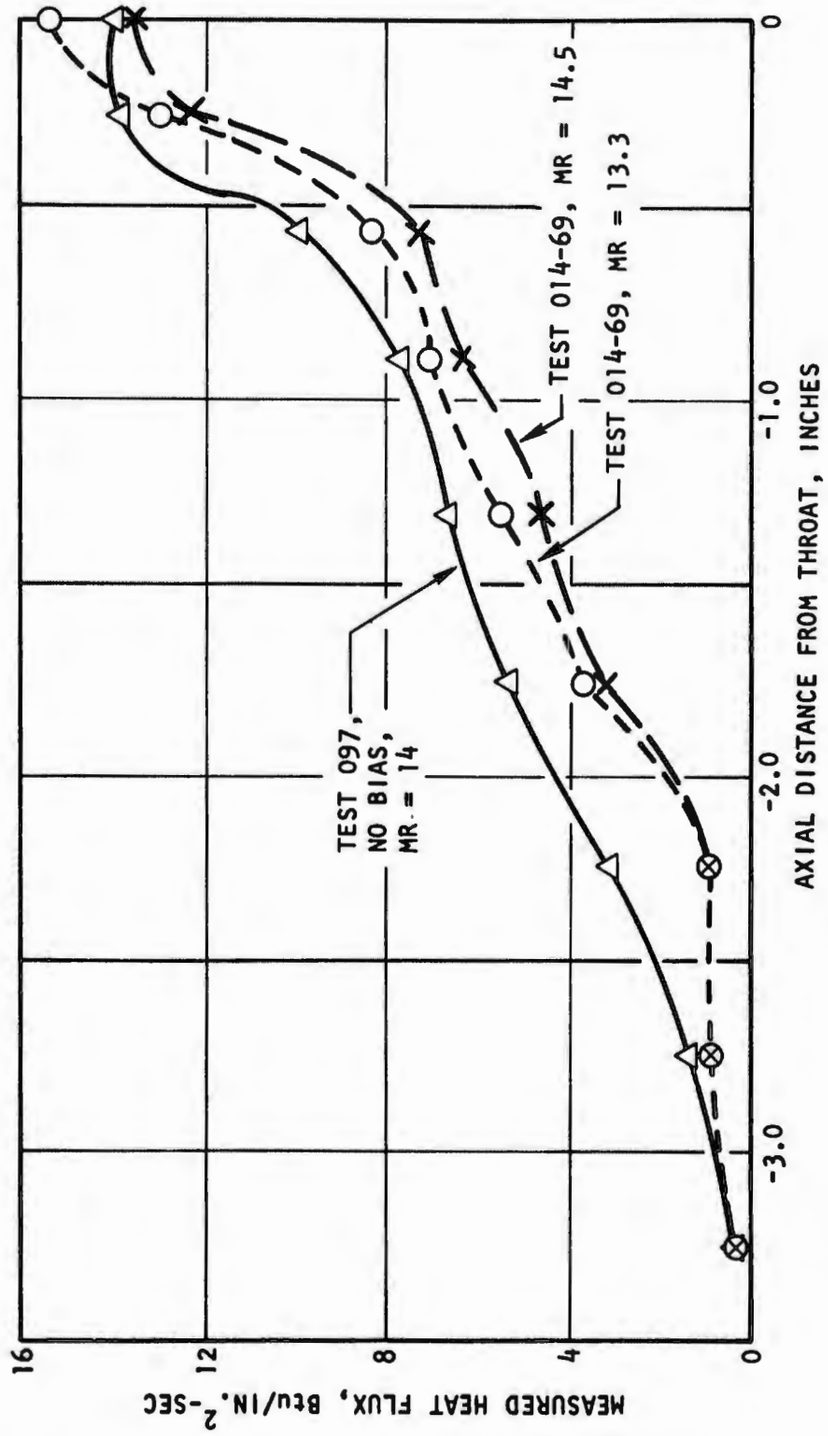

Figure 83. 30-Degree Water-Cooled Segment Heat Transfer Profile With 0.018-Inch Diameter Oxidizer Bias Holes (Chamber Pressure = 220 psia) (C)

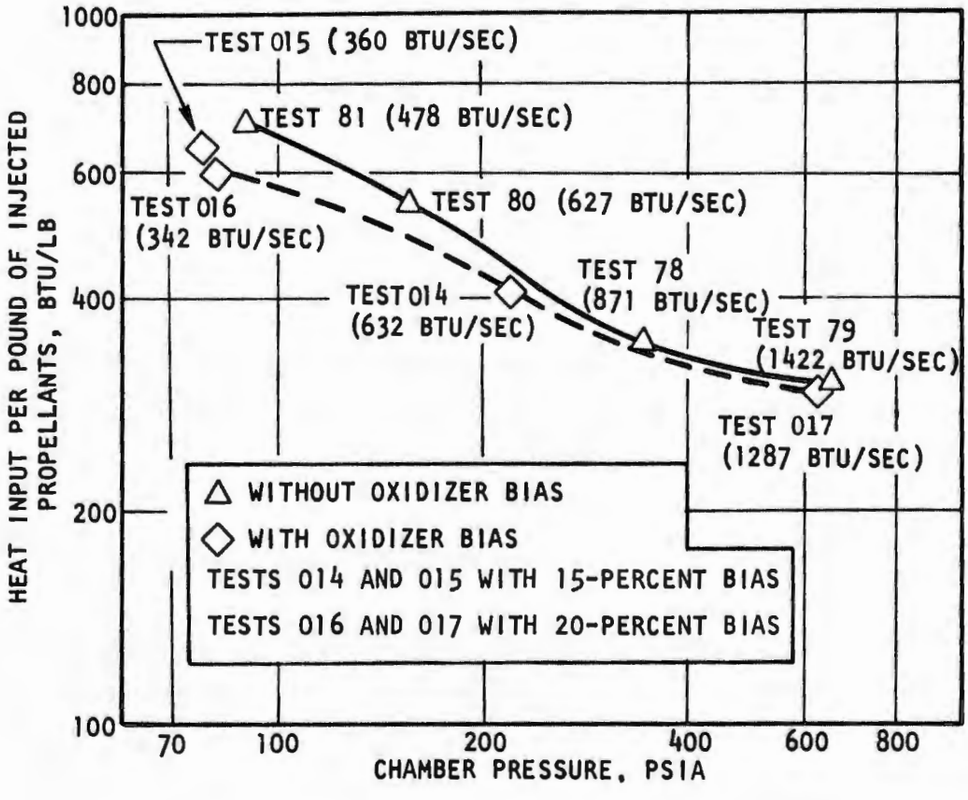

Figure 84. 30-Degree Water-Cooled Segment Heat Rejection Rate With and Without Oxidizer Bias (U)

(3) Combustion Stability Test Evaluation

(U) A combustion stability evaluation was conducted with the 30-degree water-cooled segment thrust chamber and the U/N 3 brazed-face injector which incorporated the oxidizer bias modification. A summary of this test series is provided in Table 11 . The basic requirement of the program was to evaluate the high-frequency (acoustic mode) combustion stability characteristics of the selected segment combustion chamber and injector configuration. Test 021 was a facility checkout test, and tests 022 through 028 were stability evaluation tests.

(C) Pulse guns were used to produce steep-fronted pressure disturbances in the combustion chamber. The targeted overpressure produced by the rating device was to be at least 50 percent of the mean chamber pressure with recovery from the disturbance to occur within 40 milliseconds. For the purpose of the evaluation, recovery time was defined as the elapsed time from initial chamber pressure excursion (due to the pulse) to the time when the chamber pressure oscillations return to the normal operating chamber pressure.

(U) Two basic types of high-frequency instrumentation were used:

1. The oxidizer and fuel injection manifold pressures were monitored by Photocon Type 2307 pressure transducers installed per manufacturer's recommendations to ensure sensitivity in the 0 to 20,000 Hz range.
2. The combustion chamber pressure was monitored with a Kistler-type 614A4 helium bleed pressure transducer installed per the manufacturer's recommendations to ensure sensitivity in the 0 to 20,000 Hz range.

(U) The output of the transducers was recorded on magnetic tape and also on a galvanometer oscillograph for quick posttest evaluation. The directed pulse gun and Kistler transducer locations are shown in Fig. 57, which shows the water-cooled segment thrust chamber used for all combustion stability evaluation tests. While the Kistler and Photocon transducers were commercially available products, the pulse gun assemblies were not, and these were fabricated at Rocketdyne based on Ref. 3 and 4 .

TABLE 11

30-DEGREE WATER-COOLED THRUST CHAMBER SEGMENT COMBUSTION STABILITY TEST SUMMARY (U)

TEST NO.	INJECTOR	DURATION (SEC.)	CHAMBER PRESSURE (PSIA)	INJ. FLOW (LB/SEC)	MIXTURE RATIO	FUEL INJ. TEMP. (°R)	CUTOFF	THROAT HEAT FLUX BTU/IN^2-SEC	INJ. END HEAT FLUX BTU/IN -SEC.	REMARKS
021	U/N 3	3.0	347	2.68	13.84	1242	Obser.	15.45	0.183	Facility Oxid. Main Valve Burned Out - No Pulse
022	U/N 1	5.1	330	2.52	12.76	1305	Prog.	15.40	0.929	184% Overpress. Full Rec. 30 msec.
023	U/N 3	4.8	343	2.69	14.11	1328	Prog.	15.76	0.472	111% Overpress. Full Rec. 30 msec.
024	U/N 3	8.0	72.6	0.606	11.66	1336	Prog.	6.48	0.849	230% Overpress. Full Rec. 3 msec.
025	U/N 3	4.6	213	1.66	12.86	1350	Prog.	12.4	0.794	110% Overpress. Full Rec. 15 msec.
026*	U/N 3	8.6	308	2.37	13.89	1375	Prog.	15.05	0.823	84% Overpress. Full Rec. 20 msec.
027	U/N 3	1.5	217	1.73	13.39	1175	Obser.	11.53	0.961	No Pulse Due to Observed Water Coolant Leak
028	U/N 3	2.0	600	4.38	15.2	1212	Prog.	19.8	0.889	116% Overpress. Full Rec. 25 msec.

* Throttling Transient Test
Pulse Charge - .38/10 gr/7500 psi

CONFIDENTIAL

(C) Test 022 was the first stability evaluation test and was targeted for a chamber pressure of 350 psia and duration of 5 seconds. One pulse gun was used with a 10-grain charge and a 7500-psi burst diaphragm.

(C) All test conditions were satisfactory, and the pulse was initiated immediately prior to cutoff where operation was stabilized. A steep-fronted overpressure of 184 percent was determined from the Kistler transducer that monitored chamber pressure. The system fully recovered in 30 milliseconds. The oscillograph record of the test is shown in Fig. 85, with pertinent items identified.

(C) Test 023 was conducted at a chamber pressure of 343 psia. One pulse gun with a 10-grain charge and a 7500-psi burst diaphragm was used. All test conditions were satisfactory, and the pulse was initiated immediately prior to cutoff during stabilized operation. A steep-fronted overpressure of 111 percent of operating chamber pressure was obtained with a recovery time of 30 milliseconds, as shown in Fig. 85.

(C) Test 024 was targeted for 78-psia chamber pressure. One pulse gun with a 10-grain charge and a 7500-psi burst diaphragm was used. All test conditions were satisfactory, and the pulse was initiated immediately prior to cutoff during stabilized operation. A steep-fronted overpressure of 230 percent of operating chamber pressure was obtained with a recovery time of 3 milliseconds, as shown in Fig. 86. Flame pattern photographs taken during the test are shown in Fig. 87.

(C) Test 025 was targeted for 220-psia chamber pressure. One pulse gun with a 10-grain charge and a 7500-psi burst diaphragm was used. All test conditions were satisfactory, and the pulse produced a steep-fronted overpressure of 110 percent with a recovery time of 15 milliseconds (Fig. 86).

(C) Test 026 was planned to be a transient test. A stable chamber pressure of 350 psia would be established, then chamber pressure was to be increased by simul taneous propellant tank pressurization, with the pulse occurring during the transient phase. The test was satisfactory; however, only a slight transient

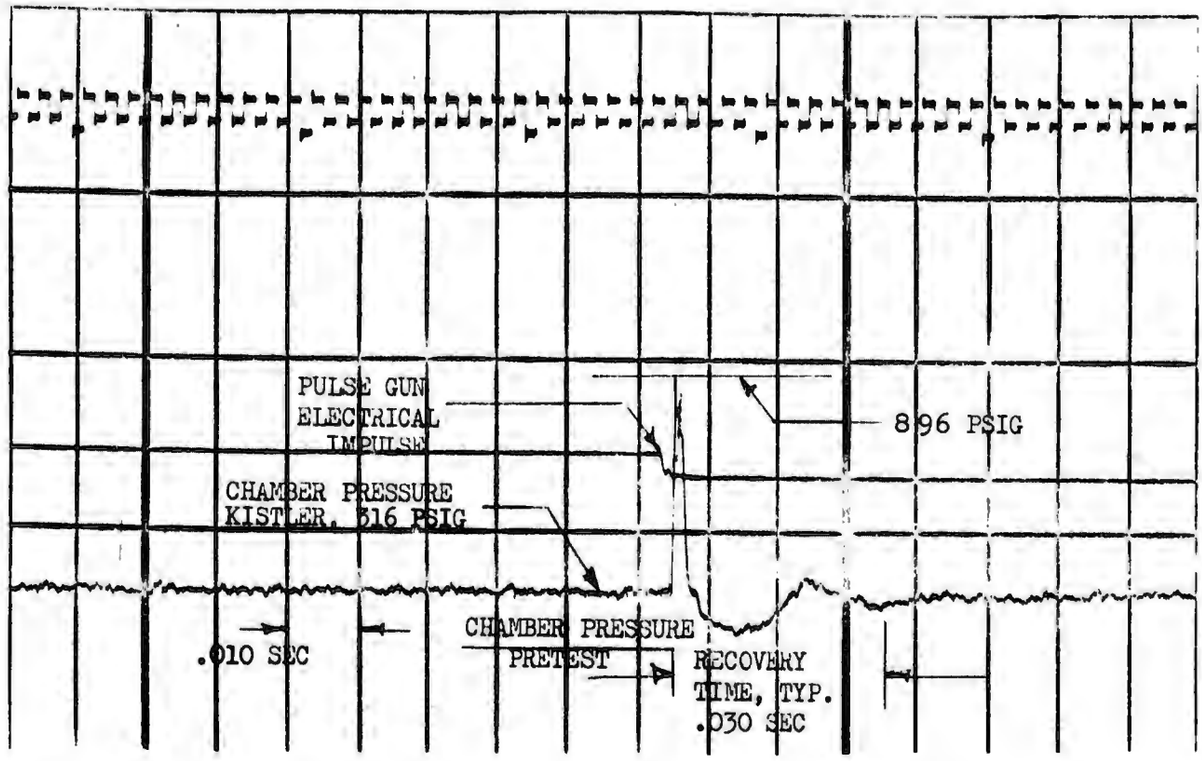

Test No. 022

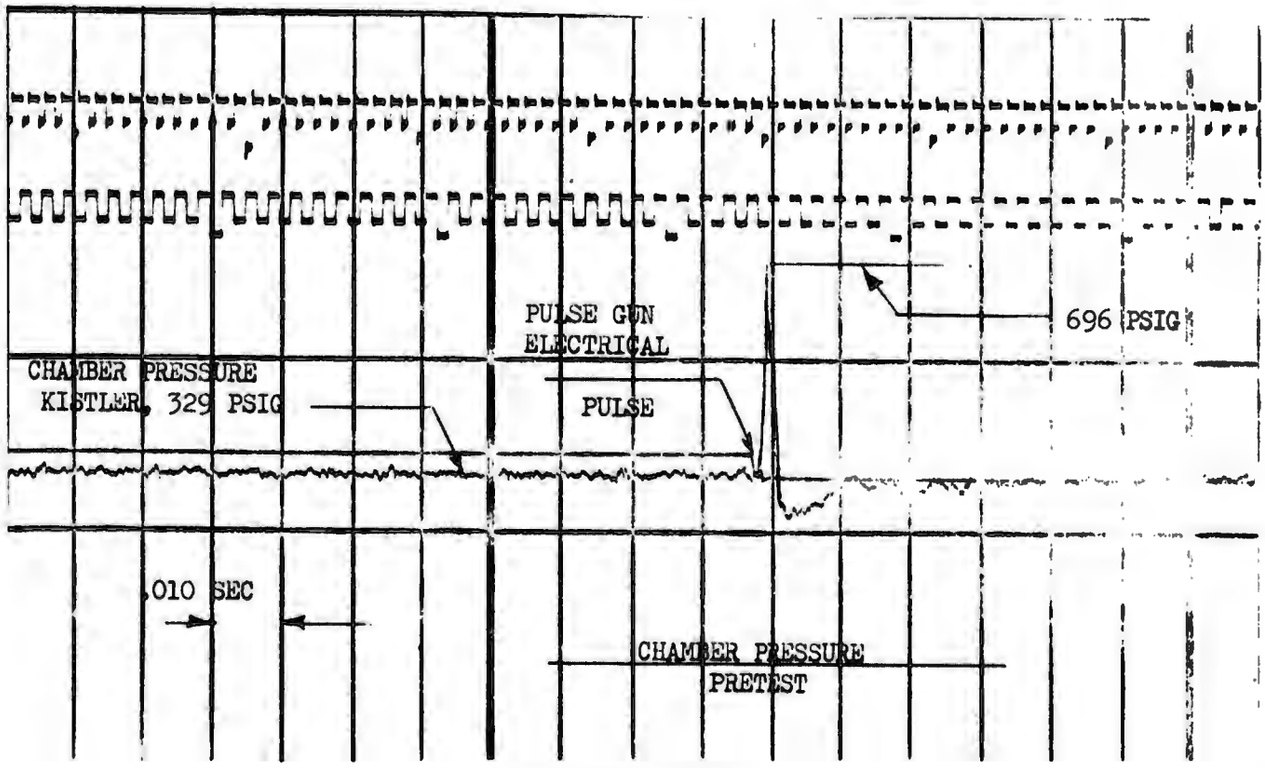

Test No. 023

Figure 85. Stability Evaluation Tests No. 022 and 023 (U)

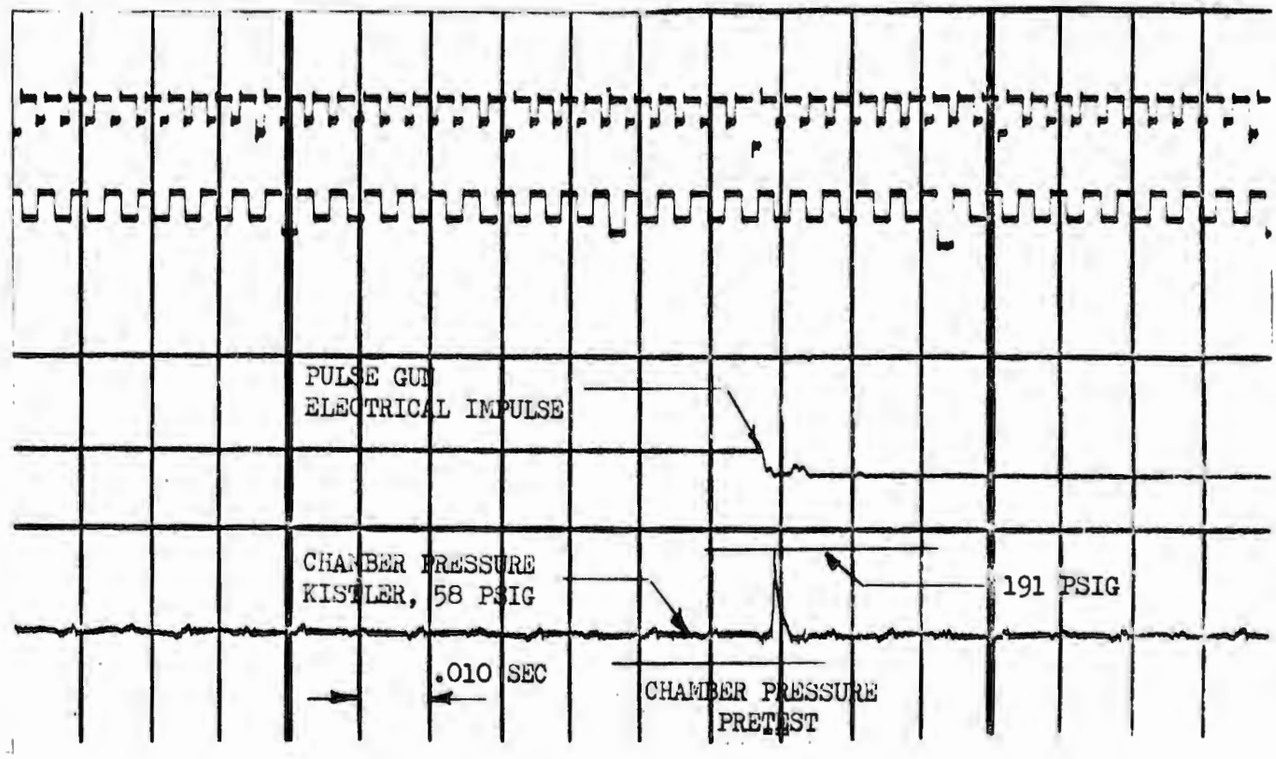

Test No. 024

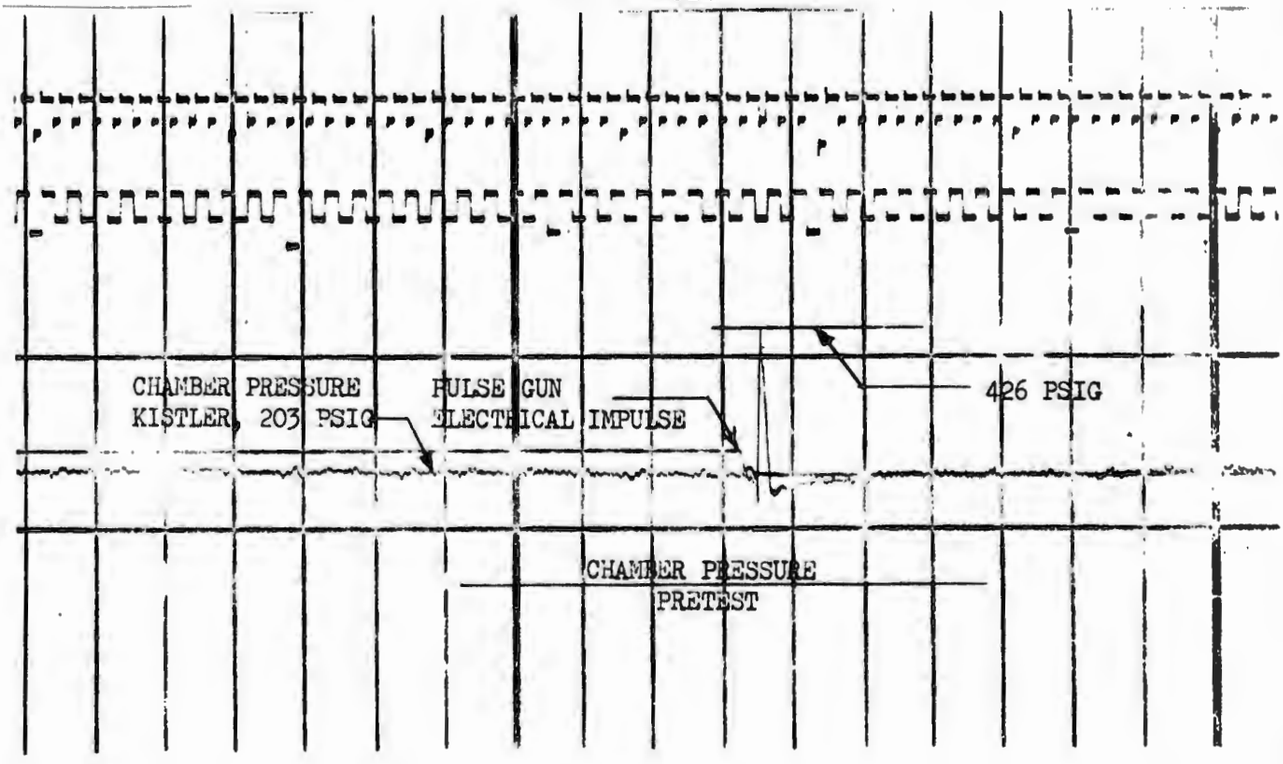

Test No. 025

Figure 86. Stability Evaluation Tests No. 024 and 025 (U)

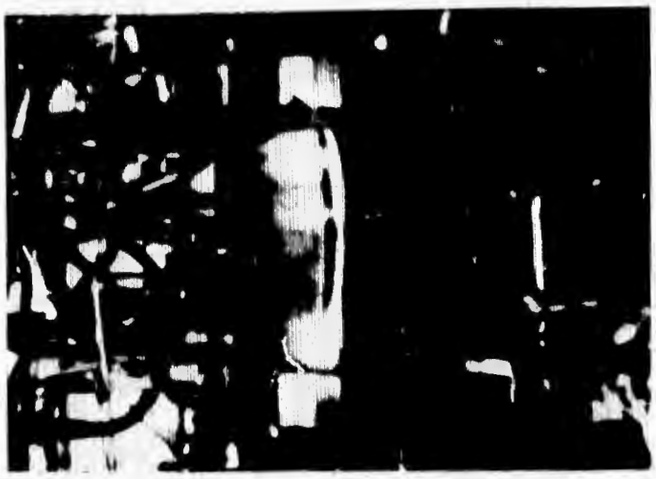

1. 5 msec before pulse

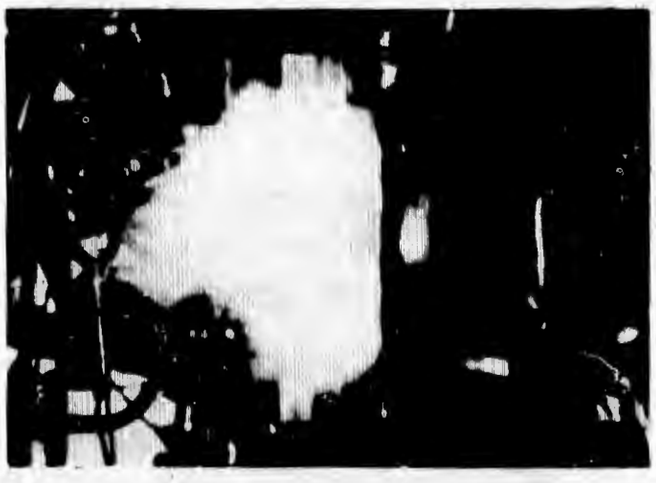

2. At time of pulse

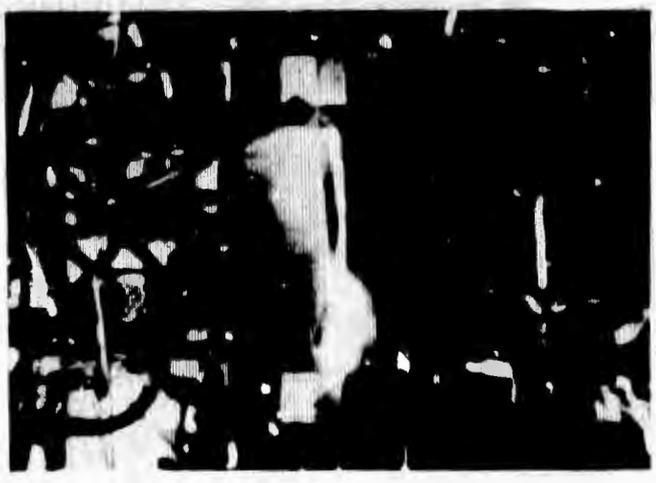

3. 40 msec after pulse

Figure 87. Test 024 Flame Patterns (P_c = 73 psia) (C)

(C) was achieved. An overpressure of 84 percent was obtained with a recovery time of 20 milliseconds (Fig. 88). Flame pattern photographs are presented in Fig. 89.

(C) Test 027 was also planned for transient throttle pulsing. The test was terminated by the test observer prior to pulsing because of a change in exhaust flame color. Posttest inspection revealed water leakage in the upper combustion zone of the thrust chamber. The leakage occurred where the coolant passage wall had been thinned during previous rework. The chamber was removed, repaired, and reinstalled.

(C) Test 028 was targeted for 650-psia chamber pressure (nontransient) with one pulse gun having a 10-grain charge and a 7500-psi burst diaphragm. The pulse resulted in 116-percent overpressure with a recovery time of 25 milliseconds, as shown in Fig. 88.

(U) No further stability evaluation testing was conducted because the 30-degree water-cooled segment thrust chamber had deteriorated due to repeated use, to the point that water leakage was excessive and chamber repair was impractical.

(C) The test results demonstrated the following:

1. The injector-combustion zone configuration exhibited excellent high-frequency combustion stability characteristics when evaluated by the directed pulse gun technique. The recovery time for every pulse was less than the desired 40 milliseconds, by conservative evaluation of the test data.
2. The transient throttling pulse test did not indicate any basic departure from the stability characteristics demonstrated at a stable fixed chamber pressure.
3. The pulse gun, charge, and burst diaphragm configuration was completely satisfactory over the chamber pressure range, and overpressures in excess of 50 percent were obtained on every pulsed test.

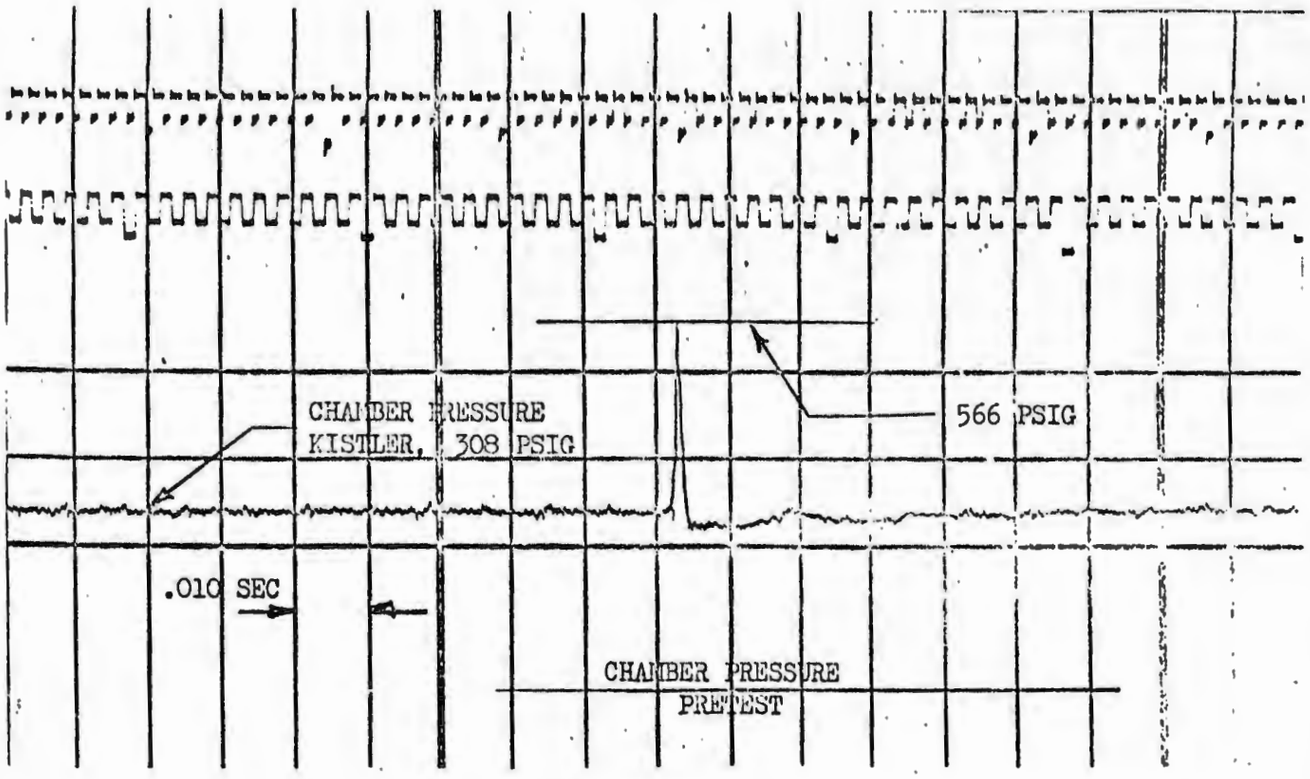

TEST NO. 026

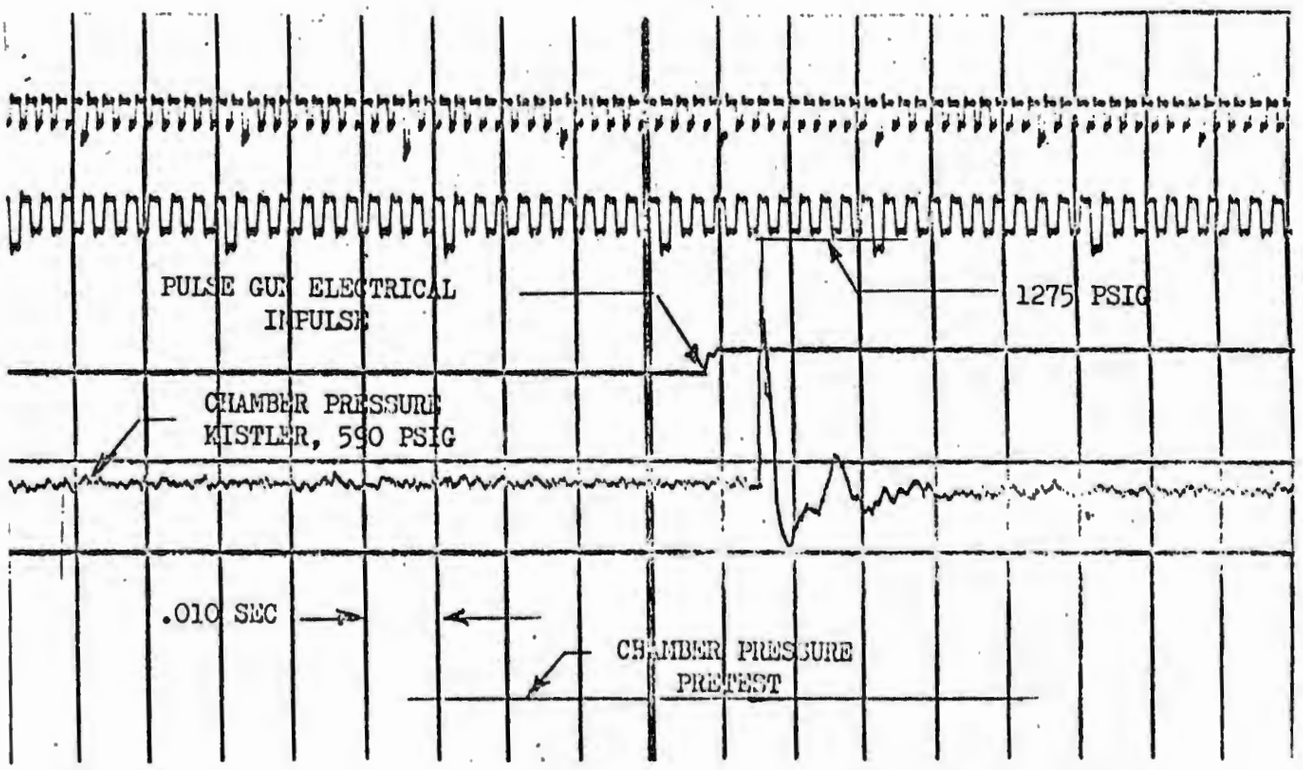

TEST NO. 028

Figure 88. Stability Evaluation Tests No. 026 and 028 (U)

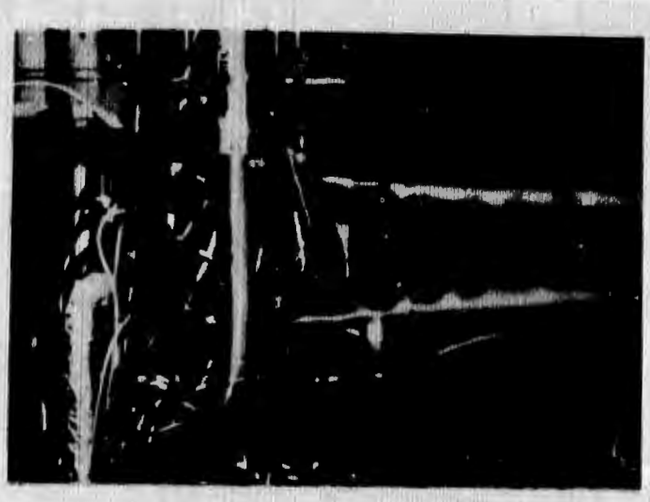

1. 5 msec before pulse

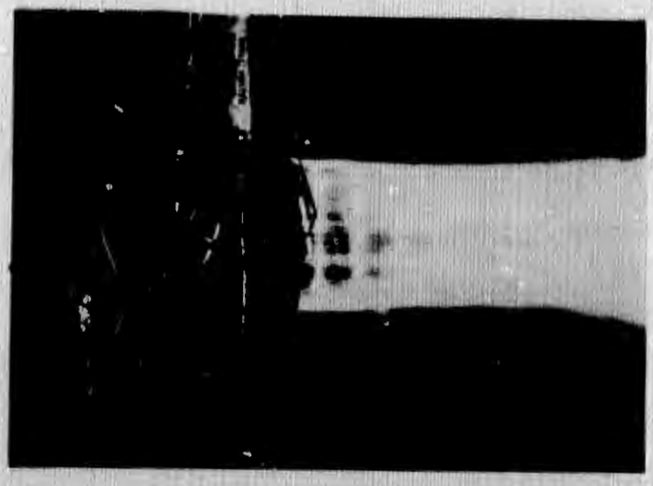

2. At time of pulse

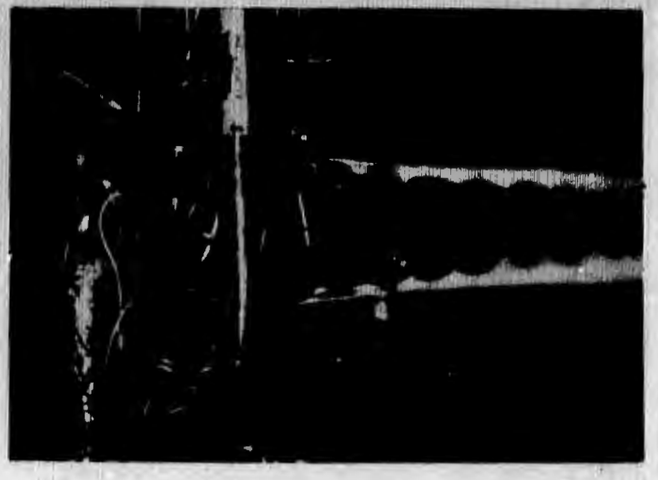

3. 40 msec after pulse

Figure 89. Test 026 Flame Patterns (P_c = 321 psia) (C)

(4) 30-Degree Water-Cooled Thrust Chamber Segment Test Summary

(C) One copper, water-cooled 30-degree chamber segment was fabricated and tested with two versions of the fan injector. The specific results are summarized as follows:

1. The brazed face injector was chosen in preference to the flat integral face injector, which exhibited detrimental heat transfer with respect to the chamber.
2. The total chamber integrated heat rejection rate and local heat transfer rates were defined as required for regeneratively cooled chamber designs and pressure loss predictions.
3. Satisfactory use of injector-provided oxidizer bias was demonstrated. The proper amount of oxidizer bias reduced the total integrated heat rejection rate without affecting the operation, performance, durability, face-cooling ability, or structural integrity of the injector.
4. The combustion stability characteristics of the 30-degree thrust chamber segment assembly were evaluated by the direct pulse (pulse gun) approach, and the injector-combustion zone configuration exhibited excellent high-frequency combustion stability characteristics. The recovery time for every pulse was less than the desired 40 milliseconds.

4. 30-DEGREE TUBE-WALL SEGMENT EVALUATION

(U) Two 30-degree tube-wall segments were designed, fabricated, and tested as an initial evaluation of regenerative cooling with full-size segment hardware. The testing was to provide total integrated heat rejection rates and pressure drop data using hydrogen as the coolant. The segment design was accomplished concurrent with the water-cooled segment test evaluations and, therefore, the coolant circuit design did not reflect the heat transfer data obtained with oxidizer mixture ratio bias.

(U) In the sections that follow, the hardware is first described, followed by a discussion of the testing, analysis, and results obtained.

a. Hardware Design and Fabrication

The segment chamber assembly consisted of four major parts:

Inner body, contoured, regeneratively cooled

Outer body, contoured, regeneratively cooled

Two Side plates, regeneratively cooled

(C) The bodies, inner and outer, consisted of a CRES structural backup to which Nickel 200, 0.017-inch wall thickness tubes were furnace braze attached (Fig. 90). The tubes (shown in Fig. 91) had an ID at the throat of 0.042 inch. The side plates were fabricated of nickel plate into which the coolant passages (channels) were electrical-discharge machined, and the hot-gas closure was electroformed nickel.

(U) The segment chamber assembly was accomplished by furnace brazing the four detail parts together. The injector mating flange was then machined to provide a flat surface and seal grooves. Following completion of machining, the coolant passages, tubes, and manifolds of the assembly were hydrostatic pressure tested to 2500 psig. No significant probelms were encountered during fabrication of the two tubular-wall segments, U/N 1 and U/N 2.

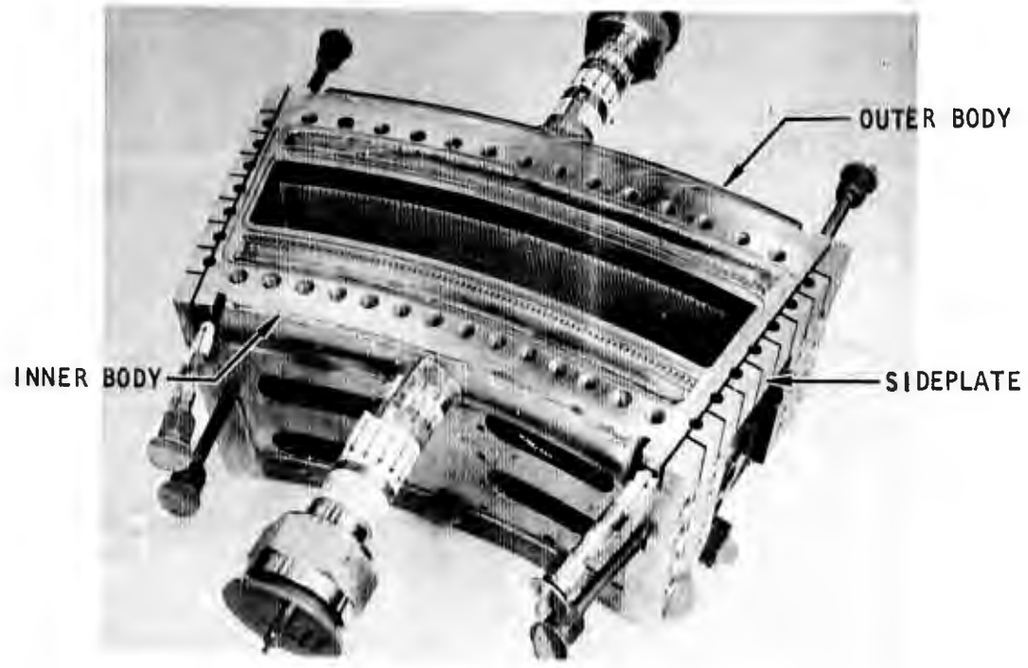

Injector End View

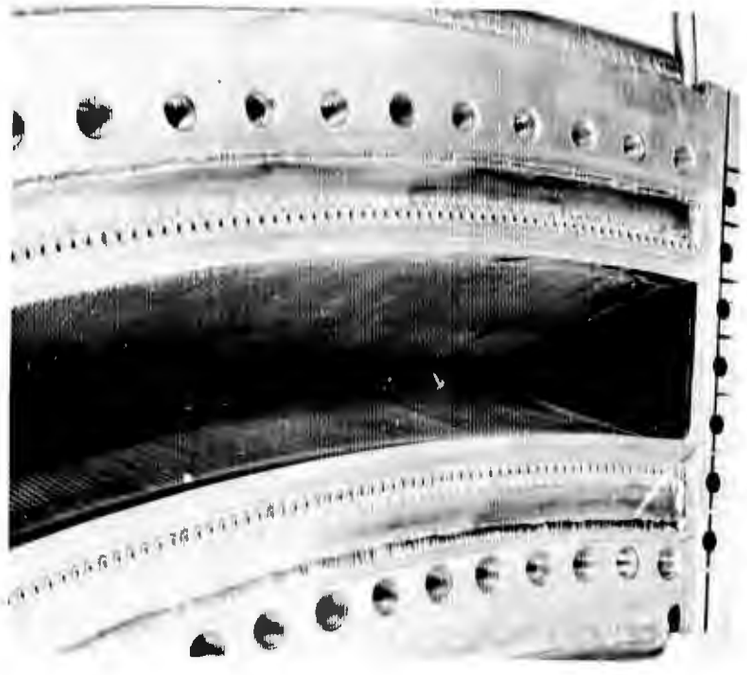

Combustion Chamber View

Figure 90. 30-Degree, Tube-Wall Segment (U)

(U) The inner and outer bodies could be cooled individually (parallel cooling circuit), or one after the other (series cooling circuit). Both techniques were used. The side plates were cooled separately in a parallel flow arrangement. The ability to individually cool any part was provided so that maximum heat transfer data could be obtained. The circuit is shown schematically in Fig. 92.

(U) Each body was designed for two-pass cooling, up and down, while the side plates were designed for single-pass down cooling.

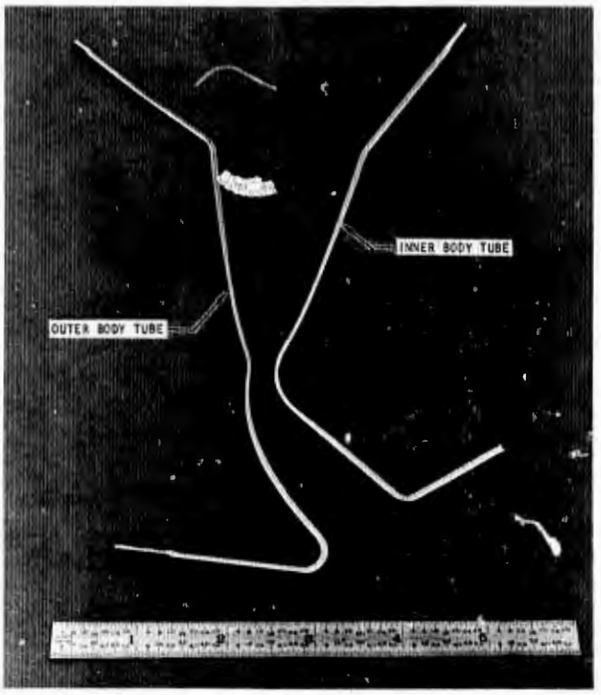

1EH32-4/8/68-C1A

Figure 91. 30-Degree Tubular Wall Thrust Chamber REgenerative Coolant Tubes (U)

b. 30-Degree Tube-Wall Segment Testing and Analysis

(C) Twenty-seven tests were conducted with the U/N 1 tubular-wall 30-degree segment, and one test was conducted with the U/N 2 tubular-wall 30-degree segment to achieve the following objectives: (1) determine the tubular-wall segment coolant enthalpy change at different chamber pressures over the throttling range (coolant enthalpy change also is referred to as a total heat rejection rate or total heat load); (2) determine the pressure loss characteristics of the tubular-wall segment design; (3) evaluate the durability of the tubular-wall segment design during repetitive tests with respect to combustion zone hot streaking, localized tube hot-gas-side surface melting, rippling, or fatigue cracking, and (4) indicate any potential problems peculiar to the segmented thrust chamber design approach in general.

(U) The tests were conducted using brazed face injectors, U/N 1 and 3, which did not have the oxidizer bias modification incorporated. The 30-degree water-cooled segment tests for evaluation of mixture ratio bias had not yet been accomplished at the time the 30-degree tube-wall tests were conducted.

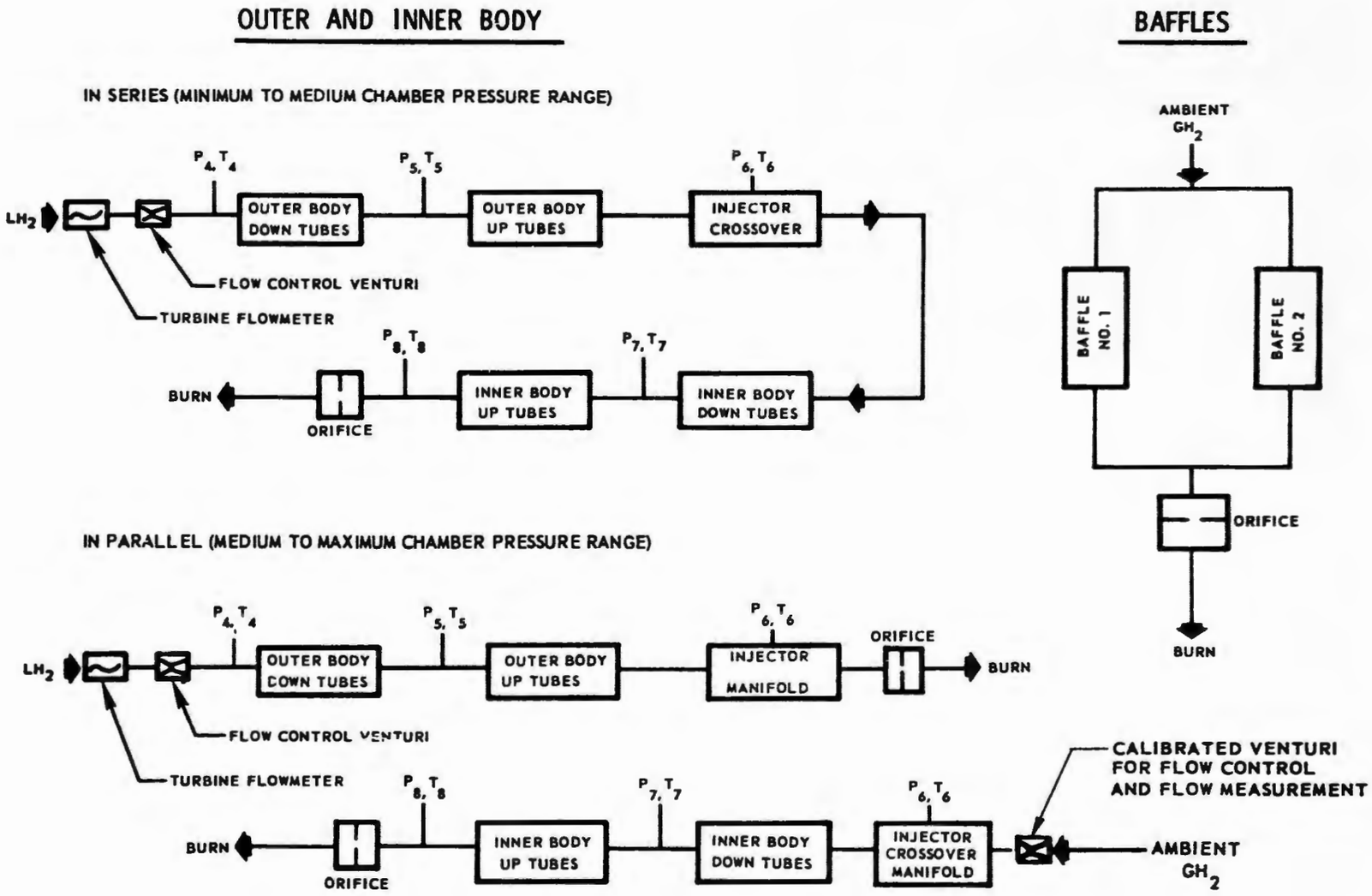

Figure 92. 30-Degree Tubular-Wall Chamber Segment Test Cooling Circuit (U)

(U) The data obtained from the 30-degree, tube-wall tests are shown in Table 12. Coolant flowrates, coolant flowrates, coolant bulk temperatures, and pressures recorded during the test are presented. The testing was accomplished at Victor stand in the Propulsion Research Area at Santa Susana. This was the same facility used for the water-cooled segment testing and is described in Appendix I.

(U) Three types of tube-cooling circuits were used during the testing of the 30-degree tube-wall segments. The circuits consisted of series cooling, reverse series cooling, and a parallel cooling. The series and parallel circuits are shown in Fig. 92. The reverse series circuit was the same as the series circuit, except that the inlets and outlets were reversed and the appropriate adjustments made in the instrumentation. The baffle cooling circuit was the same for all tests and consisted of a parallel flow of ambient gaseous hydrogen (Fig. 92). All coolant hydrogen was burned in facility burner stack after completing the coolant circuit.

(U) The series cooling circuit was used for the initial group of tests, 082 through 096 (except 091) and tests 001 through 008. (Tests 082 through 102 were conducted in 1968, and tests 001 through 008 were conducted in 1969.) The reverse series cooling circuit was used for test 091. Segment operating levels for the tests using the series circuits were in the chamber pressure range of 78 to 350 psia. The parallel cooling circuit was used for tests 098 through 102 for evaluation of operation at chamber pressures between 350 and 650 psia. The parallel cooling circuit was required at the higher chamber pressure levels because of excessive pressure drop with the series cooling circuit.

(C) The original test plan was that series cooling circuits would be used for all tests. However, heat rejection rate and pressure loss data obtained during the initial low chamber pressure range tests (78 to 350 psia) indicated that the facility liquid-hydrogen coolant tank pressure capability (2000 psig) was insufficient to provide the required coolant flowrates for the high chamber pressure range (350 to 650 psia) tests. The test stand coolant system capability was increased by adding an additional ambient gaseous supply system so that a parallel cooling circuit could be used. All the tests were conducted with some degree of

TABLE 12

30-DEGREE TUBE-WALL THRUST CHAMBER SEGMENT TEST SUMMARY (U)

TEST NO.	CHAMBER U/N / INJ. U/N	DUR. (SEC.)	CHAMBER PRESS. (PSIA)	INJ. FLOW (LB/SEC)	MIXTURE RATIO	FUEL INJ. TEMP. (°R)	W COOLANT LB/SEC	% OVER-COOL	ΔH 4-6 BTU/SEC	ΔH 6-8 BTU/SEC	$\frac{P_4}{T_4}$	$\frac{P_5}{T_5}$	$\frac{P_6}{T_6}$	$\frac{P_7}{T_7}$	$\frac{P_8}{T_8}$	ΔH TOTAL BTU/SEC	ΔH 2-BAFFLES BTU/SEC	η_{c^*}
082	1 / 1	1.0	334	2.76	14.4	1216	.295	39	760	404	1773 105	1669 610	1507 804	1180 1098	466 1198	1164	51.75	—
083	1 / 1	4	338	2.67	13.6	1305	.281	31	743	432	1828 80	1731 550	1575 786	1244 1133	543 1248	1175	56.82	97.9
084	1 / 1	8	231.6	1.81	12.5	1431	.309	106	583	361	1774 78	1684 402	1541 584	1226 830	557 918	944	46.92	101.4
085	1 / 1	10	147	1.23	13.4	1309	.264	184	460	264	1434 81	1360 358	1250 536	998 753	453 827	724	34.74	97.2
086	1 / 1	10	90	.716	14.6	1283	.113	98.6	282	117	874 88	837 574	760 755	603 991	263 1056	399	31.70	96.2
087	1 / 1	9.5	156.8	1.217	13.45	1416	.173	75.9	409	247	1205 88	1143 514	1048 715	836 1048	371 1136	656	38.70	100.0
088	1 / 1	15	83.6	.655	13.32	1296	.095	77.6	252	113	861 84	814 603	739 802	584 1088	254 1143	365	32.20	98.4
089	1 / 1	9.5	213.1	1.685	13.2	1435	.196	44.5	489	284	1401 78	1331 533	1218 750	972 1081	435 1174	773	46.38	—
090	1 / 1	2.9	343.7	2.751	14.05	1350	.353	61.7	763	349	2008 87	1897 464	1724 667	1379 862	592 962	1112	56.00	102.1
091 (R)	1 / 1	9.8	227.9	1.785	13.7	1426	.277	89.8	534	426	482 1037	1042 947	1243 479	1352 382	1446 82.5	960	42.40	100.9
092	2 / 1	10	213.5	1.775	13.92	1354	.241	78	581	317	1393 93	1323 606	1211 735	968 1096	404 1117	896	46.62	93.6
093	1 / 1	9.8	235.9	1.799	13.87	1352	.230	55	606	336	1407 79	1336 574	1220 785	980 1109	443 1214	942	46.30	100.8
094	1 / 1	10.2	146.2	1.22	14.09	1363	.220	132	479	276	1218 77	1158 466	1057 652	854 959	386 1022	755	38.92	98.7
095	1 / 1	10.2	147.4	1.22	14.00	1346	.396	350	480	351	1679 71	1586 269	1456 384	1179 555	561 629	831	32.87	101.5
096	1 / 1	10.2	346.1	2.745	14.44	1358	.321	45	800	354	1811 80	1718 534	1563 768	1262 1016	569 1100	1154	57.50	97.8

P_4, T_4 = OUTER BODY INLET MANIFOLD: PRESSURE, TEMPERATURE

P_5, T_5 = OUTER BODY RETURN MANIFOLD· PRESSURE, TEMPERATURE

P_6, T_6 = OUTER BODY DISCHARGE, OR INNER BODY INLET MANIFOLD· PRESSURE, TEMPERATURE

P_7, T_7 = INNER BODY RETURN MANIFOLD; PRESSURE, TEMPERATURE

P_8, T_8 = INNER BODY DISCHARGE MANIFOLD· PRESSURE, TEMPERATURE

P = PSIA

T = DEGREE RANKINE

TESTS 082-090, 092-096 } SERIES COOLANT FLOW

TEST 091 – REVERSED SERIES COOLANT FLOW

CONFIDENTIAL

TABLE 12 (Concluded)

TEST NO.	CHAMBER U/N / INJ. U/N	DUR. (SEC)	CHAMBER PRESS. (PSIA)	INJ. FLOW, LB/SEC	MIXTURE RATIO	FUEL INJ. TEMP. °R	% OVER-COOL O.B.	% OVER-COOL I.B.	ΔH 4-6 BTU/SEC	ΔH 6-8 BTU/SEC	P_4/T_4	P_5/T_5	P_6/T_6 O.B.	P_6/T_6 I.B.	P_7/T_7	P_8/T_8	ΔH TOTAL BTU/SEC	ΔH BAFFLES BTU/SEC	η_{c^*}
097	SOLID WALL / 3			SOLID WALL INJECTOR CHECKOUT TEST															
098	1 / 3	10	335.9	2.678	13.99	1462	119	59	762	430*	1334 73	1144 364	797 494	1528 530	1091 826	468 936	1192*	58.19	100.5
099	1 / 3	6	439.1	3.511	14.02	1428	64	37	834	510*	1524 73.5	1308 402	904 542	1720 517	1233 823	514 955	1344*	79.39	100.2
100	1 / 3	3.7	512.7	4.113	14.39	1388	36	40	875	580	1481 73	1268 513	933 585	2101 518	1450 758	639 879	1455	83.3	100.2
101	1 / 3	3.7	646.9	5.147	14.29	1455	45	14	1080	708.9	1919 76	1648 460	1128 544	2128 509	1521 816	654 942	1789	96.5	101.2
102	1 / 3	3.7	650.0	5.195	13.19	1368	9	14	1234	754.9	1668 73	1435 596	1017 802	2134 508	1503 830	659 965	1988	100.1	99.4
001	1 / 1	14.8	84.9	0.684	12.94	1322	207		392	189	902 86	849 549	741 696		640 957	213 1022	581	20.9	98.8
002	1 / 1	14.8	86.0	0.678	12.38	1362	152		338	175	824 80	776 643	679 805		588 1123	196 1172	513	24.4	98.6
003	1 / 1	9.2	84.8	0.650	13.57	1331	118		337	139	727 87	683 747	593 883		511 1194	165 1232	476	24.1	98.3
004	1 / 1	10.7	84.2	0.650	14.07	1346	77		305	122	633 87	590 886	510 964		442 1325	133 1332	427	23.8	98.0
005	1 / 1	11.2	91.5	0.674	14.03	1323	65		320	132	646 91	605 931	524 1006		450 1364	138 1388	452	24.65	103.2
006	1 / 1	11	91.9	0.670	14.03	1323	36		299	118	569 91	523 1120	458 1127		394 1537	114 1550	417	27.65	101.9
007	1 / 1	6.0	328.5	2.681	14.16	1458	17		722	334	1513 90	1425 706	1241 877		1106 1200	437 1223	1021	39.03	98.4
008	1 / 1	6.0	332.0	2.686	14.35	1362	7		690	280	1403 83	1319 761	1136 893		1002 1252	388 1253	970	38.16	101.1

P_4, T_4 = OUTER BODY INLET MANIFOLD; PRESSURE, TEMPERATURE

P_5, T_5 = OUTER BODY RETURN MANIFOLD; PRESSURE, TEMPERATURE

P_6, T_6 = OUTER BODY DISCHARGE, OR INNER BODY INLET

P_7, T_7 = INNER BODY RETURN MANIFOLD: PRESSURE, TEMPERATURE

P_8, T_8 = INNER BODY DISCHARGE MANIFOLD; PRESSURE, TEMPERATURE

P = PSIA

T = °R

TESTS 001-69 THROUGH 009-69 - SERIES COOLANT FLOW

TESTS 098 THROUGH 102 - PARALLEL COOLANT FLOW

*CORRECTED FOR INNER BODY COOLANT FLOW TO OUTER BODY OUTLET

overcooling to provide protection for the segment until the heat transfer data could be obtained and the chamber parameters (h_g, ΔH distribution, etc.) defined. The use of overcooling increased the total heat rejection rate because of the greater driving potential (adiabatic wall temperature minus tube gas-side wall temperature, i.e., $T_{aw}-T_{wg}$) from decreased tube gas-side wall temperatures.

(1) Heat Transfer Analysis

(U) The enthalpy change of the coolant that occurred during each test (Table 12) was determined by use of measured temperatures and pressures and interpolation of enthalpies from thermodynamic property charts.

(U) The measured total enthalpy change in the coolant, as determined from the minimum overcooling tests, is presented as a function of chamber pressure in Fig. 93. The heat rejection rate includes the baffle heat load.

(U) Figure 94 presents the heat rejection rate normalized by division by the injector flowrate (Btu-sec/lbm-sec) as a function of chamber pressure. This figure compares the 30-degree tube-wall heat rejection rate with the heat rejection rate determined for the 30-degree water-cooled segment (integral injector and brazed-face injectors), and the contour G solid-wall segment from the previous program (Ref. 1). As may be noted in Fig. 94, the total measured heat inputs for the 30-degree tube-wall segment were significantly greater than for the 30-degree water-cooled segment using the same injector.

(U) The measured heat rejection rate of the two baffles as a function of chamber pressure is presented in Fig. 95. Both baffles for each assembly are included. [redacted]alpy change was normalized by dividing the enthalpy change by the injector total flowrate.

(C) The data indicated that the enthalpy change in the coolant was not linear with respect to chamber pressure (i.e., $\Delta H \quad (P_c)^n$), where $n < 1.0$ and n also varied as a function of chamber pressure (Fig. 94). The variation of the exponent (n) with chamber pressure results in a turbine inlet temperature variation and fuel

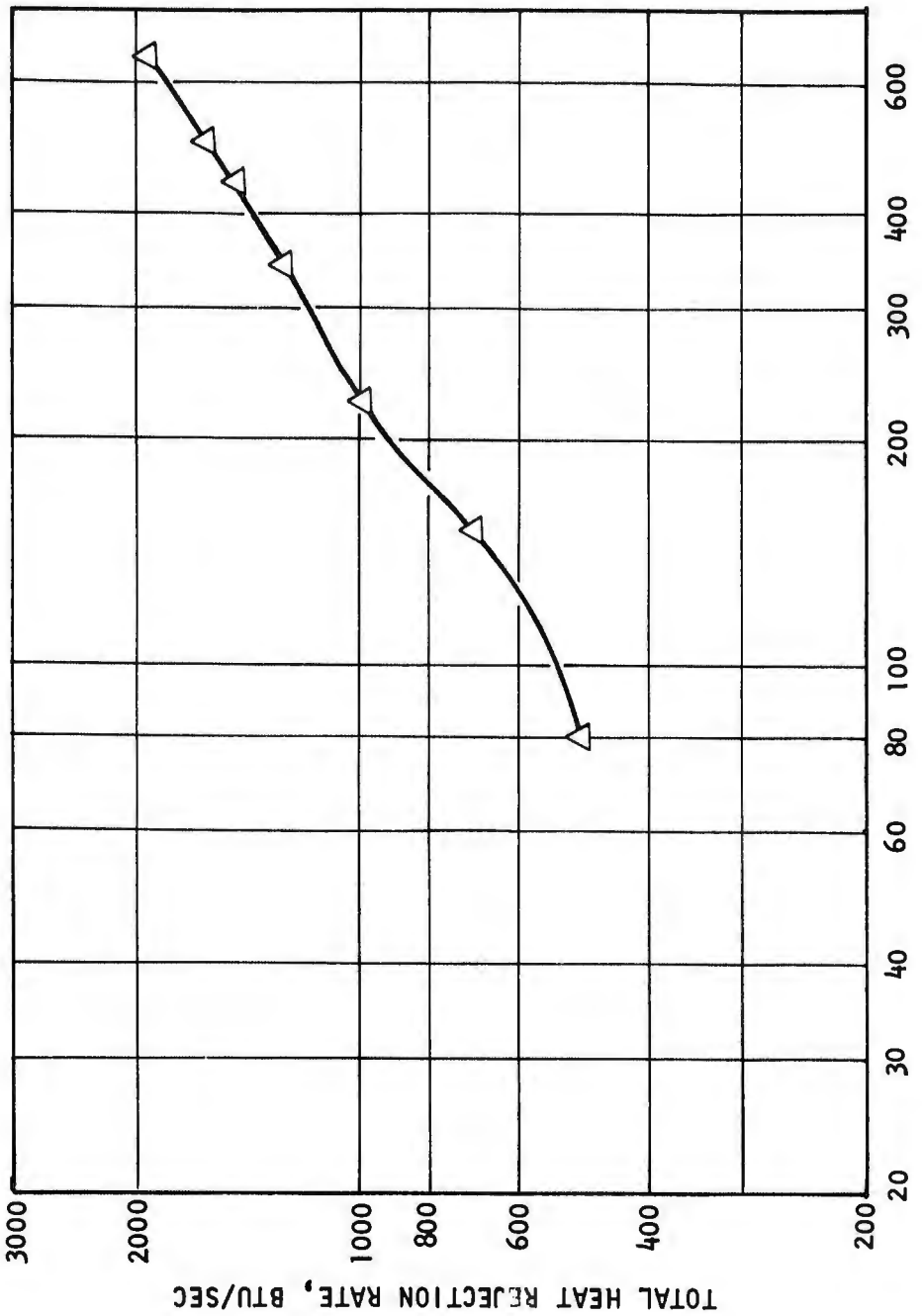

Figure 93. Total Heat Rejection Rate Versus Chamber Pressure (Baffles Included), 30-Degree Tube-Wall Segment (U)

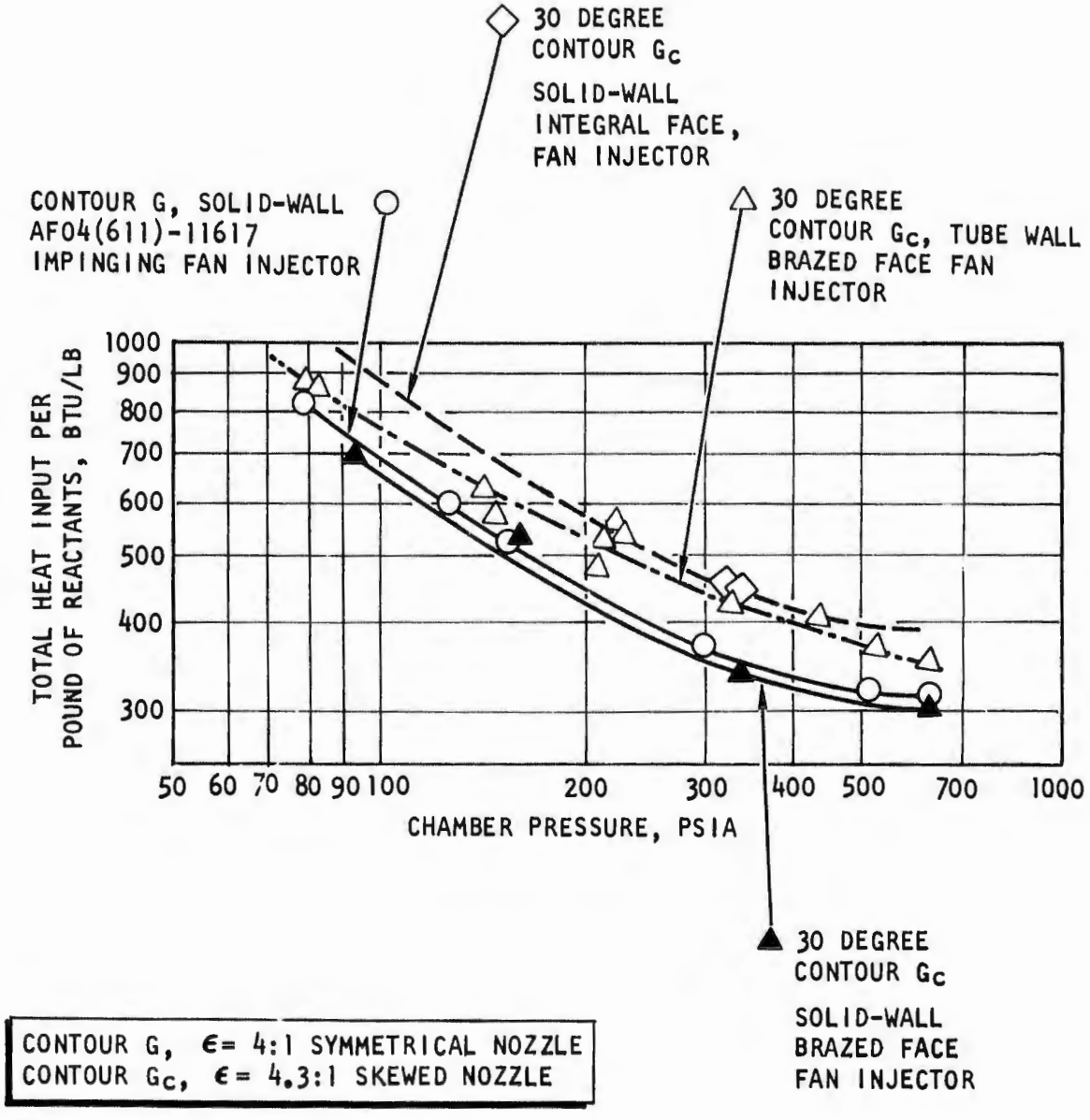

Figure 94. Comparison of Total Heat Input to Coolant (Including Baffles) Per Pound of Injected Reactants (U)

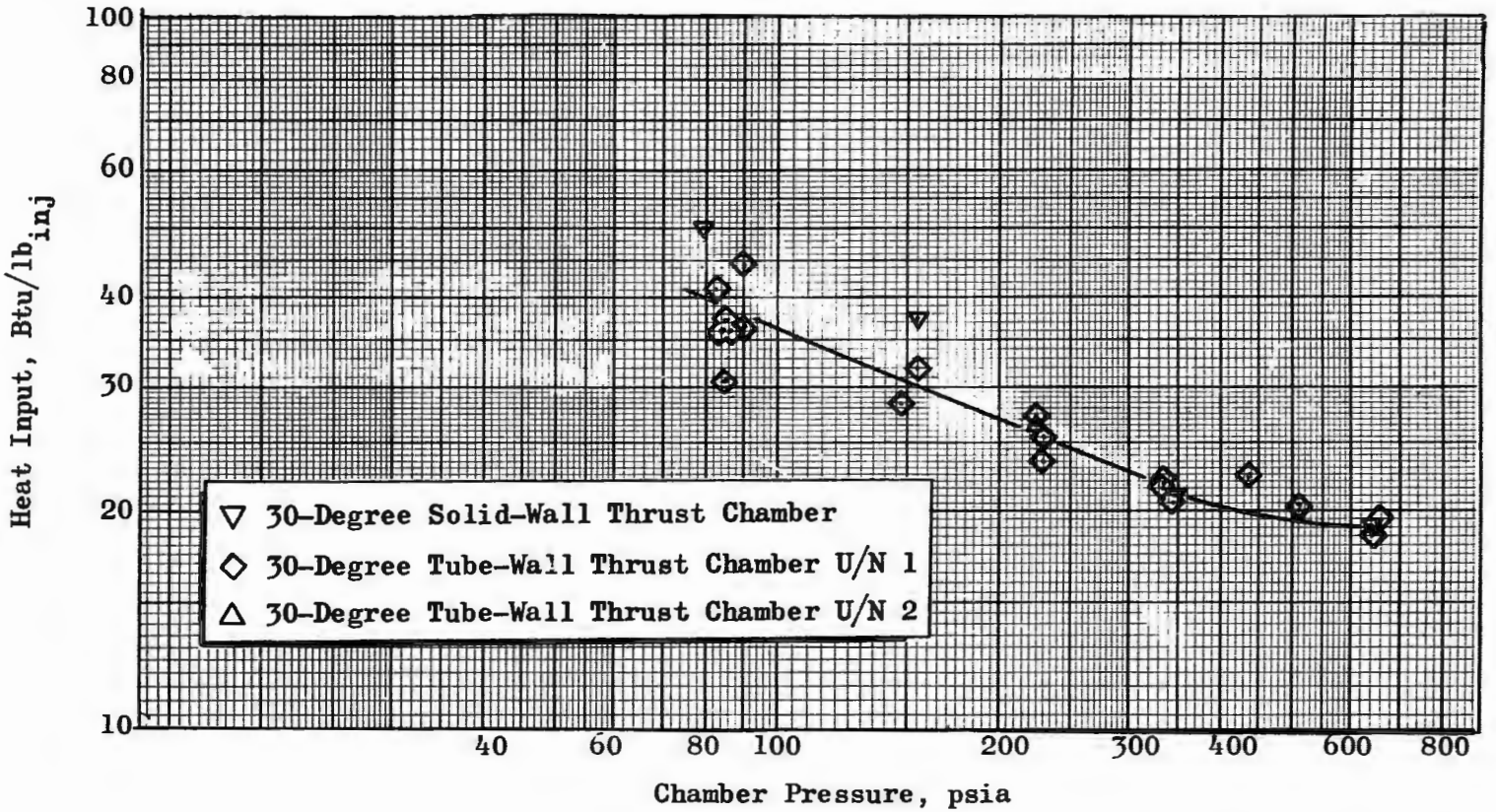

Figure 95. Heat Input to Baffles Versus Chamber Pressure (U)

(C) injection temperature will increase with decreasing chamber pressure. To maintain these temperatures constant over the throttle range may be desirable for engine operation; however, increased fuel injection velocity (which occurs with increased fuel injection temperature at low chamber pressures) can be instrumental in minimizing upper combustion zone heat loads. Increasing fluid temperatures with decreasing operating pressures does not severely penalize the systems from a structural standpoint. However, the data indicate that the injection temperature at chamber pressures below 150 psia in this chamber/injection combination would be in excess of 1500 R and, consequently, would reduce the effectiveness of the coolant in maintaining acceptable tube-wall temperatures.

(C) Figure 96 presents a comparison of the coolant enthalpy change experienced during 30-degree water-cooled solid-wall and 30-degree tube-wall thrust chamber tests. The analysis used in separating the inner and outer body heat loads for the solid-wall chamber segment was presented previously. Although the hot-gas side-wall contours were the same for the solid-wall and tube-wall segments, there was a significant difference in heat rejection rate between the two segments. As observed in Fig. 96, the tube-wall segment coolant enthalpy increase was greater than the solid wall at all chamber pressure levels.

(U) Several mechanisms have been proposed to explain the apparent difference in total heat rejection rate between the solid-wall and tube-wall segment. These mechanisms could affect several of the parameters in the heat rejection rate relationship, i.e.,

$$Q = h_g A_s (T_{aw} - T_{wg})$$

where

Q = total heat load, Btu/sec

A_s = surface area, sq in.

T_{aw} = adiabatic wall temperatures, R

T_{wg} = hot-wall surface temperature, R

h_g = gas film convective heat transfer coefficient, Btu/in.^{2}-sec-R

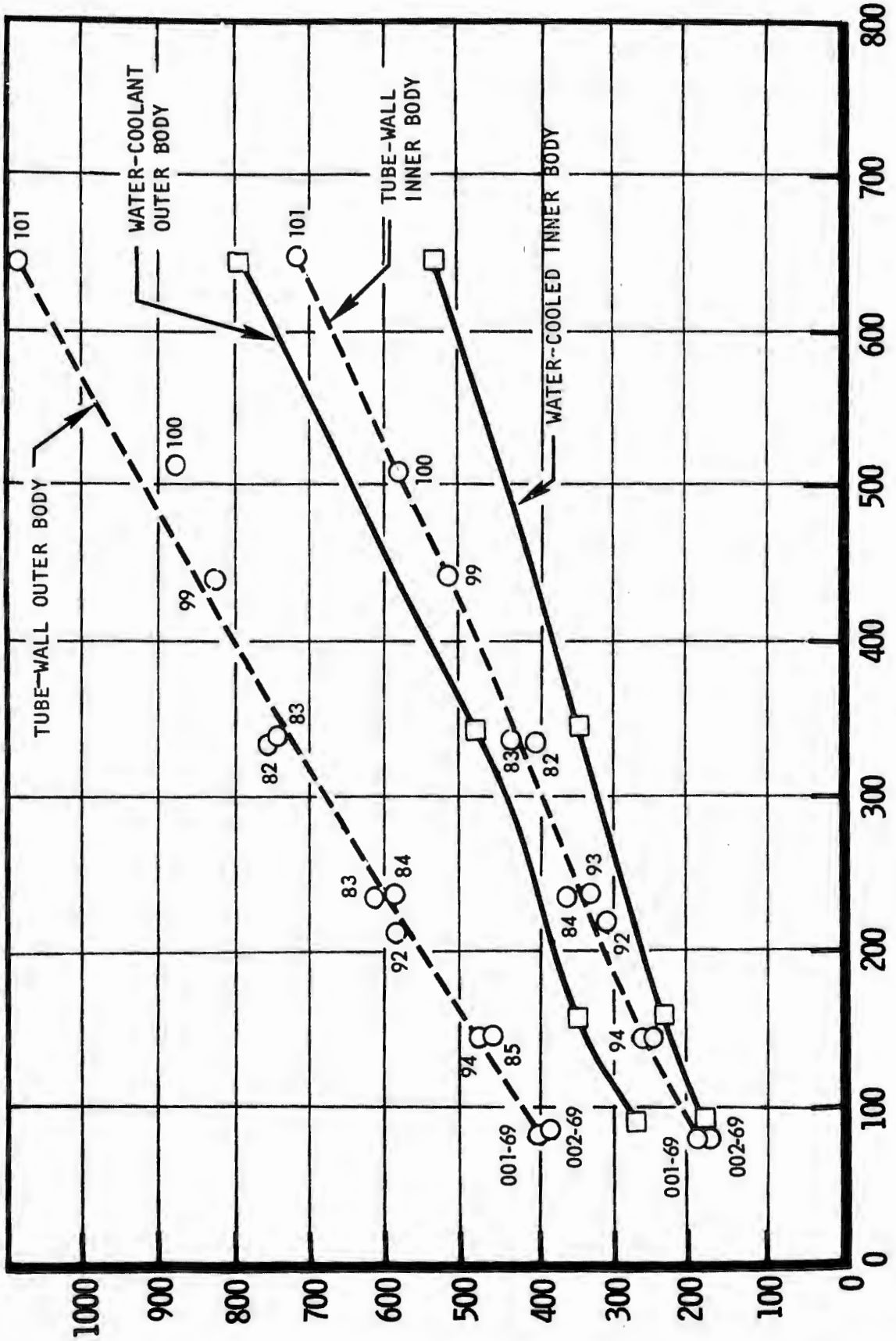

Figure 96. Comparison of Solid-Wall and Tube-Wall Heat Load vs Chamber Pressure (U)

(C) The first possible mechanism arises from the fact that the surface area (A_s) for the tube wall is greater than the solid wall. This difference is caused by the individual curved surface of each tube in the tubular-wall segment which is not present in the solid-wall segment. The magnitude of this geometrical difference has been estimated to be $A_{s_{\text{tube-wall segment}}} = 1.25\ A_{s_{\text{solid-wall segment}}}$. This estimate was made on the basis of measuring the surface area of a tube-wall imprint in a putty cast and comparing it to a flat surface with the same projected area.

(C) Because of possible unknown variation in the hot-gas-side convective film coefficient in the wetted perimeter of one tube, the 25-percent increase in area is not known to be synonomous with a 25-percent increase in total load.

(U) As indicated from Fig. 96, the geometrical A_s difference is significant, although a quantitative conclusion can be obtained only when two cryogenic cooled segments are compared. In this case, the tube-wall segment was cryogenically cooled and the solid-wall segment was water cooled.

(U) The second consideration that may provide the mechanism for the tube-to-solid-wall heat load discrepancy is that of "cold-wall effect." This effect can be illustrated simply by comparing the heat load for a wall whose gas-side wall temperature (T_{wg}) is 1100 R (cold wall), as opposed to a wall whose temperature is 1800 R (hot wall). Using the relationship $Q = h_g\ A_s\ (T_{aw}-T_{wg})$, it can be shown that:

$$Q_{\text{hot wall}} = 0.9014\ Q_{\text{cold wall}}$$

if it is assumed that $(h_g\ A_s\ T_{aw})_{\text{cold wall}} = (h_g\ A_s\ T_{aw})_{\text{hot wall}}$.

(C) The cold-wall effect is a decrease in T_{wg} (as a result of overcooling) and resultant increase in the value of $(T_{aw}-T_{wg})$, or it could be caused partly by nonoptimum tube design, both of which would result in gas-side wall temperatures being lower than the rated value (e.g., 1100 rather than 1800 R) and, consequently, a higher total heat rejection to the coolant.

(U) In addition, the lowered gas-side wall temperature results in lowered boundary layer temperatures, which tend to enhance chemical recombination in the boundary layer with resultant higher local heat fluxes.

(C) One test (091) was conducted to evaluate and demonstrate the cold-wall effect. This test was accomplished by using the reversed series-cooling circuit, thereby introducing cryogenic hydrogen into the inner body instead of the 500 to 800 R hydrogen that had previously cooled this body. This test is compared to other tube-wall tests in Fig. 97. A 33-percent increase in total Q for the inner body can be deduced from this figure as a result of the cryogenic propellant.

(C) The third mechanism affecting the tube-wall to water-cooled data was considered to be differences in the local heat flux, q/A, of the water-cooled and tube-wall segments. This difference was caused by the gas-side film convective heat transfer coefficient. The h_g in the tubular-wall segment was expected to be of the same magnitude as that in the water-cooled segment at any given local station and chamber pressure level. The basic premise upon which the tubular-wall segment coolant tube design was based was to obtain h_g's from calorimetry chamber tests and use them as tube design program input.

(C) The tubular-wall segment heat load data indicate that the local film coefficients, h_g, are larger than those of the water-cooled segment. Factors that evidently caused a difference in h_g for the two segments (solid wall versus tube wall) included relative surface roughness, a flat surface of the solid-wall segment as opposed to the rippled profile of the tube-wall segment, and the cold-wall effect in the case of the tube-wall segment.

(C) Another comparison of interest specifically pertaining to the tube-wall design is the comparison of heat loads on the individual bodies and their individual passes (up and down). The significance of these data lies in the strong effect of gas-side heat transfer coefficient and coolant bulk temperature on the tube-wall temperature levels. Table 13 presents the heat load of the inner and outer body and each cooling pass for the three tests. There are large differences in the individual passes. As shown in Table 14, a significantly higher percentage

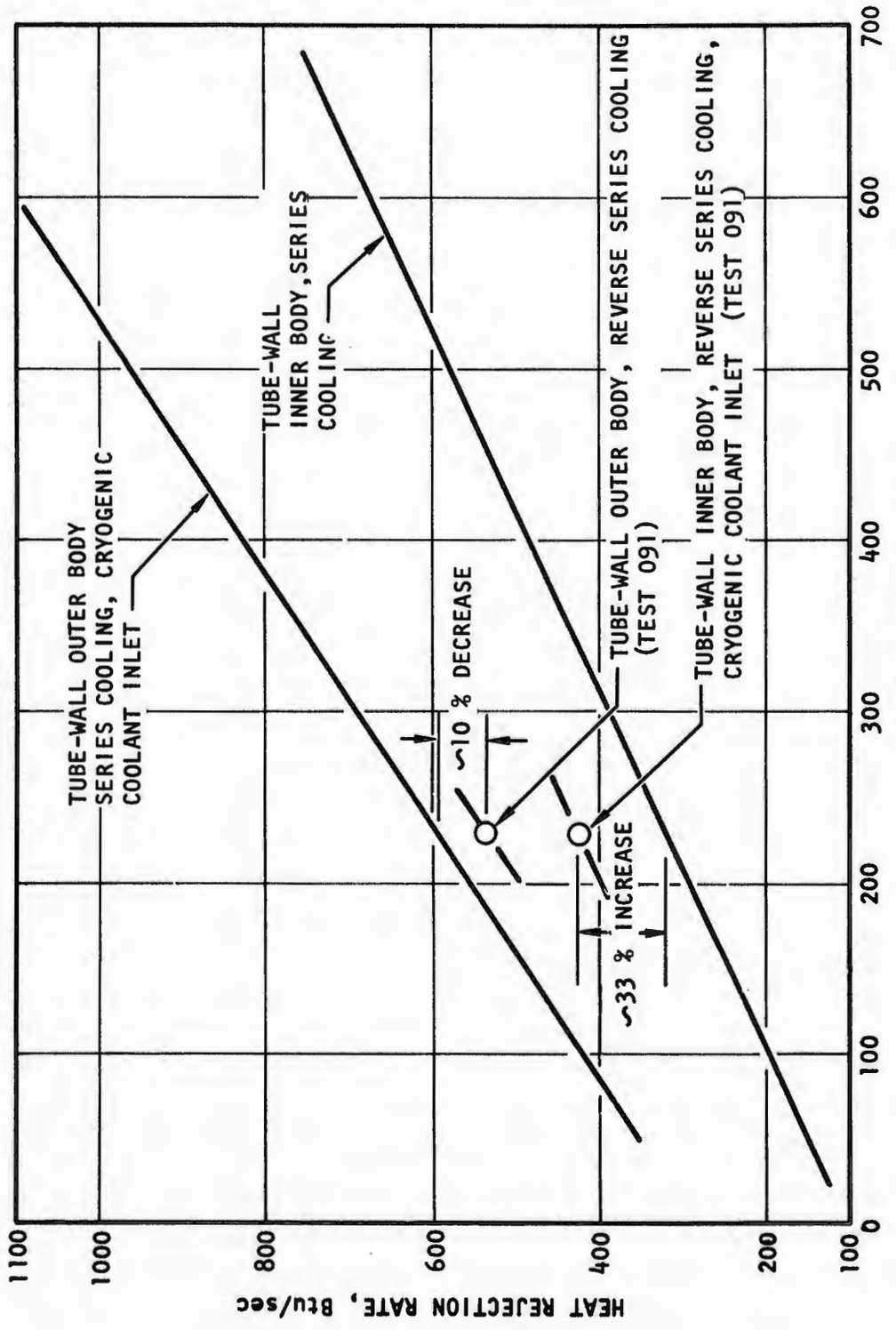

Figure 97. Demonstration of Cold-Wall Effect on Heat Rejection Rate, 30-Degree Tube-Wall Segment (U)

TABLE 13

30-DEGREE, TUBE-WALL THRUST CHAMBER SEGMENT
HEAT LOADS (U)

Test	Chamber Pressure, psia	Heat Loads, Btu/sec						Overall Total
		Outer Body Flow Pass			Inner Body Flow Pass			
		Down	Up	Total	Down	Up	Total	
083	338	504	239	743	332	100	432	1175
084	236	390	193	583	264	97	361	944
085	147	285	175	460	178	60	264	724

CONFIDENTIAL

TABLE 14

30-DEGREE, TUBE-WALL THRUST CHAMBER SEGMENT
HEAT LOAD DISTRIBUTION (U)

Test	Percent of Total Heat to Bodies		Percent of Body Heat to Individual Passes			
	Outer	Inner	Outer Down	Outer Up	Inner Down	Inner Up
083	63.2	36.8	68	32	76.7	23.3
084	61.8	39.2	66.8	33.2	73.2	26.8
085	63.5	36.5	62	38	75	25

CONFIDENTIAL

(C) of the heat load entered the outer body than the inner body. In addition, the down passes on both bodies picked up significantly more heat than the up passes.

(C) For comparison purposes with the water-cooled segment test data, test 078, performed at 340 psia on the 30-degree water-cooled thrust chamber segment, was compared with test 083 (tube-wall test). Comparisons of heat loads on the inner and outer bodies and the resultant influence on gas-side heat transfer coefficients were made.

(C) Recalling that, in the solid-wall thrust chamber there were three separate circuits for cooling, the first one cooled all the area upstream of the throat, and the remaining two cooled the inner and outer bodies aft of the throat. The water-cooled data were analyzed by considering that the gas-side heat transfer coefficients in the region upstream of the throat were identical on both bodies. The data for test 078 are shown in Table 15 and compared with that obtained from test 083.

(C) Although the total area exposed (area enhancement) to the hot gas is greater for the tube wall (because of the tube-to-tube crown effect) than that of the solid wall, the relationship between body-to-body area is the same for both configurations and, therefore, the heat load ratio between inner and outer bodies should be the same for the solid wall as that of the tube wall. Consequently, the ratios of the tube wall-to-solid wall heat loads on both bodies were considered to be caused, in part, to different gas-side heat transfer coefficients.

(C) Assuming that the water-cooled segment had the same body-to-body heat load distribution as that of the tube-wall segment, the heat to the water-cooled outer body was 63.2 percent (743/1175 x 100) of the total, or 516 Btu/sec (816 x 0.632). Thus, the heat load to the outer body forward of the throat is 288 Btu/sec (516 to 228). The remainder of the heat forward of the throat (194 Btu/sec) goes to the inner body. Thus, the gas-side heat transfer coefficients, based on water-cooled tests, would be altered in their use for tube-wall analysis by the following ratios in the subsonic portion of the thrust chamber.

TABLE 15

COMPARISON OF SOLID-WALL AND TUBE-WALL HEAT LOADS AT 340 PSIA (C)

Location	Heat Loads, Btu/sec		Solid-Wall Distribution Corrected to Tube-Wall Distribution	Ratio, Tube Wall to Solid Wall
	Solid Wall (Test 078)	Tube Wall (Test 083)		
Outer Body, Injector to Throat	245	--	288	--
Outer Body, Supersonic Region	228	--	228	--
Outer Body, Total	473	743	516	1.57
Inner Body, Injector to Throat	237	--	194	--
Inner Body, Supersonic Region	106	--	106	--
Inner Body, Total	343	432	300	1.26

(C) h_g (outer body); $\frac{288}{245}$ or 1.17 h_g (inner body), $\frac{194}{237}$ or 0.82

(C) The resultant area enhancement due to the shape of the tubes is the ratio of the total heat load or: area enhancement due to the tube shape = $\frac{1175}{816}$ = 1.43.

(C) This value is reasonable because the value is less than the maximum value possible for a tube-wall thrust chamber, which is the ratio of one-half the tube circumference to tube diameter, or 1.57 times greater than the solid-wall surface area.

(U) An apparent unequal distribution of inner- and outer-body tube-to-tube heat transfer was indicated as shown in Table 15. The tube heat transfer condition is illustrated in Fig. 98. Heat was assumed to be added both from the gas side (independent of fluid and wall temperature) and between the up-pass and down-pass fluid (proportional to fluid temperature difference). The details of the heat balances for the up- and down-tubes are shown in Fig. 99 .

(U) The solution to the tube-to-tube heat transfer analysis was based on the following assumptions:

1. Fluid has a constant heat capacity
2. Steady flow
3. Hot-gas heat addition is independent of coolant state and location
4. Up to down fluid heat transfer is proportional to the up to down fluid temperature difference
5. The up to down fluid heat transfer is described by a constant effective overall coefficient

(U) The results of the calculation are shown in Fig. 100 where local bulk temperatures relative to body inlet and body exit bulk temperature in dimensionless form along the length of the passage is plotted.

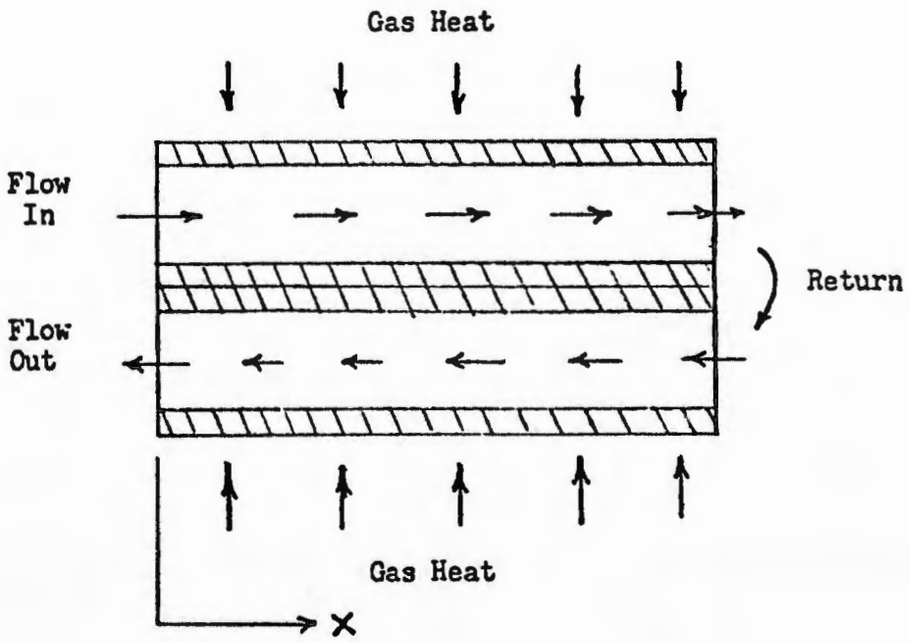

Figure 98. Tube Model Used to Estimate Up to Down Tube Heat Transfer (U)

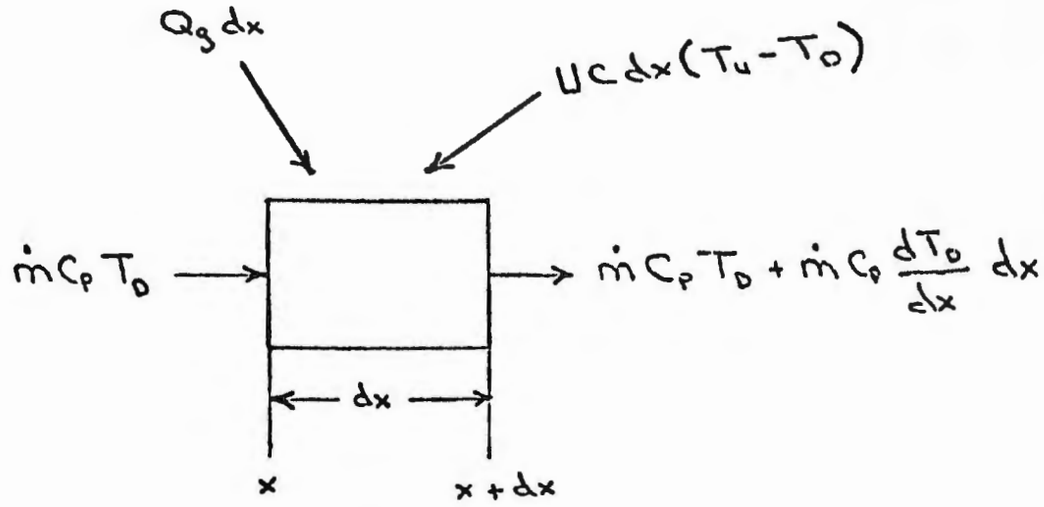

a. Down Tube Heat Balance

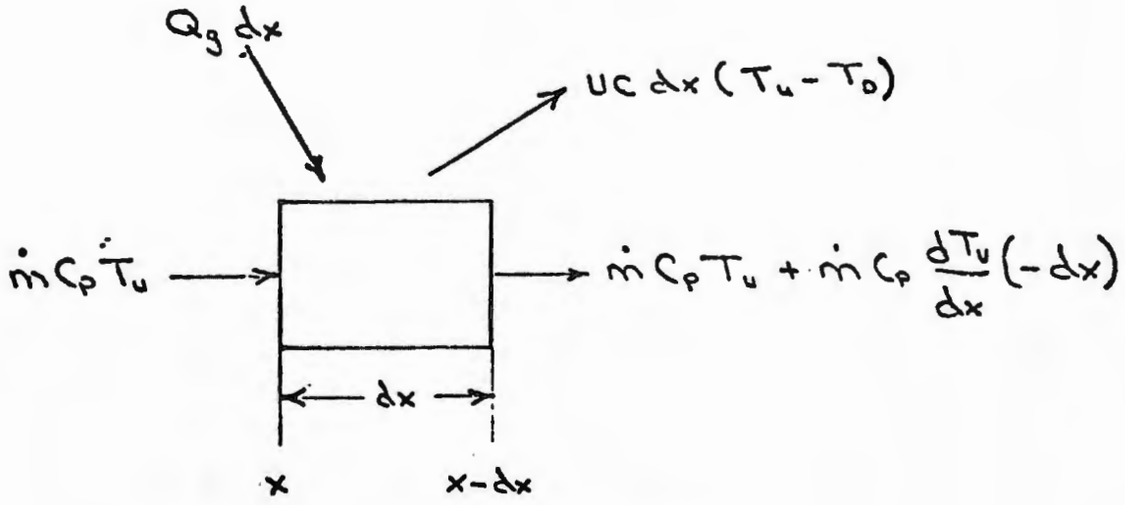

b. Up Tube Heat Balance

NOMENCLATURE

T = temperature	Q_g = gas-side heat rate per unit length
$\dot{m}$ = flowrate	
C_p = specific heat at constant pressure	Subscripts
U = tube-to-tube heat transfer coefficient	D = down
C = tube-to-tube contact height	U = up
X = distance	In = inlet
L = developed length of the tubes	Out = exit

Figure 99. Up to Down Tube Heat Transfer (U)

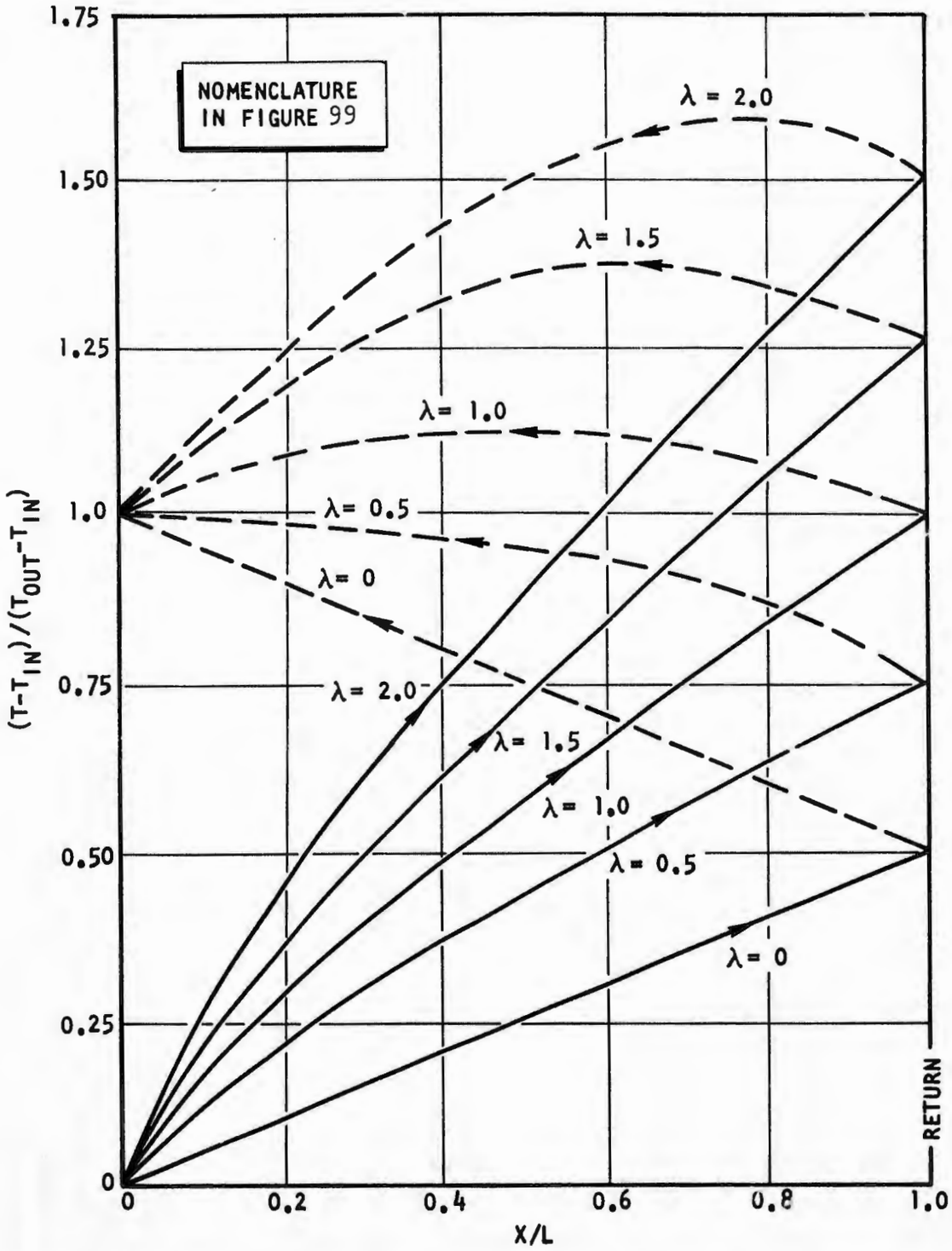

Figure 100. Dimensionless Bulk Temperature Profile in Tubes Based on Simplified Analysis of Tube-to-Tube Heat Transfer (U)

(U) The parameter (λ) used in the plot is defined as the ratio of tube-to-tube conductance to fluid internal conductance for a single interface. Because each tube in any direction is adjacent to two tubes in the opposite direction, a single interface will pertain to half the flow per tube. Thus, the parameter definition is best written as:

$$\lambda = \frac{UCL}{\dot{m}/2\ C_p}$$

and, on the basis of the total chamber flow,

$$\lambda = \frac{2\ UCLN}{\dot{m}_T\ C_p}$$

where N = number of tubes (the other nomenclature is defined in Fig. 99).

(C) Based on the results shown in Table 14 for test 083, the down-pass fractions of total heat load for the outer and inner body, respectively, are:

Outer Body, $\frac{Q_T}{Q_{OB}} = 0.68$

Inner Body, $\frac{Q_T}{Q_{IB}} = 0.767$

Q_T = total heat load

Q_{OB} = heat load of outer body

Q_{IB} = heat load of inner body

(C) The corresponding values of the parameter (λ) were computed to be:

λ (Outer Body) = 0.38

λ (Inner Body) = 0.52

(C) Based on these data, a value for the effective tube-to-tube contact height, C, was estimated because it was virtually unknown in an analysis of this type. The estimate was dependent on conditions within the tubes. For this analysis, a location of 0.6 inch upstream of the throat was chosen to estimate tube-to-tube

(C) effective heat transfer coefficients. Using the flowrates from test 083, the values obtained were (including resistance of up and down films as well as wall thermal resistance):

$$\text{Outer Body Coefficient, U} = 0.0058 \frac{\text{Btu}}{\text{in.}^2\text{-sec-F}}$$

$$\text{Outer Body Coefficient, U} = 0.0082 \frac{\text{Btu}}{\text{in.}^2\text{-sec-F}}$$

(C) The following other parameters were used:

Developed Length of Tubes (L), inches	= 6.8
Total Flowrate ($\dot{m}_T$), lb/sec	= 0.281
Heat Capacity at Constant Pressure (C_p), Btu/lb-F	= 3.5
Number of Tubes (N)	= 150

Values of tube-to-tube contact height (effective) were calculated from the λ equations as follows:

C (Outer Body) = 0.0317 inch

C (Inner Body) = 0.0306 inch

(U) The results of this calculation show a reasonable dimension in terms of the size of the tubes and a significant consistency between the inner and outer bodies. The actual contact height may be more, but the presence of braze alloy and tube-to-tube variations make this parameter difficult to estimate on a purely theoretical basis.

(C) The effect of the tube-to-tube temperature is of significant benefit in the outer body when consideration is given to wall temperatures, because the bulk temperature of the coolant is in a range where warmer fluid benefits the cooling capability. Unfortunately, the inner-body effects will be detrimental because

(C) coolant temperature and wall temperatures move in similar directions at the higher bulk temperatures. Pressure drop is similarly increased by warmer fluid and, therefore, less dense (higher velocity) fluid exists in the tubes over a greater length.

(U) To further investigate the effect of two-dimensional heat flow on the hot-gas side-wall temperature of the tubular wall thrust chamber, a 31-region model (Fig. 101) was used. Regions 15 and 31 of the model simulated the braze filler in in adjacent downpass and uppass tubes. Nickel tubes were used in the analysis. The gas-side heat transfer coefficient profile in Fig. 102 was assumed.

(U) In this analysis, the one-dimensional tube-wall temperature was assumed, the gas-side film coefficient (h_g) and coolant bulk temperatures were established from the test data for the particular chamber pressure, and the coolant-side film coefficient (h_c) was computed from the following equation.

$$h_c = \frac{1}{\frac{(T_{aw} - T_B)}{h_g\,(T_{aw} - T_{wg})} - \left(\frac{\Delta X}{k} + \frac{1}{h_g}\right)}$$

where

h_c = coolant side film coefficient

T_{aw} = adiabatic wall temperature

T_B = coolant bulk temperature

h_g = gas-side film coefficient

T_{wg} = gas side wall temperature

ΔX = wall thickness

k = wall thermal conductivity

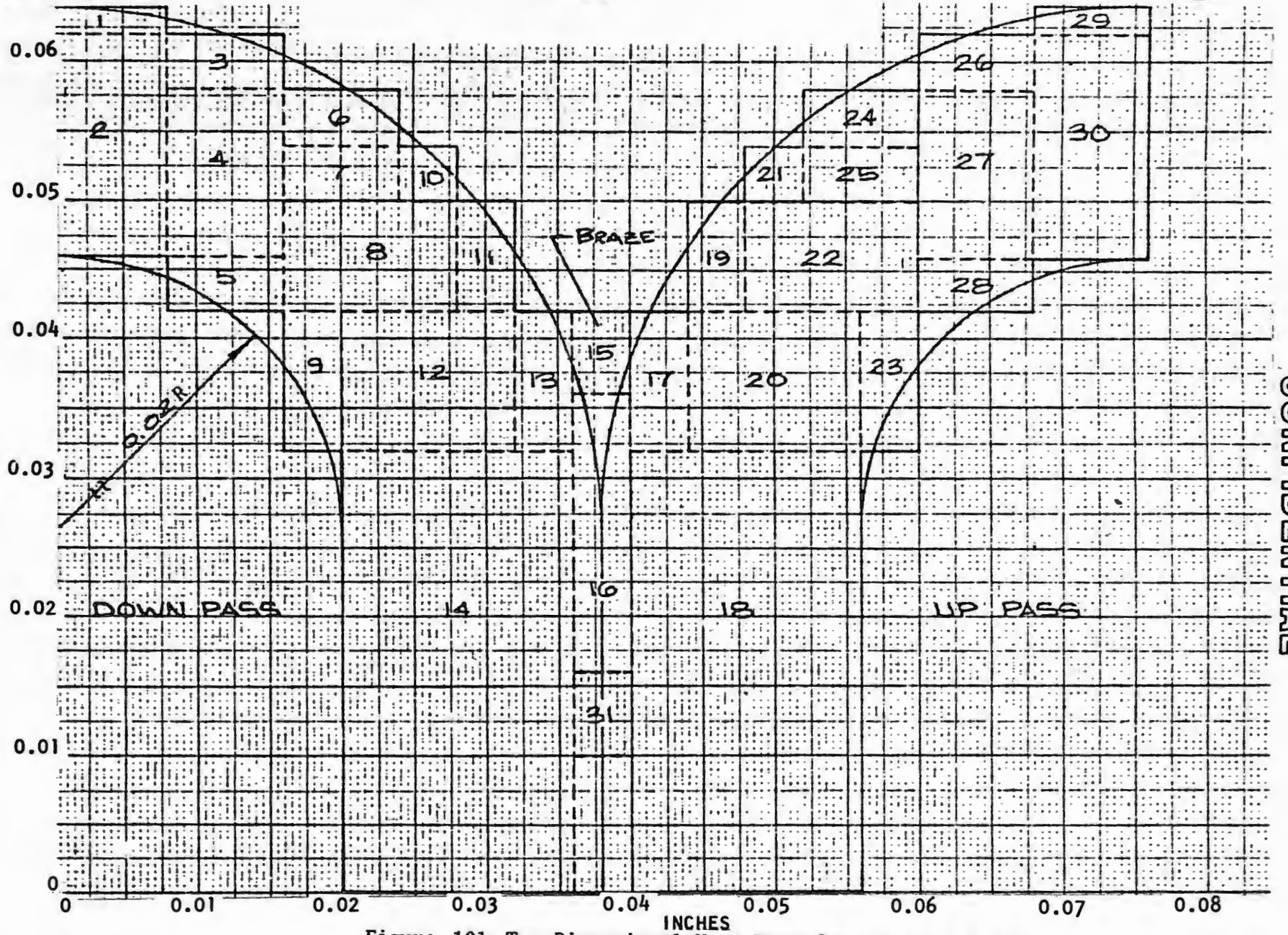

Figure 101. Two-Dimensional Heat Transfer Tube Model (U)

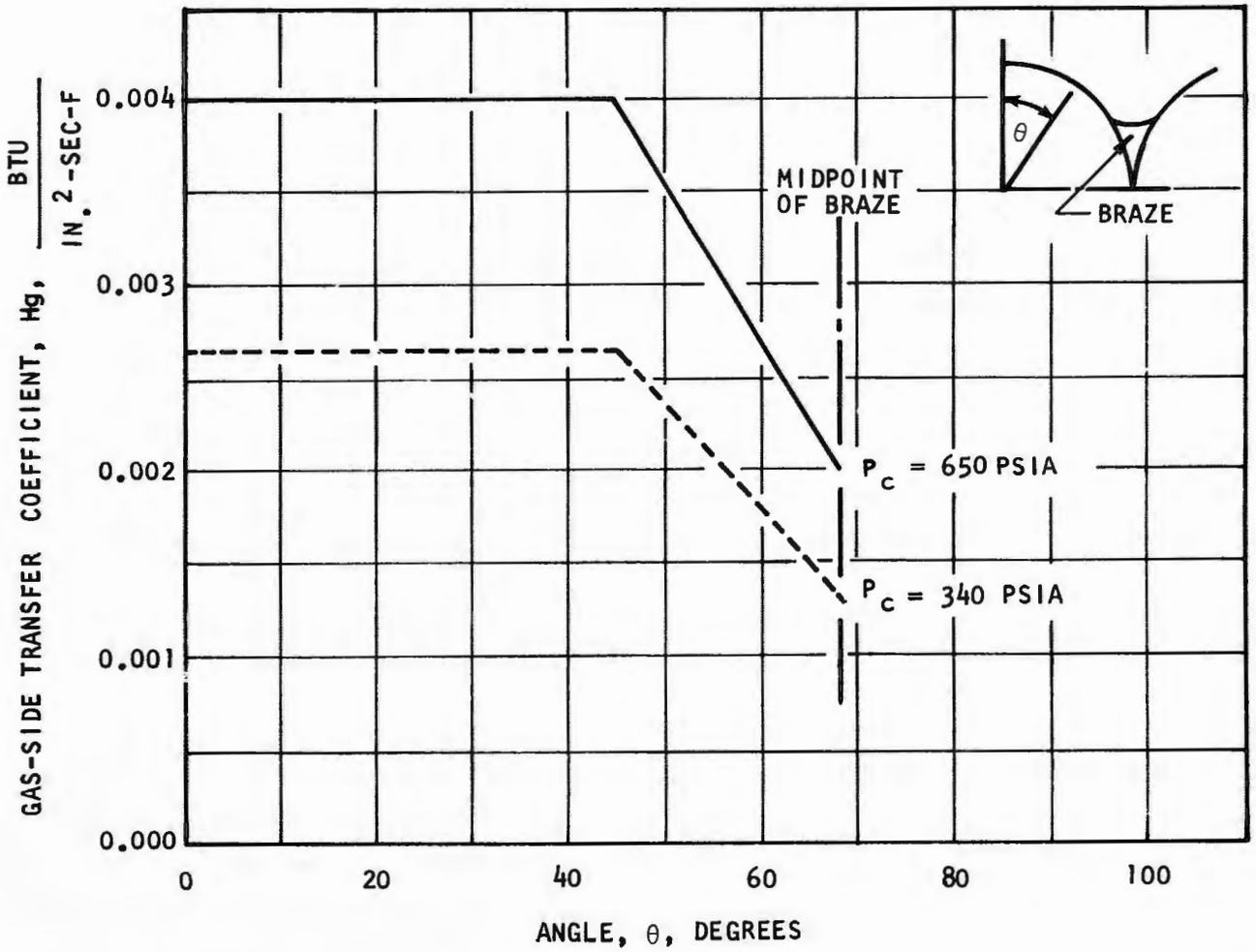

Figure 102. Assumed Gas-Side Heat Transfer Coefficient Profile at Nozzle Throat (U)

CONFIDENTIAL

(C) The analysis assumed two tube designs, the first of which had the wall temperatures of both uppass and downpass tubes at 1400 F and the second considered a 1100 F tube wall for the downpass tube and a 1400 F tube wall for the uppass tube. A summary of the results obtained for the nozzle throat with chamber pressures of 650 and 340 psia is shown in Tables 16 and 17. As shown in these tables, the maximum two-dimensional wall temperature was much higher than the one-dimensional value. The analysis showed a weak relationship between the coolant bulk temperature and two-dimensional wall temperatures at these heat flux levels (compare T_{wg}/2-D for T_B = -160 F and T_B = 300 F in Table 16). Also, a lower one-dimensional wall temperature (i.e., 1400/1100 F case) resulted in a larger temperature difference between the one- and two-dimensional analyses.

(C) A comparison of the results of two tubes designed for 1400 F and those designed for 1100 and 1400 F indicated that the cooler tube did not significantly reduce the wall temperature of the hotter tube. Figure 103 shows the isotherms for the 1100/1400 F test case. As shown by the isotherms, the cooler tube (downpass) cooled only a small fraction of the hot tube (uppass). This result is obtained because of the difference in gas-side surface area and coolant-side surface area and the high heat flux profile on the tube. A typical tube gas-side wall temperature profile is shown in Fig. 104.

(C) As the heat flux was lowered (Tables 16 and 17), the two-dimensional wall temperature tended to approach and, finally, become less than the one-dimensional value. This result is illustrated in Fig. 105. However, as noted in Fig. 105 at low heat flux levels (low gas-side heat transfer coefficient), the coolant bulk temperature significantly influences the two-dimensional wall temperatures.

(C) Based on the analysis of the test data, a number of significant phenomena were observed:

1. High outer-body heat loads (relative to the inner body); the difference is well in excess of that observed in water-cooled segment testing.

TABLE 16

TWO-DIMENSIONAL HEAT TRANSFER EFFECT AT NOZZLE THROAT P_c = 650 PSIA (C)

(P_c = 650 psia, h_g = 0.00398 Btu/in.^{2}-sec-F, T_{AW} = 8000 F)

	Downpass				Uppass			
	T_{WG}, F 1-D	T_B, F	h_c, $\frac{\text{Btu}}{\text{in.}^2\text{-sec-F}}$	$(T_{WG})_{2\text{-D}}^{\max}$, F	T_{WG}, F 1-D	T_B, F	h_c, $\frac{\text{Btu}}{\text{in.}^2\text{-sec-F}}$	$(T_{WG})_{2\text{-D}}^{\max}$, F
Outer Body	1400*	-160	0.0283	1776	1400*	200	0.0461	1780
	1400**	-160	0.0283	1764	1100**	200	0.1140	1503
	1100**	-160	0.0457	1559	1400**	200	0.0461	1773
Inner Body	1400*	300	0.0560	1751	1400*	400	0.0711	1757
	1400**	300	0.0560	1732	1100**	400	0.671	1434
	1100**	300	0.1949	1464	1400**	400	0.0711	1730

*Both up and down tubes at 1400 F

**Up tube at 1400 F, down tube at 1100 F

CONFIDENTIAL

TABLE 17

TWO-DIMENSIONAL HEAT TRANSFER EFFECT AT NOZZLE THROAT P_c = 340 PSIA (C)

(P_c = 340 psia, h_g = 0.00265 Btu/in.^{2}-sec-F)

	Downpass				Uppass			
	T_{WG}, F 1-D	T_B, F	h_c, $\frac{Btu}{in.^2\text{-sec-F}}$	$(T_{WG})_{max}$ 2-D, F	T_{WG}, F 1-D	T_B, F	h_c, $\frac{Btu}{in.^2\text{-sec-F}}$	$(T_{WG})_{max}$ 2-D, F
Outer Body	1400*	40	0.0176	1588	1400*	370	0.0268	1609
	1400**	40	0.0176	1566	1100**	370	0.0572	1393
	1100**	40	0.0276	1419	1400**	370	0.0268	1590
Inner Body	1400*	540	0.0368	1616	1400*	740	0.0655	1626
	1400**	540	0.0368	1602	1200**	740	0.0937	1424
	1100**	540	0.1279	1358	1400**	740	0.0655	1593

*Both up and down tubes at 1400 F

**Up tubes at 1400 F, down tube at 1100 F

CONFIDENTIAL

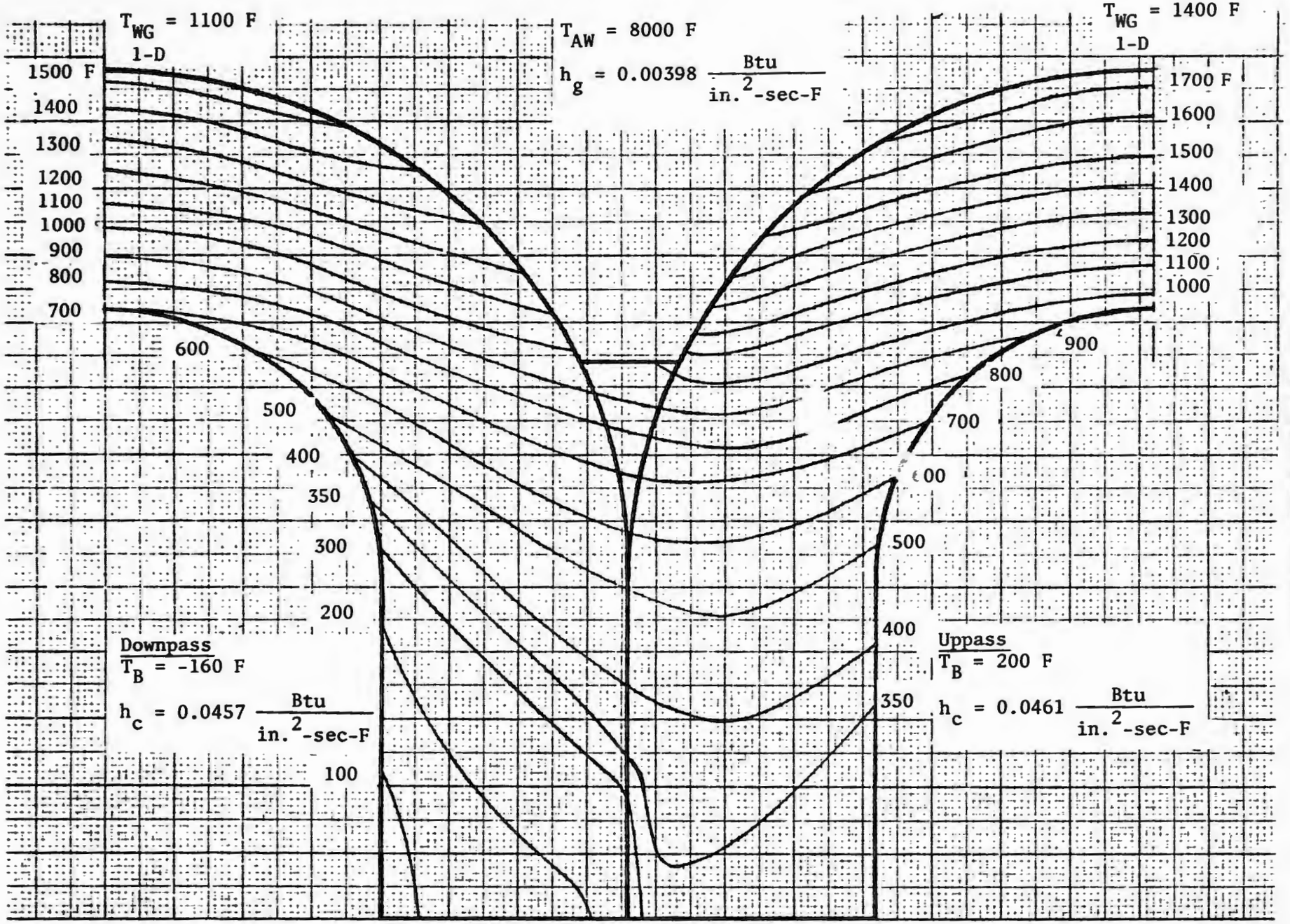

Figure 103. Typical Temperature Distribution Outer Body (P_c = 650 psia) (C)

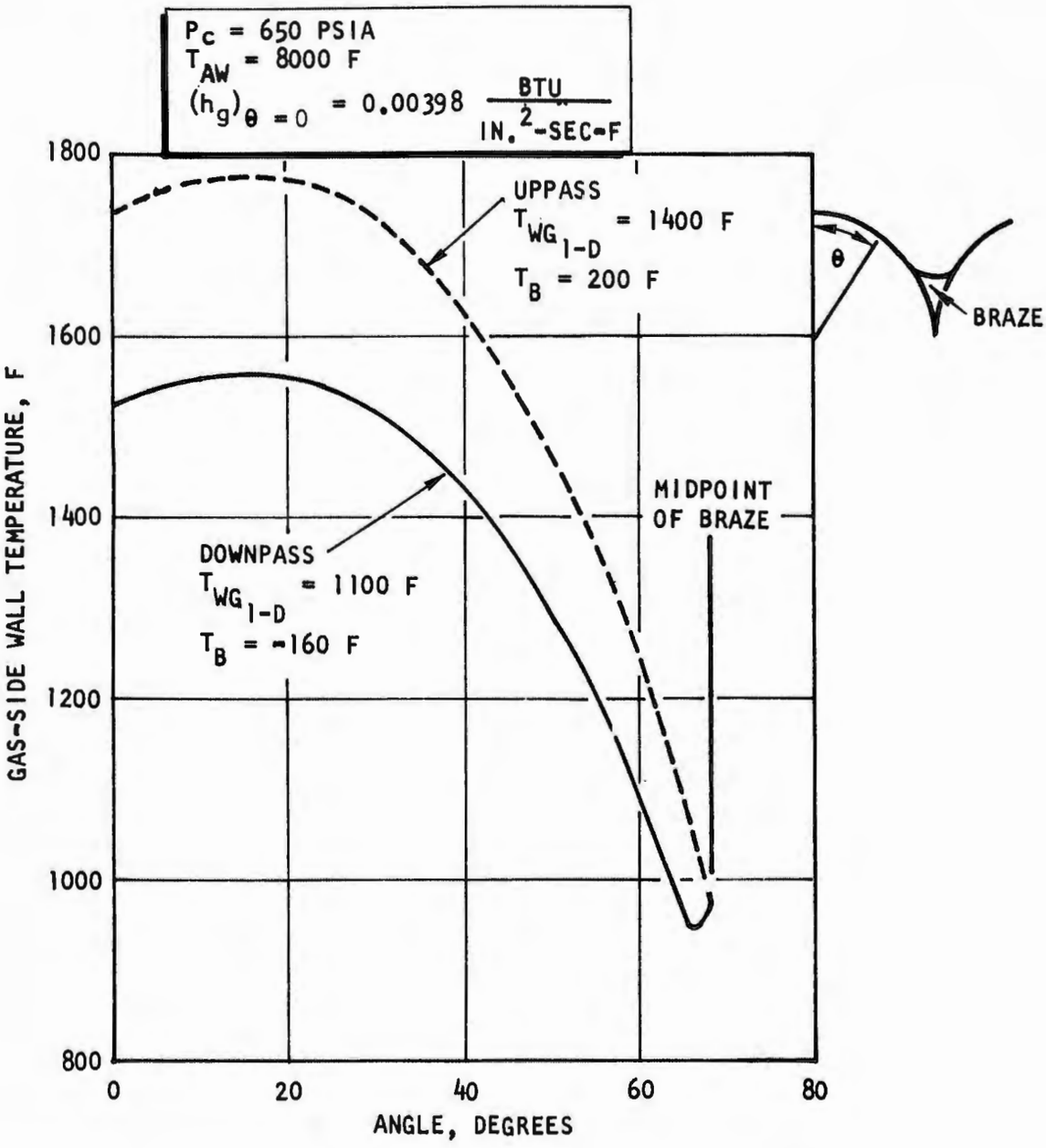

Figure 104. Outer Body Gas-Side Wall Temperature Profile (Throat) (U)

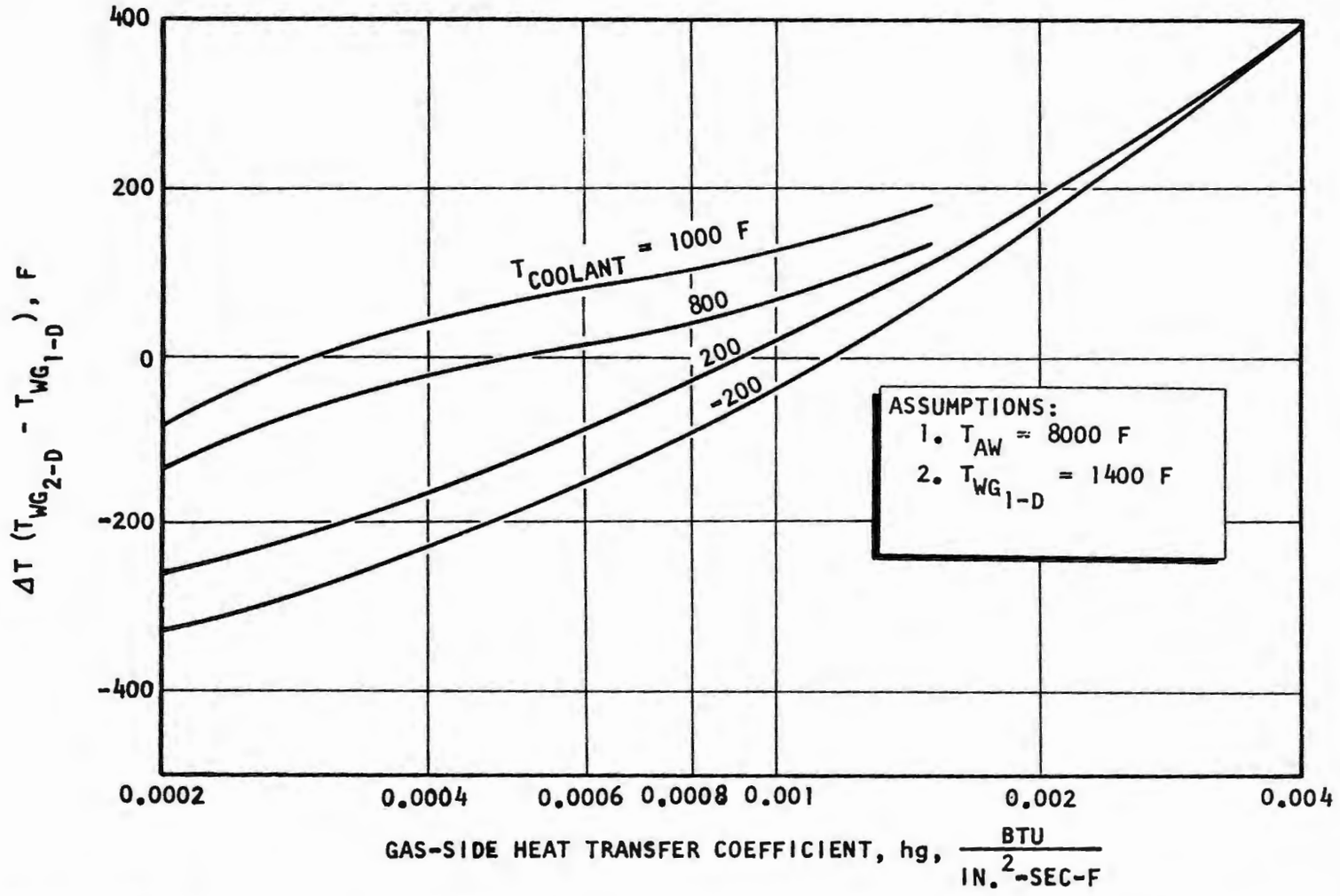

Figure 105. Two-Dimensional Tube Heat Transfer Effect With Variation of Gas-Side Coefficient (U)

(C) 2. High inner-body heat loads; observation of this phenomenon indicates a very large heat transfer from up tubes to down tubes in both bodies.

3. A higher total integrated heat load in the tube-wall as compared to the water-cooled segment test experience.

(2) Combustion Performance

(C) The characteristic velocity efficiency (η_c*) derived from the 30-degree tube-wall test data is tabulated in Table 12 and shown in Fig. 106. Some of the data resulted in values above 100 percent. This result is believed to be primarily caused by difficulty in measuring the throat area of the tube-wall segment and predicting the thermal growth of the chamber backup structure during the firing. The throat gap was measured at 20 locations along its length at various intervals during the test program; however, the measurement was made while the hardware was at ambient temperature and, consequently, the measurement would only indicate a test-to-test trend.

(C) The additional throat area that exists because of the tube interstices was estimated from tube braze samples and geometric considerations. The corrections applied to the data to account for the throat area change from transient thermal conditions considered variations in percent overcooling and burn duration and assumed a constant 5-second hydrogen prechill before ignition.

(3) 30-Degree Tube-Wall Segment Test Summary

(C) Two tube-wall thrust chamber segments were fabricated and tested. The results were:

1. Hydrogen cooling of the tube-wall chamber was demonstrated with varying amounts of overcooling.

2. Total heat rejection rate data was obtained for cryogenic cooling and exceeded the amount predicted on the basis of the previous 30-degree water-cooled segment tests.

(C) 3. The pressure drop of the tubular-wall chamber was grossly excessive.

4. The tube-wall segment test results indicated that investigation of alternate design approaches was required (refer to the tube-wall main thrust chamber analysis of Vol. I, Sections I, IV, and VI).

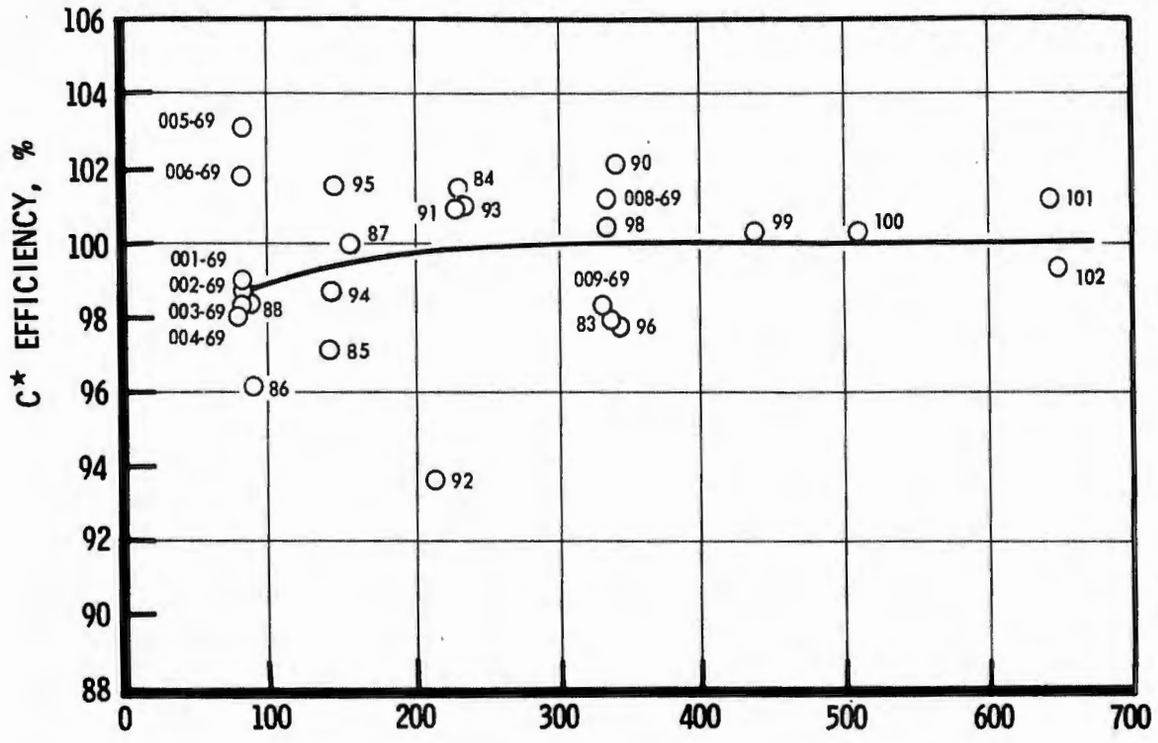

Figure 106. Combustion Efficiency, 30-Degree Tube-Wall Thrust Chamber Segment (U)

5. INITIAL 30-DEGREE CHANNEL WALL SEGMENT EVALUATION

a. General Approach

(C) Testing of the 30-degree tube-wall segments (discussed in the previous section) resulted in excessive heat loads and excessive associated required pressure drop, and indicated that investigation of alternate design approaches was necessary. Several approaches for reducing the heat load and improving the chamber cooling were considered. These approaches were:

1. Flattened tubes
2. Filled or dimpled tubes
3. Shortened combustion chamber length
4. Channel coolant passages
5. Injector mixture ratio bias (film cooling)

(U) The flattened tubes, illustrated in Fig. 107a, was an approach considered for achieving a smoother chamber hot-gas wall surface. Based on the 30-degree water-cooled segment (smooth wall) test results, compared to the 30-degree tube-wall segment (bumpy wall) test results, a considerably smaller heat load was possible with a smooth wall by virtue of a smaller hot-gas surface area. Little experience, however, was available with flattened tubes.

(U) Filled tubes and dimpled tubes, illustrated in Fig. 107b and 107c, were approaches for improving the heat transfer of the tube coolant side by virtue of reduced flow cross section, and associated increased coolant flow mass velocity. Smaller original size tubes were not considered practical for the tube tapering and forming processes. Some favorable experience existed with dimpled tubes (Atlas sustainer engine); however, experience with filled tubes was nonexistent.

(U) The shortened combustion chamber was an approach for reducing the overall heat load by reducing the chamber hot-gas wall surface area, and was described in Section III, 2, a (1) (c).

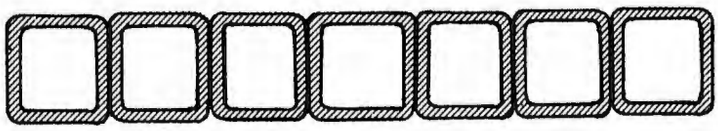

(a) FLAT TUBES

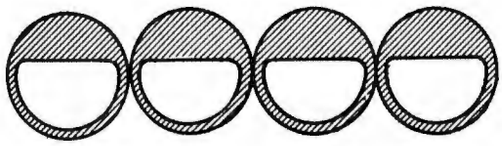

(b) FILLED TUBES

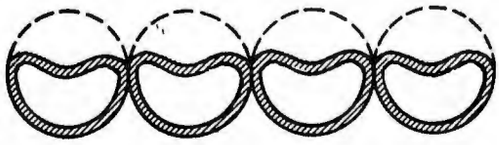

(c) DIMPLED TUBES

Figure 107. Alternate Tube Designs (U)

(U) The channel coolant passage approach was considered attractive because it achieved the desirable smooth hot-gas wall, made possible the use of smaller coolant passages than normally achievable with tubes, and offered the potential for reduced fabrication costs compared to a tube-wall design by virtue of eliminating the tapering, forming, and handling of many tubes.

(U) The injector mixture ratio bias was an approach for reducing the chamber wall heat flux and associated heat load by introducing film coolant (either oxidizer or fuel) from the outer periphery of the injector.

Of the above candidate approaches, three were selected for test evaluation:

1. Shortened combustion chamber length
2. Injector mixture ratio bias
3. Channel coolant passages

(U) The short combustion chamber length and injector mixture ratio bias evaluations were carried out with the 5-inch and 30-degree water-cooled segment hardware, and were discussed previously in Section III, 2, b (7) and Section III, 3, b (2), respectively.

(U) The evaluation of the initial segment designed with channel coolant passages (channel-wall) is discussed in the following paragraphs.

b. Hardware Design and Fabrication

(U) The purpose of this segment chamber, which was company-funded, was to provide an initial technology evaluation of a channel coolant passage chamber for AMPS. The channel wall fabrication technique offered considerably greater development versatility and lower cost than tubes and tube-wall chambers. Variations in coolant channel depth and width are easily obtained; as compared to extensive lead time and tooling required for tube configuration changes.

(U) The chamber consisted of four basic detail parts: inner body, outer body, left-hand baffle, and right hand baffle, with accessory parts such as locating pins, bolts, etc. A flow chart showing the significant manufacturing operations for the complete thrust chamber assembly is presented in Fig. 108 .

(C) The hot-gas wall contour (Gc) was the same as that used for the tube wall. The basic structure was 347 CRES forging that was initially machined to provide an ID contour that was oversize with respect to the radii, required manifolds, feed ports, and manifold weld lips. The contour was then built up with electroform nickel to approximately 0.130-inch thick (see Fig. 109), thus providing excess material on both the inner and outer bodies. The contour was then machined to within -0.010 inch of the final contour required for face attachment. The axial coolant passages, 0.036 + 0.002/-0.000 inch constant width with variable depths of 0.072 inch at the injector, 0.032 at the throat, and 0.92 at the exit end, were then machined.

(C) The outer body had 147 slots, and the inner had 145 slots. The slot cutting was accomplished by use of an air-driven-motor, single-slotting saw tool assembly. The tool assembly was attached to the ram of a Bullard vertical turret lathe equipped for tracer machining, and the slots were cut on radial lines with a vertical traverse while maintaining slot depth from a tracing template. The same machine and trace tooling also were used for all of the contour machining.

(U) After completion of the slots, they were filled with Rigidax wax, as shown in Fig. 110, and the contour was final machined by removing 0.010 inch from the face. This provided a clean, burr-free, wax-free surface to which the electroformed face could be attached. The wax was used to maintain the required passage cross-sectional flow area during electroforming of the hot-gas wall and was removed after face formation.

(C) The hot-gas side surface of the electroformed nickel (electroplated) was initially thicker than required and was machined to the required wall thickness of 0.018 inch in the throat and to 0.030 inch above and below the throat.

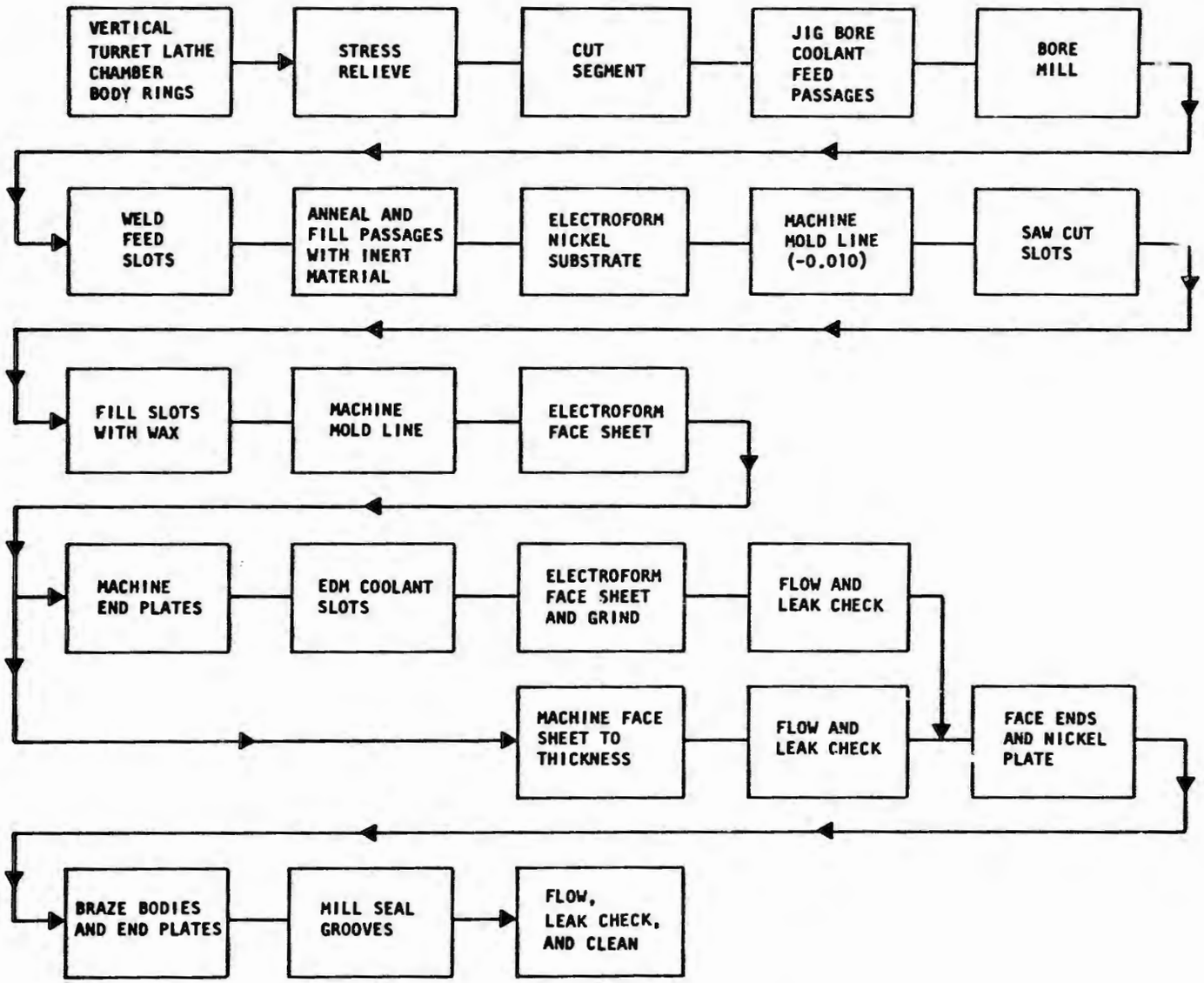

Figure 108. Fabrication Flow Chart for the 30-Degree Channel-Wall Chamber U/N 1 Thrust Chamber Segment (U)

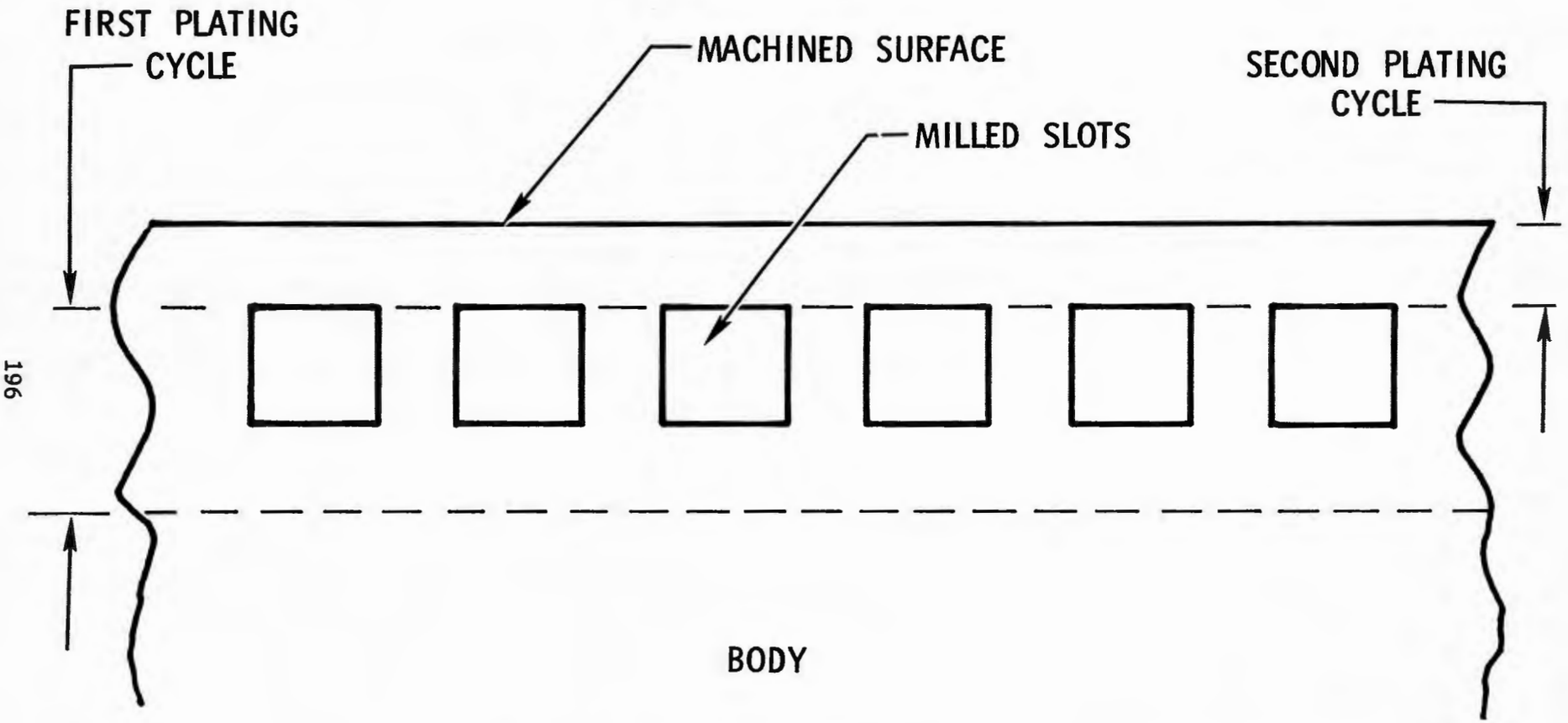

Figure 109. Channel Wall Thrust Chamber Segment U/N 1 Construction Method (U)

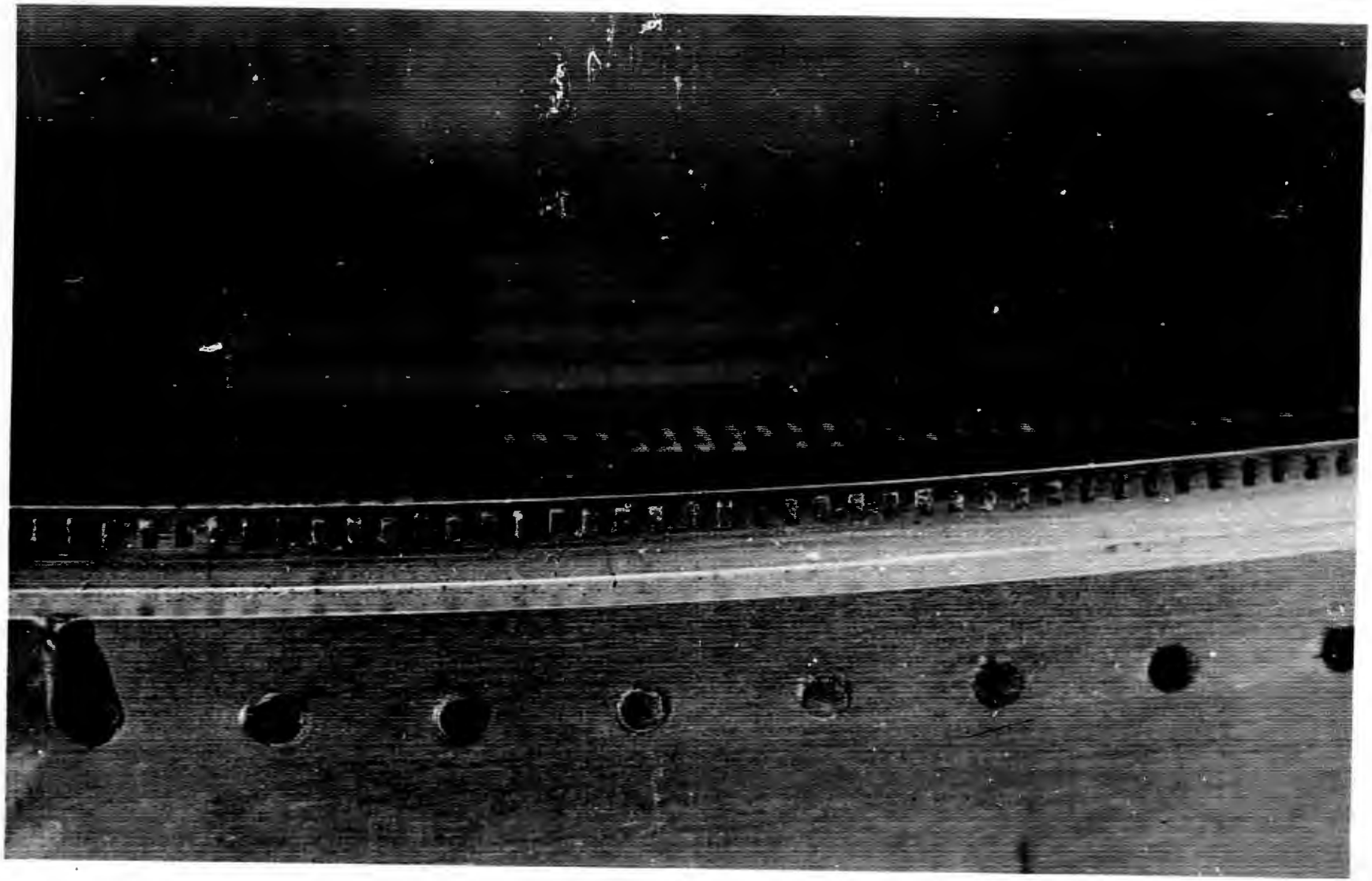

1EH32-10/21/68-C1J*

Figure 110. Wax-Filled Slots in Outer Body (U)

(U) Final machining of the segment body for furnace braze assembly completed the detail part as shown in Fig. 111.

(U) Because this chamber (U/N 1) was the first to be built at Rocketdyne by this technique, some problems were anticipated. The only problems that occurred, however, were concerned with the electroforming process development and control such as:

1. Control of the plating thickness over a contoured surface required anode and shield placement development.
2. Activation of the surface to be plated was not possible reliably and repetitively.
3. Equipment malfunctions such as filter plugging, poor agitation, pump failures, etc., occurred.
4. Laminations in the plated material occurred in random areas; some were not removed and did not prove to be detrimental.
5. Porosity occurred in certain areas because of the impingement of the plating solution on the surface being plated.

(U) The end plate baffles were designed for a four-pass cooling circuit and were a channel design also. The coolant slots were electrical discharge machined into a wrought nickel plate that had been machined to provide manifolds. The EDM machining was required because of the coolant passage pattern complexity. The hot-gas side surface was formed by electroforming nickel similar to the inner and outer bodies. Because the baffle hot-gas side surface is flat, the nickel face was surface ground to the required wall thickness. One of the completed baffles and its structural backup plate are shown in Fig. 112.

(U) The segment detail parts, inner and outer bodies, and baffles, were furnace brazed together to form the complete assembly. The views of the completed thrust chamber segment are shown in Fig. 113. One significant problem was encountered during weld closure of the inner body turnaround manifold. A series of cracks

1EH31-12/11/68-C1A*

Figure 111. Channel Wall Segment Outer Body (U)

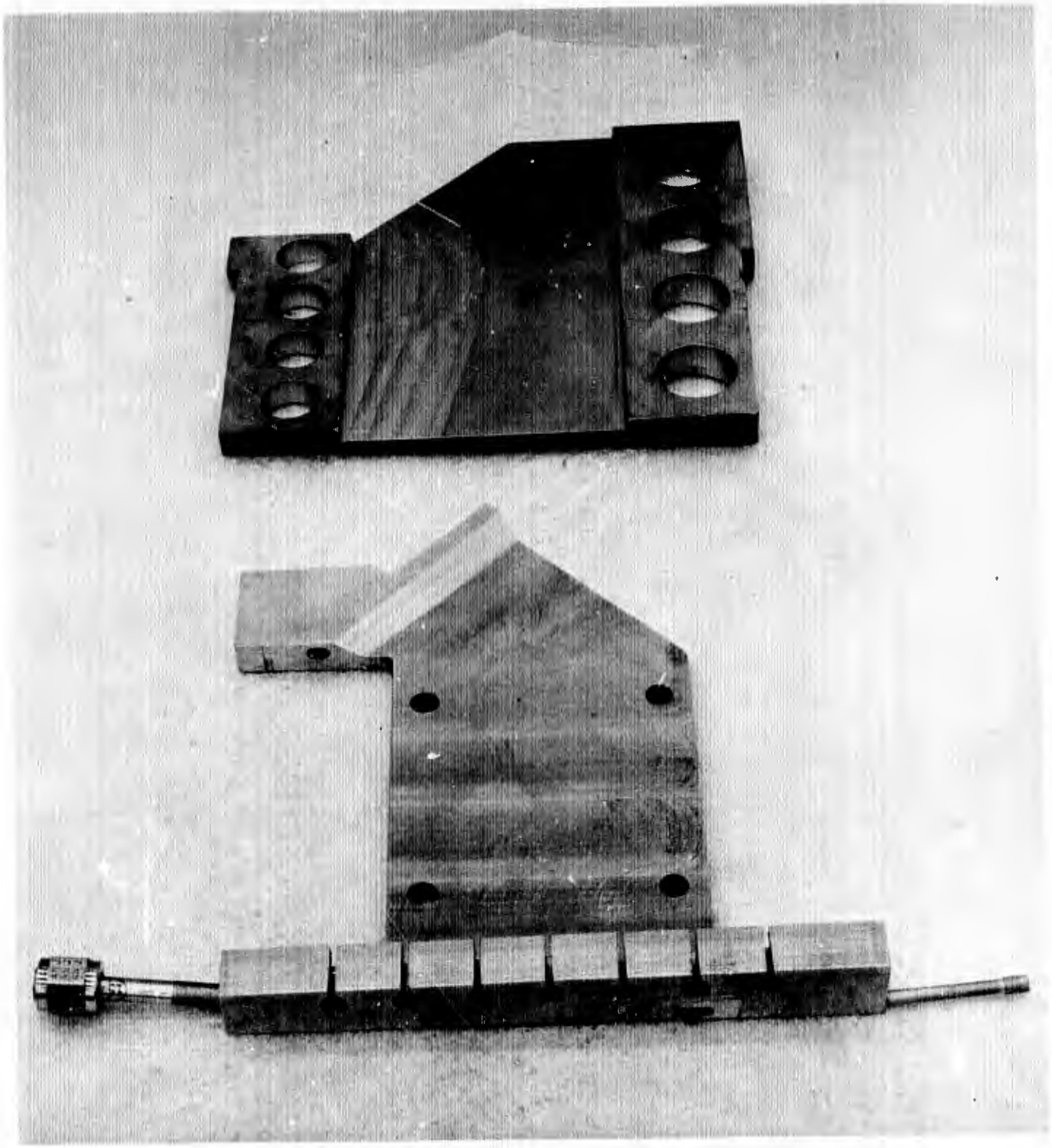

1EH31-12/11/68-C1E*

Figure 112. Baffle and Structural Backup Plate (U)

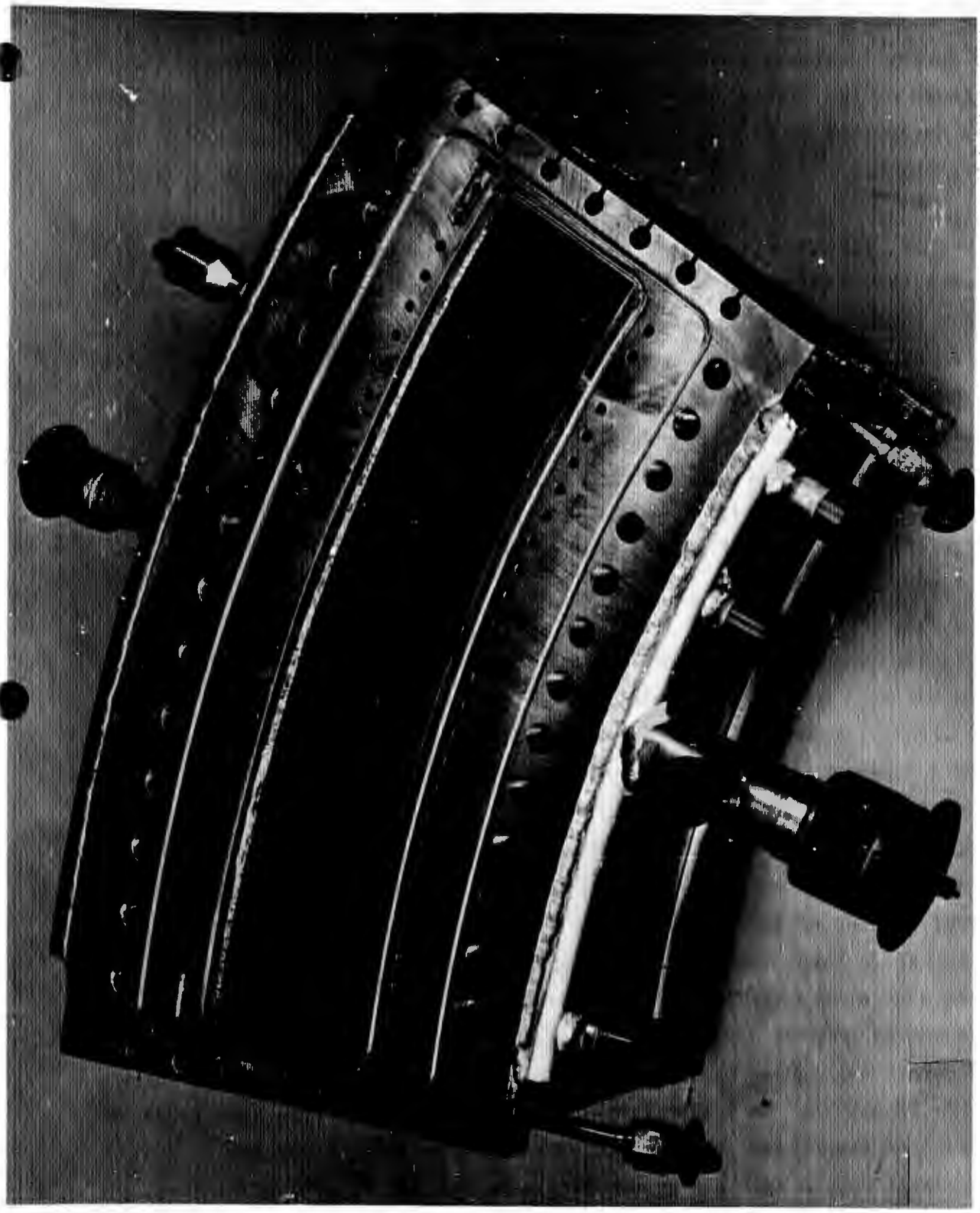

1EH32-1/10/69-C1H*

Figure 113. Channel Wall Thrust Chamber U/N 1 (U)

(U) was found emanating from the weld into the parent material. No cracks had occurred during identical welding performed on the outer body turnaround manifold, and the cause of the cracks was not immediately apparent. The condition was subsequently determined to be related to the location of circulation nozzle in the electroform bath.

(U) Many very small surface cracks were noted on the inner body face downstream of the throat prior to testing. Some cracks also occurred at the injector end where the contour curve transition runs into a straight section. The cracks were believed to have resulted from inadequate electroform process control, as was the case for the above-mentioned turnaround manifold. An attempt was made to seal the cracks aft of the throat by localized electroplating and at the injector end by plasma-sprayed nickel. The repair at the injector end was successful, but the repair aft of the throat was unsuccessful. Helium leakage tests performed prior to hot firing disclosed that many of the fine cracks leaked. No attempts were made to seal all the cracks prior to testing.

(C) A heat transfer analysis of the channel-wall chamber was conducted concurrent with the mechanical design phase. Because of the predicted throttling limitations caused by high total heat rejection rates to the coolant and the requirement tomaintain a reasonable heat transfer comparison tool, the channel wall chamber segment utilized the same coolant circuit as the previous tube-wall design. The coolant circuit is shown in Fig. 114 and had the provision for both parallel cooling and series cooling of the bodies. The chamber was designed initially for internal feeding of the baffles but with the capability of being modified to separate baffle feed. This modification was made during the test program when measurement of the baffle discharge coolant flowrate showed that an insufficient amount of coolant was being provided. The less than required baffle coolant flowrate was caused by excessive coolant leakage at the outer body discharge which is also at the injector-to-thrust chamber joint. The high-pressure coolant hydrogen leaked into the combustion zone at this joint because of poor sealing capability with this design and decreased the amount of coolant available for the baffle.

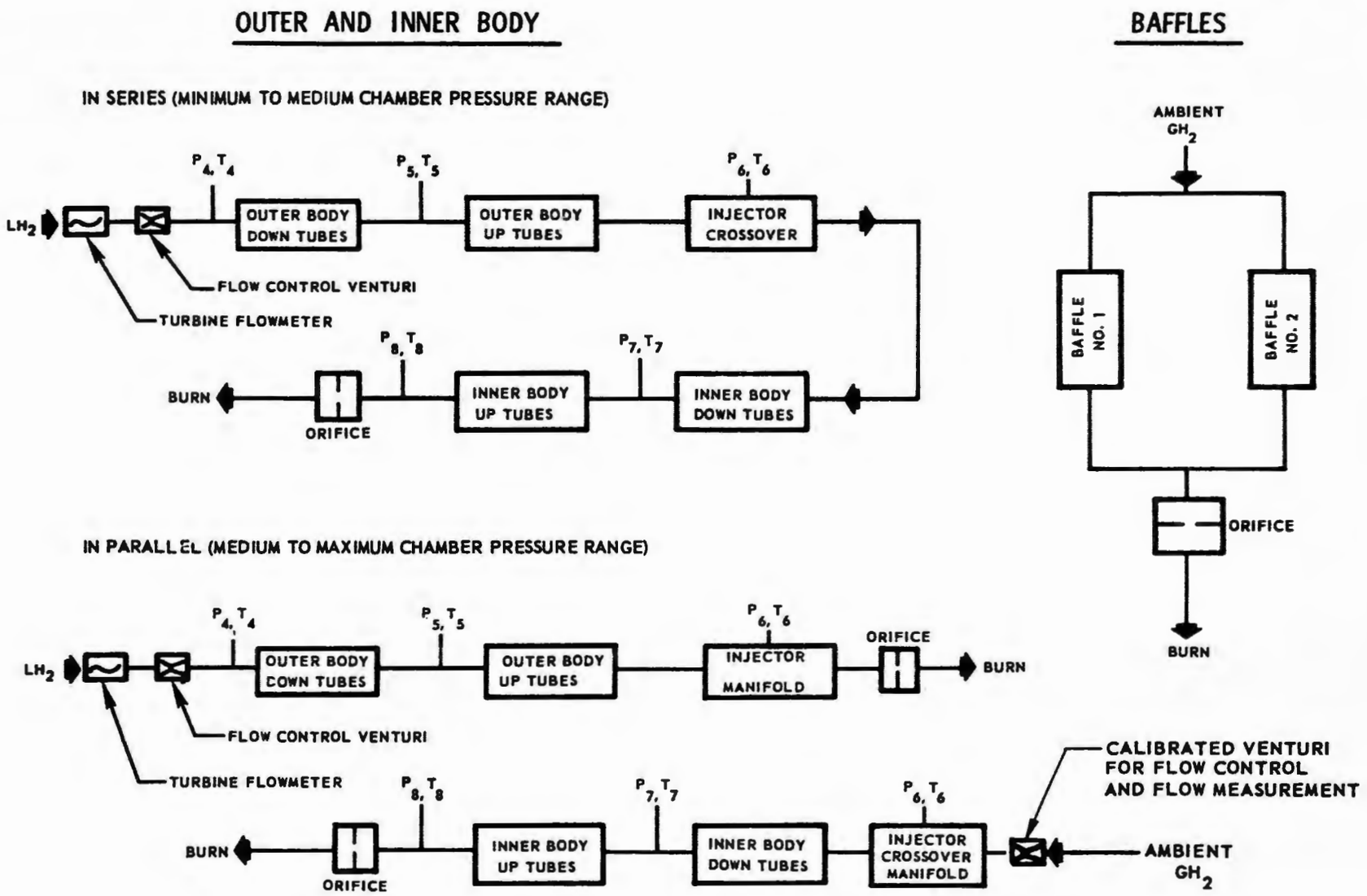

Figure 114. Channel-Wall Chamber Segment U/N 1 Test Cooling Circuit (U)

CONFIDENTIAL

(C) The local hot-gas side convective heat transfer film coefficients used for the design of the channel wall were the same as used for the tubular wall thrust chamber, realizing that the hot-gas side surface area is a minimum in the channel chamber because of the nonrippled surface and, thus, less total heat input. A maximum gas-side wall temperature of 1600 F was predicted at 650-psi chamber pressure and over approximately 50 percent of the chamber pressure range. Analytical predictions of gas-side wall temperatures slightly in excess of 1600 F were obtained for the medium to low chamber pressure range.

c. Initial 30-Degree Channel-Wall Segment Testing and Analysis

(C) Twelve tests were conducted with the initial channel-wall segment over a chamber pressure range of 610.0 to 75.8 psia. The purpose of the testing was to evaluate the channel-wall fabrication techqniue and heat load reduction potential compared to the tube-wall chamber. A summary of this test series is provided in Table 18.

(C) The first eight tests were conducted with the U/N 1 brazed-face injector and were conducted with a series-cooling circuit (Fig. 114). Localized surface cracking of the electroformed nickel-face sheet occurred on the inner body downstream of the throat (Fig. 115). This area had incipient cracks prior to testing as a result of the fabrication process and was decreased earlier. No overheating, erosion, or failure of the face sheet-to-channel land joints were noted. Slight erosion of the injector body at the inner O-ring groove, from fuel leakage into the combustion chamber and resulting hot-gas recirculation, was noted and weld-repaired.

(C) An additional test was conducted with the 30-degree U/N 3 injector using a parallel-cooling circuit (Fig. 114), so that near-maximum chamber pressure could be attained. The test was terminated by the test observer because of a change in exhaust flame color. Posttest inspection of the hardware revealed erosion of the injector body at the O-ring groove because of fuel leakage at this seal. The erosion was subsequently weld-repaired. Slight surface melting and erosion of

TABLE 18

30-DEGREE CHANNEL-WALL THRUST CHAMBER SEGMENT U/N 1 TEST SUMMARY (U)

Test No.*	Chamber U/N	Injector U/N	Duration, seconds	Chamber Pressure, psia	Injector Flow, lb,sec	Mixture Ratio	Fuel Injector Temperature, R	Percent Overcool		$-\Delta H$ 4-6 Btu/sec	ΔH 6-8 Btu/sec	$\frac{P_4}{T_6}$	$\frac{P_6}{T_6}$		$\frac{P_8}{T_8}$	ΔH Total, Btu/sec	ΔH Baffles, Btu/sec
								Outer Body	Inner Body				Outer Body	Inner Body			
1001	1	1	3	216.8	1.73	13.0	1304	136	65	485	232	1288 87	1072 491		430 779	717	23.3
1002	1	1	10	207.9	1.73	12.7	1332	138	80	466	284	1321 80	1046 451		455 792	750	30.6
1003	1	1	4.5	144.7	1.20	12.5	1340	221	131	396	260	1157 75	964 416		397 756	656	26.8
1004	1	1	10.6	82.4	0.65	13.5	1290	312	121	194	160	659 75	402 304		205 678	354	22.1
1005	1	1	8.0	79.8	0.65	13.0	1260	105	33	236	87	526 78	329 682		154 1129	323	--
1006	1	1	8.6	150.0	1.20	13.9	1347	-4	-19	255	138	643 87	535 837		184 1345	393	42.4
1007	1	1	9.5	75.8	0.62	13.8	1298	268	79	120	190	554 64.3	457 237		163 836	310	33.0
1008	1	1	4.1	420	2.90	11.8	1337	66	-9	644	422	1557 77.5	1294 447		458 938	1066	--
012-69	1	3	4.9	610	5.11	13.4	1386	190	101	980	--	1879 71	776 414	1913 512	739 688	--	83.8
018-69	1	1	21.3	87	0.653	14.72	1460	103	48	304	91	573 79	477 801		179 1125	395	20.2
019-69	1	1	18	75.8	0.650	15.00	1378	230	61	228	156	567 76	455 446		161 1018	384	21.2
020-69	1	1	5.5	417.8	3.307	14.58	1363	50	-12	891	386	1657 78	1348 664		511 1144	1277	34.2

P_4, T_4 = Outer body inlet manifold; pressure; temperature

P_6, T_6 = Outer body discharge, or inner body inlet manifold; pressure; temperature

P_8, T_8 = Inner body discharge manifold; pressure; temperature

P = psia, T = degrees R

*Test No. 1xxx refers to company-sponsored tests,
Test No. xxx-69 refers to program test in 1969

CONFIDENTIAL

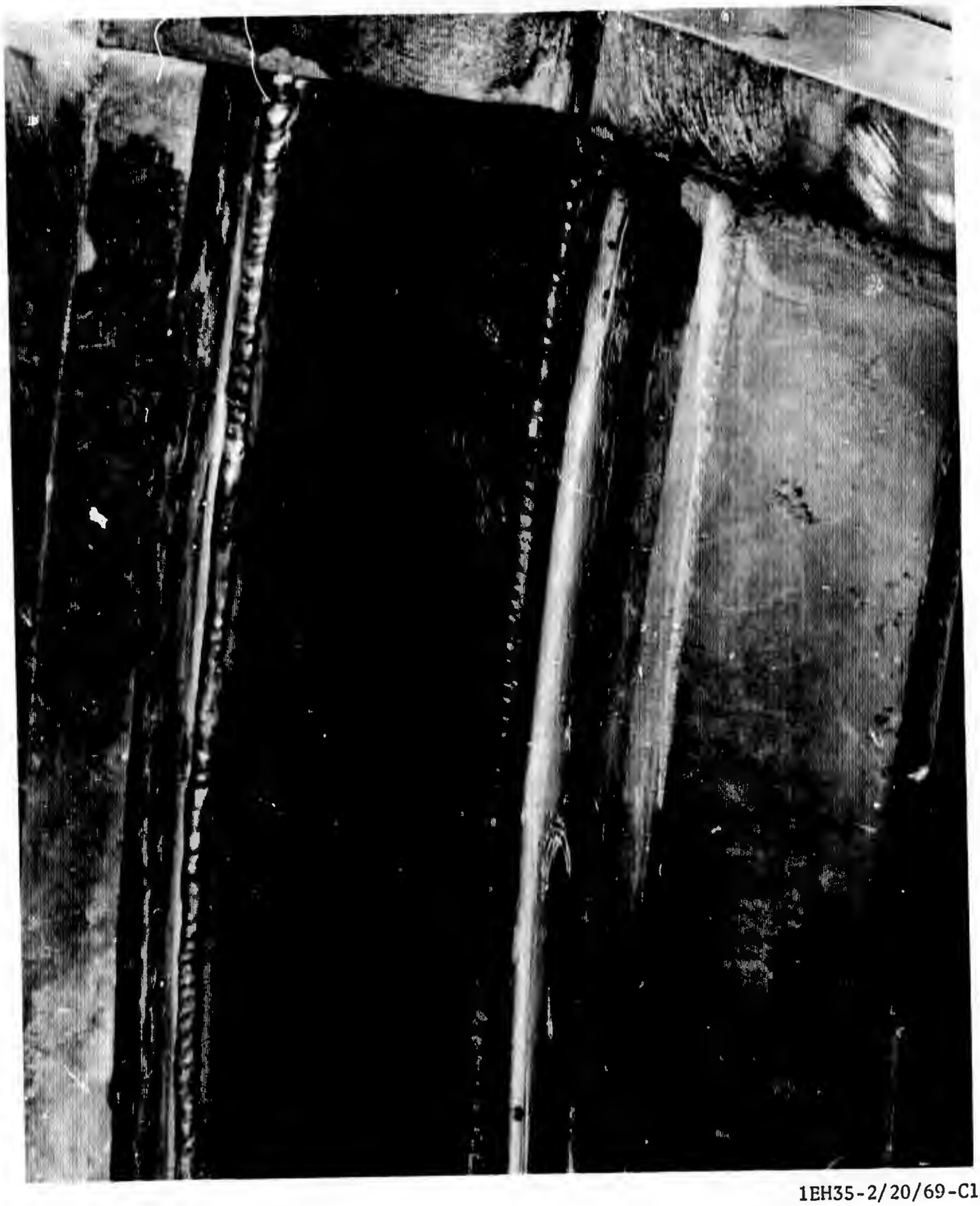

1EH35-2/20/69-C1H

Figure 115. Channel Wall Thrust Chamber U/N 1 Inner Body Cracks (U)

(C) the chamber hot-gas-side wall at one channel location also was noted. The melted region was suspected to have resulted from a partially restricted coolant channel (blockage). Other than the local damage, the general condition of the chamber was unchanged.

(C) The final three tests were conducted with the U/N 1 injector which was modified for oxidizer bias (0.021-inch diameter bias orifices. (Refer to Section III, 3, b (2).) The tests were satisfactory and of programmed duration.

(U) Prior to the tests, an attempt was made to decrease the amount of chamber-wall coolant leakage by arc-plasma spraying nickel onto the hot-gas side walls. The attempt was not completely successful because of an inability to position the spray nozzle normal to the wall because of poor accessibility, and leakage existed after the repair. During each firing test, a portion of the plating flaked off and was expelled by the exhaust gas. No other thrust chamber damage occurred, nor was there any noticeable deterioration as a result of the oxidizer bias. No visual damage to the injector was indicated.

(U) During hydrostatic pressure test of the injector face-to-body braze joints, a braze joint failure was discovered. Leakage was found to exist between an oxidizer passage and the purge passage and between a fuel passage and the purge passage. Neither leakage caused any damage becuase of the static helium purge that isolates the two propellants. As designed, if a small braze joint failure does occur (as it did in this case), the helium purge, which is at a greater pressure than either of the two propellant injection pressures, will flow into the propellant manifold, or manifolds and prevent mixing of the two propellants.

(C) Following test 020 (the final test of this series), the thrust chamber segment was sectioned and metallurgically evaluated. Metallographic analysis, including electron-microprobe investigation of the cracks, was performed and it was concluded that the cracking was the result of inferior quality electroformed nickel. An explanation for this problem was that the plating solution was directly recirculated on the part, aft of the throat on the inner body, and may have contributed to the embrittlement at elevated temperatures. The combustion zone, however, was

(U) exposed to more severe temperature conditions as compared to the nozzle, and had a minimal number of cracks. In addition, the regeneratively cooled side plates (baffles) sustained no damage during the firing tests. The side plates were fabricated by a process quite similar to the contoured segment walls, i.e., the coolant passages were EDM formed in wrought nickel sheet and the hot-gas side face was of electroformed nickel. Based on the above results, additional laboratory development work was necessary to improve the process control for electroforming.

(U) A comparison of heat transfer test results of the U/N 1 channel-wall segment to the tube-wall segment chamber test results was made. The results could not be considered entirely quantitative because of the injector seal leakage and the condition of the hot-gas walls and their unknown effect on heat transfer in the upper combustion zone. However, a qualitative comparison (Fig. 116) was made with the channel-wall data points superimposed on a plot of the tube-wall and water-cooled copper segment data. As shown, the channel-wall heat loads were much lower than for the previous tube-wall segment and approached the values of the water-cooled segment.

d. Initial 30-Degree Channel-Wall Segment Test Summary

(C) Twelve firing tests were conducted on the initial channel-wall chamber segment with an electroformed hot-gas face closure. The significant results were:

1. Qualitative heat transfer test data showed reduced heat loads compared to the tube-wall segment. The reduction was attributed to the flat versus nonflat (tubes) hot-gas wall.
2. Chamber fabrication was accomplished without difficulty, except for the nickel electroforming process. Embrittlement and cracking of the electroformed hot-gas surface indicated that additional laboratory development work was necessary before starting fabrication of additional channel-wall segments of this design.

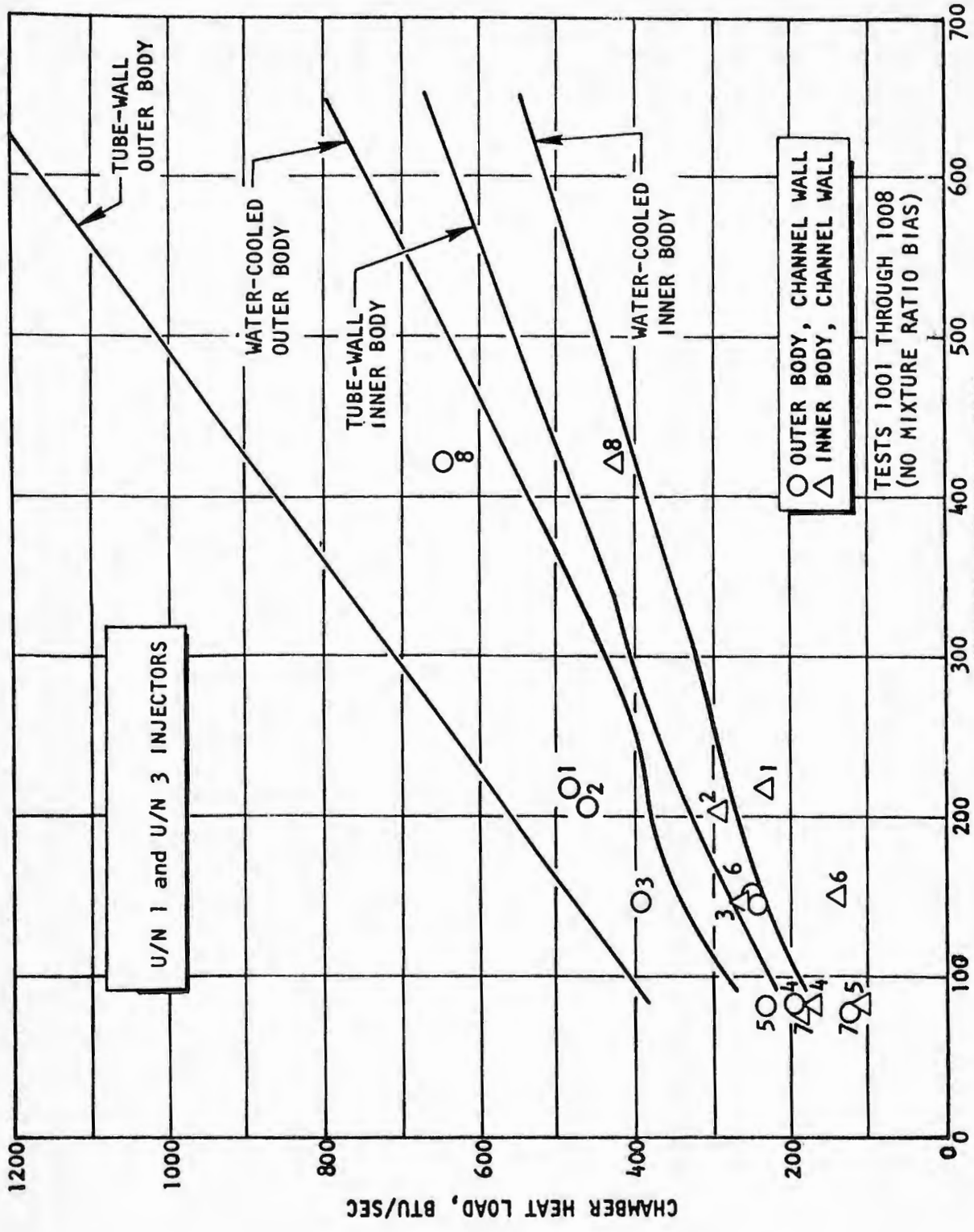

Figure 116. Chamber Heat Load vs Chamber Pressure (U)

(C)

3. Hydrogen leakage at the injector-to-chamber attachment flange dictated that a design change in this area was required.

4. The oxidizer bias was not found to be detrimental to the chamber hot-wall, even though hydrogen leakage through the cracks in the hot-gas wall existed.

6. PROTOTYPE 30-DEGREE CHANNEL-WALL SEGMENT EVALUATION

a. Configuration Definition

(U) This thrust chamber segment, which was designated the prototype 30-degree segment, incorporated all design improvements indicated by previous tubular- and channel-wall thrust chamber data. The primary purpose of the chamber evaluation was to verify satisfactory regnerative cooling (with near design coolant pressure drop) over the design throttle range. Demonstration of durability and performance also was required.

(C) The selected design was the channel-wall chamber concept utilizing a single-pass cooling circuit and G_c combustion chamber contour. The coolant circuit design selection was based on detailed analysis of the firing test data obtained with the 30-degree water-cooled and initial channel-wall segments. A relative comparison of three candidate configurations is shown in Table 19.

(U) Local heat flux values were acceptable in all three candidate configurations; however, the overall total heat rejection rates were excessive in the medium to low chamber pressure range for both the two-pass channel-wall and two-pass tube-wall segments. Excessive hot-gas-side wall temperatures were predicted because of the high coolant bulk temperature (Table 19).

(U) The relative comparison of configurations in Table 19 showed significant improvement in chamber cooling for the two-pass channel-wall design compared to the two-pass tube-wall design. This improvement was basically a result of the reduced hot-gas wall surface area for the channel-wall, which has a flat surface, and two-dimensional heat transfer effects.

(U) The single-pass channel-wall design provided further improvement by optimizing the coolant passage profile to provide less pressure losses in areas of low heat flux and sufficient pressure losses in high heat flux areas to maintain acceptable wall temperatures. The new and original profiles are shown in Fig. 117. The channel width was kept at 0.028 inch, while the depth was varied. As seen from

TABLE 19

COMPARISON OF TUBE-WALL AND CHANNEL-WALL DESIGN

(TWO-DIMENSIONAL HEAT FLOW INCLUDED)

(Oxidizer Injector Bias Not Included) (U)

CONFIGURATION	REQUIRED INLET PRESSURE FOR P_c = 650 PSIA	COOLANT BULK EXIT TEMPERATURE (F)			MAXIMUM GAS SIDE WALL TEMPERATURE (F)					
					OUTER BODY			INNER BODY		
		650 P_c	220 P_c	150 P_c	650 P_c	220 P_c	150 P_c	650 P_c	220 P_c	150 P_c
1 PASS CHANNEL-WALL CONSTRUCTION	LESS THAN 2100 PSIA	580	960	1070	1370	1270	1530	1550	1530	1670
2 PASS CHANNEL-WALL CONSTRUCTION	2100 PSIA	570	940	*	1530	1490	*	1650	1700	*
2 PASS TUBE-WALL CONSTRUCTION	2300 PSIA	1000	1310	*	1710	1750	*	1960	2000	*

CONFIDENTIAL

CONFIDENTIAL

CHANNEL DESIGN

0.028 In. Passage Width
0.018 In. Gas Side Wall Thickness
0.030 In. Land
0.00006 In. Roughness (RMS)
0.016-.080 In. Passage Depth (One Pass)
0.036-.190 In. Passage Depth (Two Pass)
2280 Channels Per Side (Complete Chamber)

TUBE DESIGN

.070-.140 In. Unformed Tube Diameter
.0165 In. Wall Thickness
.00006 In. Roughness (RMS)
.00013 In. Roughness (RMS) Throat
1920 Tubes in Outer Body (Complete Chamber)
1872 Tubes in Inner Body (Complete Chamber)

*Excessive values

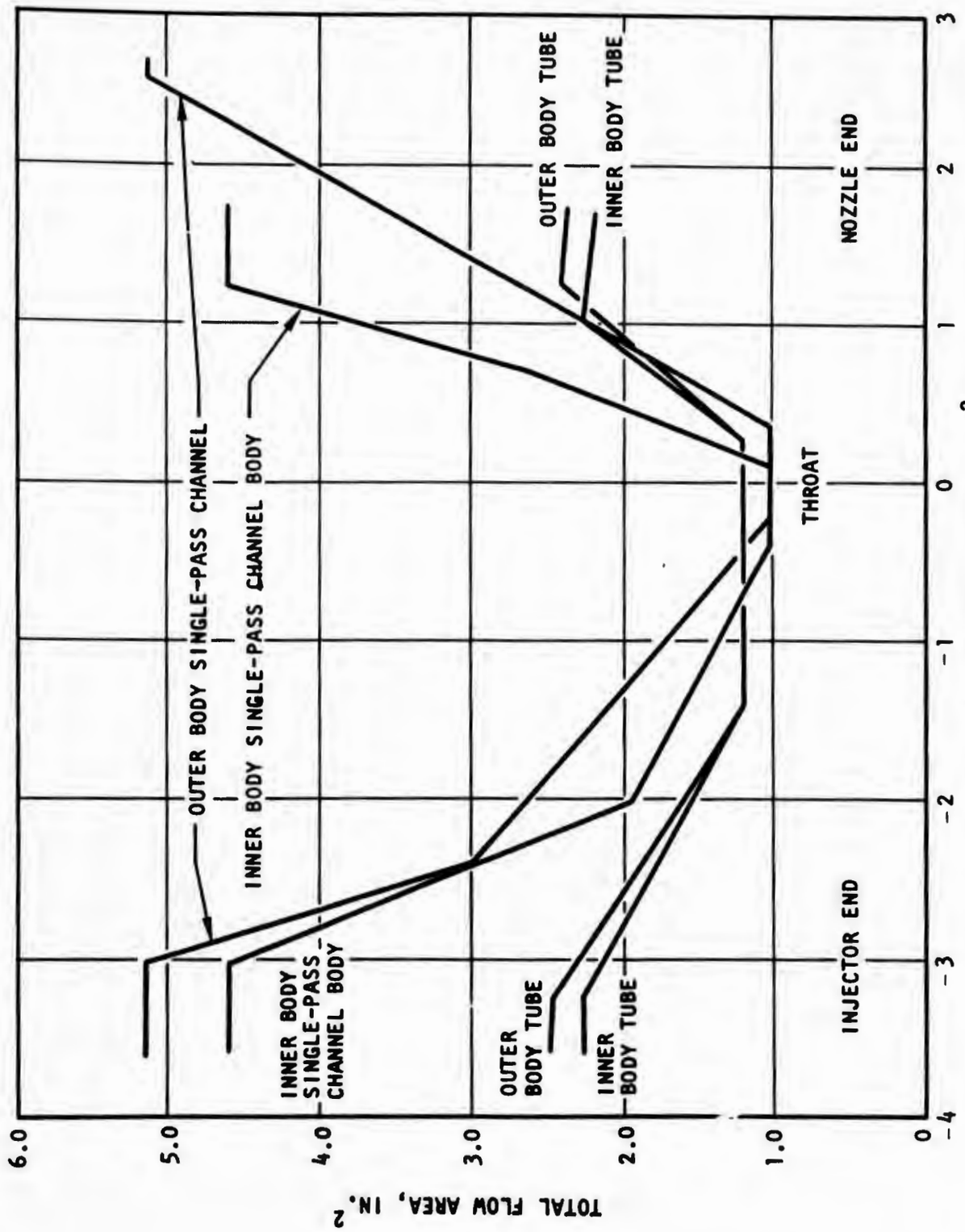

Figure 117. Outer and Inner Body Total Passage Area vs Length From Throat (Prototype Channel-Wall Segment) (U)

(U) Fig. 117, the channel area varies from a maximum value of 5 $in.^2$ at the outer body entrance to 1 $in.^2$ at the throat. The tube-wall thrust chamber flow area varied from 2.5 $in.^2$ at the entrance to 1.2 $in.^2$ at the throat. The results presented in Table 19 were derived prior to the definition of oxidizer bias capabilities and do not include this improvement. The relative gas-side wall temperature differences between the candidate configurations, however, remain the same when evaluated with the oxidizer bias included.

(C) The predicted prototype segment coolant circuit parameters are shown in Fig. 118. The data shown include the improvements of optimized coolant channel flow areas and the injector oxidizer bias. As noted, operation of the segment was predicted to be completely satisfactory with hot-gas wall temperatures less than 1400 F over the complete throttle range. The cooling circuit design utilized a single pass in each body (inner and outer) and a double pass through the nozzle (Fig. 119).

b. Hardware Design and Fabrication

(U) Evaluation of the initial 30-degree channel segment (U/N 1), discussed previously, indicated that a problem area existed in the mechanical design and fabrication of the hot-gas face. This problem area was the most critical aspect of the prototype segment design and two techniques for generation of the face were evaluated by a laboratory test program.

(C) The techniques consisted of: (1) electroformed nickel face onto an electroformed nickel substrate into which the coolant passages (of varying depth and constant width) have been machined; and (2) furnace braze attachment of explosively, or stretch formed, wrought-nickel face sheet to an electroformed nickel substrate into which the coolant passages (of varying depth and constant width) have been machined.

(U) The initial channel-wall segment, U/N 1, was fabricated by the first technique noted above. Some surface cracks of random orientation resulted with the electroformed face. These results led to the conclusion that the electroform process

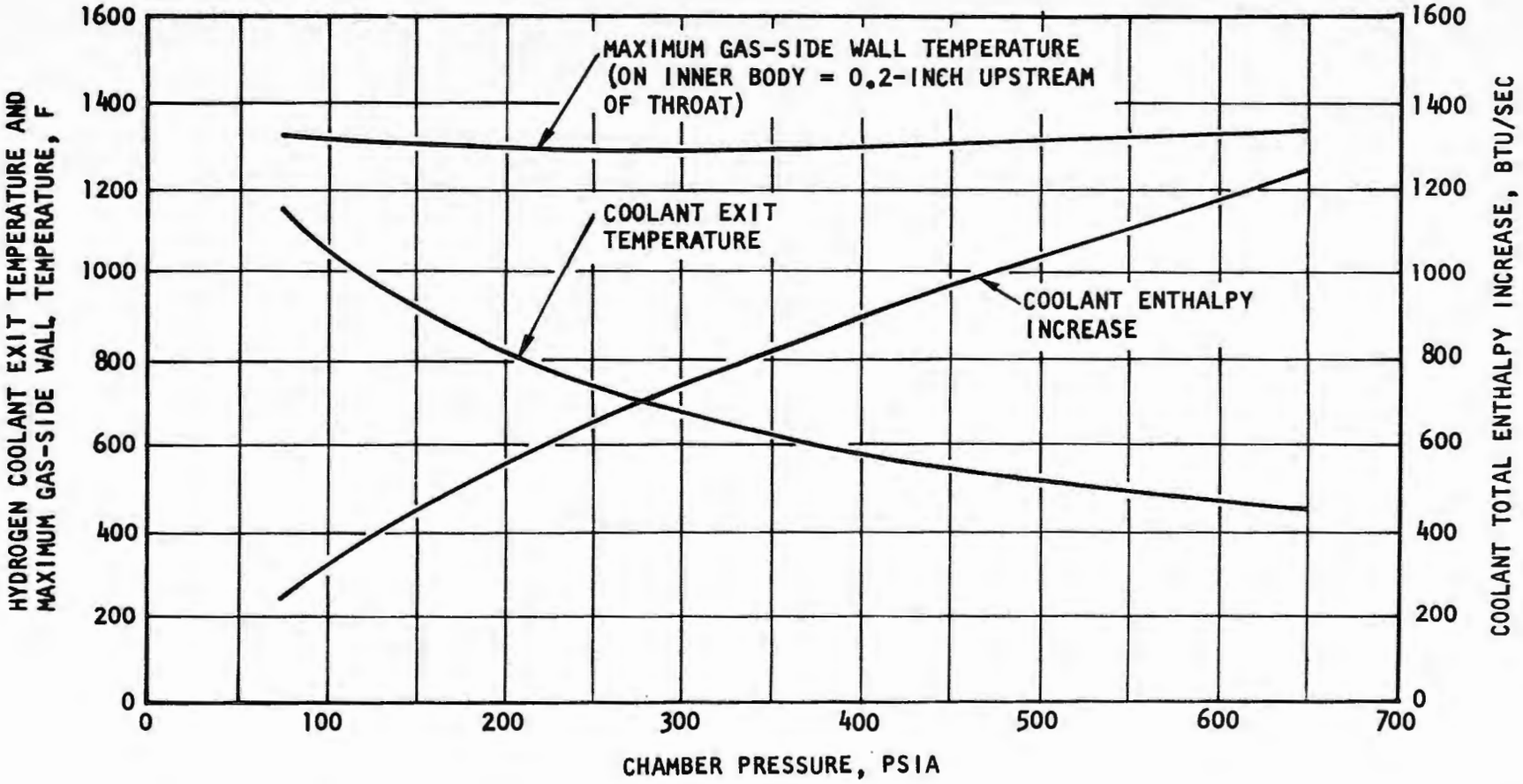

Figure 118. Prototype 30-Degree Regeneratively Cooled Segment, Predicted Cooling Circuit Parameters (U)

CONFIDENTIAL

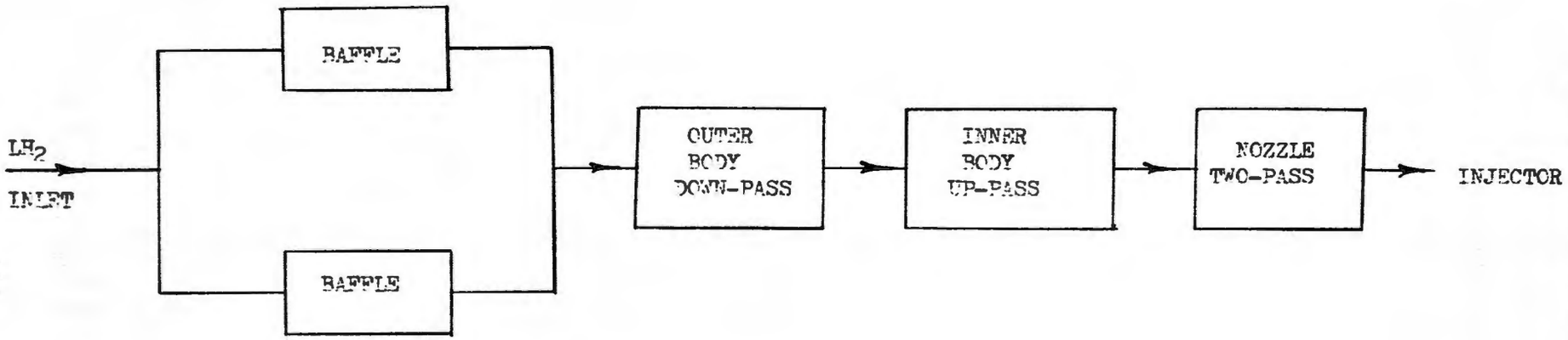

Figure 119. Prototype 30-Degree Segment Cooling Circuit (U)

(U) variables were not adequately defined (e.g., current density, bath temperature, chemical composition, and agitation rate).

(U) Both the electroformed and braze sheet for the hot-gas closure were relatively new processes, and experimental laboratory investigations were conducted on a number of samples for definition and optimization of the significant process variables. Figures 120 and 121 illustrate the brazed face samples and Fig. 122 and 123 illustrate the electroform face samples. The sample evaluations are discussed in more detail in Ref. 5.

(U) The above investigation led to the conclusion that a wrought-nickel face was superior to an electroformed nickel face because of reproducible sheet quality and mechanical properties. Although the improved electroform samples were successful, the inability to completely define the mechanism of electroform failure on the initial 30-degree channel chamber (U/N 1) was considered sufficient reason to relegate this approach to a backup classification.

(C) The following hot-gas face configuration was selected for the prototype thrust chamber segment:

1. Inner Body: stretch-formed, wrought-nickel sheet that was furnace-braze attached to the electroformed nickel substrate into which the coolant passages were machined
2. Outer Body: explosively formed, wrought-nickel sheet that was furnace-braze attached to the electroformed nickel substrate into which the coolant passages were machined
3. Side Plates: (Baffles) wrought-nickel sheet that was furance-braze attached to the wrought-nickel plate into which the coolant passages were machined.

(U) The prototype channel-wall segment layout is shown in Fig. 124. To minimize the sealing problems experienced with the initial channel-wall segment (U/N 1), no high-pressure coolant was permitted in the prototype injector-to-segment joint

SAMPLE #1

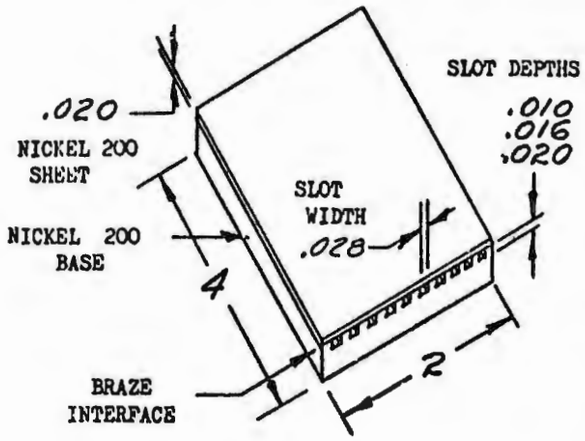

SLOT PLUGGING EXPERIMENT

SUCCESSFULLY BRAZED WITHOUT PLUGGING.
WITHSTOOD 15,000 P.S.I. PROOF TEST.
WITHSTOOD 5700 P.S.I. AT 1120°F.

SAMPLE #2

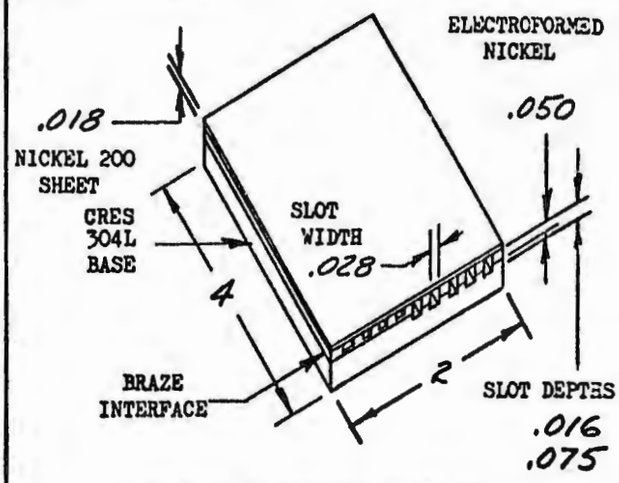

BRAZE TO ELECTROFORM EXPERIMENT

SUCCESSFULLY BRAZED WITHOUT PLUGGING.
WITHSTOOD 15,000 P.S.I. PROOF TEST.
WITHSTOOD 5,900 P.S.I. AT 1080°F.
(DEEPER SLOTS WENT INTO 304L BASE)

SAMPLE #3

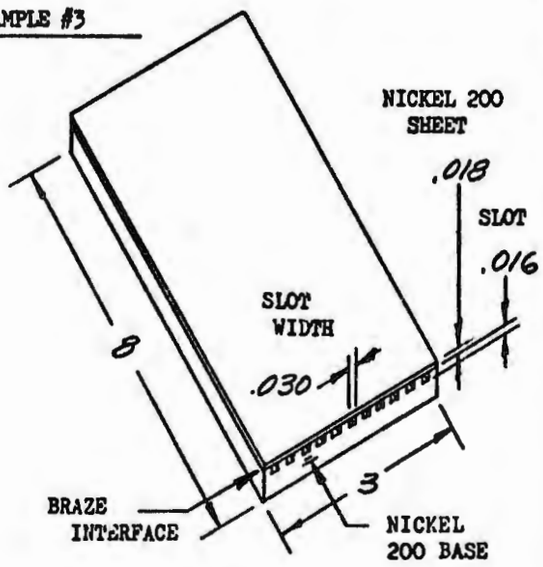

BRAZE ACCUMULATION EXPERIMENT

TO BE BRAZED ON AN INCLINE TO
EVALUATE ACCUMULATION EFFECTS
FROM GRAVITY OR CAPILLARITY.
BEING ALLOYED WITH THE STRIP
Rolling Method

SAMPLE #4

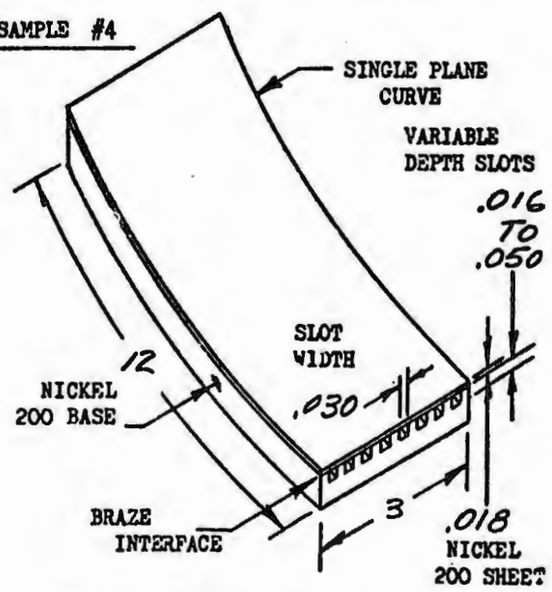

COMBINED BRAZING VARIABLES

SINGLE PLANE CURVED SAMPLE FOR
VERIFICATION OF MULTIPLE VARIABLES.
TO BE ALLOYED WITH STRIP ROLLING

Figure 120. Wrought Sheet Brazed Face Samples (No. 1, 2, 3, and 4) (U)

WROUGHT SHEET BRAZED FACE SAMPLES

SAMPLE #5

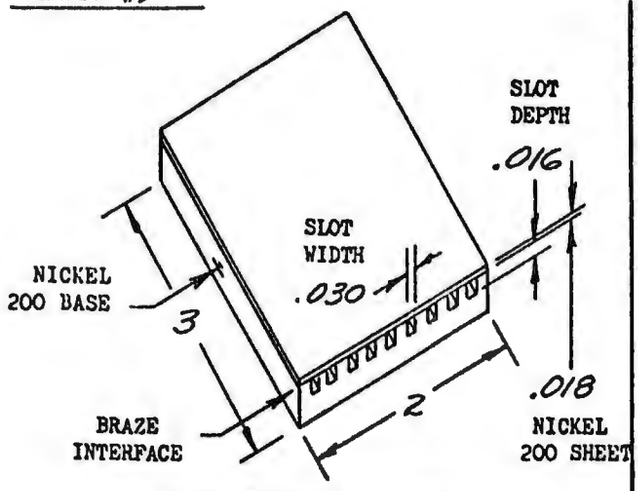

ALLOY QUANTITY EXPERIMENT

ALLOYING METHODS EVALUATED. MAXIMUM AND MINIMUM ALLOY AMOUNT DETERMINED. LACK OF BOND CHECKED BY STOP-OFF ON TWO LANDS IN TWO LOCATIONS. (UNBONDED AREA BLISTERED AT 10,800 P.S.I. PRESSURE TEST) ALL INTENDED LANDS BRAZED - NO PLUGGING. PORTION REBRAZED SUCCESSFULLY USING 50-P.S.I. BAG PRESSURE.

SAMPLE #6

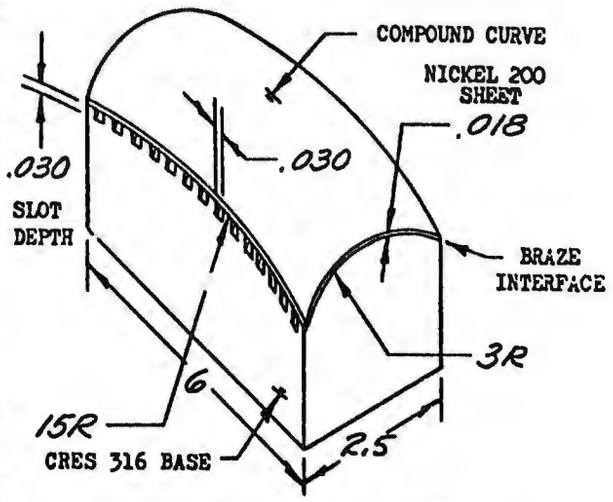

COMPOUND CURVATURE EXPERIMENT

EVALUATION OF FIT, BRAZE TOOLING, BRAZE PRESSURE, TEMPERATURE, AND EXPANSION RATES ON A THREE-DIMENSIONAL SURFACE. DETERMINES VACUUM OR PRESSURE BAG BRAZING PROCESS. FIRST BRAZE SUCCESSFUL; SECOND BRAZE WITH FOIL ALL OVER SUCCESSFUL; THIRD BRAZE TO BE STRIP ROLLED ALLOY AND 50-P.S.I. BAG PRESSURE.

SAMPLE #7

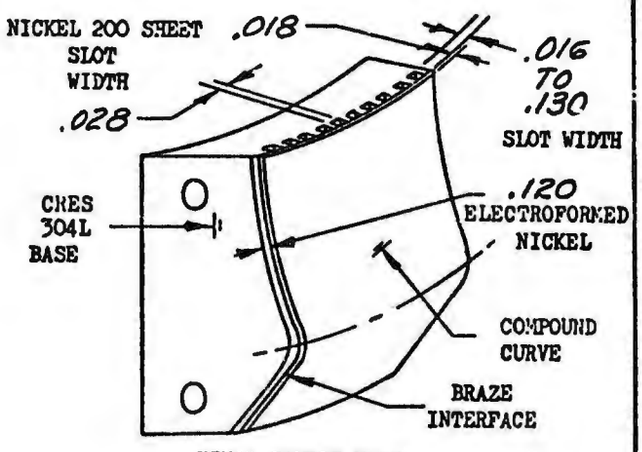

FINAL SAMPLE HALF

REPRESENTS ACTUAL CHAMBER SEGMENT HALF SECTION #1 EVALUATES ALL VARIABLES.

SAMPLE #8

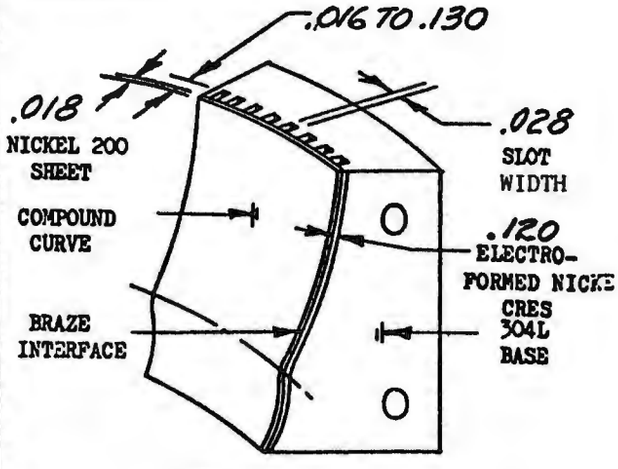

FINAL SAMPLE HALF

REPRESENTS ACTUAL CHAMBER SEGMENT HALF SECTION #2 EVALUATES ALL VARIABLES.

Figure 121. Wrought Sheet Brazed Face Samples (No. 5, 6, 7 and 8) (U)

SAMPLE #1

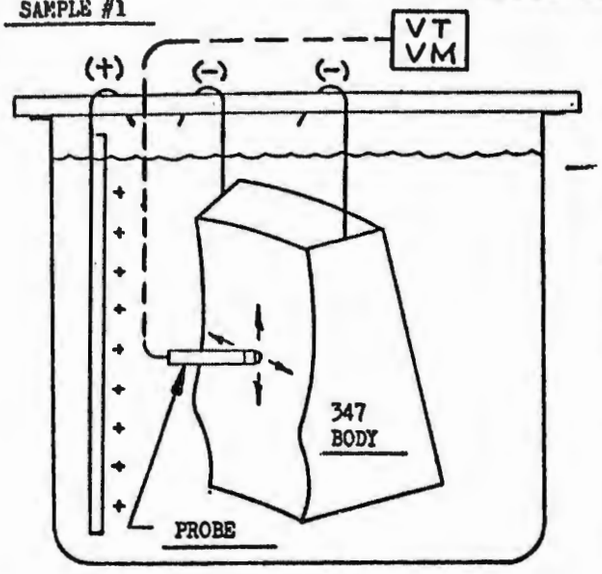

A. UNSHIELDED DEPOSITION PATTERN

SURPLUS INNER AND OUTER BODIES FOR CATHODE. DEPOSIT THIN SEPARABLE LAYERS OF NICKEL, PART OFF, AND MEASURE.

B. FACE POTENTIAL

PROBE TO DETERMINE SURFACE POTENTIAL GRID COMPLETELY SUCCESSFUL.

SAMPLE #2

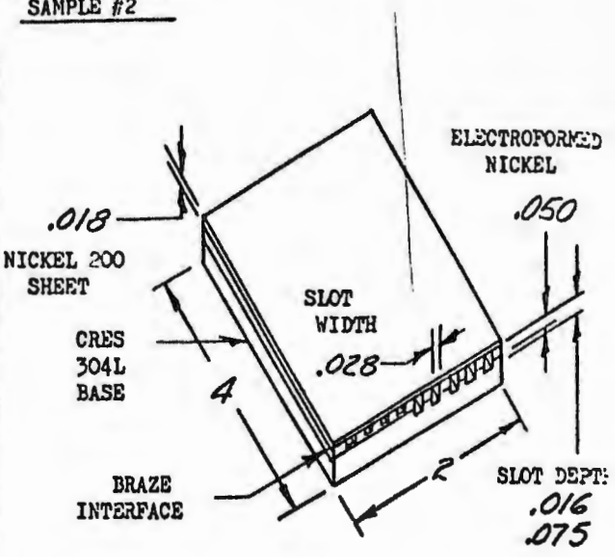

BRAZE TO ELECTROFORM EXPERIMENT

SUCCESSFULLY BRAZED WITHOUT PLUGGING.

WITHSTOOD 15,000 P.S.I. PROOF TEST.

WITHSTOOD 5,900 P.S.I. AT 1080°F.

(DEEPER SLOTS WENT INTO 304L BASE)

SAMPLE #3

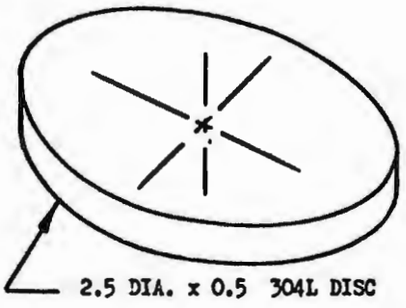

ACTIVATION AND ELECTROFORMING ON 304L MATERIAL

ACTIVATION TRIALS ON CHAMBER BODY MATERIAL COMPLETELY SUCCESSFUL.

SAMPLE #4

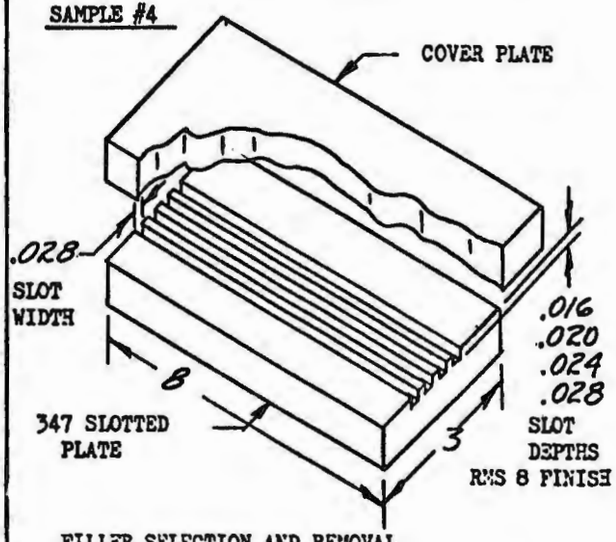

FILLER SELECTION AND REMOVAL

A. CLAMP PLATE OVER RIGIDAX FILLED SLOTS AND RUN REMOVAL TESTS

B. REPEAT WITH UNICHROME 320 WAX

C. REPEAT WITH RIGIDAX AND NO $CACO_3$ FILLER

D. DETERMINE OPTIMUM WAX FOR FILL, ADHESION, COMPATIBILITY, WORKABILITY, ETC. WORK STOPPED UNTIL FACE APPLICATION METHOD IS CHOSEN.

Figure 122. Electroformed Face Samples (No. 1, 2, 3 and 4) (U)

SAMPLE #5

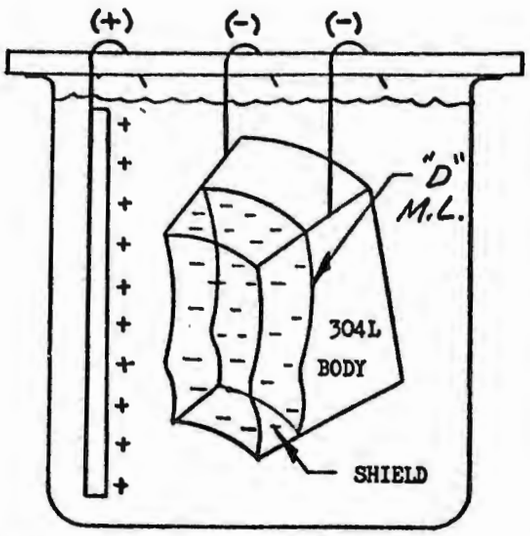

EFFECTS OF SHIELDING ON DEPOSITION RATE

A. FORMULATE SHIELD GEOMETRY FROM TESTS 1A AND 1B AND VERIFY BY ELECTROFORMING FACING ON 304L INNER AND OUTER BODIES.

B. CHECK DEPOSITION PATTERN USING SPECIAL FIXTURE.

C. OPTIMIZE FOR BASIC SHIELD GEOMETRY TO BE USED ON ALL SUBSTRATE ELECTRO-FORMING.

SAMPLE #6

NODULE CONTROL

USING SHIELDS FROM SAMPLE #5 WITH .100 x .100 SLOTS FOLLOWING "D" MOLD LINE DETERMINE EDGE SPACING FOR MOST EFFECTIVE NODULE CONTROL.

SAMPLE #7

DETERMINATION OF INITIAL CURRENT DENSITY FOR FACING

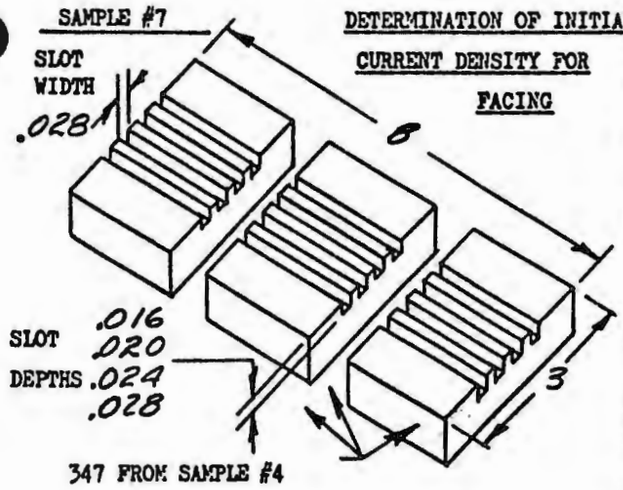

A. ACTIVATE AND E.F. WITH 5.0A/ft^2 FOR 1 HOUR, AND INCREASE TO 20.0 A/ft^2.

B. ELECTROFORM WITH 20.0 A/ft^2 INITIALLY.

C. E.F. WITH 10.0 A/ft^2 FOR 1 HOUR AND INCREASE TO 20.0 A/ft^2.

D. ETCH OFF A, B, C AND REPEAT OPTIMUM CONDITION FOR VERIFICATION.

SAMPLE #8

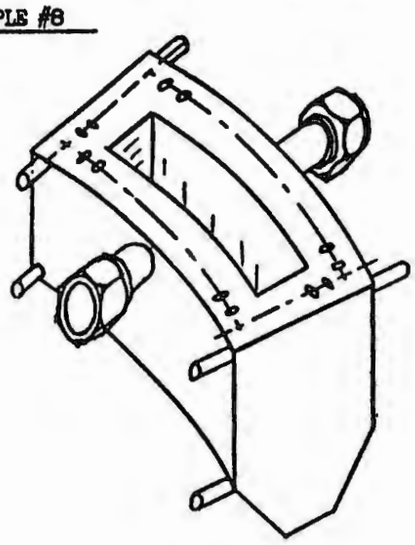

ANALYSIS OF ALL-CHANNEL CHAMBER

A. CONDUCT FAILURE ANALYSIS ON CRACKS.

B. INVESTIGATE CORRECTIVE ACTION FOR ELECTROFORMING AND/OR MACHINING PROCESS.

Figure 123. Electroformed Face Samples (No. 5, 6, 7 and 8) (U)

CONFIDENTIAL

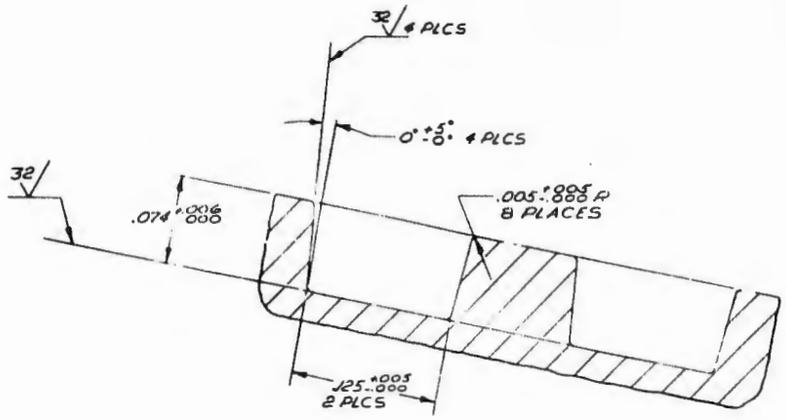

SECTION C-C
SCALE 20/1

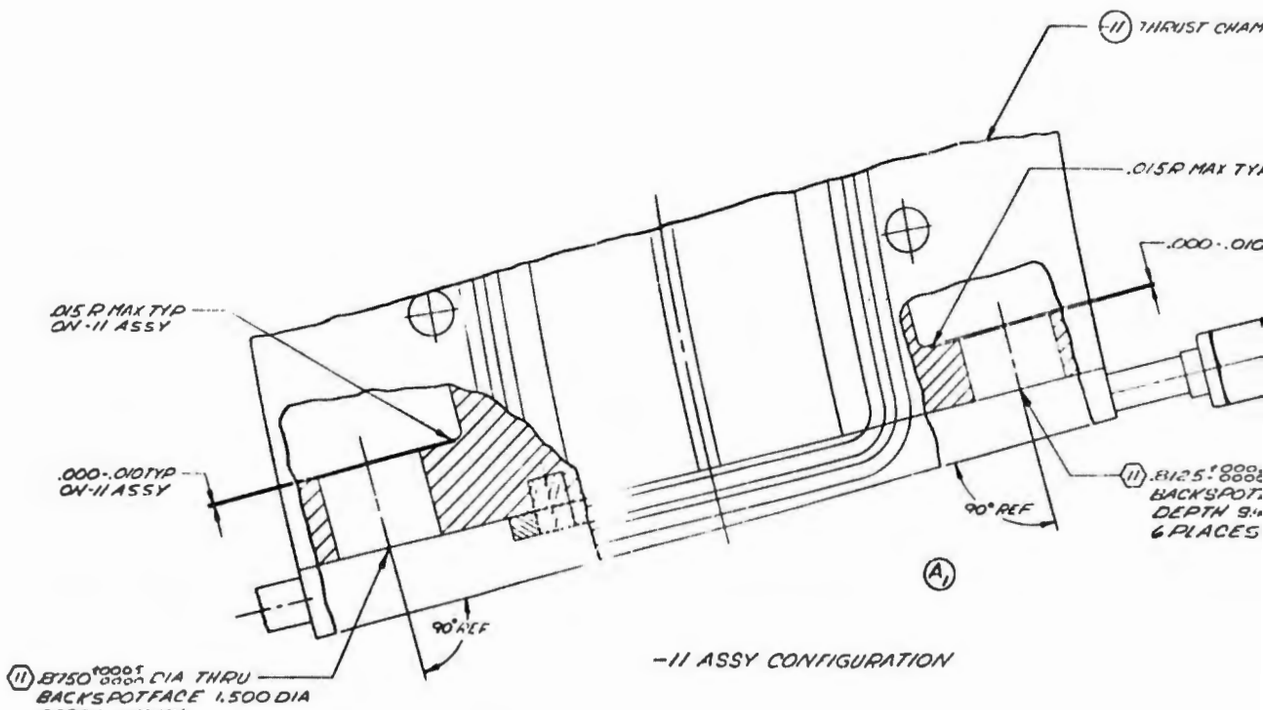

-11 ASSY CONFIGURATION

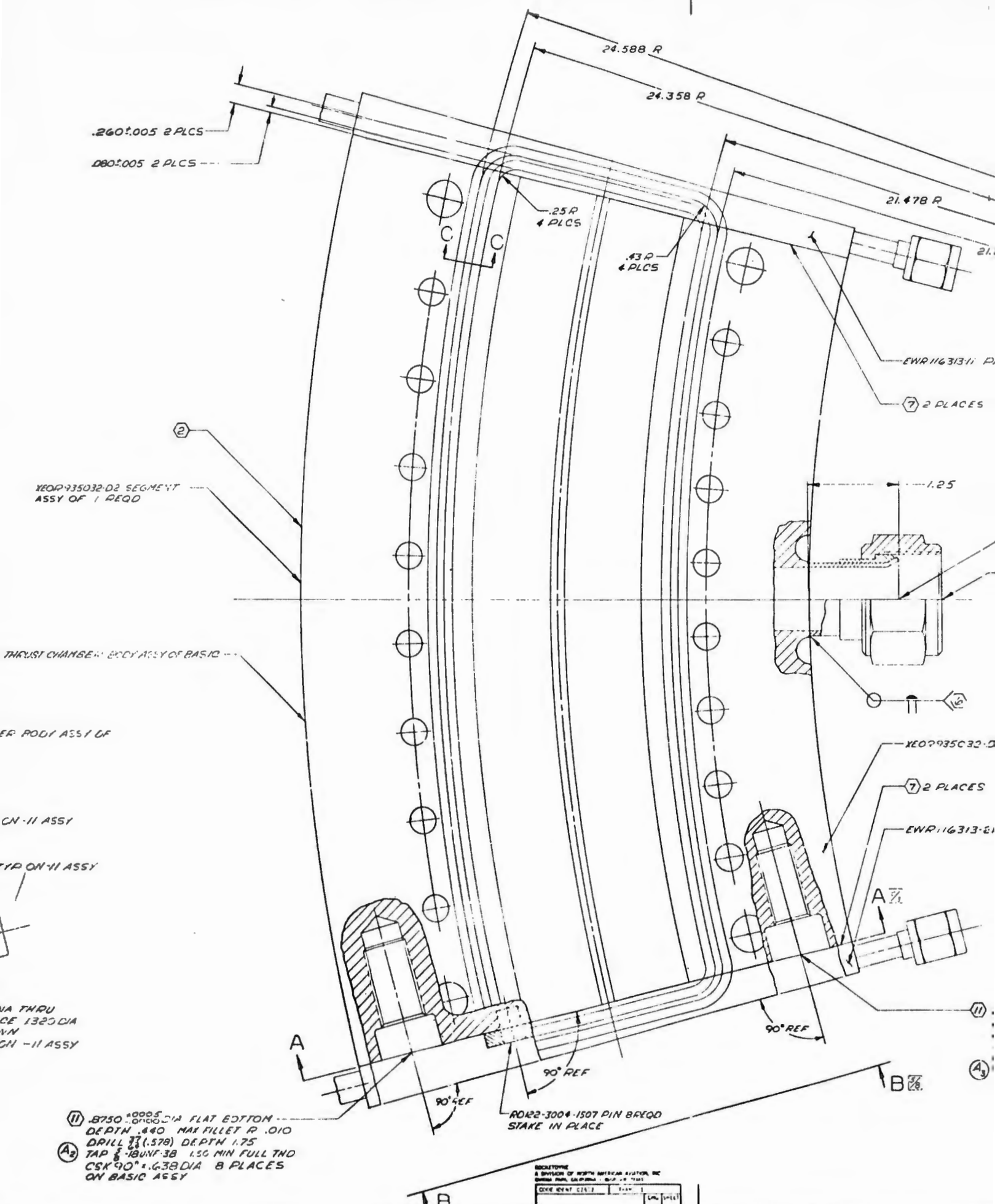
24.588 R
24.358 R
.260±.005 2 PLCS
.080±.005 2 PLCS
.25 R 4 PLCS
.43 R 4 PLCS
21.478 R
C
C
EWR 116313-11
7 2 PLACES
2
XEOP 935032-02 SEGMENT ASSY OF 1 REQD
1.25
THRUST CHAMBER BODY ASSY OF BASIC
ER BODY ASSY OF
CN -11 ASSY
TYP ON -11 ASSY
XEOP 935032-0
7 2 PLACES
EWR 116313-6
A
A
11
90° REF
90° REF
90° REF
B
B
A3
11 .8750 +.0005 -.0010 DIA FLAT BOTTOM
DEPTH .440 MAX FILLET R .010
DRILL 37/64 (.578) DEPTH 1.75
A2 TAP 5/8-18UNF-3B 1.50 MIN FULL THD
CSK 90° x .638 DIA 8 PLACES
ON BASIC ASSY
R0122-3004-1507 PIN BREQD
STAKE IN PLACE

21.248 R

11 PANEL ASSY OF 1 REQD

ES

-7 TUBE 1 REQD
FLARE PER MS 33514

MS20819-..6C SLEEVE 1 REQD
AN818 16J NUT 1 REQD

32-01 SEGMENT ASSY OF 1 REQD

ES

13-21 PANEL ASSY OF 1 REQD

(11) .3125 +.0005 -.0000 DIA FLAT BOTTOM
DEPTH .485 MAX FILLET R .010
DRILL #8 (.453) DEPTH 1.75
TAP 1/2-20UNF-3B 1.50 MIN FULL THD
CSK 90° .512 DIA 6 PLACES
(A3) IN BASIC ASSY

(A7)
-A-
22.918 R REF
.187 +.002 -.000
(3) BRAZE SURFACE — 2 PLACES
4.25
2.750 REF
(4) THROAT DATUM — (REQR 935032-02)
(5) .3125 +.0010 -.0000 DIA
.260 DEEP FLAT BOTTOM
.010 MAX FILLET R
8 PLACES
E
E
2.750 REF
-A- .005
(A7)

.030 STOCK
(A7)
.440 DIA
.940 DIA
-3 RING DETAIL

SECTION A-A

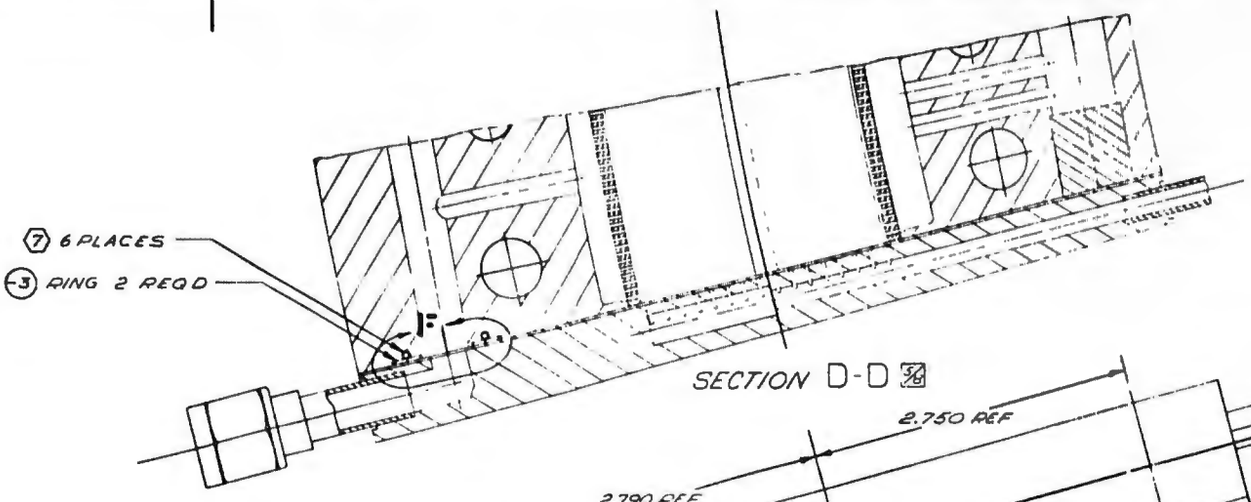

SECTION D-D

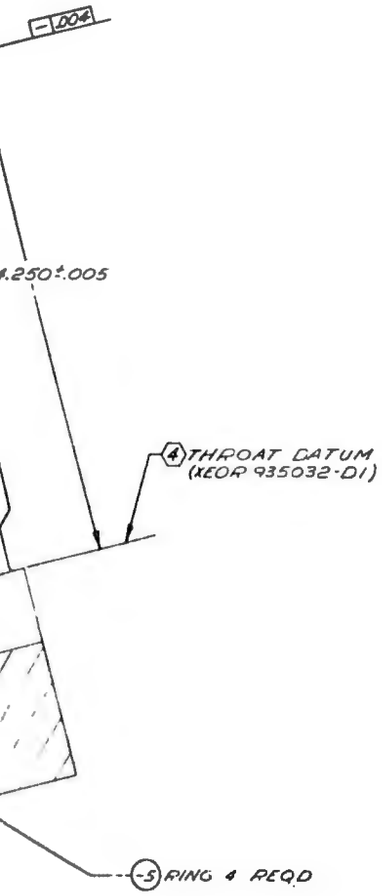

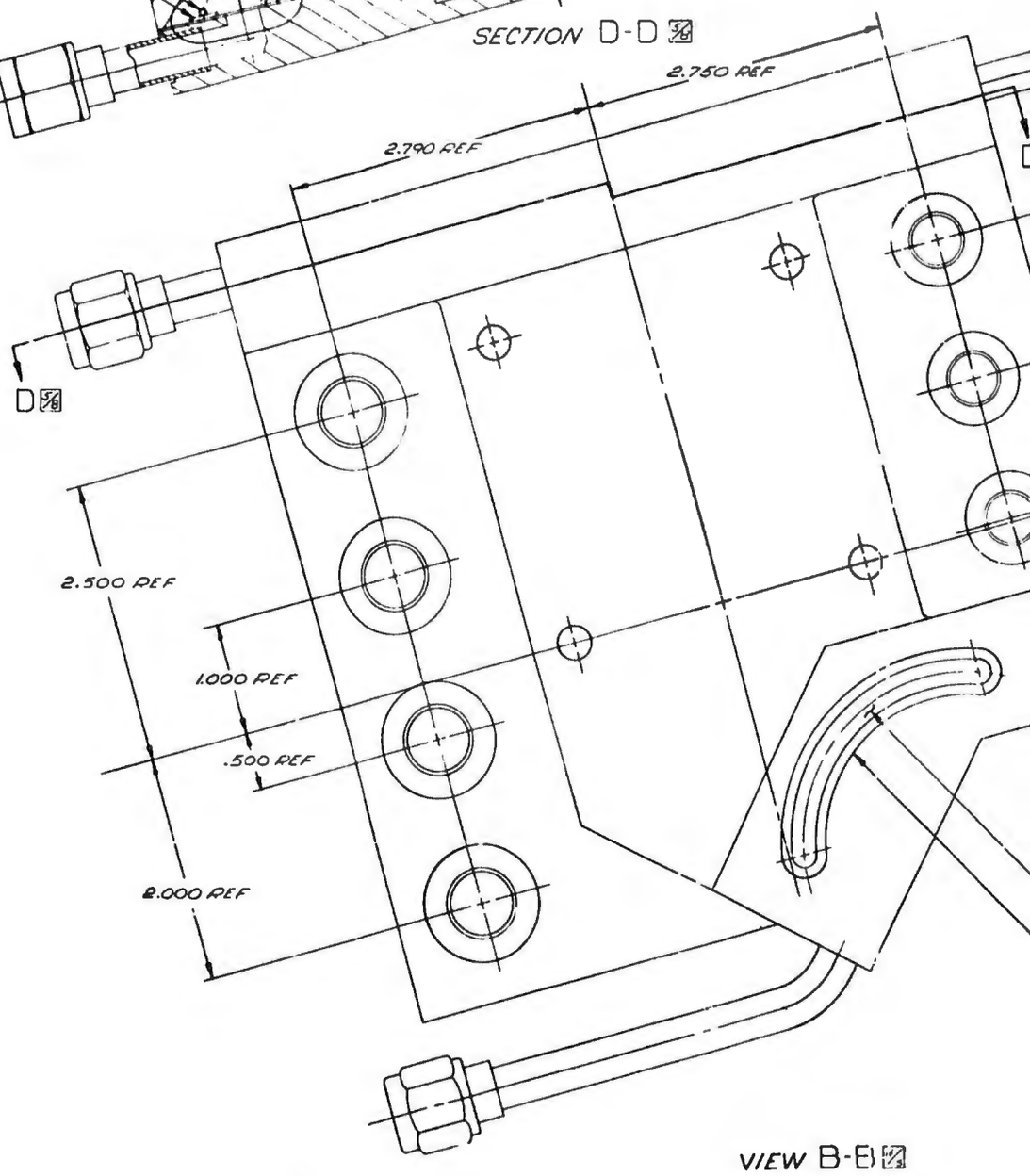

VIEW B-B

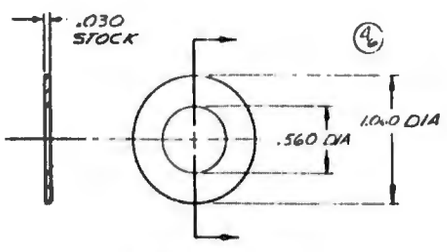

-5 RING DETAIL

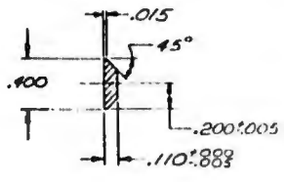

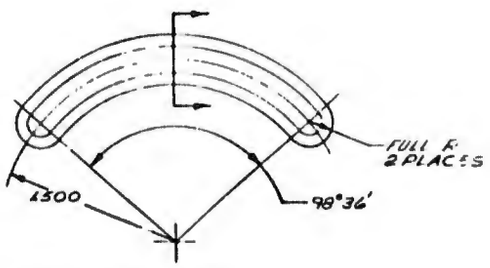

-9 COVERPLATE DETAIL

REVISIONS					
ZONE	LTR	DESCRIPTION		DATE	APPROVED
		1. MAY BE REWORKED 3. RECORD CHANGE 2. CANNOT BE REWORKED 4. NON SHOP PRACTICE 5. PARTS MADE OK			
	A				
19		1) CREATED BASIC -11 ASSY	3		
		ADDED -11 ASSY CONFIG			
19		2) .875 +.005 -.000 DIA WAS .850 +.005 -.000	12		
		ADDED ON BASIC ASSY			
15		3) ADDED ON BASIC ASSY	3		
2		4) ADDED G/N 14	1		
3-11		5) ADDED DETAIL F & SECTE-E	1		
9		6) 1.060 DIA WAS 1.06 DIA	1		
		.560 DIA WAS .56 DIA			
12		7) .440 DIA WAS .44 DIA	1		
		.960 DIA WAS 1.46 DIA			
2		8) ADDED G/N: 15 & 16	5		
11/12		9) ADDED SURFACE A &	1		
		-A- 0251			
		EFFECT ON ITEMS 2, 4, 5, 6, 7, 8, 9			
		WNOO1 & SUBS			

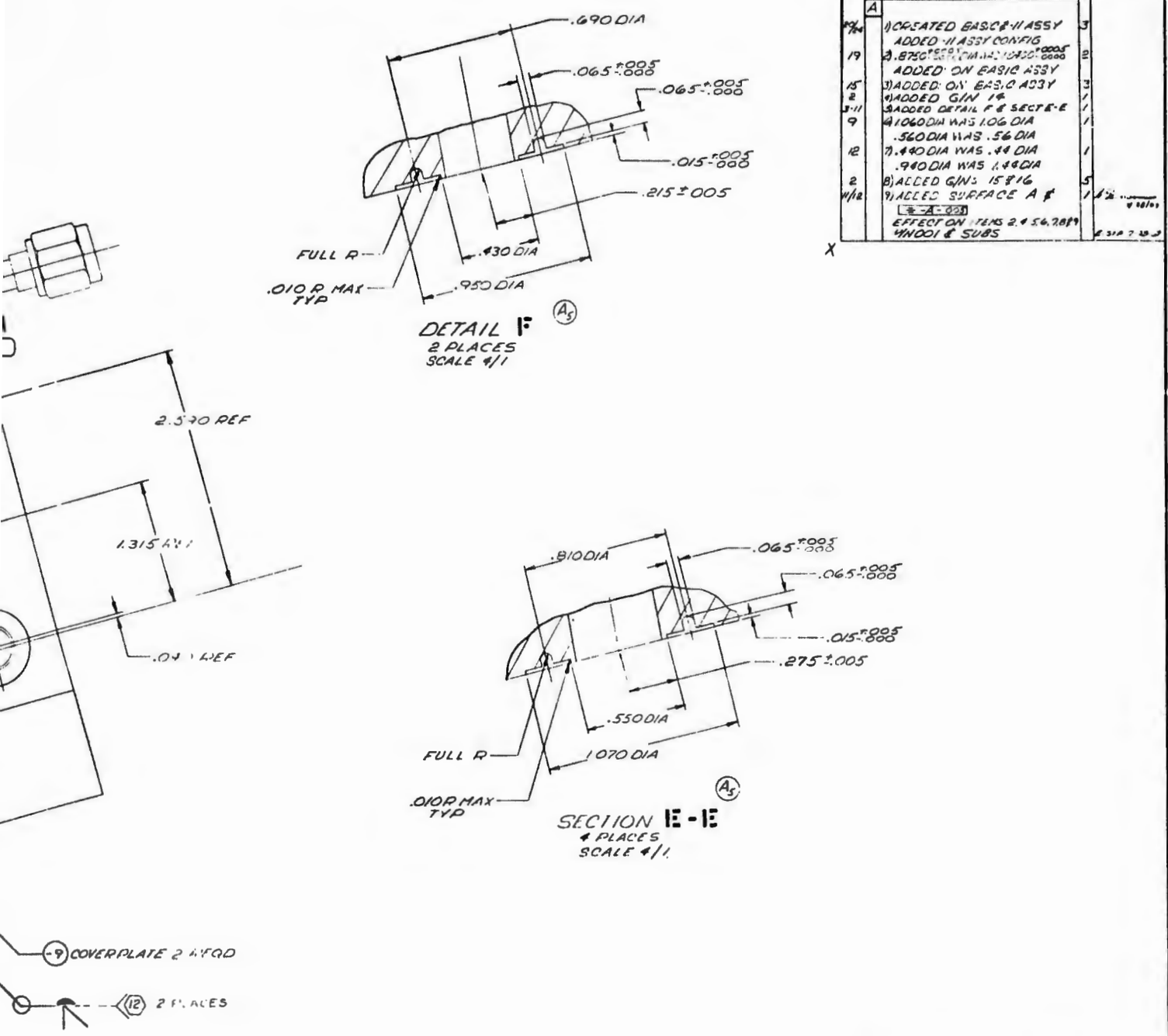

CONFIDENTIAL

(12) 75% MINIMUM BRAZE ENGAGEMENT
.5 VACUUM DRY AFTER PRESSURE TEST AT 250±20°F
14 CONTROL CONTAMINATION OF MFG. PROCESSES TO LEVEL 4 PER RA0615-003
13 HYDROSTATIC PROOF PRESSURE TEST WITH 40 MICRON FILTERED WATER TO 6700±50 PSIG MAINTAIN PRESSURE FOR 2 MINUTES REPEAT FOR A TOTAL OF 5 CYCLES NO LEAKAGE ALLOWED
(12) GTA BRAZE PER RA0107-027 USING RB0170-064 BRAZE ALLOY
(11) COORDINATE WITH PART NO XEOP 935035
10 CRITICAL PORTSTER RA0116-058 (DO NOT USE PLASTIC CAPS)
(9) FM 415 FELTMETAL 15% WROUGHT DENSITY HUYCK METAL CO, 4847 ALCOVE ST, N HOLLYWOOD CALIF.
8 ALL MATERIALS CONTACTING THIS PART MUST MEET THE REQUIREMENTS OF RA0102-014
(7) BRAZE PER MPR B-175-49
(6) WELD PER RA0107-027 CLASS II
(5) COORDINATE WITH PART NO EWR116313
(4) IN LINE WITHIN .002 TOTAL
3 VAPOR DEGREASE PER ST0110GA0002
(2) IDENTIFY PER RA0104-008
1 MACHINE PER RA0103-002

NOTE UNLESS OTHERWISE SPECIFIED

223/224

-11 BASIC DASH NO

-9	347 CRES PLATE	300 x 150 x .125	QQS763 CL 347 CONDA
-7	321 CRES TUBE	100 OD x .065 WTH x 150	MIL-T-8808 CLASS I
-5	N. 200 FELTMETAL	125 x 125 x .030	(9)
-3	N. 200 FELTMETAL	175 x 175 x .030	(9)
(4)	MATERIAL	SIZE	SPECIFICATION

HEAT TREAT: NOTED
FINISH:
MATL:

UNLESS OTHERWISE SPECIFIED DIMENSIONS ARE IN INCHES AND APPLY PRIOR TO PLATING OR ANY EACH SURF REQUIREMENTS
TOLERANCES ON ANGLES ± 0° 30'
DECIMALS ± .XX ± .03 .XXX ± .010
HOLES NOTED "DRILL" GIVES THRU TOLERANCE
DO NOT SCALE PRINT

DR BY
CHK BY
DES
MAT
DEV

ROCKETDYNE
A DIVISION OF NORTH AMERICAN AVIATION INC
CANOGA PARK CALIFORNIA · MCGREGOR TEXAS

BODY-BRAZED THRUST CHAMBER, ASSY OF

SIZE J | CODE IDENT NO 02602 | XEOP 935033
SCALE 4/1 | SHEET

Figure 124. Prototype Segment Assembly (U)

(U) region. The fuel coolant crossover passages were removed from the injector and transfer of coolant, where required, was accomplished by external lines. A fabrication flow chart is shown in Fig. 125 and the completed prototype segment assembly is shown in Fig. 126 through 128.

(U) The prototype end plates, designed for a one-pass cooling circuit, are shown in Fig. 129 and 130. The baffle coolant passages were electrically discharge machined. The hot-gas side of the end plate was made of wrought nickel and furnace-braze attached, similar to the technique used for the contoured segment halves. Preformed, felted, nickel strips were used to effect the braze joint between the baffle plates and segment bodies (Ref. 5). This method provided an improved joint and permitted removal of the baffle-to-body secondary bolts that had been used to support the baffle end plate along the wall contour on the previous segment designs. The baffles had the capability of being separately cooled in addition to being normally cooled within the basic cooling circuit.

c. Prototype 30-Degree Segment U/N 1 Testing and Analysis

(U) One hundred tests (029-128) were conducted for evaluation of the prototype channel-wall thrust chamber segment and injector assembly. The majority of the tests were conducted with complete regeneratively cooled operation. A test summary is presented in Table 20 and significant details are discussed in the following paragraphs.

(U) Tests 092-039 were conducted with the brazed-face injector U/N 4 which incorporated the 15-percent oxidizer bias modification. These tests utilized separate hydrogen flow for cooling of the chamber and were of sufficient duration to achieve the following test objectives:

1. Heat transfer data consisting of total coolant enthalpy change, and coolant enthalpy change in each component, such as baffle, inner body, and outer body.

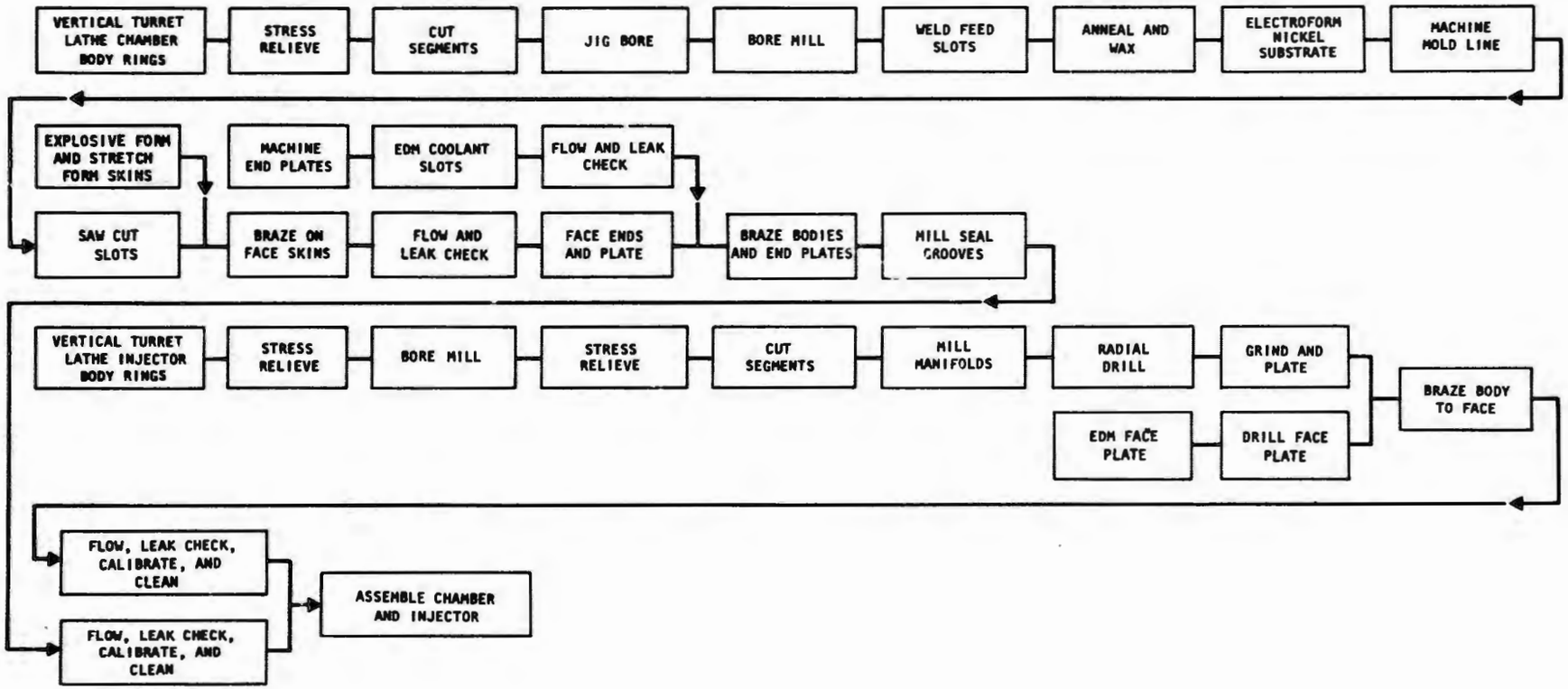

Figure 125. Typical Fabrication Flow Chart for the 30-Degree Prototype Thrust Chamber Segment Assembly (U)

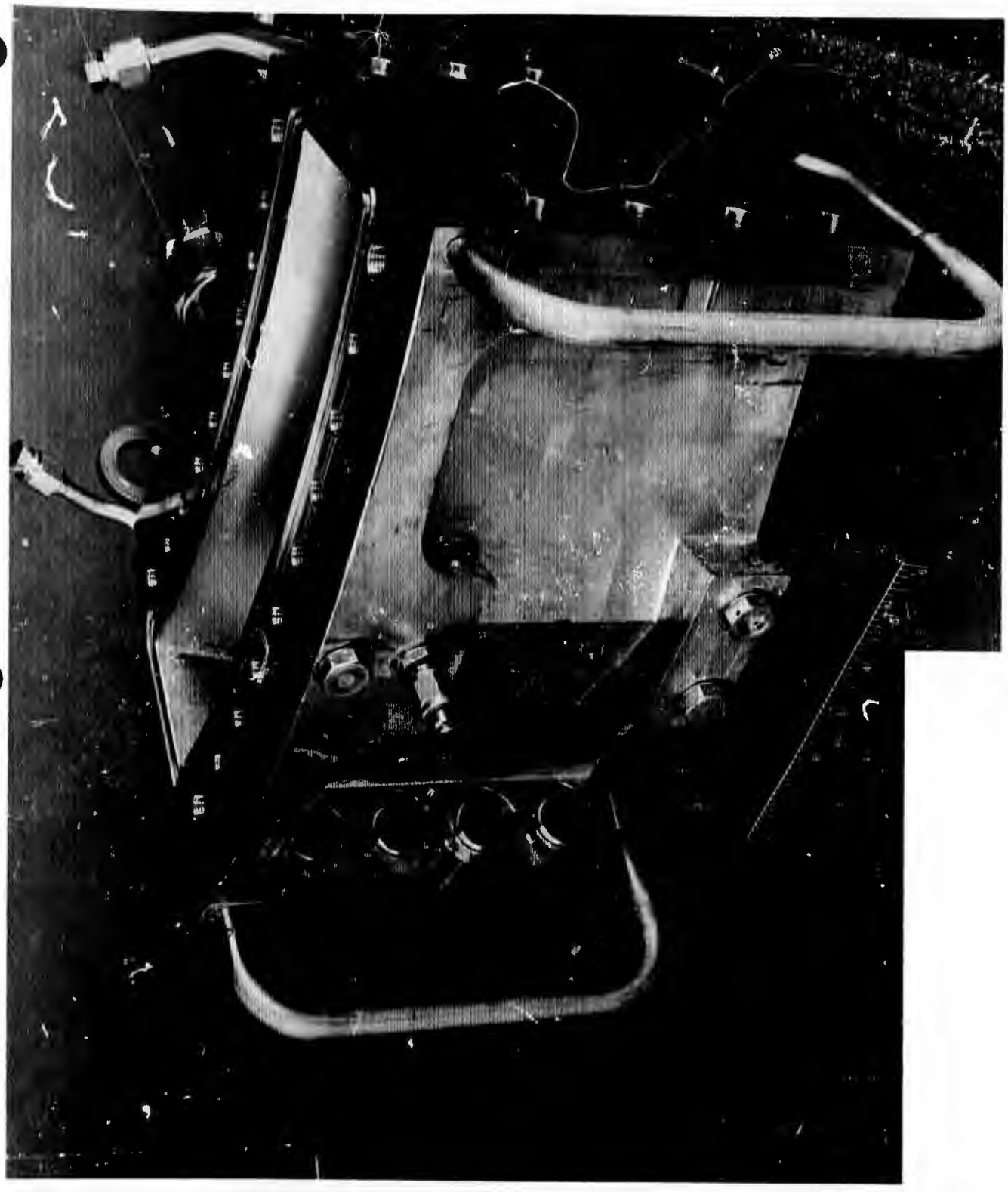

1EH22-4/7/70-C1A*

Figure 126. Prototype Segment (Outboard View) (U)

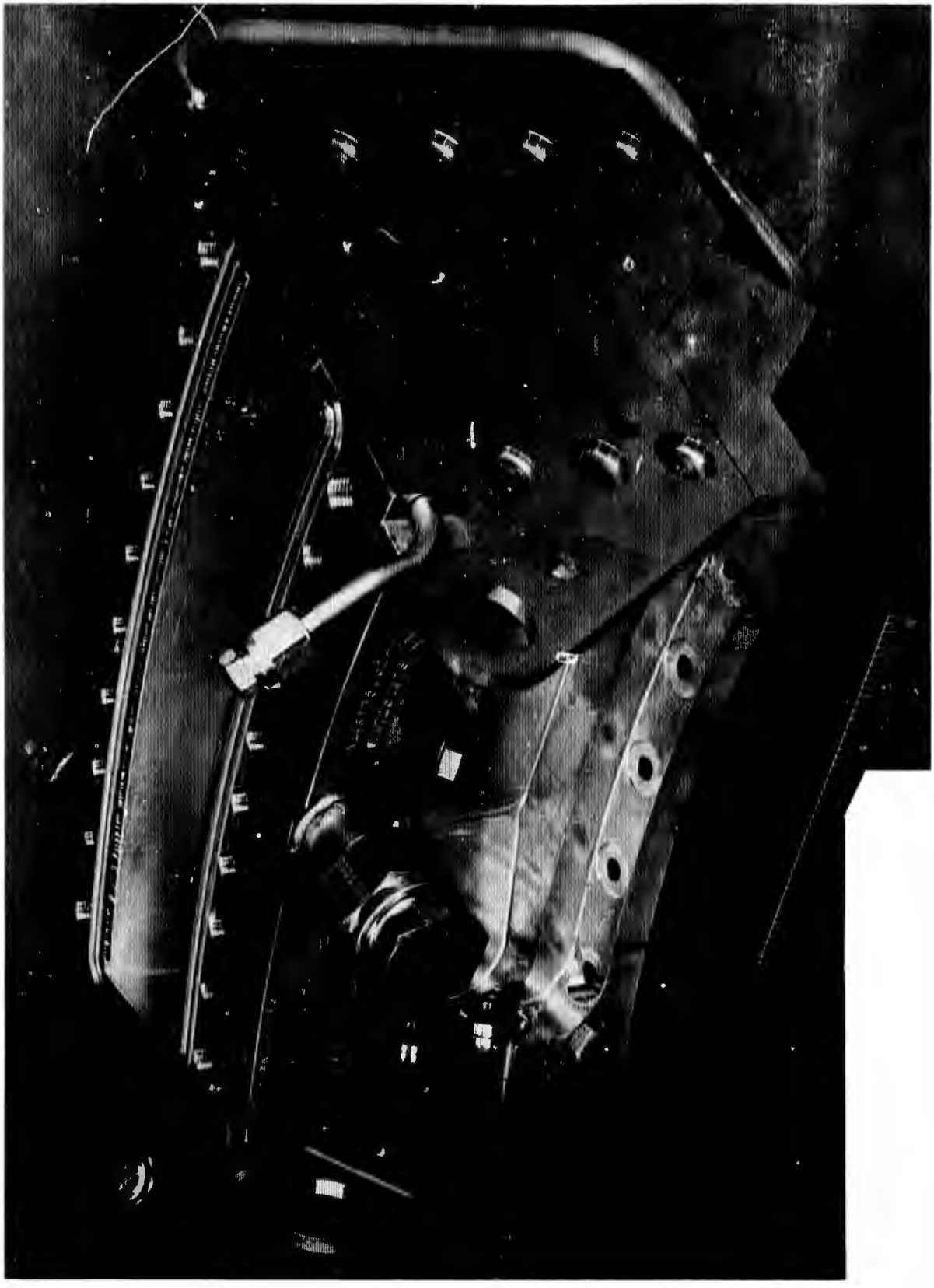

1EH22-4/7/70-C1D*

Figure 127. Prototype Segment (Inboard View) (U)

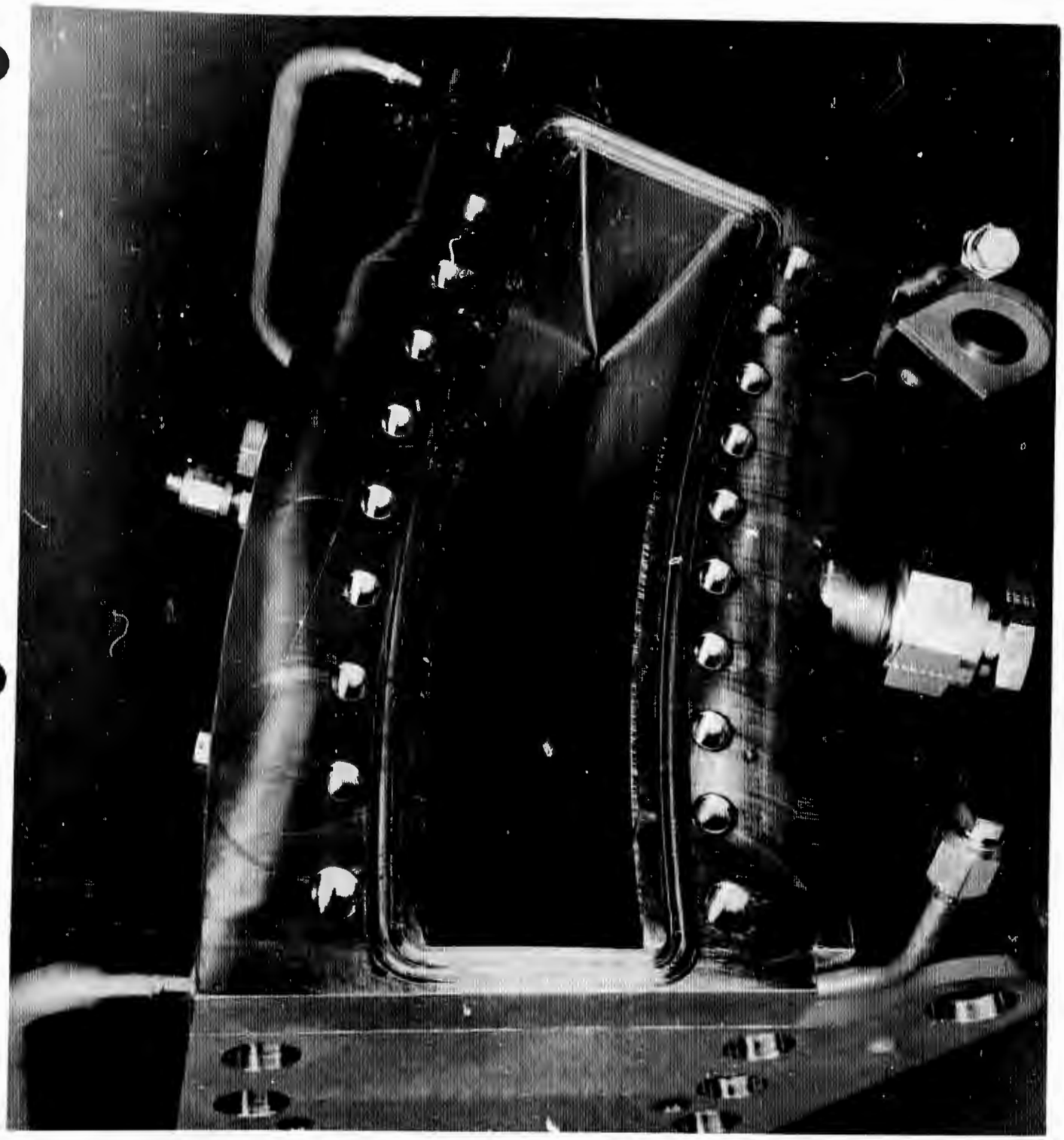

1EH22-4/7/70-C1D

Figure 128. Prototype Segment (Top View) (U)

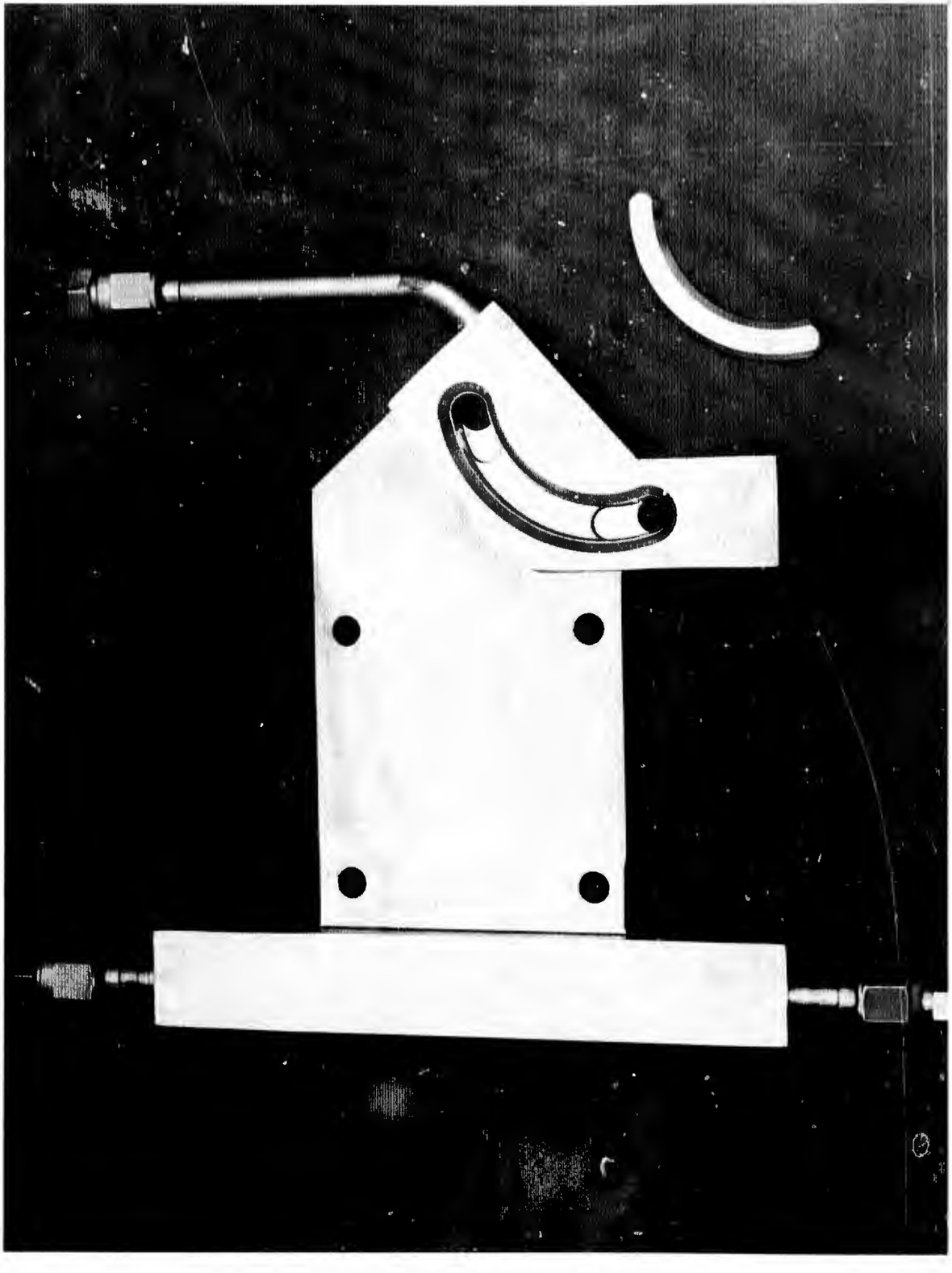

1EH32-7/31/69-C1G

Figure 129. Baffles After Final Machining (U)

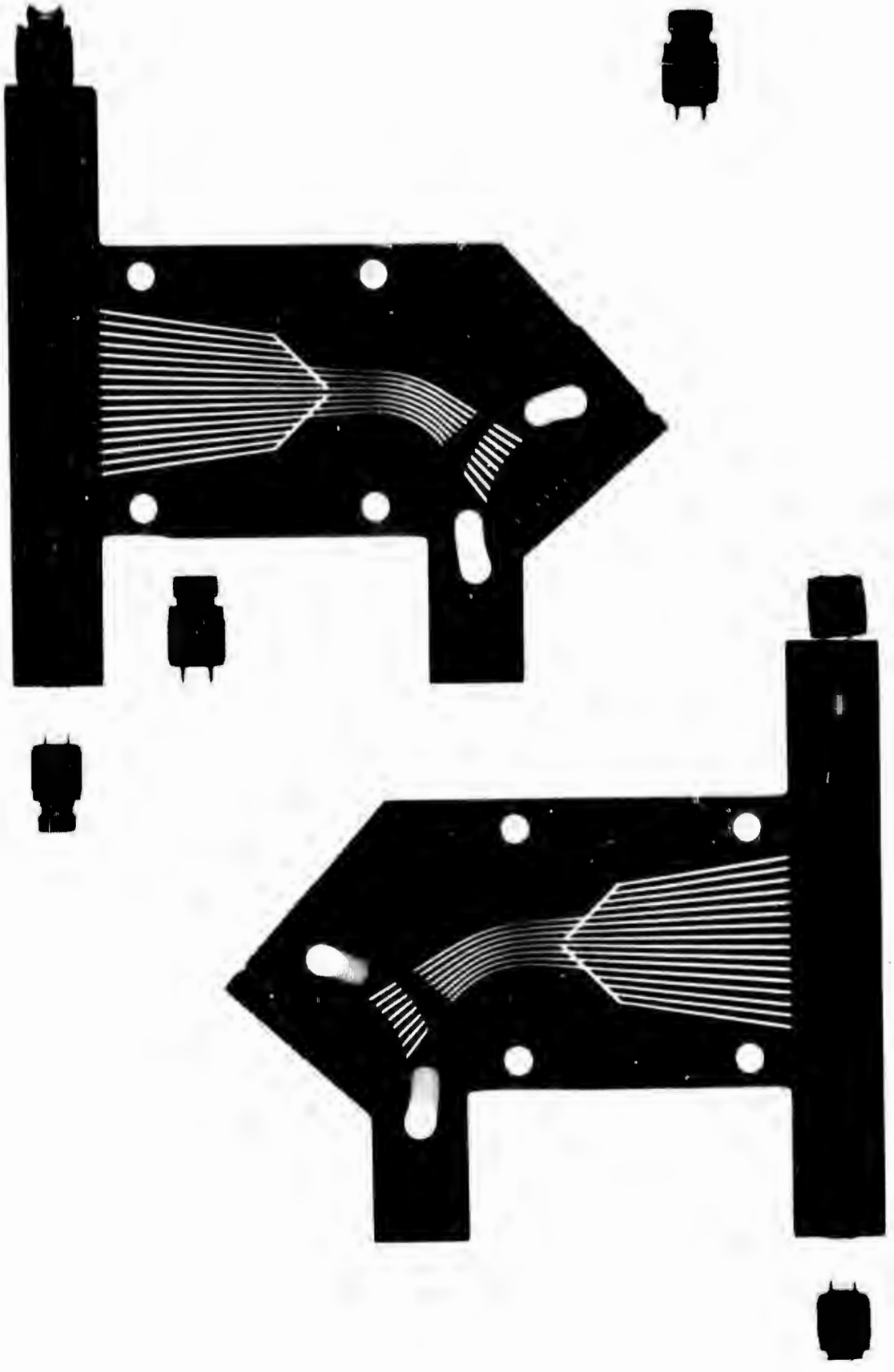

Figure 130. X-Ray of Baffle (U)

TABLE 20

TEST SUMMARY, PROTOTYPE U/N 1 30-DEGREE CHANNEL-WALL THRUST CHAMBER SEGMENT TESTING (U)

TEST NO.	CHAMBER U/N / INJ. U/N	DUR. (SEC.)	CHAMBER PRESS. (PSIA)	INJ. FLOW (LB/SEC)	MIXTURE RATIO	FUEL INJ. TEMP. (°R)	% OVER-COOL	ΔH BAFFLES BTU/SEC	ΔH O/B BTU/SEC	ΔH I/B BTU/SEC	$\frac{P_3}{T_3}$	$\frac{P_4}{T_4}$	$\frac{P_5}{T_5}$	$\frac{P_6}{T_6}$	$\frac{P_7}{T_7}$	ΔH TOTAL BTU/SEC	ΔP TOTAL PSI
029	4/4	1.0	301.2	2.478	12.87	1202	53	-	-	-	1285 89	1024 -	888 -	807	446 700	679	839
030	4/4	2.8	335.0	2.755	14.58	1000	41	-	-	-	1319 78	1097 -	972 -	891 -	534 -	775	785
031	4/4	3.0	331.2	2.715	13.99	1331	38	-	-	-	1320 76	1099 -	971 -	889 -	529 823	816	792
032	4/4	1.8	327.4	2.726	14.15	1280	40	-	-	-	1309 91	1069 -	938 -	858 -	491 821	795	818
033	4/4	3.0	338.1	2.760	14.40	1315	34	-	-	-	1302 77	1090 -	962 -	883 -	528 -	814	774
034	4/4	6.8	348.6	2.7806	14.16	1348	20	66	453	385	1252 81	1048 131	943 582	853 582	522 993	904	730
035	4/4	10.0	212.2	1.676	12.95	1480	55	49	328	321	989 74	814 124	737 539	679 539	427 976	698	561
036	4/4	4.6	499.6	4.110	15.02	1388	21	79	564	432	1738 77	1432 127	1279 507	1173 507	722 824	1073	1016
037	4/4	7.0	498.5	4.125	14.86	1358	21	130	510	430	1728 72	1433 153	1282 503	1171 503	721 820	1070	1006
038	4/4	3.2	602.1	5.054	14.61	1436	23	119	757	502	2111 71	1723 142	1542 487	1409 487	865 787	1258	1246
039	4/4	3.2	600.5	5.001	14.65	1251	10	129	724	471	1910 75	1568 160	1405 519	1284 519	779 835	1195	1131
040	4/4	13.2	81.0	.624	12.63	1342	26	61	-	-	384 79	326 332	280 -	257 -	138 1446	321	247
041	4/4	6.5	627.6	5.339	14.45	1292	-0.7	151	597	473	1877 67	1560 157	1397 559	1283 559	768 898	1221	1109
042	4/4	10.0	232.8	1.75	13.35	1360	0	81	287	323	718 105	588 248	510 768	465 768	247 1383	691	471

P_3, T_3 = Baffle Inlet; Pressure, Temperature

P_4, T_4 = Outer Body Inlet; Pressure, Temperature

P_5, T_5 = Outer Body Discharge; Pressure, Temperature

P_6, T_6 = Inner Body Inlet; Pressure, Temperature

P_7, T_7 = Inner Body Discharge; Pressure, Temperature

P = psia

T = ^{o}R

CONFIDENTIAL

TABLE 20

(Concluded)

TEST NO.	CHAMBER U/N / INJ. U/N	DUR. (SEC.)	CHAMBER PRESS. (PSIA)	INJ. FLOW (LB/SEC)	MIXTURE RATIO	FUEL INJ. TEMP. (°R)	% OVER-COOL	ΔH BAFFLES BTU/SEC	ΔH O/B BTU/SEC	ΔH I/B BTU/SEC	$\frac{P_3}{T_3}$	$\frac{P_4}{T_4}$	$\frac{P_5}{T_5}$	$\frac{P_6}{T_6}$	$\frac{P_7}{T_7}$	ΔH TOTAL BTU/SEC	ΔP TOTAL PSI
043	4/4	1.2	206.8	1.744	10.7	600	Regen.				897 79	727	636	574	318 600		579
044	4/4	1.7	210.8	1.722	12.2	680	Regen.				856 86	692	607	550	306 680		549
045	4/4	1.6	203.3	1.697	14.6	690	Regen.				745 83	610	534	484	275 690		470
046	4/4	2.0	78.8	0.644	11.1	750	Regen.				417 80	334	283	255	131 750		287
047	4/4	3.8	75.3	0.625	17.4	915	Regen.				317 101	250	210	192	104 915		214
048	4/4	1.4	321.8	2.76	11.7	610	Regen.				1250 69	1026	1007	821	472 610		778
049	4/4	1.3	368.3	3.03	7.7	530	Regen.				1810 74	1404	1234	1112	633		1177
050	4/4	1.4	484.8	4.10	12.1	630	Regen.				1834 73	1459	1292	1169	690 630		1144
051-059	4/4	1.7	218.3	1.74	13.1	811	Regen.				821 73	689	606	551	319 811		503
060-068	4/4	1.7	209.8	1.69	12.7	765	Regen.				815 65	689	602	546	306 765		509
069-077	4/4	1.7	209.8	1.69	12.7	765	Regen.				815 65	689	602	546	306 765		509
078-087	4/4	1.7	209.8	1.69	12.7	765	Regen.				815 65	689	602	546	306 765		509
088-097	4/4	1.7	209.8	1.69	12.7	765	Regen.				815 65	689	602	546	306 765		509
098-107	4/4	1.7	209.8	1.69	12.7	765	Regen.				815 65	689	602	546	306 765		509
108-117	4/4	1.7	209.8	1.69	12.7	765	Regen.				815 65	689	602	546	306 765		509
118-128	4/4	1.7	209.8	1.69	12.7	765	Regen.				815 65	689	602	546	306 765		509

P_3, T_3 = Baffle Inlet; Pressure, Temperature

P_4, T_4 = Outer Body Inlet; Pressure, Temperature

P_5, T_5 = Outer Body Discharge; Pressure, Temperature

P_6, T_6 = Inner Body Inlet; Pressure, Temperature

P_7, T_7 = Inner Body Discharge; Pressure, Temperature

P = psia

T = °R

CONFIDENTIAL

(U)

2. Injector chamber compatibility over the range of operating chamber pressures
3. Characteristic velocity efficiency (η_c*) over the chamber pressure range
4. Structural integrity of the chamber and injector
5. Determination of the pressure loss characteristics of the injector and thrust chamber segment to verify conformance with the analytically predicted values

(U) Test 040 was programmed for 20 seconds duration at minimum chamber pressure; however, the test was terminated by the test observer at 13.2 seconds because of an external fire. Posttest disassembly and inspection revealed erosion damage to the injector-to-chamber mating flange surface of both the chamber and injector (Fig. 131).

(U) Investigation of the failure revealed that:

1. The dual O-ring pressurizing system, although activated and pressurized, was not providing GN_2 to pressurize the seals because the land between the O-ring grooves was blocking the port.
2. The O-rings (Viton-A) were degraded from the combustion gas and permitted leakage that was not checked off because of the lack of GN_2.
3. The hardware erosion was caused by escaping combustion gas.

(U) To repair the damage, the complete eroded section was built up by TIG brazing with Nioro (gold-nickel alloy) and remachined to drawing requirements. The O-ring groove configuration was changed to a deeper groove and the land between the dual grooves was decreased in height to improve seal pressurization. The modified design is shown in Fig. 132. In addition to this modification, the Viton A O-rings were changed to hollow metal O-rings for improved compatibility with the combustion gases.

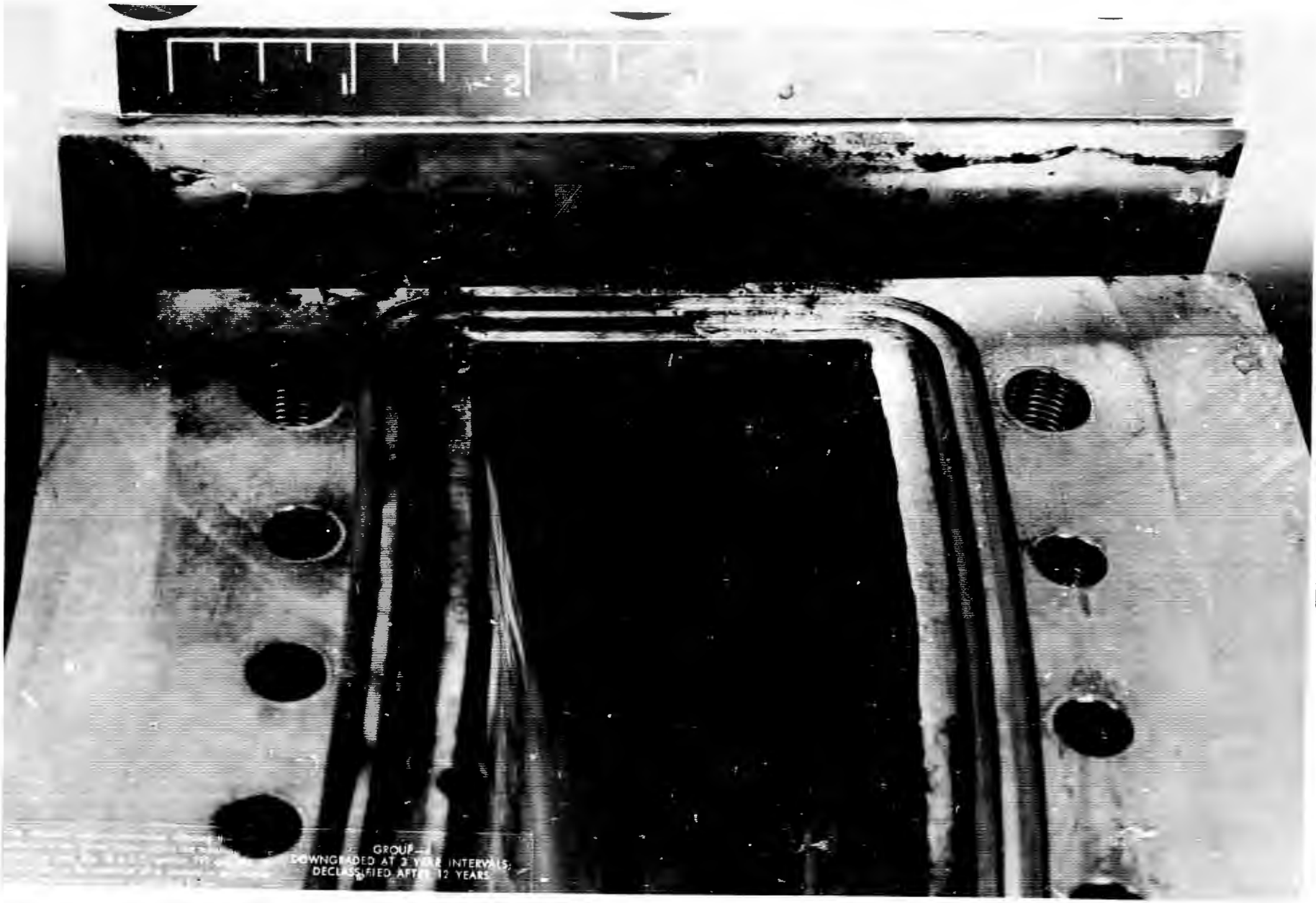

1EH45-9/9/69-C2B

Figure 131. 30-Degree Prototype Segment U/N 1, Seal Area Erosion (U)

CONFIDENTIAL

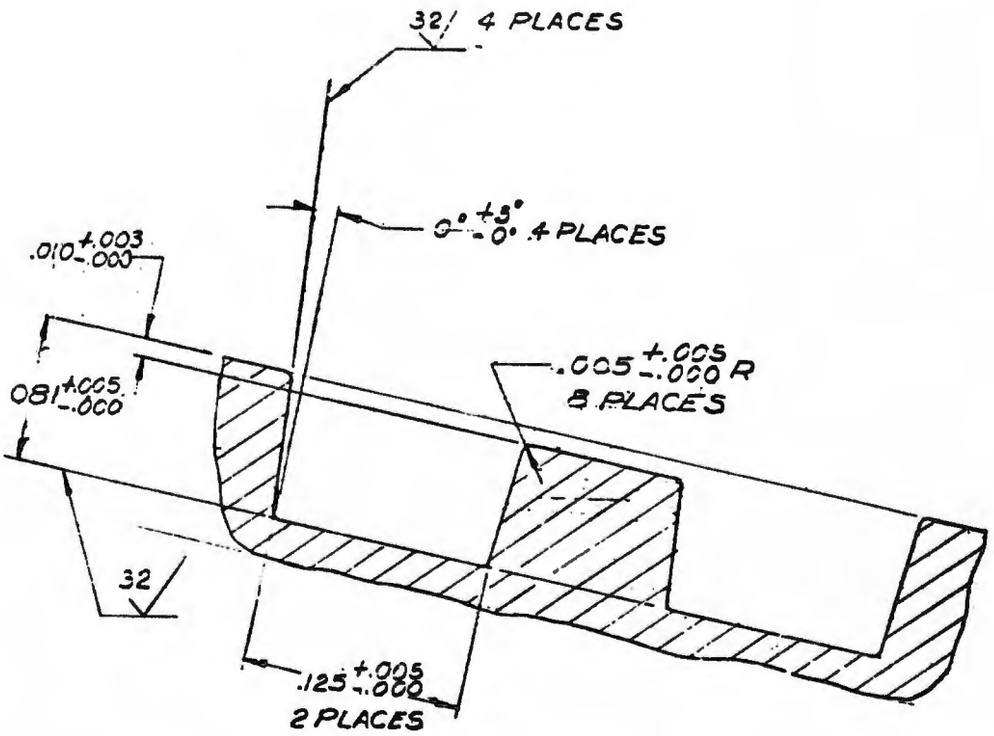

Figure 132. Modification to Land Between O-Ring Grooves on Prototype Channel-Wall Chamber Segment U/N 1 (U)

(C) Test 041 was a satisfactory, programmed test targeted for near maximum chamber pressure and utilized the hardware used during tests 029-040. Posttest disassembly revealed that the thrust chamber inner body had developed two "blisters" near the throat. The blisters (Fig. 133) were located immediately upstream of the throat. (The photo was taken after test 042.) The blisters were formed when the face sheet separated from the inner-body lands in the two small local areas. There was no surface overheating or melting of the blisters, indicating they probably occurred during test shutdown.

(U) The face sheet separation was evaluated, and three possible failure modes were determined:

1. The local areas did not have face sheet-to-land braze bonding and were hydraulically deformed.
2. The areas were locally overheated and then the braze joints failed with concurrent hydraulic deformation of the face sheet.
3. The areas were subjected to cyclic thermal straining that resulted in braze joint failure and hydraulic deformation of the face sheet.

(U) After careful examination of the hardware and test results, the first failure mode, lack of braze bonding, was determined as the most plausible explanation.

(C) Test 042 was conducted with the hardware in the posttest 041 condition. The test was a satisfactory programmed cutoff test whose main objective was to evaluate the effect of regenerative cooling on chamber start and mainstage operation. The test was targeted for 220-psia chamber pressure. The crowns of the blister protrusions burned off during transition to mainstage, as determined from motion picture coverage, and two additional protrusions occurred upstream (downstream coolant flow direction) of the throat (Fig. 133) that were the result of overheating caused by a lack of coolant flow. The protrusion in line with the largest throat plane protrusion ruptured. Examination of the test data and inspection of the injector and chamber indicated that satisfactory regenerative-cooling tests and regenerative-cooling cyclic tests could be performed without repairing the chamber.

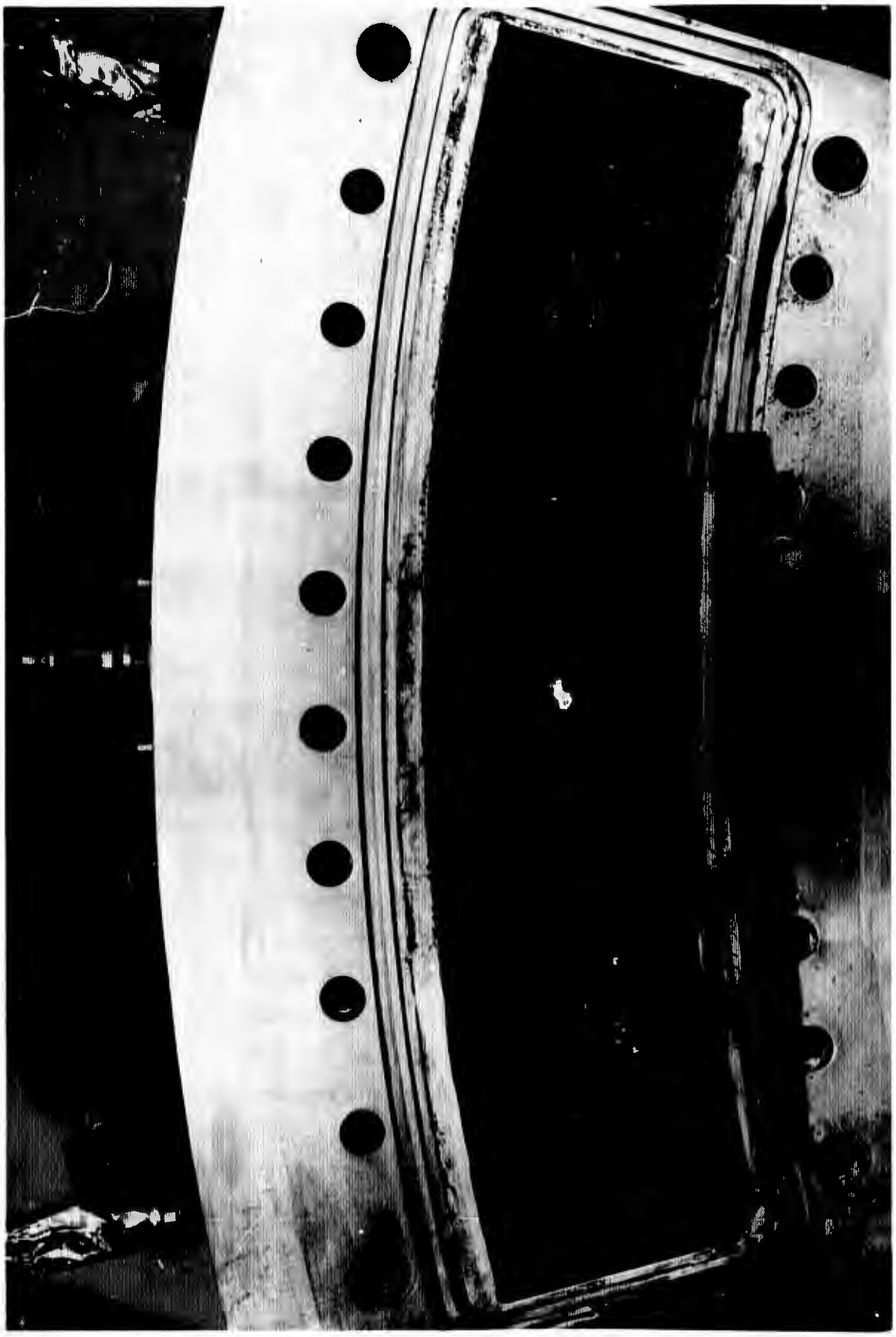

1EH35-9/19/69-C1D

Figure 133. 30-Degree Prototype Segment U/N 1; Condition Posttest 042 (U)

(C) Tests 043-050 were conducted to evaluate the operation of the injector-chamber assembly with full regenerative cooling. All hydrogen used as coolant also was injected for combustion, less the small amount lost into the chamber through the damaged areas in the face sheet. All tests were satisfactory programmed duration tests and were conducted over a range of chamber pressures (Table 20). No additional hardware damage or change was noted. Completely satisfactory start transients were obtained on all tests.

(C) Tests 051-128 were conducted for cyclic durability testing of the injector-chamber assembly. The tests were conducted by maintaining the fuel valve open and cycling the oxidizer main valve open and closed. The main oxidizer valve was opened for 1.7 seconds and closed for 1.5 seconds. The duration allowed chamber pressure and flowrates to stabilize at targeted mainstage conditions and the oxidizer shutoff time allowed full chamber pressure decay prior to the subsequent cycle. A typical test cycle is shown in Fig. 134 and shows chamber pressure trace vs time. Inspection of the hardware after the test series showed no change in the hardware condition.

(C) The segment chamber heat transfer test results are tabulated in Table 20. A comparison of these test results, with analytically predicted values and previous tube-wall segment test results, is presented in Fig. 135. The total chamber segment coolant enthalpy rise is shown as a function of chamber pressure. The results of tests 029 through 042 (with sufficient duration) are shown, together with a curve based on the previous tube-wall test results. Results of tests 043-128 are not presented in these comparisons because the chamber "blisters" had ruptured, making accurate determination of coolant flowrate throughout the chamber difficult.

(C) The results illustrate the close correlation between the predicted regenerative cooling characteristics and the actual test results of the prototype channel-wall chamber segment. Similar correlations were obtained for predicted and experimental values of injector and chamber inner and outer-body pressure losses. The data show a significant improvement over the previous tube-wall segment data and demonstrate the capability for regenerative cooling over the required throttling

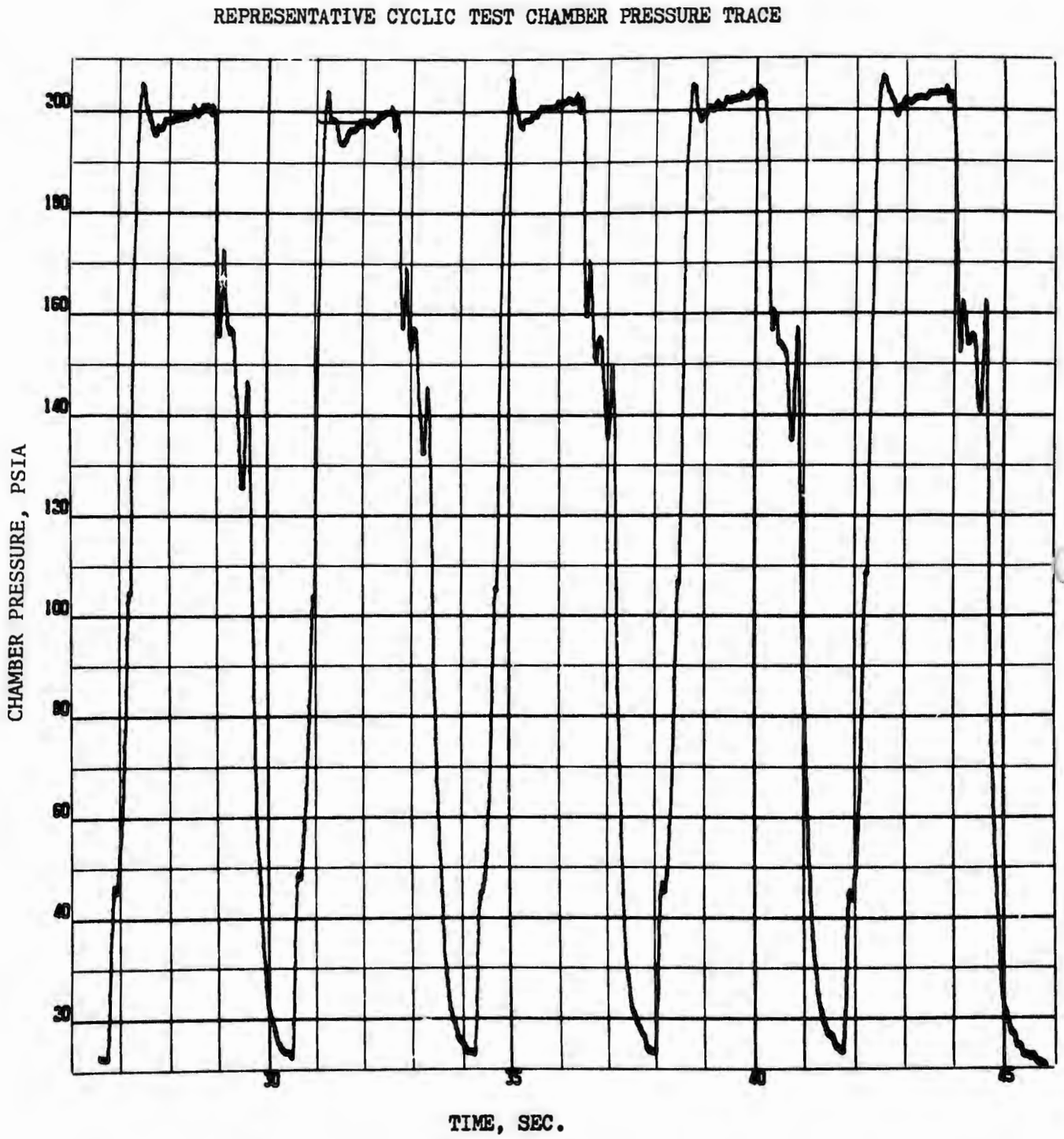

Figure 134. Typical Cyclic Tests Conducted on Prototype Segment U/N 1 (U)

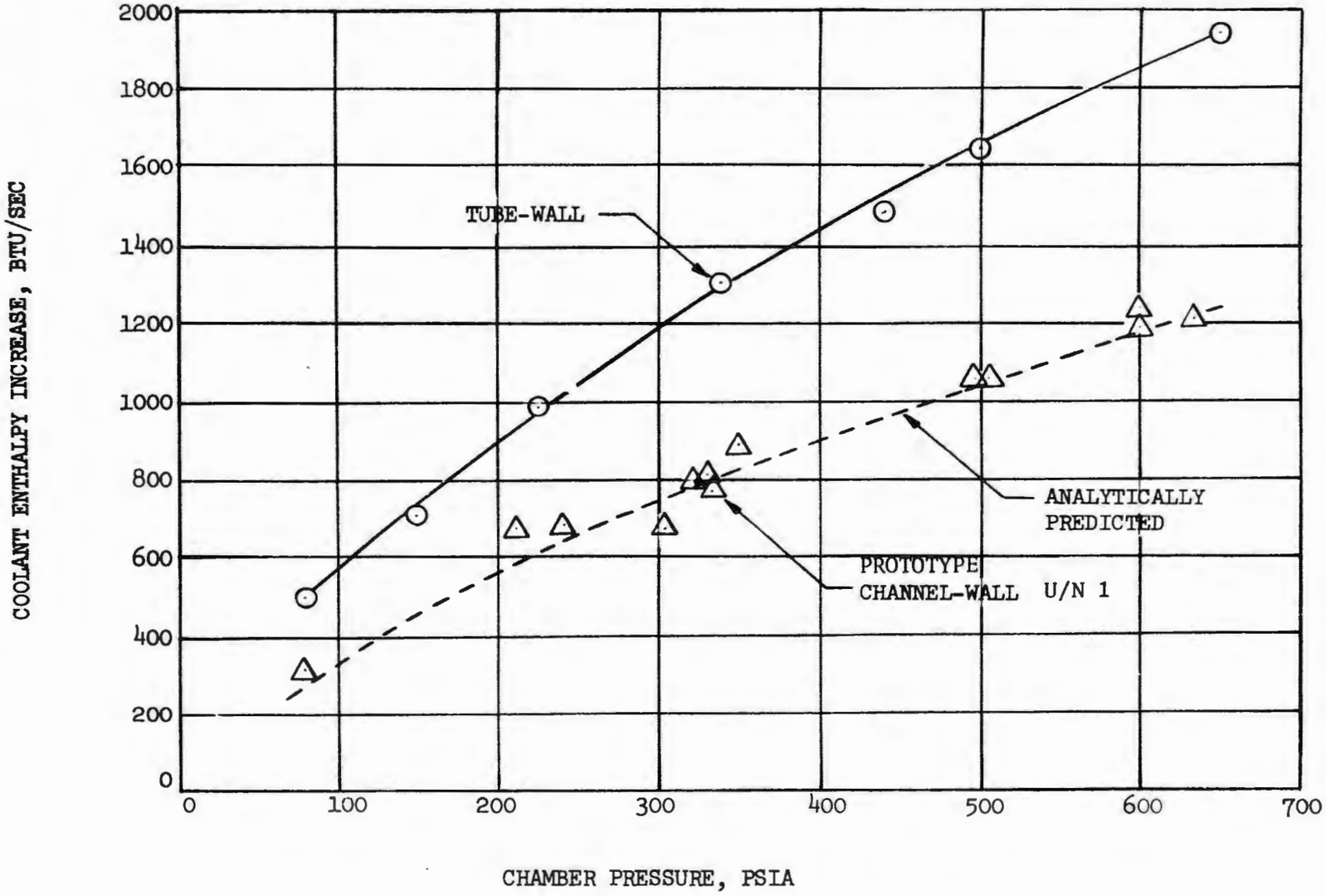

Figure 135. 30-Degree Segment Heat Load Comparison (U)

(C) range. The chamber-injector compatibility also was shown to be excellent, with no visible or apparent hot streaking, erosions, or surface melting of the chamber hot-gas face.

d. Main Chamber Segment U/N 1 Test Evaluation

(C) To provide a final verification of the prototype segment design and fabrication processes, particularly the integrity of the hot-gas face sheet to channel land braze joint, a firing test series was conducted on the U/N 1 chamber segment for the main thrust chamber assembly. During previous testing of the prototype U/N 1 segment, suspected nonbrazed regions of the inner body face sheet-to-land joint resulted. The prototype U/N 1 segment inner body had been hydrostatic pressure tested at 2750 psig, at ambient temperature, and no evidence of deficient braze bonding had been determined. A more stringent nondestructive evaluation of segment body face sheet-to-land braze joint was, therefore, indicated to be required. A review of available techniques, such as thermochromistic paints, ultrasonics, etc., was conducted, and the conclusion was that a hydrostatic test of the segments would be used at increased pressures with Stress Coat (Magnaflex Corporation) applied to the face sheet hot-gas-side surface to indicate stress characteristics. A review of all stress analysis work concerned with the joint in question was made and additional computations were performed to select a hydrostatic proof pressure for the inner and outer body that would produce a tension stress level in the nickel land commensurate with the value expected during hot firing. The calculations showed that the nickel land strength is the limiting factor, not the braze joint. Pressures of 3460 psig for the outer body and 3850 psig for the inner body were determined as the ambient pressure values which would simulate the loads in the lands during hot-firing conditions.

(C) Samples with regions that lacked braze bonding were prepared, stress coated, and pressurized to provide standards for the full segment bodies. The inner and outer body for U/N 1, main chamber segment, were stress coated and pressure tested to the values noted above. No lack of braze bond indications were noted on the inner body, while the outer body had seven regions of apparent small, nonbonded face sheet to land joints. Because of the noncritical location of the nonbonded

(C) regions and analytical stress predictions, which indicated that these small regions would not be detrimental tothe operation of the chamber, both bodies were accepted for U/N 1 assemlby. These locations were carefully mapped for future comparisons during the firing test program. (See Ref. 5 for more details on the Stress Coat procedures used.)

(C) Seven firing tests, 129-135, were conducted on the main chamber segment U/N 1 over a chamber pressure range of 658 to 78 psia (Table 21). The segment is shown installed in the test stand in Fig. 136. The tests were conducted with prototype injector U/N 4. This injector had previously accumulated 100 tests in conjunction with the 30-degree prototype chamber segment No. 1. All tests were satisfactory, and no change in hardware condition occurred. The tests were conducted with a regenerative-cooling circuit and a hydrogen tapoff flow extracted between the chamber coolant passage exit and the injector inlet manifold. The hydrogen tapoff flow was controlled to simulate the turbine drive gas flowrate that is required from each segment over the range of operating chamber pressures. The targeted or required tapoff flowrates were determined from the results of the latest engine system power balance analysis. Both engine and injector mixture ratio values are shown in Table 21 together with the corresponding hydrogen tapoff flowrate as a percentage of the total injector flowrate. The engine mixture ratio is defined as total oxidizer flowrate divided by total fuel flowrate (tapoff plus injector). The results of these tests agree favorably with the results obtained from the previous 30-degree prototype U/N 1 chamber segment and predicted values of pressure drop and bulk temperature rise.

(U) The combustion efficiencies obtained on these tests are shown in Fig. 137 and exceeded the minimum performance objective of the program.

TABLE 21

TEST SUMMARY, 30-DEGREE MAIN CHAMBER SEGMENT U/N 1 (U)

TEST NO.	DUR. (SEC)	CHAMBER PRESSURE (PSIA)	INJ. FLOW (LB/SEC)	ENGINE MIXTURE RATIO	% HYDROGEN TAPOFF	INJECTOR MIXTURE RATIO	FUEL INJ. TEMP. (°R)	ΔH BAFFLES BTU/SEC	ΔH O/B BTU/SEC	ΔH I/B BTU/SEC	$\frac{P_3}{T_3}$	$\frac{P_4}{T_4}$	$\frac{P_5}{T_5}$	$\frac{P_6}{T_6}$	$\frac{P_7}{T_7}$	ΔH TOTAL BTU/SEC	ΔP TOTAL PSI
129	2.0	216	1.79	8.86	2.81	12.2	584	64	-	-	755 113	662 214	587 -	554 -	305 816	470	449
130	11.0	227	1.77	10.85	1.63	13.3	934	59	-	-	740 81	690 180	617 -	586 -	338 1065	542	402
131	11.0	341	2.74	11.0	1.74	13.8	853	91	-	-	1124 74	1005 158	902 -	898 -	491 918	725	633
132	11.2	592	5.00	11.6	2.02	15.4	819	120	-	-	1926 70	1672 148	1508 519	1428 519	810 851	1166	1116
133	11.2	632	5.43	12.0	1.63	15.2	833	125	-	-	2035 68	1772 147	1602 -	1519 -	879 856	1231	1156
134	11.2	658	5.78	12.3	1.44	15.2	849	140	-	-	2138 66	1858 150	1680 -	1586 -	921 869	1296	1217
135	20.0	78-86 *	.62-.64	11.3-13.0	0.40-0.84	11.9-14.7	755-1220	33-44	-	-	344 87	308 354	272 -	262 -	134 1510	177-232	220-210

P_3, T_3 - BAFFLE INLET; PRESSURE, TEMPERATURE
P_4, T_4 - OUTER BODY INLET; PRESSURE, TEMPERATURE
P_5, T_5 - OUTER BODY DISCHARGE; PRESSURE, TEMPERATURE
P_6, T_6 - INNER BODY INLET; PRESSURE, TEMPERATURE
P_7, T_7 - INNER BODY DISCHARGE; PRESSURE, TEMPERATURE
' - PSIA
T - °R

* CHAMBER PRESSURE INCREASED FROM 78 TO 86 PSIA DURING TEST

CONFIDENTIAL

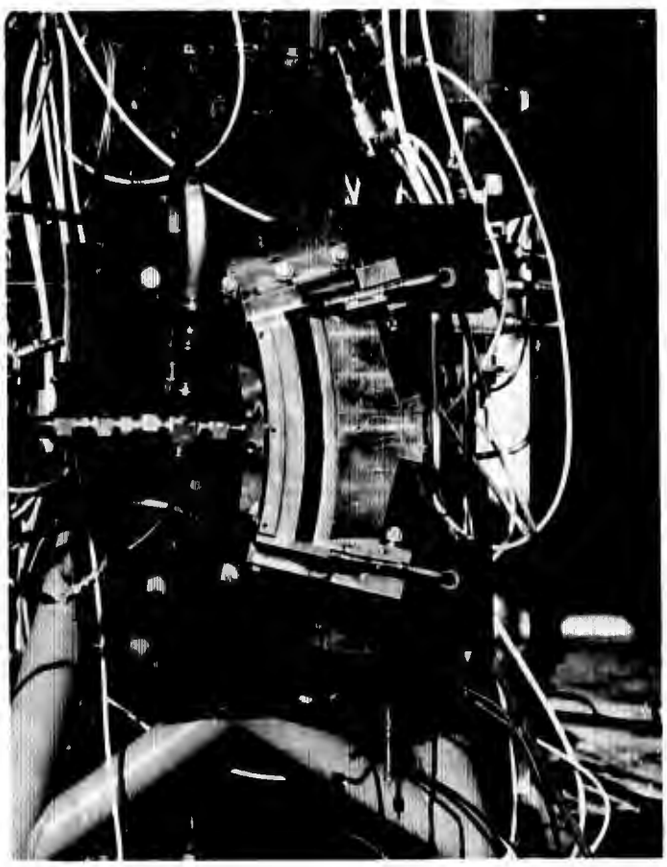

5AA31-10/27/69-S1A

Figure 136. Main Chamber Segment U/N 1 Installed in Test Stand (U)

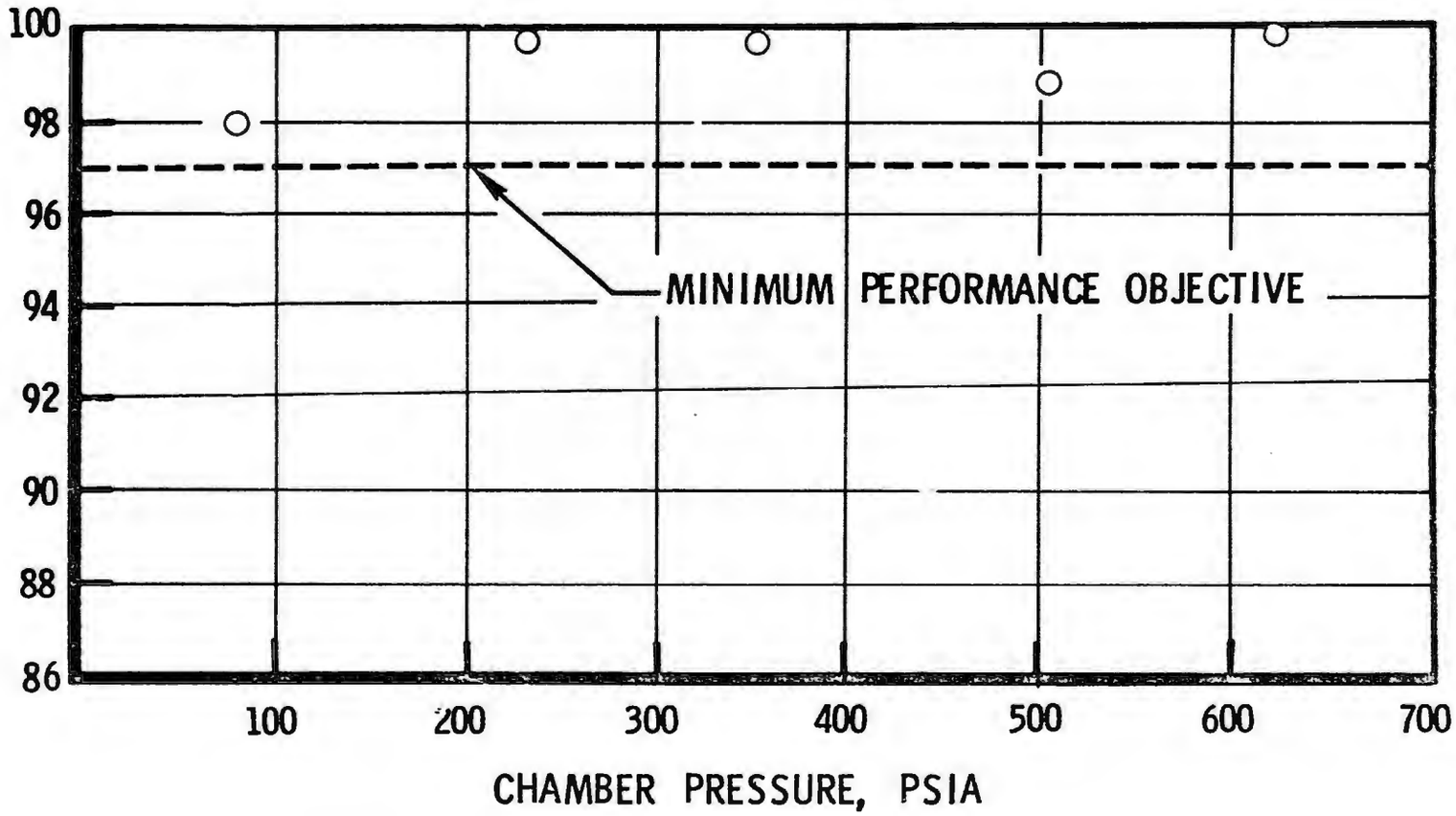

Figure 137. 30-Degree Main Chamber Segment U/N 1 Combustion Efficiency (Mixture Ratio = 13:1 to 14:1) (C)

CONFIDENTIAL

e. 30-Degree Prototype Segment Evaluation Summary

(C) The prototype segment evaluation included 107 firing tests on two segment assemblies: 30-degree prototype segment U/N 1, and 30-degree main chamber segment U/N 1. The significant results were:

1. The integrity of the segment chamber design and fabrication method was demonstrated.
2. Satisfactory segment chamber regenerative cooling was demonstrated with measured heat loads close to the analytically predicted values.
3. Measured combustion efficiencies exceeded the minimum program goal of 97 percent over the design throttle range.
4. Good injector/chamber durability was demonstrated with 100 firing tests being conducted on one segment assembly.

7. MAIN THRUST CHAMBER ASSEMBLY EVALUATION

(U) The main thrust chamber assembly included the following components:

1. Twelve 30-degree channel-wall segment assemblies
2. Thrust mount and propellant inlet manifold assembly
3. Nozzle extension and base closure
4. Associated propellant feed tubes, seals, and connecting hardware.

The complete chamber assembly was described in Section III, 1.0 and the 30-degree segment development was covered in Section III, 2.0 through 6.0 The design and fabrication of the other main thrust chamber components are discussed in the following paragraphs, and then the main thrust chamber test effort is discussed.

a. Hardware Design and Fabrication

(1) Nozzle Extension

(C) The nozzle extension was a regeneratively cooled, tubular-wall assembly design. The basic design is shown in Fig.138 and consists of 900, 347 CRES coolant tubes with an OD of 0.145-inch by 0.012-inch wall thickness, with inlet and outlet manifolding and a flange for attachment of the base closure-secondary nozzle simulator. The tubes were not required to be tapered, but required booking and forming operations. The number of tubes required in the assembly was 898. The nozzle extension was a furnace-brazed assembly.

(C) The completed nozzle assembly is shown in Fig.139 . The cooling circuit was basically a two-pass arrangement. Hydrogen flow from each of the segment inner bodies enters the nozzle upper manifold (Fig. 138), flows upward in alternate

CONFIDENTIAL

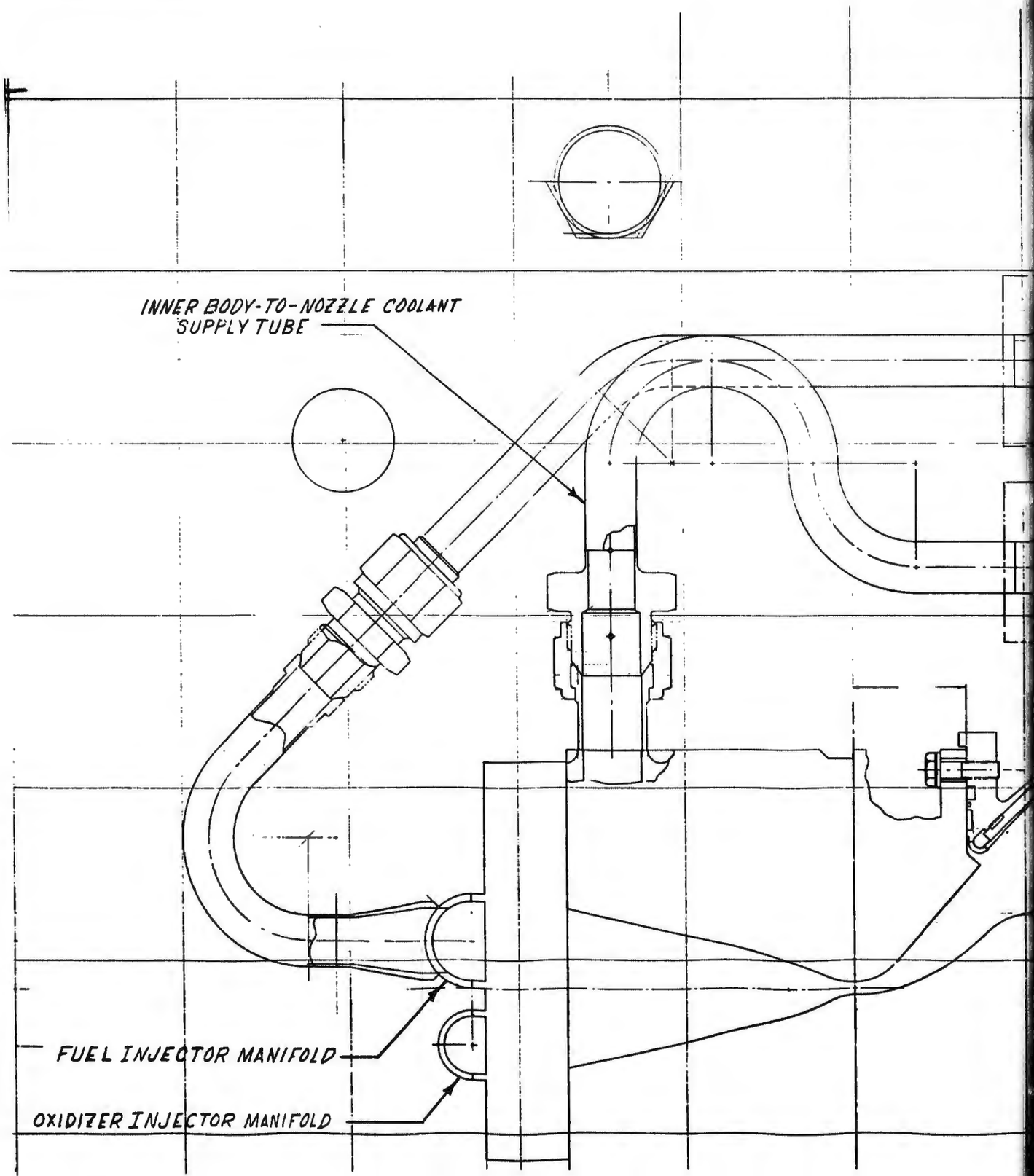

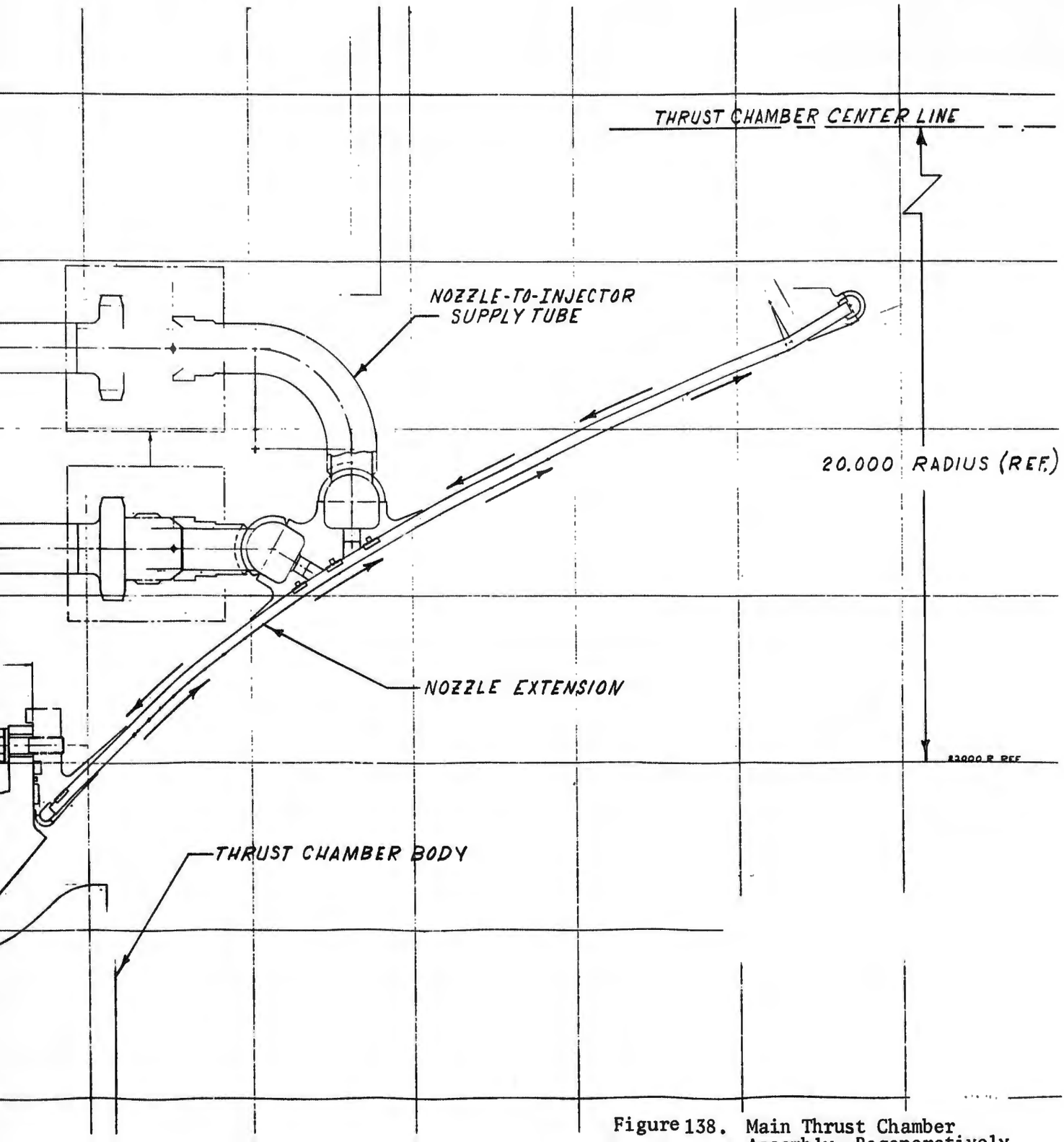

Figure 138. Main Thrust Chamber Assembly, Regeneratively Cooled Nozzle Extension (U)

CONFIDENTIAL

2

1EH32-1/30/70-C2D

Figure 139. Completed Nozzle Extension (U)

(C) tubes, flows down in alternate tubes the length of the nozzle, then returns to the lower manifold for routing back to each of the segment injector manifolds. Provision was also made to bleed some turbine-drive hydrogen from the lower manifold and route it to the base-closure annulus for simulation of turbine exhaust flow.

(U) The nozzle extension heat transfer and fluid flow calculations were made by dividing the cooling circuit into 42 increments. For each increment, iteration was made on the heat flux from the combustion gas to the coolant, the resulting temperature profile, and the coolant change of state until all were compatible with the friction and momentum pressure drop over the increment.

(U) Gas-side heat transfer coefficients were computed using a General Electric Timeshare computer to solve the equation:

$$\frac{h}{\rho v\ cp} = S_T$$

where

S_T = Stanton number (dimensionless)

h = surface heat transfer coefficient, Btu/in.^{2}-sec-F

ρ = gas density, lbm/in.^{3}

v = gas velocity, in./sec

cp = gas specific heat at constant pressure, Btu/lbm-R

The results are presented graphically in Fig. 140 and 141.

(U) The coolant surface heat transfer coefficient was determined by:

$$Nu_b = 0.025\ Re_b^{0.8}\ pr_b^{0.4}\ \left(\frac{T_b}{T_w}\right)^{0.55}$$

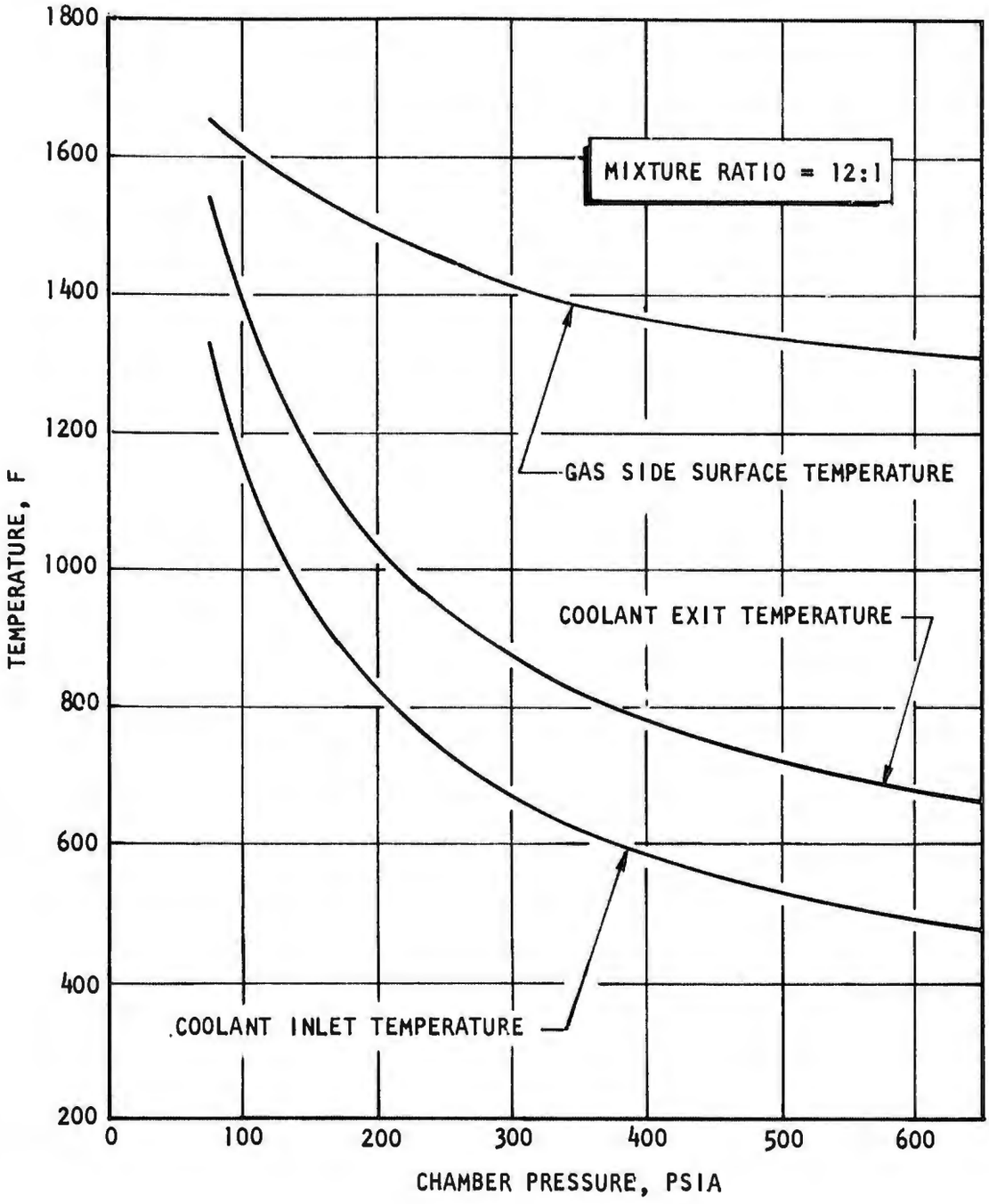

Figure 140. Nozzle Extension Gas-Side Surface Temperature and Coolant Inlet and Exit Temperature (U)

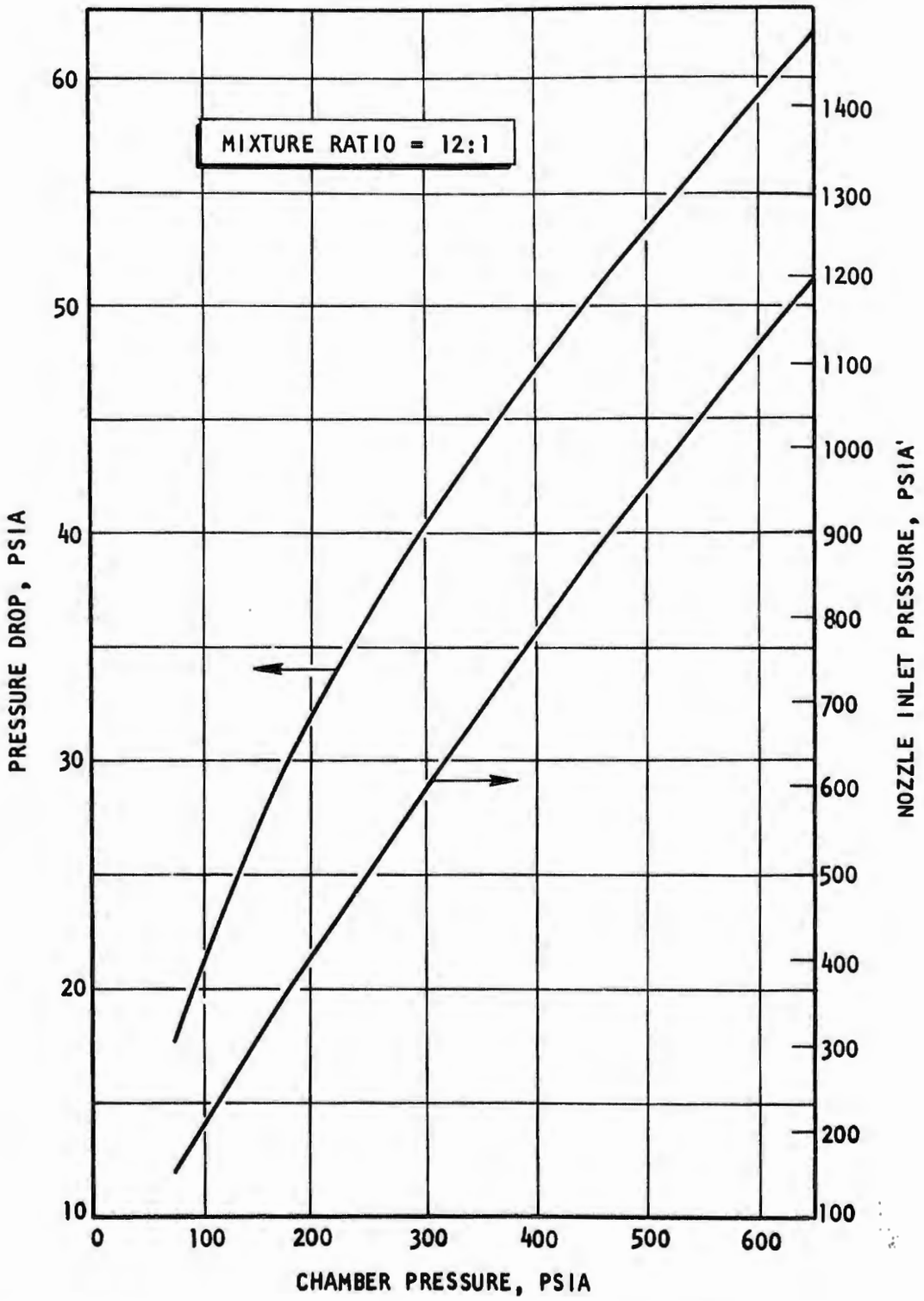

Figure 141. Nozzle Extension Tube Assembly Pressure Drop (U)

(U) where subscripts b and w indicate properties were evaluated at bulk coolant temperature and wall temperature, respectively.

(U) The fabrication process used to build the nozzle extension was similar to that used for any furnace braze assembled, tubular-wall, regeneratively cooled thrust chamber. A significant problem was encountered during the initial nozzle braze cycle at elevated temperatures because of a contaminated furnace atmosphere which severely oxidized all exposed nozzle surfaces. Several elevated temperature (1800 F) hydrogen atmoshpere cleaning cycles were used to remove the oxides. The nozzle was then successfully brazed at 1810 F using a 50 Au-50Cu braze alloy. The braze temperature of 1810 F was well below the maximum hot-gas wall temperature of 1650 F expected during firing tests of the chamber assembly (Fig. 140).

(2) Base Closure and Secondary Chamber Simulator

(U) The base closure and secondary thrust chamber simulator function was to provide a method of distributing the base flow (engine turbine exhaust gases) into the base region. The gases are injected axially and radially to provide thrust by pressure (acting on the exposed area of the base), protect the base from overheating as a result of primary flow recirculation, and protect the secondary engine thrust chamber (simulator used during thrust chamber only tests) from primary gas recirculation. Based on cold-flow-tests conducted, the radial inward flow of the secondary gases would provide the most protection for the secondary thrust chamber simulator. An objective of the Phase I testing to determine the appropriate apportionment of axial and radial flow for the protection of the secondary nozzle and the base region. Ablative material was applied to the base region for Phase I testing to obtain maximum durability during the base region investigation. The base closure assembly is shown in Fig. 142 and 143.

(3) Thrust Mount and Manifolds

(U) The main chamber thrust mount and primary propellant inlet manifold assembly is shown in Fig. 144. The assembly was designed to provide two basic functions: (1) transmit the thrust generated by the thrust chamber assembly to the facility

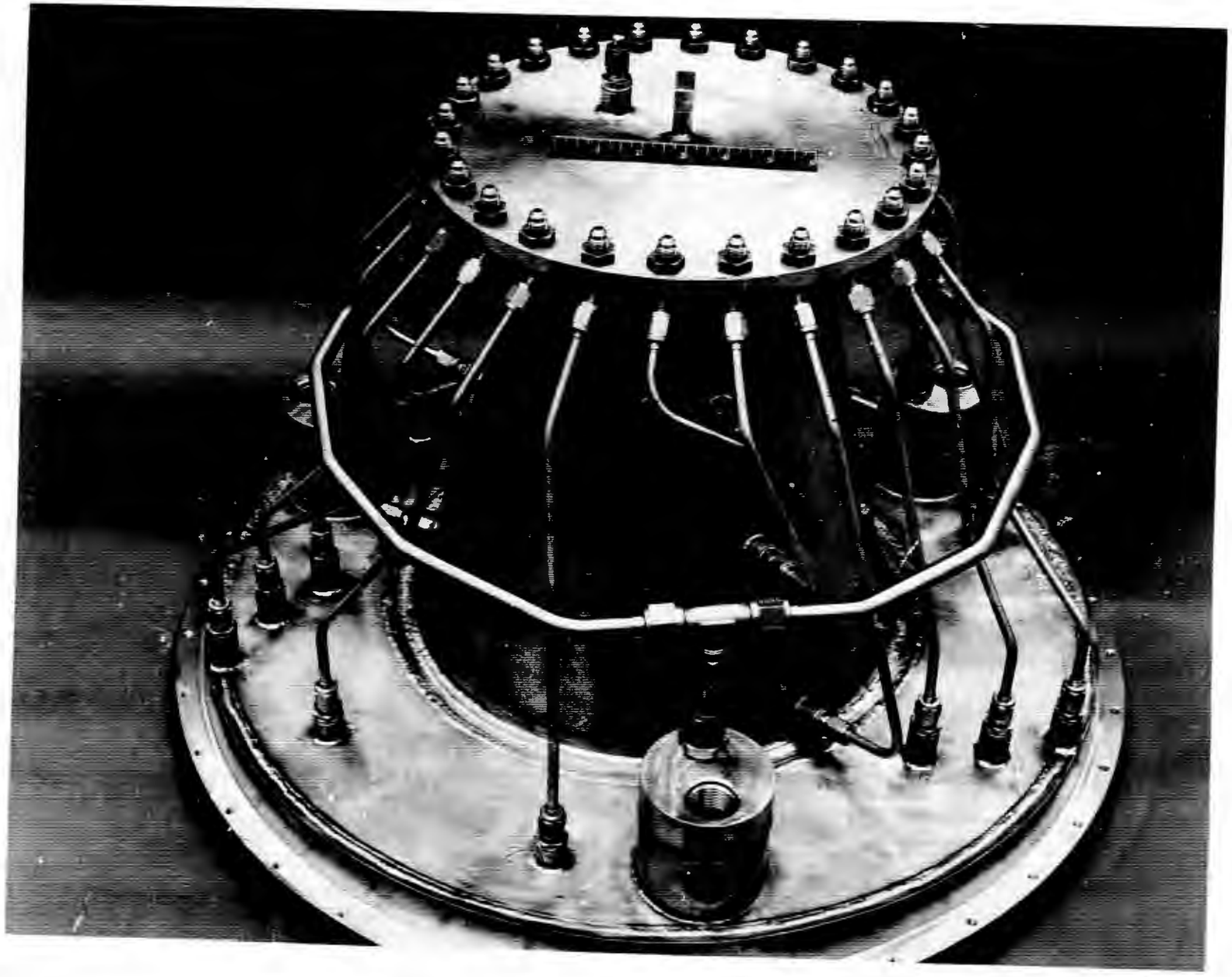

1EH32-2/3/70-C1K

Figure 142. Base Closure, Forward End (U)

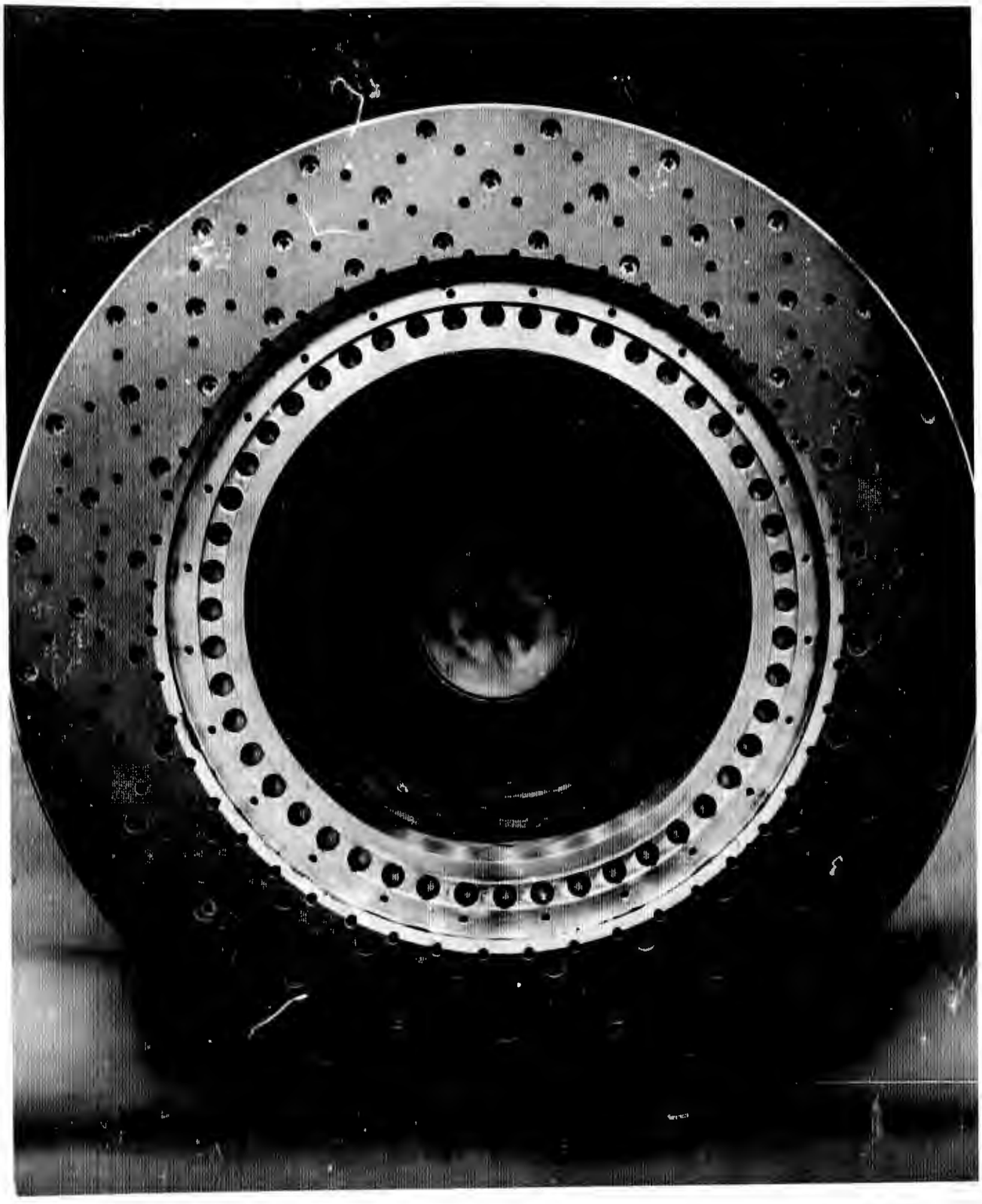

1EH32-2/3/70-C10

Figure 143. Base Closure, Aft End (U)

(U) thrust measuring system, and (2) provide the primary fuel and oxidizer distribution manifolds which would be connected to facility ducting during thrust chamber testing and the turbopump high-pressure discharge ducts during engine testing.

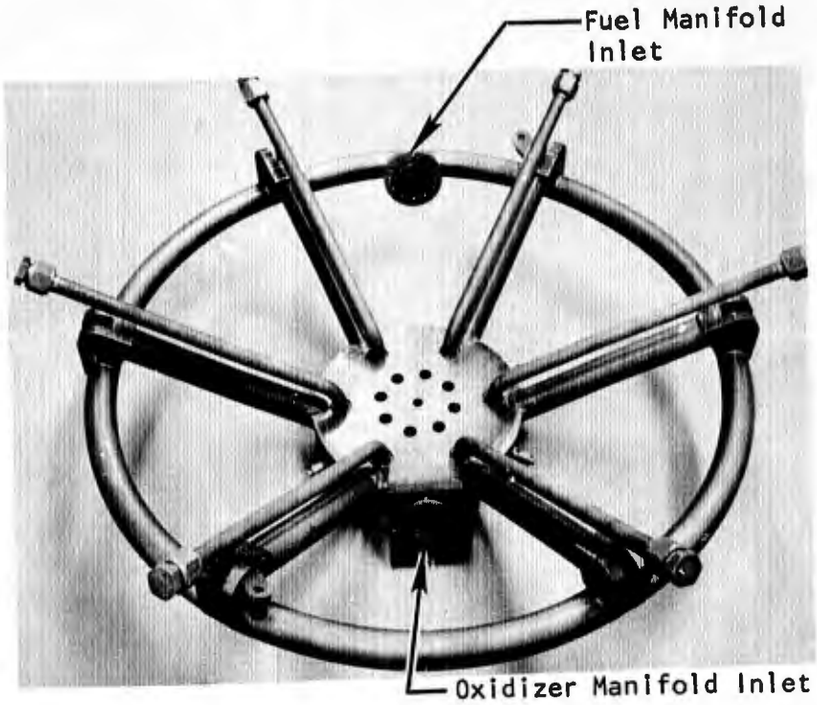

Figure 144. Thrust Mount and Propellant Manifold Assembly (Facing Downward) (U)

(U) In the design of the propellant distribution manifolding, care was taken to maintain equal length distribution lines to each segment to achieve equal priming and distribution. The oxidizer distribution manifold was included within the gimbal/thrust mount interface (Fig. 6). Six 3/4-inch OD tubes route the oxidizer from this manifold to the segments.

(C) The fuel distribution manifold, fabricated from 347 stainless steel, was 1.5 inches constant OD with an overall circular diameter of 32 inches. Twenty-four individual 1/4-inch OD tubes route the hydrogen from this manifold to the 12 segments.

(U) The thrust mount, fabricated from 718 Inconel, had attach points at six locations on the segment assembly ring.

(U) A two-segment facility thrust mount (Fig. 145) was also designed and fabricated. The purpose of the thrust mount was to permit installation of two 30-degree segments, into the Nevada Test Facility to perform the Test Stand B-4A facility activation checkout tests.

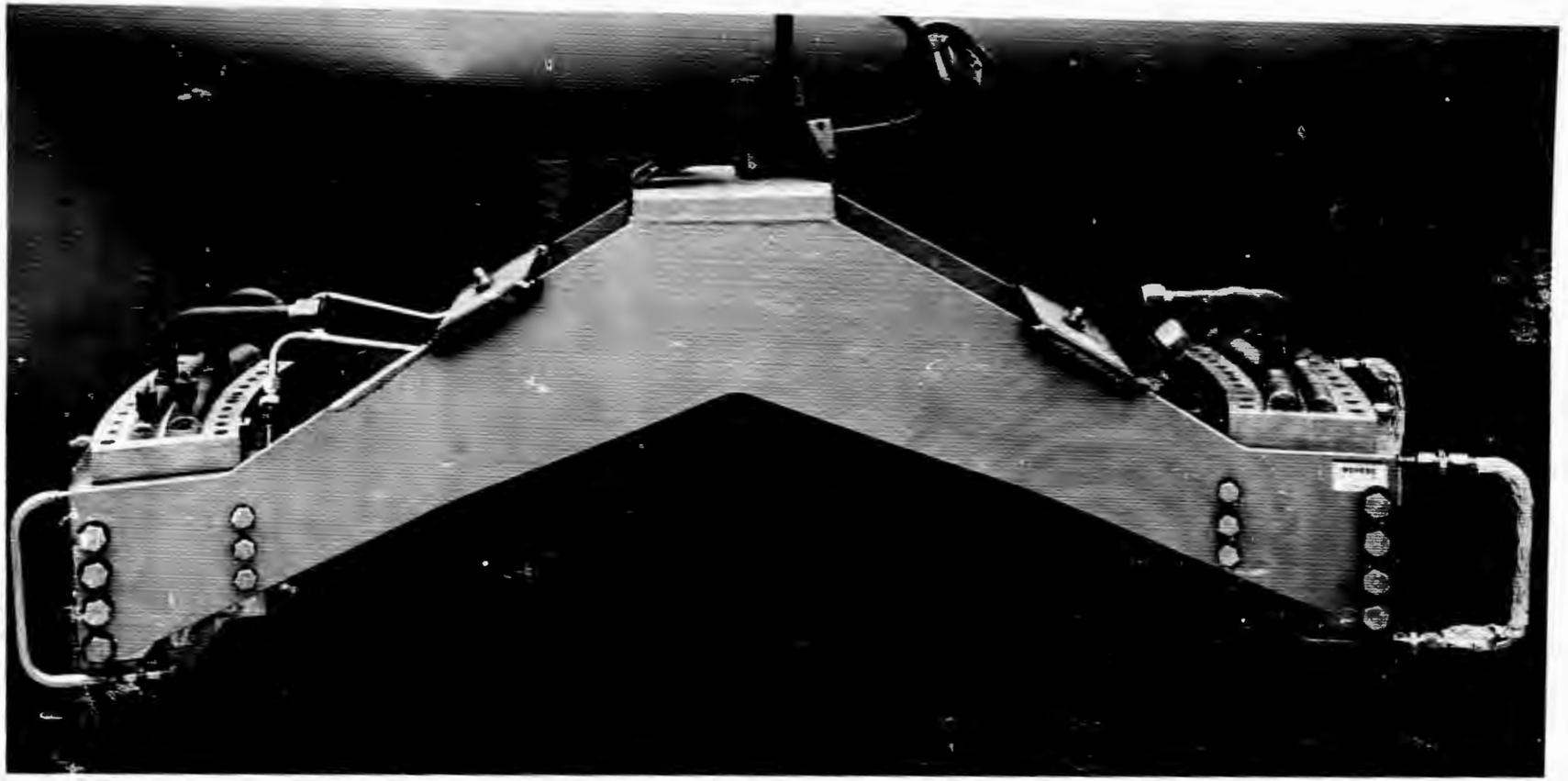

1EH83-12/23/69-C1C

Figure 145. Facility Activation Test Assembly (U)

(4) Engine and Thrust Chamber Build and Transport Dolly

(U) A build and transport dolly was designed and fabricated and is shown in Fig. 146 and 147. It was intended to serve as the holding fixture during assembly or transportation of the main engine or main thrust chamber.

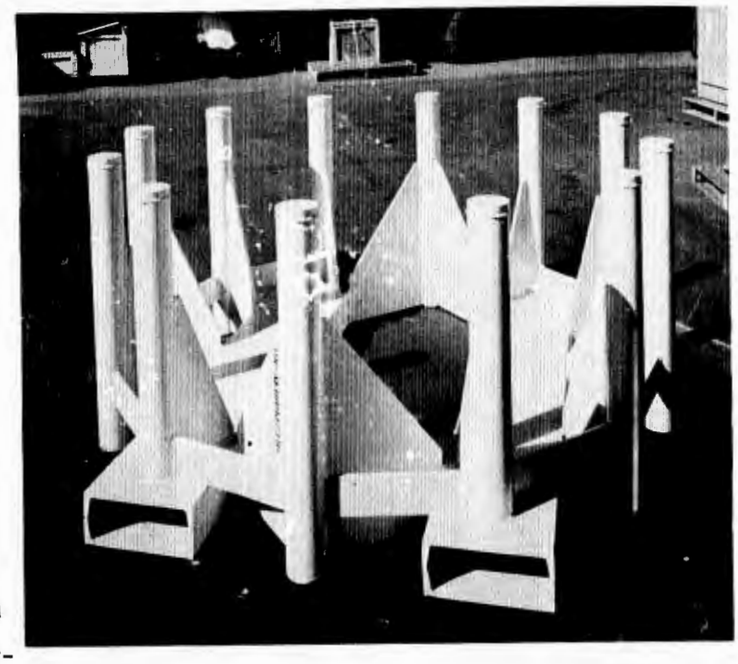

Figure 146. Build and Transport Dolly (U)

(U) The assembly consisted of the basic dolly and 12 detachable thrust chamber supporting arms. The dolly was an assembly of 12 structural tubes positioned vertically and equally about a 70-inch diameter. These were secured by a series of interconnecting structural plates and two fork lift guides. The support arms were designed to be structurally loaded as cantilever beams. Therefore, the arm weldments provided a bolting surface at each end and longitudinal rigs to maximize the section modulus. Four of these arms provided a means of attaching to a lifting device for the removal or installation of the engine or thrust chamber to or from the dolly.

(U) The main thrust chamber, when installed in the dolly, was located in the center at an elevation that places the injector on a plane with the vertical tube ends. Maintaining the engine in this position was accomplished by attachment of a support arm between each segment and its corresponding vertical tube.

(U) The dolly with the thrust chamber secured was moved by use of a fork lift. During extended transportation by truck or trailer, the chamber was secured within the dolly. The dolly with the thrust chamber assembly installed is shown in Fig. 148.

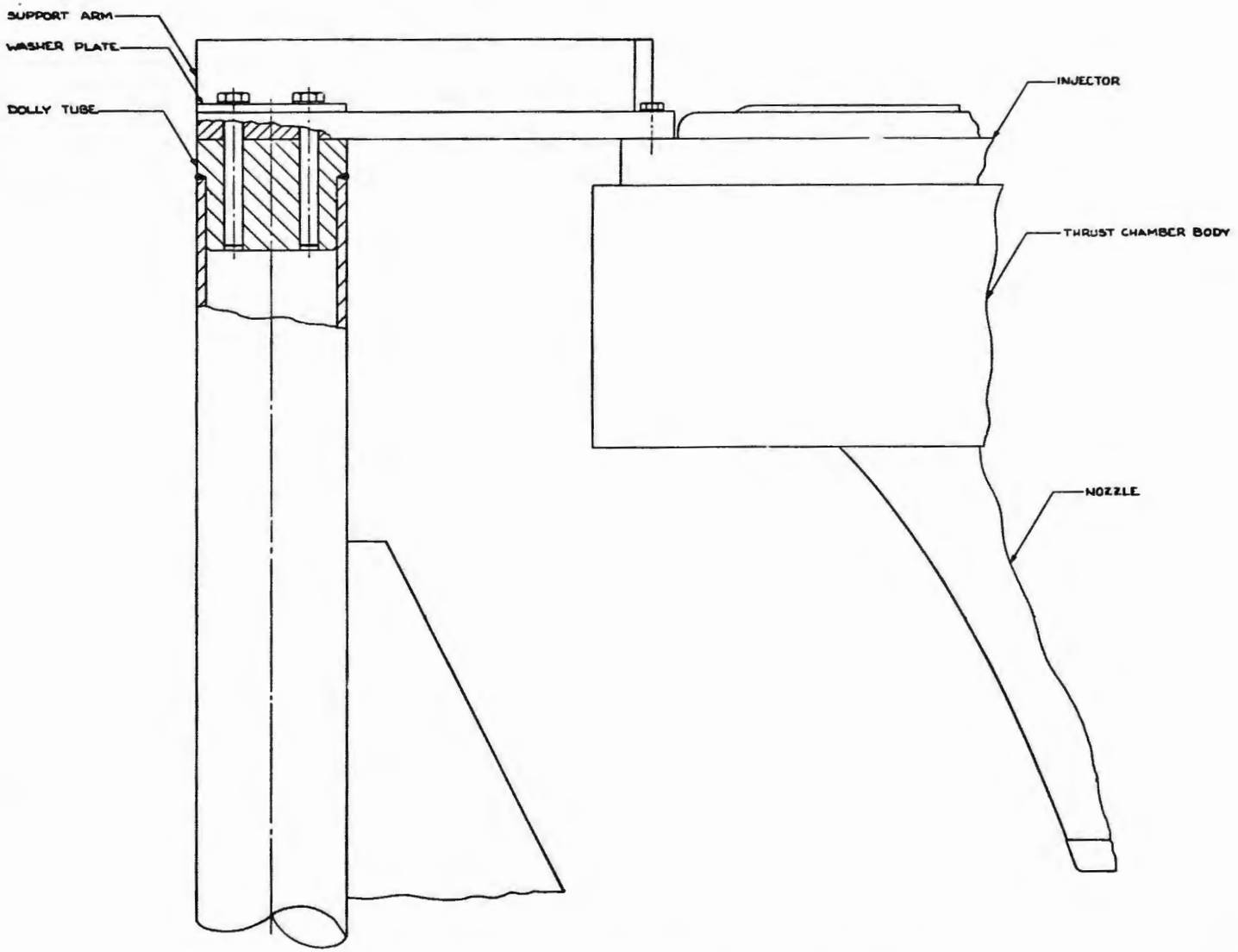

Figure 147. Build and Transport Dolly (section view) (U)

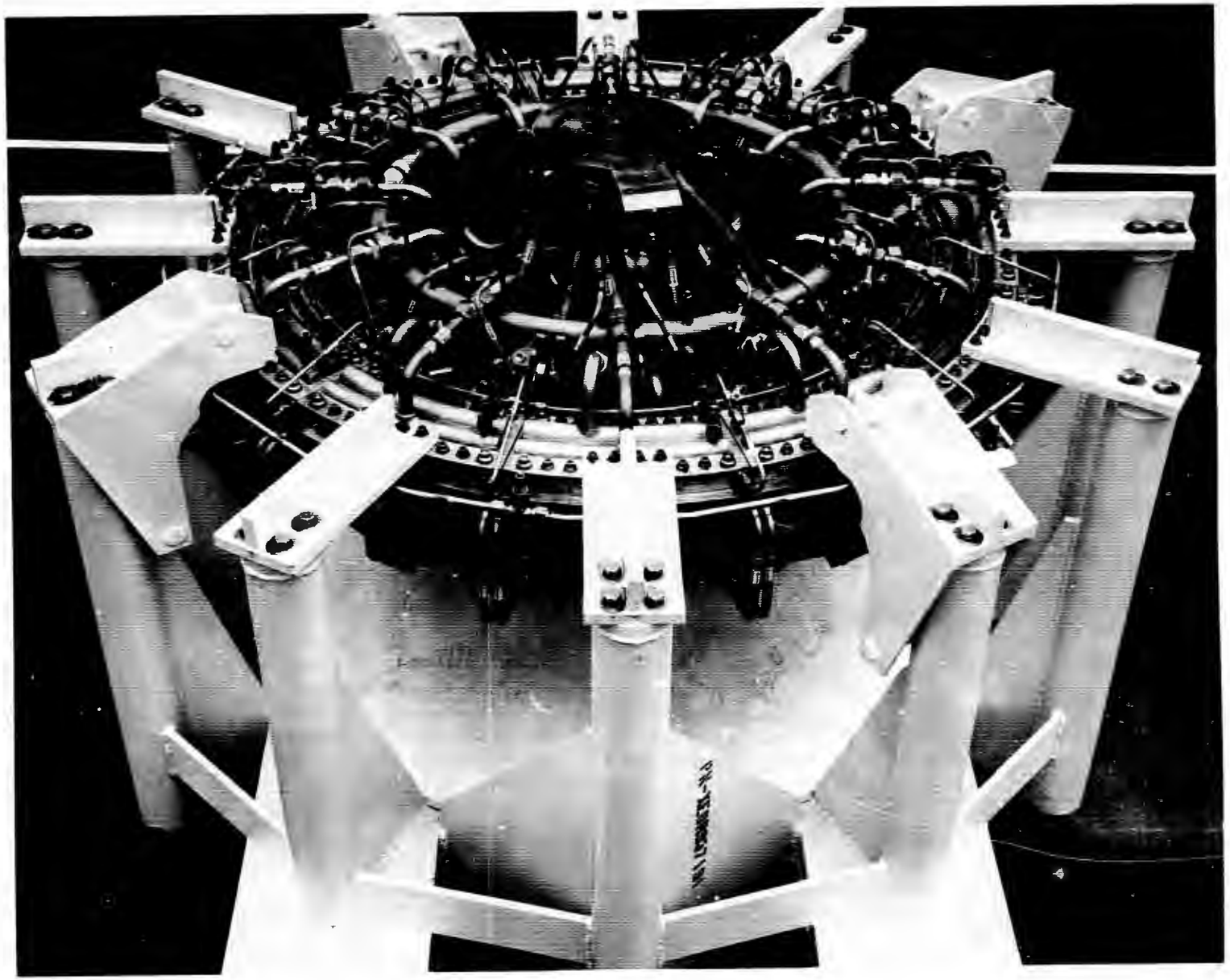

1EH32-2/20/70-C1E

Figure 148. Dolly With Main Thrust Chamber Assembly Installed (U)

b. Main Thrust Chamber Assembly Testing

(U) The main thrust chamber assembly testing was to be conducted at the B-4A Test Stand, Nevada Field Laboratory. The primary purpose of the testing was to verify the heat transfer and performance capabilities of the main thrust chamber assembly.

(U) No main chamber tests were conducted, however, because of damage of the facility oxidizer high-pressure feed system during facility activation checkouts. The activation effort and the problems encountered are discussed in the following sections.

(1) B-4A Facility Activation

(U) The facility activation effort is summarized in Table 22 . The activation was planned to include the following.

1. Fluorine systems blowdowns
2. Hydrogen system blowdown
3. Checkout of the hyperflow altitude simulation system
4. Hot-firing tests of the two-segment assembly to verify complete facility operation

(2) Initial Facility Blowdowns

(U) The oxidizer system blowdowns were accomplished by use of the oxidizer system closed-loop mode. A return line was installed that connected the oxidizer feed system downstream of the oxidizer main valve to the oxidizer storage vessel. Liquid fluorine blowdowns were conducted using oxidizer run tank pressures up to 600 psig. Oxidizer leakage was found on the downstream side of the oxidizer main valve at a fitting where the oxidizer injector purge is introduced. The leak was repaired. No other problems were encountered.

TABLE 22

B-4A TEST HISTORY (U)

Run No.	Date, 1970	Hardware Tested	Duration, seconds	Oxidizer Tank Pressure, psia	Fuel Tank Pressure, psia	Oxidizer Purge Pressure, psia	Fuel Purge Pressure, psia	Comments
---	2/20	Dual Segment Oxidizer Blowdown	14.5	180	--	--	--	Satisfactory
---	2/20	Dual Segment Oxidizer Blowdown	14.5	400	--	--	--	Satisfactory
---	2/20	Dual Segment Oxidizer Blowdown	16.0	400	--	--	--	Satisfactory
---	2/20	Dual Segment Oxidizer Blowdown	10.0	600	--	--	--	Satisfactory
001	3/5	Dual Segment Fuel Blowdown	75.0	---	875	250	500	Satisfactory; fuel tank pressure regulator leaked at body halves
002	3/11	Dual Segment Hot Fire	2.0	800	1205	350	500	Satsifactory; hot-wire burnout after cutoff; found leak at MOV
003	3/13	Dual Segment Hot fire	3.0	1200	1530	425	500	Injector bolts failed; due to ignition delay
004	3/16	Facility Fuel Blowdown (~6 lb/sec)	29.0	--	2300	--	500	Satisfactory; temperature O.K. after 20 seconds
005	4/1	Single Segment Hot Fire	1.7	1235	1460	150	150	Facility malfunction; hot-wire cutoff; oxidizer injection purge burnout
---	4/13	Single Segment Oxidizer Blowdown	2.0	60	--	--	--	Satisfactory
---	4/13	Single Segment Oxidizer Blowdown	3.0	60	--	--	--	Noted oxidizer vapors in capsule at end of burnout; MOV leak
---	4/15	Single Segment Oxidizer Passivation	~2.0	80	--	--	--	Fire in capsule at main oxidizer valve leave closed position; oxidizer injector purge check valve burned out
---	4/24	Single Segment	300	10-20	--	--	--	Satisfactory

		Oxidizer Blowdown						capsule at end of burnout; MOV leak
---	4/15	Single Segment Oxidizer Passivation	~2.0	80	--	--	--	Fire in capsule at main oxidizer valve leave closed position; oxidizer injector purge check valve burned out
---	4/24	Single Segment Oxidizer Passivation	300	10,20, 30,40, 50,75, 100	--	--	--	Satisfactory
---	4/24	Single Segment Oxidizer Blowdown	34.2	200	--	--	--	Satisfactory*
---	4/24	Single Segment Oxidizer Blowdown	40.0	300	--	--	--	Satisfactory*
---	4/24	Single Segment Oxidizer Blowdown	12	400	--	--	--	Hot wire cutoff after 12 seconds; no facility damage
---	4/24	Single Segment Oxidizer Blowdown	41	500 (increased to 640	--	--	--	At conclusion of blowdown, sparks inside can ~25 seconds later; oxidizer run line burnout
---	5/23	Single Segment Oxidizer Passivation	5	10,20,30, 40,50,75, 100	--	--	--	Satisfactory
---	5/23	Single Segment Oxidizer Blowdown	100	200	--	--	--	Satisfactory
---	5/23	Single Segment Oxidizer Blowdown	100	300	--	--	--	Satisfactory
---	5/23	Single Segment Oxidizer Blowdown	100	400	--	--	--	Satisfactory
---	5/23	Single Segment Oxidizer Blowdown	100	500	--	--	--	Satisfactory
---	5/23	Single Segment Oxidizer Blowdown	100	600	--	--	--	Satisfactory
PRE 006	5/25	Single Segment Hot Fire	5.0 (scheduled)	1235	1480	400	150	**

*Oxidizer run bleed and TCA passivation valves opened for 15 seconds during blowdown

**During pressurization of oxidizer run tank (~1150 psig), shudder in oxidizer run line, frost fell from line, and within 1 to 2 seconds, small detonation and fire at top of oxidizer run vessel. About 1 to 2 seconds later, large detonation and fire from oxidizer run tank, vertically upward with dense, pink-white smoke; shortly thereafter another unidentified small detonation.

(U) The fuel system blowdowns were conducted through the test hardware with the altitude simulation system operating. No problems were encountered.

(3) Activation Firing Tests 001, 002, and 003

(C) The test hardware consisted of the two-segment test assembly, Fig. 145. The first two tests were satisfactory. The third test was planned for 400-psig chamber pressure and 5-seconds duration.

(C) An ignition delay and detonation occurred within the combuston zone of the U/N 1 thrust chamber segment at start, and the injector was separated from the chamber by the blast. There was no damage to the other segment assembly (S/N 2). The hardware damage consisted of:

1. The injector (U/N 001) oxidizer inlet line was bent and crimped, Fig. 149. This damage was minor and repairable. There was no other damage to the injector.
2. The segment chamber (U/N 1) was slightly deformed, and the cooled side-plates were bulged, Fig. 150. The damage is nonrepairable, although the outer body of the assembly was salvaged and used as previously planned for assembly of spare segment, S/N 17.

(U) Minor facility damage consisted of burned instrumentation and control wiring and burned thrust measuring system hydraulic calibration lines.

(C) Examination of the test records indicated that the detonation, which occurred in U/N 1 segment chamber, was caused by an ignition delay. Figure 151 depicts the oscillograph traces of pertinent parameters.

(C) The data showed that ignition "pops" had occurred during starting of the thrust chamber segment, U/N 2, on both tests 002 and 003. An investigation was conducted to determine what conditions would be required to obtain an ignition delay with

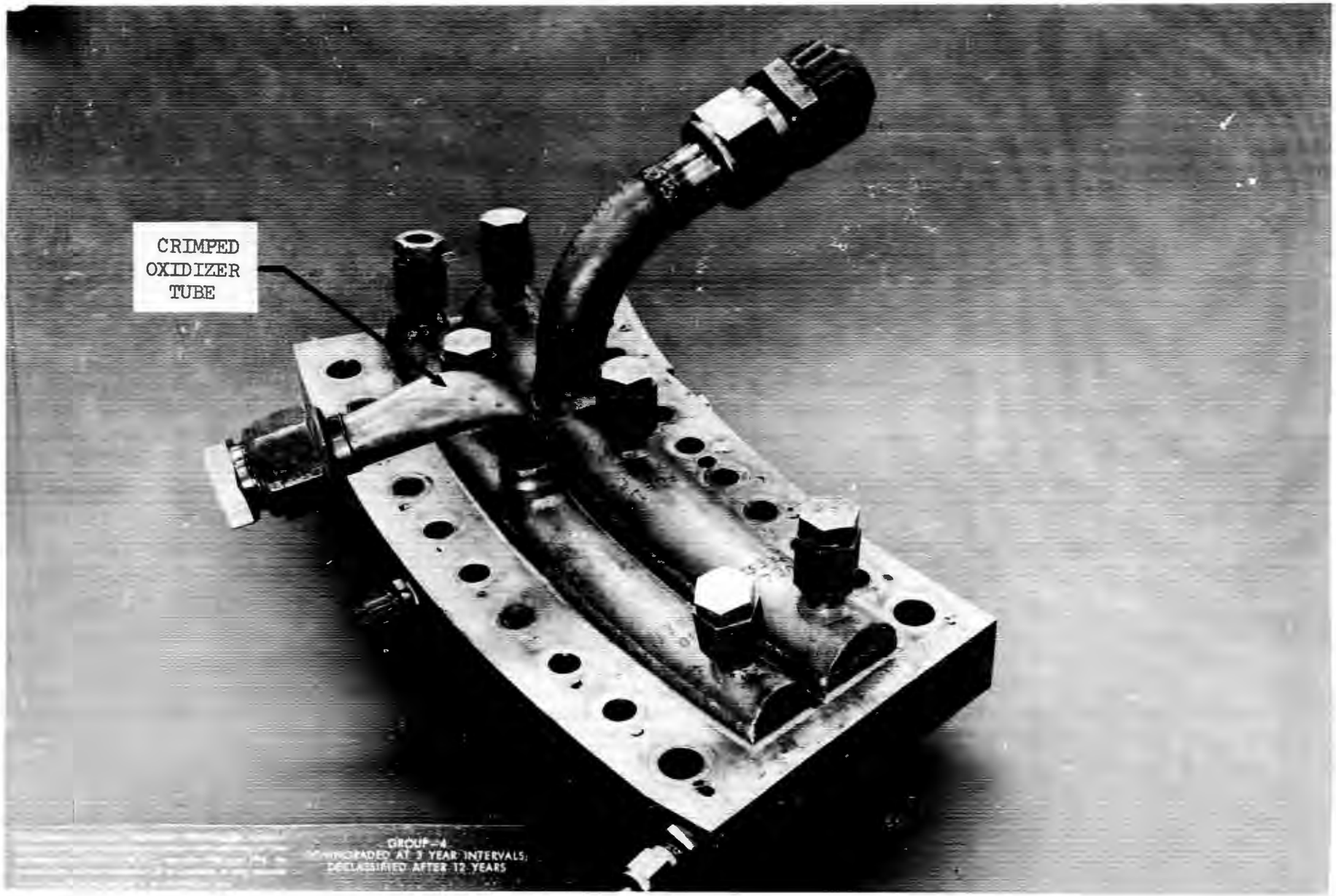

1EH35-3/20/70-C1A

Figure 149. Segment Injector U/N 001 Posttest 003 (U)

CONFIDENTIAL

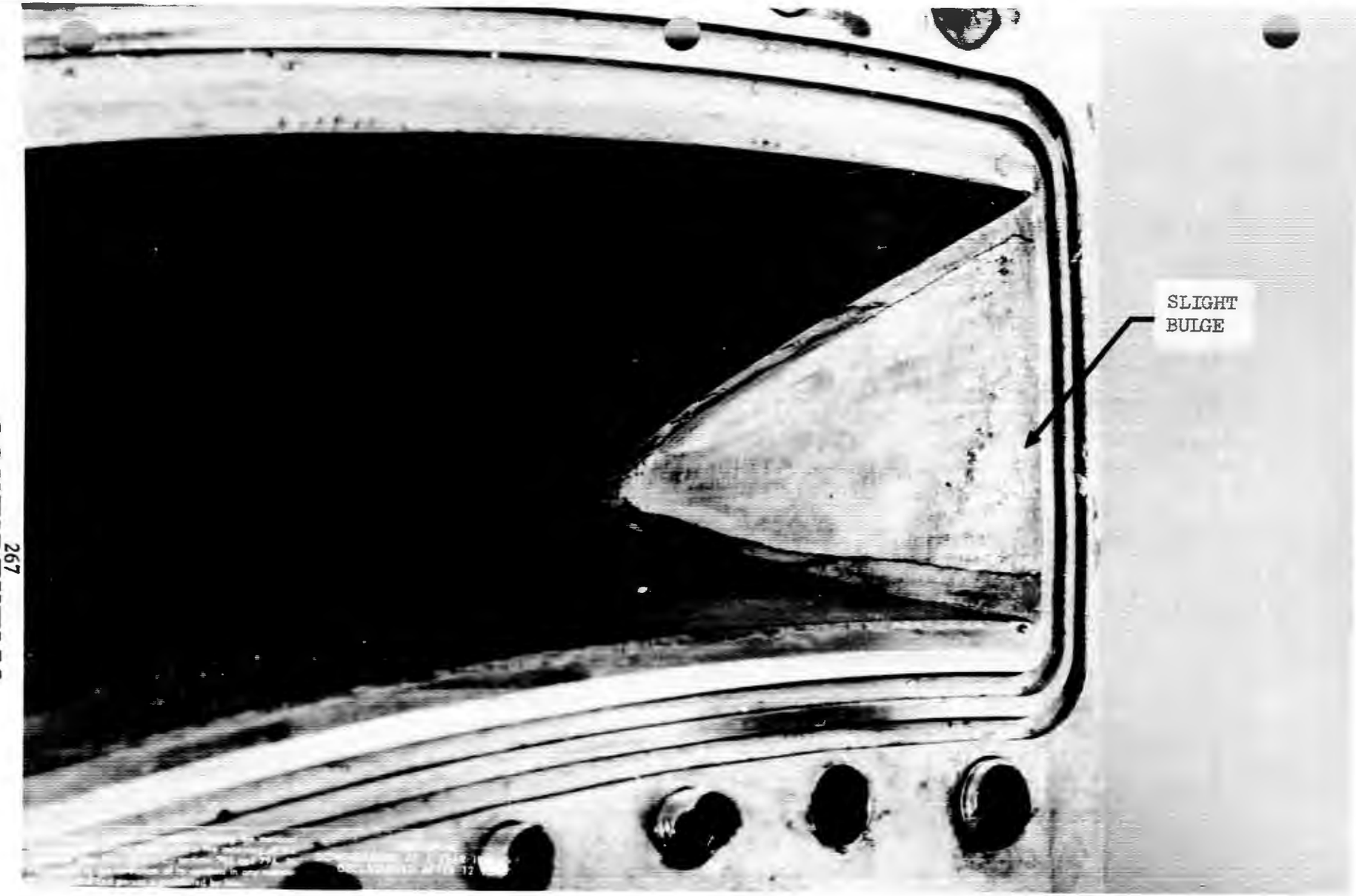

CONFIDENTIAL

1EH35-3/20/70-C1E

Figure 150. Segment Chamber S/N 1, Posttest 003 (U)

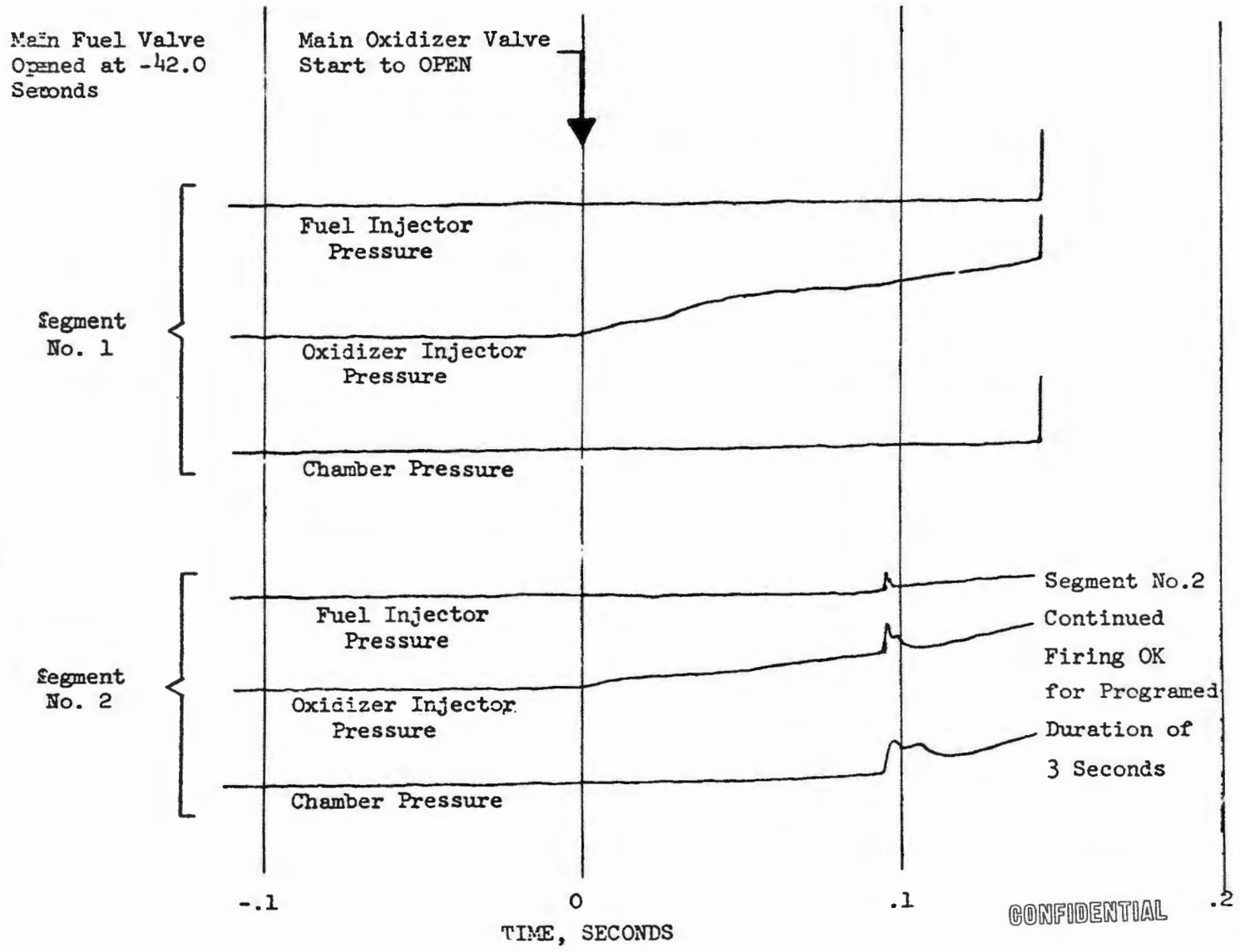

Figure 151. B-4A Facility Activation Test No. 003 (U)

CONFIDENTIAL

(C) this propellant combination. The investigation revealed that the following test conditions likely contributed to the ignition delay:

1. Extremely cold propellants and associated hardware due to a long fuel lead on test 002 and 003.
2. High volume purging during start on the oxidizer side that diluted the oxidizer and also acted as a reaction quencher.

(U) The conclusion was that the failure was caused by unique operational conditions imposed which were outside the normal operating range of the AMPS engine system design.

(C) The following facility corrective action were taken prior to the next test which was to be conducted with a single segment:

1. The oxidizer purge gas was changed from gaseous nitrogen to gaseous helium, and the purge gas supply pressure was decreased to 150 psig from 450 psig.
2. The main oxidizer valve opening time was decreased to 180 milliseconds.
3. A fuel feed system coolant bypass system was installed that decreased the fuel lead time to less than 10 seconds and prevented segment hardware overchilling. The fuel bypass flow was discharged directly into the altitude diffuser.

(4) Activation Firing Test 005

(C) The next attempted hot-fire facility activation test used a single segment assembly mounted in a new thrust mount. The test was planned for 3 seconds at 400-psig chamber pressure. The test was terminated prematurely by the automatic fire detection link cutoff device. The detected fire was a result of burnout of the oxidizer helium purge tube (Fig. 152). The tube burnout was attributed to moisture contamination. There was no segment hardware or other facility damage. Ignition and starting characteristics of the segment were smooth and normal.

1XZ35-4/2/70-R1A

Figure 152. Facility Oxidizer Purge Tube Posttest 005 (U)

(U) The purge configuration was then modified by installing the purge check valve directly into the MOV lower body and changing the purge gas from GN_2 to GH_e.

(5) Additional Oxidizer System Blowdowns

(U) Because of the oxidizer system modification, repassivation of the system, and additional blowdowns were conducted to verify system integrity.

(C) Two low-pressure, short-duration, liquid fluorine passivations and blowdowns of the oxidizer system were conducted on 13 April 1970. The basic facility oxidizer feed system is shown schematically in Fig. 153, and shows the modified oxidizer purge configuration.

(U) The first passivation and blowdown was satisfactory. At the completion of the second passivation and blowdown, leakage of oxidizer was noted from between the body halves of the MOV. The MOV was removed, disassembled, and inspected. The upper body half was found to have been incorrectly machined in the seal region. The valve was cleaned, reassembled with a different upper body half, and reinstalled in the system. The purge check valve was also removed with the MOV and was bench tested prior to reinstallation.

(a) Facility Oxidizer System Passivation and Blowdown, 15 April 1970

(U) This facility passivation and blowdown test was conducted with the liquid fluorine run vessel pressurized to 80 psig. The injector oxidizer purge check valve failed immediately upon MOV opening actuation, resulting in a detonation. Additional explosive-type damage was noted just upstream of the cavitating venturi that was located approximately 25 inches downstream of the MOV discharge flange (Fig. 153). Also, burning occurred on the MOV purge boss, presumably as post-detonation combustion.

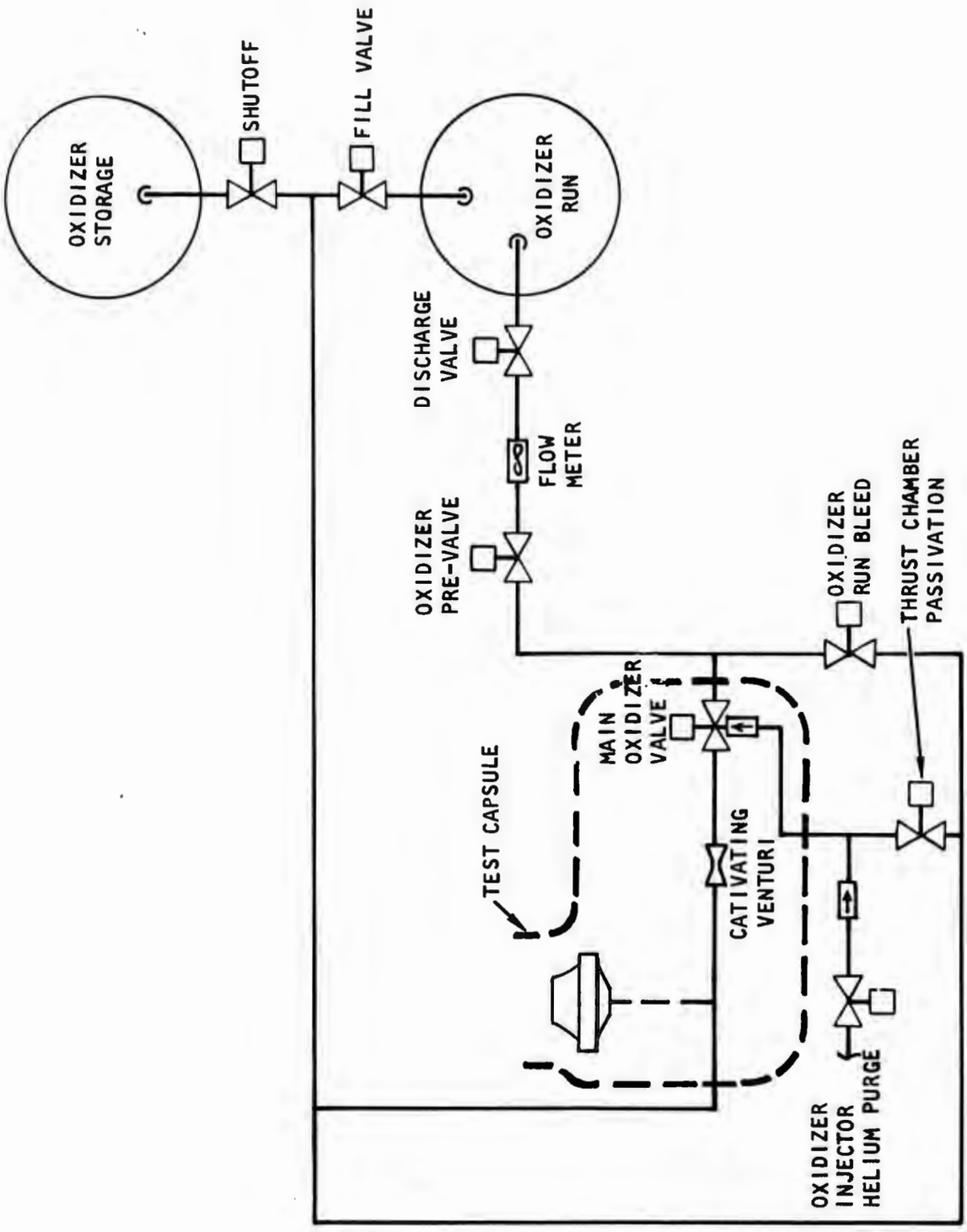

Figure 153. NFL - B-4A Oxidizer Blowdown System (U)

(U) An analysis of the incident resulted in the following conclusion. The initiation of the detonation was attributed to the presumed presence of moisture (ice) on the poppet, or spring of the check valve. This moisture was subjected to the impact of liquid fluorine upon opening of the MOV and resulted in an immediate detonation. The presence of ice in the check valve is postulated for several reasons:

1. The MOV had been removed and serviced prior to this blowdown. The system was exposed to ambient air with possible subsequent condensation in the line.
2. The system LN_2 jacket chilldown was initiated before passivation.
3. No passivation was carried out by flowing fluorine through the check valve. Limited passivation with gaseous fluorine up to the closed check valve, however, was carried out prior to initiating the blowdown.
4. The check valve, being of much lower mass than the MOV and run line, would quickly cool to LN_2 temperatures during the system chilldown and concentrate residual moisture in the check valve.

(U) The following changes were made for the next passivation and blowdown test:

1. A cold trap was installed for the helium purge gas to pass through and remove any moisture prior to introduction of the gas into the oxidizer system.
2. More rigorous passivation procedures were adopted which included ambient temperature gaseous fluorine passivation at various pressure levels prior to the final liquid fluorine passivation.

(b) Facility Oxidizer System Passivation and Blowdown, 24 April 1970

(U) Extensive passivation of the oxidizer system was accomplished in which the system was passivated at pressures up to 400 psig with fluorine gas at ambient temperature. The final step in the gaseous passivation was a 4-hour hold at 400 psig.

(U) Following system chilldown and introduction of liquid fluorine into the system, a series of 11 blowdowns through the feed system and back to the storage tank was conducted, as follows:

Tank Pressure, psig	Flow Duration, seconds
10	300
20	300
30	300
40	300
50	300
75	300
100	300
190	34
280	40
400	12
560 to 640	41

(U) The last blowdown was terminated as programmed after 41 seconds of flowing liquid oxidizer. The run tank pressure gradually increased from 560 to 640 psig during the blowdown. No anomalies, other than the tank pressure rise, were noted either by observers or on the data records until the time that the MOV closed-position microswitch picked up. At that time, observers reported that sparks and smoke appeared on the television monitor screen. The television camera was placed to view the inside of the capsule through a porthole. Several seconds after smoke first appeared inside of the capsule, observers noted that the oxidizer main run line had burned through outside of the capsule.

(U) Figure 154, which shows a composite of the Brush recorder and oscillograph records, indicates that the MOV closed in 160 milliseconds which is considered normal. The pressure at the cavitating venturi (located downstream of the MOV) started to decay 25 milliseconds after the MOV reached the closed microswitch, indicating that the MOV was closed enough to restrict the flowrate.

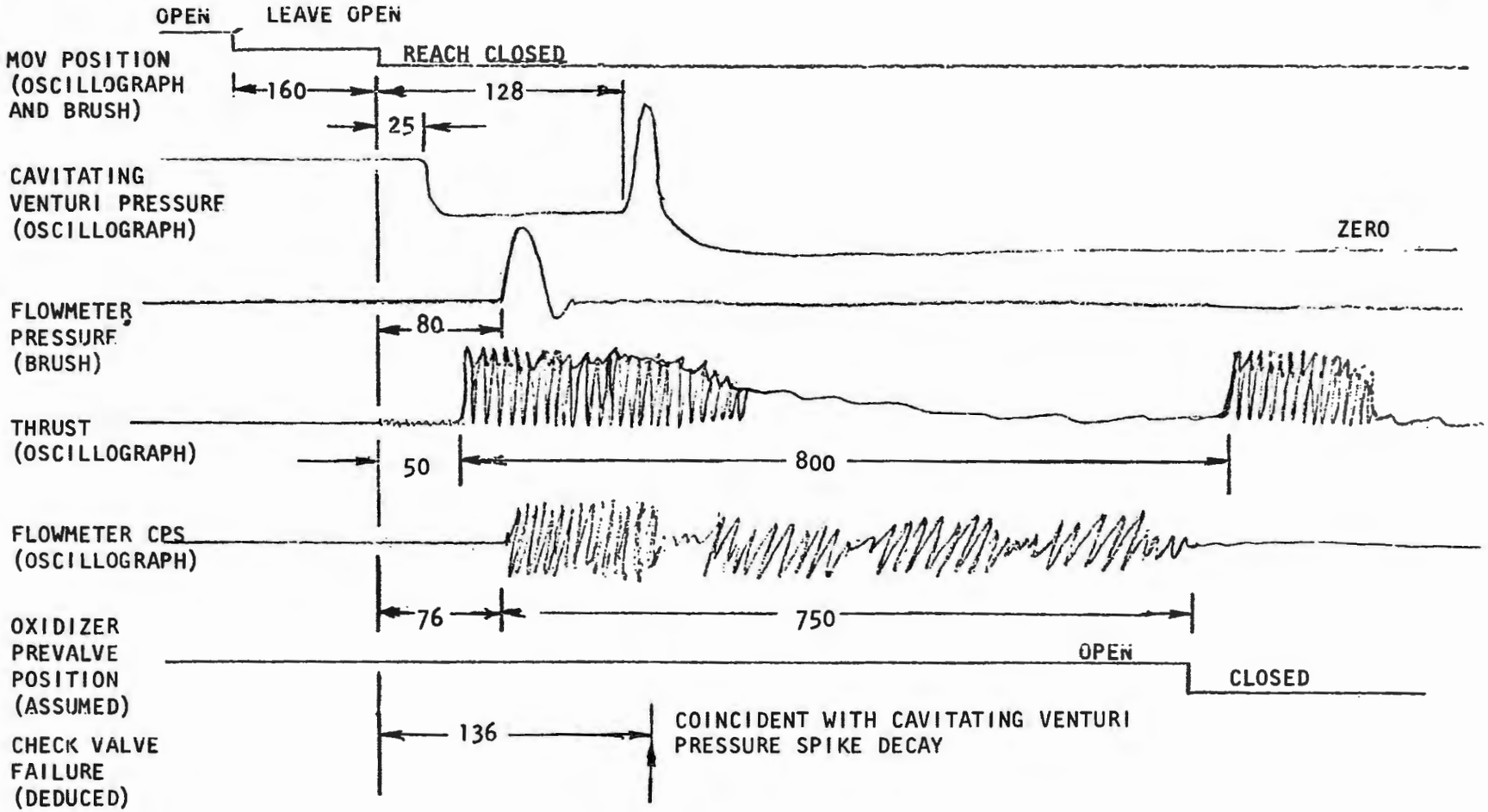

Figure 154. Sequence of Significant Events (U)

(U) The pressure at the cavitating venturi reflected a high-amplitude pressure spike of approximately 1960 psig at 128 milliseconds, after the MOV reached the closed microswitch. The cavitating venturi pressure then decayed to zero very rapidly after the pressure spike, indicating that the oxidizer purge check valve had failed and relieved the pressure in the cavity downstream of the MOV seat and plug. The previous blowdowns exhibited a slow pressure decay after closing of the MOV, and the pressure did not decay to zero.

(U) The oxidizer flowmeter apparently began spinning backwards very rapidly at 76 milliseconds after the MOV reached the closed microswitch. The interpretation of backward spinning of the flowmeter is that high-pressure gas generated by burning in the MOV area caused backflow in the run line. The pressure at the oxidizer flowmeter also shows a very high amplitude spike (in excess of 2000 psi) at that time. The flowmeter trace on the oscillograph shows that oxidizer in the line appeared to oscillate back and forth due to pressure surges in the line for approximately 750 milliseconds, after it first started spinning backward. The oxidizer flowmeter apparently stopped spinning after 750 milliseconds, because the oxidizer run line prevalve had closed. The oxidizer prevalve closed as a result of a cutoff signal given by a fire detect link break at the oxidizer injector purge check valve. As previously mentioned, the purge check valve is believed to have failed 136 milliseconds after the MOV reached the closed microswitch.

(U) The thrust trace experienced a severe disturbance 30 milliseconds prior to the high-pressure surge at the oxidizer flowmeter. The thrust trace showed another severe disturbance approximately 800 milliseconds after the first disturbance. There were no pressure disturbances seen in the flowmeter pressure or in the cavitating venturi pressure at the time of this second disturbance. The interpretation of these observations is that the thrust disturbances indicate that a reaction was occurring in the run line and that the MOV and the prevalves were closed at the time of the second disturbance.

(U) Analysis of the test films indicated that burnout of the oxidizer run line at the entrance to the altitude capsule occurred approximately 25 seconds after MOV closure.

(U) All significant damage was confined to the facility oxidizer feed system and consisted of the following:

1. Internal burning of the MOV
2. Burning of the 1-inch purge check valve located in the lower half of the MOV body (Fig. 155)
3. Burnout of the 3-inch jacketed oxidizer line at its entrance to the altitude capsule (Fig. 156.) along with burning of adjacent electrical wires and control tubing

(U) The conclusion was that the incident was initiated by burning in the stem area of the MOV while the valve was in the open position during the last blowdown. Upon closing the valve, the hot portion of the stem was exposed to liquid oxidizer resulting in a violent reaction.

(U) The evidence indicated that the sequence of events was as follows (Fig. 157 and 158):

1. Initiation of combustion occurred at the vent hole in the normalizing fin spacer (sleeve). This was evidenced by intense burning and melting noted on the normalizing fin (housing) adjacent to the hole and burning and melting at corresponding location on the stem.
2. Burning of sleeve on the inside (stem side) as evidenced by metal loss and melting.
3. Gravity flow of molten metal to the junctureof the Al-Bronze lower stem guide.
4. Burning of spacer above Al-Bronze lower stem guide and heating of the valve stem.
5. Exposure of the hot stem portion, by stem travel during valve closure, to the liquid oxidizer in the upper valve body half.
6. Ignition of stem by the liquid oxidizer.

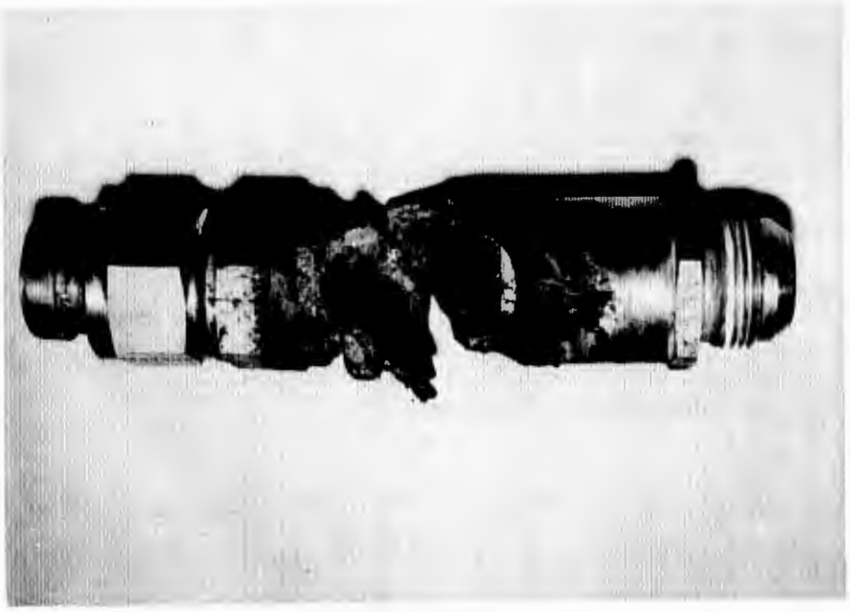

Figure 155. Oxidizer Purge Check Valve (U)

Figure 156. Main Oxidizer Valve and Inlet Line (U)

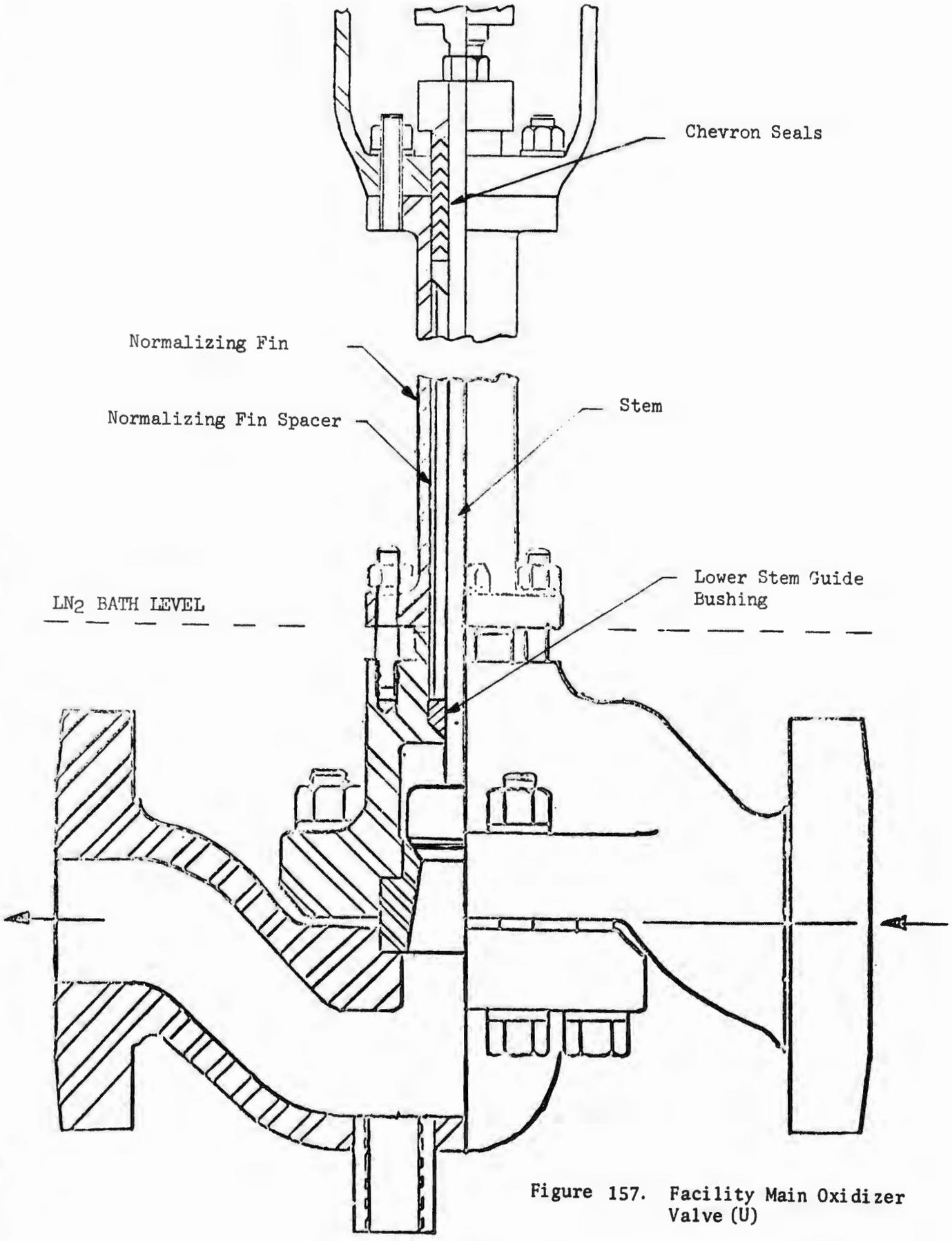

Figure 157. Facility Main Oxidizer Valve (U)

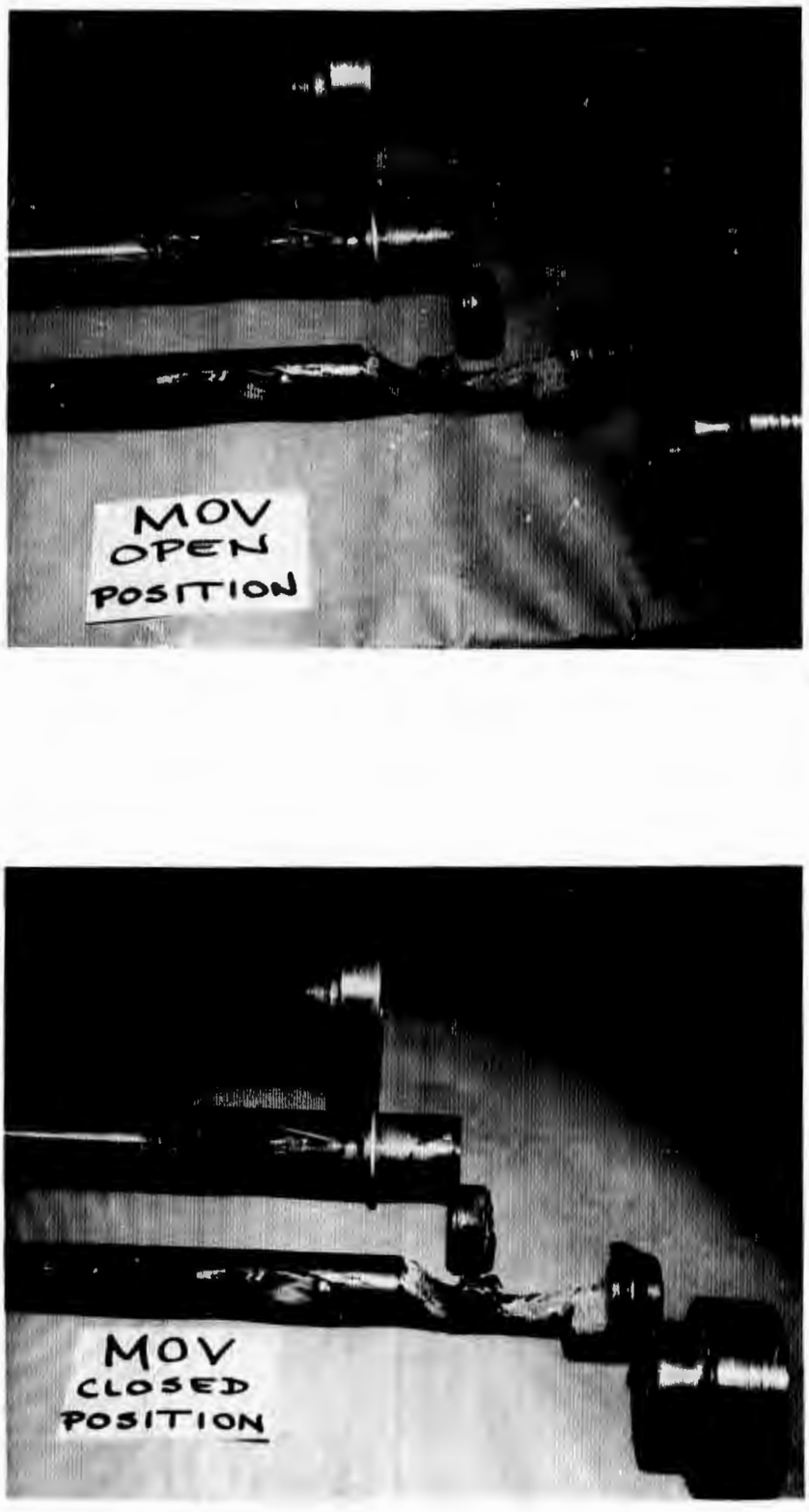

Figure 158. Main Oxidizer Valve Plug and Stem Assembly (U)

7. Combustion of stem and plug collar, lower portion of the stem above the collar, upper valve body half, inlet flange, and subsequently, the oxidizer line, LN_2 jacket, and expansion bellows.

8. Some melted metal deposition on upper rim of the valve seat with slight burning of the seat.

(U) The above modes are listed in assumed decreasing order of probability.

(U) As previously noted, the reaction in MOV became violent only when the stem was moved from the open to the closed position. The data indicate that up to this point, the oxidizer injector purge check valve, located directly below the MOV lower body half, was still intact. The failure of this check valve shortly thereafter cannot be attributed to any specific cause (a number of possibilities exists), but of significance was that the check valve was located in an area in which two previous failures had occurred.

(U) The severe damage (burning) of the check valve precluded a diagnosis as to the exact origin of the burning; however, some possible modes of initiation include the following:

1. Because extensive burning took place immediately above the MOV plug, while the MOV was open, the possibility existed that one or more hot fragments traveled through the MOV seat and lodged into the check valve. These fragments could then provide a site for the initiation of the check valve burning. The "dropping fragment" premise is supported, in part, by the observation that there were some melted metal particles seen in the MOV seat.

2. The failure may be due to the passivating fluorine not reaching all portions of the check valve and reactions starting when abnormal vibrations exposed nonpassivated areas to liquid fluorine.

3. The failure may be the result of contamination in the check valve, in the form of the water-based Teflon lube used during assembly of the check valve, which could be exposed to fluorine either when pressure is raised or during vibration.

(U) 4. The failure may be caused by particulate matter having collected at the check valve (located at the system low point in a natural trap). These particles could react with liquid fluorine when frictional energy is supplied during vibration.

(U) While failure mode of the check valve could not be conclusively determined, the location appears to be particularly vulnerable, whether a check valve is located there or not.

(U) Based on the analysis conducted, the following corrective action was accomplished prior to conducting the next oxidizer system blowdown:

(U) • Liquid Propellant Valves and Run Tank

1. Reverse upper chevron packing seals in the three main line propellant valves to minimize the entry of moisture.
2. Provide a dry atmosphere at the packing area on all oxidizer system Annin-type propellant valves (either GN_2 purge or desiccant).
3. Tighten seal packing several times before introducing oxidizer into the system, and torque the valve body bolts several times to minimize the possibility of leakage resulting from gasket relaxation.
4. Change the MOV from 3 to 2 inches to reduce oxidizer system vibrations during valve actuation.

(U) • Oxidizer Purge Configuration

1. Move the purge entry port to a location downstream of the MOV
2. Locate the purge check valves on vertical riser with a minimum of 18 inches from run line to the check valve
3. Install a restricting orifice in the purge line and use a purge pressure of 4000 psig minimum.

(U) • System Inerting and Passivation. The procedures used to passivate the systems prior to the above series of blowdowns were adequate with one exception. At the start of the passivation cycle, a vacuum was pulled on the system to remove any moisture from the system. This procedure, however, may have, in fact, introduced moisture instead. This procedure will be discontinued, because of being potentially more hazardous than beneficial.

(U) In addition, during the passivation process, the oxidizer gas was left in the system overnight at a pressure of 5 psig. The procedure will be used; however, a higher pressure will be maintained which is sufficient to assure positive internal pressure in spite of day-night temperature cycles.

(U) • Other. At any time the system is not in use, a positive pressure will be maintained in the oxidizer system with either helium or gaseous oxidizer.

All noted modifications were accomplished, and additional passivations and blowdowns were scheduled.

(c) Oxidizer System Incident of 25 May 1970

(U) The oxidizer system was thoroughly passivated with ambient temperature gaseous fluorine. The gaseous fluorine was first introduced into the system at low pressure. The pressure was held for 5 minutes and the system was inspected for anomalies. The pressure was then increased to 400 psig in small increments with 5-minute holds at each pressure level. The final hold at 400 psig was for 2-1/2 hours. The system pressure was then held at 50 psig during periods of test stand inactivity. No anomalies were noted at any time during the passivation process.

(U) Approximately 1800 pounds of liquid fluorine was transferred to the oxidizer run tank from the storage tank. Seven liquid fluorine blowdowns of 5-minutes duration each were conducted at run tank pressures of 10, 20, 30, 40, 50, 75, and 100 psig. Five additional liquid fluorine blowdowns of 100-seconds duration each were conducted at run tank pressures of 200, 300, 400, 500, and 600 psig. The oxidizer

(C) was returned to the storage tank in a closed-loop system. Each of the oxidizer valves, which are normally exposed to fluorine, was actuated several times during the blowdown series. No anomalies were noted during the blowdown series or during the test stand securing operations.

(U) Analysis of the blowdown graphic recorder and oscillograph records indicated that all operations were normal.

(U) An activation firing was to be made with a single segment assembly for the purpose of final facility checkout prior to installation of the 360-degree main chamber. During final pretest setup operations, a violent reaction(s) occurred in the oxidizer system which resulted in extensive damage to the facility. Figures 159 and 160 show overall views of the facility damage.

(U) The oxidizer system contined 1800 pounds of fluorine at the time of the incident, and the test capsule was at a simulated altitude condition.

(U) The fuel run tank appeared to sustain little damage. The fuel run line, which passed over the oxidizer run line, was severely distorted and burned through as a result of the oxidizer fires. The fuel run line valves have not been inspected but appear to be relatively undamaged and repairable.

(U) The inside of the altitude capsule sustained fire damage to lighting fixtures, wiring, and instrumentation as a result of rupture of the main oxidizer valve. The flexible boot on the outside of the capsule was damaged, but the capsule itself appeared to be relatively undamaged. The thrust chamber segment was not damaged in the incident.

(U) The complete oxidizer system schematic is shown in Fig. 161 and consists of the following subsystems.

Subsystem 1. The oxidizer storage and transfer system which contains the oxidizer storage vessel, 500-gallon, 475-psig; storage tank shutoff valve; 1-inch-diameter tubing transfer line, and oxidizer run tank fill valve; and oxidizer run tank, 360-gallon, 2000-psig maximum working pressure.

Figure 159. NFL-B4A Facility Damage (viewed from block house side) (U)

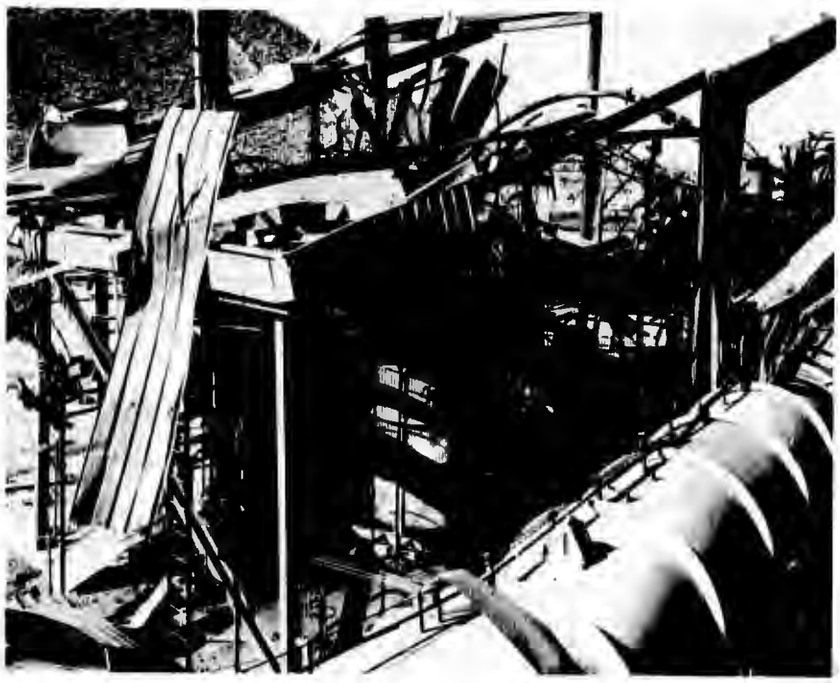

Figure 160. NFL-B4A Facility Damage (viewed from altitude simulation diffuser side) (U)

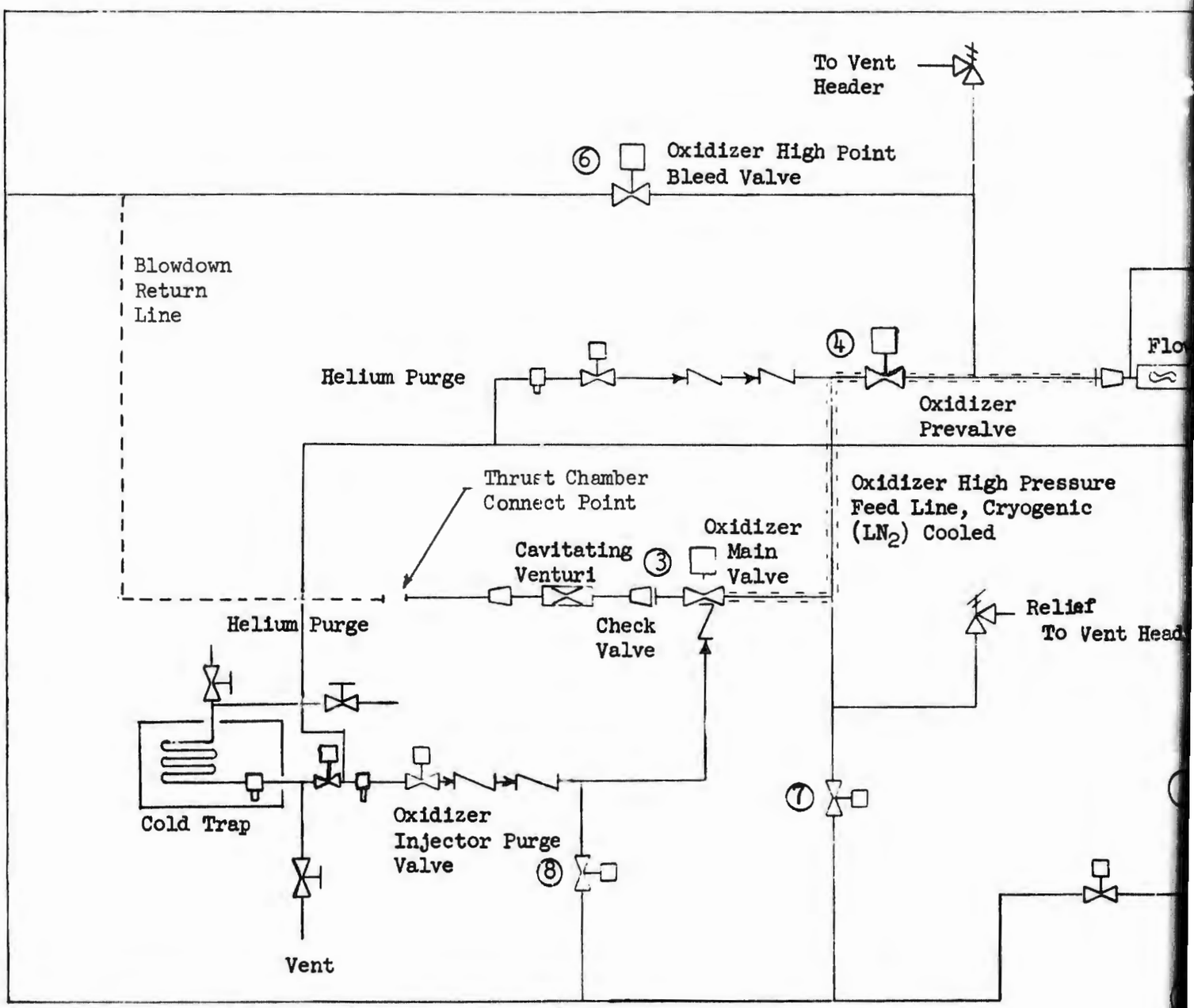
To Vent Header
⑥ Oxidizer High Point Bleed Valve
Blowdown Return Line
④
Helium Purge
Oxidizer Prevalve
Thrust Chamber Connect Point
Oxidizer High Pressure Feed Line, Cryogenic (LN_2) Cooled
Oxidizer Main Valve
③
Cavitating Venturi
Helium Purge
Check Valve
Relief To Vent Head
⑦
Cold Trap
Oxidizer Injector Purge Valve
⑧
Vent

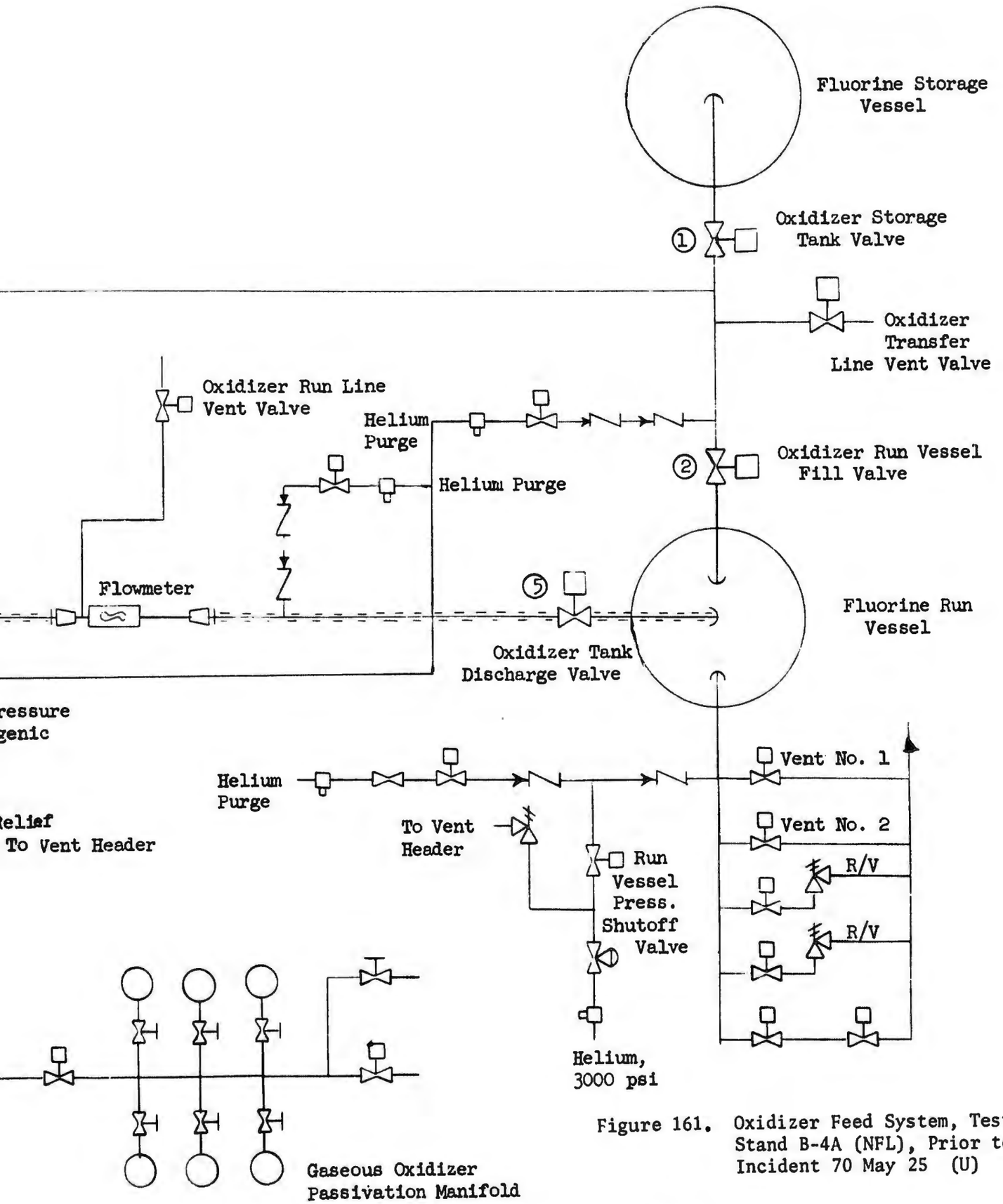

Figure 161. Oxidizer Feed System, Test Stand B-4A (NFL), Prior to Incident 70 May 25 (U)

2

(U) The oxidizer run tank (Fig. 162) was built originally for liquid-oxygen service and was modified for fluorine service. The modifications consisted of welding a "blind" flange into the tank bottom and converting to a dip-tube discharge. The dip-tube was provided with an LN_2 jacket inside of the tank as well as outside to the first pipe flange. The tank was immersed in an LN_2 bath, which in turn was enclosed in a foam-insulated jacket.

(U) Subsystem 2. The oxidizer high-pressure feed system, which contains the oxidizer run tank, run tank discharge valve, prevalve, main valve, cavitating venturi, and blowdown return line. The line terminates at the test hardware.

(U) Subsystem 3. The oxidizer run line high-point bleed, which consists of the oxidizer run line high-point bleed valve and a return line. This bleed removes oxidizer from the section of run line between the tank discharge valve and prevalve for priming of the system pretest.

(U) Subsystem 4. The oxidizer run line bleed contains the oxidizer run bleed valve. This system bleeds oxidizer from the high-pressure feed line between the prevalve and main oxidizer valve for priming pretest.

(U) Subsystem 5. The oxidizer passivation system and oxidizer high-flow helium purge system that contains the thrust chamber passivation valve and oxidizer injector purge valve. Two check valves are installed in the high-flow injector helium purge system with a soft seat check valve located near the purge valve and a metal seat check valve adjacent to the main oxidizer valve. The check valves are used to prevent backflow of oxidizer into the helium purge system.

(U) Subsystem 6. This is the remaining 1/2-inch-diameter tubing line that returns oxidizer to the storage vessel from the other various subsystems.

(U) Several liquid-fluorine blowdowns and three hot-fire tests had been conducted on test stand B-4A prior to the incident of 25 May 1970. The oxidizer system had been exposed to maximum operating conditions of 1235-psi tank pressure and approximately 4 lb/sec steady-state flowrate. The oxidizer flowrate from valve

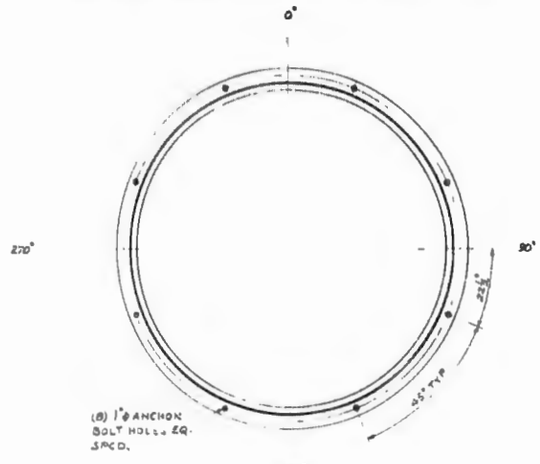

ANCHOR BOLT ORIENTATION
SCALE - 1" = 1'-0"

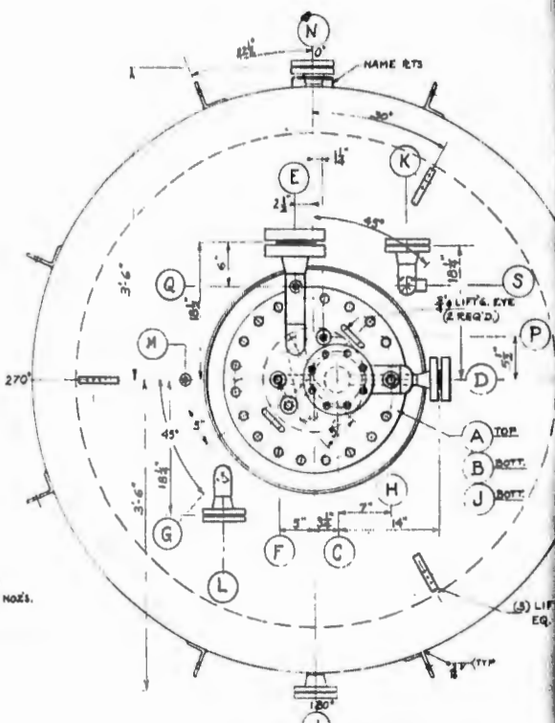

PLAN VIEW
TRUE ORIENTATION
SCALE - 1½" = 1'-0"

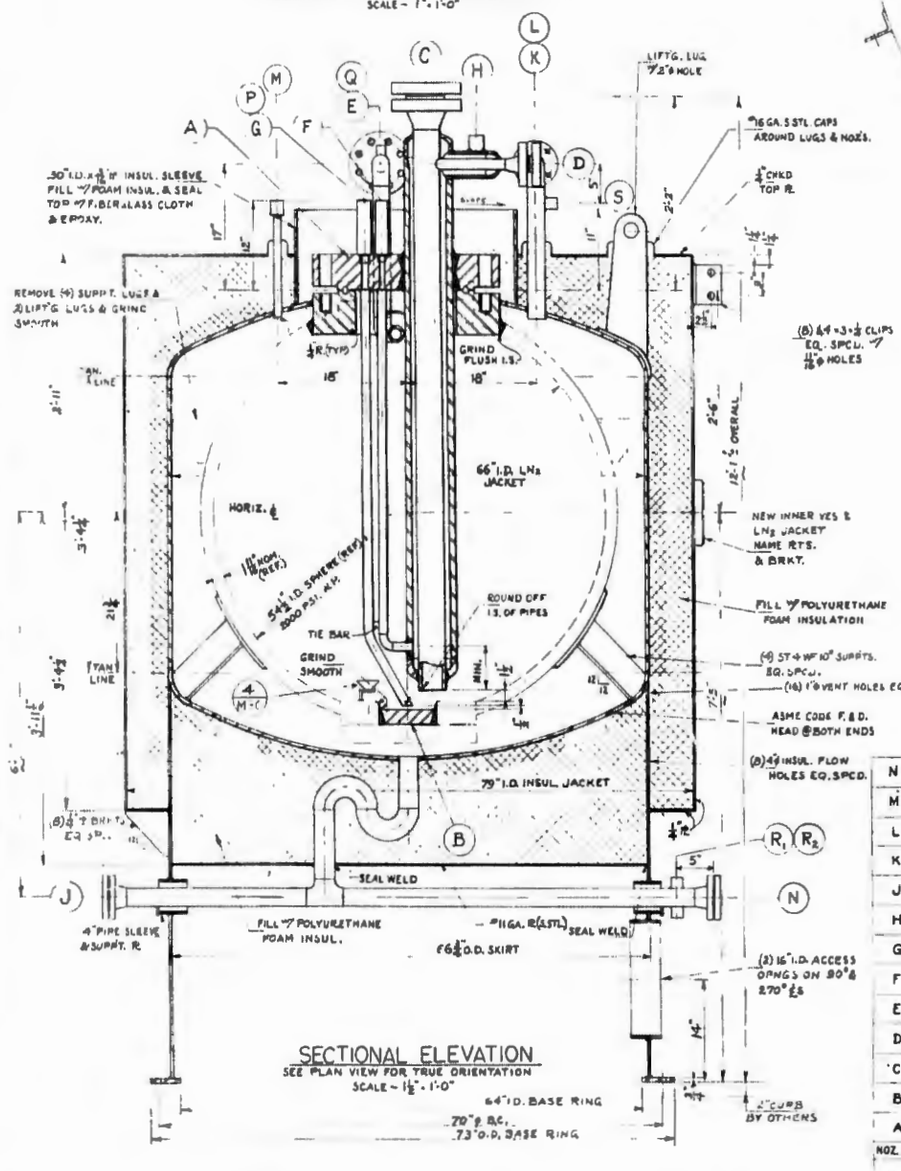

SECTIONAL ELEVATION
SEE PLAN VIEW FOR TRUE ORIENTATION
SCALE - 1½" = 1'-0"

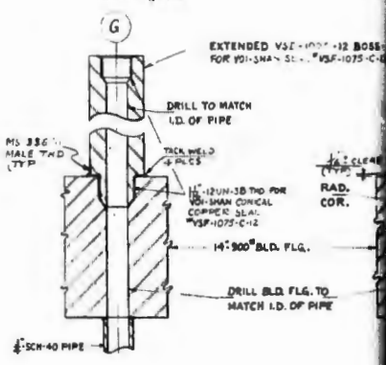

1 M3 DETAIL
SCALE - 6" = 1'-0"

NOZ. NO.	SERVICE	SIZE	DESCRIPTION	
N	LN_2 JACKET FILL	2"	150# R.F. WELD NECK FLANGE	SEE ELE
M	LN_2 LEVEL CONTROL	¾"	6000# SCWD. CPLG.	W/ BRASS
L	LN_2 JACKET VENT	2"	150# R.F. WELD NECK FLANGE	W/ EXT. 90°
K	LN_2 JACKET SPARE	2"	150# R.F. WELD NECK FLANGE	W/ EXT. 90°
J	LN_2 JACKET DRAIN	2"	150# R.F. WELD NECK FLANGE	SEE ELE
H	NOZ. "C" LN_2 JACKET VENT	1" TUBE	VSD-1000-16 BOSS (2½ø x 2")	W/ PLUG
G	SIPHON DRAIN	¾" TUBE	INSTALL EXTENDED VSD-1000-12 BOSS IN TAPPED BLD. FLG.	W/ INTERN PIPE - SE
F	NOZ. "C" LN_2 JACKET FILL	¾" TUBE	INSTALL EXTENDED VSD-1000-12 BOSS IN TAPPED BLD. FLG.	W/ INTERN NOZ. "C" L
E	PRESSURIZATION & VENT	2"	900# RTJ. WELD NECK FLANGE	W/ INTERN ELL & P
D	SPARE	1"	900# RTJ. WELD NECK FLANGE	W/ 3" SCH
C	RUN & FILL	3"	900# RTJ. WELD NECK FLANGE	W/ 6"-XX-H
B	BOTTOM HANDHOLE (EXIST.)	8"	900# ST&G PAD TYPE FLANGE	REMOVE AND PL
A	TOP HANDHOLE & ACCESS OPNG.	14"	900# RTJ. PAD TYPE FLANGE & SPECIAL BLIND FLANGE	REMOVE ETC. & I

NOZZLE SCHEDULE

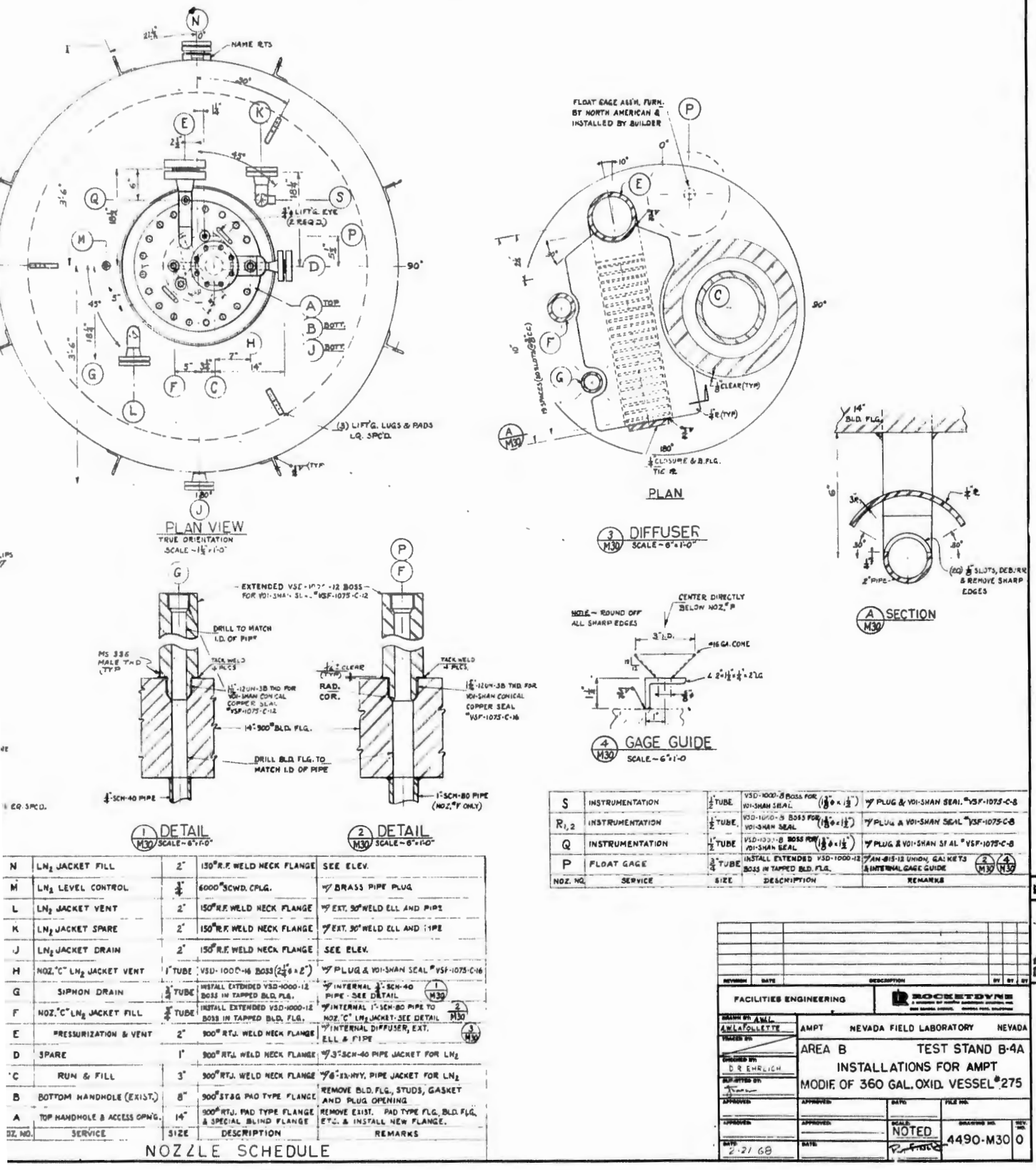

NOZ. NO.	SERVICE	SIZE	DESCRIPTION	REMARKS
N	LN_2 JACKET FILL	2"	150# R.F. WELD NECK FLANGE	SEE ELEV.
M	LN_2 LEVEL CONTROL	¾"	6000# SCWD. CPLG.	¾" BRASS PIPE PLUG
L	LN_2 JACKET VENT	2"	150# R.F. WELD NECK FLANGE	¾" EXT. 90° WELD ELL AND PIPE
K	LN_2 JACKET SPARE	2"	150# R.F. WELD NECK FLANGE	¾" EXT. 90° WELD ELL AND PIPE
J	LN_2 JACKET DRAIN	2"	150# R.F. WELD NECK FLANGE	SEE ELEV.
H	NOZ."C" LN_2 JACKET VENT	1" TUBE	VSD-1000-16 BOSS (2¼"ø x 2")	¾" PLUG & VOI-SHAN SEAL "VSF-1075-C-16
G	SIPHON DRAIN	¾" TUBE	INSTALL EXTENDED VSD-1000-12 BOSS IN TAPPED BLD. FLG.	¾" INTERNAL ¾" SCH-40 PIPE - SEE DETAIL 1 M30
F	NOZ."C" LN_2 JACKET FILL	¾" TUBE	INSTALL EXTENDED VSD-1000-12 BOSS IN TAPPED BLD. FLG.	¾" INTERNAL 1" SCH-80 PIPE TO NOZ."C" LN_2 JACKET - SEE DETAIL 2 M30
E	PRESSURIZATION & VENT	2"	900# R.T.J. WELD NECK FLANGE	¾" INTERNAL DIFFUSER, EXT. ELL & PIPE 3 M30
D	SPARE	1"	900# R.T.J. WELD NECK FLANGE	¾" 3" SCH-80 PIPE JACKET FOR LN_2
C	RUN & FILL	3"	900# R.T.J. WELD NECK FLANGE	¾" 6"-Ø-HVY. PIPE JACKET FOR LN_2
B	BOTTOM HANDHOLE (EXIST.)	8"	900# ST&G PAD TYPE FLANGE	REMOVE BLD. FLG., STUDS, GASKET AND PLUG OPENING
A	TOP HANDHOLE & ACCESS OPN'G.	14"	900# R.T.J. PAD TYPE FLANGE & SPECIAL BLIND FLANGE	REMOVE EXIST. PAD TYPE FLG., BLD. FLG. ETC. & INSTALL NEW FLANGE.

NOZZLE SCHEDULE

NOZ. NO.	SERVICE	SIZE	DESCRIPTION	REMARKS
S	INSTRUMENTATION	½" TUBE	VSD-1000-8 BOSS FOR VOI-SHAN SEAL (1⅛"ø x ½")	¾" PLUG & VOI-SHAN SEAL "VSF-1075-C-8
$R_{1,2}$	INSTRUMENTATION	½" TUBE	VSD-1000-8 BOSS FOR VOI-SHAN SEAL (1⅛"ø x 1½")	¾" PLUG & VOI-SHAN SEAL "VSF-1075-C-8
Q	INSTRUMENTATION	½" TUBE	VSD-1000-8 BOSS FOR VOI-SHAN SEAL (1⅛"ø x 1½")	¾" PLUG & VOI-SHAN SEAL "VSF-1075-C-8
P	FLOAT GAGE	¾" TUBE	INSTALL EXTENDED VSD-1000-12 BOSS IN TAPPED BLD. FLG.	7AN-815-12 UNION, GAL'KETS & INTERNAL GAGE GUIDE 2 M30 4 M30

REVISION	DATE	DESCRIPTION	BY	BY

FACILITIES ENGINEERING — ROCKETDYNE

DRAWN BY: A.W.L. — A.W.LaFOLLETTE
TRACED BY:
DESIGNED BY: D.R.EHRLICH
SUP. APPROVED BY:
APPROVED
APPROVED
APPROVED
DATE: 2-21-68

AMPT NEVADA FIELD LABORATORY NEVADA
AREA B TEST STAND B-4A
INSTALLATIONS FOR AMPT
MODIF. OF 360 GAL. OXID. VESSEL #275

APPROVED
APPROVED
DATE
DATE
FILE NO.
SCALE: NOTED
DRAWING NO. 4490-M30
REV. NO. 0

4490-M30 0

Figure 162. Details of Oxidizer Run Tank Construction

2

(U) opening to prime at the cavitating venturi exceeded 60 lb/sec for approximately 0.5 second during two of the hot-fire tests. The test stand history is presented in Table 22.

(U) Several oxidizer blowdowns were conducted on 23 May 1970 to tank pressure of 600 psi with no anomalies. The test stand was then secured over the weekend by transferring the remaining oxidizer from the run tank back to the storage tank. The run line was purged of oxidizer. The entire oxidizer system was then pressurized with 50-psi helium. The system was pressurized through a helium system cold trap into the upstream run line bleed. The oxidizer system was secured with the various system valves left in the positions indicated in Table 23. The location of the various valves is shown in Fig. 161.

(U) The oxidizer system remained pressurized to 50 psig over the weekend, as evidenced by a check of instruments immediately upon shift start Monday morning.

(U) The following operations were completed in preparation for the test on 25 May 1970:

(U) Installation of Run Line. The facility had been left in the blowdown configuration following the 23 May 1970 oxidizer blowdowns. The blowdown return line downstream of the cavitating venturi to the storage tank return line (Fig. 161) was removed after purging with helium and the run line connecting downstream of the cavitating venturi to the segment thrust chamber inlet was installed. The 50-psig pressure was maintained in the run tank and run line.

(U) Purge Cold Trap Activation. The helium purge cold trap was purged with hot gaseous nitrogen and then charged with liquid nitrogen in preparation for usage of the helium purges.

(U) Purification of the Run Line and Run Tank. The run line and run tank were purified by conducting one pressure vent cycle at 150-psig helium pressure. The helium was supplied from the helium purge system.

TABLE 23

POSITION OF VALVES DURING
SECURING OPERATION (U)

Valve	Secured Position	Normal Position
Run tank discharge valve	Open	Closed
Oxidizer prevalve	Open	Closed
Main oxidizer valve	Closed	Closed
Oxidizer run line bleed valve	Closed	Closed
Oxidizer high-point vent valve	Closed	Closed
Thrust chamber passivation valve	Closed	Closed
Storage tank discharge valve	Closed	Closed
Oxidizer transfer line vent valve	Closed	Closed
Run line transducer vent valve	Closed	Closed
Run tank fill valve	Closed	Closed
Run tank vent valve #1 and #2	Closed	Closed
Run tank relief shutoff #1 and #2	Open	Open
Run tank pressurization shutoff	Closed	Open
Oxidizer transfer line helium purge	Closed	Open
Oxidizer run line U/S and D/S helium purge	Closed	Open
Oxidizer run tank transducer shutoff	Open	Open
Oxidizer run tank transducer vent	Closed	Open
Oxidizer injector purge valve	Closed	Open
Oxidizer injector low-flow purge (GN_2)	Capped off	—

(U) Run Line and Run Tank Chilldown. The run tank and run line were pressurized with helium to 150 psig prior to starting chilldown of the run tank and run line. After completion of chill of the line and tank, the pressure had collapsed to 20 psig. The LN_2 chill in the system was normally maintained until completion of the test and transfer of oxidizer from the run to storage tank had been completed.

(U) Electromechanical Checkouts. During electromechanical checkouts, the depressurization of the run line was necessary downstream of the prevalve, but not upstream on the run vessel. This line section was repressurized, using the downstream helium purge (through a cold trap) following completion of checks.

(U) Flowmeter Pressure Transducer Prerun Zero. The run line between the tank discharge valve and prevalve was vented to ambient pressure (vent header pressure) for transducer calibration. This operation required 15 to 20 minutes, while the vent was closed. The system was then repressurized by use of the upstream helium purge through a cold trap.

(U) Vent Run Tank and Line and Transfer LF_2. In preparation for transferring LF_2 from the storage tank to the run tank through the transfer line, the transfer line, run line (tank to the main oxidizer valve), and run tank were vented to vent stack ambient pressure.

(U) The run tank vent was then closed and LF_2 was transferred into the LN_2-chilled run tank. The LH_2 was transferred through an uninsulated line.

(U) Test Countdown. The run countdown was started and included passivation of the run line downstream of the main oxidizer valve and the segment thrust chamber assembly injector. Gaseous fluorine was provided from the storage vessel, through the thrust chamber passivation valve.

(U) Pressurization of the fuel tank was completed. The oxidizer run tank was being pressurized. At approximately 600- to 700-psig tank pressure, the oxidizer high-point bleed valve and run bleed valves were opened and closed

(U) for final system bleed. Pressurization of the oxidizer run vessel was continued to 1100 psig when the incident occurred. The only activity at the time of the detonation was pressurization of the oxidizer run tank. No recorders or cameras were running at the time.

(d) Damage Description

(U) The majority of damage was confined to the oxidizer run system and the test stand structure in the vicinity of the oxidizer system.

(U) Fuel System. The fuel run tank appeared to sustain little damage. The fuel run line, which passed over the oxidizer run tank, was severely distored and burned through as a result of the oxidizer fires. The fuel run line valves have not been inspected but appear to be relatively undamaged.

(U) Altitude Capsule. The inside of the altitude capsule sustained fire damage to lighting fixtures, wiring, and instrumentation as a result of rupture of the main oxidizer valve. The flexible boot on the outside of the capsule itself appeared to be relatively undamaged.

(U) Thrust Chamber Segment. The thrust chamber segment was not damaged in the incident.

(U) Hyperflow Unit. There was no damage sustained by the hyperflow unit. The hyperflow unit was not running at the time of the incident.

(U) Oxidizer System. The burning and ruptures appeared to originate within the oxidizer system. The individual components of the oxidizer system were, therefore, thoroughly analyzed for condition in an attempt to identify the point of origin of the detonation. A summary of observations concerning facility condition is presented below. A schematic diagram showing the oxidizer run line condition is presented in Fig. 163.

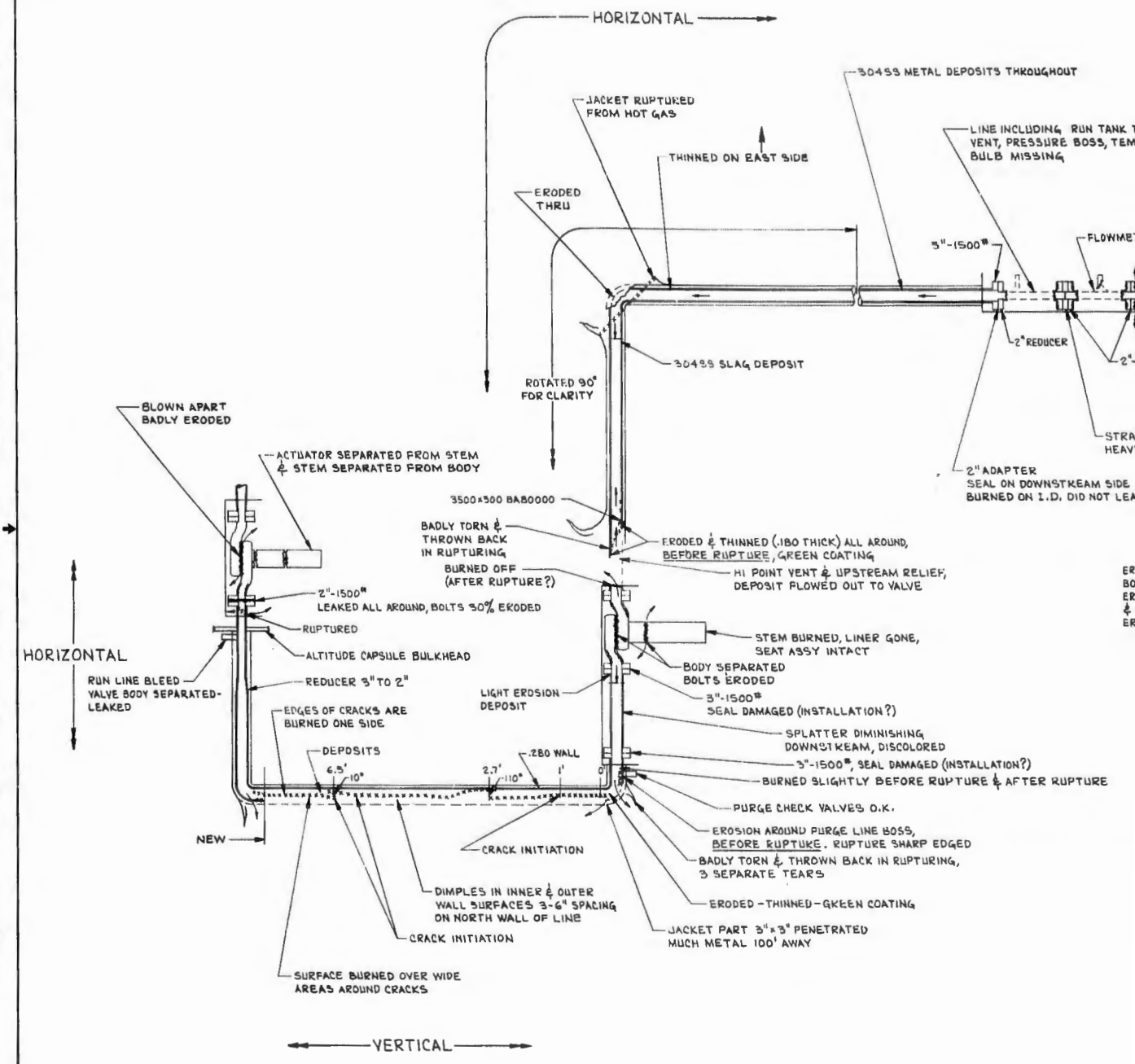
HORIZONTAL
304SS METAL DEPOSITS THROUGHOUT
JACKET RUPTURED FROM HOT GAS
THINNED ON EAST SIDE
LINE INCLUDING RUN TANK T
VENT, PRESSURE BOSS, TEM
BULB MISSING
ERODED THRU
3"-1500#
FLOWME
2"REDUCER
304SS SLAG DEPOSIT
ROTATED 90° FOR CLARITY
BLOWN APART BADLY ERODED
ACTUATOR SEPARATED FROM STEM & STEM SEPARATED FROM BODY
STRA
HEAV
2" ADAPTER
SEAL ON DOWNSTREAM SIDE
BURNED ON I.D. DID NOT LEA
3500x300 BA80000
BADLY TORN & THROWN BACK IN RUPTURING
ERODED & THINNED (.180 THICK) ALL AROUND, BEFORE RUPTURE, GREEN COATING
BURNED OFF (AFTER RUPTURE?)
HI POINT VENT & UPSTREAM RELIEF, DEPOSIT FLOWED OUT TO VALVE
2"-1500#
LEAKED ALL AROUND, BOLTS 90% ERODED
RUPTURED
STEM BURNED, LINER GONE, SEAT ASSY INTACT
ALTITUDE CAPSULE BULKHEAD
HORIZONTAL
RUN LINE BLEED VALVE BODY SEPARATED-LEAKED
BODY SEPARATED BOLTS ERODED
REDUCER 3" TO 2"
LIGHT EROSION DEPOSIT
3"-1500#, SEAL DAMAGED (INSTALLATION?)
EDGES OF CRACKS ARE BURNED ONE SIDE
SPLATTER DIMINISHING DOWNSTREAM, DISCOLORED
DEPOSITS
.280 WALL
6.5'
10°
2.7'
110°
1'
3"-1500#, SEAL DAMAGED (INSTALLATION?)
BURNED SLIGHTLY BEFORE RUPTURE & AFTER RUPTURE
PURGE CHECK VALVES O.K.
EROSION AROUND PURGE LINE BOSS, BEFORE RUPTURE. RUPTURE SHARP EDGED
NEW
CRACK INITIATION
BADLY TORN & THROWN BACK IN RUPTURING, 3 SEPARATE TEARS
DIMPLES IN INNER & OUTER WALL SURFACES 3-6" SPACING ON NORTH WALL OF LINE
ERODED - THINNED - GREEN COATING
CRACK INITIATION
JACKET PART 3"x3" PENETRATED MUCH METAL 100' AWAY
SURFACE BURNED OVER WIDE AREAS AROUND CRACKS
VERTICAL
NOTE: UNLESS OTHERWISE SPECIFIED

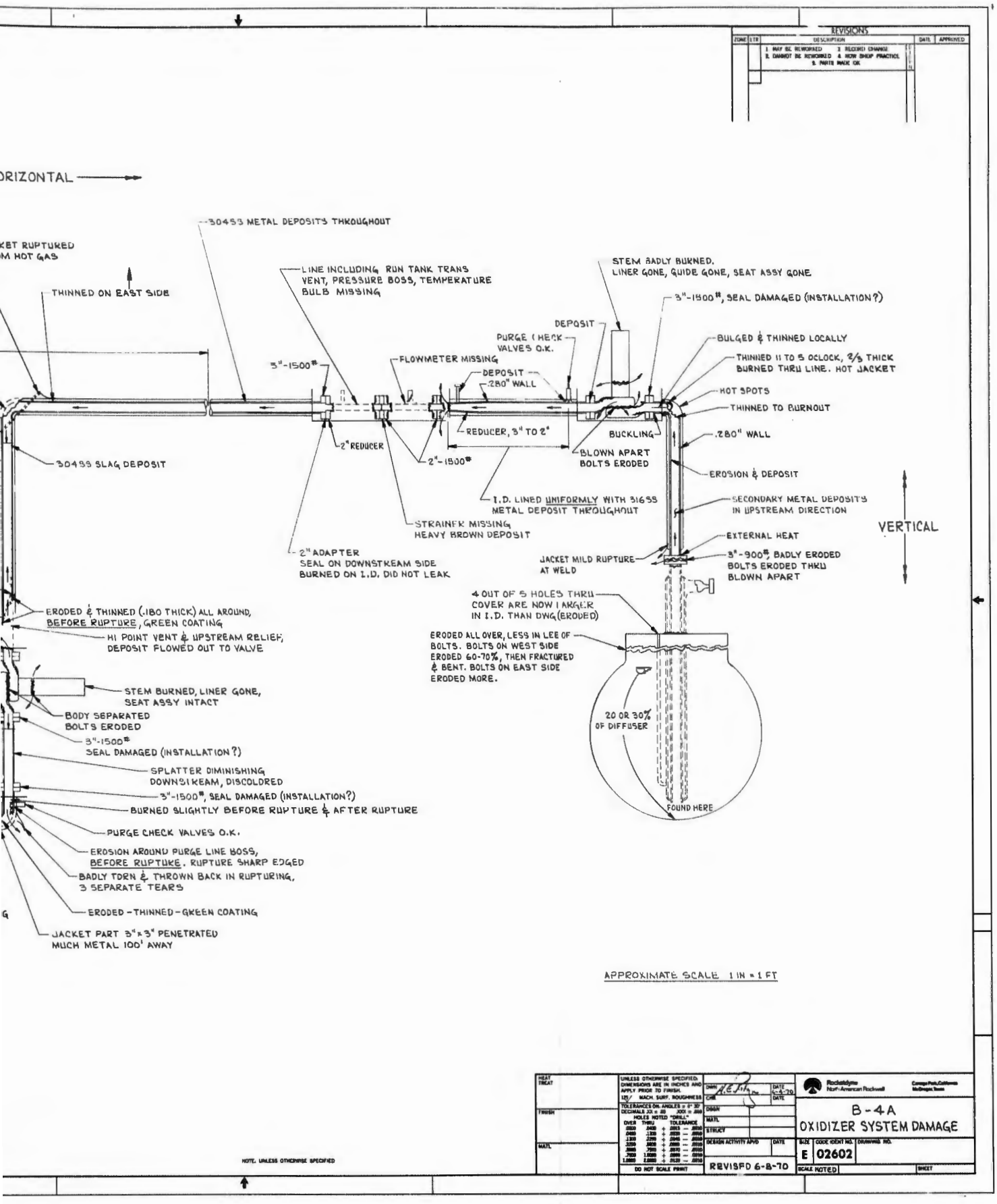

Figure 163. Sketch of Oxidizer Run Line (U)

2

(U) The following hardware conditions were observed:

1. The tank cover lifted, the bolts burned from the inside, and eventually the bolts ruptured under thinned conditions.
2. Hot gas and metal were blown up the tank fill valve line.
3. The dip tube and its jacket were burned off above and below the tank cover.
4. The tank relief valve did not see hot flow and the line upstream of it was burned out.
5. Four out of the five tank cover holes were enlarged from hot-gas flow outward, the liquid level plug being one which remained intact.
6. The tank cover was launched under a pressure of approximately 5000 psi.
7. The dip tube is gone, up to the first line flange above the tank.
8. A portion of the pressurizing diffuser was found in the tank bottom, this being the only part of equipment in the tank found.
9. The tank liquid level gage float and guide assembly is gone.
10. The tank fill and pressurization valves are burned on the outside only, and one of them shows impact from below.
11. A piece of the dip tube jacket and the run line boss remained, apparently burned off from the line outside the tank cover.
12. Erosion and deposit in the tank discharge line was in the downstream direction.
13. The elbow upstream of the tank valve was burned out in a downstream direction.
14. Deposit in the line downstream of the tank valve was in the downstream direction and was of 316 stainless steel material, the material of the tank valve.
15. All three of the run valve bodies were partially separated at the body half joint and all leaked at these separations and continued to burn internally. Also, the prevalve and tank valves separated at the normalizing fin joint.

(U) 16. The tank valve body separated completely at the bolted joint, the bolts being burned and ruptured.

17. The 3-inch 900-pound rated flange at the tank outlet separated and burned badly; other 3-inch 1500-pound rated flanges in the system remained intact.

18. A 2-inch 1500-pound rated flange at the MOV separated and leaked.

19. The flowmeter section and the venturi section, both of 2-inch line, are gone completely, apparently burned out, with the line flanges in all cases remaining and showing internal burning.

20. Erosion and deposit in the line downstream of the flowmeter and venturi section-appeared to flow in the downstream direction to the elbow, and was of 304 stainless steel.

21. Erosion of the line upstream of the prevalve appeared to flow in an upstream direction,and thinned the wall to 0.18 inch.

22. Deposit and slight erosion on the downstream side of the elbow upstream of the prevalve was in a downstream direction for a short distance.

23. The elbow upstream of the prevalve was burned out, with flow indicated in both directions at different times.

24. The fracture in the line upstream of the prevalve traveled in an upstream direction from the missing portion of the line.

25. The high point relief valve did not see hot flow and the elbow upstream of it was burned out.

26. The hot metal flowed up to the high point bleed valve and this valve separated in the body and leaked slightly.

27. Erosion and flow out of the prevalve was primarily in an upstream direction, although there was some erosion in all directions at its downstream flange.

28. The spool piece downstream of the prevalve showed light erosion at the prevalve end and did not show erosion throughout its length.

(U) 29. There were three independent ruptures in the line downstream of the prevalve, with the cracks initiating at the thin spots of the "dimples."

30. The jacket of the line downstream of the prevalve was ruptured most violently, with that upstream of the prevalve next most, and those on each side of the tank valve only sightly.

31. There were two separate fracture initiation points in the elbow downstream of the prevalve, these being at points indicating the fracture was caused by violent twisting.

32. The dimples in the line downstream of the prevalve may have been caused by some high-energy phenomenon occurring before rupture and are related, one to another.

33. The erosions in the elbow downstream of the prevalve occurred before and after rupture of the line and are independent of reactions in the prevalve or main valve, the erosions appearing centered about the purge fitting.

34. There was an erosion across the complete rupture of the line downstream of the prevalve between it and the elbow, indicating erosion prior to rupture.

35. The MOV body joint separated completely, its bolts burning and fracturing, imparting violent bending to its support on the downstream side and line on the upstream side.

36. ıe line immediately upstream of the MOV within the capsule was fractured completely, apparently from bending rather than internal pressure.

37. The general appearance of the run line immediately upstream of the prevalve is of gross internal burning, while the line downstream of the prevalve is generally ruptured with little internal burning.

38. The on-stem packing of all oxidizer valves was in good condition upon disassembly of the valves after the incident.

39. None of the pipe welds that could be found and/or inspected appeared to be points of initiation of the overall failure.

(U) 40. The internal surface of the tank was slag splattered, but there were no significant surface erosions.

(e) Comparison With Other Incidents

(U) With respect to the total damageinvolved, the incident of 25 May 1970 was significantly different from those common to fluorine facilities. The history of fluorine incidents at other installations shows a pattern of destruction which is normally limited to the point of origin of the reaction and, at most, a section of line upstream and downstream to a burned-out elbow.

(U) The fact that this incident involved the entire oxidizer system, from the run tank to the main vlave, indicates that the initial energy release was vigorous enough to create other reactions in the system which, accumulatively, created the total destruction.

(U) Oxidizer system problems encountered during NFL segment testing and similar programs at Santa Susana Field Laboratory included:

1. Burnout of MOV stem chevron packing
2. Contaminated MOV plug
3. MOV body seal leakage
4. Contaminated fittings in oxidizer line
5. Contaminated fluorine
6. Broken turbine-type oxidizer flowmeter

(U) In each case, either no fire resulted from the anomaly or the fire was almost wholly confined to the area of the point of initiation of burning. Propagation of burning was in a downstream direction and was a result of being carried by oxidizer flow conditions rather than strict propagation through the liquid fluorine. The fire in each case was put out by closing an oxidizer system valve.

(U) Pratt & Whitney has also experienced valve stem packing burnout using fluorine. The apparent result was confinement of the fire to the affected valve rather than catastrophic propagation throughout the system.

(U) NASA-Lewis has reported an incident of a detonation in fluorine line at the tank outlet (Ref. 2) as a result of introduction of moisture into the system. An explosion (as in the run line at the tank outlet) occurred as a result of fluorine reacting with ice during pressurization of the tank (approximately 900 psi). The reaction did not propagate into the tank nor was an appreciable amount of damage sustained in the downstream ducting.

(U) Aerojet General Corporation experienced a reaction in an oxidizer tank while attempting to mix fluorine and wet liquid oxygen. The theory was that the moisture in the LOX reacted with the fluorine and caused tank pressure rise. The reaction was kept under control by continual venting of the oxidizer tank. There was no damage incurred as a result of this occurrence.

(f) Possible Modes of Contamination Entry

(U) The possibility of contamination entry into the oxidizer system was investigated. The operational procedures for system rework, system cleaning, blowdowns, and test setup were reviewed in an effort to uncover invalid or violated operational procedures.

(U) Oxidizer system facility modifiactions had been made just prior to the oxidizer blowdowns conducted on 25 May 1970. These were investigated for possible modes of contamination entry.

(U) Run Line. The oxidizer system run line upstream of the oxidizer main valve had been repaired by replacing a section of 3-inch line and adding a transition piece to 2-inch line. The line section from the flowmeter to the tank valve was trichloroethylene- and acetone-wiped. The procedures for cleaning the aforementioned line sections were reviewed. No evidence that contamination had been introduced into the oxidizer system through these operations was uncovered.

(U) Oxidizer System Valves. The prevalve was removed for servicing following the 24 April 1970 incident. The individual parts were cleaned prior to stem and plug assembly. The copper seats were final-machined using Freon as the lubricant. After final-machining, the plug end of the stem was cleaned with acetone. The possibility exists that Freon or acetone could have become entrained in the threads or under the copper seat of the plug. This could not be proved to be the initiating mechanism, however.

(U) The possibility of contaminated pressurant was investigated. Several helium samples had been taken and analyzed since the test stand was activated. Samples taken in February (prior to test stand activation) showed hydrocarbon contamination levels of 0.02 and 0.08 mg. Subsequent analysis of the helium consisted of periodic dew-point readings taken at the site. The result in each case was that the dew point was less than -100 F, which corresponds to 1.5-ppm water contamination.

(U) The oxidizer purge systems are provided with filters, driers, and a cold trap to prevent the introduction of contaminant into the oxidizer system.

(U) The tank pressurization system did not utilize a cold trap and is supplied from a separate pressure bottle.

(U) Helium samples were taken from the tank pressurization system at several points and analyzed for water and hydrocarbons. The hydrocarbon content in each case was less than 0.05 mg, which is in the range expected from a clean system (0.5 mg of hydrocarbons was the maximum allowable).

(U) Water content analyses were conducted in the laboratory and showed that the water content of each sample taken after the incident was in the range of 13.3 to 16.5 ppm. The U.S. government specification for grade A helium states that the water content of the helium delivered from their facilities varies from 1.0 to 20 ppm on a volume basis with a typical value of 10 ppm H_2O on a volume basis.

(U) As noted previously, the helium sample evaluations at the facility by use of a dewpoint apparatus always indicated a dewpoint of less than -100 F, which corresponded to 1.5 ppm by volume water content. Therefore, the validity of the site evaluation technique (dewpoint method) was questionable and greater confidence was placed in the laboratory determinations.

(U) No evidence was found to indicate that the system was contaminated with hydrocarbons; however, the high water content was suspect.

(U) Moisture condensation from atmosphere also was investigated as a possible mode of contamination entry. A transducer vent valve is opened during the countdown procedure, which exposes the oxidizer run line between the tank valve and the prevalve to the ambient conditions in the oxidizer vent header. In reconstructing the countdown, a remote possibility existed that the vent valve could have been open for 15 minutes. The oxidizer vent header outlet is located approximately 300 feet from the test stand. A continuous GN_2 purge is introduced into the vent header at the test stand to keep an inert atmosphere in the vent header.

(U) No evidence was found to conclusively implicate the vent header as being contaminated. Involvement of the vent header as the initiating source would require contamination of the vent header and an operator error. Neither was found.

(U) The possibility of relief valve malfunction was considered. Examination of the relief valves after the incident tends to discount the hypothesis of relief valve failure.

(g) Failure Analysis Results

(U) From analysis of the damaged hardware and supporting structural, dynamic, thermal, metallurgical and chemical analysis, the following is known of the mechanism of the failure:

1. There were four or more fires existing in the system during the failure sequence. These four were within each of the three oxidizer run valves and in the tank dip-tube area. Independent reactions may have taken place at the flowmeter and two line locations downstream of the prevalve.

(U)

2. All of these four fires occurred before rupture of any lines or the tank, indicated by pattern and direction of erosion and metal deposit on inside of lines and valves.

3. Three or more of the fires (at the three run valves) were caused by a severe pressure pulse traveling through the system, which pulse was in turn a result of a rapid reaction, perhaps detonation, within the system. Major indication of this was the effect of separation of valve bodies without similar effects on weaker straight-through flanges and on relief valves on low-response lines. The tank fire, if not the initiating source, was believed caused by burning metal entering the tank-dip tube from the tank valve.

4. Rupture of lines upstream and downstream of the prevalve probably occurred almost simultaneously, indicated by lack of damage to the spool piece immediately downstream of the prevalve. Also, three ruptures occurred in the run line downstream of the prevalve, as indicated by the extensive erosion of this line in the upstream direction before rupture.

5. These two line ruptures resulted from hot gas generated in the system at the valves and independently from the tank fire. Evidences of erosion within the lines prior to rupture indicated a discrete time between the original pulse and the ruptures.

6. Fractures in the elbow downstream of the prevalve resulted from rupture of the line immediately downstream. Similarly, fracture of the line immediately upstream of the MOV resulted from mechanical load from the MOV body separating completely.

7. Burnout of the flowmeter section of line occurred after burnout of the elbow downstream of it and prior to complete burnout of the line at the tank and separation of tank valve flanges. This was indicated by erosion and deposit in a downstream direction toward the elbow throughout that section of line.

(U) 8. As the tank reaction progressed and tank pressure built up, the pressurization line burned out at approximately 2000 psi, the cover lifted, and the bolt burning started at approximately 3000 psi. Four out of five of the tank-cover penetrations were burned out at approximately this time, and the bolts failed and the cover was launched at approximately 5000 psi (as indicated by calculations). Structure, thermal, and cover trajectory analysis indicates these events.

9. As system pressure built up from internal fires,the relief valves did not pass hot gas because of burnout of elbows in the lines to them and/or because of the very short duration of the pulse.

10. As mentioned in item 3 above, the presence of the pressure pulse was indicated by the fact that valve body joints separated whereas straight-through flanges did not. The possible presence of a detonation wave in the system, perhaps associated with the pressure pulse, was indicated by a series of "dimples" in the line downstream of the prevalve, the only explanation for which is a high-energy shock mechanism.

(U) Whereas the analysis does point to a detonation or rapid reaction initiating a pressure surge throughout the oxidizer line, there were no positive indicators as to the location of the initial reaction. Possibilities for the location of the initial reaction were as follows:

1. The downstream purge port, indicated by an independent and separate erosion there prior to line rupture and by the "dimple" phenomenon in the line 3 feet downstream.

2. The tank dip tube at the pressurization diffuser, indicated by presence of a portion of the diffuser in the tank and the knowledge that pressurization through the diffuser was the only system activity at the time of the incident, and 13- to 16-ppm H_2O in the helium pressurant.

3. At the tank valve normalizing-fin area, indicated by large separation of this flange, as compared to the prevalve.

(U) 4. At the prevalve plug threads, indicated by burning pattern, as compared to the tank valve and possibility of slight contaminant in these threads.

5. At the flowmeter section, indicated by this section being entirely consumed, whereas the line upstream of it was lined with deposit and presence of the vent fitting perhaps serving as a source of moisture.

(U) The exact determination of the location of the initiating reaction was not possible; however possibility No. 2 above is generally considered to be the most likely location of the initial reaction.

(U) No additional effort was expended at the facility because of destruction of the oxidizer high-pressure propellant feed system and associated facility systems.

SECTION IV

OXIDIZER TURBOPUMP BEARINGS AND SEALS

1. GENERAL

(C) This section describes the results of the oxidizer turbopump bearing and seal test program of Task II. The bearing and seal program consisted of design, fabrication, and test of hardware for both the main and secondary engine liquid fluorine turbopumps. The main turbopump uses a 25-mm turbine bearing, a 20-mm pump bearing, with a full-thrust operating speed of 28,000 rpm. The secondary turbopump uses 8-mm bearings with a full thrust operating speed of 75,000 rpm. Separate testers were designed and fabricated to allow testing the two different bearing and seal configurations at the required operating conditions. The testers utilized the same test facility and drive equipment.

(C) The main bearing and seal tester was run for five tests with liquid fluorine for a total time of 697 seconds. One liquid nitrogen test of 61 seconds duration was performed.

(C) The secondary bearing and seal tester was run for six tests with liquid fluorine for a total time of 241 seconds.

2. MAIN TESTER DESCRIPTION

(U) The main tester (Fig. 164 and 165) was designed to simulate the main engine liquid fluorine turbopump bearing and seal operating conditions and allow the use of actual turbopump hardware. The tester consisted of a rotating shaft supported by the test bearings. The bearing axial load was controlled by a piston that was pressurized to maintain the desired load. The bearings were lubricated and cooled in the same manner as the turbopump by flowing liquid fluorine through the bearing cavity. The tester seals were the same as would be required on an actual turbopump to contain the liquid fluorine and maintain separation between the fluorine and hydrogen turbine gas.

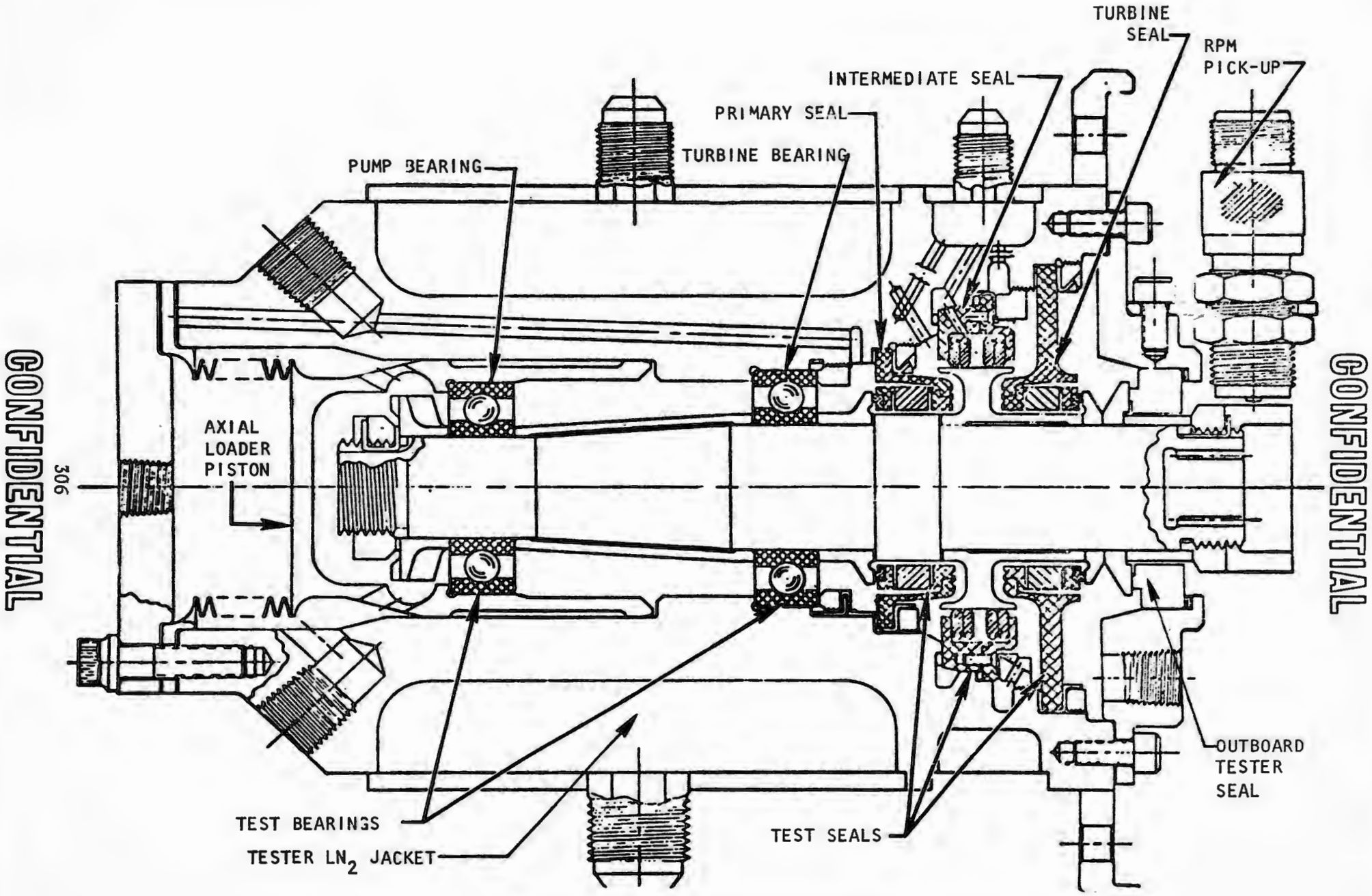

Figure 164. Main Bearing and Seal Tester (U)

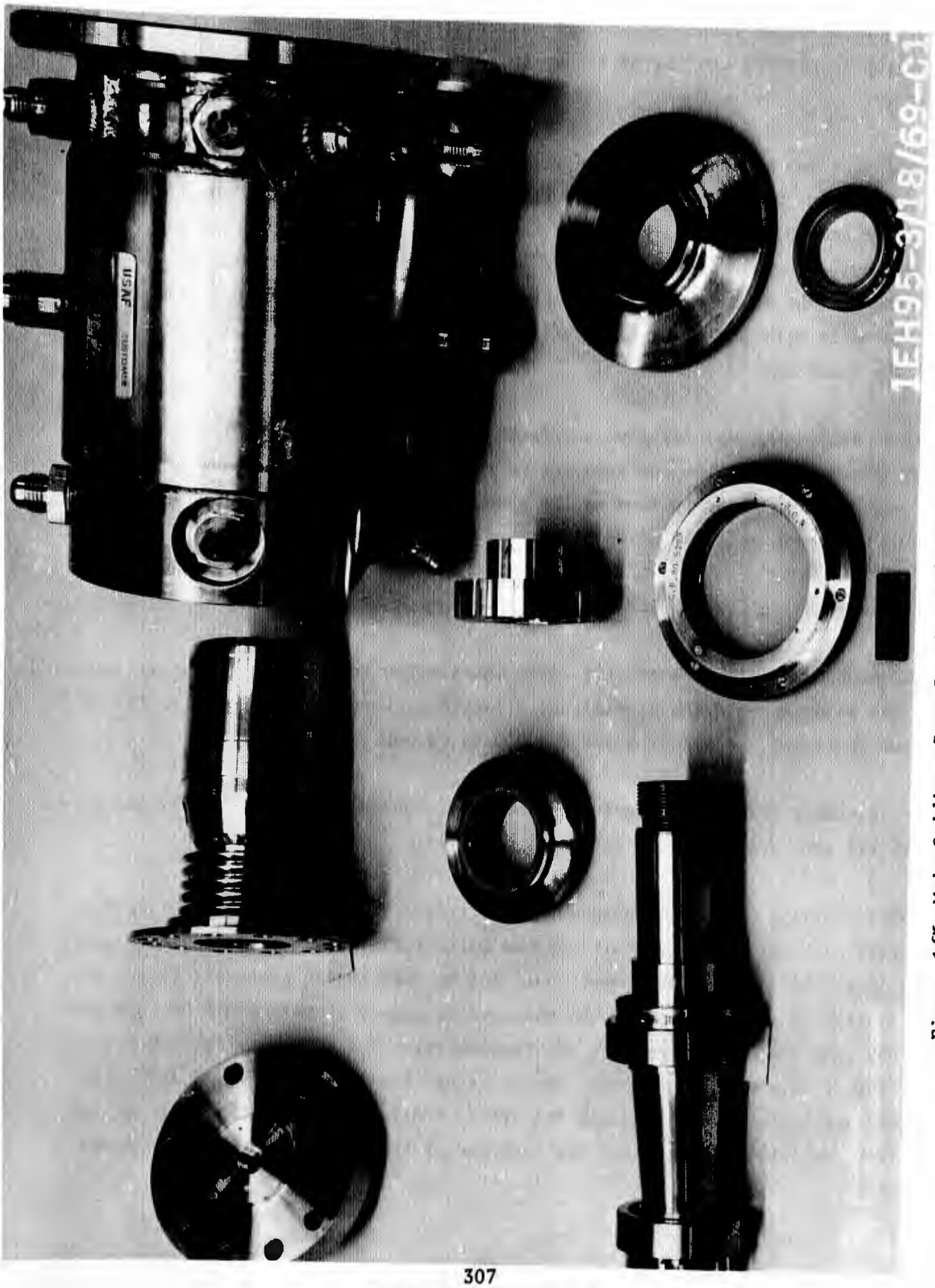

Figure 165. Main Oxidizer Pump Bearing and Seal Tester Major Components (U)

(U) A liquid nitrogen insulation jacket was utilized as an integral part of the tester housing to provide cooling necessary to maintain liquid fluorine in the bearing cavity.

(U) The tester was mounted on a cylindrical frame (Fig. 166), which also provided the drive turbine mount and maintained alignment. The tester mount was attached to a frame assembly that was bolted to the test facility slab. The tester drive was provided by a commercial turbine powered with ambient-temperature gaseous nitrogen. The drive turbine was connected to the tester through a commercial torquemeter with splined quill shafts. A long quill shaft may be used in place of the torquemeter.

(U) An air fan blower was designed and fabricated for installation in the drive system between the turbine and torquemeter for additional speed control. The air blower absorbed higher torque as the speed increased to prevent overspeed and allow more precise speed adjustments.

3. SECONDARY TESTER DESCRIPTION

(C) The secondary tester design (Fig. 167) was similar to the main tester and operated in the same manner. The significant differences were the smaller size (8- vs 25-mm bearings) and higher speed (75,000 vs 28,000 rpm).

(U) The secondary tester was mounted on the same mounting frame (Fig. 168) and driven with the same drive turbine as the main tester.

(U) A short housing mount was designed and fabricated to allow close coupling the turbine and tester with a short splined quill shaft in place of the torquemeter. The long quill shaft arrangement could not be used on the secondary tester due to a critical speed problem. The main and secondary testers could be interchanged on the same short mount without the torquemeter. The secondary torquemeter was similar to the main torquemeter, except it was smaller and designed for lower torque and higher speed. An air fan blower similar to the main tester, except smaller, was installed between the torquemeter and turbine for improved speed control.

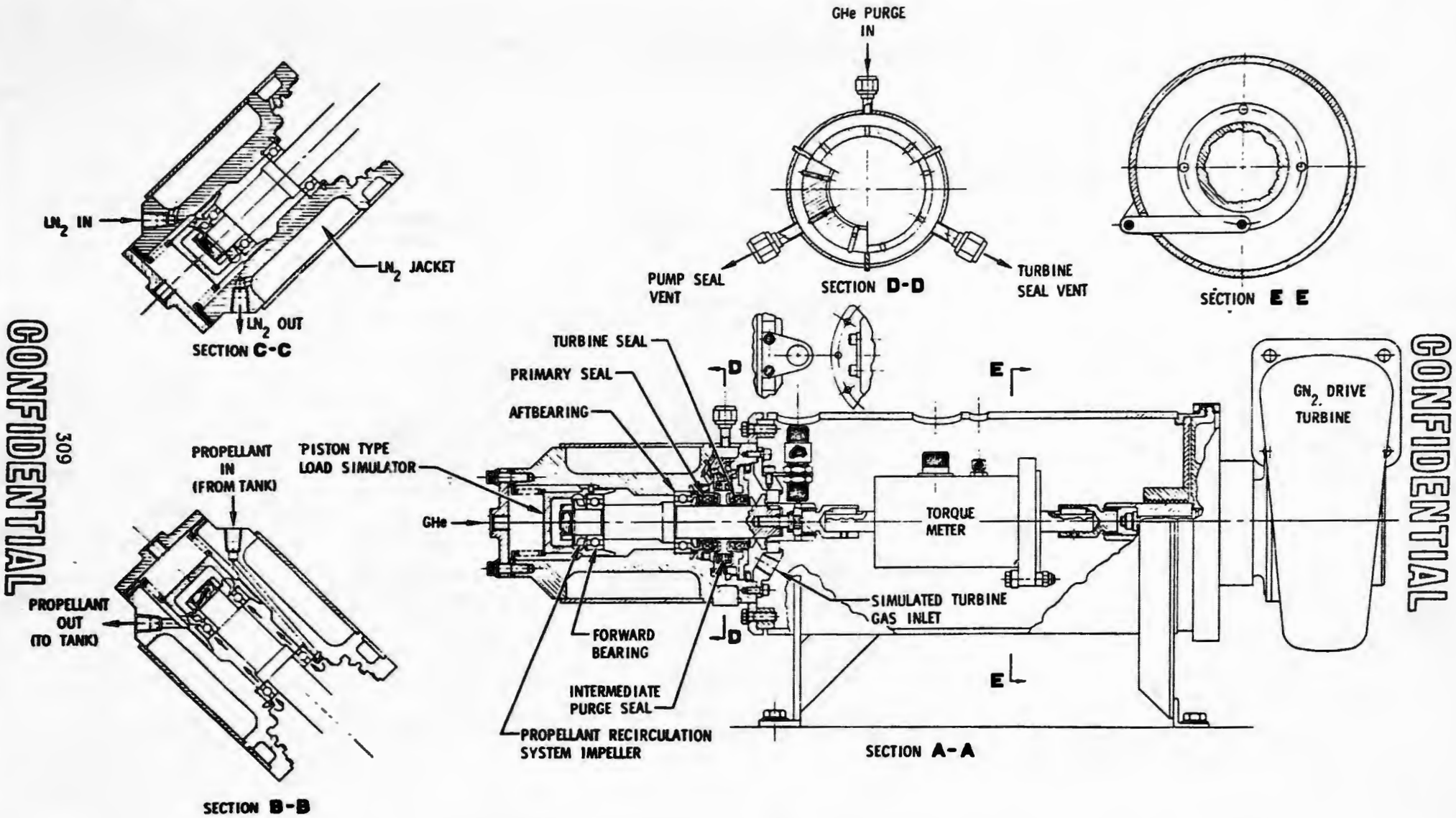

Figure 165. Main Oxidizer Bearing and Seal Tester and Drive Assembly (U)

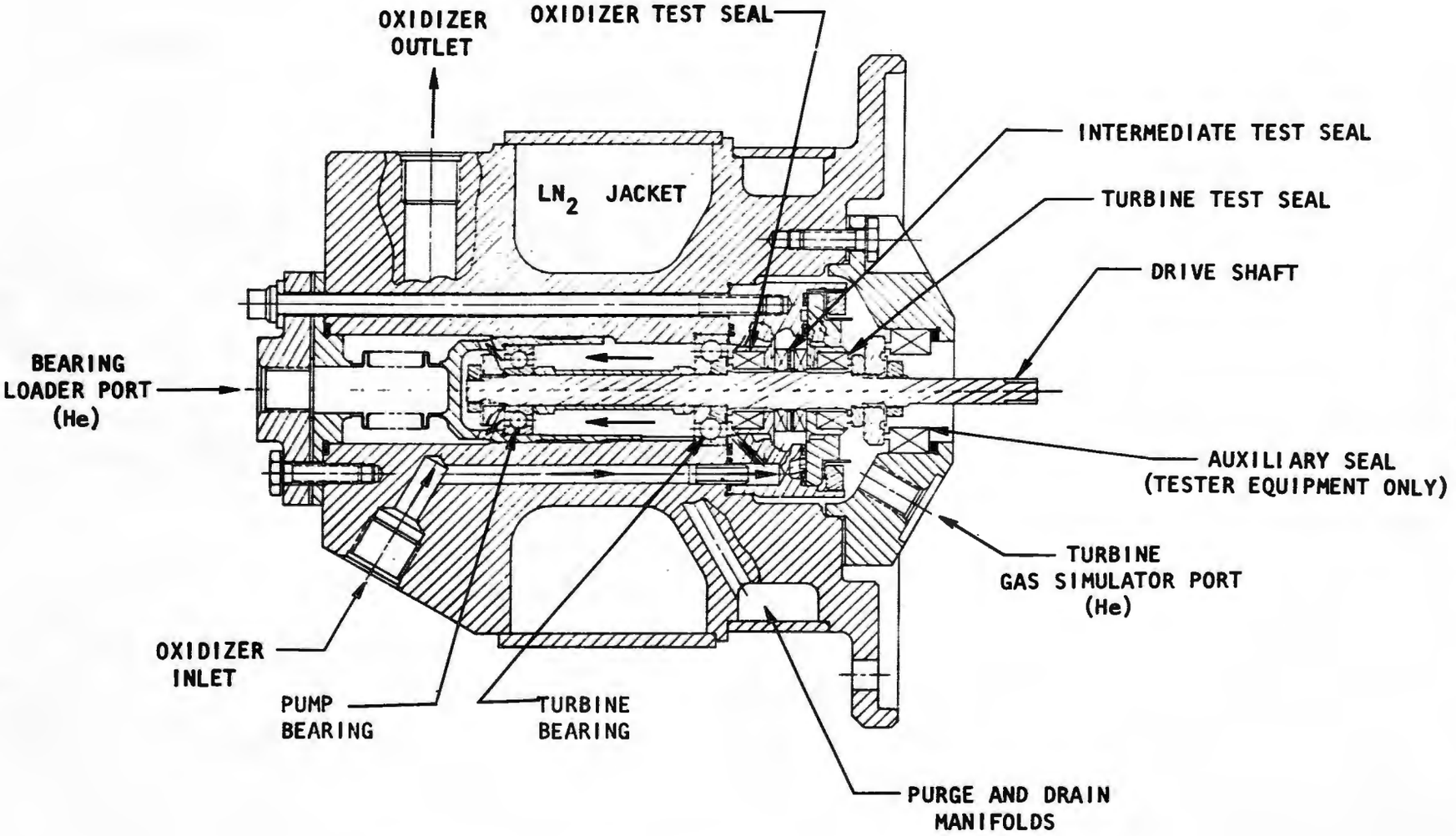

Figure 167. Secondary Bearing and Seal Tester Assembly (U)

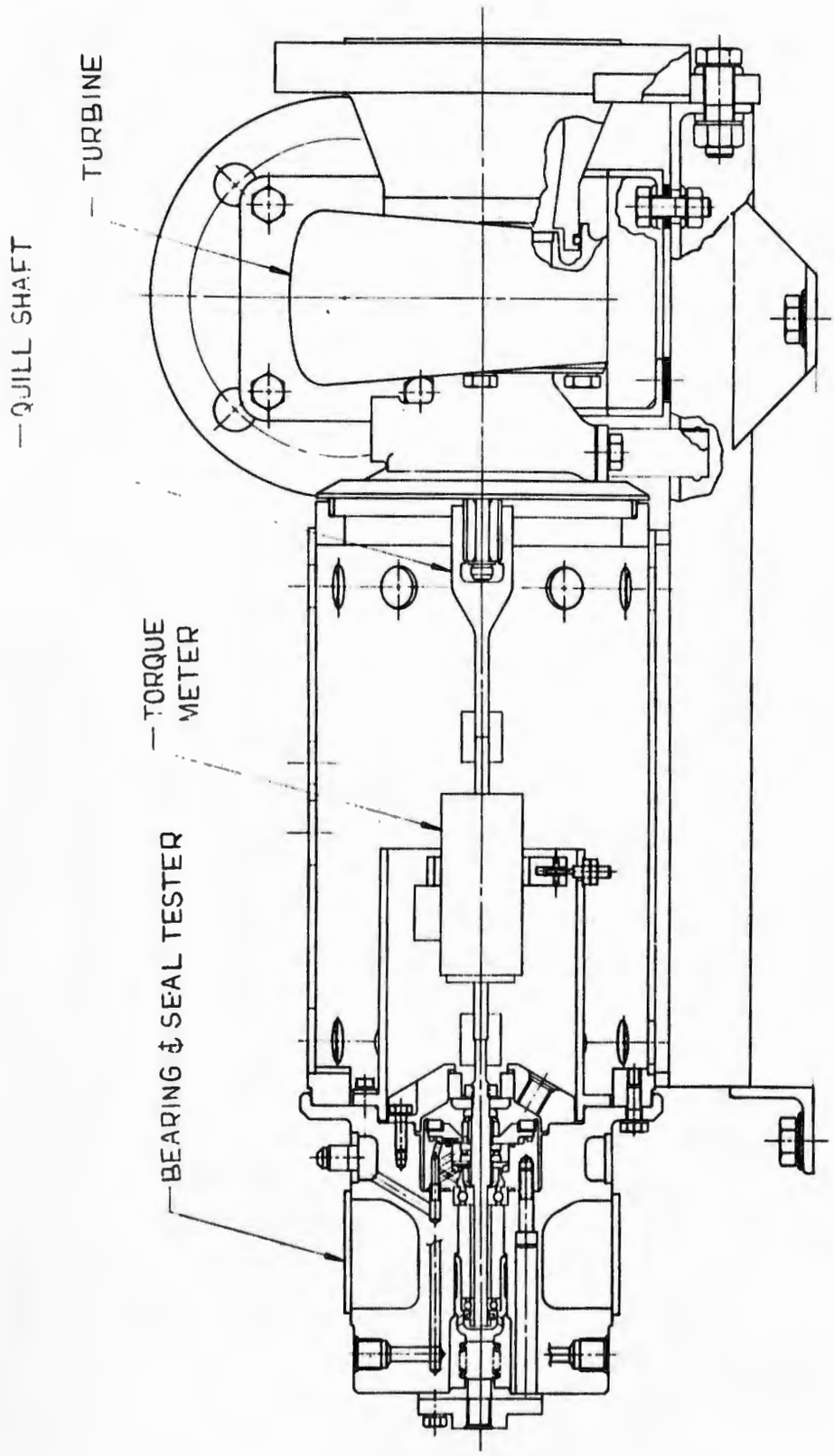

Figure 168. Secondary Engine Oxidizer Turbopump Bearing and Seal Tester and Drive Assembly (U)

4. TEST FACILITY

(U) The dynamic liquid fluorine testing was performed at the Santa Susana Field Laboratory Propulsion Research Area, Mike stand. The static seal tests with liquid and gaseous nitrogen were performed in the Engineering Development Laboratory at Canoga Park. The test facility schematic is shown on Fig. 169. The tester installation in the test facility is shown on Fig. 170

(U) The fluorine was supplied from a storage tank in the gaseous state. The fluorine was then chilled and condensed to a liquid prior to entering the run tank by flowing through a liquid nitrogen heat exchanger. The liquid fluorine lines from the tank to the tester and the tester housing were jacketed to allow liquid nitrogen to be flowed through for cooling to maintain the fluorine at liquid condition.

(U) The liquid fluorine flow was established initially by pressurizing the run tank to flow through the tester bearing cavity and out through an atmosphere bleed. The intent was to close the atmosphere bleed and recirculate the liquid fluorine back to the run tank after chilldown using an impeller on the tester shaft to develop the necessary differential pressure. However, the impeller did not develop sufficient head, and venting of the fluorine overboard was necessary to maintain adequate flow. Since the run tank capacity was 20 gallons and the desired flowrate was 3 gpm for the main tester and 1 gpm for the secondary tester, and also because approximately half of the capacity was used for chilldown, the run duration was limited to approximately 3 minutes for the main tester and 10 minutes for the secondary tester.

(U) The drive turbine was pressurized with facility gaseous nitrogen that was regulated during the test for speed control. The entire fluorine system was purged with dry gaseous helium to remove air and prevent condensation of moisture prior to introducing fluorine. The system, including the tester assembly, was then passivated with gaseous fluorine for 2 hours minimum prior to testing with liquid fluorine. Precautions were taken to prevent air or moisture from entering the fluorine system when any connections were broken.

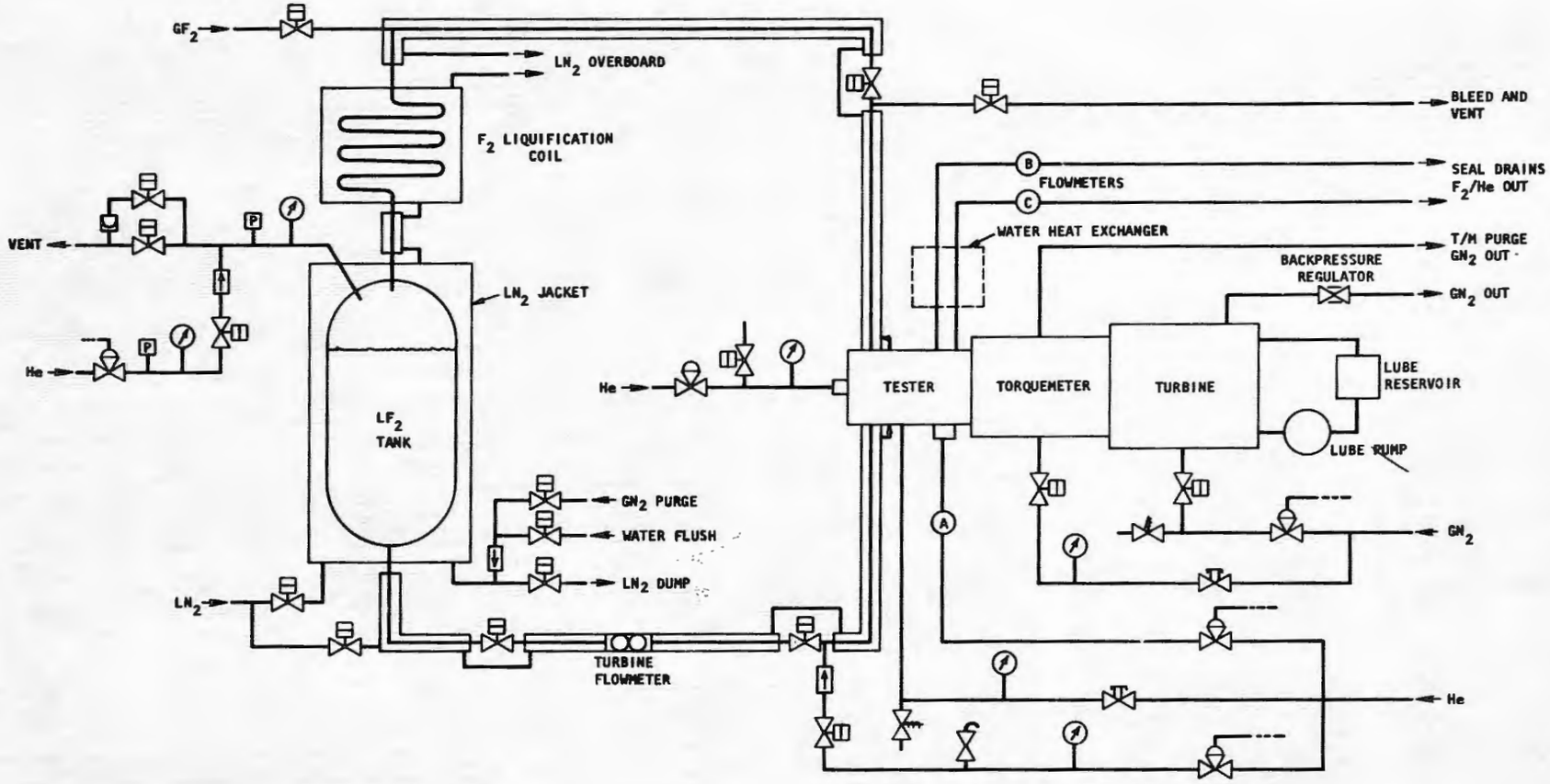

Figure 169. Test Facility Schematic (U)

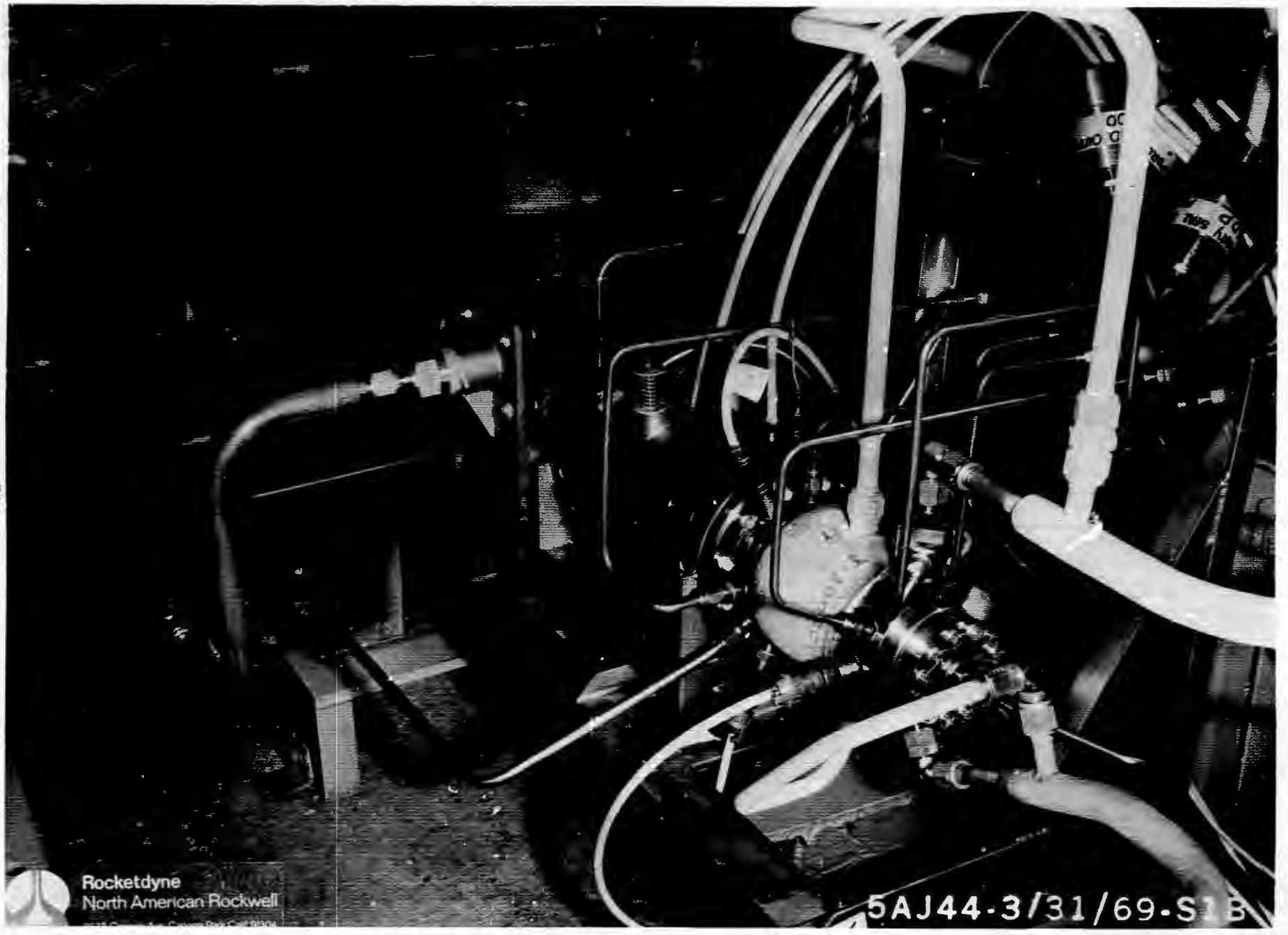

Figure 170. Main Bearing and Seal Tester Installation (U)

(U) A particle trap was installed in the liquid fluorine inlet line from the run tank to the tester to minimize the possibility of foreign particle contamination entering the tester. A filter was ordered for installation in the fluorine inlet line, but was not received in time to be used.

a. Test Instrumentation

(U) The tester was instrumented to record the following parameters utilizing a Beckman data acquisition system and a high-frequency tape recorder. The critical parameters were visually monitored during the test to detect abnormal operation. Automatic cutoff devices were used on the critical redline parameters:

1. Turbine GN_2 temperature
2. Primary seal drain orifice temperature
3. Turbine seal drain orifice temperature
4. Oxidizer outlet temperature
5. Oxidizer inlet temperature
6. Primary seal drain cavity temperature
7. Turbine seal drain cavity temperature
8. Intermediate seal purge temperature
9. Torquemeter torque
10. Oxidizer inlet pressure
11. Intermediate seal purge pressure
12. Primary seal drain cavity pressure
13. Turbine seal drain cavity pressure
14. Turbine seal pressure
15. Oxidizer outlet pressure

(U) 16. Bearing load bellows pressure

17. Turbine GN_2 inlet pressure

18. Intermediate seal purge flow orifice ΔP

19. Bearing cavity pressure

20. Primary seal leakage orifice ΔP

21. Turbine seal leakage orifice ΔP

22. Tester speed

23. Oxidizer flow

24. Bentley shaft displacement transducer

25. Tester vibration (accelerometer)

(U) The intermediate seal purge flowrate and the seal leakage flowrates were measured with calibrated flow orifices installed in the line. The seal drains were routed through a heat exchanger to convert the liquid fluorine leakage to ambient temperature gas for measurement of the differential pressure at the flow orifice.

(U) The liquid fluorine bearing coolant flowrate was measured with two separate turbine type flowmeters installed in series in the inlet line.

(U) The tester shaft deflection was measured with a Bentley proximity position transducer mounted at the drive shaft. Calibration slots were machined into the shaft to allow in-place calibration of the signal.

(U) The liquid fluorine temperatures were measured with Rosemont temperature bulbs.

(U) The tester speed was measured with a magnetic speed pickup installed on the drive shaft.

(U) The tester shaft torque was measured with a Himmelstein strain gage torquemeter modified for this specific application. The torquemeter was calibrated by the manufacturer.

5. MAIN SEAL DESIGN

(U) The main engine oxidizer turbopump seal arrangement is shown on Fig. 171. A summary of the seal design values is shown in Table 24.

(C) The purposes of the seal system were to contain the liquid fluorine and turbine hydrogen gas and to maintain separation of the fluorine and hydrogen. Two face-contact Inconel-X welded bellows seals were used to contain the fluorine and hydrogen. A purged double floating ring intermediate seal was used to separate the drain cavities. Both drains were vented overboard.

(C) Primary fluorine seal designs (Fig. 172) were completed and hardware was fabricated for the following seal face materials:

1. Aluminum oxide (AL_2O_3) plasma spray on a nickel-chrome mixture base
2. Aluminum oxide solid insert
3. Kentanium K162B solid insert

(C) Primary seal mating rings of the following materials were designed and fabricated:

1. Kentanium K162B
2. Aluminum oxide (AL_2O_3) coated INCO 718

(C) The aluminum oxide plasma spray nose on a nickel-chrome mixture base offered the highest probability of meeting the leakage objectives without mechanical failure. The spray coating eliminated the problem of sealing between the solid insert and metal carrier and also minimized face distortion due to thermal contraction which was a problem when a solid insert with a different coefficient of contraction was pressed into a steel carrier.

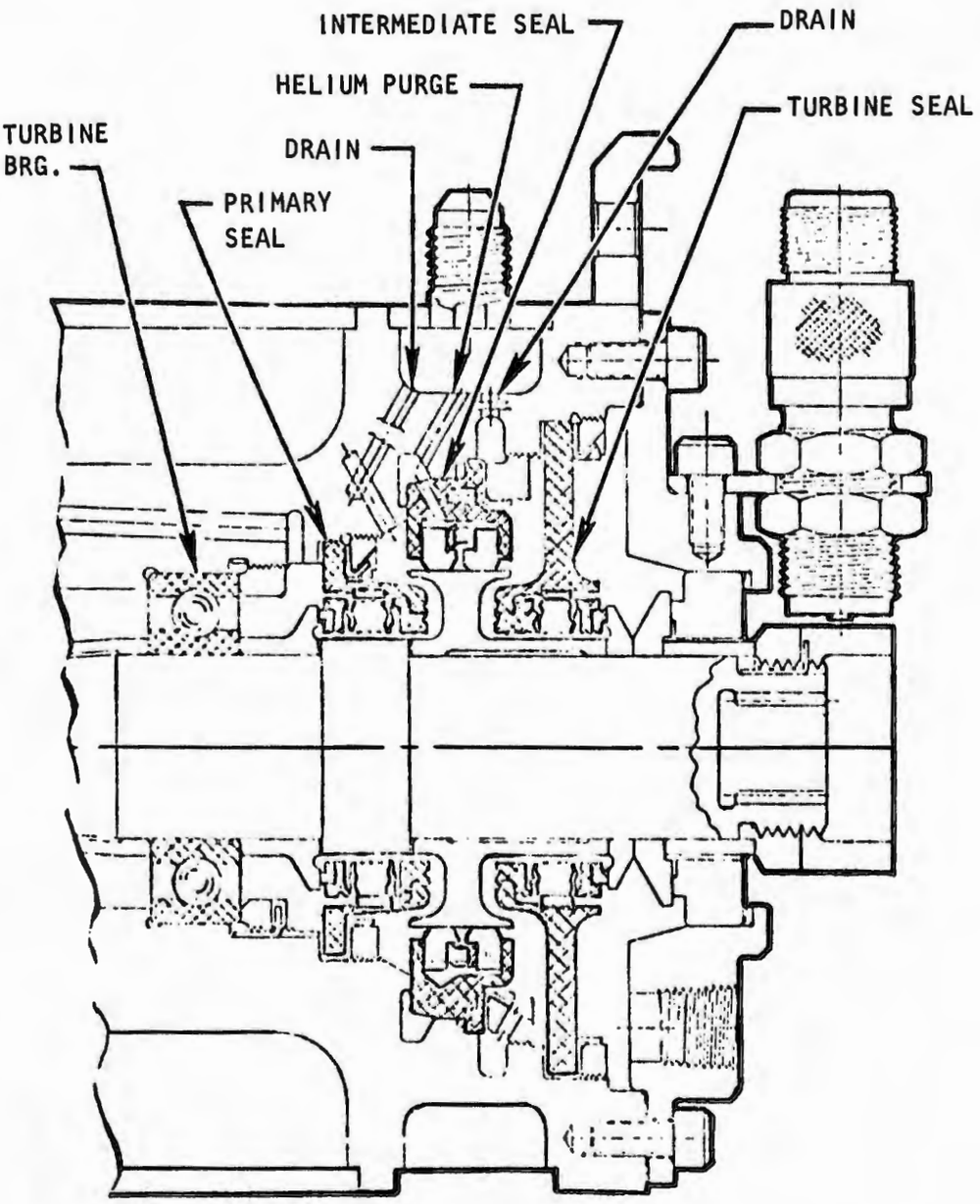

Figure 171. Main Oxidizer Turbopump Seal Arrangement (U)

TABLE 24

OXIDIZER TURBOPUMP SEAL DESIGN VALUES (U)

Design Value	Main Turbopump Seals				Secondary Turbopump Seals		
	Primary	Intermediate		Turbine	Primary	Intermediate	Turbine
NA5 Specification No.	NA5-260265	NA5-260266		NA5-260306	NA5-260306	NA5-260307	NA5-260308
Seal Type	Bellows Face	Purged Floating Gap	Purged Segmented	Bellows Face	Bellows Face	Purged Floating Gap	Bellows Face
Fluid Pressures, psia	200	50	50	50	200	50	50
Spring Load, pounds	5/26	---	.2	5.8/19.4	1.4/6.8	---	1.4/6.8
Pressure Balance Ratio	0.6	---	---	0.6	0.6	---	0.6
Hydraulic Load, pounds	10.5/14.0	---	10.5/46	0/3.6	0.8/1.1	---	0.2/0.27
Total Load, pounds	15.5/40.0	---	10.7/46.2	5.8/23.0	2.2/7.9	---	1.6/7.1
Surface Speed, ft/sec	173	244	244	173	205	125	205
Unit Load, psi	34/88	---	13.4/57.8	13/51	30/125	---	22/114
PV Factor, psi x fps	5900/15300	---	2280/14100	2260/8850	5780/25500	---	4150/23000
Materials Seal Face	AL_2O_3 Spray K162B Insert AL_2O_3 Insert	BaF_2-CaF_2 Composite	Barium B-10 K162B BaF_2-GaF_2	Carbon P5N	Al_2O_3 Spray	BaF_2-CaF_2 Composite	Carbon P5N
Mating Ring	K162B Solid Al_2O_3 Spray	BaF_2-CaF_2 Spray	INCO 718 BaF_2-CaF_2 AL_2O_3	Chrome Plate	AL_2O_3 Spray	BaF_2-CaF_2 Spray	Chrome Plate
Bellows	Inconel-X	---	---	Inconel-X	INCO 718	---	INCO 718
Vibration Damper	Inconel-X Wave Spring	---	---	Inconel-X Wave Spring	None	---	None

CONFIDENTIAL

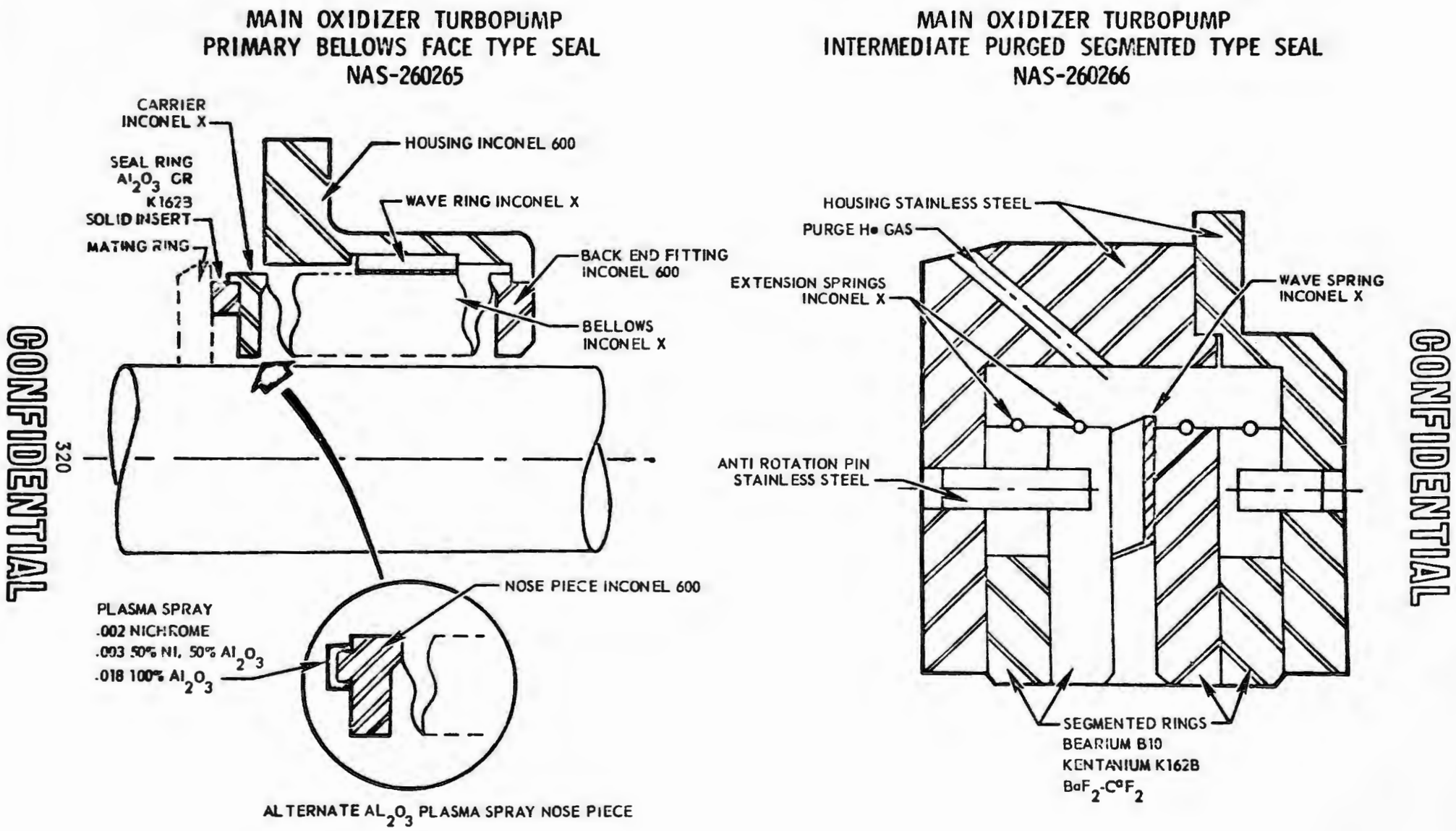

Figure 172. Main Oxidizer Turbopump Seal Details (U)

(C) The aluminum oxide spray was applied by coating the Inconel carrier with 0.002 inch nickel-chrome, then 0.003 inch 50-50 mixture of nickel-chrome and aluminum oxide and finally 0.018 inch 100 percent aluminum oxide. The nickel-chrome mixture base provided a flexible bond of the aluminum oxide to the Inconel carrier to minimize bond failure or flaking due to high thermal gradients or impact loading. The initial design utilized Inconel shoulders at the ID and OD edge of the seal nose to prevent edge chipping; however, the shoulders were eliminated when the test results indicated that the Inconel tended to score and damage the seal face.

(C) The solid insert designs using aluminum oxide or Kentanium K162B potentially have lower wear rates and may be necessary to meet the 10-hour life objective.

(C) The primary liquid fluorine seal was designed with a 0.6 pressure balance ratio and minimum spring load to minimize the face loading for maximum wear life consistent with satisfactory leakage. The seal face materials necessary for compatibility with fluorine have higher coefficients of friction (0.4 to 0.5) than the usual carbon materials (0.1 to 0.2) and the heat generation is proportionally higher; therefore, the total face load must be minimized and the maximum possible cooling of the faces provided. The PV factor (unit face load, psi x velocity, fps) was within the current state of the art for this type of seal.

(C) The primary (Fig. 172) and turbine seals both utilized an Inconel-X wave spring at the bellows convolutions to provide vibration damping.

(C) The main intermediate seal design was initially a purged double-segmented type (Fig. 172). Three designs were completed and hardware was fabricated for the following material combinations:

1. Bearium B-10 versus INCO 718
2. Kentanium K162B versus AL_2O_3 coated INCO 718
3. BaF_2-CaF_2 composite versus BaF_2-CaF_2 coated INCO 718

(U) The purged segmented seal design provided positive separation of the drain cavities and minimum purge gas leakage; however, the segments were loaded against the mating ring surface by the differential pressure load from the purge pressure and, therefore, significant heat was generated at the rubbing surface. The heat generation may be sufficient to cause ignition of the segments and/or mating ring when exposed to fluorine. The loaded segments may also cause a relatively high and irregular drag torque which can be a significant problem with the relatively low horsepower turbines used on the AMPT turbopump.

(C) The main intermediate seal design was changed to a purged double floating gap type, similar to the secondary intermediate seal (Fig.173). The floating rings were designed to provide 0.004/0.006 inch diametrical clearance and were free to be centered by the shaft location; therefore, drag torque and heat generation were negligible. The rings were constructed of BaF_2-CaF_2 composite material and the mating ring surface was plasma-spray coated with BaF_2-CaF_2 and baked in an oven to fuse the matrix.

(C) The main turbine seal design was similar to the primary seal, except a carbon P5N insert pressed into an Inconel carrier was used for the seal face. The mating ring was hard chrome-plated INCO 718.

6. SECONDARY SEAL DESIGN

(U) The secondary engine oxidizer turbopump seal arrangement is shown in Fig. 174. A summary of the seal design values is shown in Table 24.

(U) The seal arrangement and principle of operation was similar to the main turbopump. The smaller size and critical speed requirements necessitated compromising the design to use the surface of the bearing inner race for the primary seal mating ring and the surface of the turbine wheel for the turbine seal mating ring.

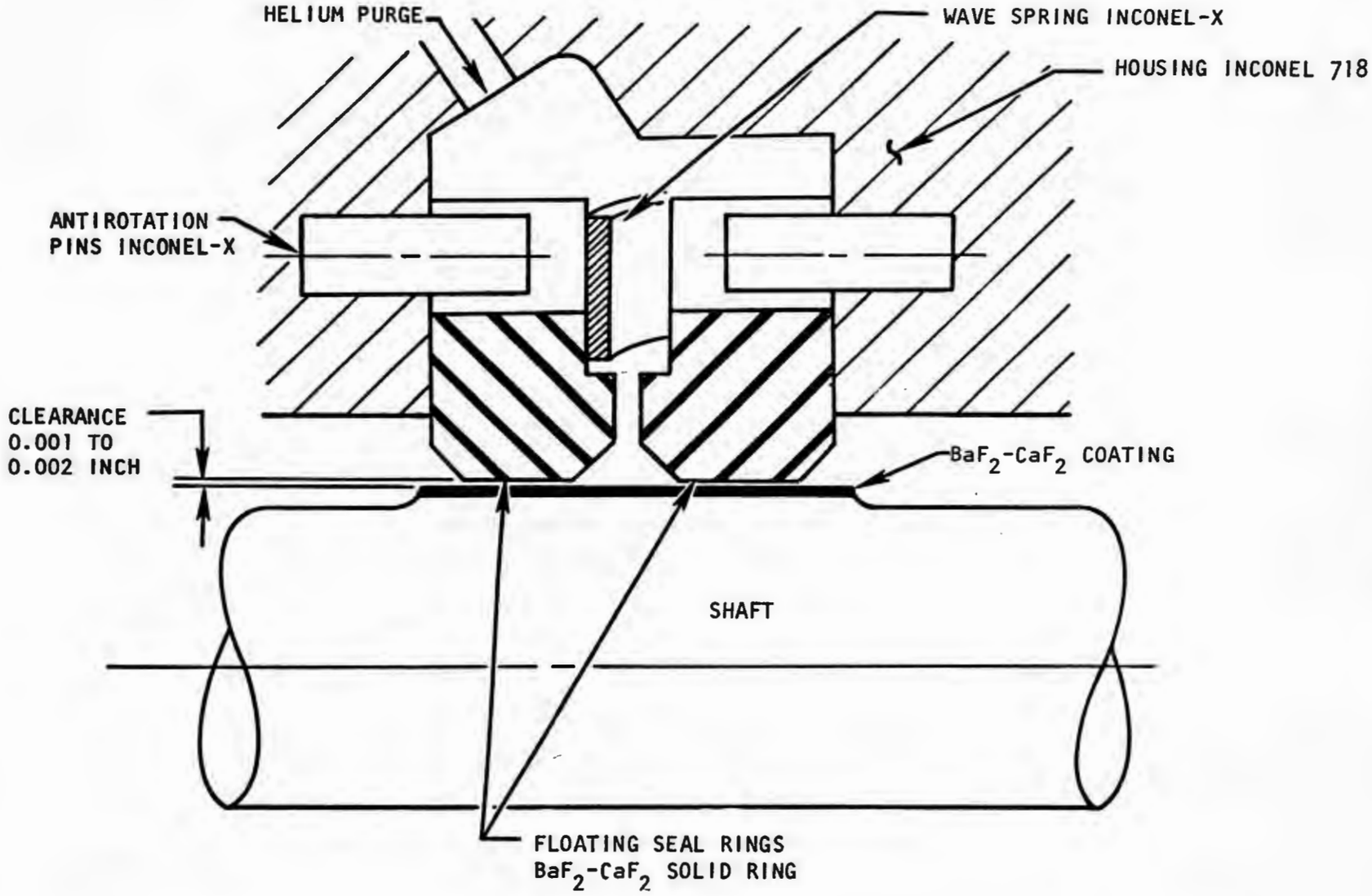

Figure 173. Secondary Oxidizer Turbopump Intermediate Floating Gap Low-Friction-Type Seal Detail (NA5-260307) (U)

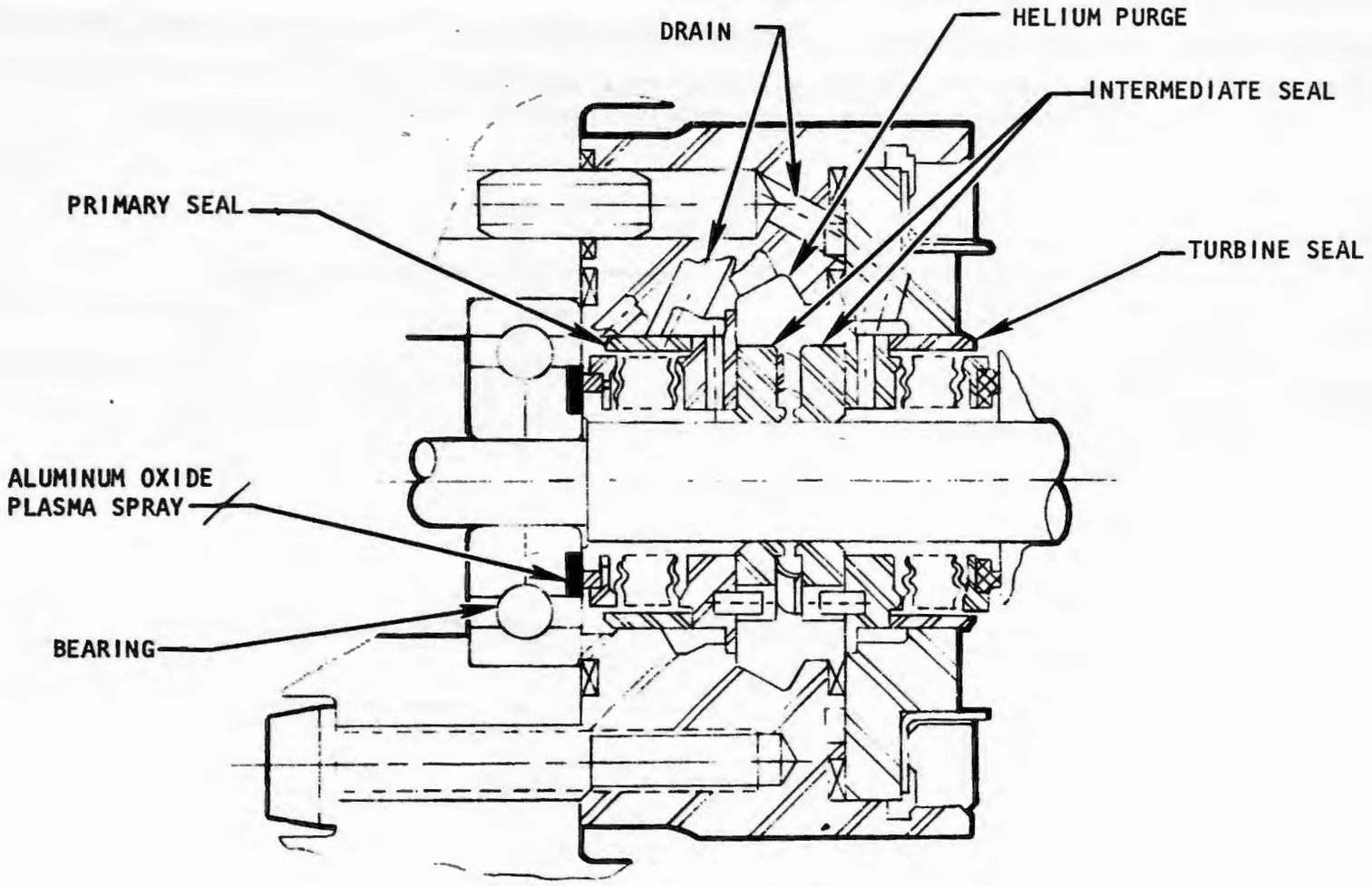

Figure 174. Secondary Turbopump Seal Arrangement (U)

CONFIDENTIAL

(C) The primary seal was a face-contact-type INCO 718 welded bellows with a plasma-sprayed AL_2O_3 on nickel-chrome mixture base nose rubbing against a plasma-sprayed AL_2O_3 surface on the 440C bearing inner race.

(C) The intermediate seal (Fig. 173) was a purged double floating gap type with 0.002/0.004 inch diametrical clearance. The rings were BaF_2-CaF_2 composite material and the shaft surface was spray coated with BaF_2-CaF_2.

(C) The turbine seal was a face-contact type INCO 718 welded bellows with a carbon P5N nosepiece insert rubbing against a chrome-plated surface on the INCO 718 turbine wheel. The tester utilized a separate mating ring since there was no turbine wheel.

(C) The design principles were the same for the secondary seals as for the main seals, except that vibration dampers were not used on the primary or turbine bellows seals due to the limited space available. The test results indicated that a vibration damper was necessary on the dry running turbine seal to prevent resonant frequency vibration of the bellows which resulted in fatigue failure of the bellows weld after short time periods.

7. BEARING DESIGN

(U) The bearing designs for the oxidizer turbopumps were selected with minimum departure from available experience in materials choice and optimized bearing geometry for the intended application, while maintaining external dimensions required for matching with the seal package. The design values are presented in Table 25.

(C) The bearing materials were selected on the basis of materials found to be successful in screening tests conducted in an IR&D program at Rocketdyne in October 1966. In those tests, ball bearings with 440C balls and races and K-monel cages were

TABLE 25. OXIDIZER TURBOPUMP BEARING DESIGN SUMMARY (U)

NA5 SPEC NO.	MAIN TURBOPUMP		SECONDARY TURBOPUMP	
	260268	260269	260311	260310
ITEM	POSITION		POSITION	
	TURBINE	PUMP	TURBINE	PUMP
TYPE	ANGULAR CONTACT BALL BEARING	ANGULAR CONTACT BALL BEARING	SPLIT INNER RING BALL BRG	ANGULAR CONTACT BALL BEARING
BORE, mm	25	20	8 (10 EFFECTIVE)	8
OD, mm	47	42	27	22
WIDTH, mm	12	12	8	7
CLASS, ABEC	5	5	7	7
BALL COMPLEMENT				
NUMBER OF BALLS	13	11	8	7
BALL DIAMETER, INCH	1/4	1/4	3/16	5/32
PITCH DIAMETER, INCH	1.42	1.22	.755	.591
INITIAL CONTACT ANGLE, DEGREES	25	25	25	25
RACE CURVATURES				
INNER	.52	.52	.52	.52
OUTER	.53	.53	.53	.53
CAGE				
O.D. CLEARANCE	.015-.020	.015-.020	.055-.010	.005-.010
POCKET CLEARANCE	.020-.025	.020-.025	.015-.020	.015-.020
MATERIALS				
BALLS	440-C	440-C	440-C	440-C
RACES	440-C	440-C	440-C	440-C
CAGE	K-MONEL	K-MONEL	K-MONEL	K-MONEL
DN @ SPEED	$.7 \times 10^6$	$.56 \times 10^6$	$.6 \times 10^6$ ($.75 \times 10^6$ EFFECTIVE)	$.6 \times 10^6$
COOLANT FLOW (GPM)	3	3	1	1
AXIAL LOAD (LBS)	300	70	65	65

CONFIDENTIAL

(C) operated for 2 hours and 48 minutes at 5000 rpm (0.225×10^6 DN). Further confirmation of the suitability of 440C rings and balls and high nickel content alloy cages was demonstrated in a NASA test program (Contract NAS3-11201).

(C) The bearings for both main and secondary engine oxidizer pumps had conservative DN values (0.56×10^6 to 0.75×10^6). Therefore, optimizing the geometry for load capacity and life required maximizing ball size, contact angle, and minimizing curvatures. Bearings with extremely close curvatures (51 percent and lower) were sensitive to geometric changes caused by temperature differentials; therefore, a standard geometry of 52-percent inner race curvature and a 53-percent outer race curvature with 25-degree contact angles was chosen. Dynamic analysis of this bearing geometry at design speed and load conditions indicated satisfactory stress and life levels. Bearings with similar internal geometry have been successfully tested in LF_2 at Rocketdyne at 0.225×10^6 DN.

(C) The external dimensions of the front (pump end) bearing of the secondary pump were standard for an 8-mm-bore R38 bearing. The rear (turbine end) bearing was nonstandard as follows:

1. The outer race OD was set by the turbine and static seal requirements
2. The inner race OD was set by the primary seal diameter because one-half of the split inner race was used as the mating ring (equivalent to a 10-mm-bore bearing)
3. The bore was 0.002 larger than standard for an 8-mm bore to avoid the problems arising from pressing the inner race over the pump bearing journal first, and then onto its own journal.
4. Tolerances were specified as ABEC-7 (Annular Bearing Engineering Committee Dimension Standard)

(C) The external dimensions for the main engine pump end bearing and the turbine bearing were standard for a 104 (20-mm bore) bearing and a 105 (25-mm bore) bearing, respectively.

8. MAIN SEAL STATIC TEST RESULTS

(U) Static tests were performed in the Engineering Development Laboratory at Canoga Park on each test seal to measure the spring load, static leakage, and drag torque. The following tests were conducted.

a. Spring Load Versus Compression

(U) The seal spring load was measured through the operating length range for compression and release to establish the limits of face load. The results are shown in Table 26 and Fig. 175 and 176.

TABLE 26

MAIN SEAL SPRING LOAD (U)

CONFIDENTIAL Seal Type	Seal P/N	Seal S/N	Load (pounds) at Nominal Length
Primary AL_2O_3 Insert	80-5326	CR1	15.4
Primary AL_2O_3 Spray	80-5329	CR1	17.0
Primary AL_2O_3 Spray	80-5329	CR2	15.6
Primary K162B	80-5313	CR1	14.9
Primary K162B	80-5313	CR2	17.3
Turbine	80-5314	CR2	15.6
Turbine	80-5314	CR4	13.7

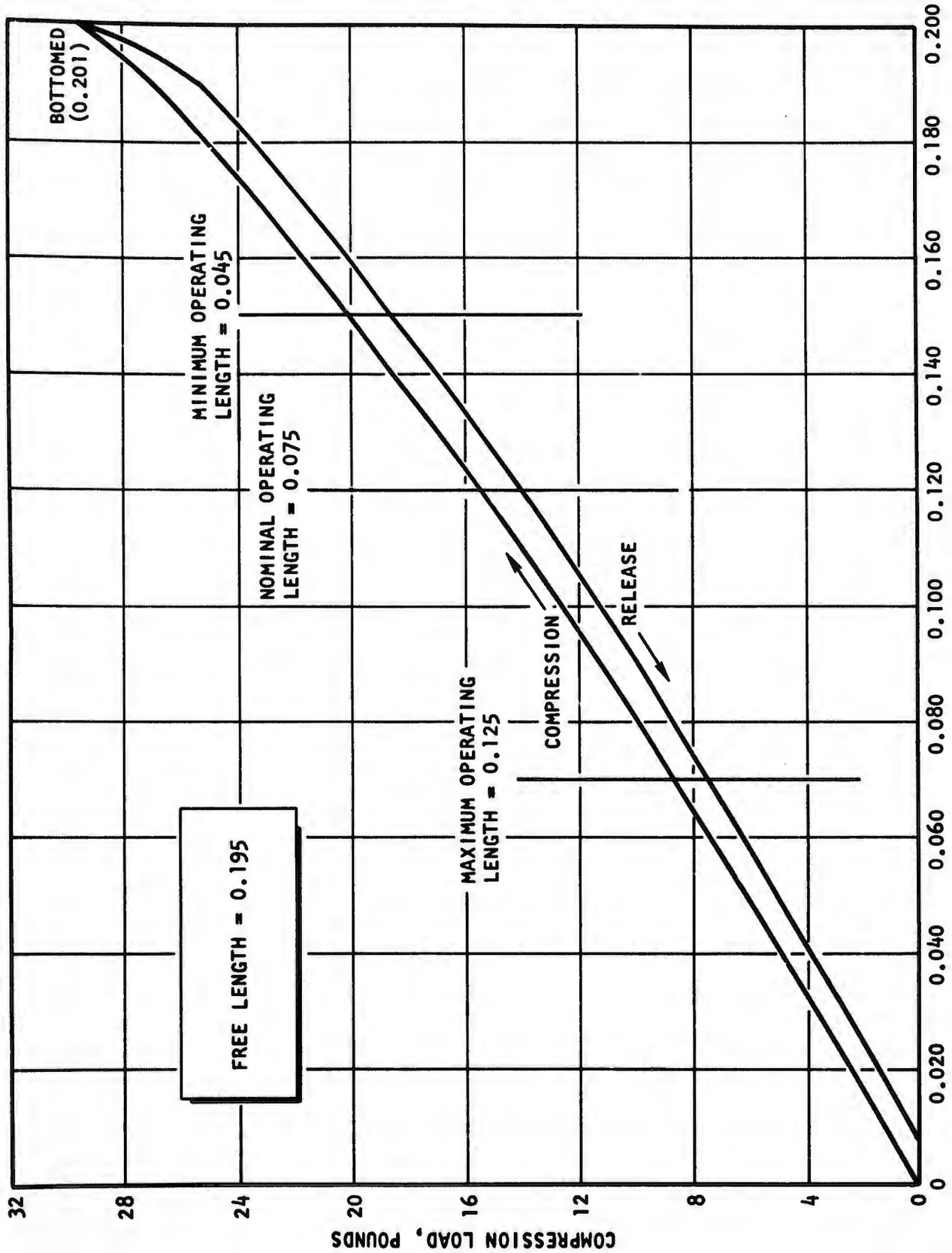

Figure 175. Main Turbopump Primary Seal Load vs Compression (Al_2O_3 Solid-Nose Insert) (C)

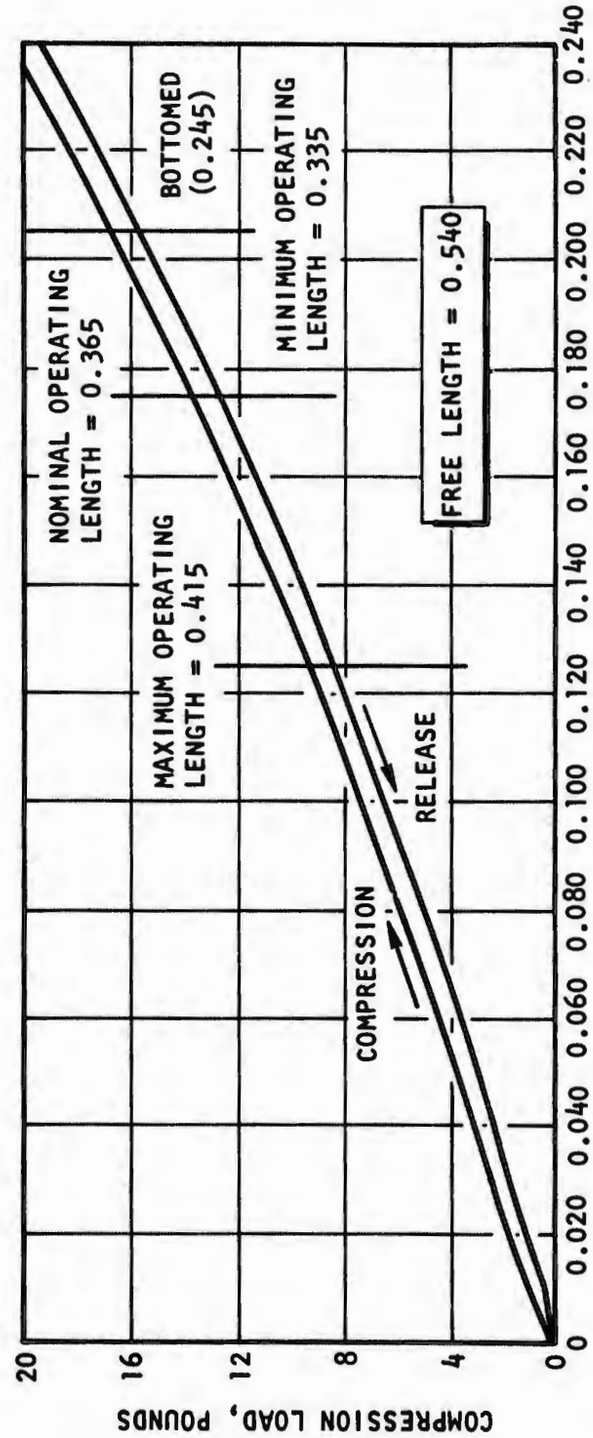

Figure 176. Main Turbopump Turbine Seal Load vs Compression (U)

b. Primary Seal Static Leakage Versus Pressure

(U) The primary seal static leakage was measured with gaseous helium and liquid nitrogen to establish the ambient-temperature and chilled-down leakage characteristics. The results are shown in Table 27 and Fig. 177 through 179.

(C) The results of the LN_2 static leakage tests indicated that the solid insert designs leaked excessively at high pressure due to thermal distortion of the seal face caused by the Inconel carrier contracting faster than the AL_2O_3 or K162B insert. The insert was twisted by the thermal load such that the ID was higher than the OD. This distortion allowed a higher effective pressure separating force across the seal face and caused the face to separate when the differential effective pressure load exceeded the spring load. The excessive leakage occurred at lower pressure when the seal was installed at a longer operating length due to the lower spring load.

(C) The sprayed AL_2O_3 design did not appear to be affected by thermal distortion as the leakage was much lower at high pressure and there was no face separation.

c. Intermediate Seal Static Leakage Versus Pressure

(C) The intermediate seal static leakage was measured with gaseous helium to establish the purge gas leakage rate. The results are shown in Table 28 and Fig. 180 through 182.

TABLE 27

MAIN PRIMARY SEAL STATIC LEAKAGE VERSUS PRESSURE (U)

Seal Type	Seal P/N	Seal S/N	Installed Length, inch	Pressure, psid	GHe Leak, scim	LN_2 Leak, scim
AL_2O_3 Insert	80-5326	CR1	0.125	30	8	400
				50	16	730
				100	60	(1)
				150	120	(1)
				200	220	(1)
				250	-	(1)
			0.079	30	2	150
				50	4	315
				100	15	116
				150	28	320
				200	-	4400
				250	-	(1)
AL_2O_3 Spray	80-5329	CR2	0.075	30	3	3
				50	6	12
				100	24	32
				150	45	86
				200	-	150
				250	-	250
K162B Insert	80-5313	CR2	0.125	30	5	70
				50	10	550
				100	45	(1)
				150	-	(1)
				200	-	(1)
				250	-	(1)
			0.075	30	3.5	25
				50	7.5	60
				100	18.5	265
				150	44	(1)
				250	-	(1)

CONFIDENTIAL

(1) Excessive leakage (> 5000 scims)

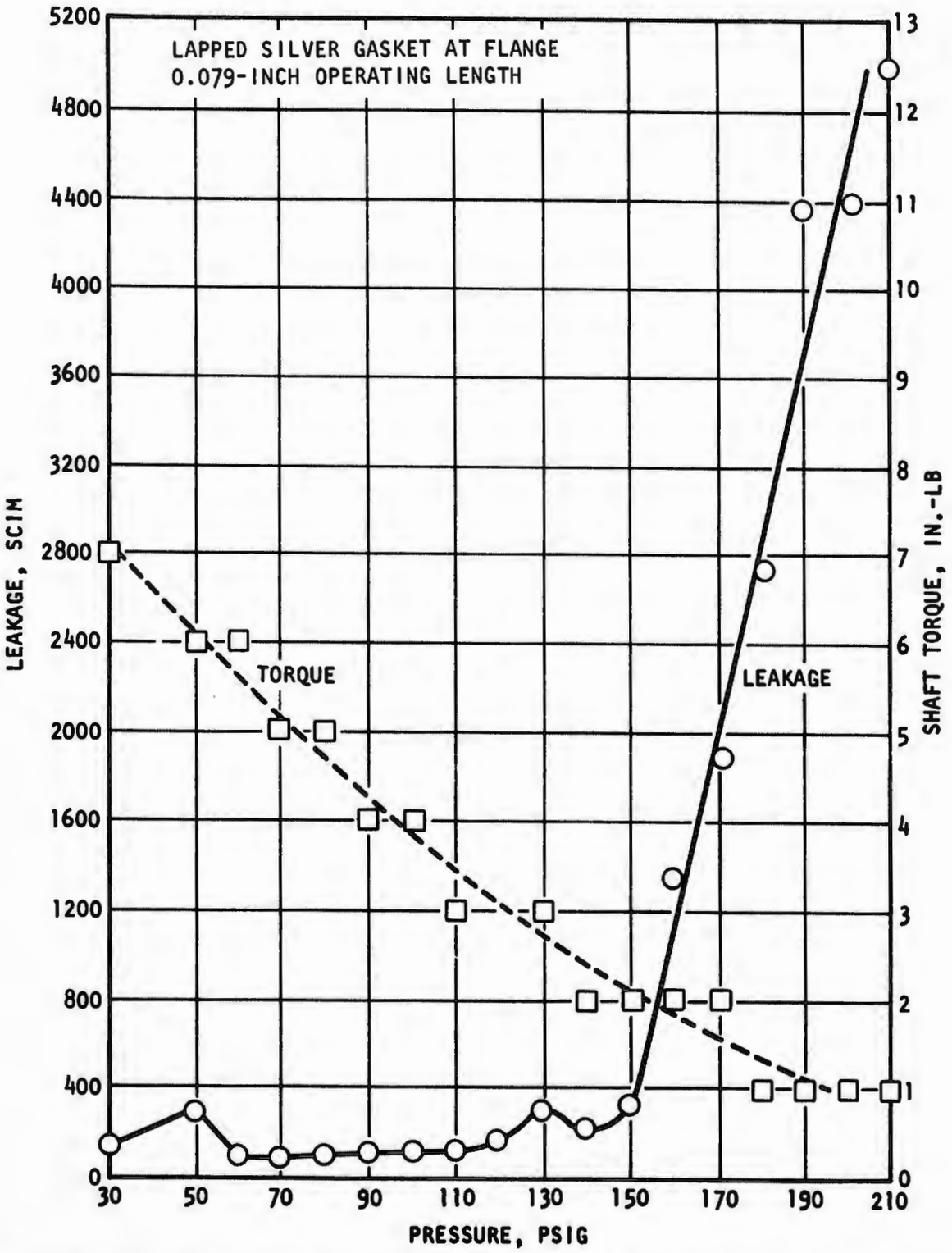

Figure 177. LN_2 Leakage and Torque vs Pressure, Main Pump Primary Seal, Al_2O_3 Insert (P/N 80-5326, S/N CR1) (C)

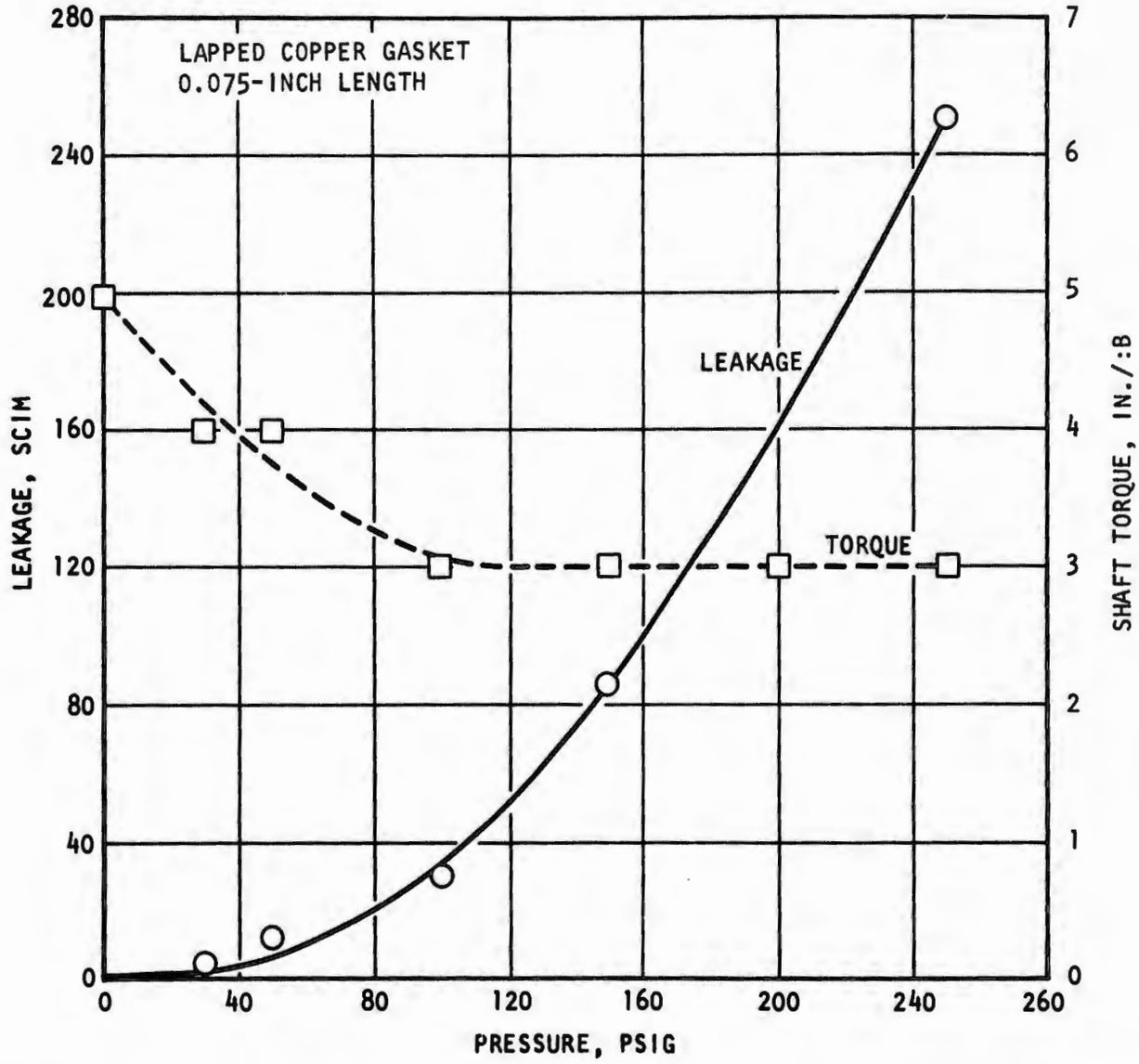

Figure 178. LN_2 Leakage and Torque vs Pressure, Main Pump Primary Seal Al_2O_3 Spray (P/N 80-5329, S/N CR2) (C)

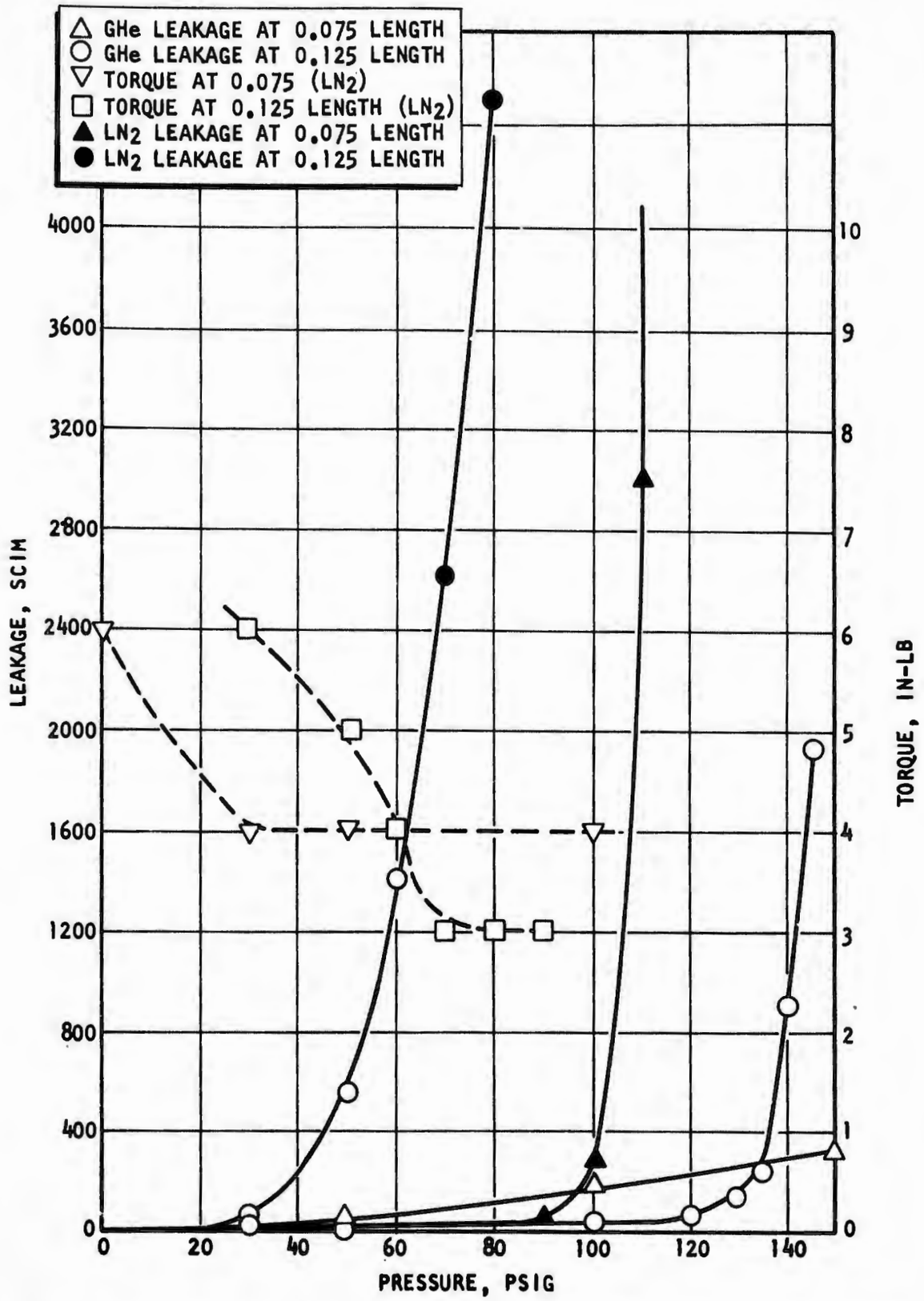

Figure 179. Main Oxidizer Pump Primary Seal Static Test, K162B Insert (P/N 80-5313, S/N 2) (C)

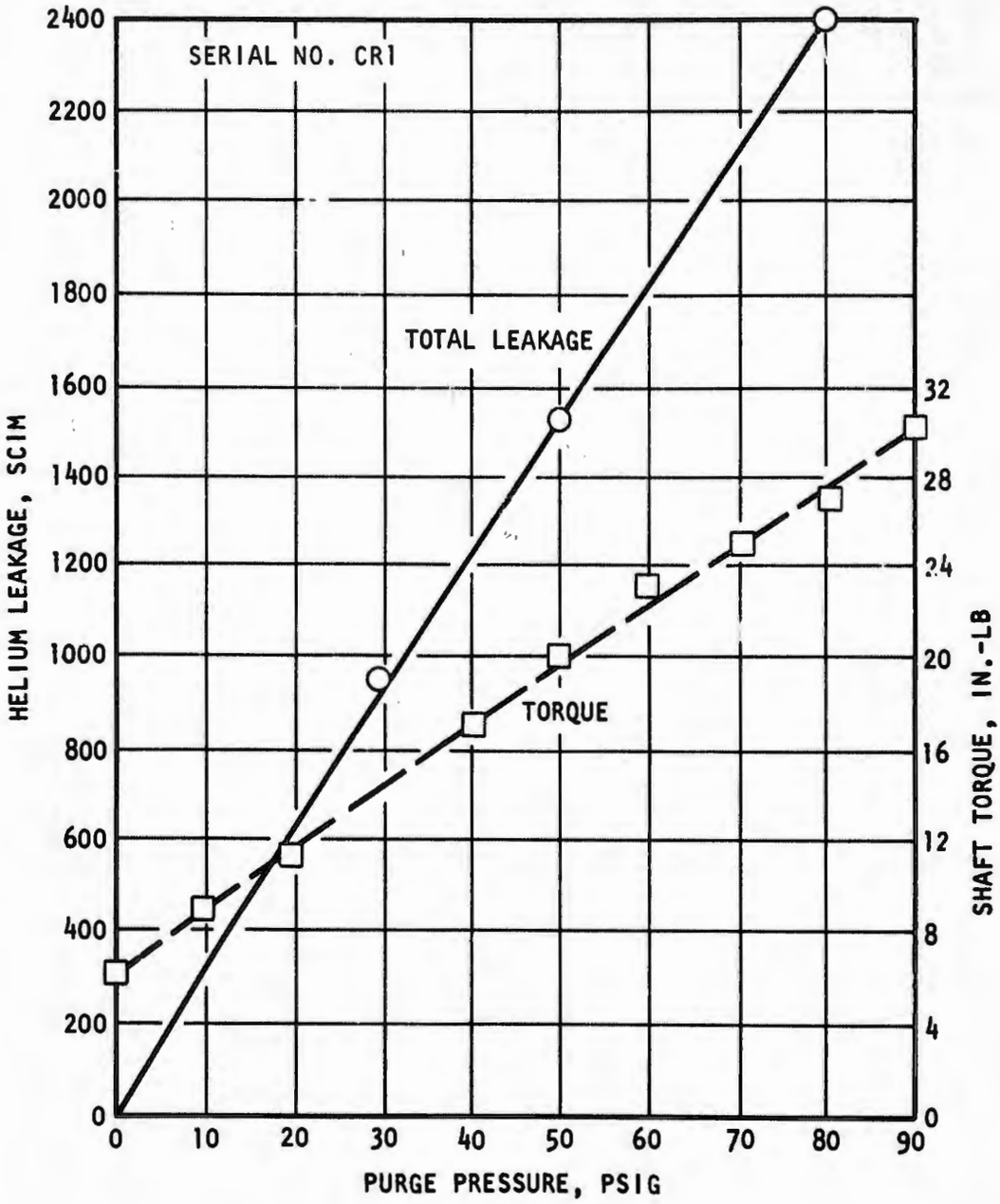

Figure 180. Main Pump Intermediate Seal Leakage and Torque vs Pressure (Bearium B-10), P/N 80-5292 (C)

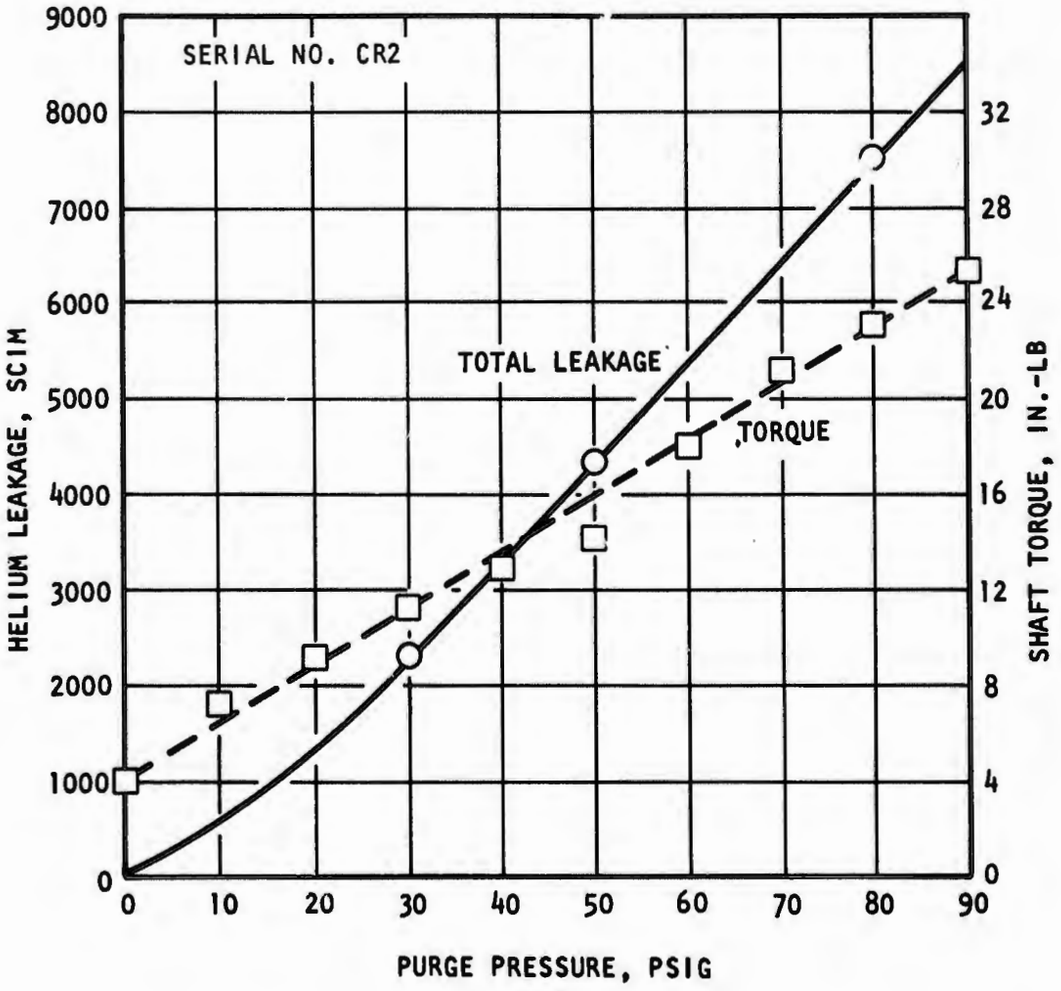

Figure 181. Main Pump Intermediate Seal Total Leakage and Torque vs Pressure (Bearium B-10), P/N 80-5292 (C)

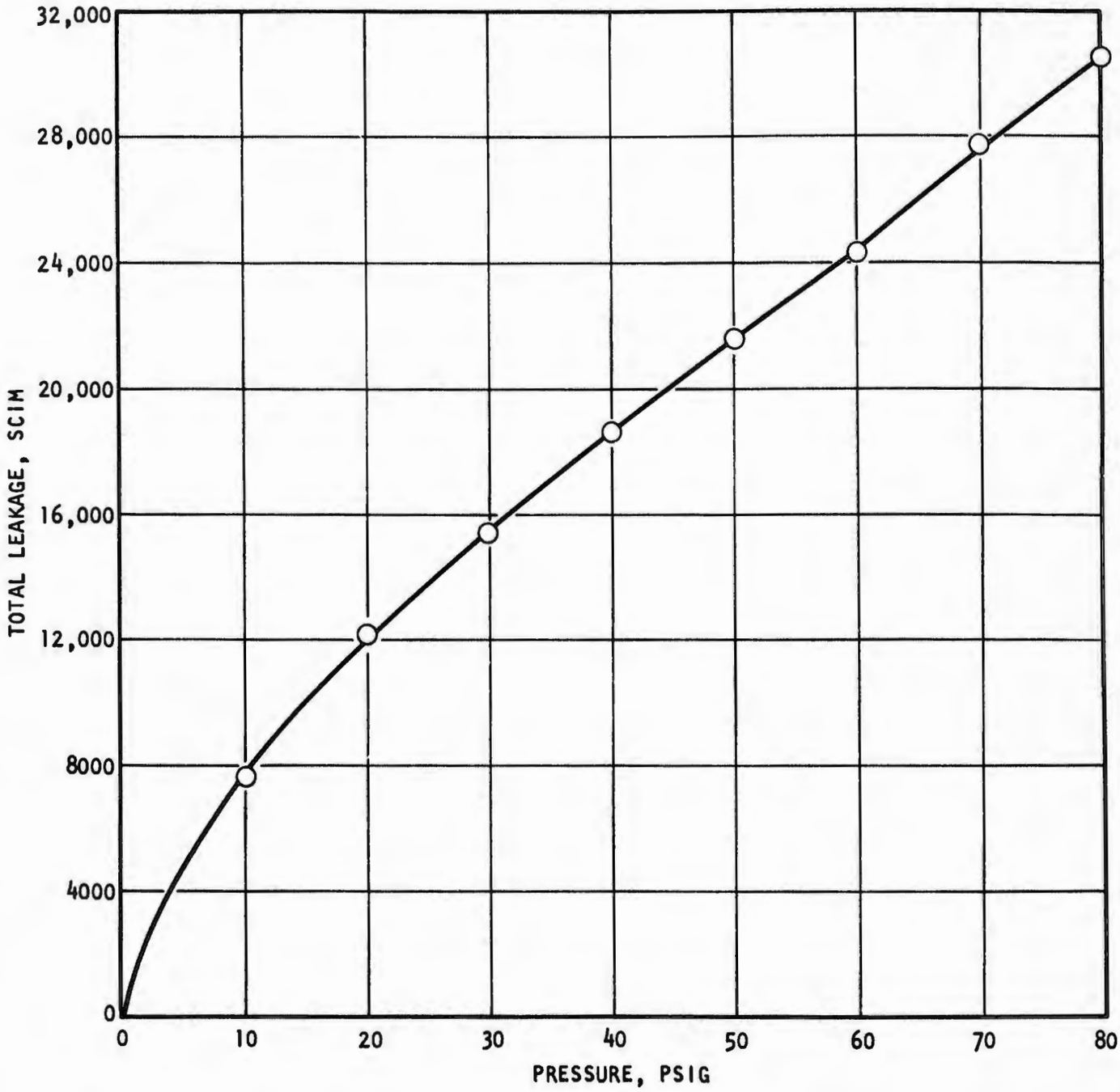

Figure 182. Main Oxidizer Pump Intermediate Seal (BaF_2-CaF_2 Floating Ring), S/N 1 (0.0037-inch-diameter clearance), P/N 80-5391 (C)

TABLE 28

MAIN INTERMEDIATE SEAL STATIC LEAKAGE (U)

Seal Type	CONFIDENTIAL Seal P/N	Seal S/N	GH_e Leak at 50 psid, scim
Segmented Bearium B-10	80-5292	CR1	1500
Segmented Bearium B-10	80-5292	CR2	4940
Floating Gap BaF_2-CaF_2	80-5391	CR2	21500

d. Seal Friction Torque Versus Pressure

(U) The seal friction torque versus pressure was measured at ambient temperature and LN_2 chilled conditions to determine the seal drag for estimating horsepower losses. The results are shown on Fig. 177 through 181.

(C) The AL_2O_3 insert primary seal (P/N 80-5326 CR1) torque decreased from 10 in.-lb at zero pressure to 1 in.-lb as the pressure was increased (chilled with LN_2) due to loss of contact load (Fig. 177). The AL_2O_3 spray seal (P/N 80-5329 CR2) torque dropped slightly then held constant at 3 in.-lb, indicating the pressure load was nearly balanced (Fig. 178). The normal trend was for greater frictional drag at higher pressures due to increased face contact load.

(U) The segmented intermediate seal (P/N 80-5292) torque followed the predictable trend with 4 to 6 in.-lb at zero pressure and 16 to 20 in.-lb at the nominal purge pressure of 50 psig (Fig.180 and 181). There was no measurable torque drag with the floating-gap intermediate seal design (P/N 80-5391).

(U) The turbine seal torque was approximately 4 in.-lb at 50 psig.

9. SECONDARY SEAL STATIC TEST RESULTS

(U) Static tests were performed in the Engineering Development Laboratory at Canoga Park on each test seal to measure the spring load, static leakage, and drag torque. The following tests were conducted.

a. Spring Load Versus Compression

(U) The seal spring load was measured through the operating length range for compression and release to establish the limits of face load. The results are shown in Table 29 and Fig. 183 and 184.

TABLE 29

SECONDARY SEAL SPRING LOAD (U)

Seal Type	Seal P/N	Seal S/N	Spring Load (pounds) at Nominal Length
Primary	80-5533	1	4.2
		2	2.8
		3	2.5
Turbine	80-5535	1	3.5
		6	4.0
		11	4.7

b. Primary Seal Static Leakage Versus Pressure

(U) The primary seal static leakage was measured with gaseous helium and liquid nitrogen to establish the ambient-temperature and chilled-down leakage characteristics. The results are shown in Table 30 and Fig. 185.

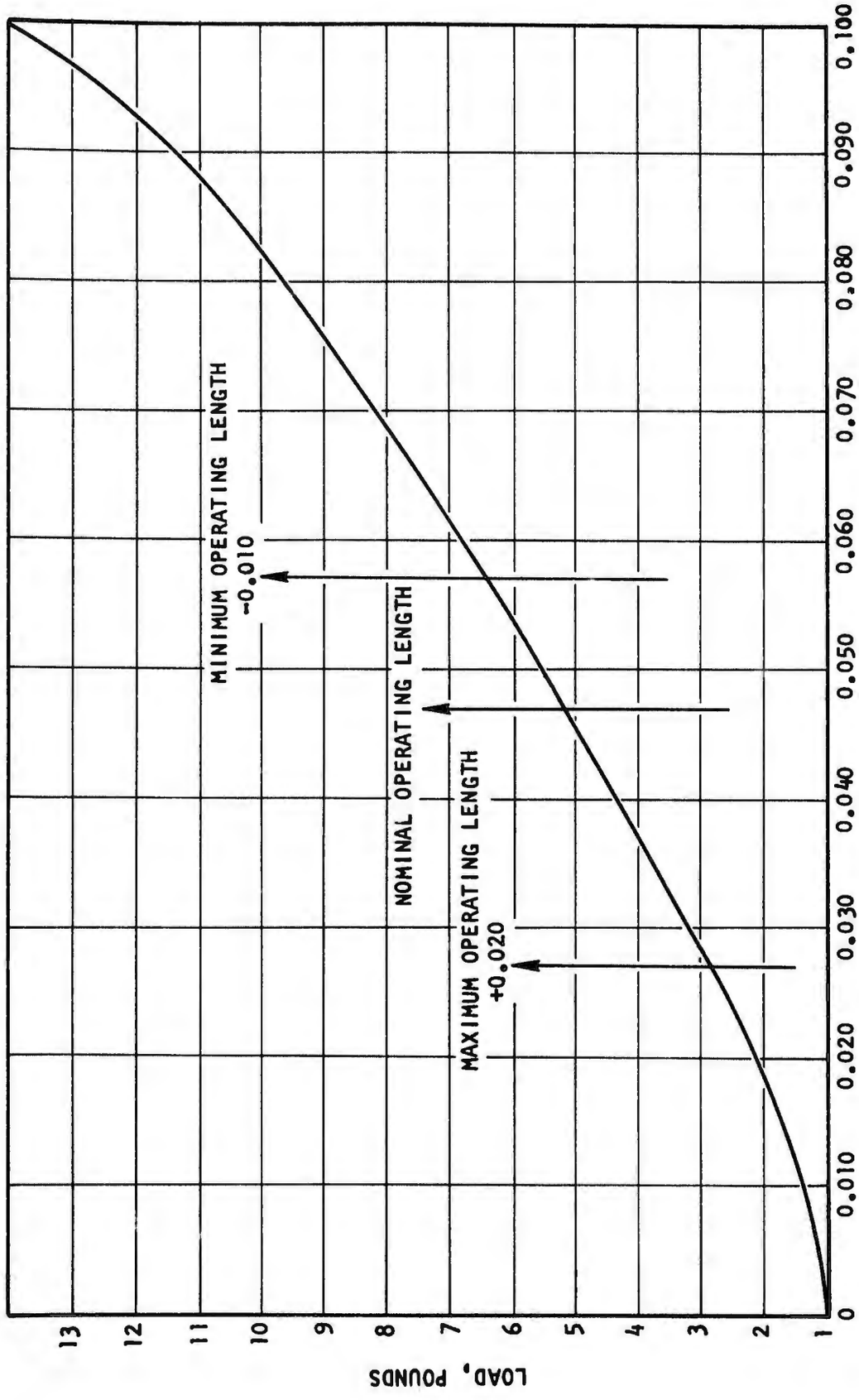

Figure 183. Secondary Primary Seal Load vs Compression (P/N 80-5533, S/N 1) (U)

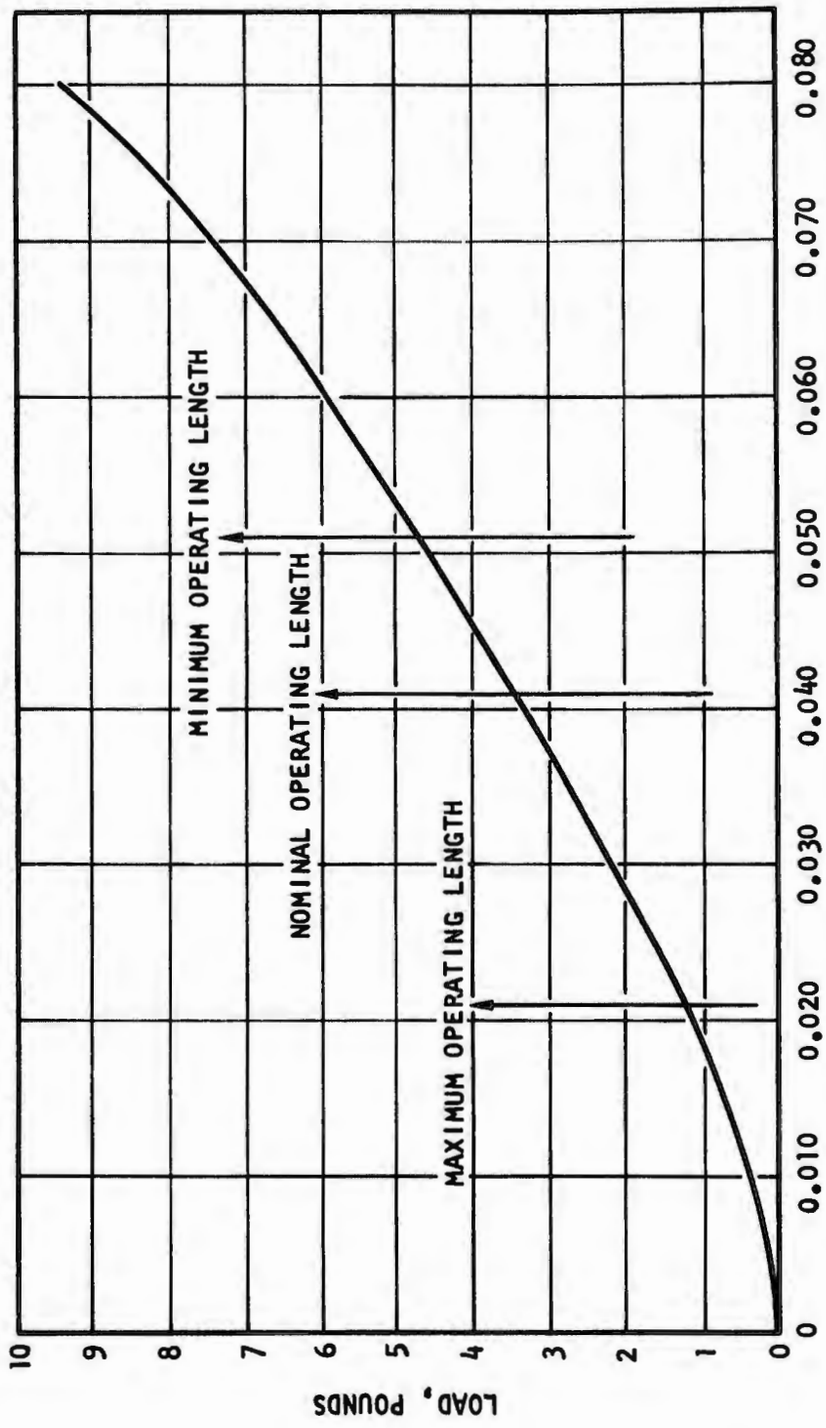

Figure 184. Secondary Turbine Seal Load vs Compression (P/N 80-5535, S/N 1) (U)

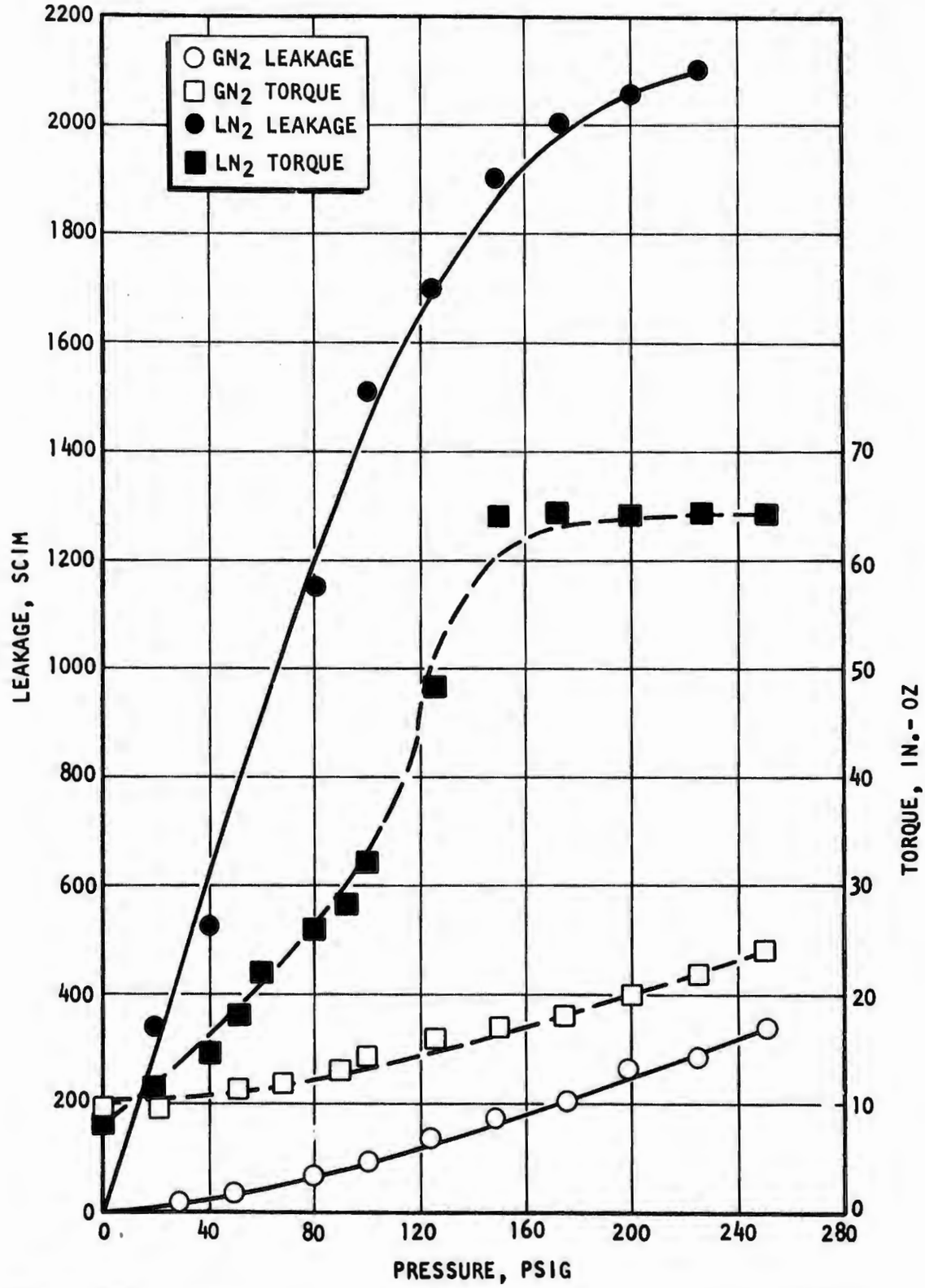

Figure 185. Secondary Primary Seal Leakage and Torque (P/N 80-5533, S/N 1) (AL_2O_3 Spray) (C)

(C) The results of the liquid nitrogen leakage tests indicated that the AL_2O_3-coated nose was not significantly affected by thermal distortion. There was no indication of seal face separation as occurred on the main seal solid insert designs.

TABLE 30

SECONDARY PRIMARY SEAL STATIC LEAKAGE (U)

Seal Type	Seal P/N	Seal S/N	Pressure, psid	GHe Leak, scim	LN_2 Leak, scim
AL_2O_3 Spray	80-5533	CR1	30	(1) 19.5	460
			50	35	700
			100	96	1500
			150	170	1900
			200	260	2050
			250	340	2350
		CR2	30	10	15
			50	18	32
			100	45	80
			150	90	155
			200	140	250
			250	190	--

CONFIDENTIAL

(1) GN_2 leakage

c. Intermediate Seal Static Leakage Versus Pressure

(U) The intermediate seal static leakage was measured with gaseous helium to establish the purge gas leakage rate. The results are shown in Table 31 and Fig. 186.

TABLE 31

SECONDARY INTERMEDIATE SEAL STATIC LEAKAGE (U)

Seal Type	Seal P/N	Seal S/N	GHe Leak at 50 psid, scim
Floating Gap BaF_2-CaF_2	80-5534x	CR1	7450
Floating Gap BaF_2-CaF_2	80-5534x	CR5	8400

CONFIDENTIAL

d. Seal Friction Torque Versus Pressure

(U) The primary seal friction torque versus pressure was measured at ambient temperature and chilled with LN_2. The results are shown on Fig. 185. The primary seal ambient torque increased from 10 in.-oz at zero pressure to 24 in.-oz at 250 psig. The cold torque increased from 8 in.-oz at zero pressure to 64 in.-oz at 250 psig.

(U) There was no measurable torque drag on the floating-gap intermediate seal.

(U) The turbine seal torque was between 8 and 16 in.-oz at the 50-psig operating pressure.

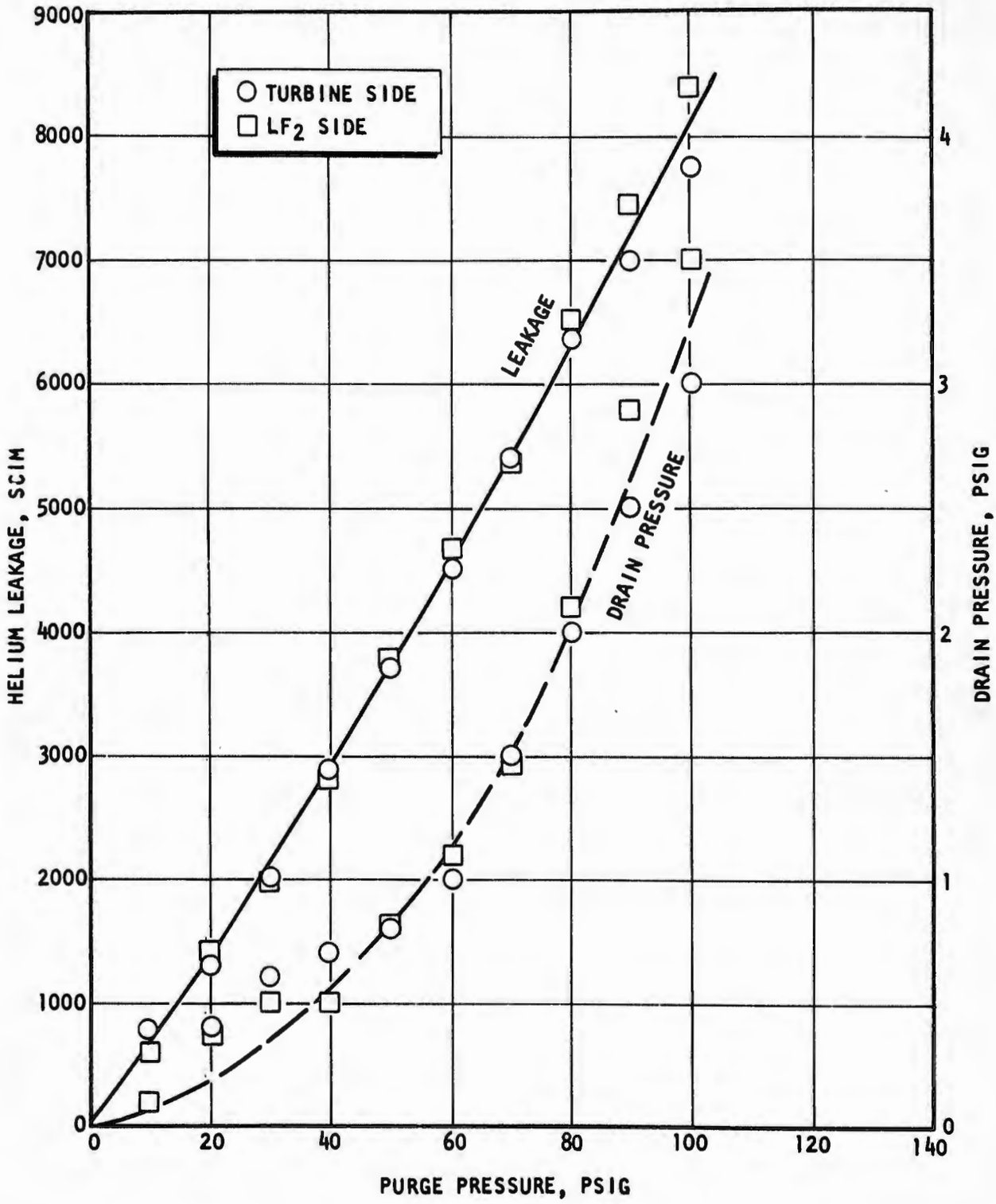

Figure 186. Secondary Intermediate Seal Leakage and Drain Pressure (Diametral Clearance = 0.0023 in.) (P/N 80-5534X, S/N 1) (U)

10. MAIN BEARING AND SEAL DYNAMIC TEST RESULTS

(C) The main bearing and seal tester was run for five tests with liquid fluorine for a total time of 697 seconds. One liquid nitrogen test of 61 seconds duration was performed. The main bearing and seal testing is summarized in Table 32. The bearing and seal test hardware summary is shown in Table 33. Data from two of the tests are summarized in Tables 34 and 35.

TABLE 32

MAIN BEARING AND SEAL TEST SUMMARY (U)

Test No.	Date, 1969	Number of Starts	Time, seconds	Speed, rpm	Remarks
001 (LF_2)	4-2	0	0	0	No rotation; turbine valve not open
002 (LF_2)	4-3	1	3	42,500	Torquemeter seized; rebuilt tester with new bearings and seals; used solid shaft in place of torquemeter and added air fan for speed control
LN_2 Starts	4-25	5	61	6,400 53,700	Speed control erratic; damaged bearings and seals due to LN_2, rebuilt tester, and added bigger air fan
003 (LF_2)	5-10	8	56	33,000	Speed control erratic; suspect intermediate seal torque variation
004 (LF_2)	5-12	5	518	16,700 47,000	Fire started at intermediate seal and burned through tester housing
005 (LF_2)	11-17	5	120	20,000	Fire started at rear bearing and damaged tester due to internal burning

CONFIDENTIAL

TABLE 33

MAIN BEARING AND SEAL HARDWARE SUMMARY (U)

Test No.	Time, sec	Primary Seal			Intermediate Seal			Turbine Seal			Bearings	
		Type	S/N	Condition	Type	S/N	Condition	Type	S/N	Condition	Set No.	Condition
001	0	AL_2O_3 insert 80-5326 versus AL_2O_3	CR1	(1)	Bearium segmented 80-5292 versus Inconel	CR1	(1)	Carb P5N 80-5314 versus chrome	CR4	(1)	1	(1)
002	3	↓	CR1	(2) Nose insert broken, mating ring worn	↓	CR2	(2) Mating surface scored & pins bent	↓	CR4	Satisfactory (relapped seal & installed new mate ring)	1	(2) Failed
LN_2 Starts	61	AL_2O_3 Spray 80-5329 versus K162B	CR2	(3) Rubbing surface galled	↓	CR1	Satisfactory	↓	CR4	Satisfactory (relapped seal)	2	(3) Rough
003	56	↓	CR1	(1)	↓	CR1	(1)	↓	CR4	(1)	3	(1)
004	518	↓	CR1	(4) Housing burned	↓	CR1	(4) Burned out	↓	CR4	(4) Burned out	3	(4) Rough
005	120	K162B Insert 80-5313 versus K162B	CR2	(5) Burned out	BaF_2-CaF_2 floating gap versus BaF_2-CaF_2	CR1	(5) Satisfactory	↓	CR2	Satisfactory	4	(5) Burned

(1) No inspection
(2) Damaged due to high rotating load caused by torquemeter failure
(3) Damaged due to lack of lubrication from running with liquid nitrogen
(4) Damaged by fire which started at intermediate seal Bearium B-10 segments
(5) Damaged by fire which started at rear bearing

TABLE 34

MAIN TESTER DATA SUMMARY (TEST 002) (U)

	Time Slice, seconds			
	Before (98,914)	Maximum (101.396	After (103.080)	End (250)
Primary Seal Drain Flow, scfm	*	*	*	*
Turbine Seal Drain Flow, scfm	1.1	6.2/7.2	5.5	2.2
LF_2 Tester In Temperature, F	-255	-255	-256	-256
LF_2 Tester Out Temperature, F	-244	-245	-245	-245
Primary Seal Drain Temperature, F	-40	-45	-35	-140
Turbine Seal Drain Temperature, F	-45	-30	-35	--
Intermediate Seal Purge Temperature, F	30	30	30	--
Torquemeter torque, in.-lb	0	15	0	0
LF_2 Tester In Pressure, psig	26.5	26.5	26.4	26
Intermediate Seal Purge Pressure, psig	49.3	27.3	83.0	43.5
Primary Seal Drain Pressure, psig	21.1	14.6/17.8/21.8	20.3	16
Turbine Seal Drain Pressure, psig	0.7	4.6/15.5/18.8	3.0	0
LF_2 Tester Out Pressure, psig	29.5	28.9	29.1	29
Load Bellows Pressure, psig	79.4	79.4	79.4	79
Intermediate Seal Purge Flow, scfm	15.1	17.0	12.0	5.5
Bearing Cavity Pressure, psig	25.5	22.4/23.1	25.2	25
Tester Speed, rpm	0	42,560	0	0
LF_2 Tester Flow, gpm	0	2.64	1.85	2.3

CONFIDENTIAL

*Posttest checkout revealed measurement to be incorrect.

CONFIDENTIAL

TABLE 35

MAIN TESTER DATA SUMMARY, TEST 004 (U)

Parameter	Time Slice, seconds								
	First Start	Second Start	Third Start	Fourth Start		Fifth Start			
	230	470	540	590	635	660	675	963.5	980.5
Oxidizer Inlet Temperature, F	-267	-240	-260	-277	>-200	-255	-255	-279	-277
Oxidizer Outlet Temperature, F	-269	-266	-261	-261	-259	-226	-216	-273	-282
Primary Seal Drain Temperature, F	-217	-174	-126	-164	-140	- 91	- 70	-164	**
Turbine Seal Drain Temperature, F	*-304	*-140	*-114	*-100	*-106	*-80	*-55	*+165	**
Internal Seal Purge Temperature, F	-142	-122	-114	-116	-110	-110	-108	- 55	+ 85
Oxidizer Inlet Pressure, psig	93.5	114.9	131.0	132.5	132.0	161.9	162.1	70.2	66.8
Internal Seal Purge Pressure,psig	6.9	4.7	5.4	40.4	0.17	17.5	10.9	0.46	0.8
Primary Seal Drain Pressure, psig	7.2	5.7	6.5	41.5	0.21	17.8	11.6	1.5	0.77
Turbine Seal Drain Pressure, psig	6.5	3.1	1.6	28.5	0.32	14.6	7.9	0.7	1.8
Oxidizer Outlet Pressure, psig	95.2	116.4	132.4	134.3	133.7	162.9	163.2	70.4	36.5
Load Bellows Pressure, psig	104.1	132.5	132.4	152.0	151.6	151.5	151.4	151.3	151.3
Turbine Inlet Pressure, psig	39.5	33.4	37.0	50.3	58.4	46.8	33.6	45.5	44.1
Bearing Cavity Pressure, psig	94.9	116.2	132.3	134.7	132.8	163.2	163.1	64.9	35.7
Tester Speed, rpm	28,889	16,952	17,329	43,255	10,788	43,669	22,314	29,640	46,993
Oxidizer Flow, gpm	<0.1	<0.1	0.7	0.4	<0.1	0.3	<0.1	<0.1	1.4

*Questionable measurement
**Pegged off-scale

(U) The following tests were performed on the main bearings and seals using the dynamic tester.

a. Test 001 (No Start)

(U) The tester was chilled down by flowing LN_2 through the tester jacket. Liquid fluorine was then flowed into the tester, and an attempt was made to start the drive rotation by pressurizing the turbine GN_2 system. The test was terminated when the turbine did not rotate. Investigation revealed that the GN_2 valve upstream of the turbine inlet had not actuated open; therefore, no GN_2 pressure had reached the turbine. The tester was not disassembled.

b. Test 002 (1 Start for 3 Seconds)

(C) The tester was chilled down with LN_2. Liquid fluorine was then flowed into the tester, and the turbine inlet pressure was increased in increments. The drive suddenly broke loose and spiked up to a maximum speed of 42,500 rpm and back to zero. Investigation revealed that the drive torquemeter was binding up on the turbine end and not transmitting the turbine torque to the tester, until the turbine starting torque increased enough to break the torquemeter loose. The torquemeter apparently failed and seized tight as the speed spiked up causing an excessively high rotating radial load on the tester shaft which failed both tester bearings and broke the primary seal AL_2O_3 nosepiece (Table 34).

(U) The tester was rebuilt using new bearings and seals, and the drive assembly was rebuilt using a solid quill shaft in place of the torquemeter. (The torquemeter was returned to the vendor for analysis.) Also, a special air fan was installed on the turbine shaft to absorb torque and prevent overspeed after breakaway.

(U) To check out the use of the air fan (air brake) for improved tester speed control, a series of start tests was conducted with LN_2 simulating LF_2 in the tester. The LN_2 was used as a safety precaution because of the lack of tester speed control which had occurred on the two previous test attempts.

(C) The speed control checkout tests were conducted by increasing the turbine inlet pressure gradually until rotation started; then the speed was adjusted by venting the pressure. The results of the initial start tests indicated that the air fan improved the speed control; however, additional speed control was necessary. Therefore, a larger air fan was installed and the following start tests were conducted.

- Start No. 1 (7 seconds). Speed spiked up to 53,700 rpm and leveled off for 3 seconds
- Start No. 2 (3 seconds). Speed spiked up to 41,600 rpm
- Start No. 3 (5 seconds). Speed increased to 24,700 rpm
- Start No. 4 (18 seconds). Speed increased erratically to 38,400 rpm
- Start No. 5 (28 seconds). Speed increased to 33,300 rpm, dropped to 25,600 rpm when pressure was vented, then varied erratically from 26,900 rpm to 6400 rpm

(C) Inspection of the tester hardware after the LN_2 start tests revealed that both tester bearings were damaged because of lack of lubrication from running with LN_2. The primary seal face was severely damaged from rubbing against the K162B mating ring in LN_2. The bearing and seal materials depended on formation of a fluoride film for proper lubrication when operating in LF_2, and such a film was not present when operating in LN_2.

c. Test 003 (8 Starts for 56 Seconds)

(C) The tester was chilled down by flowing LN_2 through the tester jacket. Liquid fluorine was then flowed into the tester and the turbine inlet pressure was increased to 64 psig and the speed suddenly spiked to 33,000 rpm. The pressure was vented to 45 psig and the speed dropped to 15,000 rpm, then decayed to zero with no change in pressure. The pressure was increased again to 77 psig, and the speed spiked to 33,000 rpm, then dropped to zero when the pressure was vented to 66 psig. The speed spiked from zero to approximately 30,000 rpm six more times with the turbine pressure constant at approximately 90 psig. The test was terminated because of erratic speed control.

(C) The intermediate seal purge pressure decayed from approximately 50 to approximately 45 psig at the same time the speed increased, then gradually recovered to approximately 50 psig at the same time the speed dropped to zero (Fig. 187). The erratic speed control was caused by a variation in the tester torque resulting from the segmented intermediate seal drag torque changing from the loading caused by the purge pressure.

(U) The purge pressure, which loaded the segments against the shaft, decayed gradually, reducing the seal drag, and allowed the turbine to start rotation. The seal leakage increased as rotation started, which further reduced the purge pressure because of the slow response of the pressure regulator. A progressive speed increase resulted until the pressure regulator responded and started to build up the purge pressure. The speed then decreased and stopped after repressurization because of the additional seal drag.

(U) Part of the speed control problem was related to variation of the intermediate seal drag torque from the loading caused by the purge pressure and, it was, therefore, decided to run the initial portion of test 004 with no purge pressure to eliminate that variable. This method of operation was not considered to be a hazard because the main function of the purge was to provide a pressure barrier between the oxidizer and fuel-rich drain cavities to maintain separation, and there was no combustible gas in the tester. The purge also provided some cooling and lubrication for the rubbing segments; however, the load decrease with no purge pressure was expected to compensate for the lack of cooling.

d. Test 004 (5 Starts for 518 Seconds)

(C) Test 004 included five starts for a total rotation time of 518 seconds (Fig. 188).

(1) First Start (56 Seconds)

(C) After chilling the tester with LN_2 and introducing LF_2 to the tester, the turbine inlet GN_2 pressure was increased gradually with no intermediate seal purge pressure, and the bearing cavity pressure was set at 95 psig. The turbine broke loose

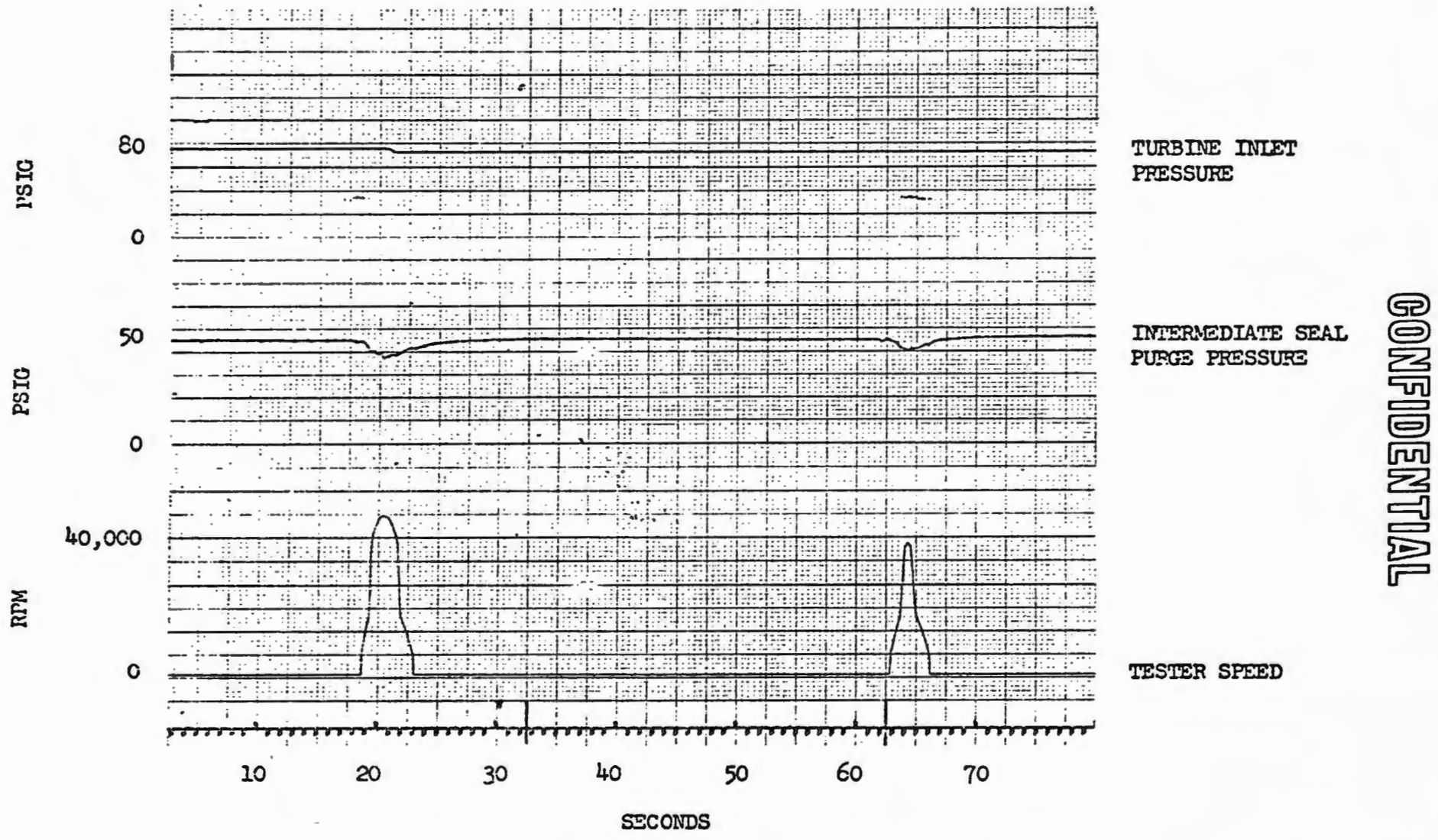

Figure 187. Segmented Intermediate Seal Stability, Test 003 (U)

CONFIDENTIAL

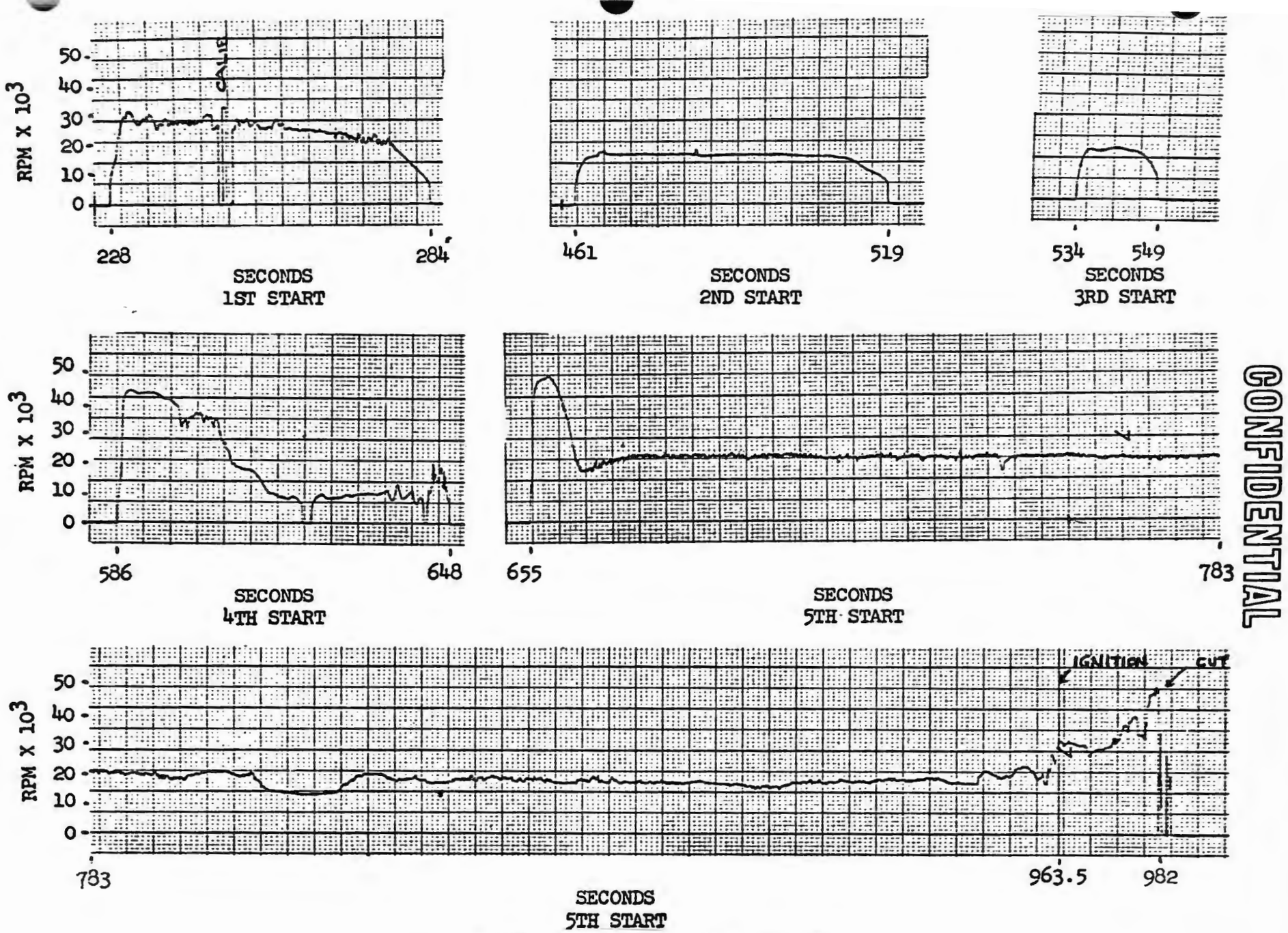

Figure 188. Rpm vs Time, Test 004 (U)

(C) at 40-psig inlet pressure, spiked up to 29,000 rpm, then leveled off at 28,000 rpm when the turbine pressure was vented to 38 psig, and gradually dropped to 21,000 rpm while the turbine pressure was constant at 38 psig. The speed was relatively steady, but there was no indicated oxidizer flow through the bearings; therefore the turbine pressure was vented to stop rotation until the cause of no flow was determined.

(C) Investigation showed that the recirculation impeller on the tester shaft was not pumping because of cavitation or vapor lock of the oxidizer at the impeller inlet. The bearing cavity pressure was increased to 114 psig to improve the NPSH at the impeller inlet.

(2) Second Start (58 Seconds)

(C) Turbine rotation started at an inlet pressure of 34 psig, leveled off at 17,000 rpm for 58 seconds, and then dropped to zero at a constant inlet pressure of 34 psig. The oxidizer bearing flow was intermittent and the bearing cavity pressure was increased again to 132 psig approximately 20 seconds before the speed dropped to zero.

(3) Third Start (15 Seconds)

(C) The turbine inlet pressure was increased from 34 to 37.5 psig, and the turbine restarted and leveled off at 17,000 rpm for 15 seconds, then dropped to zero again with no change in turbine inlet pressure. The oxidizer flow was initiated by cycling the bleed valve open, which vented the oxidizer return line to atmospheric pressure and caused flow through the tester because of the pressure differential between the oxidizer tank and ambient conditions.

(4) Fourth Start (62 Seconds)

(C) The turbine inlet pressure was increased gradually to 52 psig, and the speed spiked up to 43,000 rpm and gradually decayed to zero as the inlet pressure was slowly vented to 42 psig, then restarted and increased to 10,000 rpm as the turbine

(C) inlet was repressurized to 53 psig. The inlet pressure was increased to 58.5 psig, and the speed increased to 11,000 rpm, then dropped to zero. The bearing cavity pressure was increased from 130 to 163 psig at the same time by remotely adjusting the pressure regulator. Oxidizer flow was maintained intermittently by cycling the bleed valve open.

(5) Fifth Start (327 Seconds)

(C) The turbine suddenly restarted and spiked to 48,000 rpm at a constant inlet pressure of 58 psig, then dropped to 21,000 rpm when the inlet pressure was vented to 34 psig and remained relatively steady for 300 seconds with a gradual decay to 18,000 rpm while the inlet pressure was constant at 34 psig.

(C) Oxidizer flow was maintained intermittently by cycling the bleed valve open. The bearing cavity pressure was vented to 105 and then to 75 psig because of the oxidizer flow out the bleed.

(C) The decision was then made to increase the speed to 28,000 rpm, leave the oxidizer bleed open to maintain flow, and gradually increase the intermediate seal purge pressure to determine the effect of seal drag on speed.

(C) The turbine inlet pressure was increased from 34 to 38 psig and the speed increased to 21,000 rpm. The pressure was increased again from 38 to 42 psig, and there was no change in speed. Another pressure increase from 42 to 47 psig resulted in a speed increase to 23,000 rpm. The pressure gradually decayed to 45.5 psig (regulator drift) and the speed followed with a decrease to 17,000 rpm. Then the speed suddenly increased to 31,000 rpm while the pressure was constant at 45.5 psig. Also, at approximately the same time, the Bentley scope showed excessive shaft deflection, which was suspected to have been caused by running at a critical speed. An attempt was made to change the operating speed, however, before any adjustment to the pressure could be made, the speed increased again to 40,000 rpm. The pressure was vented from 45.5 to 43.5 psig, and the speed dropped to 33,000 rpm, then spiked to 48,000 rpm. At this time, the test observer saw fire and sparks coming from the tester, and the test was terminated.

(U) Posttest inspection of the tester revealed a hole burned through the tester housing in the area of the primary seal drain. There also was a secondary fire caused by ignition of lubricating oil that had leaked from the turbine and collected in the torquemeter housing.

(U) The turbine and tester shaft could be turned freely after the test with approximately 2 to 4 in.-lb torque.

(C) Inspection of the tester hardware revealed the following (see Fig. 189 and 190).

1. The major portion of the burning was centered in the primary seal drain and intermediate seal area, indicating that the origin of the fire was on the primary side of the intermediate seal.
2. There was no burning in the intermediate seal purge cavity area of the tester housing, indicating that the fire did not start inside of the intermediate seal.
3. There was no burning in the turbine seal drain area of the tester housing, indicating that the fire did not start at the turbine seal.
4. The primary seal drain cavity portion of the tester housing was completely burned out through the housing, indicating that combustion was supported by oxidizer leakage through the primary seal.
5. The seal portion of the tester housing was partially burned and covered with molten metal and slag.
6. The bearing cavity portion of the tester housing was not damaged by the fire and appeared to be completely isolated from the burning in the seal area by the primary seal.
7. The primary seal housing was partially burned away from the drain side, but the sealing face was in good condition and the seal was still functional enough to maintain adequate sealing of the oxidizer.

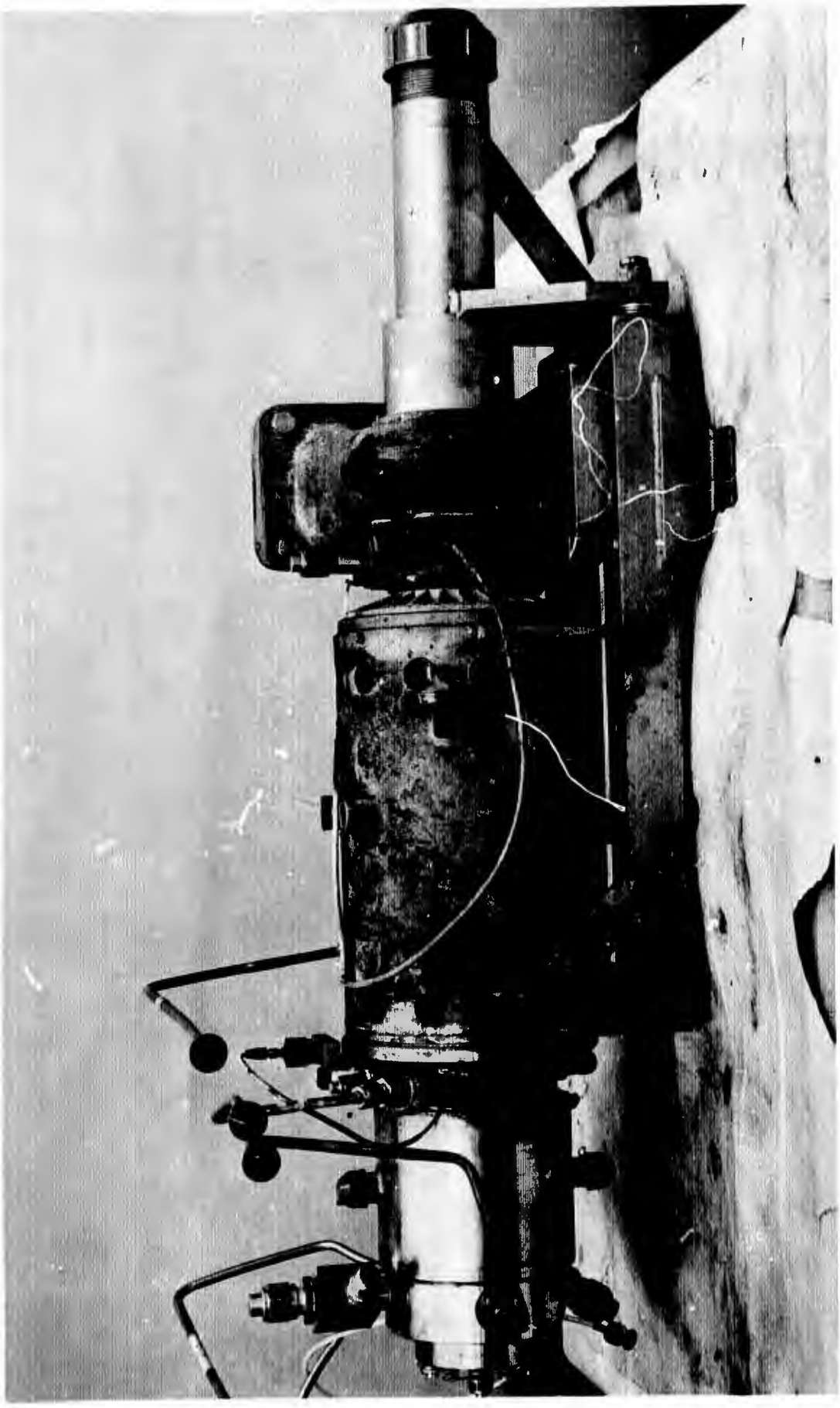

1EH95-5/13/69-C1A

Figure 189. Main Tester and Drive Assembly (Posttest 004) (U)

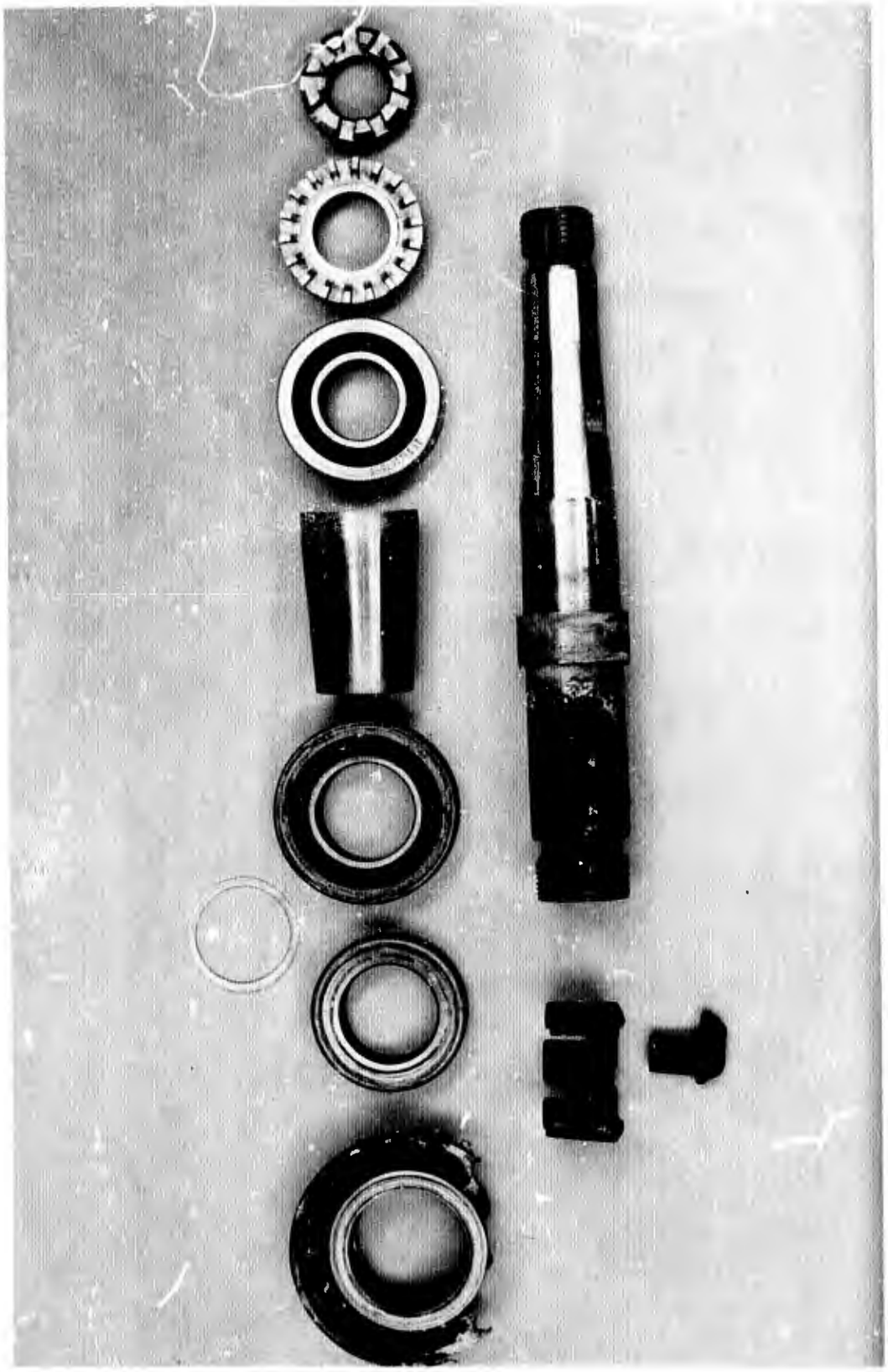

1EH95-5/15/69-C1B

Figure 190. Main Tester Seals, Bearings, and Shaft (Posttest 004) (U)

(C) 8. The tester bea gs sounded slightly rough (noisy) when rotated but were not damaged by the fire and appeared to be in reasonably good condition. The roughness was probably caused by the high speed and high loads from the excessive shaft deflection during the failure.

(C) The test data indicated that the fire started in the primary seal drain cavity at 963.5 seconds, which was 18.5 seconds before the test was cut (see Fig. 191, and Table 35).

(C) The first indication of the fire was a pressure and temperature increase in the primary seal drain. The pressure spiked to 3.0 psig, and the temperature spiked off scale and went erratic. There was a temperature and pressure increase in the turbine seal drain at about the same time, but the pressure only reached 1.0 psig, indicating the origin of the pressure source was in the primary seal drain.

(C) There was a second ignition in the primary seal drain approximately 1 second later at 964.7 seconds, which caused a pressure spike of 11.5 psig in the primary drain, 2.7 psig in the intermediate purge cavity, and 0.7 psig in the turbine drain. The progressive decrease in the pressure levels indicated that the pressure source originated in the primary seal drain.

(C) The data indicated that the most probable cause of the failure was ignition of the Bearium B-10 intermediate seal segments on the primary drain side, followed by complete combustion of the intermediate and turbine seals with the gaseous oxidizer that had leaked through the primary seal and accumulated throughout the seal area. The greater amount of burning in the primary drain was caused by the fire starting in that area and from the combustion being supported by the additional oxidizer which was leaking through the primary seal. The fire apparently burned out after approximately 10 seconds because of depletion of the oxidizer in the seal drain area.

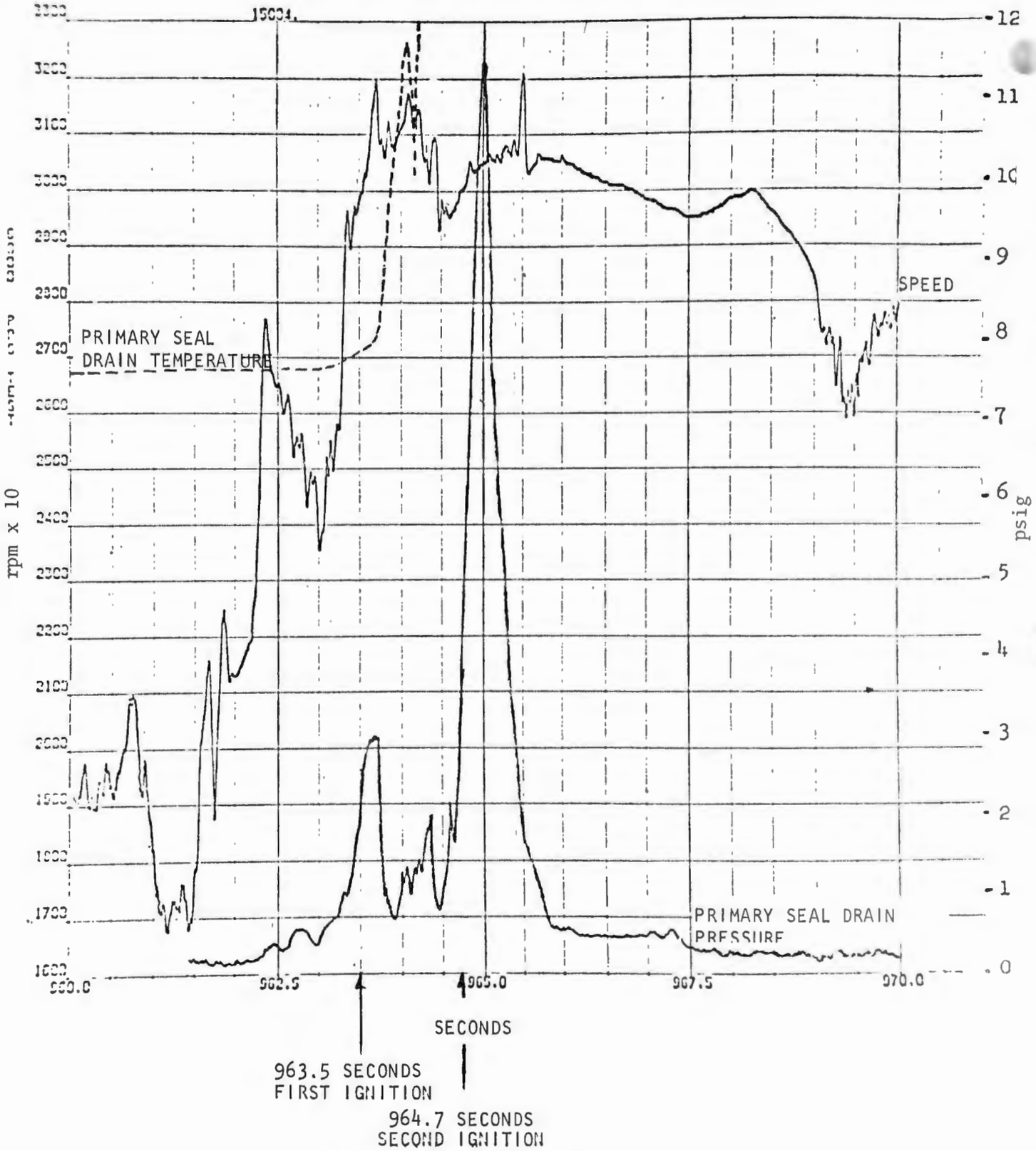

Figure 191. Test 004 Failure, Fifth Start (U)

(C) Ignition of the Bearium B-10 segments in a highly oxidizing atmosphere was possible because of the heat generation between the rubbing surface of the segments and the rotating mating ring. The excessive shaft deflection was believed to have caused a high load on the rubbing surface of the segments, which resulted in a surface temperature sufficiently high to ignite the Bearium in the oxidizing atmosphere.

(C) The conclusion was that the Bearium B-10 segmented intermediate seal was the cause of the failure because of the high drag torque and the torque variation of the segmented-type seal. The intermediate seal design was changed to a floating ring-type design fabricated from AmCerMet 701-65 composite material. The seal design is shown in Fig. 173 and was used for the subsequent main bearing and seal test.

e. Test 005 (5 Starts for 120 Seconds)

(C) Replacement tester components were fabricated, the tester reassembled with the new intermediate seal design, and test 005 was conducted. The tester was chilled down by flowing LN_2 through the tester jacket. Liquid fluorine was then flowed into the tester, and an attempt was made to bring the speed up to idle (approximately 5000 rpm) by slowly pressurizing the drive turbine. The plan was to start the test from idle speed after instrumentation and redline verification. The turbine pressure was increased, and the speed pickup instrumentation did not indicate any rotation; however, the Bentley scope showed that there was rotation for approximately 60 seconds; then the rotation stopped and restarted three times during a period of approximately 60 seconds.

(U) The test was terminated when the oxidizer outlet temperature suddenly increased and pegged off the chart in excess of -200 F. At approximately the same time, the oxidizer inlet pressure started oscillating, and there was a flash of fire at the tester. The Bentley and accelerometer scopes did not show any abnormal deflection or vibration. The oxidizer flow was approximately 2 gpm during rotation.

(C) Posttest inspection of the tester assembly revealed that two holes were burned through the housing at the primary seal drain (Fig. 192). The shaft was locked solid (Fig. 193). There was a heavy deposit of fluoride coating in the oxidizer outlet port.

(C) Disassembly of the tester revealed the following:

1. Turbine seal and mating ring were in good condition.
2. Intermediate seal and mating ring were in good condition except for slight burn damage and a crack in the oxidizer side ring.
3. Primary seal housing was burned through to the drain cavity for approximately 90 degrees at one location, and the internal portion of the seal was burned away. The rubbing surface of the mating ring was not burned and approximately 270 degrees of the seal nose was still intact. The portion of the mating ring under the seal nose was protected from burning; therefore, the fire did not start at the seal rubbing surface.
4. The turbine end bearing was completely consumed by the fire, except for a portion of the outer race.
5. The tester shaft was completely burned away and separated in the area of the turbine end bearing. The rear portion of the shaft was fused to the turbine end bearing retainer nut with molten metal.
6. The tester housing was partially burned away in the area of the oxidizer inlet at the turbine end bearing and at the primary seal drain.
7. The pump end bearing was in good condition, except for one area at the cage which was damaged by burning.

(C) Analysis of the damaged hardware indicated that the fire started in the rear bearing and burned the shaft away in both directions from the bearing, finally burning a hole under the primary seal mating ring which allowed the seal and drain area to be damaged by fire. The majority of the burning occurred after cutoff while the shaft was stationary. The burning apparently continued until the available oxidizer was consumed.

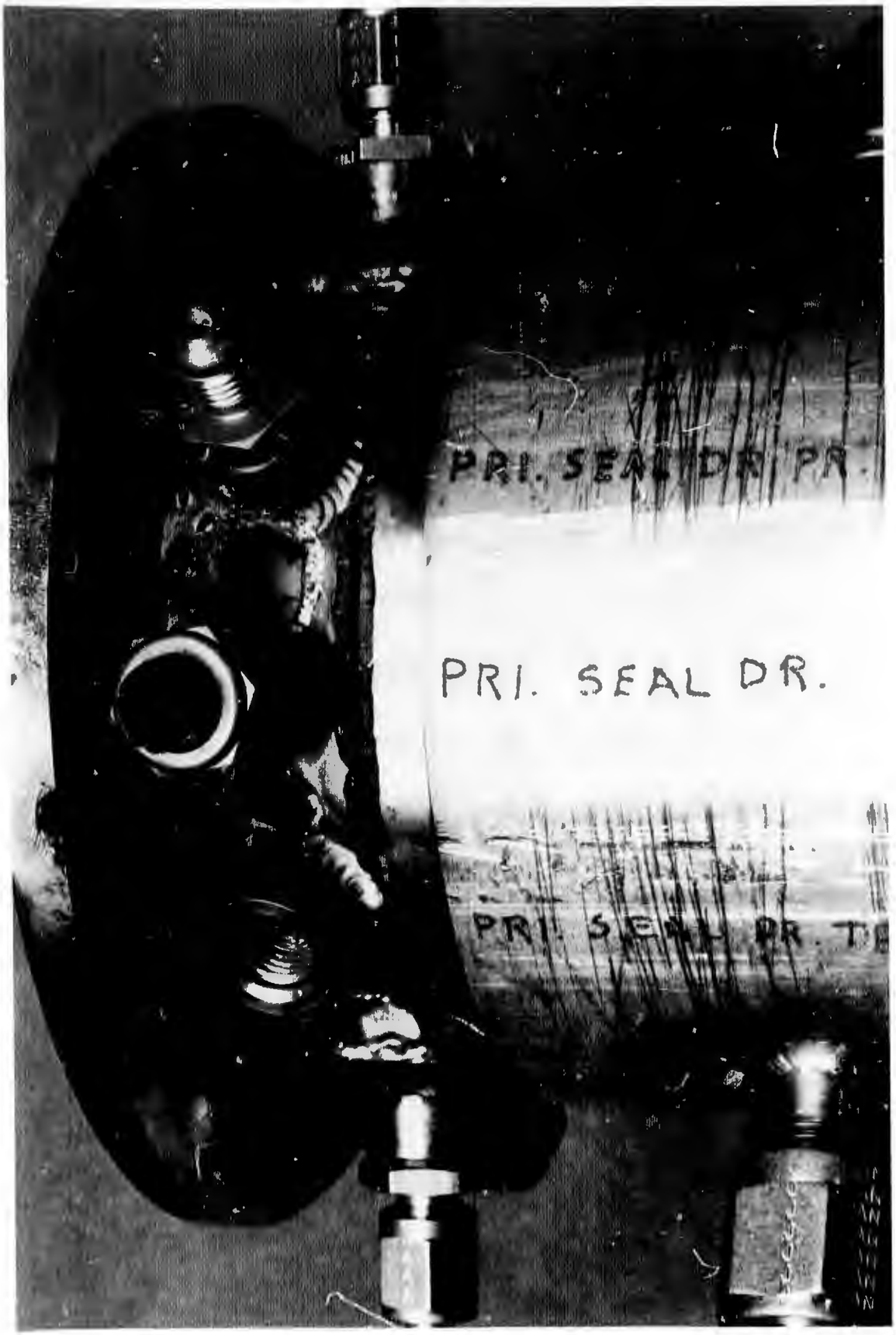

1EH95-11/20/69-C1D

Figure 192. Main Tester Damage--View of Outer Housing Seal End (U)

1EH95-11/20/69-C1B

Figure 193. Main Tester Damage--View of Seal Cavity (U)

(C) The most probable cause of ignition in the bearing was a piece of foreign material wedging between the bearing cage and outer race, causing the cage to seize and stop rotating with the balls. The cage seizure would cause the balls to skid on the inner race, and the resultant frictional heat could cause ignition. The skidding balls also could cause an intermittent high torque, which would explain why the tester stopped and restarted just prior to the fire. This conclusion is substantiated by a similar incident on another program, where the test was terminated due to a torque increase before ignition occurred (Ref. 6).

(U) Also, the possibility existed that friction between the balls and cage pockets either caused excessive heat generation at the ball-cage contact or caused the balls to skid on the inner race, and resulted in ignition due to frictional heat. Previous test experience indicates that this failure mode is unlikely.

(U) Program analysis showed that repair of the tester for further main bearing and seal testing was impractical; therefore, all remaining testing was directed to the secondary bearings and seals.

11. SECONDARY BEARING AND SEAL DYNAMIC TEST RESULTS

(C) The secondary bearing and seal tester was run for six tests with liquid fluorine for a total time of 241 seconds. The secondary bearing and seal testing is summarized in Table 36. The bearing and seal test hardware summary is shown in Table 37. The test data are summarized in Table 38.

(U) The following dynamic tests were performed on the secondary bearing and seal program.

a. Test 005, 125 Seconds (11-10-69)

The test objective was 5 minutes of operation at 75,000 rpm to check out the tester and drive operation. The speed was increased gradually up to 21,000 rpm, then ramped quickly to 66,000 rpm, increased gradually to 72,000 rpm within 90 seconds, and was constant for the remainder of the test.

TABLE 37

SECONDARY BEARING AND SEAL TEST HARDWARE SUMMARY (U)

Test No.	Time, seconds	Primary Seal			Intermediate Seal			Turbine Seal			Bearings	
			S/N	Condition	Type	S/N	Condition	Type	S/N	Condition	Set No.	Condition
005	125	AL_2O_3 Spray 80-5533 versus Al_2O_3	CR1	(1) Nose Chipped and broken	BaF_2-CaF_2 floating gap 80-5534X versus BaF_2-CaF_2	CR1	(1) ID worn out of round	Carb P5N 80-5535 versus Chrome	CR1	Nose chipped, bellows cracked	1	(2) Rough, but not failed
001	6	↓	CR2	Satisfactory	↓	CR5	Satisfactory	↓	CR10	Satisfactory	2	Satisfactory
002	0		CR2	Satisfactory		CR5	Satisfactory		CR10	Satisfactory	2	Satisfactory
003	20		CR2	Face distorted (relapped)		CR5	Satisfactory		CR10	Nose chipped, bellows cracked	3	Satisfactory
004	71		CR2	(1) Nose worn at outer edge		CR5	Satisfactory		CR11	Nose chipped, bellows cracked	3	Satisfactory
005	19		CR3	Satisfactory		CR5	Satisfactory		CR6	Nose chipped, bellows cracked	4	Satisfactory

(1) Damaged due to excessive shaft deflection
(2) Damaged due to being run unloaded

CONFIDENTIAL

TABLE 38

SECONDARY BEARING AND SEAL TEST DATA SUMMARY (U)

Parameter	Test Number 001	002	003	004	005
Date	1-5-70	1-13-70	1-24-70	1-19-70	2-6-70
Data Slice Time, seconds	20.483	No rotation	32.275	80.910	20.013
Turbine GN_2 Temperature, F	-9		-29.2	-45	-33
Primary Seal Temperature, F	-2.7		-9.7	-10	-8
Turbine Seal Temperature, F	2.6		9.2	12	10
Oxidizer Outlet Temperature, F	-232		-298	-291	-289
Oxidizer Inlet Temperature, F	NG		-304	--	-307
Primary Seal Drain Temperature, F	-135		-205	-218	-180
Turbine Seal Drain Temperature, F	-135		-140	-144	-160
Intermediate Seal Purge Temperature, F	-50		-55	-55	-45
Torque, in.-lb	3		2.7	3.6	--
Oxidizer Inlet Pressure, psig	79.6		319	324	NC
Intermediate Seal Purge Pressure, psig	42.7		47.5	55.5	64
Primary Seal Drain Pressure, psig	1.0		2.2	9.0	1.4
Turbine Seal Drain Pressure, psig	0.7		0.8	1.2	1.3
Turbine Seal Cavity Pressure, psig	37.7		50.7	44.2	41
Oxidizer Outlet Pressure, psig	55.3		56.3	60.4	58
Load Bellows Pressure, psig	112		128	209	213
Turbine GN_2 Pressure, psig	2.9		4.0	11.6	17.4
Intermediate Seal Purge Flow, scfm	5.5		6.0	7.0	9.2
Bearing Cavity Pressure, psig	51.2		47.1	40.7	47
Primary Seal Leakage, scfm	Nil		Nil	1.5	Nil
Turbine Seal Leakage, scfm	Nil		Nil	Nil	Nil
Speed, rpm	1161		21,700	47,000	61,380
Oxidizer Flow A, gpm	0.9		1.06	1.08	1.09
Oxidizer Flow B, gpm	NG		NG	1.2	1.2

TABLE 36

SECONDARY BEARING AND SEAL TEST SUMMARY (U)

Test No.	Date	Number of Starts	Time, seconds	Speed, rpm	
005	11-10-69	1	125	72,000	Bearings unloaded, damaged bearings and seal
001	1-5-70	1	6	1,161	Satisfactory rotating passivation test
002	1-13-70	--	--	--	High and erratic inlet pressure. No rotation
003	1-24-70	2	20	22,350	Improper turbine pressure adjustment and bearing cavity pressure redline
004	1-29-70	1	71	47,000	Excessive shaft deflection Damaged torquemeter
005	2-6-70	1	19	63,000	Excessive shaft deflection. Broke turbine and tester shafts
				1	CONFIDENTIAL

(U) The test was terminated prematurely due to loss of the Bentley shaft deflection transducer signal. The signal was lost when the shaft rubbed and broke the transducer, which had been set at 0.030-inch clearance.

(C) Inspection of the tester assembly revealed that the tester shaft was loose and could be moved approximately 0.030 inch in the radial direction. Pressurizing the bearing load piston did not affect the shaft radial clearance; therefore, the tester was disassembled for inspection with the following results:

1. The primary seal sprayed AL_2O_3 nose was chipped excessively around the OD edge, and approximately 30 degrees of the nose was broken off.

(C)

2. The primary seal sprayed AL_2O_3 mating surface was in good condition.
3. The intermediate seal was in good condition, except that the ID of the floating rings was worn out-of-round.
4. The intermediate seal BaF_2-CaF_2 coated shaft surface was worn away on one side (approximately 120 degrees arc).
5. The turbine seal carbon nose was chipped excessively around the OD edge and the bellows was cracked approximately 180 degrees at the lower ID plate weld.
6. The turbine seal chrome-plated mating ring was in good condition. The wear pattern showed excessive radial runout.
7. The bearings were in fair condition. The bearing race wear tract showed that the bearings were run unloaded.
8. The bearing load piston was stuck in the unloaded position due to AL_2O_3 from the primary seal wedging between the piston and housing.

(C) Investigation revealed that the bearings were unloaded due to the bearing cavity pressure being higher than the load bellows pressure. Because the bearings were an angular contact design which required preload to maintain alignment, the unloaded bearings allowed the tester shaft to rotate off center and wobble. Excessive shaft movement was believed to have caused the damage.

(U) The tester was rebuilt with new seals and bearings.

b. Test 001 (6-Second Duration)

(C) The test objective was to accomplish a rotating passivation and static fluorine flow test. Fluorine was flowed through the tester for 6 seconds with shaft rotation at 1160 rpm maximum. The fluorine flow was then continued for another 5 minutes.

(U) The test objective was satisfactorily accomplished. The tester was disassembled, and the hardware was in good condition. The tester was reassembled with the same seals and bearings.

c. Test 002 (No Rotation)

(C) The test objective was a 1-minute checkout at 20,000 rpm with a posttest inspection. The test was terminated after approximately 8 minutes of fluorine flow through the tester due to high and unstable fluorine inlet pressure. No rotation occurred.

(C) Disassembly of the tester revealed a residue deposit from an apparent reaction in the area of the fluorine inlet passage through the primary seal. Machining burrs were found at the housing fluorine passage inlet. A piece of the Inconel burr was suspected to have broken loose and lodged in the seal passage, then ignited and burned.

(U) The burrs were removed from the passage, and the parts were cleaned. The tester was reassembled with the same hardware, except that new bearings were installed because there was no assurance that all burr particles could be removed from the bearings.

(C) The high inlet pressure (200 psig), shown in Table 38 for this test, was determined to be normal for liquid flow conditions. The erratic and unstable pressure was apparently caused by ignition of a small burr in the fluorine inlet passage.

d. Test 003 (20-Second Duration)

(C) The test objective was a 1-minute checkout at 20,000 rpm with a posttest inspection. The test was terminated by the automatic overspeed device when the speed exceeded the 20,000-rpm redline and reached 22,350 rpm maximum due to the drive turbine GN_2 pressure adjustment.

(C) An attempt was made to restart the test; however, as the bearing cavity pressure was being adjusted to 50 psig, the cavity pressure suddenly spiked from 47 to 105 psig while the fluorine inlet pressure was constant at 320 psig. The test was terminated to inspect the facility bleed and tester for a flow restriction.

(C) Disassembly of the tester revealed the following:

1. The bearings were in good condition.
2. The primary seal Al_2O_3 face was distorted out-of-flat (ID higher than OD).
3. The primary seal mating surface was out-of-flat (higher at OD), but otherwise in good condition.
4. The intermediate seal and shaft surfaces were in good condition.
5. The turbine seal carbon nose was chipped excessively around OD edge, and the bellows was cracked at the lower ID plate weld.

(C) Inspection of the tester fluorine passages and facility fluorine bleed did not reveal any discrepancy that would explain the bearing cavity pressure spike.

(U) The tester was reassembled with the same hardware, except the primary seal face and mating surface were lapped flat and a new turbine seal was installed.

e. Test 004 (71-Second Duration)

(C) The test objective was a 1-minute checkout at 75,000 rpm with a posttest inspection. The tester speed was increased gradually up to 24,000 rpm, then an attempt was made to accelerate quickly to 50,000 rpm to avoid dwelling in the critical speed region; however, the drive turbine GN_2 pressure could not be increased quickly enough and excessive shaft deflection occurred. The test was terminated after 71 seconds of rotation due to a sudden speed drop from 45,000 to 31,500 rpm while the drive turbine GN_2 pressure was being increased. The speed drop was apparently caused by excessive shaft seal rubbing due to shaft deflection.

(C) The tester was disassembled for inspection with the following results:

1. Turbine seal carbon nose was chipped excessively around the OD edge, and the bellows was cracked at the lower ID plate weld.

(C) 2. Turbine seal mating ring wear pattern showed excessive radial runout.

3. The intermediate seal and mating surface were in good condition. The measured wear was 0.0002 to 0.0005 inch.

4. The primary seal AL_2O_3 nose was worn off approximately 0.002 inch lower around the outer surface. The contact pattern at the inner surface was irregular and had 0.002 to 0.004 inch of wear.

5. The primary mating surface appeared to be in good condition.

6. The bearings were in good condition.

(U) The torquemeter output shaft was bent due to excessive deflection of the tester shaft.

(U) The tester was reassembled with a new primary seal, new turbine seal, new bearings with same cages, and the same intermediate seal.

(U) The tester was installed on a short housing mount with the air fan blower and no torquemeter.

f. Test 005 (19 Second Duration)

(C) The test objective was a 5-minute checkout at 75,000 rpm with a posttest inspection. The test was terminated after 19 seconds of rotation by the automatic cutoff device on the intermediate seal purge pressure redline. The purge pressure dropped to 20 psig (minimum redline is 35 psig) due to the seal rings being unseated by excessive shaft deflection. At the same time, the Bentley transducer signal indicated excessive shaft deflection, the tester accelerometer signal indicated high vibration levels, and the speed was not responding to the drive turbine pressure increase. The test was terminated after 19 seconds of operation. Inspection of the tester and drive assembly revealed the following:

1. The drive turbine shaft was broken off flush with the mounting plate.

2. The tester shaft was broken off at the turbine seal mating ring shoulder.

(C)

3. The Bentley transducer was broken due to rubbing.
4. The speed pickup transducer was broken due to rubbing.
5. The turbine carbon seal was broken and the seal ID had been rubbed by the shaft. The mating ring wear pattern showed excessive radial runout.
6. The turbine seal carbon nose was chipped around the OD edge, and the bellows was broken all around at the lower ID plate weld. The mating ring wear pattern showed excessive radial runout (Fig. 194).
7. The intermediate seal rings and the shaft surface were in good condition, except the seal antirotation slots were bent slightly by the excessive shaft deflection (Fig. 195).
8. The primary seal and mating ring surfaces were in good condition. The AL_2O_3 surface was polished with no apparent wear (Fig. 196 and 197).
9. The bearings were in good condition (Fig. 198).

(C) Analysis of the Bentley displacement transducer high-frequency data revealed that the maximum peak-to-peak shaft displacement at the Bentley location (tester end of the air fan coupling) was 0.050 inch at 60,000 rpm just prior to the failure. The excessive shaft deflection resulted in failure of the tester shaft and the turbine shaft due to the high cyclic loading.

(U) Continued testing would require modification of the tester drive equipment and, therefore, the above test was the final test of the program.

12. CONCLUSIONS RESULTING FROM BEARING AND SEAL TESTING

(U) Dynamic testing was limited due to difficulties with the tester equipment. While sufficient durations were not accumulated at design conditions to demonstrate feasibility and durability of the bearings and seals, some favorable test results were obtained.

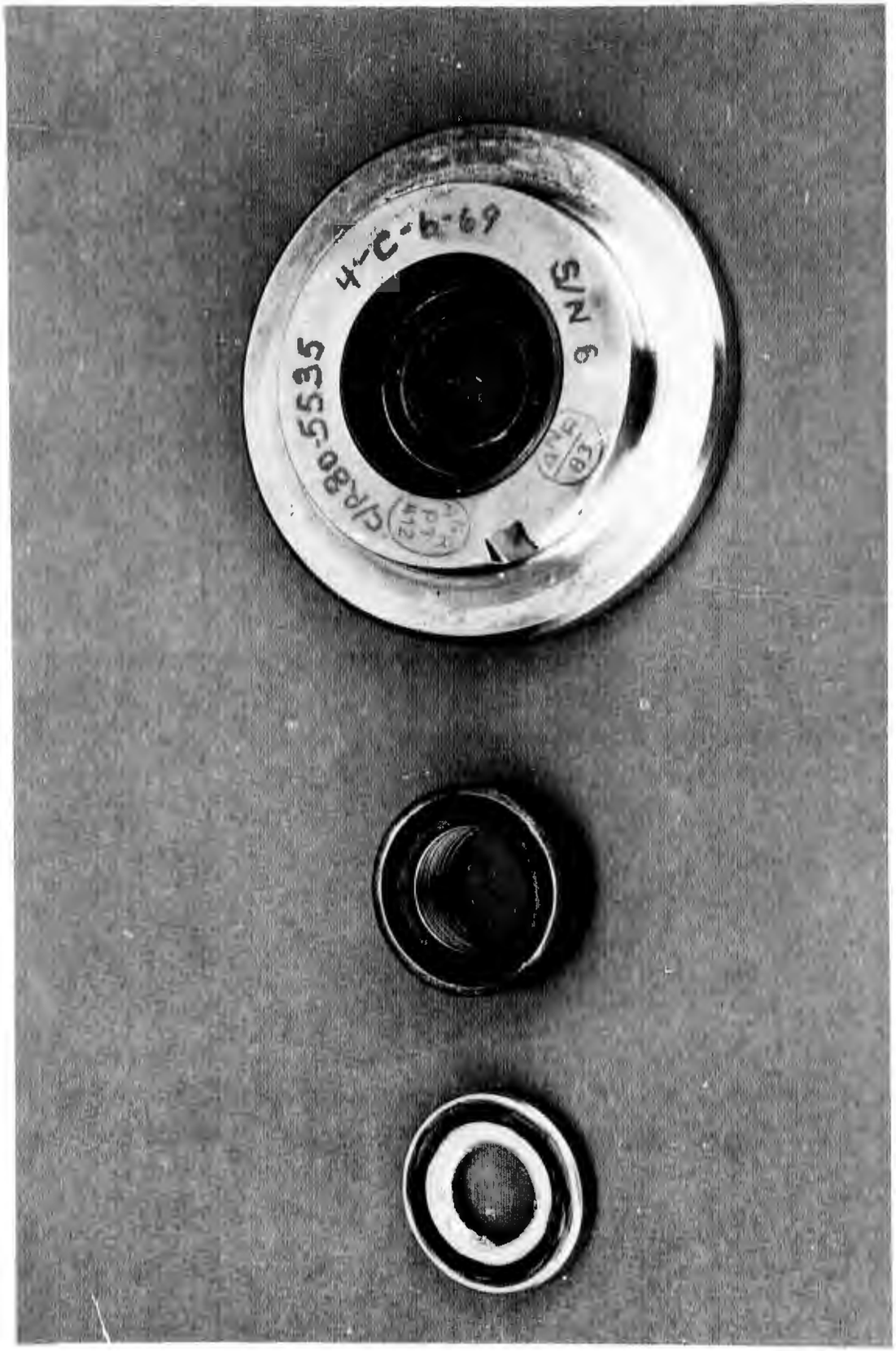

1EH95-2/11/70-C1D

Figure 194. Secondary Pump Turbine Seal After Test 005 (U)

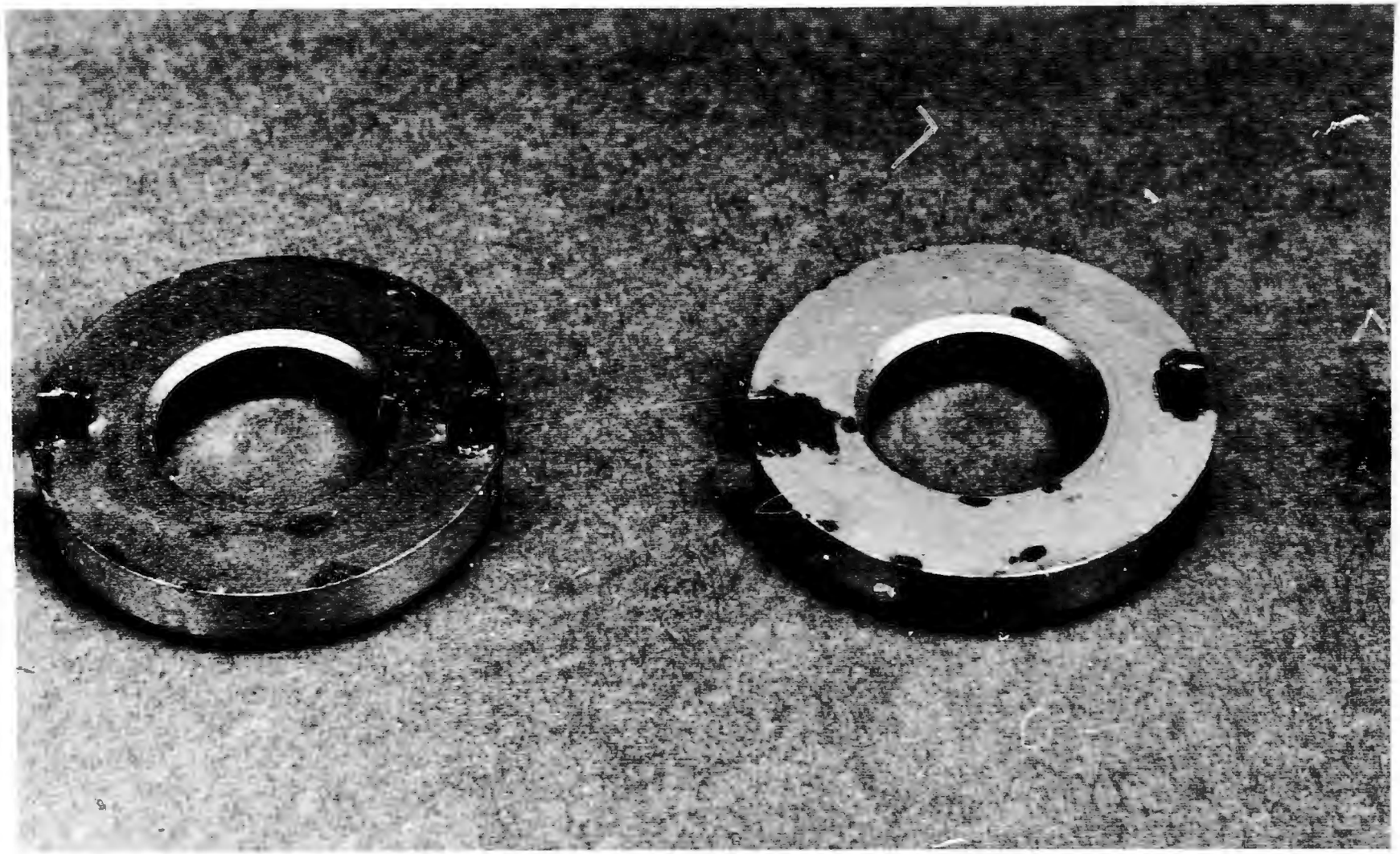

1EH95-2/11/70-C1E

Figure 195. Secondary Pump Intermediate Seal Rings After Test 005 (U)

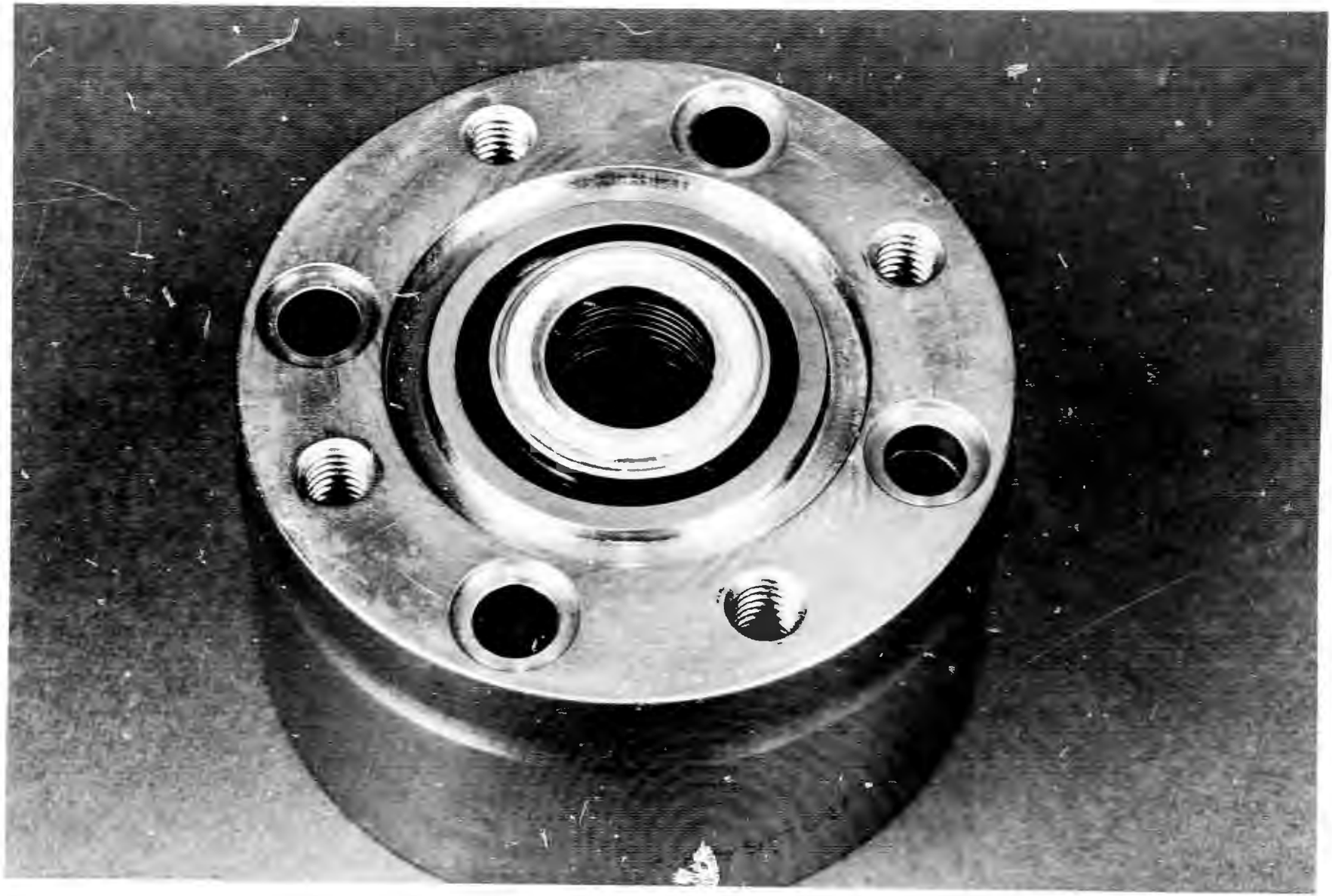

1EH95-2/11/70-C1B

Figure 196. Secondary Pump Primary Seal Assembly After Test 005 (U)

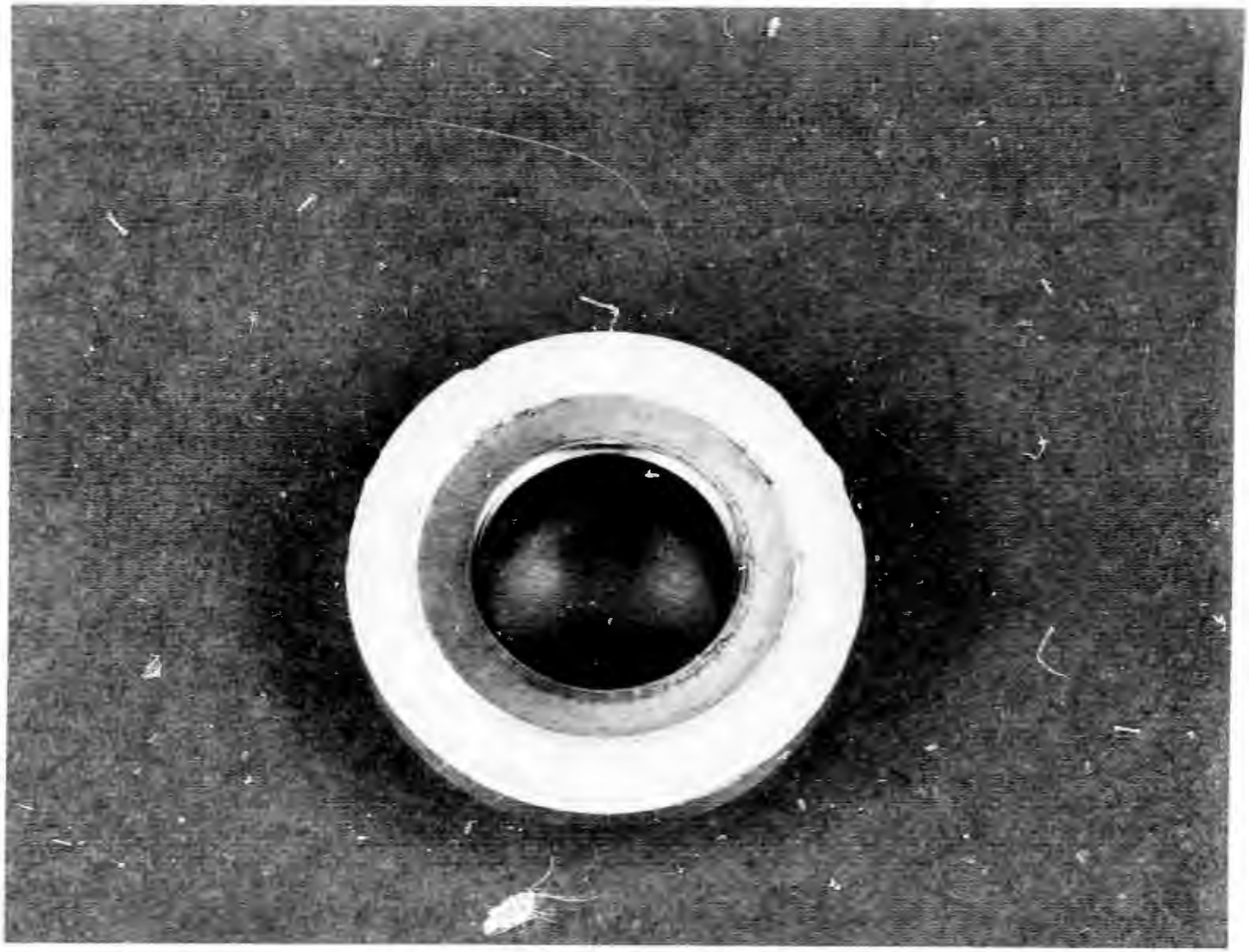

1EH95-2/11/70-C1c

Figure 197. Secondary Pump Primary Seal Mating Ring After Test 005 (U)

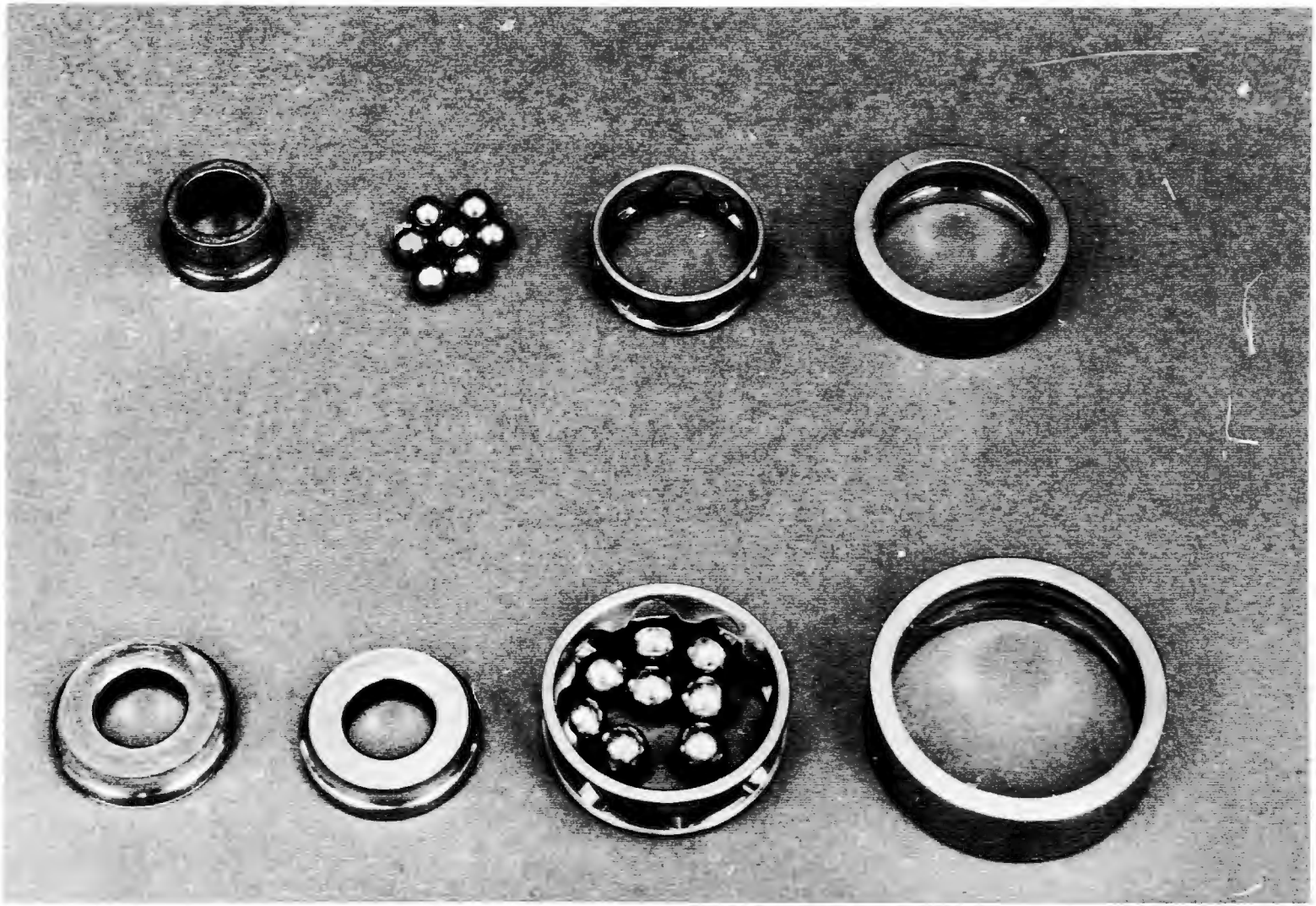

1EH95-2/11/70-C1G

Figure 198. Secondary Pump Bearings After Test 005 (U)

(C) Except where damage attributed to other causes occurred, the bearings were in satisfactory condition after each test, in spite of overspeed, lack of coolant flow, and abnormal loading conditions. Insufficient testing was accomplished to demonstrate durability; however, the bearings were run for short periods at full load and speed without failure.

(C) The primary fluorine seal with the plasma-sprayed AL_2O_3 nose performed satisfactorily during the limited testing at normal operating conditions. Insufficient testing was accomplished to establish wear rates and demonstrate durability; however, the sealing efficiency was satisfactory. The Kentanium K162B and solid AL_2O_3 insert configurations leaked excessively at high pressure due to thermal distortion of the seal face; however, the wear life was expected to be better, and the higher leakage may be acceptable.

(C) The AmCerMet 701-65 floating-ring purged intermediate seal proved to be very effective for the separation of the oxidizer and turbine drain cavities. The seal survived extremes of operation with very little damage and performed very satisfactorily. The rubbing characteristics of the material against the BaF_2-CaF_2 coating mating surface were satisfactory. The Bearium B-10 segmented seal was unsatisfactory due to high torque and excessive heat generation which resulted in ignition of the material.

(C) The main turbine bellows face-type carbon seal performed satisfactorily during the limited testing; however, the secondary turbine seal bellows failed after short periods on all the seals tested. The failure mode appeared to be fatigue of the bellows plate adjacent to the weld due to resonant vibration in the bellows assembly which was excited by running the seal in a dry atmosphere of GN_2. Nonlubricated seal faces will initiate a resonance frequency vibration due to a stick-slip condition (difference between static and dynamic coefficient of friction) at the rubbing face. The secondary seal did not have vibration dampers due to the small size and limited space available. The recommended corrective action would be to redesign the seal to add a vibration damper similar to the one used on the main seal. Sufficient lubrication would likely be present in the actual turbine from the hot-gas products to prevent the stick-slip condition.

(U)

REFERENCES

1. AFRPL-TR-67-214, Advanced Thrust Chamber for Space Maneuvering Propulsion, H. G. Diem and R. P. Pauckert, July 1967.

2. NASA SP3037, Fluorine and Fluorine-Oxygen Mixtures in Rocket Systems, Schmidt, H. W.

3. AFRPL-TR-68-18, Improvement of Bombs and Pulse Guns as Combustion Stability Rating Devices, Rocketdyne, a division of North American Rockwell, 1968.

4. AFRPL-TR-67-280, Final Report, Advanced Cryogenic Rocket Engine Program, Aerospike Concept, Rocketdyne, a division of North American Rockwell, 1967.

5. AFRPL-TR-70-126, Advanced Maneuvering Propulsion Technology Program Interim Materials and Processes Report, R-8285, Rocketdyne, a division of North American Rockwell, Canoga Park, California, October 1970, CONFIDENTIAL.

6. Contract NAS3-11201, F_2 Lubricated Bearing Technology.

APPENDIX I

TEST FACILITIES

(U) Three test facilities were utilized during the AMPS program:

Victor Test Stand, Propulsion Research Area, Santa Susana Field Laboratory--for 5-inch and 30-degree segment testing

Mike Test Stand, Propulsion Research Area, Santa Susana Field Laboratory--for oxidizer turbopump bearing and seal testing

B-4A Test Stand, Nevada Field Laboratory--for main thrust chamber testing

(U) Each of the facilities required some modification to meet the specific program requirements. The modifications and the description of the Victor and B-4A facilities are provided in the following paragraphs. A description of the Mike test stand was presented in the Oxidizer Turbopump Bearing and Seal section.

1. VICTOR TEST STAND

(U) The Victor test stand had been used for segment testing in previous programs involving LH_2 and LF_2. As a result, facility modifications for the main engine segment testing consisted primarily in providing the propellant capacity requirements. The modifications consisted of installation of a 2000-psig rating, LN_2-jacketed oxidizer tank, installation of an LN_2-jacketed, high-pressure, oxidizer propellant feed line with two 1-inch turbine flowmeters in tandem in the line, and installation of platinum resistance bulb temperature sensors. Also, a heater to provide 1000 F fuel to the injector was designed, fabricated, and installed in the hydrogen supply line.

(U) Figure I-1 is a schematic representation of the Victor test stand following the modifications. Figure I-2 shows the test stnad with the G_c contour thrust chamber installed.

a. Oxidizer Tank and Related Systems

(U) A high-pressure (2000-psi), 43-gallon fluorine tank was installed to fulfill the high-pressure requirements of this program. The tank is shown in the test stand schematic (Fig.I-1) and in the test stand photo (Fig. I-3).

(U) The oxidizer flowmeters originally selected for the program were 1-inch 50 RF pickup-coil-equipped meters, which according to manufacturer's (Fisher-Porter) specification, were capable of measuring flows from 0.3 to 15 lb/sec fluorine. Because of the special drag-free rotor design of RF flowmeters, an excellent flat response results over the entire calibration. This operation was believed to be ideal for the AMPS engine segment program, which required a wide range of oxidizer flows. Unfortunately, the first few runs made with these 1-inch 50 RF meters gave poor flowmeter recordings. The outputs were either intermittent or null. Other programs had similar problems when employing RF meters in cryogenic systems. Therefore, a dual change was made--(1) 1/2-inch flowmeters were used and (2) the RF coils were replaced with standard coils in these flowmeters so that they could operate as more dependable standard meters. In addition to the tandem 1/2-inch flowmeters, cavitating venturis were also used for flow measurement. The cavitating venturis also suppressed chamber pressure spiking during the test start transient.

(U) Oxidizer delivered to the test stand hardware must be kept at a uniform temperature. Changes in propellant temperature during a run will complicate flowrate calculations because of density transients. This occurred in several hot firings on Victor test stand. A warm "slug" of oxidizer build up in a section of unchilled line after approximately 2 seconds of

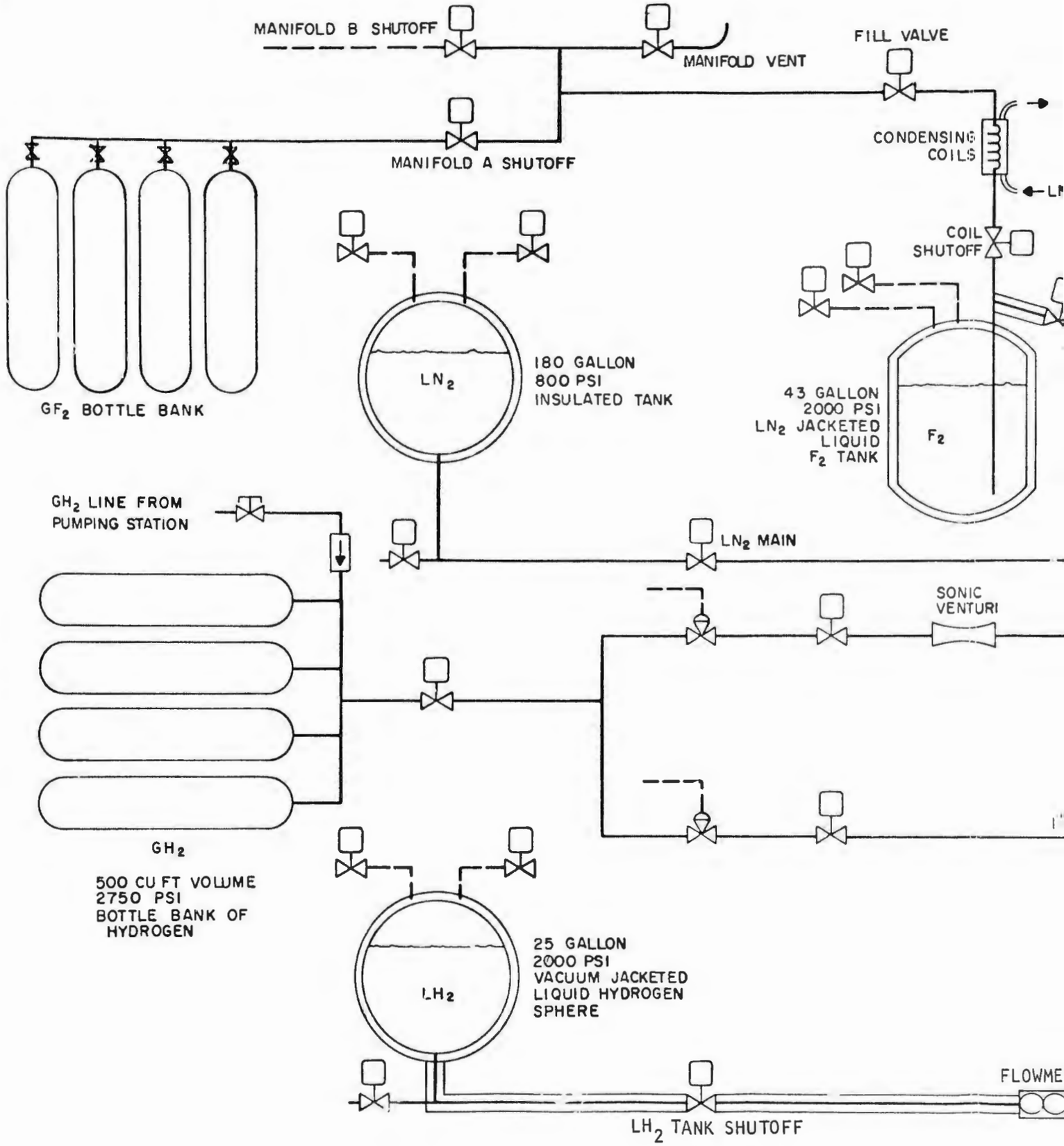
MANIFOLD B SHUTOFF
MANIFOLD VENT
FILL VALVE
MANIFOLD A SHUTOFF
CONDENSING COILS
COIL SHUTOFF
GF_2 BOTTLE BANK
LN_2
180 GALLON
800 PSI
INSULATED TANK
43 GALLON
2000 PSI
LN_2 JACKETED
LIQUID
F_2 TANK
F_2
GH_2 LINE FROM
PUMPING STATION
LN_2 MAIN
SONIC
VENTURI
GH_2
500 CU FT VOLUME
2750 PSI
BOTTLE BANK OF
HYDROGEN
LH_2
25 GALLON
2000 PSI
VACUUM JACKETED
LIQUID HYDROGEN
SPHERE
LH_2 TANK SHUTOFF

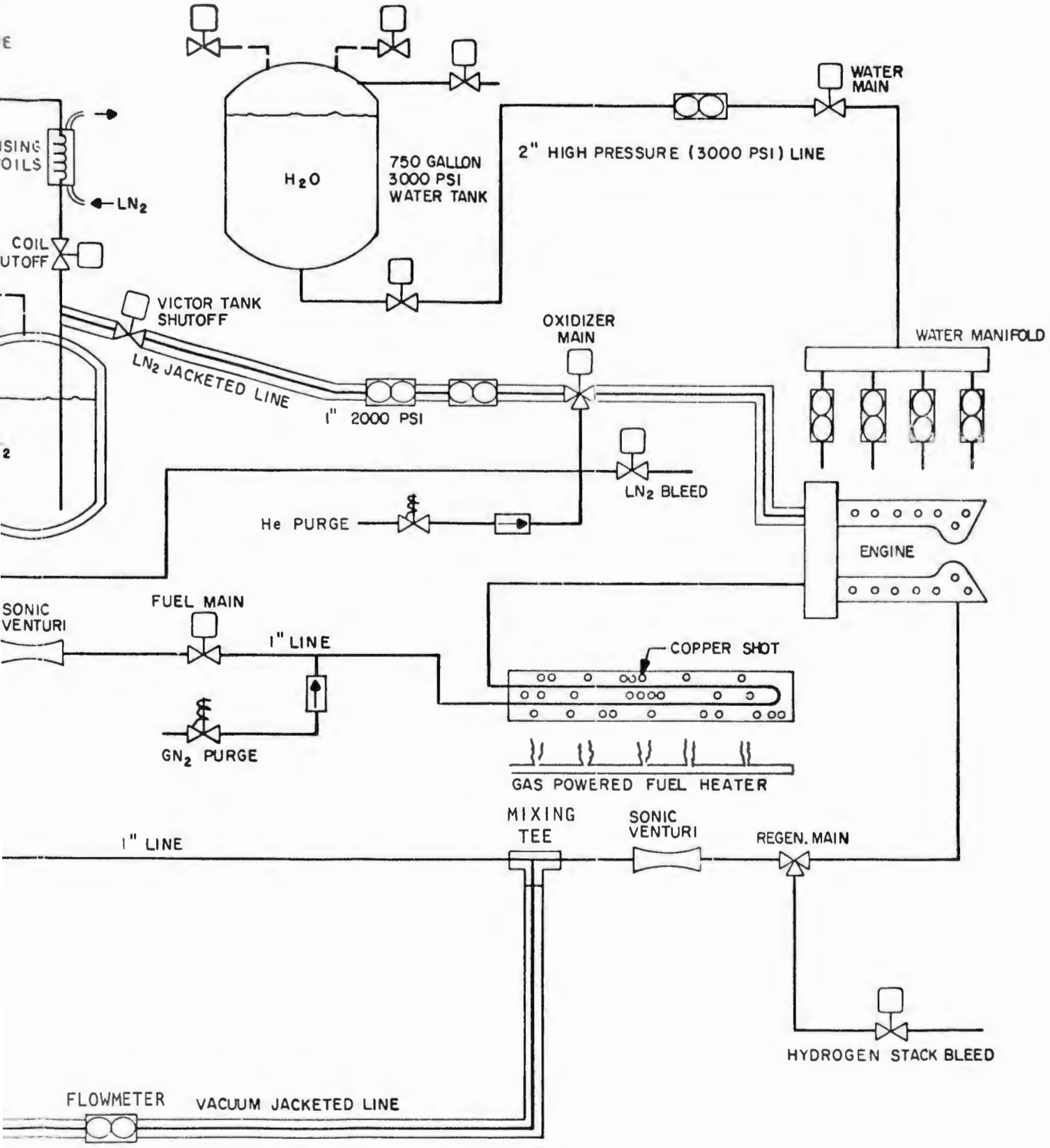

Figure I-1. Schematic Diagram of Test Stand Victor, PRA (U)

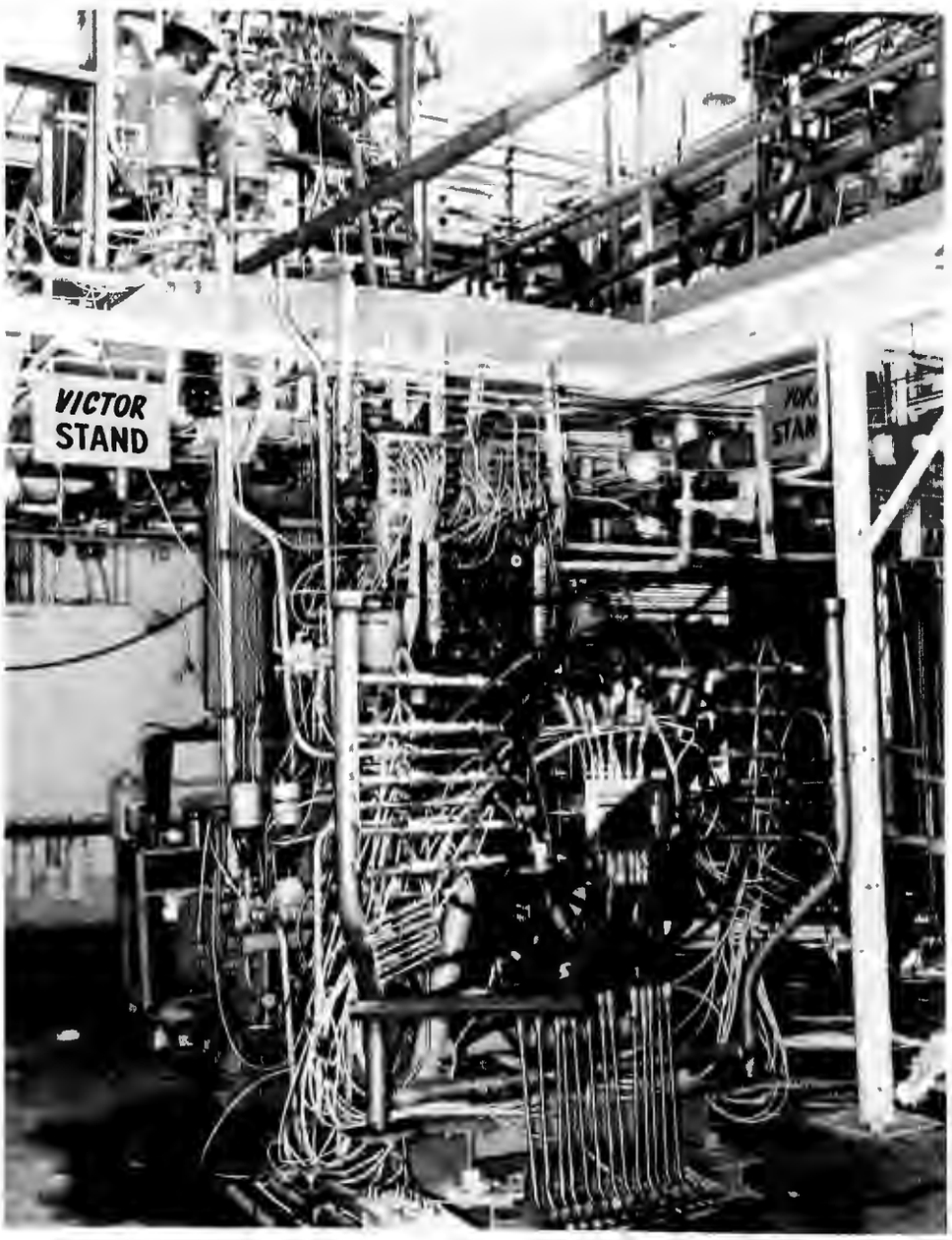

5AA21-1/5/68-S1C

Figure I-2. Victor Test Stand Installation With Solid-Wall Segment Installed (U)

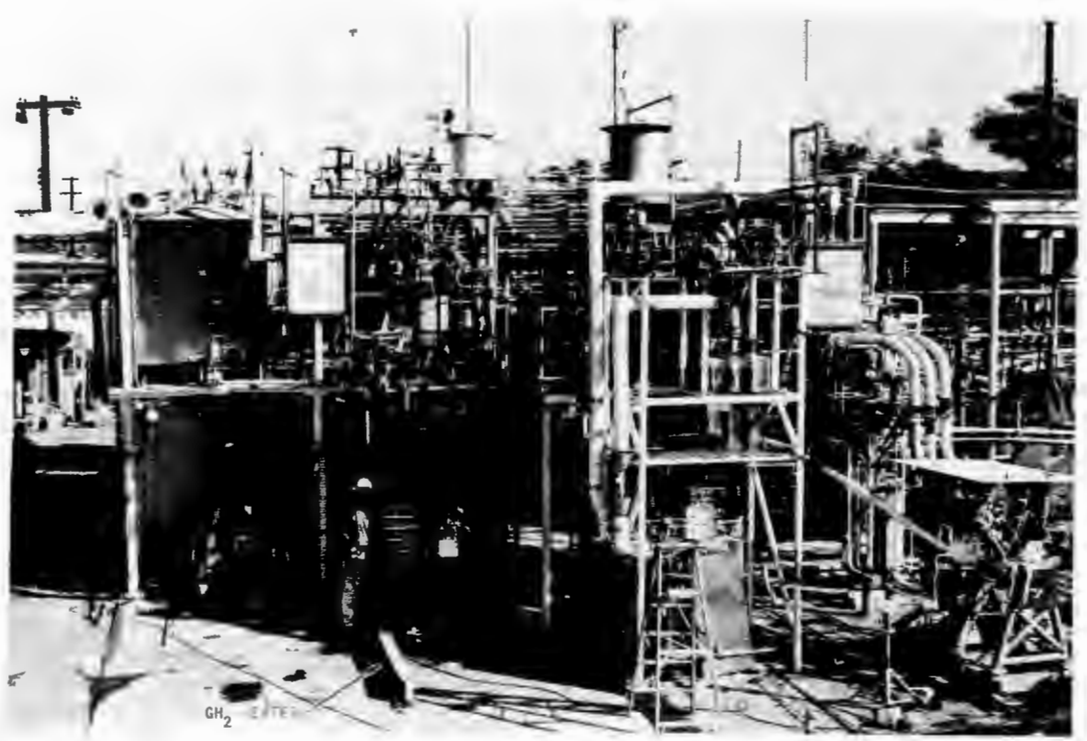

5AA21-1/5/68-S1B

Figure I-3. Victor Test Stand Showing Fluorine Tank and Hydrogen Heat Exchanger Installation (U)

(U) run duration. This warm slug of oxidizer reached the thrust chamber segment and affected the oxidizer flowmeters, oxidizer injection pressure, and chamber pressure. During system analysis, the conclusion was reached that this warm slug of oxidizer formed in the oxidizer tank shutoff valve, which was only partially chilled, and in the run tank dip tube, which was not chilled. This condition was slightly improved by completely jacketing the valve; however, the tank dip tube could not be economically modified. For this reason, the decision was made to place large-volume LN_2-jacketed run line downstream of these undesirable heat sinks to eliminate the warm oxidizer problem. This new line extended the steady-temperature run duration from 1 to 5 seconds and was installed after test 040.

(U) Some of the run data exhibited oxidizer injection pressure surges that occurred soon after oxidizer main valve opening as shown in Fig. I-4. To avoid possible hardware damage, a reduction in this surge was desirable. The magnitude of the pressure surge depended on the starting conditions.

(U) Previously, the oxidizer line from main valve to injector was chilled with liquid nitrogen, and then primed with liquid nitrogen just before oxidizer main valve opening. To attenuate the oxidizer pressure surge in the injector at starting, the run operating procedure was changed. To force out the liquid nitrogen used to chill the injector, a 2-second helium purge was introduced in the oxidizer main line between the stand oxidizer main valve and injector. This change provided a cavity for the liquid fluorine to fill during startup to avoid liquid fluorine ramming. This change was initiated after test 037.

(U) During prerun oxidizer line priming, some two-phase flow and flowmeter overspinning occurred. Recalibrations were performed on these flowmeters when possible. A cavitating venturi in the oxidizer line provided a backup oxidizer flow measurement.

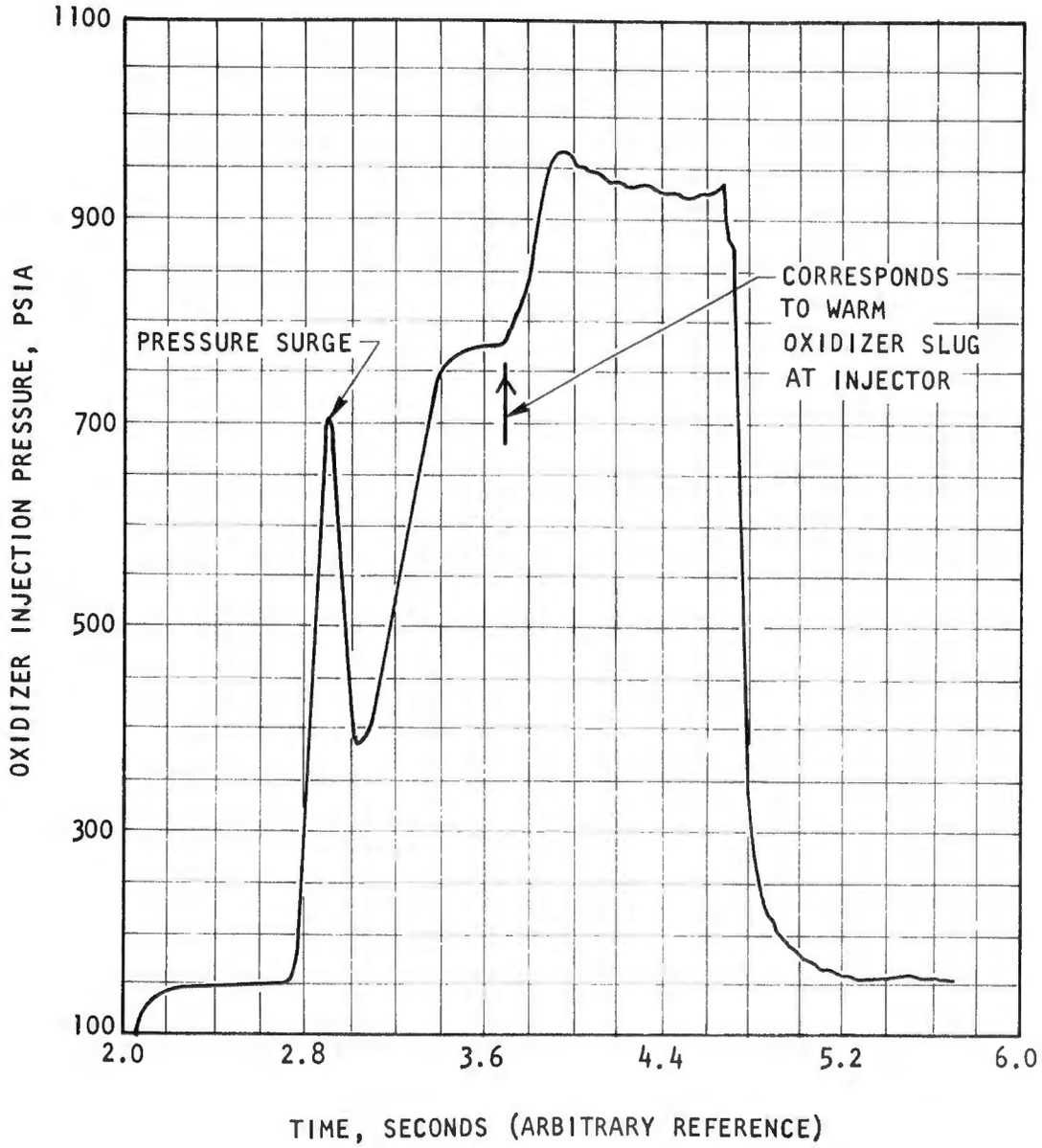

Figure I-4. Oxidizer Injection Pressure During Start of Test 36 (U)

(U) During tests 047 through 050, the performance data indicated that either one or both of the propellants used was contaminated. Samples were taken of the propellants in storage following test 050. The posttest sample of (test 050) oxidizer contained 6.8 percent (by weight) air. Because the majority of the air content is nitrogen, the presence of this air percentage could have a significant effect on injector performance. Fuel purity was found to be satisfactory. There was no way of determining the actual content of the oxidizer used during the individual tests in question as no samples were taken during the test period. The practice has been to sample the delivered oxidizer on a spot basis only. The frequency of these spot checks depends on the rate of use and uniformity of delivery source.

(U) The impurity content on the tests in question may not have been the same, and possibly some preferential sampling may have occurred that may not be completely representative of the total delivered oxidizer.

(U) Because the oxidizer storage system is maintained at pressures above atmospheric pressure, the conclusion was that the air was received in the oxidizer as delivered. All storage bottles suspected of contamination were removed from the system.

b. Fuel System

(U) The GH_2 was stored in a bottle bank that was filled on demand by a remote pumping station. The high-pressure (2000-psi) 25-gallon LH_2 tank was used for regenerative-cooling tests. A set of sonic venturis, with throat diameters of 0.1, 0.12, 0.14, and 0.16 inch, was used to measure gas flowrates. LH_2 flowrates were measured by a turbine flowmeter and a subsonic venturi in series.

c. Hydrogen Heat Exchanger

(U) A heat exchanger was required to heat ambient GH_2 for nonregeneratively cooled segment tests, up to 1000 F, which was the main thrust chamber design fuel inlet temperature. The original heat exchanger used in previous programs consisted of a packed 1-inch pipe wrapped with a nichrome heater. This heat exchange was not adequate for the AMPS program because of the higher hydrogen flowrates required. Thus, a new heat exchanger consisting of a 12-foot, 2-1/2-inch-diameter, schedule 80 pipe and packed with 100 pounds of 3/8-inch-diameter steel shot was fabricated. Because the test area was not equipped with adequate electrical power for a heater, the new heat exchanger incorporated gas heating. This gas-powered heater is shown in Fig. I-3. To operate the heater, the 2-1/2-inch pipe and packing was brought up to temperature (1000 F) by heating with a GH_2 burner. Then, the scheduled hot firing was performed with a GH_2 lead. With an adequate fuel-to-oxidizer lead, the fuel temperature measured downstream of the heat exchanger and that measured inside the injector fuel manifold reached steady state in approximately 2 seconds. On occasions, a shortened fuel lead was preferred, thus the fuel had to be overheated to compensate for the resulting transients.

d. Water-Coolant System

(U) The water-cooled segment hardware (G_c contour has 13 coolant passages; K contour has 17) each required 1 to 2 lb/sec coolant. A high-pressure, 750-gallon water tank furnished the required water through a 2-inch line plumbed to the stand. From this line, thirteen 1/2-inch flex hoses were plumbed to the thrust chamber (Fig. I-2). To determine heat flux in the thrust chamber during hot firings, the coolant flowrate and temperature rise was measured. Therefore, a separate coolant feed line, flowmeter, and differential thermocouple was recorded on the Beckman Data Acquisition System. Pressure measurements at four of the coolant passage discharge ports were made to determine the boiling point of coolant for wall temperature determinations.

e. Special Instrumentation

(U) High-frequency chamber pressure readings were made with a Kistler model 614A helium-bleed rocket transducer, which utilized a helium-gas-filled passage to transmit both static and dynamic pressures to a protected, acceleration-compensated, miniature quartz element. Helium flow was metered by a preadjusted internal orifice in the gage. The gas flowed around the pressure sensor and through the small passage at the conical end of the adapter. This helium flow extended the frequency response of the pressure measurement from near dc to over 10,000 cps, while simultaneously providing the necessary cooling for local heat fluxes up to 30 Btu/in.^{2}-sec.

2. B-4A TEST STAND

(U) The B-4A test stand modification was quite extensive and involved all facility systems. An overall view of the B-area test facility is presented in Fig. I-5. The B-4A test position is shown in more detail in Fig. I-6 and I-7. Figures I-8 and I-9 show the interiors of the altitude capsule with respect to the engine diffuser and thrust-measuring system.

a. Oxidizer System

(U) The run tank for the B-4A test stand was a 360-gallon, 2000-psi LN_2-jacketed tank. Significant design modifications of the tank included the addition of an LN_2 jacket, a jacketed dip tube, and enclosure of the tank in a polyurethane insulation jacket. The requirement of the jacket on the dip tube was the result of an investigation during the segment test program at Victor test stand, which revealed the probable source of warm slugs of oxidizer was the uninsulated dip tube in the Victor test stand run tank (Ref. Appendix I, 1.0, a).

6RE11-10/29/69-R1

Figure I-5. B Area Test Facility, NFL (U)

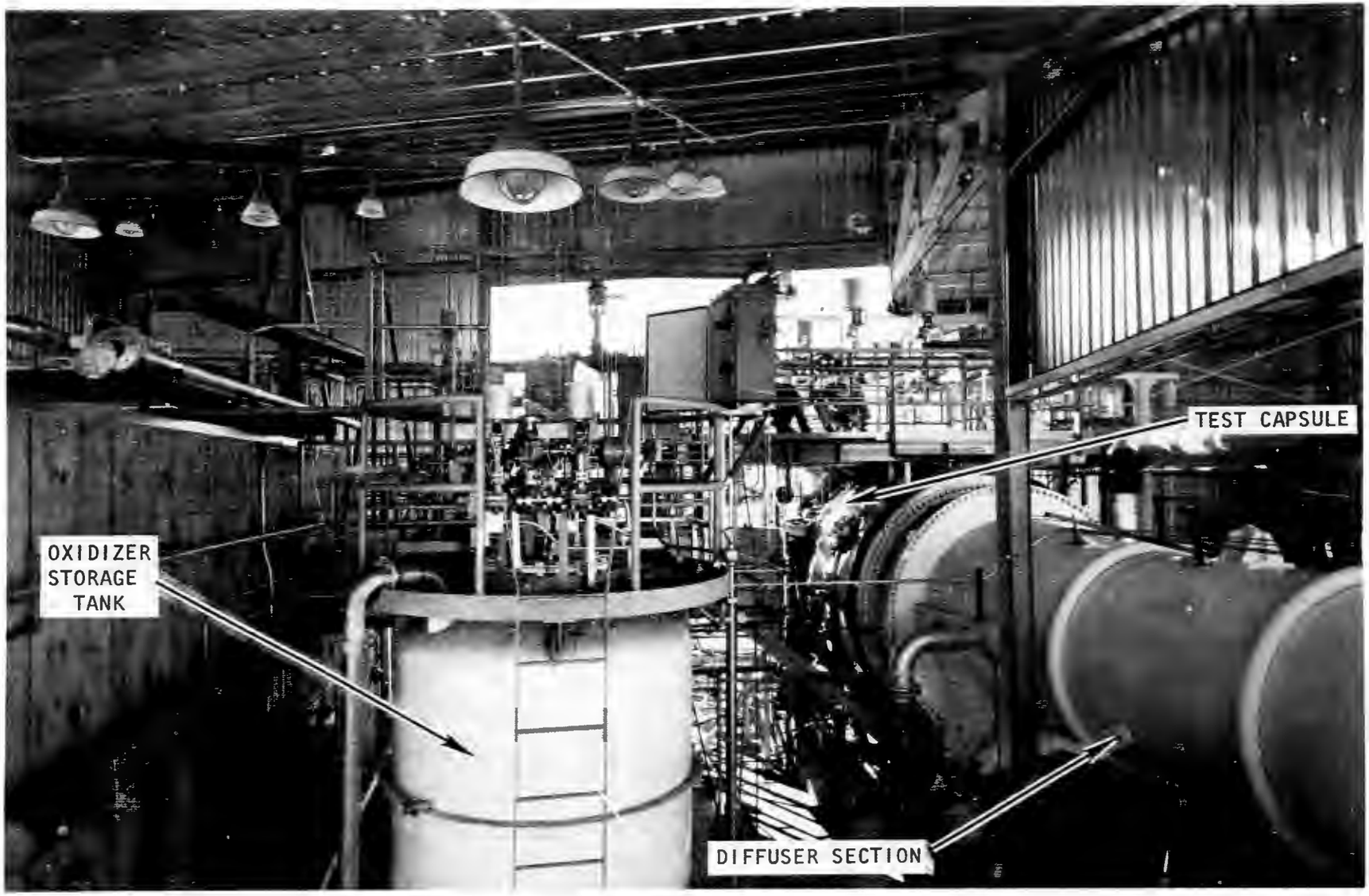

6RE36-11/14/69-R1F

Figure I-6. B-4A Main Thrust Chamber Test Facility (U)

6RE36-11/7/69-R1B

Figure I-7. B-4A Test Position, View of Test Capsule (U)

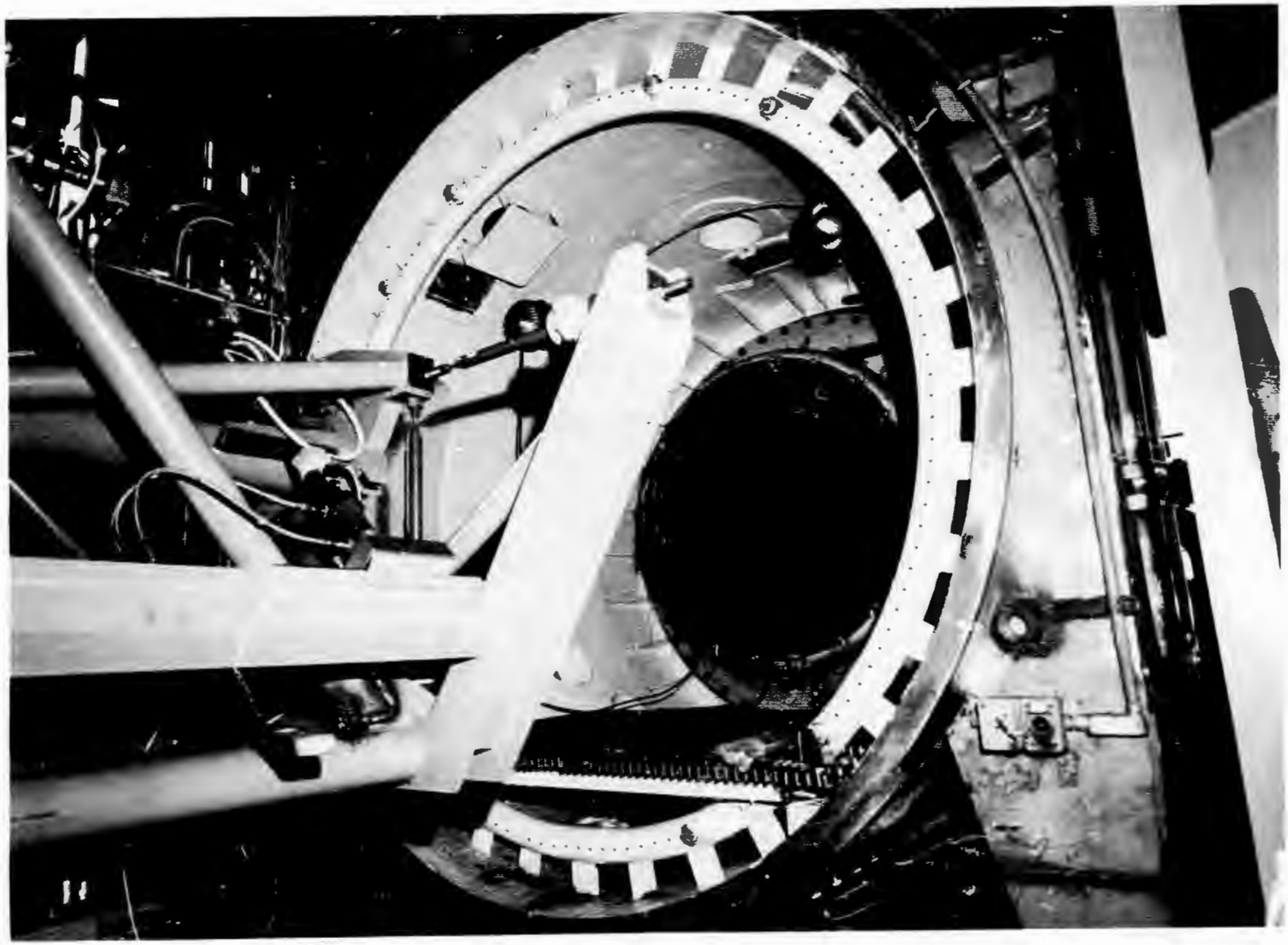

6RE36-2/4/70-R1A

Figure I-8. Altitude Capsule Interior and Diffuser Inlet (U)

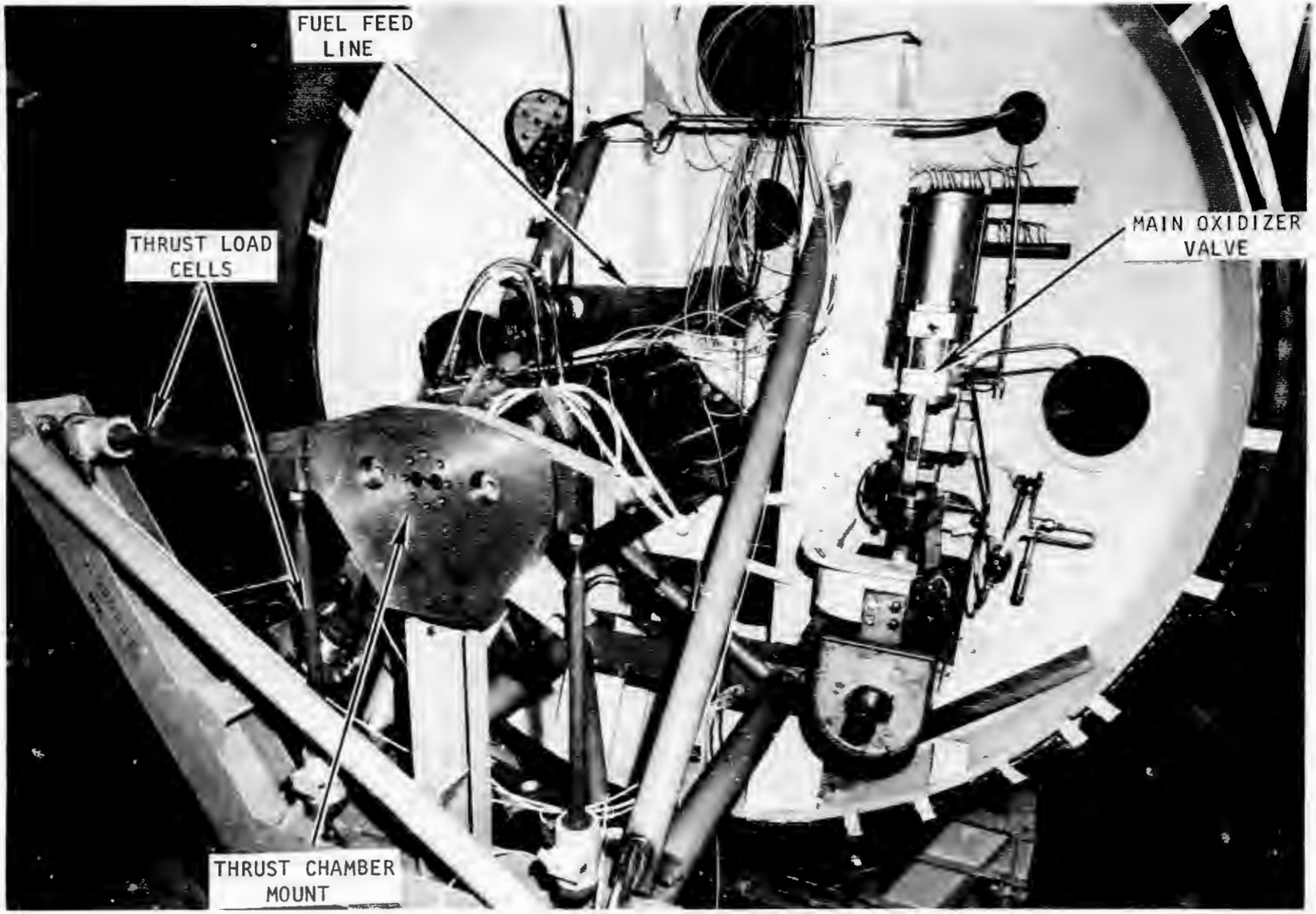

6RE36-2/4/70-R1B

Figure I-9. Altitude Capsule Thrust Mount (U)

(U) The oxidizer storage tank used at NFL, test stand B-4A, was a 525-gallon LN_2-jacketed tank originally located at NFL test stand B-3A. The tank required no internal modifications. All high-pressure feed ducting and pressurizing and purge systems were newly fabricated and installed by an outside contractor. The oxidizer storage vessel is shown in Fig. I-6.

(U) The oxidizer system was completely disassembled, cleaned, and dried after completion of the construction subcontractor's effort. As discussed in Section III, 7.0, b, modifications were made to the oxidizer system to overcome difficulties encountered during facility activation.

b. Fuel System

(U) The fuel run tank was a 1000-gallon, vacuum-jacketed vessel rated for 3000-psi service. Significant design modifications included the addition of Perlite in the vacuum jacket, the addition of polyurethane insulation around the tank and inlet and outlet ducting, and modifications to the inlet and outlet flanges.

(U) The fuel storage tank was a 28,000-gallon, vacuum-jacketed dewar. This tank required no modifications.

c. Altitude Facility Design

(U) The use of the existent altitude simulator facility for the AMPS engine required that the facility be tailored to the AMPS engine size and flowrates. The design provided for a water-jacketed diffuser insert to be installed inside the existing diffuser section (Fig. I-10) with access to the diffuser for inspection and repairs. The existing water system was modified to provide control for proper cooling flowrates for the variable-thrust operation.

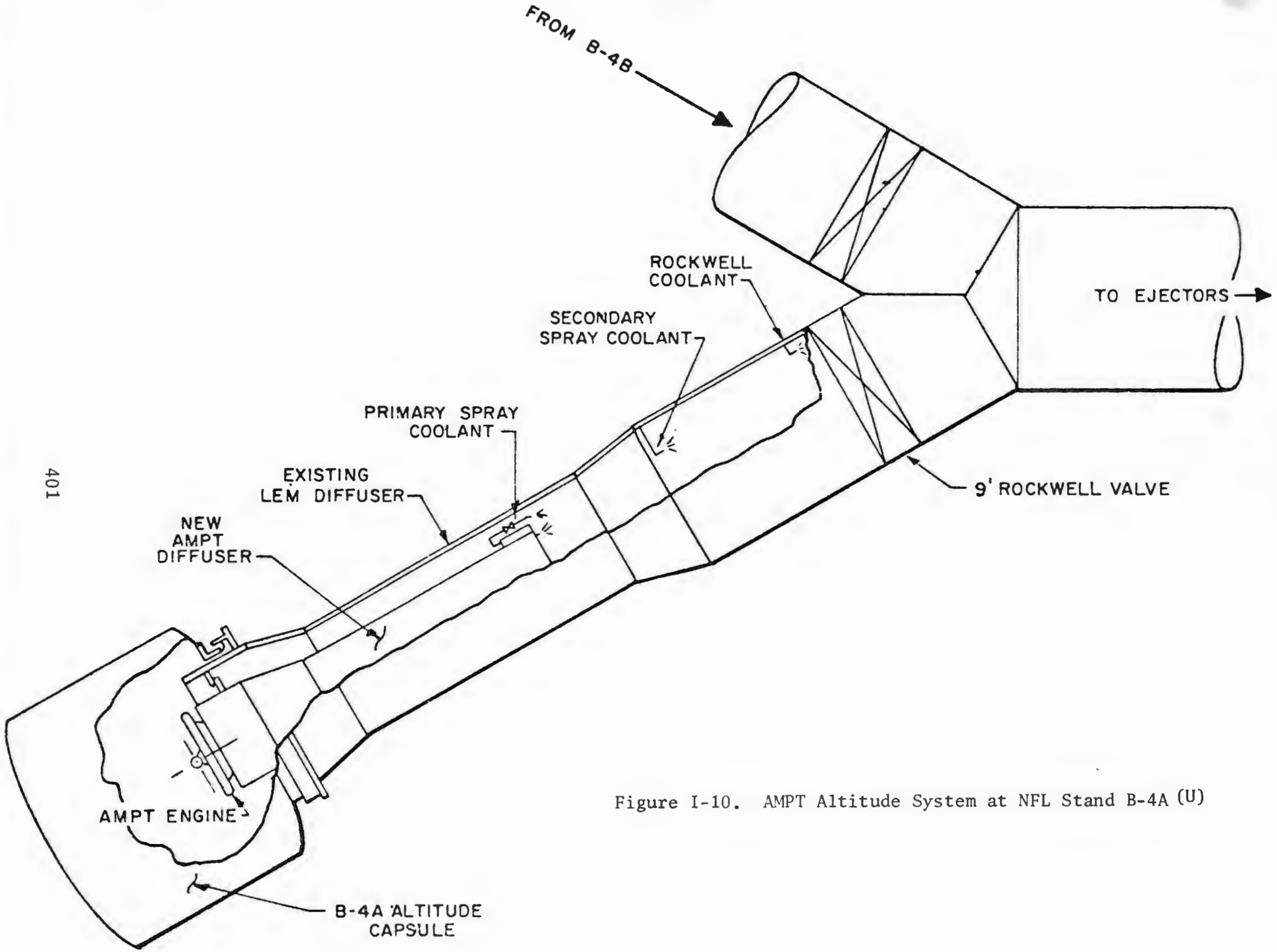

Figure I-10. AMPT Altitude System at NFL Stand B-4A (U)

d. Thrust Measuring System

(U) The thrust measuring system (Fig. I-9) design included provisions for measuring angular misalignment and thrust vector displacement in addition to measuring total axial thrust. Because the firing attitude of the thrust chamber was horizontal, the "side" load cells served the dual purpose of supporting the thrust mount and thrust chamber. The thrust-measuring system was attached to the movable head of the capsule.

APPENDIX II

PERFORMANCE ANALYSIS PROCEDURE

(U) The basis of comparison of combustion performance was characteristic velocity (c*) efficiency (percent of theoretical chemical equilibrium characteristic velocity at the thrust chamber conditions). Delivered characteristic velocity was calculated based on the method of measured chamber pressure and on the method of measured thrust. Standard performance equations were used, with corrections applied to the measured values for energy losses and departure from ideal, one-dimensional flow.

(U) The method of measured thrust was not applicable to tests where the chamber pressure was below 200 psia. This was due to nozzle separation that occurred below that chamber pressure and voided the thrust measurement. Below 200-psia chamber pressure, the method of measured chamber pressure only was used. In addition, the measured thrust method was not used for the 30-degree segment test due to nonaxial thrust caused by the skewed divergent nozzle.

1. c* BASED ON CHAMBER PRESSURE

(U) The delivered value of c*:

$$c^*_{\text{delivered}} = \frac{P_{c_o} A^* g}{w} \qquad (1)$$

where

P_{c_o} = free stream stagnation pressure at throat, psia

A^* = aerodynamic throat area, in.^2

g = gravitational constant, 32.174 ft/sec^2

w = total injector propellant flowrate, lb/sec

$$\eta_{c^*} = \frac{c^*_{\text{delivered}}}{c^*_{\text{theoretical chemical equilibrium}}} \qquad (2)$$

where

$c^*_{\text{theoretical chemical equilibrium}}$ = theoretical value associated injection enthalpy of the propellants diminished by heat loss prior to boundary layer attachment

$$\eta_{c^*} = \frac{P_{c_o} A^* g}{w\, c^*_{\text{theoretical chemical equilibrium}}} \qquad (3)$$

(U) The parameters used in Eq. 1 are not all measured directly, but are obtained by application of suitable correction factors to the measured parameters. Application of these factors to Eq. 3 gives:

$$\eta_{c^*} = \frac{(P_{c_{\text{injector end}}})(A_T)(F_G)(F_{TE})(F_{PR})(F_{HL})}{(w_o + w_f)(c^*_{\text{theoretical chemical equilibrium}})}$$

where

$P_{c_{\text{injector end}}}$ = measured chamber pressure at the injector face, psia

A_T = measured throat area, ambient temperature, in.^2

F_G = factor to account for geometric throat effect

F_{TE} = factor to account for thermal shrinkage of throat gap due to thermal growth of the backup structure of the thrust chamber

F_{PR} = factor to account for enlargement of the throat gap due to chamber pressure

F_{HL} = factor to account for heat loss to chamber wall prior to boundary layer attachment

w_o = measured injector oxidizer flowrate, lb/sec

w_f = measured injector fuel flowrate, lb/sec

(U) The applicable correction factors for η_{c*} based on chamber pressure are listed below.

a. Correction for Conversion of Measured Injector End Chamber Pressure to Free Stream Stagnation Pressure at the Throat

(U) The free stream stagnation pressure at the throat was assumed to be equal to the measured injector end chamber pressure. Analysis had shown the total correction to be less than 0.8 psia verifying that this is a valid assumption for a throat chamber with a contraction ratio in the range of 11:1.

b. F_{TE}, Correction for Thermal Throat Shrinkage

(U) A correction factor to account for the throat gap change due to heating of the inner and outer body backup structure by the regenerative coolant was required. The throat structure temperature of the individual bodies was calculated by interpolation of individual body delta temperature from coolant inlet to coolant outlet for the regeneratively cooled thrust chamber and calculated mean wall temperatures for the water-cooled chambers. The proper proportion ratio was determined by measurement of individual body total integrated heat rejection rate of the 30-degree water-cooled thrust chamber segment. The stress analysis techniques are detailed in Ref. 1. The corrections are shown in Fig. II-1 and II-2.

c. F_{PR}, Correction for Throat Gap Change Due to Chamber Pressure

(U) A correction factor to account for the theoretical throat gap change due to pressure loading was calculated for the tubular wall and channel wall thrust chamber segments and is shown in Fig. II-3 and II-4. There was no throat deflection of the copper-solid-wall, 5-inch or 30-degree water-

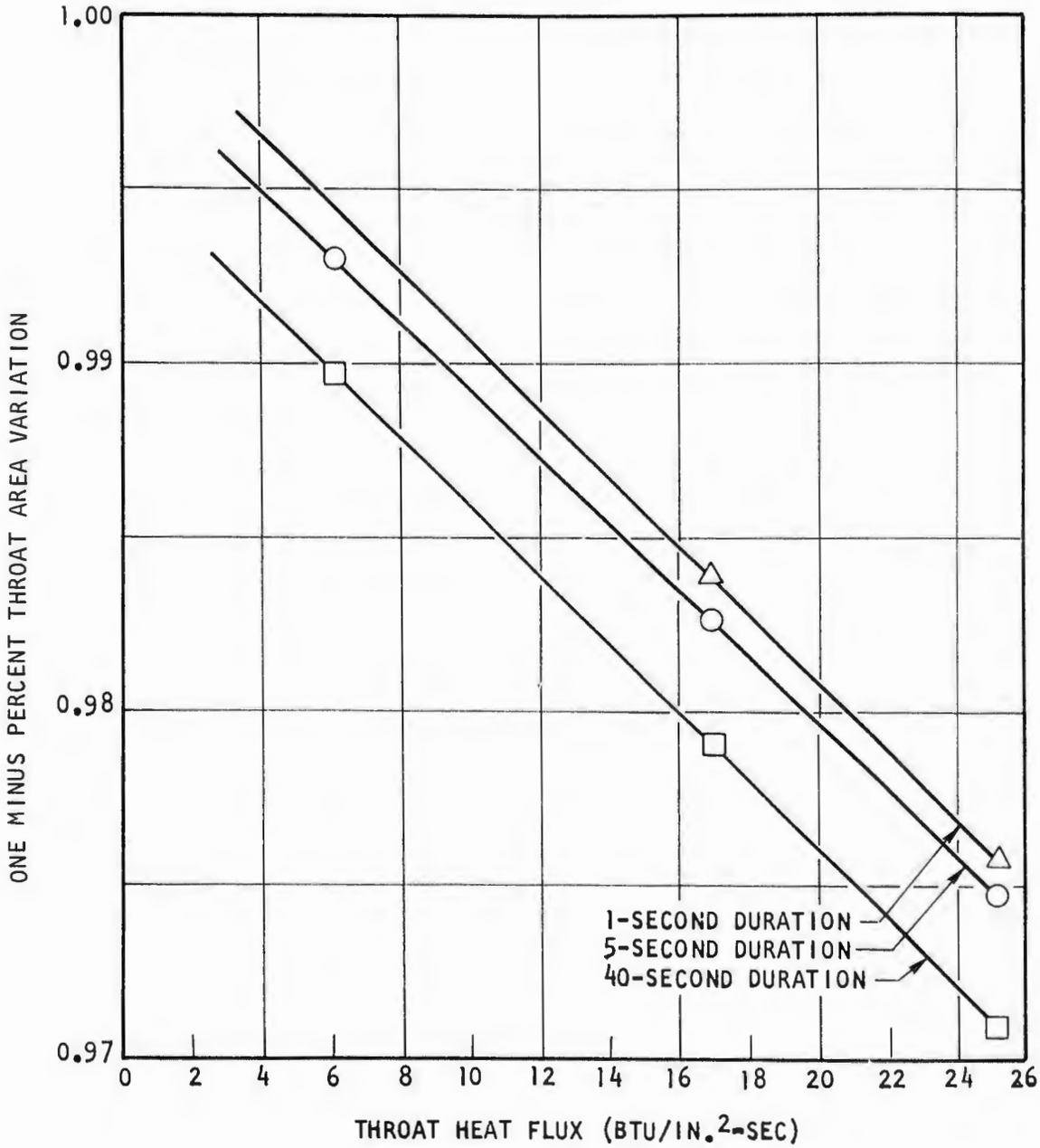

Figure II-1. Throat Thermal Shrinkage Correction Factor for 30-Degree Water-Cooled Segment (U)

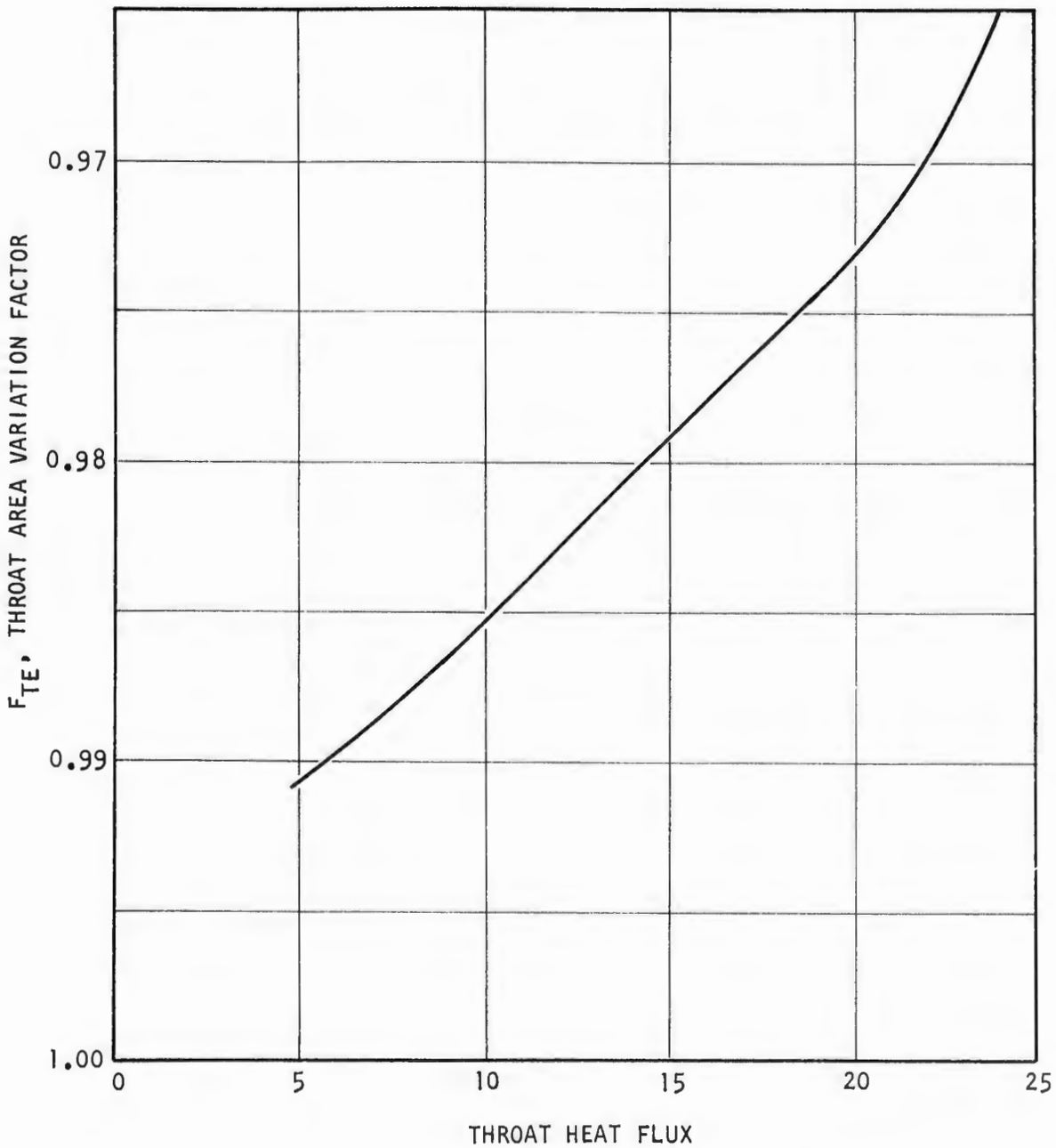

Figure II-2. Throat Correction Factor for Thermal Deflection, 5-Inch and 30-Degree, Solid-Wall Thrust Chambers (U)

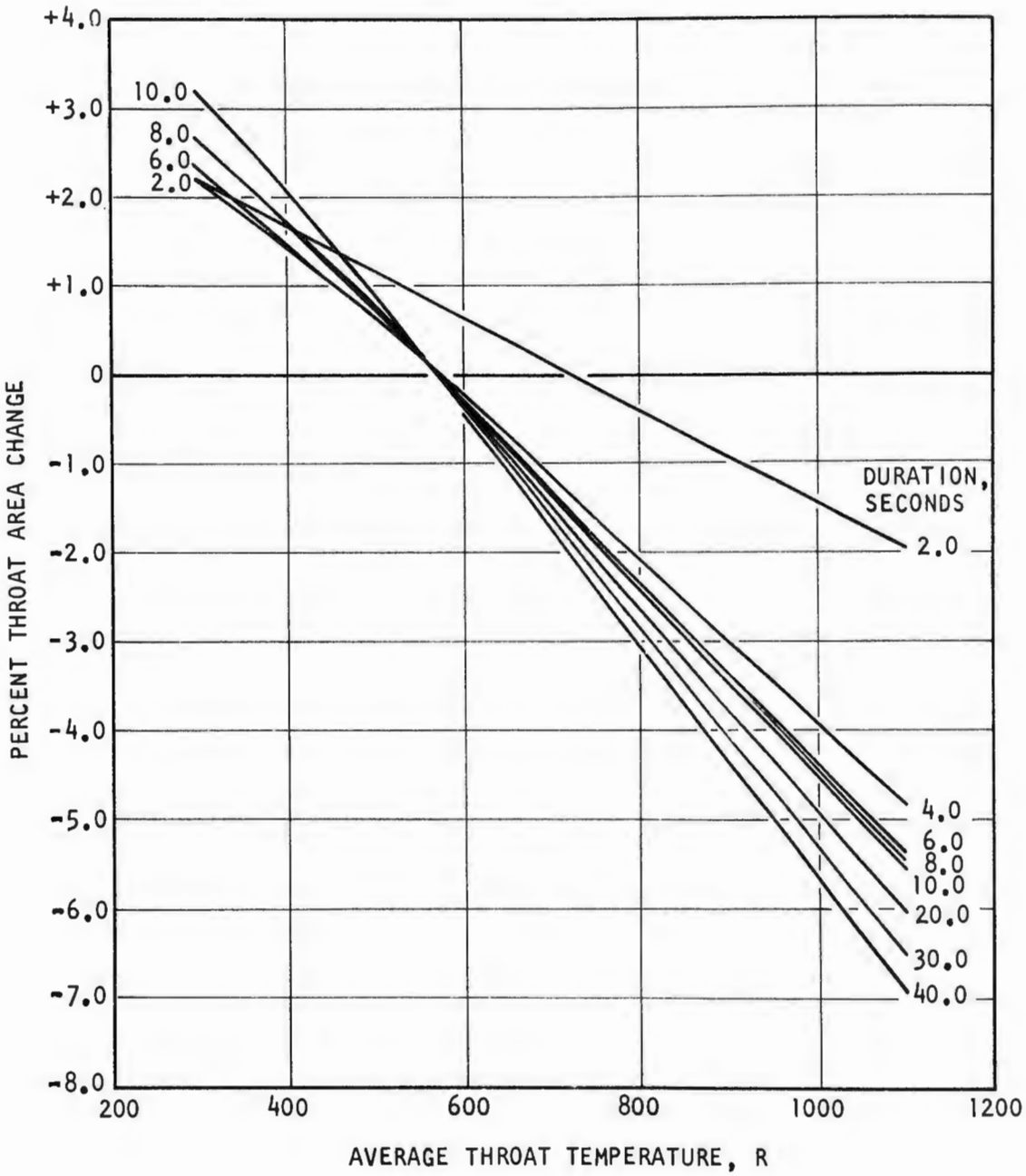

Figure II-3. 30-Degree Regeneratively Cooled Segment (Inner Body Throat Area Change) (U)

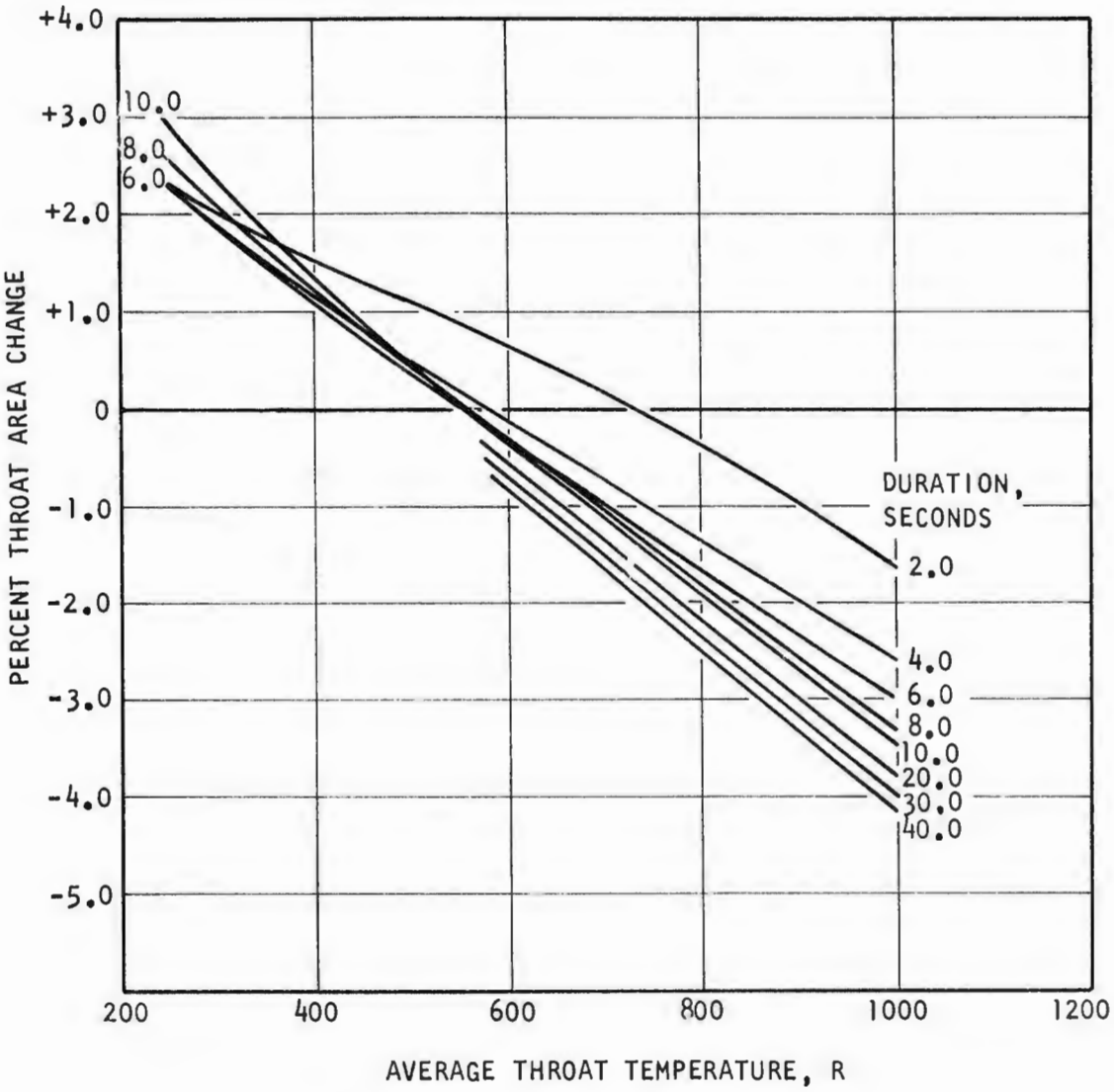

Figure II-4. 30-Degree Regeneratively Cooled Segment (Outer Body Throat Area Change) (U)

(U) cooled thrust chambers because of their more rigid construction. The material properties of the regeneratively cooled thrust chamber backup structure at the operating temperatures were used during analysis.

d. F_{HL}, Correction for Heat Loss to the Upper Combustion Zone

(U) Boundary layer and heat transfer losses are covered in the same section since they are virtually inseparable and either presented alone may confuse their effect on the delivered performance. For purposes of analysis, the thrust chamber wall is divided into two regions: the region between the injector and the point where boundary-layer attachment occurs, and the region between the attachment point and the nozzle exit.

(U) The region before the boundary layer growth begins is marked by the presence of violent turbulence and combustion. In this region, the heat transferred to the thrust chamber wall is lost uniformly by all of the gas; a molecule that transfers heat to the wall may reach the center of the flow field or by a series of collisions receive some energy from the gas in the center of the flow field. The reaction rates are high in this area, and stay time is long; thus, the gas composition will achieve the equilibrium associated with the reduced energy level. The gas will then proceed through the remaining length of the thrust chamber as though the lost heat had never been present. Therefore, in relation to the potential performance at the injector conditions, a heat loss has occurred. This heat loss is defined as the difference in the one-dimensional isentropic expansion (ODIE) specific impulse values at the two energy levels divided by the value at injection conditions.

(U) Once boundary layer growth is initiated, the heat transferred to the wall is lost entirely from the boundary layer. Gross diffusion, conduction, and radiation between boundary layer and core gas is assumed to be negligible. The core gas proceeds through the nozzle without further loss of

(U) heat. As heat is lost, the boundary layer grows to include an increasing portion of the total flow, but for any boundary layer thickness, the portion of the mass outside the boundary layer has lost no heat or it would become part of the boundary layer. For realistic nozzles, the boundary layer never contains more than a very small fraction of the total fluid mass.

(U) As stated in the philosophy of correction, there are two heat transfer regions--one is the region prior to boundary layer development and the other is the region that is subject to boundary layer mechanics. It is assumed that heat lost in the first region is removed from the bulk of the flow and affects its general energy level. This effect is to be taken while allowing the flow to conform to shifting equilibrium. Therefore, when choosing the correct theoretical value to use with a given corrected experimental c*, one must account for the amount of heat which was not available to the "core" flow at the time it passed through the throat. The values of para-hydrogen theoretical c*'s multiplied by the correction factor obtained at the injection temperature of the hydrogen are, therefore, too high.

(U) There are several ways that this heat loss can be included in theoretical c* determination. One method is to remove the heat from the propellants prior to running the theoretical, thermochemical equilibrium calculation. Essentially, this is the technique that is used here. However, instead of recalculating the entire theoretical number, the heat loss prior to boundary layer development will be removed from the hydrogen by artificially adjusting the measured injection temperature of an "effective injection temperature." The effective temperature is then used to determine a "corrected" value of the correction factor to para-hydrogen data. The technique is outlined in Table II-1 and the values are shown in Fig. II-5.

(U) The heat loss to the region prior to the boundary layer attachment was determined experimentally for both the 5-inch and 30-degree segment thrust chambers.

TABLE II-1

ESTIMATION OF THEORETICAL c* INCLUDING EFFECTS OF HEATED FUEL AND HEAT LOSS PRIOR TO BOUNDARY LAYER DEVELOPMENT (U)

Step 1: Look up the para-hydrogen theoretical c* value that corresponds to the proper P_c and MR

Step 2: Look up the value of ξ at the proper P_c and MR but use the following temperature ($\xi = c^*_{\text{theoretical correct}}/c^*_{\text{theoretical para-hydrogen}}$)

$$T_{H_2}{}_{\text{effective}} = T_{H_2}{}_{\substack{\text{measured} \\ \text{injector}}} - \frac{\Delta \dot{Q}}{C_{p_{H_2}} \dot{w}}$$

where:

$T_{H_2}{}_{\text{effective}}$ = effective H_2 injection temperature, F

$T_{H_2}{}_{\substack{\text{measured} \\ \text{injector}}}$ = measured H_2 injection temperature, F

$\Delta\dot{Q}$ = heat flowrate removed prior to boundary layer development, Btu/sec

C_p = specific heat of H_2 at $T_{H_2}{}_{\substack{\text{measured} \\ \text{injector}}}$, Btu/lbm-F

$\dot{w}$ = measured hydrogen flowrate, lbm/sec

then:

$$c^*_{\text{theoretical}} = (c^*_{\text{para-hydrogen}})\ (\xi)$$

(see Fig. II-5 for values of ξ)

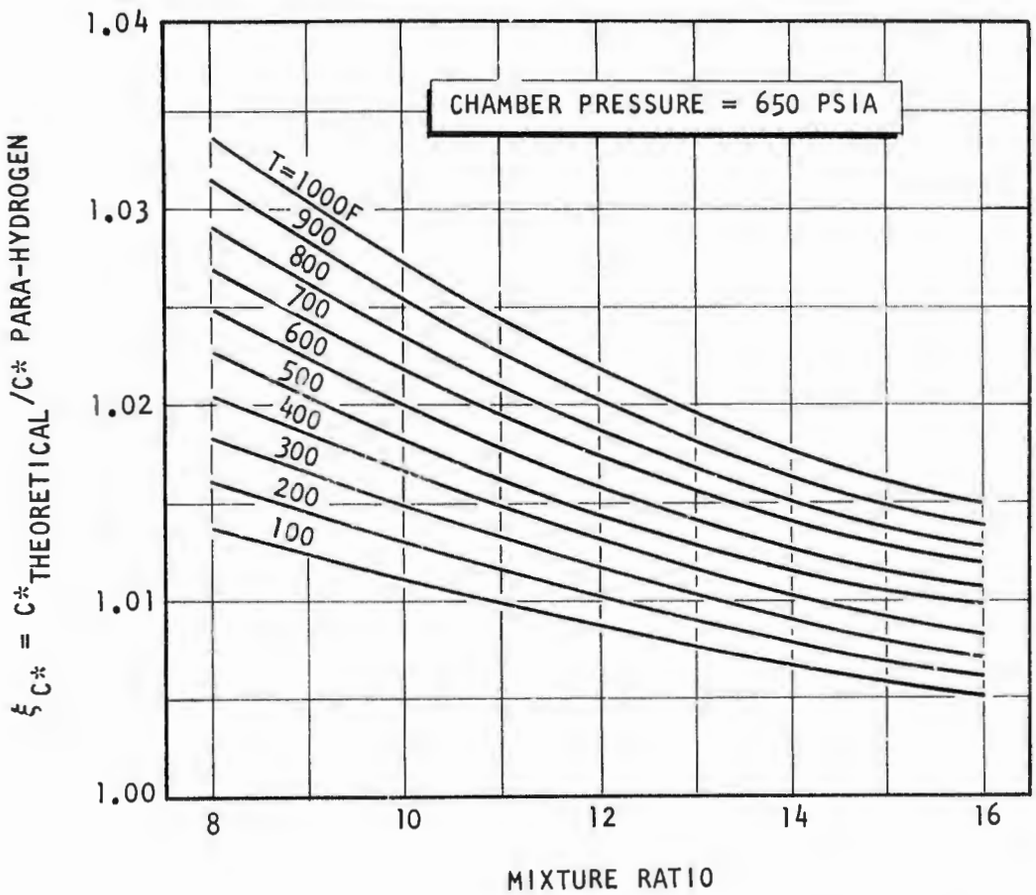

Figure II-5. c* Correction vs Mixture Ratio (U)

(U) The heat loss through the boundary layer from the boundary layer attachment point to the throat was considered from the boundary layer only and no correction was applied for this.

3. F_G, Correction for Geometric Efficiency

(U) Analytical and experimental determination of the factor to be applied to the geometric throat area to account for boundary layer effects and deviation from one-dimensional flow. This factor is shown in Fig. II-6 for the 5-inch and 30-degree segments as a function of chamber pressure.

2. c* BASED ON THRUST

(U) The alternate determination of c* efficiency, from 200 to 650 psia chamber pressure, for the 5-inch segment assembly, is based on the following:

$$c^*_{\text{delivered}} = \frac{(F_{\text{vacuum}})(G_c)}{(C_{F_{\text{theoretical vacuum}}})(W_T)} \tag{4}$$

and

$$\eta_{c^*} = \frac{c^*_{\text{delivered}}}{c^*_{\text{theoretical chemical equilibrium}}} \tag{5}$$

and

$$\eta_{c^*} = (C_{F_{\text{theoretical vacuum}}})(W_T)(c^*_{\text{theoretical chemical equilibrium}}) \tag{6}$$

where

F_{vacuum} = vacuum thrust, pounds

$C_{F_{\text{vacuum}}}$ = theoretical chemical equilibrium thrust coefficient (vacuum) corrected for fuel injection temperature and heat loss from the products of reaction to the thrust chamber segment walls (coolant)

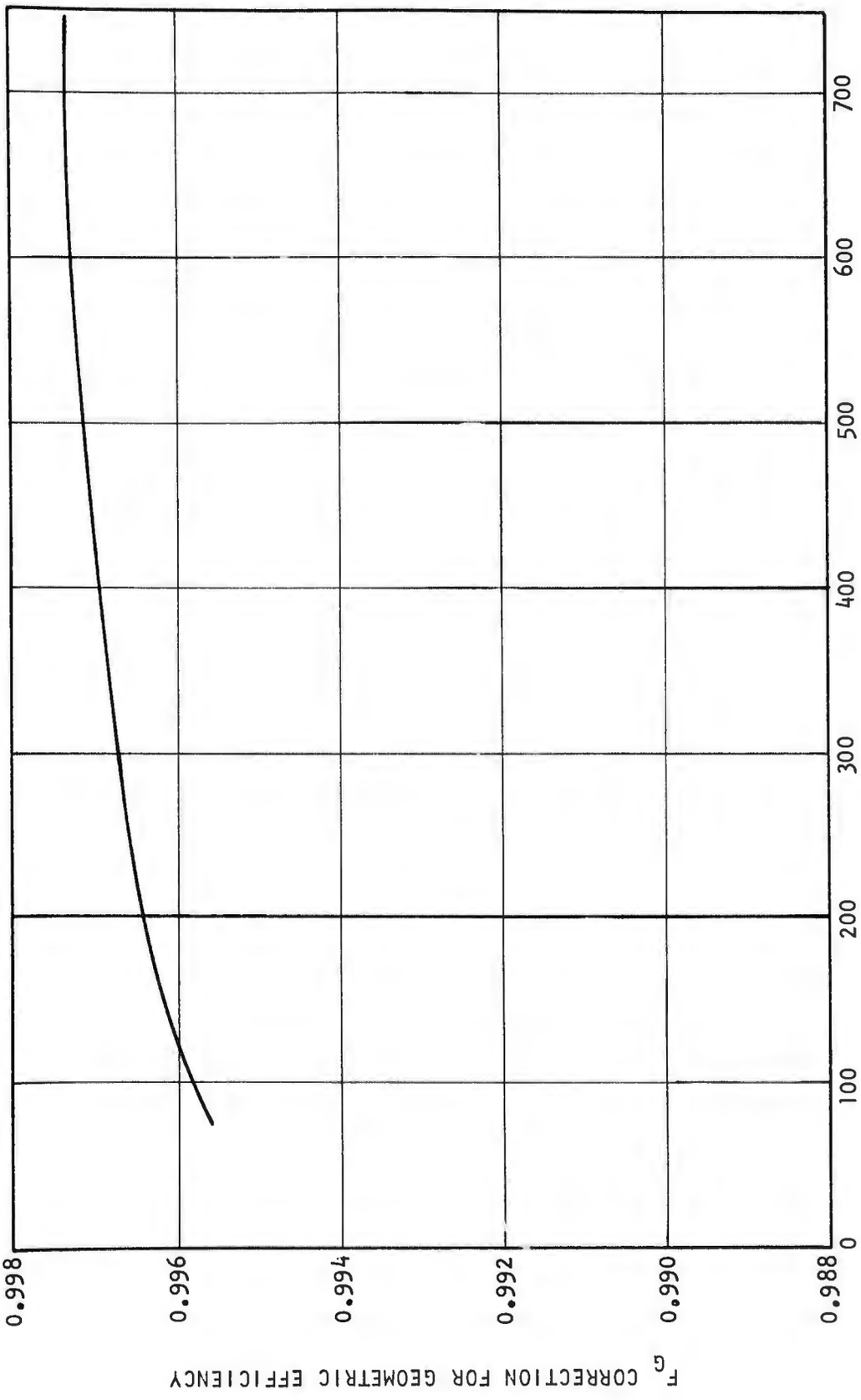

Figure II-6. Chamber Pressure vs Throat Discharge Coefficient (U)

(U) As noted previously, not all parameters are measured directly; therefore, certain corrections must be applied. Equation 6 is therefore modified:

$$\eta_{c^*} = \frac{(F_{site} + P_e A_e - P_b A_b)(G_c)\left(1 + \sum_{i=1}^{n} F_i\right) - n}{(C_{F_{\substack{\text{theoretical vacuum} \\ \text{corrected}}}})(w_o\ w_f)(c^*_{\substack{\text{theoretical chemical} \\ \text{equilibrium}}})} \qquad (7)$$

where

$$\sum_{i=1}^{n} F_i = F_{FR} + F_{DIV} + F_K$$

and

F_{site} = measured total effective thrust, pounds

$P_e A_e$ = thrust due to discharge pressure at chamber hot-gas exit plane

$P_b A_b$ = thrust due to pressure acting on the thrust chamber exit base

a. F_{FR}, Correction for Frictional Drag

(U) This factor corrects for the energy losses due to drag forces resulting from the viscous action of the combustion gases on the thrust chamber walls. Its magnitude, which is the integral of the local friction forces over the chamber and nozzle inside wall, was determined by means of a boundary layer analysis utilizing the integral momentum equation for turbulent flow. This analysis accounts for boundary layer effects from the injector to the nozzle exit by suitable description of the boundary layer profile and local skin friction coefficient. This analysis was conducted as described in Ref. 1.

b. F_{DIV}, Correction for Divergence

(U) The one-dimensional theoretical performance calculations assume that flow at the nozzle exit is uniform and parallel to the nozzle axis. The

(U) correction factor, F_{DIV}, allows for nozzle divergence (i.e., for nonaxial flow and for non-uniformity across the nozzle exit plane). The factor was calculated for the 30-degree segment assembly by means of a computer program which utilized the axisymmetric method of characteristics for a variable property gas. Computation begins with a transonic analysis using series expansions of the differential equations of motion near Mach 1 to calculate irrotational flow field. This procedure provides a characteristic line for use in the analysis of the supersonic portion of the nozzle. The resulting pressures are integrated over the given geometry. This analysis was conducted as described in Ref. 1.

c. F_K, Correction for Kinetic Loss

(U) A correction to account for kinetic losses in the nozzle which consists of a deviation from full chemical equilibrium expansion was calculated by computer program as described in Ref. 1. The values are presented in Fig. II-7. The kinetic losses in the expansion were negligible for chamber pressures above 350 psia.

d. C_F, Theoretical Chemical Equilibrium Correction for Heat Loss

(U) The theoretical C_F was corrected for heat lost from the products of reaction to the upper combustion zone between the injector face and point of boundary layer attachment. The point of boundary layer attachment and the rate of heat loss (Btu/sec) were determined experimentally for both the 5-inch solid-wall, water-cooled; and 30-degree solid-wall, water-cooled, calorimetry thrust chamber segments. The heat loss rate as a function of chamber pressure was determined as is presented in Fig. II-8.

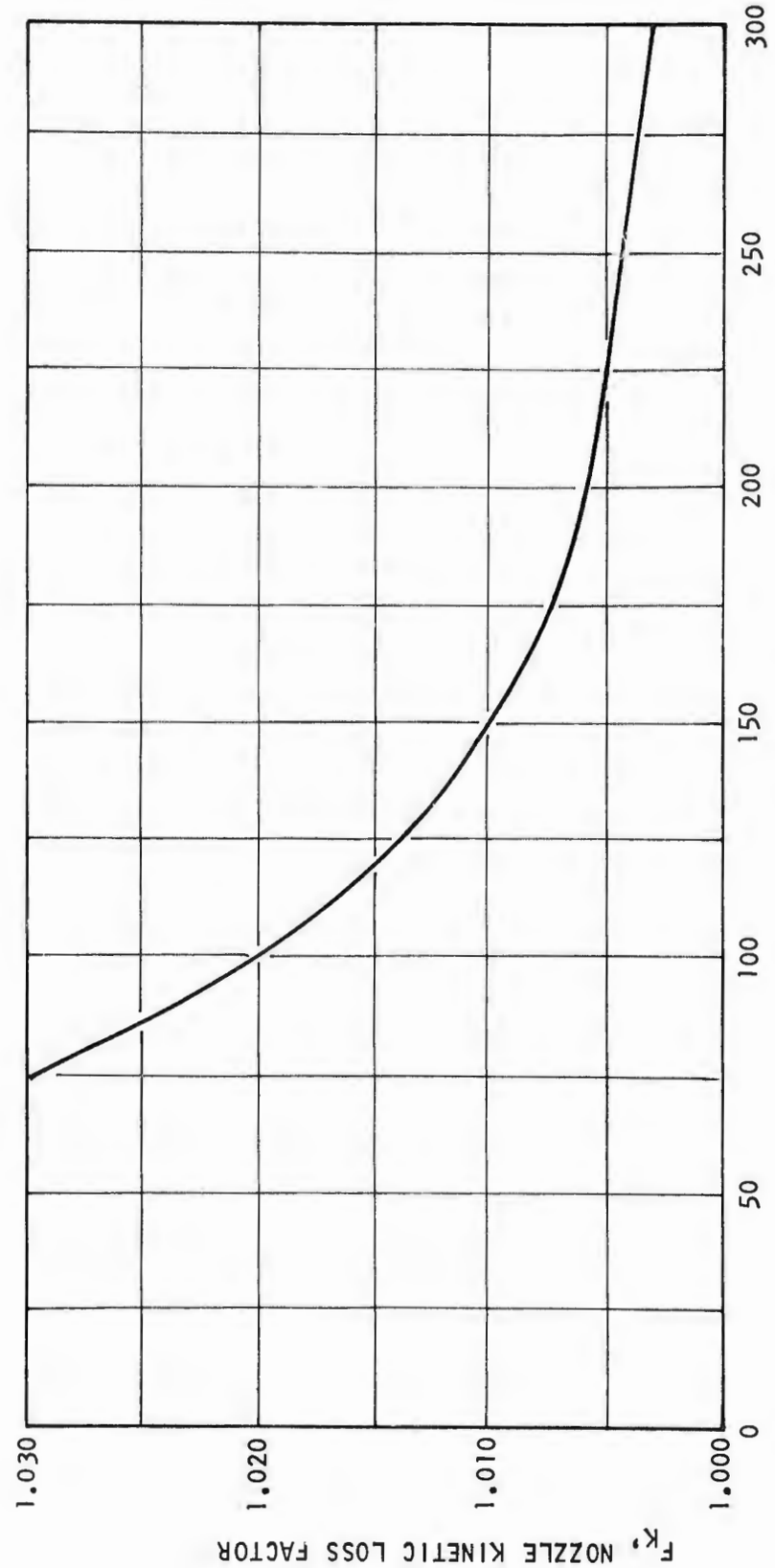

Figure II-7. Chamber Pressure vs Nozzle Kinetic Loss Factor for the Nozzle (U)

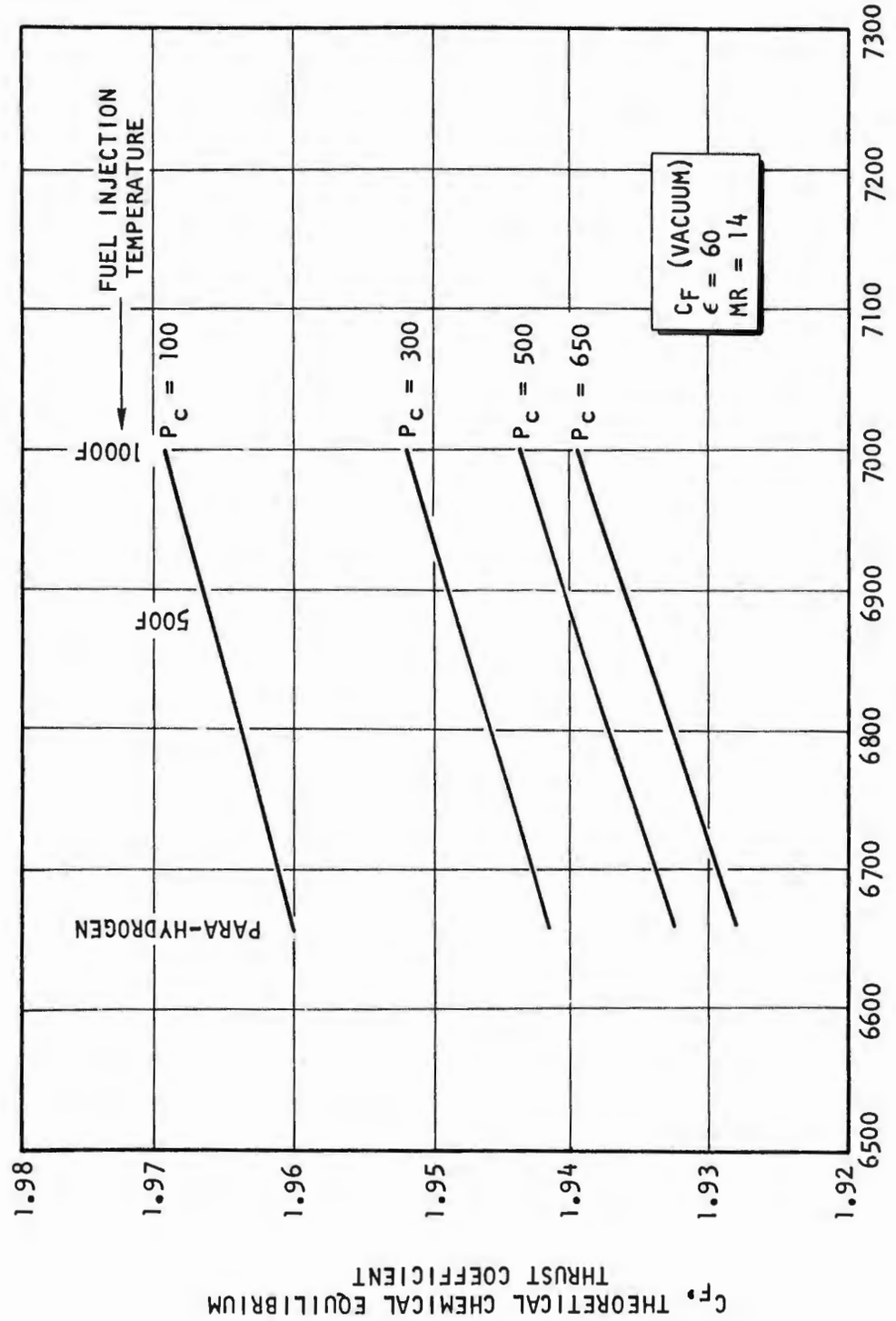

Figure II-8. Theoretical C_F and Enthalpy Relationships at Various P_c Levels (U)

(U) The heat lost from the products of reaction prior to boundary layer attachment is considered to have come from the total products (core) and decreases their sensible heat (enthalpy) accordingly. Since there is a decrease in the sensible heat of the products, there will be a commensurate decrease in C_F. For purposes of the analysis (for ease of computation), the theoretical $C_{F_{vacuum}}$ was corrected (decreased approximately 1 percent maximum) as follows, noting that:

$$c^*\left(C_{F_{\substack{\text{theoretical vacuum} \\ \text{corrected}}}}\right)(W_T)\left(c^*_{\text{theoretical}}\right)$$

$$C_{F_{\substack{\text{theoretical vacuum} \\ \text{corrected}}}} = C_{F_{\substack{\text{theoretical} \\ \text{vacuum}}}} - \frac{U\,K}{w_{\substack{\text{total injected} \\ \text{propellants}}}}$$

where

U = upper combustion zone heat loss as determined during segment testing, Btu/sec

K = $\frac{C_F}{\text{enthalpy}}$ as derived from Fig. II-8.

(U) The assumption was also made that there was no heat loss from the core downstream of the boundary layer attachment point. The heat is lost from the boundary layer only; therefore, there is no effect on C_F.

UNCLASSIFIED
Security Classification

DOCUMENT CONTROL DATA - R & D

(Security classification of title, body of abstract and indexing annotation must be entered when the overall report is classified)

1. ORIGINATING ACTIVITY (Corporate author)	2a. REPORT SECURITY CLASSIFICATION
Rocketdyne, a Division of North American Rockwell Corporation, 6633 Canoga Avenue, Canoga Park, California 91304	CONFIDENTIAL
	2b. GROUP 4

3. REPORT TITLE

Advanced Maneuvering Propulsion Technology Program--Interim Final Report (Volume II: Fluorine/Hydrogen Engine Critical Component Demonstration Testing

4. DESCRIPTIVE NOTES (Type of report and inclusive dates)

Interim Final Report (November 1967 through June 1970)

5. AUTHOR(S) (First name, middle initial, last name)

Rocketdyne Engineering

6. REPORT DATE	7a. TOTAL NO. OF PAGES	7b. NO. OF REFS
October 1970	440	6

8a. CONTRACT OR GRANT NO.	9a. ORIGINATOR'S REPORT NUMBER(S)
F04611-67-C-0116	R-8280 Vol. II
b. PROJECT NO.	
c.	9b. OTHER REPORT NO(S) (Any other numbers that may be assigned this report)
d.	AFRPL-TR-70-127

10. DISTRIBUTION STATEMENT

Qualified users may obtain copies of this report from the Defense Documentation Center

11. SUPPLEMENTARY NOTES	12. SPONSORING MILITARY ACTIVITY
	AFRPL AFSC-USAF Edwards AFB, California

13. ABSTRACT

(U) The results of the Advanced Maneuvering Propulsion System (AMPS) engine critical component evaluations are presented. The components included segments of the main aerospike thrust chamber, complete main aerospike thrust chamber assembly, and main and secondary engine LF_2 pump bearings and seals.

Performance, regenerative cooling, and combustion stability were demonstrated on aerospike thrust chamber segment firing tests. Fabrication of a complete 12-segment thrust chamber assembly was completed.

Dynamic testing of the pump bearings and seals was accomplished; however, sufficient durations were not accumulated at design conditions to demonstrate feasibility and durability of the bearings and seals.

DD FORM 1 NOV 1473

UNCLASSIFIED
Security Classification

14 KEY WORDS	LINK A		LINK B		LINK C	
	ROLE	WT	ROLE	WT	ROLE	WT
Maneuvering						
ΔV						
Channel-Wall Cooling						
Liquid Fluorine Pump Bearings and Seals						
Aerospike Thrust Chamber						
Segmentation						